Diversité morphologique, formation et évolution des bedforms sous-glaciaires : implications pour la compréhension des interactions glace-eau-sédiments

Jean Verité

DOCTORAT ECOLOGIE BRETAGNE GEOSCIENCES LOIRE AGRONOMIE ALIMENTATION

Le Mans Université

université angers

THESE DE DOCTORAT DE

LE MANS UNIVERSITE

DELIVREE CONJOINTEMENT AVEC

L'UNIVERSITE D'ANGERS

ECOLE DOCTORALE N° 600

Ecole doctorale Ecologie, Géosciences, Agronomie et Alimentation

Spécialité : Sciences de la Terre et de l'Environnement

Par

Jean Vérité

Diversité morphologique, formation et évolution des bedforms sous-glaciaires :

Implications pour la compréhension des interactions glace-eau-sédiments

Thèse présentée et soutenue à Le Mans, le 8 décembre 2022
Unité de recherche : UMR 6112
Thèse N° : 2022LEMA1041

Rapporteurs avant soutenance :

Chris Stokes	Professeur – Université de Durham
Clément Narteau	Professeur – Institut de Physique du Globe de Paris

Composition du Jury :

Président :	Clément Narteau	Professeur – Institut de Physique du Globe de Paris
Examinateurs :	Laurie Barrier	Maître de Conférences – Institut de Physique du Globe de Paris
	Florent Gimbert	Chargé de Recherche – IGE Grenoble
	Anna Grau Galofre	Chargée de Recherche – LPG Nantes
Dir. de thèse :	Régis Mourgues	Professeur – Le Mans Université
Co-enc. de thèse :	Édouard Ravier	Maître de Conférences – Le Mans Université
	Olivier Bourgeois	Professeur – Nantes Université

Remerciements

Ça y est, l'écriture de ces remerciements marque définitivement la fin de cette belle aventure qui m'aura animée durant ces trois dernières années. Ce moment m'offre la possibilité de remercier des professeurs passionnants et passionnés qui ont jalonnés mon parcours scolaire – qui se termine enfin à presque 26 ans –, les personnes avec qui j'ai collaborées durant ces trois années de thèse mais aussi et surtout toutes les personnes qui m'ont soutenues de près ou de loin, sans qui je ne serai pas là, sans qui ce travail n'existerait pas ou ne serait pas aussi abouti.

First, I would like to thank **Chris Stokes** and **Clément Narteau** for agreeing to report my PhD thesis work, and **Laurie Barrier**, **Anna Grau Galofre**, and **Florent Gimbert** for agreeing to be the examiners. Your expertise and your final evaluation are fundamental to give meaning to this work. So thank you very much for accepting to be in this jury.

Ensuite, un grand merci à tous les membres de mon encadrement officiel comme officieux, vous vous êtes, chacun dans votre rôle, impliqués pour que – je l'espère – cette thèse soit une réussite et je m'estime chanceux d'avoir pu compter sur vous. Merci d'avoir initié ce beau projet qu'est l'ANR, merci pour vos idées, vos relectures, nos discussions, votre temps, votre investissement … J'espère ne pas vous avoir trop usé ! Merci aussi pour la constance de votre encadrement qui m'aura permis de tenir bon scientifiquement notamment durant les deux premières années marquées par le Covid. En détails, je tiens à remercier :

- **Régis Mourgues**, qui aura été mon professeur de licence avant de devenir mon directeur de thèse. L'orientation scientifique prise par ce travail se sera un peu éloigné de ton domaine de recherche de prédilection mais tu as toujours su apporter ton expertise sur des aspects de mécanique et de modélisation analogique, qui ont été fondamentaux dans mon travail. Je serais systématiquement ressorti moins ignorant de nos échanges, alors merci !

- **Stéphane Pochat** et **Paul Bessin** d'avoir été ces si importants encadrants « officieux ».

Merci à toi Stéphane d'avoir été ce tonton nantais très humain, d'avoir été titillant/stimulant et d'avoir apporté ton expertise de géomorphologue multitâche ; tes idées parfois déroutantes au début auront toujours fait un bout de chemin positif dans mon esprit, alors merci ! En revanche, je suis désolé, tes références musicales resteront un peu abstraites pour moi.

Un grand merci à toi Paul qui aura été mon professeur en licence avant de devenir collègue. Je pourrais parler de ta contribution scientifique dans ce travail de thèse ou de ton organisation parfaite des UEs, qui rendent à coup sûr les enseignements de TP/TD plus faciles pour les doctorants. Mais j'ai surtout envie de parler de ton humanité et de ta bienveillance qui sont, à mon sens, essentielles dans un laboratoire et qui l'auront assurément été pour moi durant ces trois ans de thèse. Merci pour toutes ces discussions sur le boulot ou sur la vie, au bureau passé 19h (on n'est pas du matin que veux-tu), autour

d'une bière ou sur mon balcon avec une tisane. Merci pour ta porte toujours ouverte, pour tous tes conseils et pour tes mots sur nombre de mes maux de doctorants. Merci pour tous ces moments partagés, pour ce dernier été de rédaction et bien d'autres choses …

- **Olivier Bourgeois** d'avoir été ce co-directeur tant impliqué et précieux. Merci Olivier pour ton expertise et ton expérience, et d'avoir été ce géologue pluridisciplinaire capable de relier des disciplines et concepts à priori irréconciliables. Tes nombreuses idées, tes remarques pertinentes et ta justesse scientifique auront contribuées de façon majeure à la construction de ce travail. Merci également pour ton calme, ta rigueur et ton esprit critique ; un doctorant reste avant tout un étudiant et j'aurai énormément appris grâce à toi ! Merci pour cette mission dans les Alpes, pour ton flegme, ton sens de l'observation et tes connaissances partagées sur le terrain.

- et enfin **Edouard Ravier**, mon co-directeur mais surtout mon directeur officieux. Édouard, tu auras été la personne déterminante et inspirante dans mon parcours universitaire, un MENTOR au sens noble du terme, celui qui génère une vocation et avec qui j'ai eu envie de travailler. Merci de m'avoir fait confiance en acceptant de me confier les clés de ce doctorat sur ton projet ANR. J'aime à me dire que tu donnes énormément aux étudiants – comme moi – en cours, en transmettant ta passion pour la recherche et la sédimentologie, et j'espère avoir pu te rendre au moins un tout petit peu en donnant le maximum sur ce projet. Merci pour ta disponibilité de tous les instants, nos innombrables discussions de travail ou non, au bureau, autour d'une bière ou au pied d'un glacier en Islande. Merci d'avoir été ce scientifique rigoureux, hyper impliqué, regorgeant d'idées et de conseils toujours pertinents. Le mérite de la qualité scientifique de ce travail te revient grandement. Merci d'avoir été l'être humain si bienveillant, à l'écoute, constamment de bonne humeur et ayant toujours un mot juste pour encourager, réconforter ou faire rire (parfois chambreur mais c'est de bonne guerre). Avant d'être une aventure scientifique, la thèse est avant tout une aventure humaine dont la réussite tient pour beaucoup de la relation entre le doctorant et son encadrant ; je ne pouvais pas espérer mieux que toi dans ce rôle, sincèrement. Je pourrai encore m'étaler, mais je résumerai en disant que si ma thèse a été si épanouissante tant humainement que scientifiquement, tu en es largement responsable. Une aventure se termine, d'autres s'ouvrent … mais j'espère vraiment qu'on aura l'occasion de retravailler ensemble un jour !

Few words in English to thank **Chris Clark** and **Stephen Livingstone**. Thank you Chris for having opened the doors of your Sheffield's PalGlac team to me with these weekly videoconferences during these first two years of thesis marked by the lockdown, which will have allowed me to present my thesis work twice and to enlarge my culture in glacial sciences. I didn't think you would be so enthusiastic to bring your expertise and to collaborate on my first two papers. Thanks also to Stephen for your interest in my work, your input to the Murtoo paper, and then allowing me to collaborate on this exciting review paper; I am truly grateful.

Je continuerai ces remerciements en adressant un message à tous les membres et collègues du laboratoire LPG Le Mans – enseignant-chercheurs, gestionnaires, ingénieurs, doctorants, ATER et

stagiaires – que j'ai pu côtoyer, qui ont rendu la vie quotidienne plus douce au travail durant ces trois ans ou qui m'ont rendu de fiers services ; notamment Alain, Christelle, João, Leonel, Coraline … et d'autres. Un mot particulier pour Thomas ; merci de m'avoir laissé ton « bébé » et ton modèle analogique. La qualité de ta thèse et du développement du modèle mené avec David m'auront permis de démarrer efficacement ces trois années. Une pensée pour Inna, avec qui j'aurai partagé le bureau pendant quasiment un an ; je ne compte plus nos discussions toujours passionnantes et diverses autour d'un thé. Mention spéciale à Perrine qui aura effectué deux stages avec moi, en L2 et en L3 ; tu auras fait un travail très utile et de grande qualité, alors merci. Et enfin, les plus importants, mes frérots d'aventure – Loïc puis Jimmy – avec qui ont à peu près tout partagé, les moments d'excitation de découvertes comme les baisses de moral, les joies des soumissions comme les déprimes de retours/corrections d'articles. Merci pour votre écoute, toutes nos discussions, les moments de rire au bureau ou en dehors, les services rendus, nos innombrables soirées au Septante Deux et nos diners chez Lolo Lulu qui ont ponctués nos fins de semaine. Merci les gars pour toutes ces journées de travail qui – grâce à vous – ont rendu mon quotidien de thésard très agréable, merci d'avoir globalement toujours été présents même quand le labo était vide ; vivre une aventure pareille bien entouré est essentiel, vous y avez largement contribué.

J'adresserai ensuite un mot à **mes amis**. Un immense merci à mes amis du Mans en particulier Marie R., Lou, Marie B., Aymeric, Elena et Alric. Vous n'aurez probablement que retenu de ces trois années que je traçais des milliers de patates sur mon écran durant les confinements dans mon salon … mais êtes des piliers de ma vie dont la présence et le soutien au quotidien auront été ESSENTIELS afin de garder mon équilibre de vie et le moral dans les bons comme les mauvais moments de la thèse ! Sans vous je n'aurai clairement pas pu tenir durant ces trois ans notamment durant les confinements ; je vous suis infiniment reconnaissant pour ça ! Merci pour tous ces moments partagés et pour toutes nos soirées au Mans, à Paris ou ailleurs, qui m'ont permis de me vider la tête en dehors du travail et d'égayer ma vie le week-end … et parfois aussi la semaine ! Merci aussi à mes amis de Master – Madeline, Thomas et Marine – qui m'auront permis à distance de partager mon quotidien de thésard en géologie et de comprendre bien de mes petits tracas trop techniques pour des non-lécheurs de cailloux.

Enfin merci à **ma famille**. Merci à mes parents. Merci pour votre soutien infini, votre intérêt indéfectible pour ma vie et mon travail et toutes vos petites attentions de parents aimants. Merci d'avoir toujours pensé à prendre de mes nouvelles pour savoir comment j'allais quand je ne pensais pas à en prendre. Merci d'être toujours là pour nous avec Natty et de nous avoir toujours encouragés à faire un métier qui nous plait. Merci à ma sœur, Natty (et Aurélien), d'avoir participé à me faire vivre des bons moments les week-ends tout du long de la thèse et pour ton soutien, dont les preuves – je le sais – ne se limitent à l'intérêt que tu portes aux cailloux et à mes patates. Merci à ma famille au sens large, mes oncles et tantes, mes cousins et mes grands-parents, pour votre présence et votre intérêt sincère.

Table des matières

INTRODUCTION GENERALE

Introduction (*english version*)

Subglacial bedforms are sedimentary mounds and ridges resulting from the remobilization of a sedimentary bed by ice and/or meltwater flow at the base of glaciers (***Rose & Letzer, 1977; Menzies & Rose, 1987***). Due to their size and shape diversity, subglacial bedforms have been categorized into multiple classes (e.g. ribbed, circular and streamlined bedforms, hummocks, murtoos). First examples of bedforms were identified ~ 200 years ago in Ireland (i.e. drumlins; ***Bryce, 1833***), but were not interpreted as subglacial until the late 19th century (***Chamberlain, 1883; Davis, 1884***). Although their existence at the base of modern ice sheets has been demonstrated by geophysical studies for the last 20 years (***O Cofaigh et al., 2002; Smith et al., 2007; King et al., 2009; Franke et al, 2020***), most of the knowledge comes from glacial geomorphology, studying subglacial bedforms exposed after the retreat of ice sheets (***Aylsworth & Shilts, 1989; Greenwood & Clark, 2008; Lewington et al., 2020***). Glacial geomorphology has experienced an exponential growth since the beginning of the 1990s with the development of satellite imagery, allowing to refine their morphological characteristics, their large-scale spatial distributions and their formation processes. The scientific interest of subglacial bedforms depends largely on the difficulties in studying modern subglacial environments, providing only punctual spatial and temporal information on subglacial interactions and processes (***King et al., 2007; Larter et al., 2009; Franke et al., 2020***). Because subglacial interactions and processes directly control ice and meltwater flow dynamics, subglacial bedforms and the information they record are critical features for understanding ice-water-sediment interactions. Since they also provide crucial information for the reconstruction of palaeo-ice sheets (***Kleman & Hättestrand, 1999; Margold et al., 2015***), especially during late deglaciation periods, the study of subglacial bedforms allows us to better understand the contemporaneous and future dynamics of these ice masses in response to climate change.

Given subglacial bedforms are observed in various palaeo-glaciological contexts and geographic locations, their size and shape variabilities have led to the description of numerous bedform classes and even subclasses that are sometimes morphologically very similar, such as for ribbed bedforms (***Dunlop & Clark, 2006; Wagner, 2014***), drumlins (***Knight, 1997; Maclachlan & Eyles, 2013***), murtoos (***Ojala et al., 2021***) or hummocks (***Peterson et al., 2017***), questioning the relevance of classifications based on current morphological descriptions. Furthermore, preconception regarding their shapes (i.e. linear, circular, or triangular) and orientations (i.e. parallel or perpendicular) relative to the direction of ice displacement have commonly led researchers to under-consider complex bedforms, yet commonly observed along glacial paleo-

beds. The variety of subglacial bedform shapes and sedimentary compositions have also led to a multitude of formation hypotheses, whether associated with ice flow or meltwater flow dynamics (e.g. ***Smalley and Unwin, 1968; Boyce and Eyles, 1991; Hättestrand & Kleman, 1999; Linden et al, 2008; Utting et al, 2009; Clark, 2010; Möller, 2010; Eyles et al, 2016; Möller & Dowling, 2016, 2018; Peterson Becher & Johnson, 2021***). This multiplicity of formation hypotheses implies that a single bedform class is often related to different formation processes sometimes arising from different ice flow dynamics, thermal regimes or hydrological systems.

In order to unify this multiplicity of morphological classes and formation hypotheses, the idea of morphological continuum (i.e. morphological sequence characterized by a morphometric continuity between different bedform classes) and even genetic continuum (i.e. evolutionary model dependent on a process or a set of processes) has progressively emerged. The idea has been theoretically conceptualized by ***Aario (1977)*** at the end of the 1970s in order to unify ribbed, circular and streamlined bedforms. This continuum hypothesis is now supported by (i) the observation of morphometric and spatial continuity within bedform fields (***Ely et al., 2016; Sookhan et al., 2021***), (ii) common formation processes between different bedform classes, whose morphological characteristics are thought to be modulated by ice flow velocity (***Stokes et al., 2013a***) and (iii) numerically-reproduced sequences of bedforms arising from instabilities depending on ice-water-sediment interactions (***Fowler & Chapwanya, 2014; Fannon et al., 2017***). In contrast, morphological and genetic continuum hypotheses have never included complex bedforms, yet spatially associated with common bedforms classes, and have never been tested for bedforms associated with meltwater flow dynamics (murtoos, hummocks).

In this manuscript, the morphological characteristics, the spatial distribution and the formation processes of subglacial bedforms – whose the current state of knowledge is preliminary described in Chapitre I – are investigated through a new morphometric analysis developed to jointly study subglacial bedforms mapped along palaeo-ice sheet beds and reproduced by a new analog model (Chapitre II). Supported by 5 articles (2 published, 2 submitted and 1 in preparation), this work explores the existence of morphometric and genetic continuums unifying subglacial bedforms associated with ice flow dynamics (Chapitre III) and meltwater flow dynamics (Chapitre IV). Finally, a synthesis of main results is presented and an evolutionary model unifying the diversity and morphological continuity of subglacial bedforms and depending on spatio-temporal variations of ice and meltwater flow dynamics is proposed (Chapitre V).

1. Introduction

1.1. Contexte général de l'étude

Les bedforms (i.e. modelés '*-forms*' de lit '*bed-*') sous-glaciaires sont des monticules sédimentaires formés par la remobilisation du lit sédimentaire par un écoulement de glace et/ou d'eau de fonte à la base des glaciers (***Rose & Letzer, 1977; Menzies & Rose, 1987***). Au vu de leur diversité de formes et de tailles, ces bedforms ont été divisés en de multiples classes (e.g. ribbed bedforms, drumlins, MSGLs, hummocks, murtoos, etc…). Les premiers exemples de bedforms ont été identifiés il y a près de deux siècles au Nord de l'Irlande (i.e. drumlins ; ***Bryce, 1833***), mais n'ont été interprétés comme sous-glaciaires qu'à partir de la fin du 19ème siècle (***Chamberlain, 1883 ; Davis, 1884***). Bien que leur existence à la base de calottes glaciaires actuelles ait été mise en évidence par des études géophysiques depuis une vingtaine d'années (e.g. ***O Cofaigh et al., 2002 ; Smith et al., 2007 ; King et al., 2009 ; Franke et al., 2020***), l'essentiel des connaissances provient d'étude géomorphologique de bedforms sous-glaciaires mis à nu par le retrait glaciaire ou la disparition d'anciennes calottes (e.g. ***Aylsworth & Shilts, 1989 ; Greenwood & Clark, 2008 ; Lewington et al., 2020***). La géomorphologie glaciaire a connu un véritable essor depuis le début des années 1990 grâce à l'utilisation des images satellites, permettant d'affiner leurs caractérisations morphologiques, leurs distributions spatiales à grande échelle et leurs processus de formation. Leur intérêt scientifique repose essentiellement sur les difficultés d'accès et d'observations à la base des calottes glaciaires, n'offrant que des informations ponctuelles en termes d'espace et de temps sur les interactions et processus sous-glaciaires (e.g. ***King et al., 2007; Larter et al., 2009; Franke et al., 2020***). Puisque ces interactions et processus contrôlent directement la dynamique d'écoulement de la glace et de l'eau de fonte, les bedforms sous-glaciaires et les informations qu'ils enregistrent constituent des objets d'étude privilégiés pour la compréhension des interactions entre la glace, l'eau et les sédiments. Parce qu'ils fournissent également des informations cruciales pour la reconstruction des paléo-calottes glaciaires (e.g. ***Kleman & Hättestrand, 1999 ; Margold et al., 2015***), notamment durant les dernières phases de déglaciation, l'étude des bedforms sous-glaciaires permet d'appréhender avec une meilleure précision les dynamiques actuelles et futures de ces masses glaciaires en réponse au dérèglement climatique.

1.2. Problématiques générales

Dans la littérature, l'étude des bedforms sous-glaciaires se cantonne fréquemment à la description de leurs caractéristiques morphologiques. Conjuguée à des contextes paléoglaciologiques et des localisations géographiques diverses, leurs variabilités de formes a conduit à la description d'une multitude de classes et sous-classes de bedforms souvent très proches morphologiquement à l'instar des ribbed bedforms (e.g. ***Dunlop & Clark, 2006 ; Wagner, 2014***), des drumlins (e.g. ***Knight, 1997 ; Maclachlan & Eyles, 2013***), des murtoos (***Ojala et al., 2021***) ou des hummocks (e.g. ***Peterson et al., 2017***), questionnant la pertinence des classifications actuelles basées sur les paramètres de forme classiques. Par ailleurs, les a-prioris portant sur leurs formes (i.e. linéaire, circulaire ou triangulaire) et leurs orientations (i.e. parallèle ou perpendiculaire) par rapport à la direction de déplacement de la glace ont communément amenés les paléo-glaciologues à ne pas considérer des bedforms de forme complexe, pourtant couramment observés le long des paléo-lits glaciaires.

La grande diversité de formes et de compositions sédimentaires des bedforms sous-glaciaires ont abouti à une multitude d'hypothèses et de processus de formation, qu'ils soient associés à la dynamique d'écoulement de la glace ou de l'eau de fonte (e.g. ***Smalley and Unwin, 1968; Boyce and Eyles, 1991; Hättestrand and Kleman, 1999; Lindén et al., 2008; Utting et al, 2009 ; Möller, 2010; Eyles et al., 2016; Möller & Dowling, 2016, 2018 ; Peterson Becher & Johnson, 2021***). Cette multiplicité des modèles de formation impliquent qu'une même classe de bedform est souvent reliée à divers processus de formation découlant parfois de dynamiques d'écoulement de la glace, de régimes thermiques ou de systèmes hydrologiques différents.

Afin d'unifier cette grande diversité de classes morphologiques et de modèles de formation, l'idée qu'un continuum morphologique (i.e. séquence d'évolution caractérisée par une continuité morphométrique entre les différentes populations de bedforms) et même génétique (i.e. modèle d'évolution dépendant d'un processus ou d'un set de processus) a progressivement émergé. L'idée d'un continuum a été développé depuis la fin des années 1970 afin d'unifier les différentes catégories de bedforms associés à la dynamique d'écoulement de la glace (i.e. ribbed bedforms, bedforms circulaires, drumlins et MSGLs) (***Aario, 1977***). Cette hypothèse de continuum est notamment fondée sur (i)

l'observation d'une continuité morphométrique et spatiale au sein de champs de bedforms (***Ely et al., 2016 ; Sookhan et al., 2021***), (ii) des processus de formation communs dont l'impact morphologique serait modulée par la vitesse de déplacement de la glace (e.g. ***Linden et al., 2008 ; Clark, 2010 ; Stokes et al., 2013a***) et (iii) des séquence d'évolution reproduites par des modèles numériques résultant d'un unique modèle d'instabilités issues d'interactions entre la glace, l'eau et les sédiments (***Fowler & Chapwanya, 2014 ; Fannon et al., 2017***). En revanche, ces hypothèses de continuum morphologique et génétique n'ont jamais inclues les bedforms de formes complexes, pourtant associés spatialement aux bedforms communément décrits dans la littérature, et n'ont jamais été testés pour les bedforms associés à la dynamique d'écoulement de l'eau de fonte (i.e. murtoos, hummocks).

2. Organisation du manuscrit

Ce manuscrit est décomposé en 5 chapitres, s'appuyant sur 5 articles scientifiques, organisés de la façon suivante :

- Le **Chapitre I** s'attèle à définir l'état des connaissances sur les caractéristiques des environnements sous-glaciaires (i.e. glaciodynamiques, hydrologiques, sédimentologiques) et sur les processus de remobilisation de sédiments – responsables de la formation des bedforms – opérant au sein de ces environnements. Ce chapitre établit ensuite un état des connaissances sur les caractéristiques morphologiques, les processus de formation et les distributions spatiales des bedforms en fonction que leur formation soit attribuée à la dynamique d'écoulement de la glace ou de l'eau de fonte. Enfin une synthèse des modèles de continuité morphologique et génétique entre certains types de bedforms sous-glaciaires sera présentée.

- Le **Chapitre II** présente le matériel et les méthodes utilisés dans cette thèse pour l'étude des processus de formation, des caractéristiques morphologiques et de l'évolution des bedforms sous-glaciaires. Ce chapitre décrit notamment le modèle analogique et les outils de post-traitements des données expérimentales développés afin de reproduire et suivre l'évolution des bedforms sous-glaciaires. Enfin, ce chapitre présente le nouveau protocole d'analyse morphométrique développé pour mieux caractériser l'intégralité de la diversité de forme des bedforms sous-glaciaires expérimentaux et naturels.

- Le **Chapitre III** explore les processus de formation et la continuité morphologique et génétique existant entre les bedforms dont la formation est principalement gouvernée par la dynamique d'écoulement de la glace. Dans une première partie, en prenant le cas d'étude des ribbed bedforms et en utilisant la modélisation analogique, leur processus de formation et les relations entre leur diversité morphologique et la dynamique d'écoulement de la glace sont explorées. Dans une seconde partie, les résultats de l'application du nouveau protocole d'analyse morphométrique sur ~ 13 500 bedforms cartographiés en Irlande et au Canada sont présentés afin d'étudier la diversité et la continuité morphologique existant entre les ribbed bedforms, les bedforms circulaires, les drumlins, les MSGLs et les bedforms complexes. Enfin, dans une troisième partie, à partir des résultats des deux parties précédentes et de données originales, nous proposons un modèle d'évolution (i.e. continuum génétique) gouverné par la dynamique d'écoulement de glace et les interactions glace-eau-sédiments et contrôlant la continuité morphologique des bedforms sous-glaciaires préalablement démontrée. Ces trois parties sont ainsi structurées par 3 articles scientifiques :

→ **Article n°1**. Vérité, J., Ravier, É., Bourgeois, O., Pochat, S., Lelandais T., Mourgues, R., Clark, C.D., Bessin, P., Peigné, D., and Atkinson, N. (2021). Formation of ribbed bedforms below shear margins and lobes of palaeo-ice streams. *The Cryosphere, 15, 2889–2916*.

→ **Article n°2**. Vérité, J., Ravier, É., Bourgeois, O., Bessin, P., and Pochat, S. New metrics reveal the evolutionary continuum behind the morphological diversity of subglacial bedforms. (*Submitted in Geomorphology*).

→ **Article n°3**. Vérité, J., Ravier, É., Bourgeois, O., Bessin, P., Pochat, S., and Mourgues, R. Ice-meltwater-bed interactions control directions and quantity of bed deformation and subglacial bedform evolution. (*En preparation*)

- Le **Chapitre IV** explore les processus de formation et la continuité morphologique et génétique existant entre les bedforms associés à la dynamique d'écoulement de l'eau de fonte. Une première partie, utilisant la modélisation analogique et la cartographie de paléo-routes de drainage d'eau de fonte, explore la continuité morphologique et le processus d'évolution entre les murtoos et les ribbed bedforms à partir desquels ils se développent. Dans une seconde partie, un modèle d'évolution gouverné par la pression d'eau de fonte basale et la connectivité hydraulique est proposé afin d'expliquer les

caractéristiques morphologiques et sédimentaires de l'intégralité des bedforms cartographiés et formés le long des routes de drainage d'eau de fonte sous-glaciaires. Ces deux parties sont ainsi structurées par deux articles scientifiques :

→ **Article n°4**. Vérité, J., Ravier, É., Bourgeois, O., Bessin, P., Livingstone S.J., Clark, C.D., Pochat, S., and Mourgues, R. (2021). Formation of murtoos by repeated flooding of ribbed bedforms along subglacial meltwater corridors. *Geomorphology, 408, 108248*.

→ **Article n°5**. Livingstone, S.J., Vérité, J., Ravier, E., McMartin, I., Campbell, J., Lewington, E.L.M., Dewald, N., Clark, C.D., Sole, A.J., Storrar, R.D. Variable ice-water-sediment coupling provides unifying explanation for diverse landforms in subglacial meltwater corridors. (*Submitted in Earth Surface Processes and Landforms*)

- Enfin le **Chapitre V** propose une synthèse des Chapitres III et IV et un modèle d'évolution unifiant la diversité et la continuité morphologique des bedforms sous-glaciaires et dépendant des variations spatio-temporelles de dynamiques d'écoulement de la glace et de l'eau de fonte. Pour terminer des perspectives sont présentées.

3. Contexte de la thèse

Ce travail de thèse a été initié en octobre 2019. Ce travail fait partie du projet Ice Collapse « *Ice sheet collapse in deglaciation periods* », démarré en avril 2019, porté par Édouard Ravier et financé par l'Agence National de la Recherche. Cette thèse a été encadrée par **Édouard Ravier** (Maître de Conférences, LPG Le Mans), **Olivier Bourgeois** (Professeur des Universités, LPG Nantes) et **Régis Mourgues** (Professeur des Universités, LPG Le Mans).

Ce travail a donné lieu à de nombreuses collaborations avec **Paul Bessin** (Maître de Conférences, LPG Le Mans), **Stéphane Pochat** (LPG Nantes, Maître de Conférences), **Chris Clark** (Profesor) & **Stephen Livingstone** (Senior Lecturer) (Département de Géographie de Sheffield), et **Nigel Atkinson** (Senior Quaternary Scientist, Service Géologique de l'Alberta).

Dans le cadre du projet Ice Collapse, ce travail a bénéficié du travail de Post-Doctorat de **Thomas Lelandais** (janvier 2019-octobre 2019) et de **David Peigné** (Ingénieur, LPG Le Mans) sur les aspects

de modélisation analogique (design et construction du modèle expérimental, réalisation des premiers tests et optimisation du modèle).

CHAPITRE I

LES BEDFORMS SOUS-GLACIAIRES : PRODUITS ET MARQUEURS DES INTERACTIONS GLACE–EAU–SEDIMENTS SOUS LES CALOTTES GLACIAIRES

Introduction

Au sein des systèmes glaciaires terrestres, qui couvrent près de 10% de la surface du globe, on distingue différents types d'édifices en fonction de leurs dimensions, de leurs formes et de leurs localisations (inlandsis, calottes glaciaires, champs de glace, glaciers de vallées, glaciers de piedmont, etc.). Parmi ces édifices glaciaires, les calottes glaciaires (e.g. Vatnajökull en Islande et Austfonna au Svalbard) et les inlandsis (e.g. Antarctique et Groenlandais) sont des étendues de glace d'échelle continentale dont la distinction s'opère par leurs dimensions respectivement inférieures et supérieures à 50 000 km² (***Benn and Evans, 2010***) (**Figure 1.1A**). Les édifices glaciaires représentent près de 70% de l'eau douce sur Terre, et stockent l'équivalent de près de 66 m de niveau marin dont 57.9 m pour l'inlandsis Antarctique (***Morlighem et al., 2020***), 7.42 m pour l'inlandsis Groenlandais (***Morlighem et al., 2017***) et 0.32 m pour l'ensemble des autres édifices glaciaires (***Farinotti et al., 2019***). Dans ce manuscrit, nous ferons indistinctement référence à ces étendues de glace d'échelle continentale sous le terme de calottes glaciaires ('*ice sheet*').

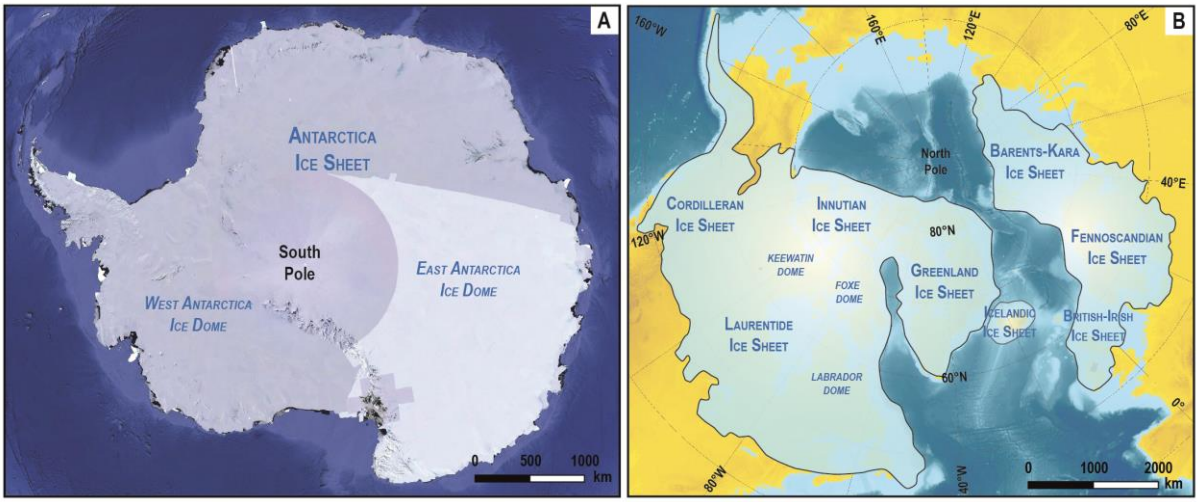

Figure 1.1*. Examples of (A) a modern ice sheet with the Antarctica Ice Sheet (© Google Earth) and (B) palaeo-ice sheets with reconstructed maximal extensions of Northern Hemisphere ice masses during the Last Glacial Maximum (~20ka BP) (ice sheets coverage after* ***Batchelor et al., 2019****).*

Identifier et comprendre les processus opérant à la surface, au sein et à la base des calottes glaciaires est capital pour appréhender les dynamiques actuelles et futures des calottes glaciaires, notamment afin d'anticiper leurs potentielles contributions à l'augmentation du niveau marin. Au cours du Quaternaire, les fluctuations climatiques liées aux cycles astronomiques ont généré de multiples

phases glaciaires et interglaciaires, favorisant les croissances et décroissances répétées de paléo-calottes glaciaires (***Batchelor et al., 2019***). Le retrait des paléo-calottes glaciaires, telles que les calottes Laurentide en Amérique du Nord et Fennoscandinave en Europe du Nord lors **du dernier** maximum glaciaire (‘*Last Glacial Maximum’*, LGM) (**Figure 1.1B**), a mis à jour de très nombreux bedforms sous-glaciaires (e.g. ***Aylsworth & Shilts, 1989 ; Hättestrand and Kleman, 1999 ; Clark et al., 2010***).

Ces bedforms sont le produit de la remobilisation de sédiments sous-glaciaires, contrôlée par les variations spatio-temporelles des processus de couplage et de découplage entre la glace, l’eau de fonte et les sédiments (***Allen, 1968 ; Aario, 1977***). Les bedforms sous-glaciaires constituent ainsi d’excellents témoins des processus sous-glaciaires, dont l’étude permet de mieux appréhender les relations entre les caractéristiques de la dynamique d’écoulement de la glace, du réseau hydrologique sous-glaciaire et de la couche de sédiments sous-glaciaires.

Dans ce chapitre, un état de l’art sur les variabilités spatiales de la dynamique d’écoulement de la glace (Chapitre I - Partie A §1), de la dynamique d’écoulement de l’eau de fonte (Chapitre I - Partie A §2) et des caractéristiques des substrats (Chapitre I - Partie A §3) à la base des calottes glaciaire sera établi afin d’étudier la variabilité des processus sous-glaciaires agissant sur la remobilisation de sédiments (Chapitre I - Partie A §4) et donc le développement de bedforms.

Puis dans un second temps, un inventaire sur la diversité des bedforms sous-glaciaires actuellement décrits dans la littérature comme étant associés respectivement à la (i) dynamique d’écoulement de la glace (Chapitre I - Partie B §1) et à la (ii) dynamique d’écoulement de l’eau de fonte (Chapitre I - Partie B §2) sera présenté en détaillant leurs caractéristiques morphologiques, leurs compositions, leurs distributions spatiales, leurs éventuelles associations avec d’autres bedforms et leurs hypothèses de formation. Une synthèse des modèles et théories qui stipulent l’existence d’un continuum morphologique et génétique entre certains types de bedforms sous-glaciaires sera ensuite présentée (Chapitre I - Partie B §3).

Enfin les problématiques soulevées par cet état de l’art et développées durant ce travail de recherche seront présentées dans un dernier temps.

Partie A. Environnements et processus sous-glaciaires

Eyjabakkajökull, Vatnajökull Ice Sheet, Iceland (2021) (personal photography).

1. Dynamique d'écoulement de la glace des calottes glaciaires

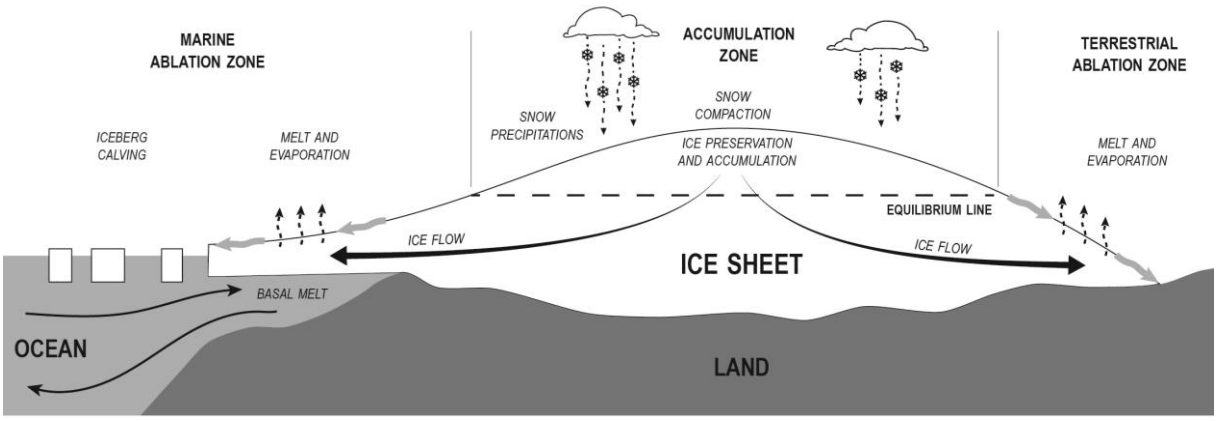

Figure 1.2. *Schematic representation of the mass balance organization within an ice sheet. Ice flow is controlled by the mass balance between accumulation zones (dominated by processes of snow precipitation and compaction, and ice preservation) and ablation zones (dominated by processes of ice melt, evaporation and iceberg calving) (adapted from* ***Sudgen & John, 1976****).*

La dynamique d'écoulement d'une calotte glaciaire, comme celle de tout autre glacier, est fondamentalement modulée par un bilan de masse défini par l'équilibre entre l'accumulation de glace, contrôlée par la compaction et la préservation des précipitations neigeuses, et les pertes, contrôlées par la fonte, la sublimation, l'évaporation et le vêlage d'icebergs (**Figure 1.2**). Ce bilan de masse est ainsi matérialisé par deux zones, une zone d'accumulation et une zone d'ablation, séparées par une ligne d'équilibre matérialisant l'altitude où accumulation et ablation se compensent parfaitement (***Sudgen & John, 1976***). Toutes les calottes glaciaires, en raison de variations de température et de précipitations neigeuses à grande échelle, sont caractérisées par un profil d'altitude de forme parabolique avec une diminution de l'épaisseur de la glace depuis l'intérieur (i.e. zone d'accumulation) vers les marges (i.e. zone d'ablation). Ce profil d'altitude est le facteur de contrôle principal de l'écoulement de la glace, la pente du glacier générant un écoulement gravitaire. Parallèlement, de nombreuses forces de résistance (e.g. forces de friction basale et latérale) agissent aux bordures des masses glaciaires et tendent à contrebalancer l'écoulement gravitaire de la glace.

1.1. Mécanique de l'écoulement de la glace

1.1.1. Forces motrices

En chaque point d'une calotte glaciaire, la colonne de glace exerce une contrainte verticale dépendante de sa hauteur H_i sur son substrat (σ_i, '*normal stress*'). La force motrice qui gouverne le

processus d'écoulement de la glace entre deux points d'une calotte glaciaire est régie par la gravité et la pente de surface entre ces deux points. Cette force motrice est définie par la contrainte d'entrainement gravitaire σ_d ('*driving stress*') (**Figure 1.3A**):

$$\sigma_d = \sigma_i \times \tan(\alpha) = \rho_i \times g \times H_i \times \tan(\alpha)$$

où ρ_i est la masse volumique de la glace, g est la constante d'accélération de la pesanteur (~9.81m/s²) et α est la pente de surface de la glace (***van der Veen & Payne, 2004 ; Hooke, 2005***). Cette force motrice, qui permet à la glace de s'écouler, peut être modulée en fonction des interactions basales entre la glace, l'eau et le substrat. Il existe ainsi 3 processus d'écoulement régis par: la déformation interne de la glace ('*ice deformation'*), le glissement basal ('*basal sliding'*) et la déformation du substrat sous-glaciaire ('*bed deformation'*) (***Benn & Evans, 2010 ; Cuffey & Paterson, 2010 ; Chandler & Evans, 2019***).

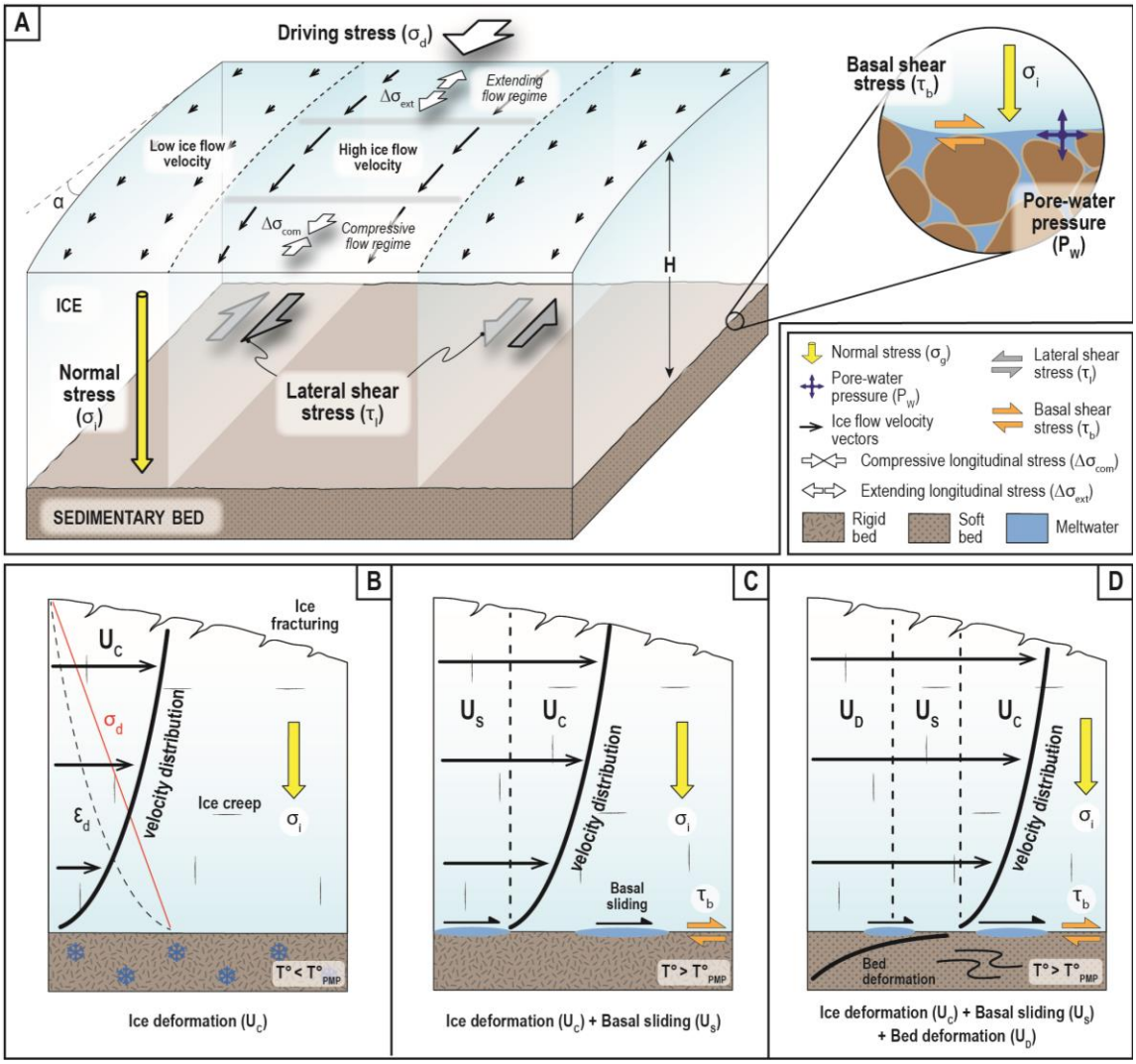

Figure 1.3. *(A) Synthetic diagram of stresses controlling ice motion. Configurations of ice motion controlled by (B) ice deformation only (i.e. creep and fracturing), (C) ice deformation and basal sliding, or (D) ice deformation, basal sliding and bed deformation (modified after* ***Boulton, 1996****).*

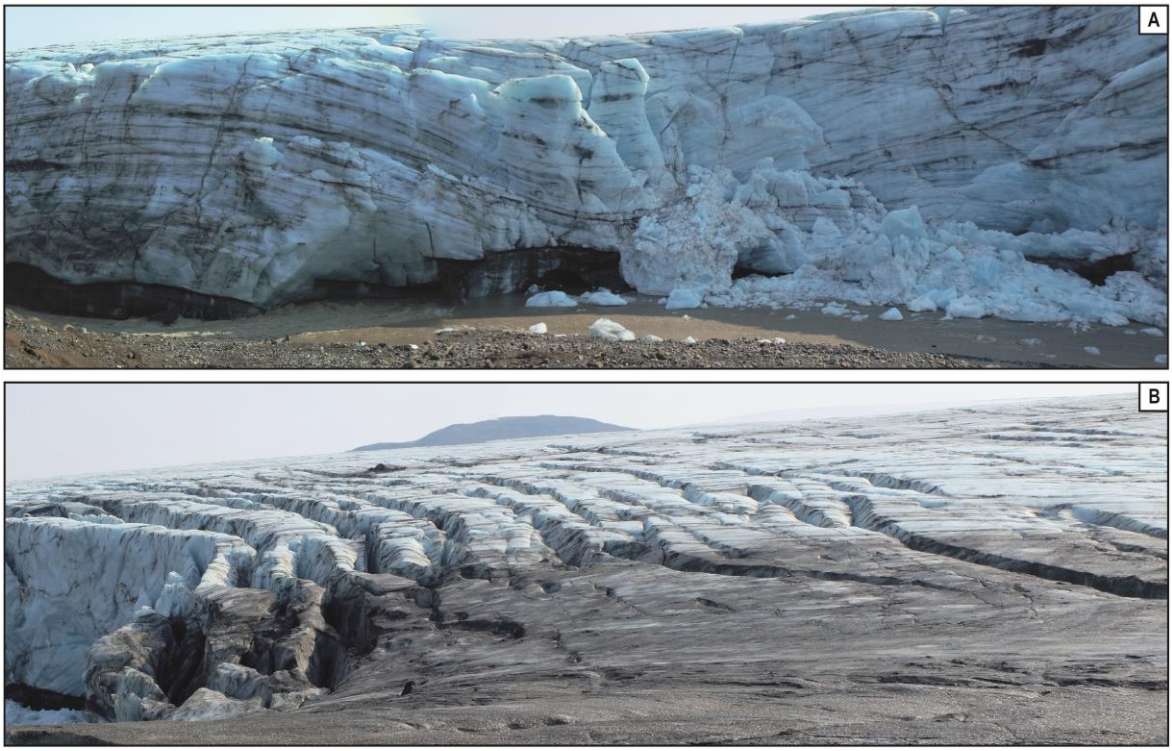

***Figure 1.4**. Ice deformation and motion by (A) creep and (B) fracturation in crevasses (Eyjabakkajojüll, Iceland) (personal photographs).*

D'un point de vue mécanique, la glace est peut être considérée comme un matériau élasto-visco-plastique. Pour des contraintes comprises inférieures à la limite d'élasticité (entre 10 et 60 kPa selon le type de glace), la glace se déforme de façon élastique et la déformation est réversible. Pour des contraintes comprises entre la limite d'élasticité et la limite de plasticité (3.5 MPa), la glace se déforme par fluage ('*Glen flow law'*)[1] au travers de mouvements intra- et inter-cristallins, avec une vitesse de déformation non-proportionnelle à la contrainte en raison de son caractère non-newtonien[2] (***Glen, 1955 ; Nye, 1957***) (**Figure 1.4A**). Ainsi à mesure que la contrainte d'entrainement gravitaire σ_d augmente avec l'augmentation de l'épaisseur de glace depuis la surface vers la base des calottes glaciaires, la vitesse de déformation de la glace augmente de façon non linéaire selon une loi de puissance (cf. '*Glen flow law*'[1]). Ainsi, la vitesse de déplacement de la glace – correspondant à la somme des vitesses de déformation à chaque altitude z entre la surface et la base de la colonne de glace – diminue de façon non linéaire depuis la surface vers la base des calottes glaciaires, expliquant la distribution des vitesses d'écoulement au sein de la colonne de glace (**Figure 1.3B**).

[1] La loi de fluage la plus couramment utilisée est la loi de fluage de Glen ($\varepsilon = A\sigma_d^n$) qui relie selon une loi de puissance (exposant $n \sim 3$) la vitesse de déformation ε de la glace à la contrainte d'entrainement gravitaire σ_d s'appliquant sur une masse glaciaire.

[2] La glace, qui est un fluide non-newtonien, possède un caractère rhéofluidifiant se traduisant par une diminution non linéaire de la viscosité apparente (i.e. augmentation de la déformabilité de la glace) avec l'augmentation de la contrainte.

Lorsque la contrainte dépasse la limite de plasticité, la glace se déforme de manière cassante, créant des fractures à l'origine de la formation des crevasses et des icebergs (**Figure 1.4B**). En l'absence d'eau de fonte à la base de la colonne de glace, générant un couplage intégral avec le substrat rigide (i.e. gelé ou rocheux), seuls les processus de déformation interne (essentiellement par fluage) permettent la mise en mouvement de la glace (**Figure 1.3B**).

Lorsque de l'eau de fonte circule le long de l'interface basale et induit un découplage entre la glace et un substrat rigide, la force de friction basale ('*basal drag'*) entre la base de la colonne de glace et le substrat est fortement réduite, permettant l'écoulement de la glace par glissement basal au-dessus du substrat (U_S). Cette configuration requiert que la base de la colonne de glace soit à une température supérieure ou égale au point de fusion sous pression de la glace ('*pressure melting point'* ; $T°_{PMP}$) (**Figure 1.3C**). Enfin, dans une configuration où de l'eau de fonte est présente de façon hétérogène – formant une mosaïque de zones de couplage ou de découplage – à la base d'une colonne de glace reposant sur un substrat sédimentaire meuble ('*soft warm bed'*), une partie de l'écoulement de la glace peut s'effectuer par la déformation d'un substrat sédimentaire saturé en eau (U_D) (<u>Chapitre I - Partie A §4.1</u>) (**Figure 1.3D**).

1.1.2. Forces de résistance

De nombreuses forces s'opposent à l'écoulement de la glace au sein des calottes glaciaires (**Figure 1.3A**). Dans la plupart des cas, la principale force de résistance qui s'oppose à l'écoulement de la glace est la force de friction basale ('*basal drag'*). La force de friction basale s'opère entre la glace en mouvement et le substrat, et génère une contrainte de cisaillement basal τ_b ('*basal shear stress'*) (***Whillans & van der Veen, 1997 ; Rolstad et al., 2000 ; O'Neel et al., 2005***). Au sein des calottes glaciaires, à la transition entre des lignes d'écoulement de glace de vitesses différentes, les forces de friction latérale ('*lateral drag'*) tendent à inhiber l'écoulement de glace et à générer des contraintes cisaillantes latérales τ_l ('*lateral shear stress'*). Ces forces de friction latérale se développent lorsque la glace s'écoule contre des parois comme dans le cas des glaciers de vallées. Au sein des calottes glaciaires, des variations de vitesse responsables de forces de friction latérale peuvent aussi se développer en réponse à des variations spatiales de la température de la glace, de l'hydrologie sous-

glaciaire (Chapitre I - Partie A §2.2) ou de la lithologie du substrat (Chapitre I – Partie A §3.2) (***Raymond, 1996 ; Raymond et al., 2001***). Enfin, les forces longitudinales ('*longitudinal drag'*) se développent parallèlement à la direction d'écoulement de la glace en réponse à des variations longitudinales de la vitesse d'écoulement et génèrent ainsi des gradients de contrainte longitudinale ('*longitudinal stress*', $\Delta\sigma$). Ces derniers sont la plupart du temps des facteurs de résistance à l'écoulement dans le cas de gradients longitudinaux compressifs $\Delta\sigma_{com}$ ('*compressive flow/longitudinal stress')*, mais peuvent aussi être des facteurs d'entrainement pour l'écoulement dans le cas de gradients longitudinaux extensifs $\Delta\sigma_{ext}$ ('*extending flow/longitudinal stress')* (**Figure 1.3A**).

1.2. Variations spatiales de la dynamique d'écoulement au sein des calottes glaciaires

Au sein d'une calotte glaciaire, la dynamique et la vitesse d'écoulement de la glace sont très variables (**Figure 1.5**). Au-delà du caractère ubiquiste de l'écoulement gravitaire de la glace, de multiples forces de résistance, dépendantes de l'hydrologie sous-glaciaire, des propriétés du substrat (e.g. lithologie, température) et de la nature des terminaisons glaciaires (terrestre ou marine) tendent à contrôler les processus et la vitesse d'écoulement de la glace et la répartition des contraintes qui s'exercent sur le substrat (***Kleman & Borgström, 1996***).

1.2.1. Dômes de glace

Les dômes de glace ('*ice domes'*) sont les régions situées au centre des calottes glaciaires dont l'altitude est située au-dessus de la ligne d'équilibre (**Figure 1.5**). Ces régions sont des zones d'accumulation, où l'épaisseur de glace est la plus forte. Malgré leur faible pente de surface, la forte épaisseur de glace au niveau des dômes génère de fortes σ_d et τ_b. Mais, malgré ces contraintes élevées et en raison des conditions de base froide communément observées pour les dômes de glace ($T° < T°_{PMP}$), l'absence d'eau de fonte basale limite les processus de glissement basal et de déformation du substrat. Par conséquent, au sein des dômes de glace, la vitesse d'écoulement de la glace est très faible en surface (< 50m/an) et nulle à la base puisque l'écoulement de la glace ne s'effectue que par fluage interne (***Dyke, 1993***) (**Figure 1.6**).

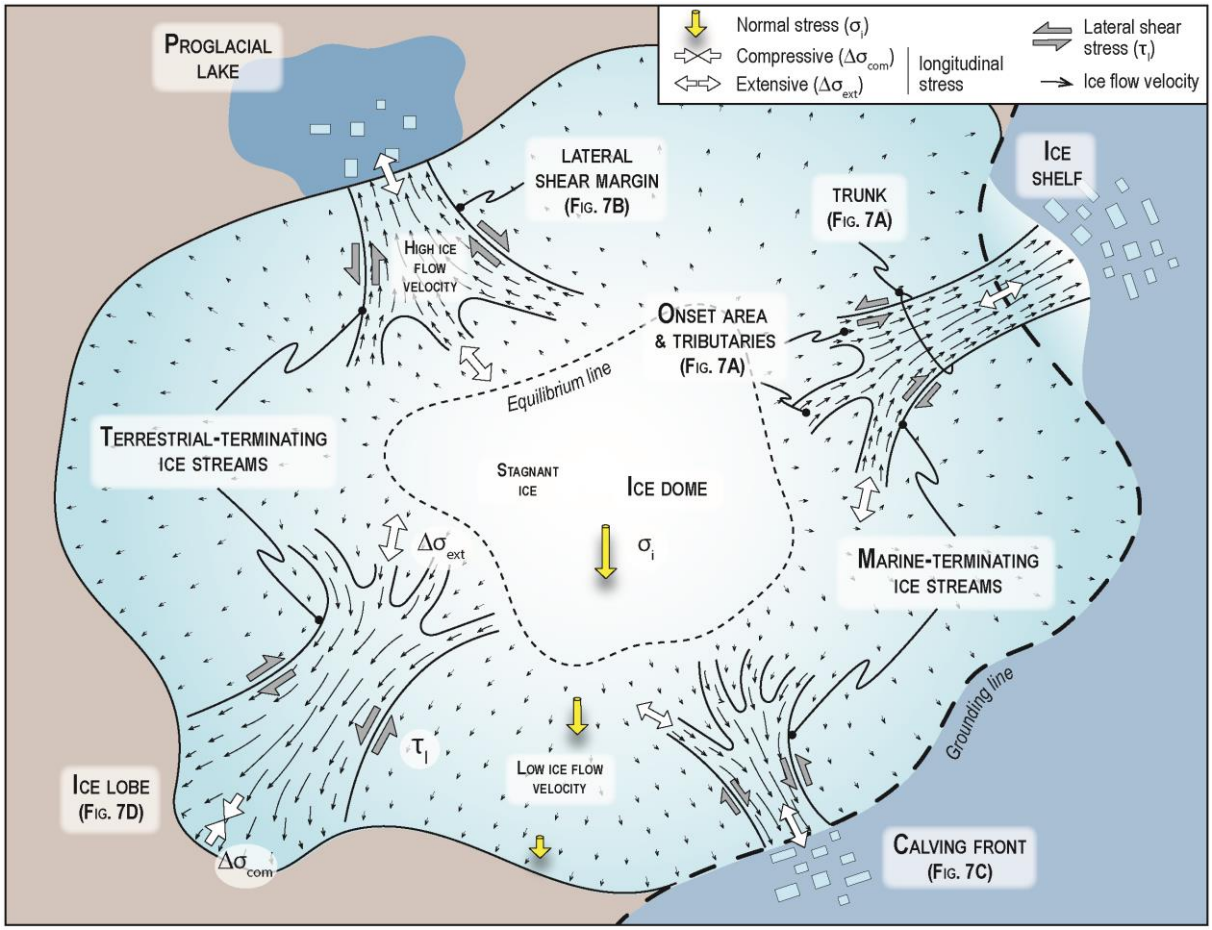

***Figure 1.5**. Schematic map of variations in ice flow dynamics and stresses depending on glaciological environments within an ice sheet.*

1.2.2. Fleuves de glace

La dynamique des calottes glaciaires est largement contrôlée par l'activité de **couloirs,** 1–10^{nes} km de large et 10^{nes}–100^{nes} km de long – situés dans des régions à base tempérée et caractérisés par de fortes vitesses d'écoulement de la glace, nommés fleuves de glace ('*ice streams*') (**Figure 1.5**) (***Paterson, 1994***). En Antarctique, ces fleuves de glace ne couvrent en moyenne que 10% de la surface des calottes glaciaires mais drainent jusqu'à 90% des flux de glace (***Bamber et al., 2000***). Leur vitesse d'écoulement en surface est supérieure à 300 m/an et dépasse fréquemment 1000 m/an, générant des contraintes cisaillantes basales τ_b (***Clark & Stokes, 2003 ; Sergienko & Hindmarsh, 2013; Zheng et al., 2019***) (**Figure 1.6**). En amont des fleuves de glace, la zone d'enracinement ('*onset area')*, correspond à la région ou un flux de glace plus rapide s'initie en lisière du dôme de glace, formant une zone parsemée de couloirs de vitesse d'écoulement modérée (**Figure 1.5**). Les zones d'enracinement des fleuves de glace sont caractérisées par un large spectre de directions d'écoulement de la glace en raison des multiples affluents ('*tributaries*'), petits couloirs convergeant vers le couloir principal (*trunk*)

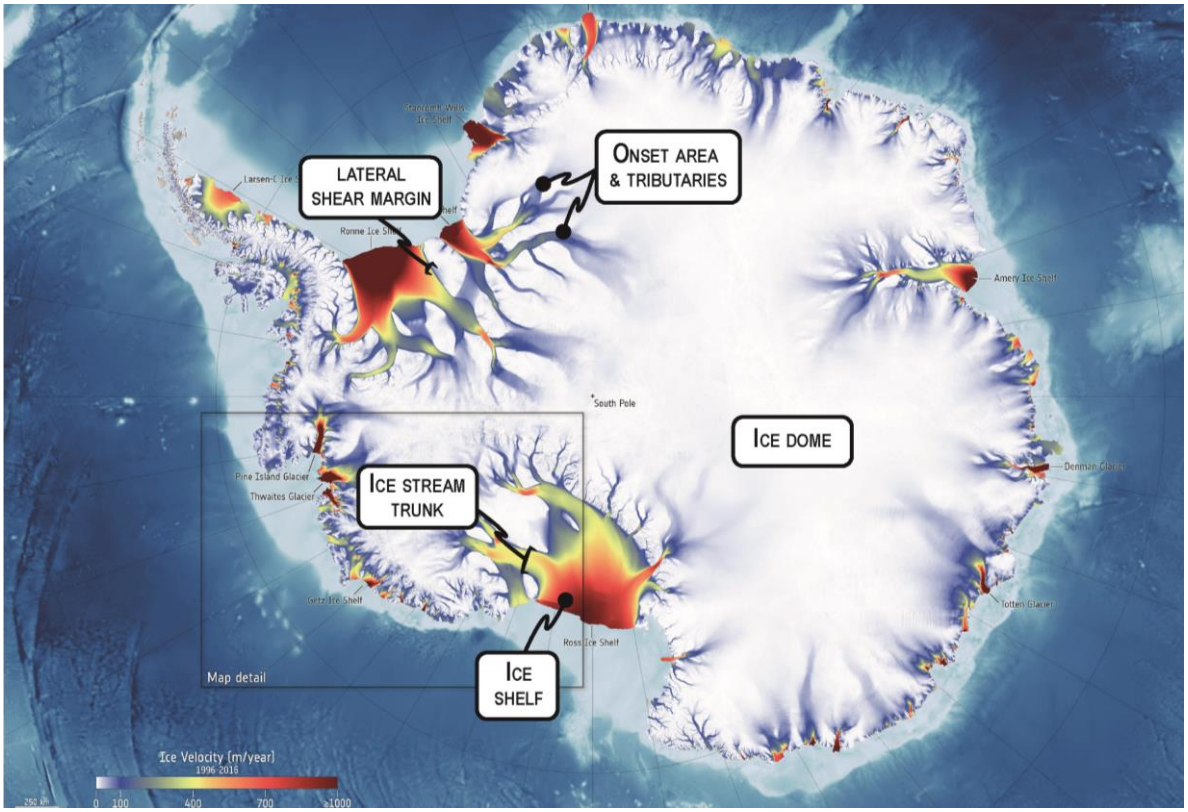

Figure 1.6. *Map of velocity magnitude (m/year) of ice surface in Antarctica measured between 1996 and 2016. Corridors of high ice flow velocity correspond to ice streams, rooted in ice domes of low ice flow velocity (© ESA - 2021).*

d'un fleuve de glace (**Figure 1.7A**). Puisque les zones d'enracinement sont des régions d'accélération de la vitesse d'écoulement de la glace, elles sont communément associées à des gradients longitudinaux extensifs ($\Delta\sigma_{ext}$) (**Figure 1.5**). Les fleuves de glace génèrent également de très forts gradients latéraux de vitesse d'écoulement avec la glace environnante qui s'écoulent à de faibles vitesses, et sont par conséquent caractérisés par des marges latérales cisaillantes ('*lateral shear margins'*) (**Figure 1.5**) (***Raymond et al., 2001 ; MacGregor et al., 2013 ; Hunter et al., 2021***). Les marges cisaillantes accommodent une grande partie des forces motrices responsables de la forte vitesse d'écoulement des fleuves de glace par l'intermédiaire des forces de friction latérale. Les fortes contraintes cisaillantes latérales ($\tau_l > 5.10^{-5}$ j^{-1}), résultant des forces de friction latérales, se traduisent par la formation de bandes latérales de quelques km de large de glace fortement crevassées (**Figure 1.7B**) (***Alley et al., 2018 ; Jennings & Hambrey, 2021***).

1.2.3. Terminaisons marines et terrestres des fleuves de glace

Les dynamiques d'écoulement des fleuves de glace diffèrent selon la nature de leurs terminaisons (i.e. terrestre ou marine) (***Stokes & Clark, 2001***). Les fleuves de glace à terminaison marine débouchent

sur des plateformes glaciaires (‘*ice shelf*’) ou des fronts de vêlage d’icebergs (‘*calving front*’) (***Depoorter et al., 2013 ; Rignot et al., 2013***) (**Figure 1.7C**). Les terminaisons marines – dont l’eau induit de très faibles forces de friction basale – sont communément caractérisées par des contraintes longitudinales extensives ($\Delta\sigma_{ext}$) et des vitesses d’écoulement de la glace très élevées (> 1000m/an).

Les fleuves de glace à terminaison terrestre débouchent, quant à eux, sur des lacs pro-glaciaires en formant des fronts de vêlage d’icebergs (***Stokes & Clark, 2003, 2004***) ou sur des plaines alluviales en formant des lobes évasés (***Patterson, 1997***) (**Figure 1.7D**). Dans le cas des fleuves de glace à terminaison lobée, la diminution de la hauteur de la colonne de glace combinée à l’augmentation de la surface de couplage entre la glace et le substrat tendent respectivement à diminuer les forces motrices et à augmenter les forces de friction basale. Dans cette configuration, la diminution de la vitesse d’écoulement de la glace le long de la marge du lobe génère des contraintes longitudinales compressives ($\Delta\sigma_{com}$) (***Patterson, 1997***).

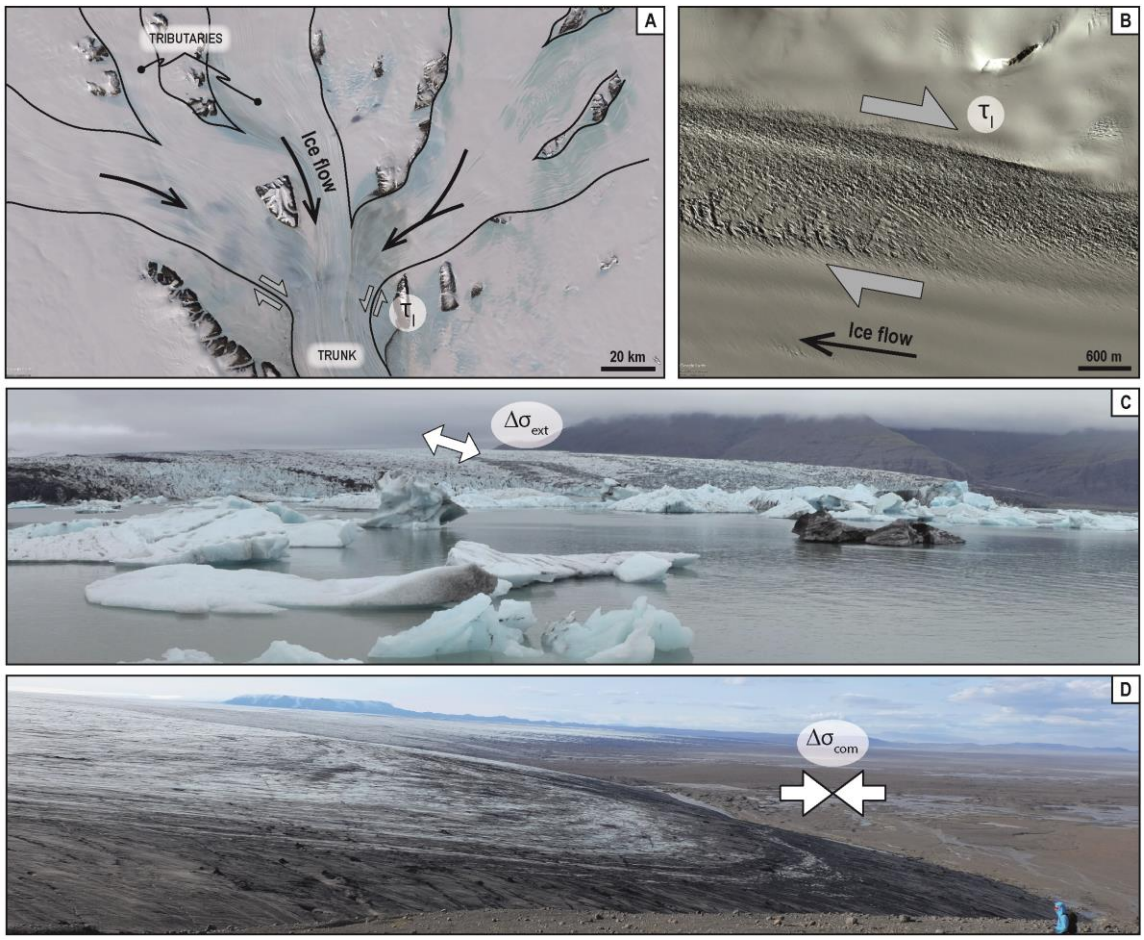

Figure 1.7. *(A) Onset area of Lambert Glacier where ice masses flowing within tributaries converge into ice stream trunk (Antarctica – © Google Earth). (B) Highly-crevassed lateral shear margin of David Glacier (Antarctica – © Google Earth). (C) Calving front of Breiðamerkurjökull Glacier and (D) terrestrial lobe of Bruarjökull Glacier (Vatnajökull Ice Sheet, Iceland) (personal photographs).*

2. Dynamique d'écoulement de l'eau de fonte à la base des calottes glaciaires

La circulation d'eau de fonte dans la porosité du lit sédimentaire et le long de l'interface glace-sédiments contrôle les interactions à la base des calottes glaciaires. La pression d'eau interstitielle (P_w) (*'pore water pressure'*) dans le substrat modulent l'amplitude des forces de résistance, la déformation des sédiments (modification de la déformabilité des sédiments) et les processus de glissement (contrôle du couplage et découplage de la glace). La notion de contrainte effective N (*'effective stress'*) fait référence à la différence entre la contrainte verticale exercée par la colonne de glace (σ_i, *'normal stress'*) et la pression d'eau interstitielle (P_w) (**Figure 1.3A**) :

$$N = \sigma_i - P_w = \rho_i \times g \times H - P_w$$

Lorsque la pression d'eau interstitielle dépasse localement la pression exercée par la colonne de glace ($P_w > \sigma_i$), la pression effective *N* est négative et permet le découplage entre la glace et le substrat. Au sein des calottes glaciaires, les dynamiques de production et de circulation d'eau de fonte sous-glaciaire sont très variables spatialement et temporellement, formant des systèmes hydrologiques complexes et capable d'influer sur les interactions glace-eau-substrat à différentes échelles de temps et d'espace (**Figure 1.8A**).

2.1. Mécanismes de production d'eau de fonte et variabilités spatio-temporelles

A la base des calottes glaciaires, la production in situ d'eau de fonte (de l'ordre du mm/an) est liée à la chaleur générée par le flux géothermique, par les frictions dues à l'écoulement de la glace sur le substrat, et par l'écoulement d'eau contre la glace. Les calottes glaciaires sont caractérisées par une grande variabilité du régime thermique basal ; celui-ci est régi par le point de fusion de la glace sous pression ($T°_{PMP}$) et influence directement la production d'eau de fonte sous-glaciaire. Ainsi, on distingue les calottes glaciaires (i) à base tempérée ($T° > T°_{PMP}$; *'warm-based'*) permettant la production d'eau de fonte sous-glaciaire, (ii) à base froide ($T° < T°_{PMP}$; *'cold-based'*) ne permettant pas la production d'eau de fonte sous-glaciaire, et (iii) polythermales, composées d'une mosaïque de bases tempérées et froides (***Engelhardt, 2004 ; Kleman & Glasser, 2007***). Le régime thermique basal contrôle la circulation d'eau de fonte le long de l'interface basale et au sein du substrat sous-glaciaire et module la déformabilité du substrat sous-glaciaire et de la transportabilité des sédiments à l'interface.

La production supra-glaciaire d'eau de fonte représente la source principale d'eau de fonte circulant au sein des systèmes glaciaires (de l'ordre du m/an) et résulte essentiellement de la **fonte** de la neige, des névés et de la glace à la surface des zones d'ablation. Les processus de fonte supra-glaciaire sont directement contrôlés par la quantité d'irradiation par les rayonnements solaires (***Lewis et al., 1998 ; Zeng et al., 2012***) et les effets d'albédo de surface (***Mayer et al., 2011 ; Ryan et al., 2022***), et sont donc sujets à de fortes fluctuations temporelles – à des échelles diurnes, saisonnières ou de cycles climatiques – et spatiales en raison de variations météorologiques régionales (***Greenwood et al., 2016***).

Au sein des calottes glaciaires, l'eau de fonte circule depuis le lieu de production vers la marge (**Figure 1.8A**), en suivant les gradients de pression (qui sont essentiellement contrôlés par la pente de la surface des calottes), selon une grande variété de chemins : supra-glaciaires (bédières, moulins) (**Figure 1.8B-C**), intra-glaciaires (crevasses, chenaux) et sous-glaciaires (chenaux et cavités sous-glaciaires). L'eau de fonte peut aussi être stockée, soit (i) en surface des calottes glaciaires, au sein de la neige et des névés (i.e. neige durcie) ou de lacs supra-glaciaires, soit (ii) à l'intérieur, au sein de cavités, ou (iii) à la base, au sein de la porosité des sédiments, de cavités ou de lacs sous-glaciaires. La durée de résidence de l'eau de fonte – courte (heures à jours), moyenne (jours à saisons) ou longue (> an) – au sein des différents lieux de stockage influence directement la récurrence et l'amplitude des épisodes de vidange et donc la dynamique de circulation d'eau de fonte, notamment sous-glaciaire.

2.2. Circulation d'eau de fonte sous-glaciaire et systèmes de drainage

Les variations de dynamique de circulation d'eau sous-glaciaire modulent les évolutions spatio-temporelles d'efficacité et de connectivité des systèmes hydrologiques sous-glaciaires (***Bell, 2008 ; Sundal et al., 2011 ; Bartholomew et al., 2012 ; Andrew et al., 2014 ; Davison et al., 2019***), qui contrôlent le degré de lubrification de l'interface basale et les processus sous-glaciaires (e.g. glissement basal, déformation du substrat, transport sédimentaire) (***Zwally et al., 2002; Das et al., 2008; Joughin et al., 2008; Palmer et al., 2011; Fitzpatrick et al., 2013; Vijay et al., 2021***).

Les systèmes hydrologiques sous-glaciaires sont communément divisés en deux grandes catégories : efficace/chenalisé et inefficace/distribué. L'efficacité de drainage est définie comme la capacité d'un système hydrologique à transférer de façon plus ou moins rapide de l'intégralité de

l'apport d'eau de fonte transitant au sein du système, en fonction de la balance entre l'apport, le stockage et la décharge d'eau de fonte (***Schoof, 2010 ; Bartholomew et al., 2012 ; Flowers, 2015 ; Greenwood et al., 2016 ; Davison et al., 2019***). L'efficacité de drainage dépend de la topographie et la lithologie du substrat sous-glaciaire, de l'épaisseur, de la température et de la pente de surface de la glace, et du débit d'eau de fonte circulant vers le substrat (***Fountain et Walder, 1998***).

2.2.1. Systèmes hydrologiques efficaces / chenalisés

Dans le cas d'un système de drainage efficace, l'intégralité de l'eau de fonte est acheminée et transférée rapidement – i.e. sans stockage – vers la marge de la calotte glaciaire au sein de structures de drainage chenalisées caractérisées par de faibles pressions (***Davison et al., 2019;Chandler et al., 2021***). Ce type de système est associé la concentration des écoulements d'eau dans des structures chenalisées, induisant une augmentation de la surface de couplage entre la glace et le substrat sous-glaciaire et une réduction des vitesses d'écoulement de la glace (***Lliboutry, 1968, Tedstone et al., 2015***).

L'eau de fonte peut circuler au sein de réseaux de chenaux incisés dans un substrat rigide et peu perméable (i.e. chenaux de Nye, **Figure 1.8D**) (***Nye, 1976***), ou dans un substrat sédimentaire meuble et perméable (i.e. vallées tunnels ou chenaux d'eau de fonte, **Figure 1.8E**) (***Sugden et al., 1991 ; Kehew et al., 2012***). En raison de la circulation d'eau sous pression, les chenaux sous-glaciaires ont des profils en long ondulant avec des inversions de pente ; ils font entre 0.1–100^{nes} km de longueur, 10^{nes}–1000^{s} m de largeur et 10^{nes}–100 m de profondeur (***Cutler et al., 2002 ; Greenwood et al., 2007 ; Kirkham et al., 2020***). Classiquement, les chenaux d'eau de fonte de petites dimensions sont définis comme des chenaux sous-glaciaires ('*subglacial channels'*) tandis que ceux de plus grandes dimensions sont définis comme des vallées tunnels ('*tunnel valleys'*), sans pour autant qu'un seuil de dimensions soit défini dans la littérature.

Lorsque le substrat sous-glaciaire est rocheux, rigide et/ou peu perméable, l'eau de fonte sous-glaciaire peut s'écouler au sein de conduits incisés dans la glace de forme semi-circulaire (i.e. chenaux de Röthlisberger, **Figure 1.8F**) (***Rothlisberger, 1972***), ou semi-lenticulaire (i.e. chenaux de Hooke ; ***Hooke et al., 1990***) ('*englacial conduits'*). L'ouverture de ces conduits est déterminée par l'équilibre entre la fonte par friction liée à l'écoulement d'eau de fonte et la contraction des conduits par fluage de la glace

liée à la contrainte normale σ_i exercée par la colonne de glace (‘*creep closure’*). Le transport de sédiments sous-glaciaires au sein de ces conduits est suivi du dépôt lorsque la pression d’eau de fonte, et donc de la vitesse d’écoulement, décroît à proximité de la marge, ce qui induit un comblement progressif et la formation de cordons sédimentaires, nommés *‘*eskers*’* (**Figure 1.8G**) (***Hewitt & Creyts, 2019***). Les **eskers** sont essentiellement sableux et graveleux, et sont en moyenne 10^{nes}–100^{nes} km de long, 10^{nes}–100^{nes} m de large et 1–10 m de haut (***Aylsworth & Shilts, 1989 ; Huddart et al., 1999 ; Storrar et al., 2013***).

2.2.2. Systèmes hydrologiques inefficaces / distribués

Dans le cas d'un système de drainage inefficace, la capacité de circulation de l’eau de fonte est réduite, rendant le transfert jusqu’à la marge de la calotte glaciaire plus lent et favorisant le stockage temporaire de l’eau. Les systèmes de drainage inefficaces – aussi qualifiés de distribués – sont associés à de fortes pressions d'eau sous-glaciaire et à une accélération de la vitesse d’écoulement de la glace en raison de l’augmentation de la surface de découplage entre la glace et le substrat (***Bindschadler, 1983 ; Hewitt, 2011 ; Davison et al., 2019***).

Parmi les systèmes de drainage distribués, des films d’eau (‘*water film’* ; aussi qualifiés d’écoulements pelliculaires ou de films de Weertman) d’épaisseurs millimétriques se développent à l’interface entre le substrat et la colonne de glace lorsque $P_w > \sigma_i$ (***Hallet, 1979 ; Lappegard et al., 2006***). Les films d’eau favorisant les processus de glissement basal et de découplage sont souvent associés aux fleuves de glace (***Breemer et al., 2002 ; Le Brocq et al., 2009***), mais sont des acteurs limités dans les processus de transport de sédiments. Ces films d’eau tendent à être associés à de faibles productions d’eau de fonte, probablement in situ (***Weertman, 1972 ; Fountain & Walder, 1998***). Des réseaux de cavités connectées peuvent également sur former à l’interface entre la colonne de glace et le substrat (***Fountain and Walder, 1998***). Leur formation est associée à l’existence de dépressions dans le substrat sous-glaciaire ou à la formation de surcreusements à la base de la glace en aval de hauts topographiques du substrat (***Lliboutry, 1979 ; Fowler, 1987***). Ces cavités sont plus ou moins interconnectées par un réseau de petits chenaux (*‘connected or disconnected subglacial cavities’* ; ***Kamb, 1987 ; Hooke, 2005***).

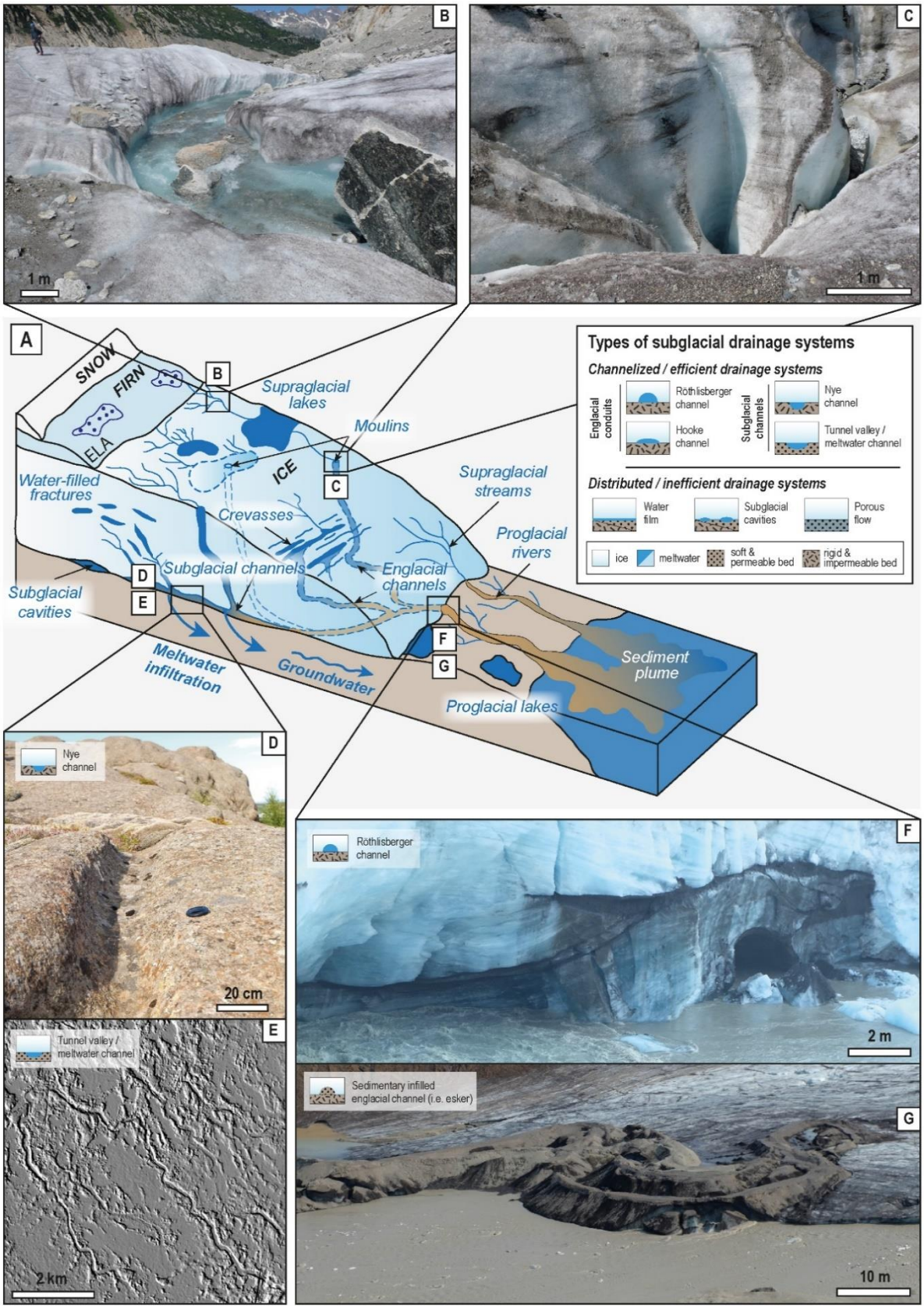

Figure 1.8. *(A) Ice sheet hydrological system with a focus on the variety of subglacial drainage systems (**Ravier & Buoncristiani, 2018** modified after **Cuffey & Paterson, 2010**). (B) and (C) Elements of supra-glacial hydrological system: (B) supra-glacial stream and (C) moulins (Mer de Glace, France). Elements of sub-glacial hydrological system: (D) Nye channel (Egilsstadir, Iceland), (E) meltwater channels (Fort Simpson, Great Slave Lake Ice Stream, Canada), (F) Röthlisberger channel (Eyjabakkajökull, Iceland), (G) esker as a morphological relic of an englacial channel (Eyjabakkajökull, Iceland) (all pictures are personal photographs).*

Alors que la circulation d'eau de fonte au sein des substrats rocheux, rigides et peu perméables est très limitée, la majorité des calottes glaciaires possèdent un lit sédimentaire non-consolidé et perméable à leur base formant des aquifères sous-glaciaires au sein desquels l'eau de fonte circule dans la porosité. La circulation d'eau de fonte s'effectue essentiellement par écoulement darcien en réponse au gradient hydraulique généré par la pente de surface de la glace (***Clarke, 1987 ; Boulton et al., 1995***).

2.2.3. Variabilité spatio-temporelle des systèmes de drainage

Bien qu'il soit commode de décrire individuellement les différents types de systèmes hydrologiques sous-glaciaires, ces derniers sont en réalité interconnectés et associés à une multitude de configurations évoluant de façon continue dans l'espace[3] (**Figure 1.9A**) et le temps (***Hubbard et al., 1995 ; Andrews et al., 2014***).

- **Variabilité spatiale des systèmes de drainage sous-glaciaire**

Les systèmes de drainage inefficaces dominés par les cavités sous-glaciaires plus ou moins connectées et les films d'eau tendent à se développer dans les environnements sous-glaciaires où le lit sédimentaire est de faible épaisseur ou absent, tandis que les systèmes inefficaces dominés par l'écoulement poral tendent à se développer en relation avec des lits sédimentaires de forte épaisseur (***Stone & Clarke, 1993 ; Kyrke-Smith & Fowler, 2014 ; Davison et al., 2019***). D'une façon générale, les systèmes de drainage distribué sont prédominants dans les régions caractérisées par une forte épaisseur de glace, une faible pente de surface de la glace et de faibles circulations d'eau de fonte (i.e. dôme de glace, zones d'accumulation), limitant le développement de systèmes de drainage chenalisé (***Meierbachtol et al., 2013 ; Dow et al., 2014***). Bien que certains systèmes de drainage distribués soient directement connectés aux zones de production d'eau de fonte supra-glaciaire par des conduits intra-glaciaires et forment des réseaux de cavités connectées, la majeure partie d'entre eux sont spatialement isolés et déconnectés des chemins d'apport d'eau de fonte (**Figure 1.9A**) (***Meirbatchol et al., 2013, 2016 ; Andrews et al., 2014 ; Hoffman et al., 2016***).

[3] Il est communément admis que l'eau de fonte transite depuis les systèmes à forte pression d'eau de fonte (inefficaces/distribués) vers les systèmes à faible pression d'eau de fonte (efficaces/chenalisés).

Les systèmes de drainage chenalisés tendent quant à eux à se développer au niveau des zones d'ablation dans des régions situées au maximum à une 50^{nes} de km de la marge des calottes (**Figure 1.9A**). Dans ces régions, la faible épaisseur de glace diminuant la contrainte normale σ_i (< 900-1200 m), la plus forte pente de surface de la glace et les plus forts apports d'eau de fonte supra-glaciaires limitent la fermeture des conduits/chenaux par fluage de la glace (effet de '*creep closure*') et augmentent la fonte de leurs parois (***Chandler et al., 2013, 2021 ; Dow et al., 2014 ; de Fleurian et al., 2016 ; Kozio & Arnold, 2018 ; Nanni et al., 2021***). Les structures de drainage chenalisé se développent ainsi rapidement en réponse à l'augmentation du débit d'eau de fonte circulant à la base de ces environnements sous-glaciaires (***Cowton et al., 2013 ; Banwell et al., 2016***).

Ainsi, sous les calottes glaciaires à base tempérée, des systèmes composites peuvent se développer à partir (i) de cavités connectées par des petits conduits/chenaux dans les zones intermédiaires des calottes glaciaires (épaisseur de glace forte, pente faible, apport d'eau de fonte modéré), interagissant (ii) latéralement avec des systèmes distribués de plus faible connectivité hydraulique stockant l'eau de fonte dans des cavités isolées (épaisseur de glace forte, pente faible, pas d'apport d'eau de fonte), et (iii) longitudinalement – en direction de la marge – avec des systèmes de drainage chenalisé (épaisseur de glace faible, pente forte, apport d'eau de fonte élevé) (**Figure 1.9B**). Ces systèmes hydrologiques sous-glaciaires composites sont interprétés comme des routes de circulation d'eau fonte ('*subglacial meltwater routes*') (***Andrews et al., 2014; Tedstone et al., 2014; Hoffman et al., 2016; Davison et al., 2019; Vore et al. 2019 ; Nanni et al., 2021***). Ces routes – larges de quelques centaines de m à quelques km et faisant jusqu'à plusieurs centaines de km de longueur – sont organisées radialement par rapport à la marge des calottes glaciaires (**Figure 1.9A**) (***Peterson et al., 2017 ; Lewington et al., 2020 ; Dewald et al., 2022***). Ces routes à forte connectivité hydraulique sont plus rares sous les fleuves de glace (***Lewington et al., 2020***), en raison des plus faibles gradients hydrauliques (plus faibles pentes de glace en surface) (***Kamb, 1987; Bell, 2008***). En revanche, d'après des études menées sur la calotte Antarctique, les films d'eau et l'écoulement poral sont prédominants sous les fleuves de glace (**Figure 1.9A**), impliquant l'existence de fortes pression d'eau interstitielle dans les sédiments sous-glaciaires et favorisant de fortes vitesses d'écoulement de la glace par glissement basal et déformation des sédiments (***Engelhardt et al., 1990 ; Engelhardt, 1998***).

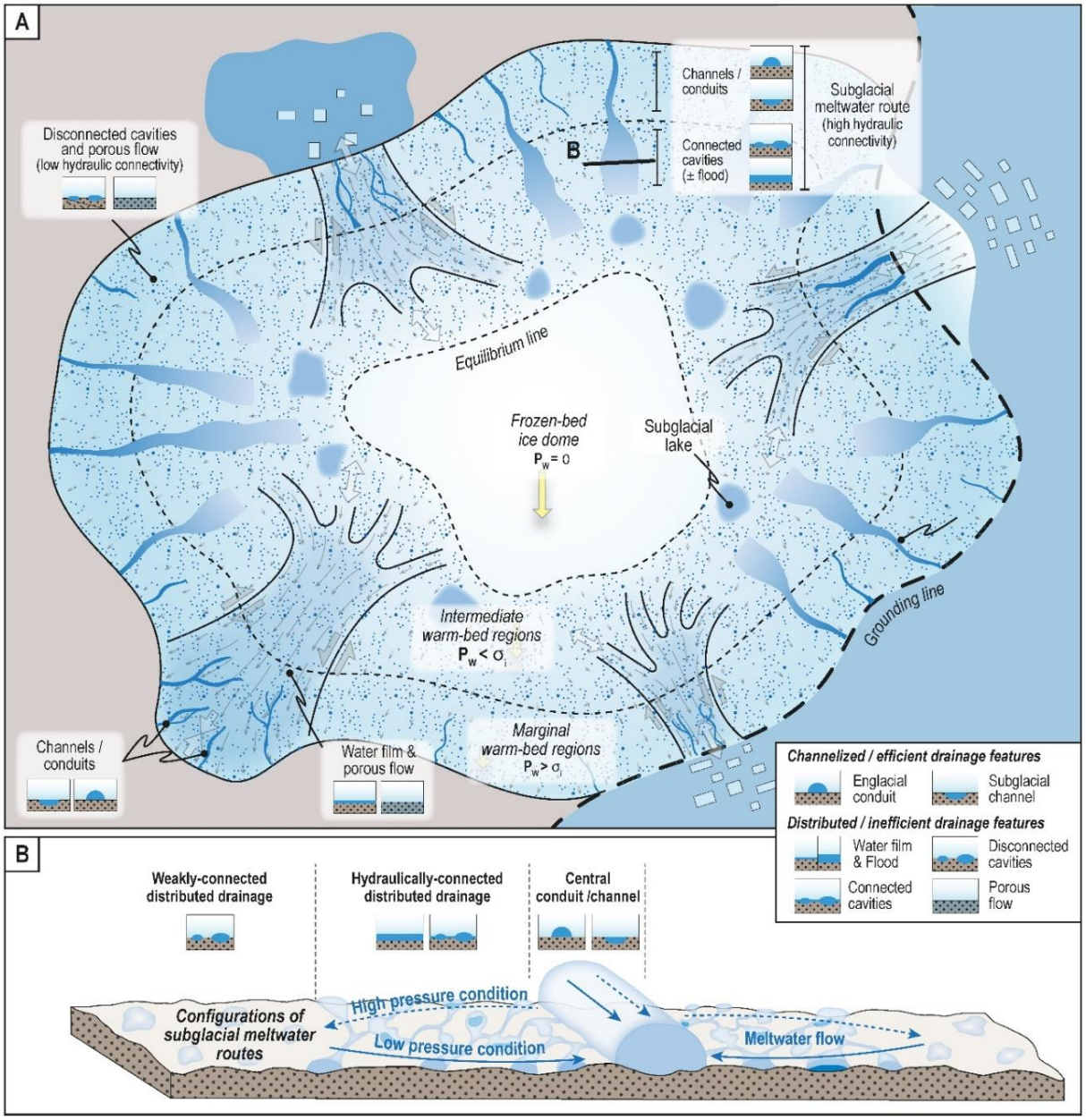

***Figure 1.9**. (A) Schematic map of meltwater drainage systems below an ice sheet. (B) Cross-section of a subglacial meltwater route. Note changes of meltwater flow configurations depending on meltwater drainage events and pressure conditions.*

- **Variabilité temporelle des systèmes de drainage sous-glaciaire**

Dans le temps, la configuration des systèmes de drainage sous-glaciaires évolue à l'échelle diurne et saisonnière, mais aussi à plus long terme, en raison de la variabilité de la production et des apports d'eau de fonte supra-glaciaire (***Hubbard et al., 1995 ; Andrews et al., 2014 ; Rada & Schoof, 2018 ; Mejia et al., 2021 ; Smith et al., 2021***). Les phases d'augmentation du débit et de la pression d'eau de fonte sont rapides, comme lors des phases de vidange de lacs supra-glaciaires, et induisent un dépassement de la capacité hydraulique des systèmes de drainage durant quelques heures à quelques

jours produisant des crues sous-glaciaires (‘*flood*’) (***Iken & Bindschadler, 1986; Hubbard et al., 1995; Das et al., 2008; Bougamont et al., 2014***). Durant ces phases, les structures de drainage chenalisé peuvent déborder en direction des systèmes de drainage distribué environnants (**Figure 1.9B**) (***Schoof, 2010 ; McGrath et al., 2011 ; Tedstone et al., 2014***). L’augmentation du débit et de la pression au sein de systèmes de drainage distribué tels que les routes de circulation d’eau de fonte peut produire un large film d’eau, qui tend à évoluer en des structures de drainage chenalisé et efficace à mesure que le débit et la pression diminuent (***Pimentel & Flowers, 2010 ; Dow et al., 2015 ; Andrews et al., 2018 ; Rada & Schoof, 2018; Nanni et al., 2021***). Malgré l’existence de reliques de systèmes chenalisés (e.g. ***Kehew et al., 2012 ; Stewart et al., 2013 ; Storrar et al., 2013***), l’empreinte morphologique associée au développement et à la dynamique de systèmes de drainage distribués et notamment des routes de drainage d’eau de fonte reste encore sporadique et mal contrainte (Chapitre I - Partie 2 §2.1). Même si des réseaux de cavités sous-glaciaires souvent désignés comme corridors de circulation d’eau de fonte sous-glaciaire (‘*subglacial meltwater corridors*’) sont identifiés dans la littérature (***Walder & Hallet, 1979 ; Sharp et al., 1989 ; Ojala et al., 2019 ; Lewington et al., 2019, 2020***), ces lacunes limitent les reconstitutions précises de la distribution spatiale et de la dynamique temporelle des circulations d’eau sous-glaciaire.

3. Distribution et caractéristiques des sédiments sous-glaciaires

A la base des calottes glaciaires, un lit sédimentaire ('*subglacial bed*') issus de l'érosion du substrat sous-glaciaire (cristallin ou sédimentaire ; rigide ou meuble) se forme sous la majorité des calottes glaciaires à base tempérée. Outre le fait de permettre l'écoulement poral de l'eau de fonte, les sédiments sous-glaciaires sont d'une importance capitale pour la dynamique d'écoulement de la glace, mais également pour la formation de bedforms, de par leur faculté à être remobilisés selon une variété de processus d'origine glaciogénique ou fluvio-glaciaire.

3.1. Mécanique et propriétés physiques des sédiments sous-glaciaires

La rhéologie d'ensemble des sédiments sous-glaciaires saturés en eau est souvent considérée comme ductile (e.g. plissement, foliation, boudinage) et modélisée par des lois de comportement visqueux (***Owen, 1987 ; Tulaczyk et al., 2000a ; Fannon et al., 2017***). Cependant, à l'échelle granulaire, leur déformation se produit essentiellement par du cisaillement intergranulaire qui est communément modélisé par une loi de type Mohr-Coulomb :

$$\tau_0 = N \times \tan\ (\varphi) + C$$

où τ_0 est la résistance au cisaillement basal ('*basal shear strength'*), *N* est la contrainte effective, φ est l'angle de friction interne et C est la cohésion du sédiment. La déformation des sédiments intervient lorsque la contrainte cisaillante basale τ_b dépasse la résistance au cisaillement basal τ_0 (***Oda & Konishi, 1974 ; Owen, 1987 ; Bestman & Prior, 2003***). La dépendance à l'angle de friction φ et à la cohésion C illustre le fait que les variations lithologiques contrôlent directement les processus de déformation des sédiments sous les calottes glaciaires. La pression d'eau interstitielle (P_w) est également un facteur de contrôle majeur car elle intervient directement dans le calcul de la pression effective (N). La déformation des sédiments sous-glaciaires est favorisée lorsque P_w est élevée puisque l'eau interstitielle tend à diminuer la résistance au cisaillement basal τ_0 ; des P_w très élevées peuvent même aller jusqu'à produire de la fracturation hydraulique au sein des sédiments et/ou le découplage de l'interface basale ($P_w > \sigma_i$). La granulométrie, le tri et la densité des sédiments contrôlent également leurs capacités de remobilisation via des processus de transport et de dépôt sédimentaire par l'eau de fonte.

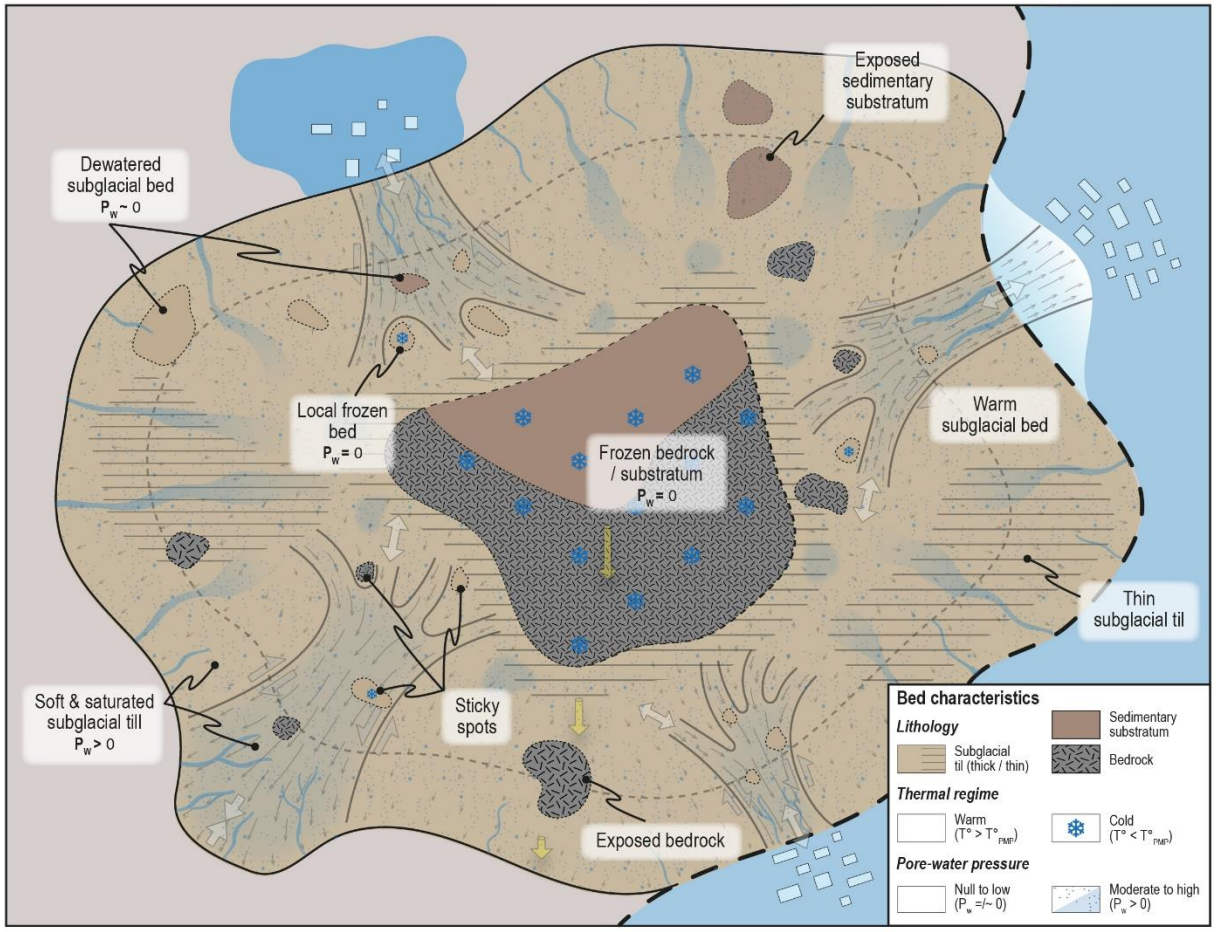

***Figure 1.10**. Schematic of variability in bed characteristics at the scale of an ice sheet*

3.2. Variabilités spatiales des caractéristiques des sédiments sous-glaciaires

Les variabilités spatiales de distribution et de caractéristiques des sédiments sous-glaciaires contrôlent directement et localement les processus sous-glaciaires (**Figure 1.10**) (***Hodgson, 1993***). En l'absence de sédiments sous-glaciaires, l'écoulement de la glace sur un substrat rigide ou gelé tend à limiter les processus de déformation basale et de glissement basal, inhibant la vitesse d'écoulement basal de la glace (i.e. dômes). En revanche, les substrats sédimentaires meubles et les sédiments sous-glaciaires meubles et saturés en eau ont quant à eux tendance à se déformer, favorisant de fortes vitesses d'écoulement de la glace (i.e. fleuves de glace). La lithologie du substrat semble également contrôler la déformabilité des sédiments sous-glaciaires issus de son érosion : des sédiments sous-glaciaires issus de roches carbonatées sont plus déformables que des sédiments dérivés de grès ou de roches ignées (***Wellner et al., 2001 ; O Cofaigh et al., 2002 ; Greenwood & Clark, 2010***). L'épaisseur des sédiments sous-glaciaires, qui est fortement contrôlée par la nature et l'érodabilité du substrat, est également très variable à l'échelle d'une calotte glaciaire, conditionnant les processus de déformation des sédiments et

le stock sédimentaire disponible pour le transport sédimentaire par l'eau de fonte (***Aylsworth & Shilts, 1989 ; Clark & Stokes, 2001***). ***Alley (2000)*** souligne notamment l'importance de la continuité spatiale de la disponibilité des sédiments sous-glaciaires pour la mise en place des fleuves de glace.

Le mode de circulation (conduits/chenaux sous-glaciaires, cavités, film d'eau) de l'eau de fonte et la pression d'eau interstitielle au sein des sédiments sous-glaciaires sont également très variables à l'échelle d'une calotte glaciaire (Chapitre I - Partie 1 §2.2.3) et modulent notamment la résistance au cisaillement basal et la capacité de transport des sédiments (***Lesemann et al., 2010 ; Sergienko & Hindmarsh, 2013 ; Lewington et al., 2020***). Au sein des fleuves de glace, alors que les sédiments meubles et saturés en eau favorisent de fortes vitesses d'écoulement de la glace par glissement basal et déformation sédimentaire, de plus faibles pressions d'eau interstitielle, des sédiments sous-glaciaires plus rigides ou absents (i.e. couplage direct avec le substrat rigide affleurant) ou une température située en dessous du point de fusion de la glace peuvent localement inhiber les processus de glissement basal et de déformation basale, formant des zones dites 'collées' ('*sticky spots'*) (***Alley, 1993 ; Piotrowski et al., 2004 ; Smith et al., 2015***).

4. Remobilisation et dépôt des sédiments sous-glaciaires en réponse aux interactions glace-eau-sédiments

Les interactions entre la glace, l'eau et le substrat / lit sédimentaire sous une calotte glaciaire sont à l'origine d'une grande variété de processus de remobilisation de sédiments (i.e. déplacement de grains ou de corps sédimentaires par l'action de l'écoulement de la glace et/ou de l'eau de fonte). Dans l'environnement sous-glaciaire, l'érosion du substrat sous-glaciaire (**Figure 1.11A**) est suivie d'un processus de transport pouvant être intra- (**Figure 1.11B**) ou sous-glaciaire (**Figure 1.11C-D**). La variété des processus de remobilisation puis de dépôt des sédiments sous-glaciaires détermine directement la lithologie, la structuration des dépôts sédimentaires et l'étendue spatiale des lits sédimentaires sous-glaciaires.

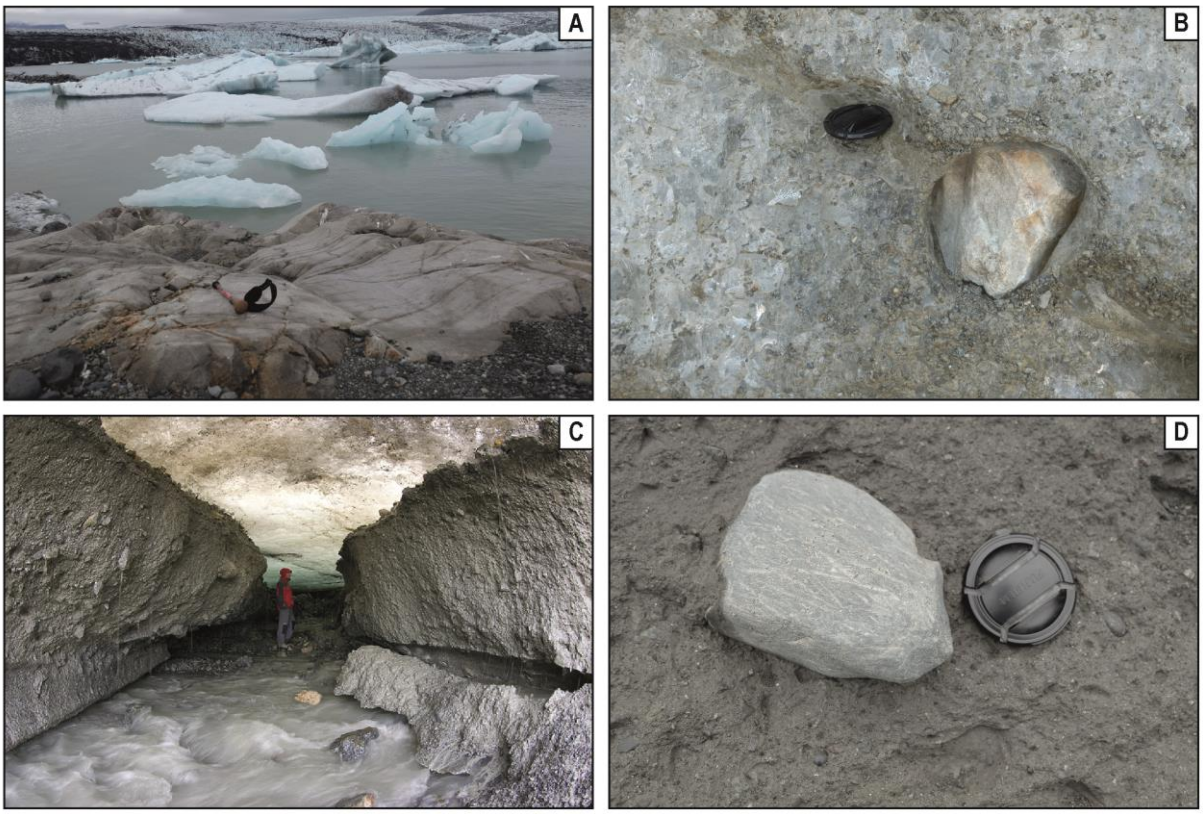

Figure 1.11. *Erosional and transport processes of glacial sediments below ice sheets. (A) Eroded, polished and striated subglacial bedrock (Breiðamerkurjökull Glacier, Iceland - personal photography). (B) Intraglacial (Glacier des Bossons, France - personal photography) and (C) subglacial transport of glacial sediments (© swisseduc.ch - Midtre Lovénbreen, Svalbard). (D) Striated and polished boulder in a subglacial till (Breiðamerkurjökull Glacier, Iceland - personal photography).*

4.1. Processus de remobilisation et de dépôt d'origine glaciogénique

Le principal moteur de remobilisation de sédiments sous une calotte glaciaire est d'origine glaciogénique, impliquant le transport puis le dépôt des sédiments uniquement par l'écoulement ou le non-écoulement de la glace. Les processus glaciogéniques dépendent du taux de fonte basale, de l'équilibre entre les forces motrices et de résistance, des caractéristiques du substrat / lit sédimentaire sous-glaciaire et des modalités de circulations de l'eau de fonte sous-glaciaires. Parmi les sédiments sous-glaciaires issus de processus glaciogéniques, on distingue ainsi les tills sous-glaciaires ('*subglacial traction till'*) et les substrats sédimentaires glaciotectonisés (***Bennett & Glasser, 2009 ; Chandler & Evans, 2019***).

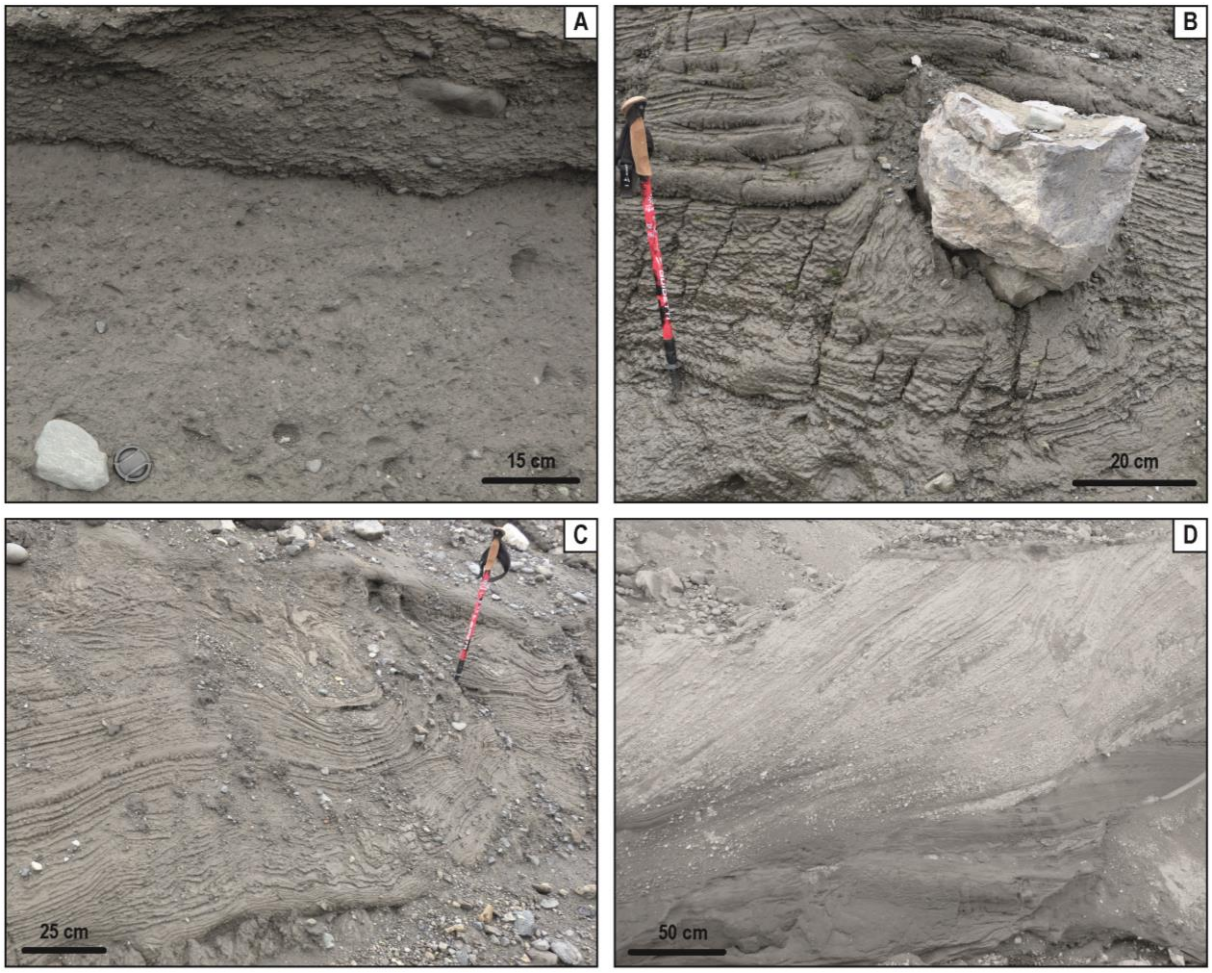

Figure 1.12. *Glaciogenic and glaciofluvial processes of subglacial sediment remobilization below ice sheets (Breiðamerkurjökull Glacier, Iceland). (A) Subglacial lodgment tills with fissile (top) and massive (bottom) structures. (B) Boulder deposited in and deforming glacial sediments, as it occurs within subglacial cavities by melt-out processes. (C) Soft sediment deformation (i.e. folding) affecting glacial sediments. (D) Foreset beds of sorted sandy sediments deposited in a glaciofluvial environment (all pictures are personal photographs)*

Les tills sous-glaciaires sont des lits sédimentaires de granulométrie variée ('diamicton' en l'absence de connotation génétique), issues de la remobilisation de sédiments transportés de façon sous-glaciaire ou intra-glaciaire et déposées essentiellement sous les calottes glaciaires à base tempérée.

Dans le cas de sédiments transportés le long de l'interface basale, ces derniers forment une couche de till sous-glaciaire tractée et déformée de façon pervasive sous l'effet de la contrainte cisaillante basale τ_b. Bien que les tills sous-glaciaires soient communément de structure massive en raison de leur hétérogénéité granulométrique, l'observation d'une structure fissile (i.e. plans horizontaux similaires à des plans de foliation) est le principal témoin de la déformation des tills sous-glaciaires et des processus de cisaillement basal (**Figure 1.12A**). Plusieurs conditions peuvent être responsables de l'arrêt du processus de remobilisation et du dépôt :

- (i) Lorsque la force de friction générée entre le substrat, le lit sédimentaire et la base de la glace devient supérieure à la contrainte cisaillante basale τ_b, cette dernière devient insuffisante pour poursuivre le processus de remobilisation de la couche de sédiments ('*lodgment till'*) (***Dreimanis, 1989 ; O Cofaigh et al., 2007***). Ce processus intervient de manière identique lorsque qu'une couche de glace basale riche en sédiments/débris génère une force de friction avec le substrat excédant la contrainte cisaillante basale τ_b (***Boulton, 1982***). Les débris grossiers charriés à la base de la glace peuvent générer des surcreusements dans le substrat lorsque ce dernier est suffisamment meuble ('*ploughing'*) (***Thomason & Iverson, 2008***).
- (ii) Lorsque la résistance au cisaillement basal dépasse la contrainte cisaillante basale ($\tau_0 > \tau_b$) à mesure que P_w augmente ou lorsque la colonne de glace et les sédiments sous-glaciaires sont découplés ($P_w > \sigma_i$), l'arrêt du processus de remobilisation engendre le dépôt du till sous-glaciaire (***Evans et al., 2006 ; Evans, 2017***).
- (iii) Lorsque la couche de till sous-glaciaire tractée à la base de la colonne de glace subit un glissement/dépôt gravitaire au sein de cavités sous-glaciaires ('*gravity deposition'*) (***Boulton, 1982 ; Bennett et al., 2006***).
- (iv) Lorsqu'un différentiel de pression effective génère un processus de succion du till sous-glaciaire ('*till squeezing*'), souvent au sein de cavité (***Evans et al., 2006 ; Kyrke-Smith & Fowler, 2014***).

Dans le cas d'un transport intraglaciaire, le dépôt intervient lorsque la base d'une colonne de glace – stagnante ou à faible vitesse et riche en sédiments – fond sur place ou au sommet d'une cavité sous-

glaciaire au contact de l'eau de fonte. Dans le second cas, la chute des sédiments les plus grossiers déforment les sédiments non-consolidés déposés à la base de la cavité ('*melt-out till'*) (***Paul & Eyles, 1990 ; Bennett et al., 2006 ; Larson et al., 2016***) (**Figure 1.12B**).

Lorsqu'une calotte glaciaire s'écoule sur un substrat composé de sédiments pré/pro-glaciaires non ou semi-consolidés, ces derniers se déforment en accommodant les contraintes cisaillantes basales tout en préservant en partie leurs structures sédimentaires préexistantes : on parle alors de substrats sédimentaires glaciotectonisés (***Evans et al., 2006 ; Chandler & Evans, 2019***) (**Figure 1.12C**).

4.2. Processus de remobilisation et de dépôt d'origine fluvio-glaciaire

Les sédiments remobilisés et déposés par des processus fluvio-glaciaires sont ubiquistes sous les calottes glaciaires à base tempérée en raison de l'abondante circulation d'eau de fonte au sein de conduits, chenaux, cavités et films d'eau. Les sédiments fluvio-glaciaires sont communément caractérisés par des couches et lentilles de sédiments sableux et graveleux, plus ou moins stratifiés et triés, intercalées au sein de tills sous-glaciaires (***Eyles et al., 1982 ; Boyce & Eyles, 2000 ; Lesemann, et al., 2010 ; Ravier et al., 2014***). En aval d'obstacles (e.g. bedform, haut topographique du substrat, boulder) ou de dépressions sous-glaciaires, des lits obliques de sédiments ('*foreset*') sont fréquemment formés par accrétion (***McCabe & O Cofaigh, 1994 ; Linden et al., 2008 ; Clerc et al., 2012***) (**Figure 1.12D**).

Lors des périodes de circulation d'eau de fonte à l'interface entre la glace et le substrat sédimentaire, des particules sédimentaires sont transportées par l'eau de fonte par charge de fond ou par charge en suspension, pouvant favoriser respectivement le dépôt de couches massives de sédiments non-triés et non-stratifiés ou de couches de sédiments typiquement sableux ou graveleux présentant des stratifications sédimentaires (***Eyles et al., 1983 ; Mulder & Alexander, 2001***). Hors période de drainage, des dépôts glacio-lacustres issus de la décantation de particules sédimentaires en suspension se mettent en place au sein lacs ou cavités sous-glaciaires déconnectés (***Smith & Ashley, 1985 ; Livingstone et al., 2012***).

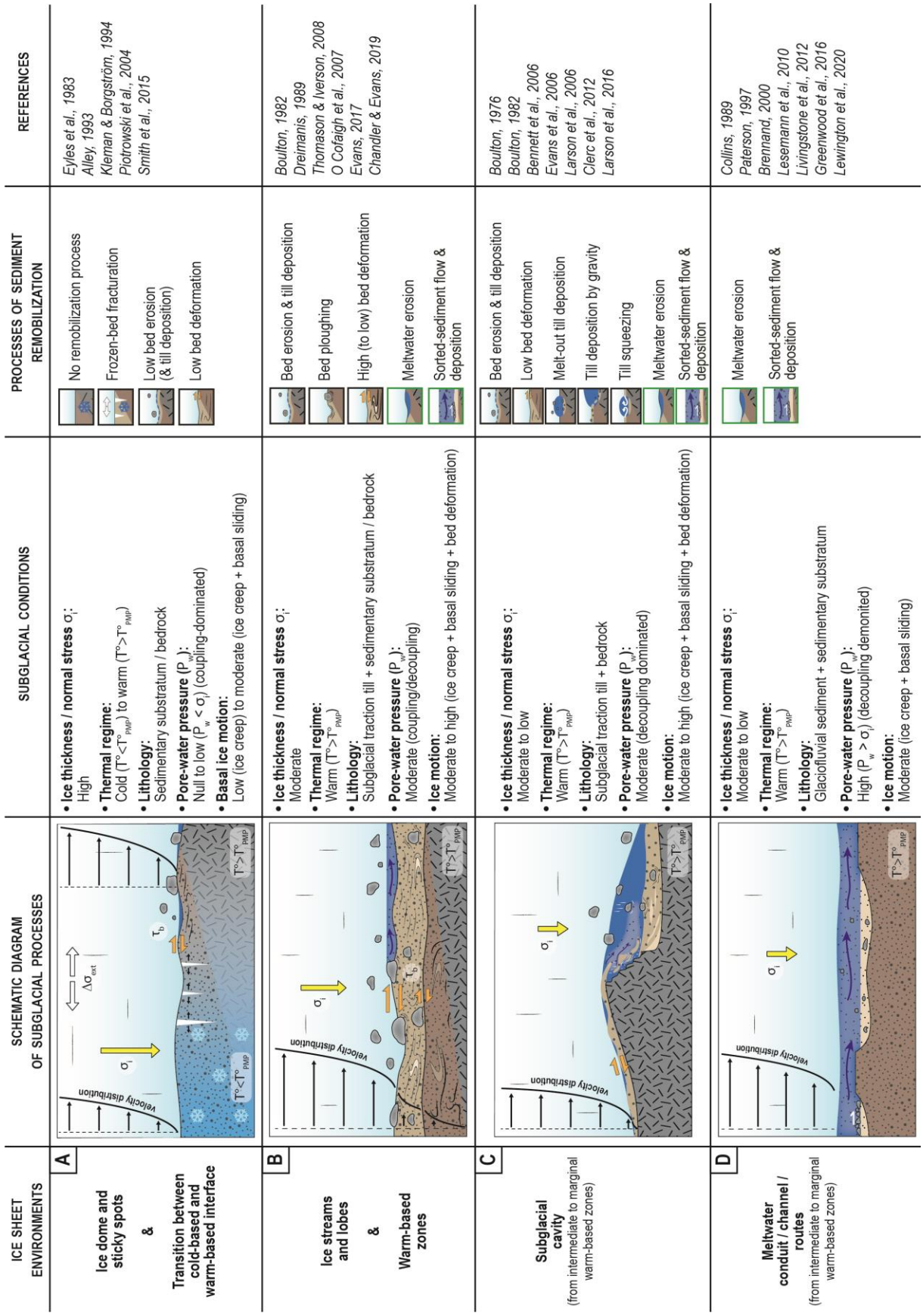

Figure 1.13. *Schematic diagrams illustrating the dominant subglacial processes of sediment remobilization below several ice sheet environments: (A) ice dome and sticky spots, (B) ice streams and lobes (and warm-based zones), (C) subglacial cavities and (D) subglacial conduits and channels.*

4.3. Variabilités spatio-temporelles de la remobilisation des sédiments sous-glaciaires

Les variations temporelles de la production d'eau de fonte et de sa circulation sous les calottes glaciaires (Chapitre I - Partie A §2.2.3) génèrent une cyclicité entre (i) les processus de remobilisation d'origine fluvioglaciaire, fortement contrôlés par les épisodes de décharge d'eau de fonte et les variations de débits durant ces épisodes, et (ii) les processus de remobilisation d'origine glaciogénique, plus constants dans le temps et plus ubiquistes à l'échelle d'une calotte glaciaire.

4.3.1. Dômes de glace, régions de base froide et 'sticky spots' (Figure 1.13A-14)

Les régions sous-glaciaires caractérisées par une base froide, en raison de l'absence d'eau de fonte à la base ($T° < T°_{PMP}$; $P_w = 0$; $\tau_b < \tau_0$), sont caractérisées par l'absence d'érosion du substrat et donc la plupart du temps dépourvues d'une lit sédimentaire sous-glaciaire. Les rares présences de sédiments remobilisables par l'écoulement de la glace sont associées au recouvrement de sédiments marginaux ou à la congélation d'eau de fonte et de sédiments circulant depuis des régions à base tempérée (***Shaw, 1977 ; Eyles et al., 1983***). Près des zones d'enracinement des fleuves de glace et/ou des zones de glace à base tempérée – où la présence d'eau de fonte à la base accélère la vitesse d'écoulement de la glace – le gradient longitudinal extensif ($\Delta\sigma_{ext}$) peut initier un faible mouvement de la glace basale par entrainement malgré l'absence d'eau, favorisant des processus d'érosion et de déformation de faible intensité et la fracturation du substrat sous-glaciaire gelé (***Kleman & Borgström, 1994***). Ces processus d'entrainement de la glace, d'érosion et de déformation de faible intensité interviennent aussi en aval des '*sticky spots'* (Chapitre I - Partie A §3.2) (***Alley, 1993 ; Piotrowski et al., 2004 ; Smith et al., 2015***).

4.3.2. Fleuves de glace et régions à base tempérée (Figure 1.13B-14)

Sous les régions à base tempérée reposant sur un substrat meuble ou rigide, la formation de lits sédimentaires sous-glaciaires est ubiquiste ('*subglacial traction till'*). Sous les fleuves de glace, des rétroactions thermomécaniques[4] (***Payne & Dongelmans, 1997 ; Hindmarsh, 2009***) et des conditions hydrologiques sous-glaciaires particulières (***Winsborrow et al., 2010 ; Kyrke-Smith et al., 2014***)

[4] En raison du caractère rhéofluidifiant de la glace – impliquant une diminution de la viscosité (i.e. augmentation de la capacité d'écoulement) lorsque la contrainte augmente – l'initiation d'une augmentation locale de la vitesse d'écoulement se traduit par une augmentation des contraintes motrices et des contraintes de cisaillement basal. L'augmentation de ces contraintes génère une boucle de rétroactions positives augmentant la vitesse d'écoulement de la glace à l'échelle régionale.

génèrent de fortes vitesses d'écoulement. Puisque la pression d'eau interstitielle P_w est communément élevée sous les fleuves de glace (***Denis et al., 2010 ; Damsgaard et al., 2016)***, les contraintes cisaillantes basales τ_b sont très supérieures à la résistance au cisaillement des sédiments τ_0 ($\tau_b >> \tau_0$), et induisent des processus de traction et de déformation du lit sédimentaire sous-glaciaire (i.e. tills) de forte intensité. Ces processus sont d'intensité modérée dans les régions à base tempérée entre les fleuves de glace ('*inter-ice stream areas'*) en raison de plus faibles vitesses d'écoulement de la glace à la base. Les variations temporelles de la dynamique et de la distribution spatiale des fleuves et lobes de glace favorisent la superposition de plusieurs phases de remobilisation et de dépôt de tills sous-glaciaires, dont les phases les plus antérieures sont partiellement ou non préservées en fonction du degré d'érosion et de surimpression par l'écoulement de glace ('*overprinting and superimposition*') (***Eyles et al., 1983 ; Evans & Hiemstra, 2005***).

Au niveau des terminaisons lobées des fleuves de glace, les gradients longitudinaux compressifs ($\Delta\sigma_{com}$), entraine la remobilisation par déformation sous-glaciaire de sédiments antérieurs non-consolidés (d'origine proglaciaire ou non glaciaire) sur lesquels le front avance (***Le Heron et al., 2005 ; Thomas and Chiverrell, 2007 ; Waller et al., 2011***).

4.3.3. Systèmes de drainage d'eau de fonte sous-glaciaires

Les variations temporelles de débit et de pression d'eau de fonte s'écoulant au sein des systèmes de drainage sous-glaciaires sont à l'origine de phases de couplage/découplage entre la glace et le substrat. Consécutivement à des périodes de vidanges de lacs sous- et supra-glaciaires (***Das et al., 2008***) ou aux variations diurnes et saisonnières de productions d'eau de fonte supra-glaciaires (***Hubbard et al., 1995 ; Andrews et al., 2014 ; Smith et al., 2021***), les débits élevés d'écoulement d'eau de fonte favorisent le développement de films d'eau de grande étendue spatiale (***Lai et al., 2021***), la croissance des cavités sous-glaciaires isolées (***Cowton et al., 2016***), l'augmentation de la connectivité hydraulique de routes de drainage (***Nanni et al., 2021***) et le développement / l'activité de chenaux/conduits sous-glaciaires, favorisant les processus de remobilisation fluvio-glaciaire.

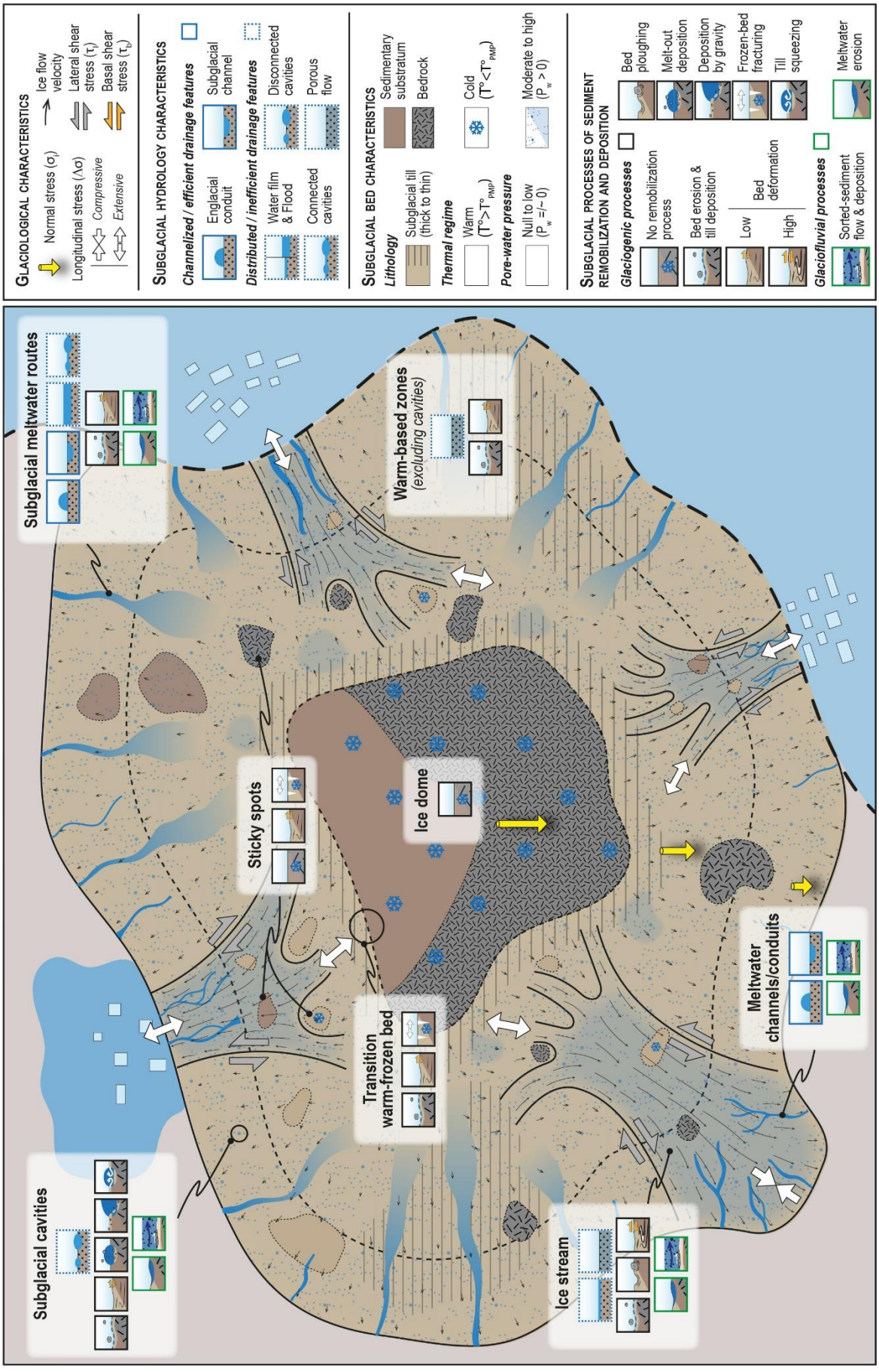

Figure 1.14. *Spatial variability of subglacial processes of sediment remobilization below ice sheets.*

Durant les périodes de quiescence de circulation d'eau de fonte, les cavités sous-glaciaires isolées sont caractérisées par une dominance des processus de remobilisation d'origine glaciogénique (i.e. glissement gravitaire de till, dépôt de till par fonte basale). En revanche, les périodes de circulation active d'eau de fonte induisent la croissance des cavités et une augmentation de la connectivité favorisant l'érosion du substrat, le transport et le dépôt de sédiments triés (***Collins, 1989 ; Clerc et al., 2012 ; Livingstone et al., 2012***) (**Figure 1.13C-14**).

Durant les périodes de circulation active d'eau de fonte, l'augmentation de la connectivité hydraulique des routes de drainage sous-glaciaires et le développement de systèmes chenalisés, le plus souvent incisés dans les lits sédimentaires / substrats sous-glaciaires, engendrent une augmentation des processus d'érosion et de transport sédimentaires (i.e. phase de crue sous-glaciaire, '*subglacial flood'*), puis de dépôt de dépôt de sédiments fluvio-glaciaires lors de la diminution du débit (***Paterson, 1997 ; Brennand, 2000; Lewington et al., 2020***) (**Figure 1.13D-14**). Au sein de ces systèmes hydrologiques distribués ou chenalisés, caractérisés par un découplage souvent temporaire entre la glace et les sédiments, les processus glaciogéniques (i.e. traction basale de sédiments sous-glaciaires) sont interrompus au détriment de processus glacio-fluviatiles (***Clark & Walder, 1994 ; Evans et al., 1995***). Ces sédiments triés et stratifiés sont souvent déformés ultérieurement et recouverts par des tills sous-glaciaires durant les périodes de recouplage dominées par les processus glaciogéniques (***Larsen et al., 2004; Piotrowski et al., 2006; Lesemann et al., 2010; Menzies and Ellwanger, 2011; Reinardy et al., 2011***).

Partie B. Bedforms sous-glaciaires : diversité morphologique, distribution spatiale et processus de formation

M'Clintock Ice Stream bed, Canada Arctic (© Google Earth)

Introduction

Les terrains découverts par le retrait des calottes glaciaires mettent à jour un ensemble de formes sous-glaciaires (i.e. *subglacial landforms*). Ces formes sous-glaciaires sont les témoins directs des processus opérant à la base des glaciers et des interactions entre la glace, l'eau de fonte et le substrat sous-glaciaire ; les étudier est donc crucial pour identifier les facteurs de contrôle de la dynamique des calottes glaciaires. Certaines de ces formes sont des monticules sédimentaires formés par la remobilisation des lits sédimentaires à la base des calottes glaciaires par l'action directe de l'écoulement de glace (processus glaciogéniques) et/ou de l'eau de fonte (processus fluvio-glaciaires) et sont donc qualifiées de modelés de lits : dans le manuscrit, j'utiliserai le terme anglais équivalent, *bedforms* (***Allen, 1968 ; Aario, 1977***),

Des investigations géophysiques ont permis d'identifier des bedforms sous-glaciaires sous les calottes glaciaires actuelles et de mettre en évidence des relations entre leur formation, les dynamiques d'écoulement de la glace (***King et al., 2007 ; Franke et al., 2020***), de l'eau de fonte (***Smith et al., 2007 ; Larter et al., 2009***) et les caractéristiques du substrat sous-glaciaire (***O Cofaigh et al., 2002***). En revanche, la faible résolution de détection des bedforms sous-glaciaires et la ponctualité spatio-temporelle des observations géophysiques ne permettent actuellement de décrire précisément ni leurs morphologies, ni leurs distributions spatiales, ni leurs processus de formation/évolution.

Pour contourner ce problème, la géomorphologie glaciaire étudie les bedforms découverts après le retrait des paléo-calottes glaciaires. A partir de leur architecture sédimentaire, de leur distribution spatiale, de leur morphologie et de la connaissance des processus de remobilisation de sédiments sous-glaciaires, de nombreuses études ont proposé des modèles de formation des bedforms associés à des configurations de l'écoulement de la glace et de l'eau de fonte spécifiques. La géomorphologie glaciaire s'est enrichie au début des années 1990 avec l'utilisation des images satellites (***Clark, 1993 ; Punkari, 1995***), puis a connu un essor considérable depuis les années 2000 avec la croissance de la résolution et de la disponibilité des images satellites et des données topographiques[5] (***Stokes, 2018***). La cartographie

[5] Le projet « Arctic DEM », démarré en 2016 et visant à produire automatiquement des modèles numériques de terrain à haute résolution (2 m) de l'entièreté des surfaces continentales au-dessus de 60°N à l'aide d'imagerie optique stéréo et de logiciels de photogrammétrie, a permis de mettre à disposition une base de données hautes résolutions et libres de droit sans précédents.

et l'étude des bedforms sous-glaciaires combinées à celles des autres morphologies glaciaires témoignant de la dynamique d'écoulement de la glace (e.g. shear moraines, complexes morainiques, fronts de fleuves de glace ou de glaciers actuels) (Chapitre I - Partie A §1.2) et de la dynamique d'écoulement de l'eau de fonte (e.g. esker, chenaux, vallées tunnels, corridor érosif) (Chapitre I - Partie A §2.2.1) permettent d'identifier différentes catégories de bedforms.

Dans cette partie, un état des connaissances actuelles est réalisé sur les caractéristiques morphologiques, la distribution spatiale et les processus de formation des bedforms sous-glaciaires selon que leur formation est attribuée principalement à (i) la dynamique d'écoulement de la glace (i.e. linéations, ribbed bedforms, bedforms circulaires) (**Figure 1.15A**) ou à (ii) la dynamique d'écoulement de l'eau de fonte (i.e. murtoos, hummocks) (**Figure 1.15B**). Enfin, des hypothèses de continuité morphologique et génétique – tentant d'unifier la diversité apparente de morphologie et de processus de formation des bedforms sous-glaciaires – seront présentées.

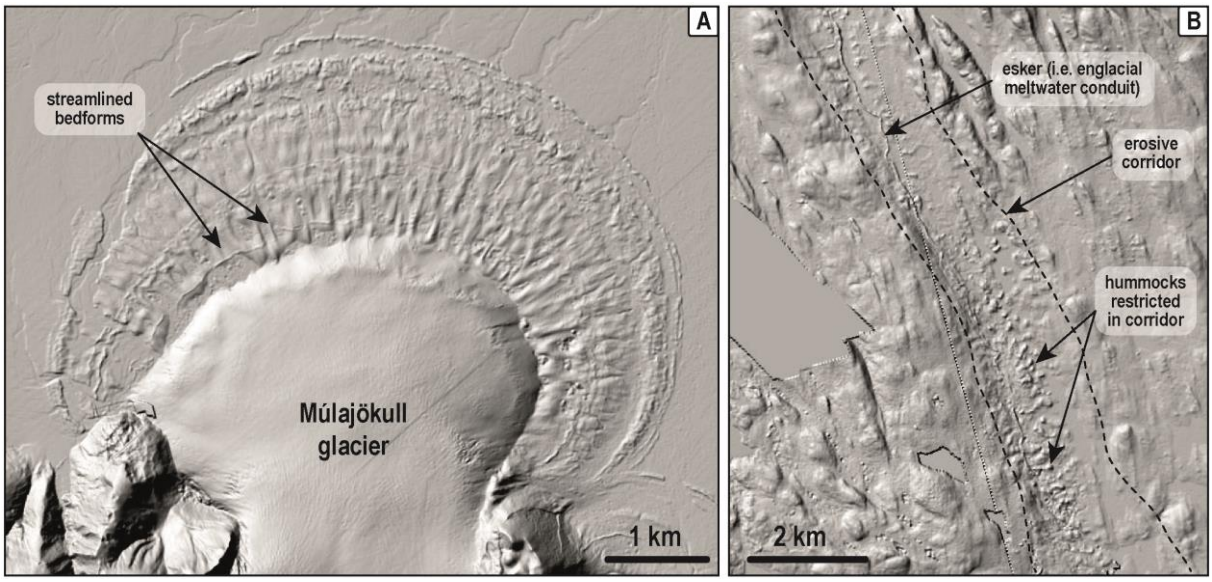

Figure 1.15. *(A) Examples of bedforms, referred to as streamlined bedforms, attributed to ice flow dynamics. Streamlined bedforms are arranged in a radial pattern around the Múlajökull glacier margin (64°39'N, 18°41' W – Iceland) (© Arctic DEM). (B) Examples of bedforms, referred to as hummocks and attributed to meltwater flow dynamics. Hummocks are gathered along an erosive corridor at the bottom of which is an esker, corresponding to the sedimentary relic of a Röthlisberger channel (60°10'N, 104°0' W – Canada) (© Arctic DEM).*

1. Bedforms sous-glaciaires associés à la dynamique de déplacement de la glace

En fonction de leurs orientations par rapport aux directions de déplacement de la glace, les géomorphologues glaciaires distinguent classiquement (i) les linéations glaciaires, rectilignes et supposément parallèles à la direction de déplacement, (ii) les ribbed bedforms, ondulés et supposément transverses (i.e. perpendiculaires) à la direction de déplacement, et (iii) les bedforms circulaires, sans orientation par rapport à la direction de déplacement.

1.1. Linéations glaciaires (‘*Streamlined bedforms*’)

Parmi les bedforms sous-glaciaires, certains sont rectilignes et parallèles les uns aux autres. L’orientation de ces bedforms rectilignes, nommés linéations glaciaires (‘*streamlined bedforms*’), a été interprétée comme indicateur de la direction de déplacement de la glace. Les linéations glaciaires sont subdivisées en plusieurs sous-catégories en fonction de leurs dimensions et de leur rapport longueur / largeur : les drumlins (***Hill, 1973 ; Menzies, 1979***), les MSGLs (‘*mega-scale glacial lineations*’ ; ***Clark, 1993 ; Canals et al., 2000***) et les flutes (***Shaw et al., 2000 ; Eyles, 2012***). Leur longueur (L) et leur largeur (W) sont mesurées respectivement parallèlement et transversalement à la direction de déplacement de la glace, et permettent de calculer un ratio d’élongation (L/W).

1.1.1. Drumlins

Terminologie. Les drumlins sont les linéations les plus communément observées et anciennement étudiées le long des paléo-lits glaciaires (***Hall, 1815 ; Bryce, 1833***). Le terme ‘drumlin’ recouvre une variété de morphologies sous-glaciaires de forme ovoïde (***Menzies, 1979 ; Stokes et al., 2011***) formées par : (i) l’érosion d’un substrat rocheux par l’écoulement de la glace (‘*rock drumlin*’ ou ‘*whaleback*’) (***Evans, 1996 ; Eyles, 2012***), (ii) le dépôt de sédiments sous-glaciaires au front ou autour d’un haut topographique du substrat rocheux (i.e. ‘*crag-and-tail drumlin*’, ‘*obstacle drumlin’*, ‘*rock-cored drumlin*’) (***Evans & Hansom, 1996 ; Hattestrand et al., 2004 ; Jakobsen et al., 2012***), ou (iii) la remobilisation de substrats sédimentaires, de tills sous-glaciaires et/ou de sédiments fluvio-glaciaires (‘*emergent drumlin*’) (***Clark et al., 2010***). Dans ce manuscrit, je ne m’intéresse qu'aux drumlins ‘*emergent*’, en cohérence avec la définition des bedforms que j’ai adoptée dans le Chapitre I - Partie B § Introduction).

Morphométrie et composition. Les drumlins sont des linéations de forme ovoïde, caractérisées par une symétrie longitudinale et allongées parallèlement dans la direction de déplacement de la glace (**Figure 1.16**) (***Menzies, 1979 ; Spagnolo et al., 2010, 2011***). En moyenne, les drumlins font en moyenne 687 ± 176 m de long, 226 ± 34 m de large (correspondant à un ratio d'élongation L/W ~ 3) et 7.0 ± 0.4 m d'amplitude (**Table 1.1** - **Figure 1.17**). Les drumlins sont constitués de couches de tills sous-glaciaires, de roches sédimentaires sous-jacentes non-consolidées et/ou de sédiments sableux/graveleux, présentant ou non des évidences de déformation (e.g. ***Wysota, 1994 ; Moller & Dowling, 2016 ; Hermanowski et al., 2019***).

Distribution spatiale. Bien que les drumlins soient parfois distribués aléatoirement le long des paléo-lits glaciaires (***Smalley & Unwin, 1968 ; Francek, 1991***), ils sont le plus souvent caractérisés par une distribution spatiale régulière, avec de fréquents alignements transverses ou obliques, dits 'en-échelon' (**Figure 1.16B**) (***Hill, 1973 ; Patterson & Hooke, 1995***), suggérant l'existence de motifs réguliers et organisés au sein des champs de drumlins (***Clark et al., 2018***).

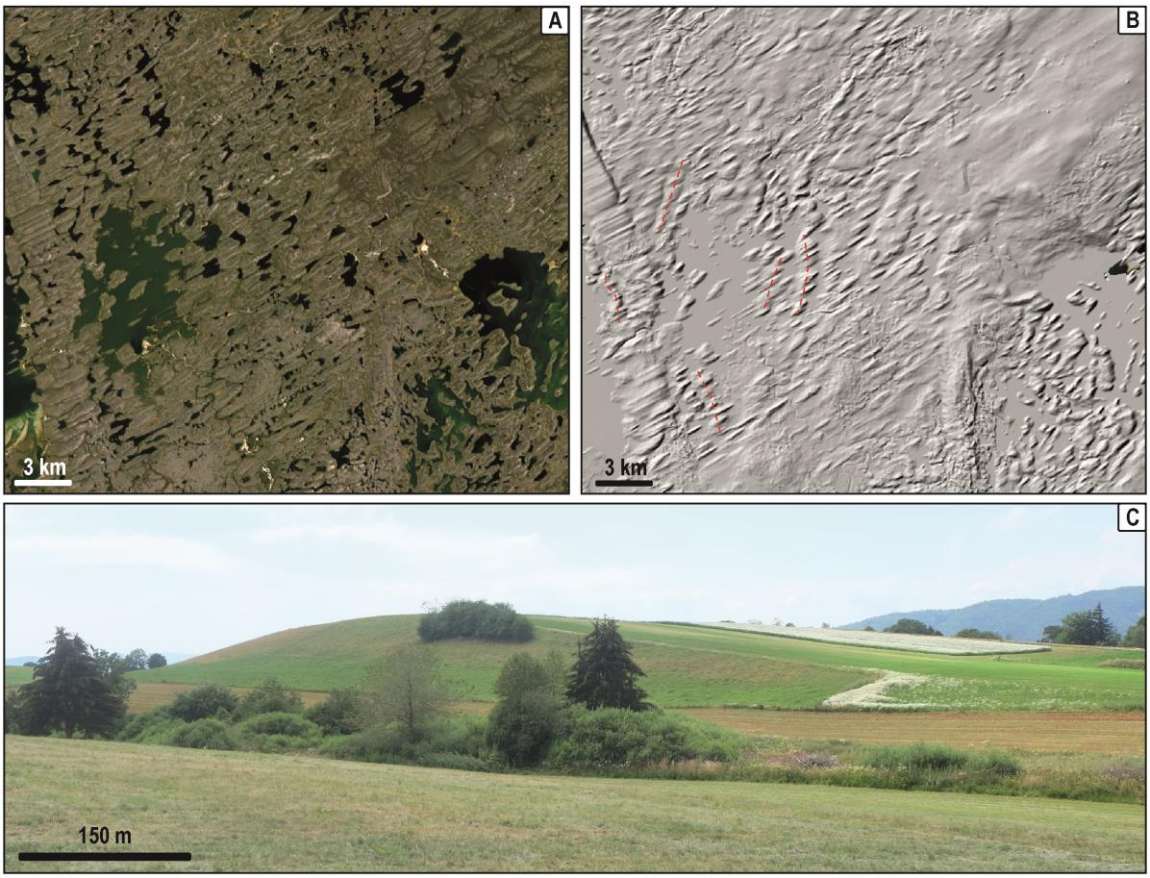

Figure 1.16. *(A) & (B) Satellite imagery (© Google Earth) and hillshaded DEM (© ArcticDEM) of drumlin field in Canada (63°4'N, 104°28' W). Note the frequent transverse to oblique alignment of drumlins in (B) (dotted red lines), suggesting patterns in the spatial organization of drumlins. (C) Illustration of the ovoid and elongated shape of a drumlin in Menthonnex-en-Bornes (Alpes, France – personal photography).*

***Table 1.1**. Morphological statistics of subglacial bedforms compiled from the literature with mean values of length, width and amplitude.*

	References	Location	n	Length (m)	Width (m)	Amplitude (m)
MSGLs ***(n = 54466)***	***(1) O Cofaigh et al., 2005***	Antarctica	313			3
	(2) Greenwood et al., 2012	Antarctica	200	982		
	(3) Winsborrow et al., 2012	Norway	650	2200		
	(4) Spagnolo et al., 2014	Antarctica; Norway; Canada (*NWT & Alberta*)	3068 *(1929)* *(1697)*	2750	270	4
	(5) Ely et al., 2016	Canada (*Quebec, NWT, Nunavut, Alberta*)	31668	1102	150	
	(6) Sookhan et al., 2016	USA (*Minnesota*)	158	3107	209	8.2
	(7) Norris et al., 2017	Canada (*Saskatchewan*)	15192	1040		
	(8) McKenzie et al., 2022	USA (*WA, NY, PA*); Canada (*Nunnavut*); Iceland; Norway; Sweden	3217	1269		
			Mean (± 1σ)	**1206 (± 415)**	**159 (± 27)**	**4.2 (± 1.2)**
Drumlins ***(n = 78525)***	***(9) Wysota, 1994***	Poland	517	138	51	4.2
	(10) Knight, 1997	N Ireland	1562	420	250	
	(11) Jørgensen, & Piotrowski, 2003	Denmark	161	1111		
	(12) Greenwood & Clark, 2008	Ireland	24049	678		
	(13) Clark et al., 2009	Britain	37043	601	209	
	(14) Smith et al., 2009	Scotland	175			9.3
	(15) Spagnolo et al., 2012	Britain	*(25848 from n°11)*			7.1
	(16) Benediktsson et al., 2016	Iceland (*Mulajökull*)	155	206	86	7.7
	(6) Sookhan et al., 2016	USA (*Minnesota*)	5624	728	267	6.7
	(17) Benediktsson et al., 2022	Iceland (NE)	797	719	185	
	(8) McKenzie et al., 2022	USA (*WA, NY, PA*); Canada (*Nunnavut*); Iceland; Norway; Sweden	8442	1147	275	
			Mean (± 1σ)	**687 (± 176)**	**226 (± 34)**	**7.0 (± 0.4)**
Ribbed bedforms ***(n = 70204)***	***(18) Dunlop & Clark, 2006a***	N Ireland; Canada (*Quebec*); Sweden	800			17
	(19) Greenwood & Kleman, 2010	Canada (*Nunavut*)	733	9512	1474	15
	(20) Hughes et al., 2010	Britain	1829	920	400	
	(21) Wagner, 2014	Canada (*Nunavut*)	45879 *(200)*	652	319	29
	(5) Ely et al., 2016	Canada; Ireland; USA (NY); Sweden	18384	701	197	
	(22) Stokes et al., 2016	Canada (*Alberta, Saskatchewan*)	1478 *(85)*	2973	700	15
	(23) Möller & Dowling, 2018	Sweden	1286	484	166	9.9
	(24) Helgadottir, 2020	Iceland (*East*)	241	112	66	6.4
	(25) Benjaminsdottir, 2021	Iceland (*N East*)	78	157	21	3.6
	(26) Vérité et al., 2021	Canada (*Alberta, Victoria Island*)	307	3190	919	
	(27) Vérité et al., 2022	Sweden; Finland	2692	229	87	
	(28) Boyes et al., 2021	Russia (*Kola Peninsula*)	8125	1258	397	
			Mean (± 1σ)	**857 (± 918)**	**281 (± 216)**	**13.5 (± 7.0)**
Circular bedforms ***(n = 1955)***	***(5) Ely et al., 2016***	Ireland	1955	417	409	
	(27) Vérité et al., 2022	Sweden; Finland	232	82	64	
	(28) Boyes et al., 2021	Russia (*Kola Peninsula*)	189	641	3493	
			Mean (± 1σ)	**402 (± 121)**	**382 (± 107)**	
Flutes ***(n = 664)***	***(29) Evans & Twigg, 2002*** ***(30) Waller et al., 2008*** ***(5) Ely et al., 2016***	Iceland (Skeiðararjökull, Breiðamerkurjökull) ; Svalbard	664	30	2	

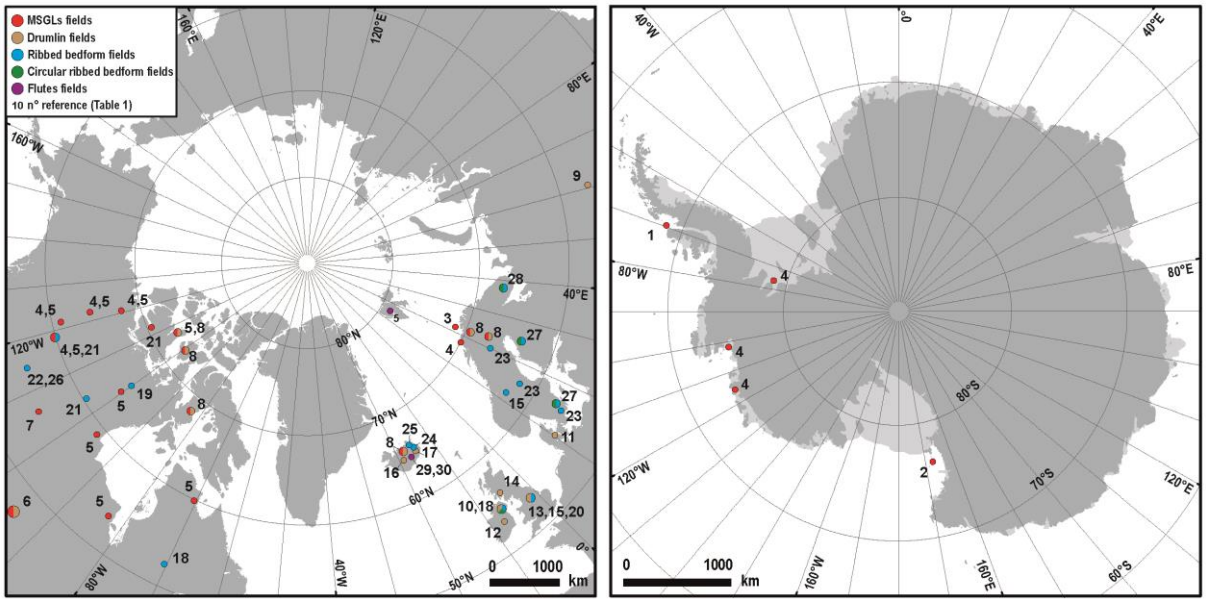

***Figure 1.17**. Location of subglacial bedform fields compiled in Table 1.*

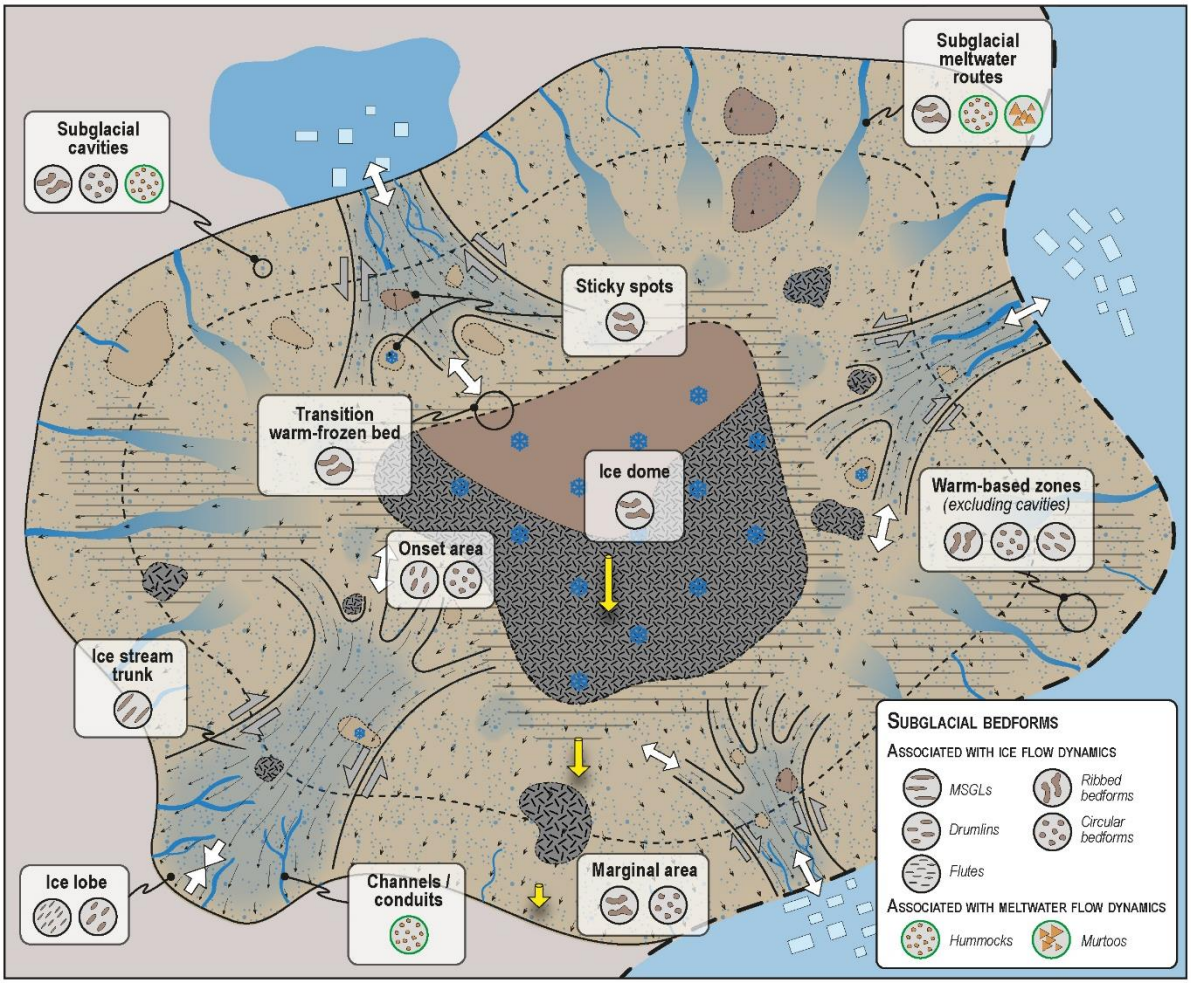

***Figure 1.18.** Spatial distribution of subglacial bedforms depending on glaciological and hydrological environments of an ice sheet. MSGLs, drumlins, flutes, ribbed bedforms and circular bedforms are predominantly-associated with the dynamics of ice flow (i.e. formation dominated by glaciogenic processes), while hummocks and murtoos are predominantly-associated with the dynamics of meltwater flow (i.e. formation dominated by glaciofluvial processes).*

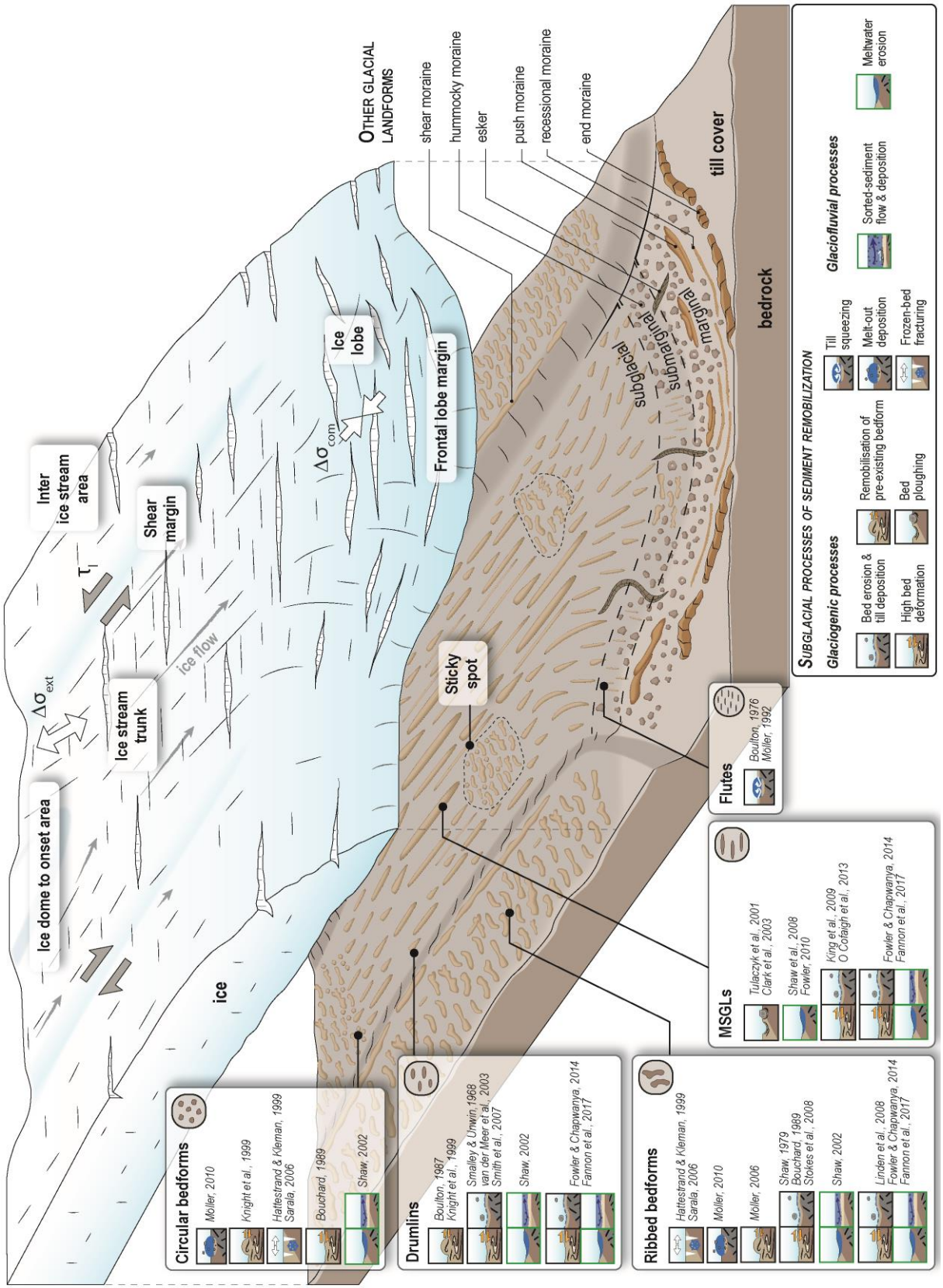

Figure 1.19. *Assemblage of subglacial bedforms – MSGLs, drumlins, flutes, ribbed bedforms and circular bedforms – predominantly-associated with the dynamics of ice flow in land-based ice stream. The hypotheses of formation of subglacial bedforms are dominated by glaciogenic processes and extremely various.*

La présence de champs de drumlins est indépendante de la topographie et de la lithologie du substrat sous-glaciaire (***Reed, 1962 ; Patterson & Hooke, 1995***), mais les variations lithologiques semblent contrôler la longueur moyenne des drumlins (***Greenwood & Clark, 2010***). A l'échelle des calottes glaciaires, les champs de drumlins sont essentiellement identifiés au niveau des zones d'enracinement des fleuves de glace ('*onset area'*) (**Figure 1.18**), illustrant, avec leur large éventail d'orientations, la zone de convergence des flux de glace au sein des affluents ('*tributaries*') en direction du couloir principal d'écoulement de la glace ('*trunk*') (Chapitre I - Partie A §1.2.2.) (**Figure 1.19**) (***Stokes & Clark, 1999; King et al., 2007; Anderson & Fretwell, 2008; Eyles, 2012***).

Formation. L'origine des drumlins est étudiée depuis le début du 20ème siècle et a donné lieu à de multiples hypothèses dont le nombre et la diversité peuvent s'expliquer par la grande diversité de leur composition sédimentaire interne (***Stokes et al., 2011***). D'autres modèles de formation de drumlins ont émergé de l'étude de la rhéologie des tills sous-glaciaires en fonction des dynamiques d'écoulement de la glace et de l'eau. Les hypothèses de formation des drumlins (**Figure 1.19**) peuvent ainsi être classées selon 3 types de modèles impliquant :

- (i) la déformation et l'érosion par l'écoulement de la glace d'un lit de sédiments sous-glaciaires en réponse à des hétérogénéités rhéologiques (e.g. lithologie, pression d'eau interstitielle) (***Smalley & Unwin, 1968 ; Bluemle et al., 1993 ; van der Meer et al., 2003 ; Smith et al., 2007 ; Clark, 2010 ; Eyles et al., 2016 ; Hermanowski et al., 2019 ; Zoet et al., 2021 ; McKenzie et al., 2022 ; Sookhan et al., 2022***) ou de landforms sédimentaires préexistants (***Boutlon, 1987 ; Hart & Roberts, 1994 ; Hart, 1995 ; Knight et al., 1999 ; Kjaer et al., 2003***).
- (ii) la déformation et l'érosion de sédiments sous-glaciaires combinées à l'érosion et au dépôt de sédiments fluvio-glaciaires par l'action conjointe de l'écoulement de la glace et de l'eau de fonte (***Fowler, 2009 ; Fowler & Chapwanya, 2014 ; Hillier et al., 2016 ; Fannon et al., 2017***)
- (iii) la circulation massive d'eau de fonte responsable de l'érosion de cavités allongées dans le sens de circulation de l'eau de fonte à la base de la colonne de glace, ultérieurement comblées par des sédiments sous-glaciaires (***Shaw, 1983, 2002***).

1.1.2. Mega-Scale Glacial Lineations (MSGLs)

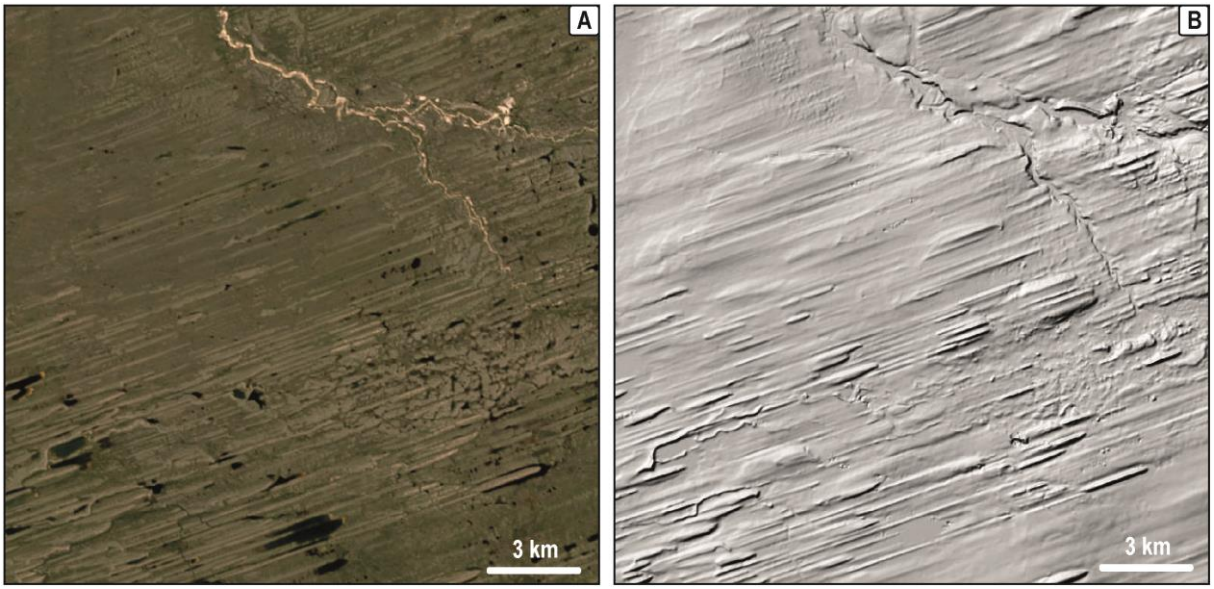

Figure 1.20. *(A) & (B) Satellite imagery (© Google Earth) and hillshaded DEM (© ArcticDEM) of a MSGL field along the palaeo-Dubawnt Lake ice stream in Canada (64°2'N, 101°52' W). Note the high elongation and the regular transverse spacing of MSGLs.*

Morphométrie et composition. Les MSGLs – aussi appelées 'mega-flutes' (***Evans, 1996 ; Jansson & Glasser, 2005***) – sont des bedforms rectilignes, parallèles les uns aux autres, très allongés dans la direction de déplacement de la glace et composés essentiellement de tills sous-glaciaires déformés (***Clark, 1993 ; Wellner et al., 2001 ; O Cofaigh et al., 2005***) (**Figure 1.20**). En moyenne, les MSGLs font 1206 ± 415 m de long, 159 ± 27 m de large (correspondant à un ratio d'élongation L/W ~ 7) et 4.2 ± 1.2 m d'amplitude (**Table 1.1** - **Figure 1.17**).

Distribution spatiale. Les MSGLs sont regroupées au sein de champs formant fréquemment des couloirs larges de 10s de km et longs de 10-100s de km. Au sein de ces champs, le ratio d'élongation des MSGLs varie transversalement et longitudinalement (***Stokes et al., 2013a***), mimant les gradients de vitesse observés au sein des fleuves de glace (***Patterson, 1997; Sergienko & Hindmarsh, 2013; Zheng et al., 2019***). Les MSGLs sont associées à de fortes vitesses d'écoulement de la glace et sont le principal critère morphologique de reconnaissance[6] des paléo-fleuves de glace ('*ice stream trunks*') (***Stokes & Clark, 2001; Clark & Stokes, 2003 ; Livingstone et al., 2013***) (**Figure 1.18**). Cette interprétation est

[6] Les '*shear moraines'* correspondant à de longs cordons morainiques bordant les couloirs de linéations glaciaires sont interprétées comme des reliques morphologiques des marges latérales cisaillantes et constituent – après les MSGLs – l'un des principaux critères morphologiques de reconnaissance des fleuves de glace (***Dyke & Morris, 1988 ; Dyke et al., 1992 ; Stokes & Clark, 2002b ; Riverman et al., 2019***).

supportée par l'observation de MSGLs mis à jour par le retrait récent de fleuves de glace actuels (***King et al., 2009 ; Smith & Murray, 2009***).

Formation. Quatre catégories d'hypothèses de formation tentent d'expliquer l'élongation et l'organisation spatiale des MSGLs (**Figure 1.19**) :

- (i) des corrugations à la base de la glace – créées par son écoulement sur un substrat rocheux présentant des irrégularités topographiques – forment en aval des surcreusements en forme de tôle ondulée dans un lit sédimentaire meuble (***Tulaczyk et al., 2001 ; Clark, et al., 2003***)
- (ii) la chenalisation d'un film d'eau à l'interface entre la glace et un lit sédimentaire produit de longs couloirs érosifs parallèles les uns aux autres (***Shaw et al., 2008 ; Fowler, 2010***)
- (iii) la déformation et l'érosion de sédiments sous-glaciaires en raison de fortes vitesses d'écoulement de la glace (***King et al., 2009 ; O Cofaigh et al., 2013 ; McKenzie et al., 2022 ; Sookhan et al., 2022***)
- (iii) la combinaison de la déformation/érosion de sédiments sous-glaciaires et de processus fluvio-glaciaires (érosion et dépôt de sédiments par l'eau de fonte) (***Fowler & Chapwanya, 2014*** ; ***Hillier et al., 2016 ; Fannon et al., 2017***).

1.1.3. Flutes

Morphométrie et composition. Les flutes sont des linéations faisant en moyenne 30 m de long, 2 m de large et moins d'1 m d'amplitude (**Table 1.1** – **Figures 1.17, 1.21**), et possédant un espacement de quelques dizaines de mètres (***Boulton, 1976 ; Gordon et al., 1992 ; Kjaer et al., 2006 ; Hart et al., 2018***). Les flutes sont donc des linéations très étroites et très allongées, dont le ratio d'élongation L/W varie de 2 à 60. Les flutes sont composées majoritairement de tills sous-glaciaire (*'lodgment tills'*) mais peuvent aussi contenir des sédiments triés silto-sableux. Un bloc rocheux ou un haut topographique du substrat rocheux – de même amplitude et largeur que la flute – est fréquemment observé au niveau de leur terminaison amont (***Boulton, 1976; Ely et al., 2017 ; Ives & Iverson, 2019***).

Distribution spatiale. Les petites dimensions induisent un faible potentiel de préservation au sein de paléo-lits des calottes glaciaires. Lorsque ces dernières sont bien préservées, les flutes ne sont observables qu'à partir de données cartographiques de très hautes résolutions et sont regroupées en champs avec d'autres linéations glaciaires. Les flutes sont fréquemment observées en superposition sur des bedforms sous-glaciaires ou sur des moraines frontales d'orientation différente et de plus grandes

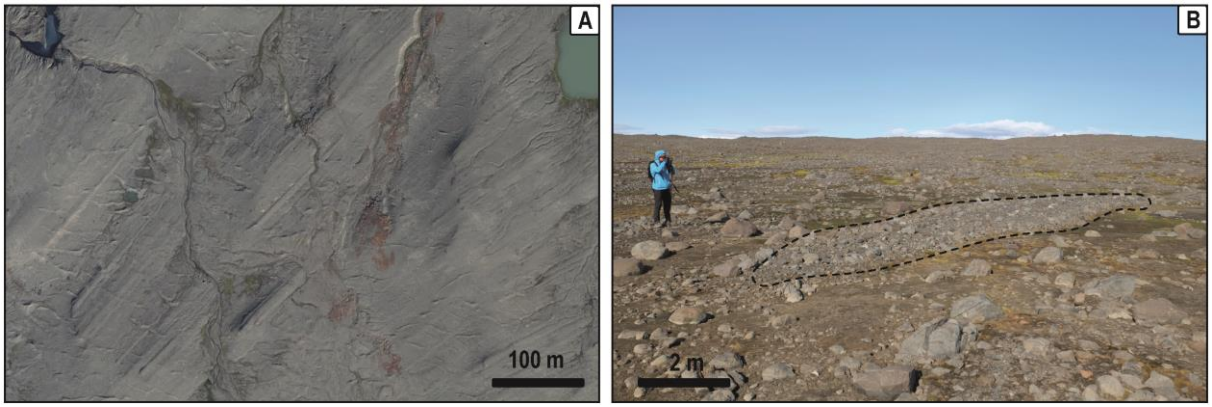

***Figure 1.21**. (A) Satellite imagery (© Loftmyndir) of a field of flutes occurring along the recently retreated ice front of the Eyjabakkajökull Glacier (Iceland). (B) Flute depicted along the recently retreated ice front of the Bruarjökull Glacier (Iceland – personal photography). Note the human-scale dimensions of flutes, compared with other large-scale lineations such as drumlins and MSGLs.*

dimensions, et sont ainsi interprétées respectivement comme illustrant des changements de direction d'écoulement de la glace (Chapitre I - Partie B §2.1.4.) ou des phases de ré-avancée du glacier. Les flutes sont communément observées au-devant des glaciers et calottes glaciaires récemment retirés (***Evans & Twigg, 2002 ; Evans et al., 2015***) (**Figures 1.18, 1.19, 1.21**).

Formation. En raison de la présence fréquente d'un obstacle rocheux au niveau de la terminaison amont, la principale hypothèse de formation des flutes repose sur la formation d'une petite cavité sous-glaciaire en aval d'un bloc rocheux / haut topographique (i.e. agent exogène), dont le comblement par du till sous-glaciaire s'effectue par effet de succion *('till squeezing')* (**Figure 1.19**), et éventuellement par des sédiments sableux déposés par l'eau de fonte (***Boulton, 1976 ; Möller, 1992 ; Rose, 1992 ; Eyles et al., 2015 ; Ives & Iverson, 2019***). Bien que les flutes soient issues de la remobilisation des sédiments par l'écoulement de la glace et de l'eau, leur processus de formation impliquant un agent exogène et contrôlant directement leurs dimensions est incohérent avec la définition des bedforms adoptée dans ce manuscrit, expliquant que les flutes soient exclues des analyses réalisées dans ce travail.

1.2. Ribbed bedforms

Terminologie. Les ribbed bedforms sont des bedforms sous-glaciaires périodiques et côtelés ('ribbed' en anglais), dont l'orientation est transverse (i.e. ~ 80-90°) à la direction de déplacement de la glace (**Figure 1.22**) (***Aylsworth & Shilts, 1989; Dunlop and Clark, 2006 ; Stokes et al., 2016***). Dans ce manuscrit, le terme 'ribbed bedform' regroupe sous un seul terme sans connotation génétique plusieurs sous-catégories de bedforms côtelés. ***Hughes (1964)*** et ***Lundqvist (1969)*** décrivent pour la première

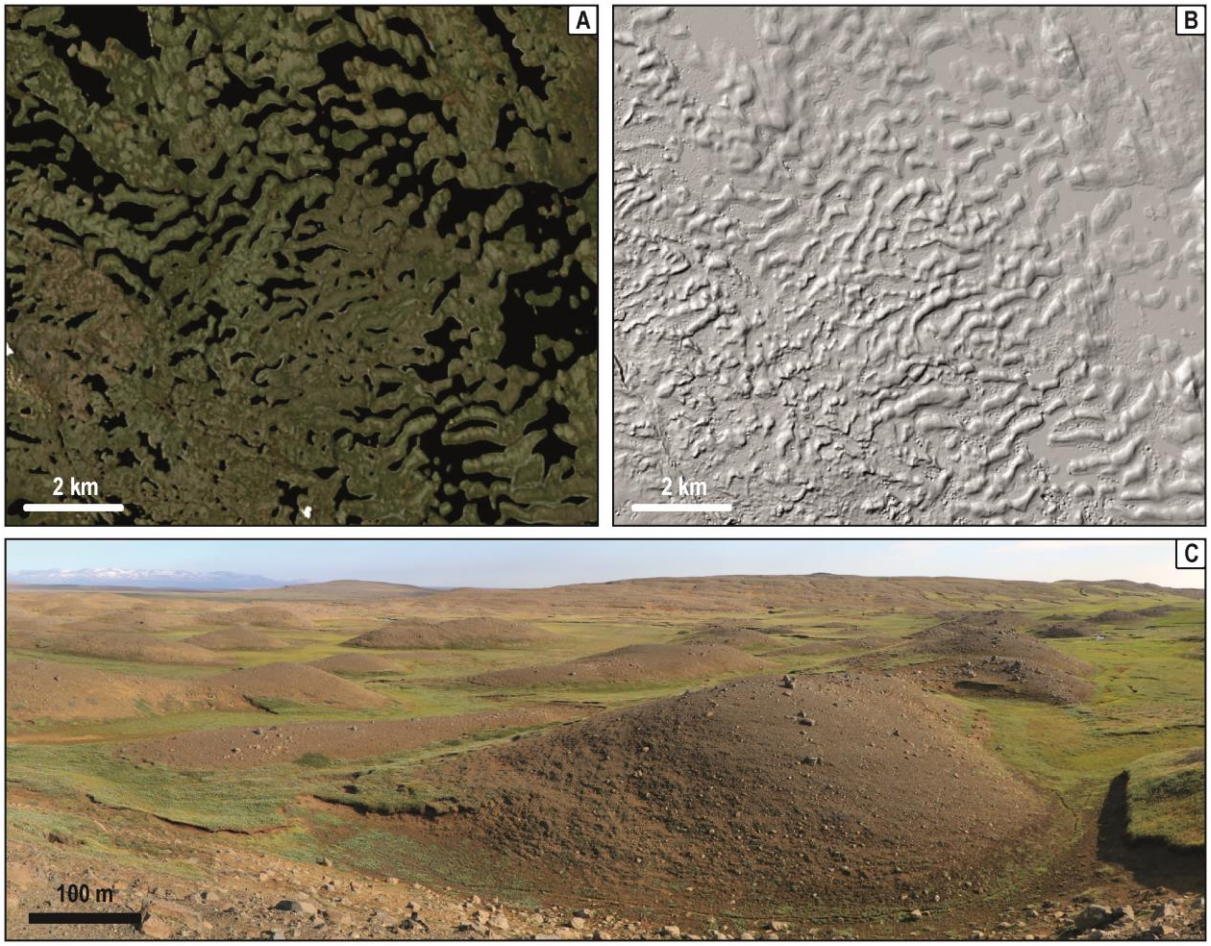

***Figure 1.22**. (A) & (B) Satellite imagery (© Google Earth) and hillshaded DEM (© ArcticDEM) of a ribbed bedform field in Canada (60°26'N, 101°9' W). The wavelength highlights the periodic pattern of ribbed bedforms. (C) Undulating and transverse sedimentary ridges corresponding to ribbed bedforms, in Vopnafjördur (Iceland - 65°35'N, 15°28'W – personal photography).*

fois ces bedforms côtelés au Canada et en Suède (près du Lac Rogen) et les nomment '*ribbed moraines'* et '*Rogen moraines*', à tort puisque qu'il ne s'agit pas de dépôts morainiques à proprement parler. Des bedforms transverses de grandes dimensions appelés *'mega-ribs'* (***Greenwood & Kleman, 2010***), et des bedforms correspondant à l'expression topographique de motifs de taux de cisaillement basal élevé identifiés sous les calottes Antarctique et Groenlandaise appelés '*traction ribs'* (***Sergienko & Hindmarsh, 2013 ; Sergienko et al., 2014 ; Stokes et al., 2016***) sont également regroupés dans la catégorie des ribbed bedforms.

Morphologie et composition. En moyenne, les ribbed bedforms font 857 ± 918 m de longueur (mesurée transversalement à la direction de déplacement de la glace), 281 ± 216 m de large et 13.5 ± 7.0 m d'amplitude (**Table 1.1** - **Figure 1.17**). En revanche, les bedforms rentrant dans la sous-catégorie de 'mega-ribs' sont en moyenne longs de 9300 m et larges de 2000 m (***Greenwood & Kleman, 2010 ; Ely et al., 2016***). ***Dunlop & Clark (2006a)*** et ***Wagner (2014)*** ont par ailleurs démontré que de grandes

variabilité et complexité morphologiques existaient au sein des ribbed bedforms, soulignant le caractère parfois sinueux des contours des ribbed bedforms (e.g. 'blocky angular', 'lumpy-type', 'jagged-type') (**Figure 1.23**). ***Stokes et al. (2016)*** ont également montré que des '*traction ribs*' identifiés au Canada pouvaient présenter des orientations obliques (< 80°) à la direction de déplacement de la glace. Les ribbed bedforms sont essentiellement composés de tills sous-glaciaires déformés, mais des intercalations de sédiments sableux/graveleux peuvent aussi être observés (***Hattestrand & Kleman, 1999 ; Linden et al., 2008 ; Trommelen et al., 2014 ; Möller & Dowling, 2018***).

Distribution spatiale. D'après certaines reconstitutions paléoglaciologiques, les ribbed bedforms sont associés à d'anciennes zones caractérisées par une base froide, une pression interstitielle nulle ou très faible, par un substrat rigide et/ou un faible taux de cisaillement basal τ_b (***Stokes, 2018***). Pour ces raisons, les ribbed bedforms sont communément associés à des régions de faible vitesse d'écoulement de la glace au sein des calottes glaciaires (**Figure 1.18**). Les ribbed bedforms sont notamment observés depuis d'anciennes positions de dômes de glace (***Aylsworth & Shilts, 1989; Dyke et al., 1992; Hättestrand & Kleman, 1999; Greenwood & Kleman, 2010***) jusqu'au zones d'enracinement des fleuves de glace, où la transition entre une base froide à une base tempérée génère des contraintes longitudinales extensives (**Figure 1.19**) (***Bouchard, 1989; Dyke et al., 1992; Hättestrand & Kleman, 1999 ; Van Landeghem & Chiverrell, 2020***). Bien que les ribbed bedforms soient globalement absents des fleuves de glace, ils correspondent à des marqueurs morphologiques de zones localement caractérisées par une forte friction basale ('*sticky spot'*) (***Cowan, 1968; Aylsworth & Shilts, 1989; Bouchard, 1989; Dyke et al., 1992; Stokes & Clark, 2003; Stokes et al., 2006a, 2008, 2016***). Les ribbed bedforms ont également été associés à des zones de faible vitesse d'écoulement de la glace situées entre les fleuves de glace (***Szuman et al., 2021***) et dans les régions marginales des calottes (***Marich et al., 2005; Möller, 2006, 2010 ; Middleton et al., 2020 ; Rabassa et al., 2022***), en raison de leur association avec des hummocky moraines et des complexes morainiques[7].

[7] Les zones marginales des calottes glaciaires à terminaison terrestre sont typiquement identifiées par des ceintures morainiques constituées de hummocky moraines (***Johnson & Clayton, 2003 ; Ebert & Kleman, 2004***) et de rides morainiques (moraines terminales, de récession ou de poussée) (***Evans & Hiemstra, 2005 ; Chandler et al., 2016***).

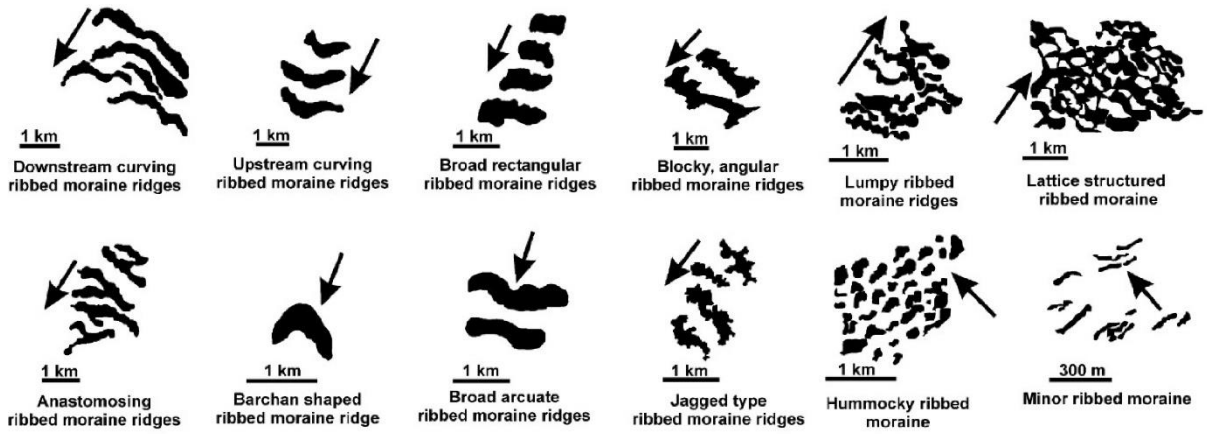

***Figure 1.23**. Classification of ribbed bedforms based on morphological distinctions (**Dunlop & Clark, 2006**).*

Formation. Excepté ***Shaw (2002)***, qui a proposé que des crues sous-glaciaires de grande échelle puissent produire des bedforms sous-glaciaires (<u>Chapitre I - Partie B §1.1.1</u>), la formation des ribbed bedforms est généralement attribuée à la déformation sous-glaciaire. Cependant, des divergences existent sur l'importance du régime thermique basal de la glace, l'implication de la circulation d'eau de fonte et la nature de la déformation du lit sédimentaire lors de la formation et l'évolution des ribbed bedforms. Les hypothèses de formation des ribbed bedforms peuvent ainsi être réparties en quatre catégories :

- (i) la fracturation par extension d'un substrat sédimentaire gelé le long des zones de transition entre les bases froides et tempérées, caractérisées par contraintes longitudinales extensives (***Hattestrand & Kleman, 1999 ; Sarala, 2006***)

- (ii) le dépôt par fonte basale ('*melt out*') d'une couche de glace basale déformée et riche en sédiments (***Möller, 2010***)

- (iii) la déformation et l'érosion d'un lit de sédiments sous-glaciaires d'une base tempérée (***Shaw, 1979 ; Bouchard, 1989 ; Stokes et al., 2008 ; Sommerkorn, 2020***) ou de landforms sédimentaires préexistants (e.g. linéations, moraines marginales) (***Lundqvist, 1989 ; Möller, 2006***) sous l'action de l'écoulement cisaillant de la glace

- (iv) la déformation et l'érosion de sédiments sous-glaciaires produites par l'écoulement de la glace combinées à de processus fluvio-glaciaires (érosion et dépôt) liés à l'écoulement d'eau de fonte (***Linden et al., 2008 ; Fowler & Chapwanya, 2014*** ; ***Fannon et al., 2017 ; Middleton et al., 2020***).

1.3. Bedforms circulaires (‘*circular bedforms*’)

Terminologie et morphométrie. Certains bedforms de forme subcirculaire possédant un diamètre moyen de 400 m (**Table 1.1** - **Figure 1.17**) ont été communément décrits au sein de champs de ribbed bedforms et de linéations et diversement appelés ‘*mammilary hills*’ (***Aario, 1977***), ‘*Blattnick moraines*’ (***Markgren & Lassila, 1980***), ‘*circular forms*’ (***Knight et al., 1999***), ‘*hummocky-ribbed moraines*’ (***Hattestrand, 1997 ; Dunlop & Clark, 2006***) ou ‘*ovoid forms’* (***Smith & Wise, 2007***).

Distribution spatiale et formation. D’après certaines études, les bedforms circulaires seraient plus densément observés à la transition entre des champs de ribbed bedforms et des champs de linéations (***Aario, 1977 ; Knight et al., 1999 ; Ely et al., 2016***). Certains bedforms circulaires apparaissent en superposition sur des ribbed bedforms, suggérant que leur formation résulte de la fragmentation/érosion des ribbed bedforms (***Knight et al., 1999 ; Greenwood & Clark, 2008***). Bien que très peu étudiés et décrits dans la littérature, leur association très fréquente avec les ribbed bedforms suggère qu’ils sont génétiquement liés à ces derniers (***Hattestrand, 1997 ; Dunlop & Clark, 2006a ; Möller & Dowling, 2015***).

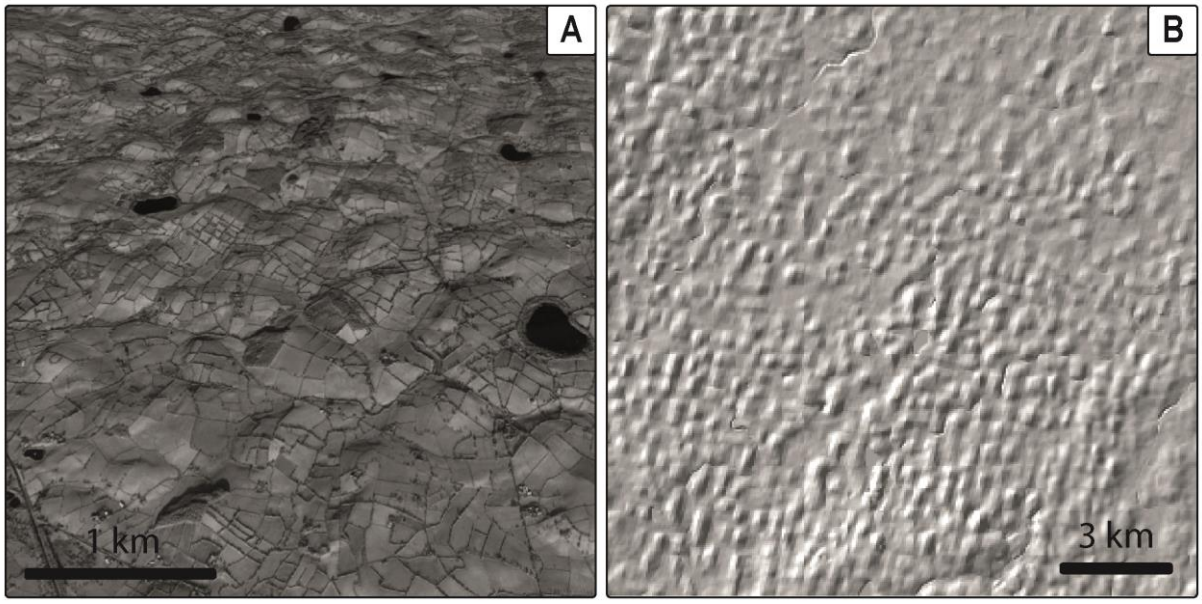

Figure 1.24. *(A) & (B) Hillshaded aerial imagery (© Google Earth) and hillshade (© ArcticDEM) of a field of circular bedforms in Ireland (54°24’N, 6°53’W). Note the periodic mammillary pattern and the intimate association with elongated transverse ridges, i.e. ribbed bedforms.*

1.4. Bedforms complexes

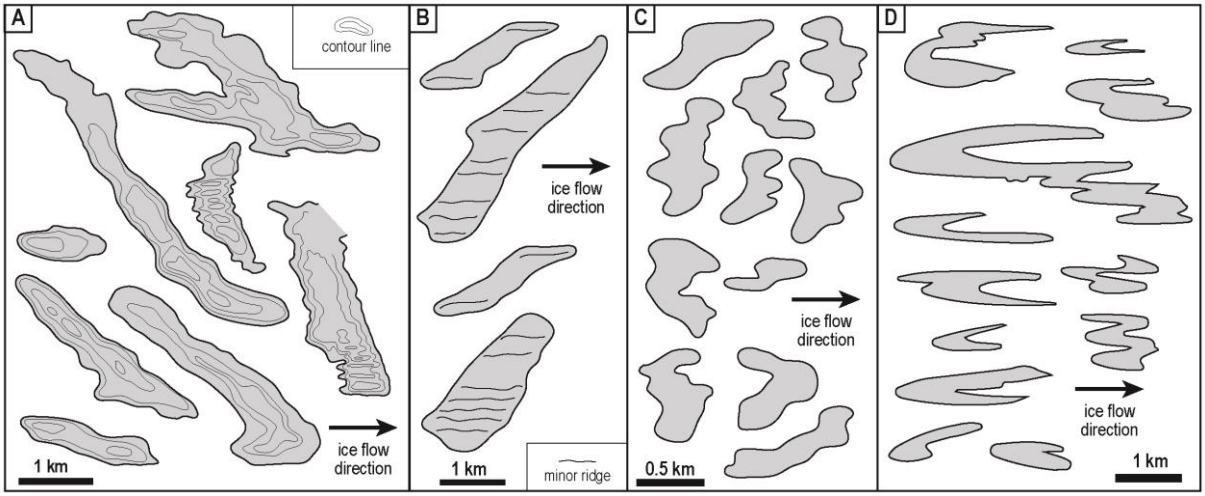

Figure 1.25. *Examples of complex bedforms that have often been excluded from classical bedform categories due to their shape complexities although they appear to be commonly associated with streamlined bedforms, ribbed bedforms and circular bedforms. Some of them are referred to as (A) smoothsided / drumlinized ribbed bedforms (**Carl, 1978**), (B) transverse asymmetrical drumlins (**Shaw, 1983**), (C) Blattnick moraines (**Markgren & Lassila, 1980**) and (D) crescentic/ parabolic ridges and drumlins (**Boulton, 1987**).*

Terminologie et morphométrie. Hormis les trois catégories précédentes de bedforms sous-glaciaires associés à la dynamique d'écoulement de glace, d'autres bedforms de forme plus complexe sont observés au sein des paléo-lits glaciaires (**Figure 1.25**). Ces bedforms complexes ont été variablement décrits comme :

- '*smoothsided / drumlinized ribbed bedforms*', correspondant à des bedforms particulièrement ondulés mais principalement transverses, ayant une apparence globale de ribbed bedform « beurré » et sur lesquels sont superposés des drumlins (i.e. drumlinisation), parfois disposés en échelon (**Figure 1.25A**) (***Carl, 1978 ; Lundqvist, 1981 ; Dunlop & Clark, 2006***)

- '*transverse asymetrical drumlins*', correspondant à des bedforms obliques à la direction de déplacement sur lesquels sont superposées des flutes d'orientation discordante et de petites dimensions (**Figure 1.25B**) (***Shaw, 1983 ; Boulton, 1987***)

- '*Blattnick moraines*', correspondant à la fois à (i) des bedforms subcirculaires similaires à des drumlins très peu allongés dans la direction de déplacement de la glace et à (ii) des bedforms transverses ayant subi un processus de drumlinisation (**Figure 1.25C**) (***Markgren & Lassila, 1980***)

- '*crescentic/ parabolic ridges and drumlins*', correspondant à des bedforms souvent en forme de U dont les branches – jointes au niveau d'une terminaison en amont ou en aval – sont allongées parallèlement

à la direction de déplacement de la glace (**Figure 1.25D**) (***Shaw, 1983 ; Boulton, 1987 ; Lundqvist, 1989 ; Smalley & Warburton, 1994 ; Eyles et al., 2016***).

Distribution spatiale. Bien que parfois situés au cœur de champs de linéations glaciaires (***Shaw, 1983 ; Eyles et al., 2016***), ces différents types de bedforms complexes sont la plupart du temps localisés au niveau de zones de transitions latérales (***Dunlop & Clark, 2006***) et longitudinales (***Carl, 1978 ; Lundqvist, 1981, 1989 ; Markgren & Lassila, 1980***) entre des champs de ribbed bedforms et de linéations glaciaires (notamment de drumlins).

Formation. Les bedforms complexes ont classiquement été interprétés comme résultant du recoupement[8], de la superposition ou de l'évolution de plusieurs générations de bedforms (***Dunlop & Clark, 2006 ; De Angelis & Kleman, 2007 ; Greenwood & Clark, 2009***) (**Figure 1.26A**), reflétant des changements de directions (***Clark et al., 1993 ; Stokes et al., 2006a ; Brown et al., 2011***) (**Figure 1.26B**) et/ou de vitesses d'écoulement de la glace (***Stokes et al., 2006b, 2008***), ou des processus d'érosion progressive des bedforms (***Knight et al., 1999 ; Eyles et al., 2016***).

Problématiques cartographiques liées l'interprétation de l'orientation des bedforms. Puisque les bedforms complexes sont interprétés comme résultant du recoupement de plusieurs générations de bedforms, ces derniers sont rarement cartographiés et représentés avec leurs véritables contours topographiques.

Ces bedforms sont la plupart du temps subdivisés et déconstruits en une superposition de plusieurs bedforms de forme simple, i.e. linéations, ribbed bedforms, bedforms circulaires (***Clark, 1993 ; Dunlop & Clark, 2006 ; Stokes et al., 2006a ; De Angelis & Kleman, 2007 ; Greenwood & Clark, 2009***). Cette subdivision et cette déconstruction des bedforms qui présentent des formes et des orientations complexes, repose sur le fait que – à l'exception des bedforms subcirculaires – les géomorphologues glaciaires ont admis des a-prioris sur l'orientation des bedforms sous-glaciaires, supposément transverse

[8] Au sein d'une calotte glaciaire, lorsqu'un changement de dynamique interne intervient (i.e. migrations de la ligne de partage des glaces ('*ice divide migration*') ou des fleuves de glace ('*ice stream migration*')), de nouvelles populations de bedforms sous-glaciaires peuvent se former en fonction de la réorganisation de la configuration d'écoulement de la glace ('*time-transgressive dynamics*'). En conséquence d'une nouvelle configuration d'écoulement de la glace, les générations de bedforms préexistants peuvent donc (i) ne pas être affectées lorsque la vitesse basale est très faible (e.g. dôme de glace), (ii) être totalement érodées et remplacées par une nouvelle génération lorsque la vitesse basale est élevée (e.g. fleuves de glace), ou (iii) être recoupées et superposées par une nouvelle génération de bedforms.

(i.e. perpendiculaire) ou parallèle à la direction de déplacement de la glace. Alors que l'interprétation des linéations glaciaires comme marqueurs de la direction de déplacement de la glace – puisque supposément parallèles à cette dernière – a été confirmée par la découverte de bedforms parallèles à la direction de déplacement de la glace sous la calotte Antarctique (e.g. ***King et al., 2007***) et sous des lobes fraîchement retirés d'une calotte islandaise (e.g. ***Johnson et al., 2010***) (**Figure 1.15A**), aucune étude n'a jusqu'à présent démontré que des bedforms sous-glaciaires pouvaient avoir des orientations complexes (e.g. obliques) par rapport à la direction de déplacement de la glace. Excluant ainsi la possibilité que les bedforms sous-glaciaires puissent présenter des formes et des orientations complexes, aucune étude approfondie de leurs caractéristiques morphologiques et de leurs genèses n'a donc été effectuée.

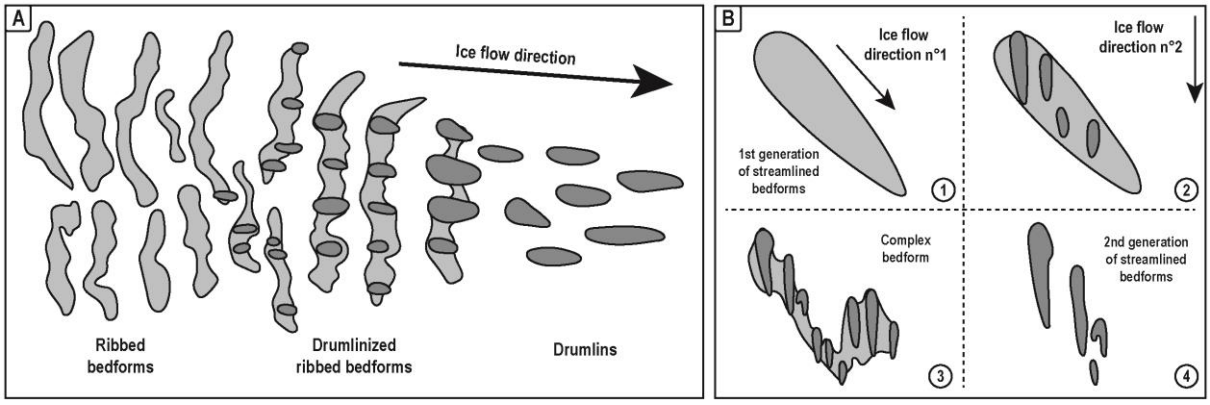

Figure 1.26. *(A) and (B) Hypotheses of formation for bedforms with complex shapes associated with cross-cutting and superimposition of several generations of ribbed bedforms and/or streamlined bedforms (**Clark, 1993; Dunlop & Clark, 2006**).*

2. Bedforms associés à l'écoulement d'eau de fonte sous-glaciaire : exemple des routes de drainage d'eau de fonte

Les routes de drainage d'eau de fonte font partie des environnements sous-glaciaires ayant la plus grande étendue spatiale sous les calottes glaciaires (***Lewington et al., 2020 ; Dewald et al., 2022***). La dynamique de ces routes fluctue au cours du temps car elle est contrôlée par la périodicité de la production et de la circulation de l'eau de fonte (Chapitre I - Partie A §2.2). En fonction des périodes de circulation ou de non circulation d'eau de fonte, les routes de drainage enregistrent une périodicité des phases de découplage et de recouplage entre la glace et le substrat sous-glaciaire favorisant respectivement des processus fluvio-glaciaires (érosion, transport, dépôt de sédiments triés) et glaciogéniques (érosion, déformation des sédiments) (Chapitre I - Partie A §4.3).

L'empreinte morphologique de ces routes de drainage, initialement identifiées par la présence de reliques morphologiques de systèmes de drainage chenalisé (e.g. esker, chenaux, vallées tunnels), de sédiments d'origine fluvio-glaciaire et de hummocks, a été définie sous les termes de « corridor glacio-fluviatile » (‘*glacio-fluvial corridor’*) (***St-Onge, 1984 ; Rampton, 2000 ; Utting et al., 2009***) et de « corridor de hummocks » (‘*hummock corridors’*) (***Peterson & Johnson, 2018***) avant d'être récemment redéfinie comme « corridor d'eau de fonte sous-glaciaire » (‘*subglacial meltwater corridors*’) (***Ojala et al., 2019 ; Lewington et al., 2019, 2020 ; Sharpe et al., 2021***). Ces routes de drainage comportent également de nombreux bedforms dont l'étude morphologique permet de mieux contraindre la dynamique d'écoulement de l'eau de fonte et la nature des processus de remobilisation de sédiments sous-glaciaires associés.

2.1. Hummocks et bedforms associés

Morphométrie et composition. Les hummocks sous-glaciaires associés à la dynamique d'écoulement de l'eau de fonte[9] sont décrits comme des buttes désorganisées et de forme irrégulières, faisant en moyenne 10^{nes}–100^{nes} m de diamètre et 1–10 m d'amplitude mais présentant une forte

[9] Une confusion peut exister entre plusieurs types de morphologies glaciaires de forme subcirculaire / mamelonnée (‘hummocky’ en anglais) : les ‘*hummocky moraines*’ (marginales ou sub-marginales, résultant essentiellement de la fonte de glace « morte » ou stagnante à la périphérie des masses glaciaires), les ‘*hummocky-ribbed bedforms*’ (sous-glaciaires, dont la formation est attribuée à la dynamique d'écoulement de la glace) et les ‘*hummocks*’ (sous-glaciaires, dont la formation est attribuée à la dynamique d'écoulement de l'eau de fonte).

variabilité de formes et de dimensions (**Figure 1.27A**) (***Utting et al., 2009; Peterson & Johnson, 2018; Lewington et al., 2019***). La composition sédimentaire des hummocks est très variable et peut être caractérisée par des sédiments sableux d'origine fluvio-glaciaire, des diamictons sableux ou des sédiments glaciaires antérieurs érodés (***Dahlgren, 2013; McMartin et al., 2015b ; Haiblen, 2017; Peterson & Johnson, 2018; Campbell et al., 2020***).

Distribution spatiale. Les hummocks sous-glaciaires sont regroupés sous la forme de corridors (10^{nes}–100 km de long et 1–5 km de large), subparallèles à la direction de déplacement de la glace. Ces corridors sont la plupart du temps perpendiculaires aux complexes morainiques matérialisant d'anciennes positions de lobes glaciaires durant les phases de déglaciation, formant des motifs radiaux autour des anciens dômes des paléo-calottes glaciaires Laurentides et Scandinaves (**Figure 1.27B**) (***Peterson et al., 2017 ; Lewington et al., 2020 ; Dewald et al., 2022***).

Hypothèses de formation. Les corridors de hummocks sont interprétés comme des reliques de routes de drainage d'eau de fonte sous-glaciaire (**Figures 1.18-1.19**). La formation de ces hummocks a été variablement associée à (i) des processus de dépôt de matériel fluvio-glaciaire au sein de cavités durant des périodes de forte décharge d'eau de fonte (***Utting et al., 2009***), (ii) d'écoulements sédimentaires hyper-concentrés au sein de cavités permettant le dépôt de diamictons sableux ultérieurement érodés par des circulations d'eau de fonte (***Haiblen, 2017 ; DesRosiers, 2021***), ou (iii)

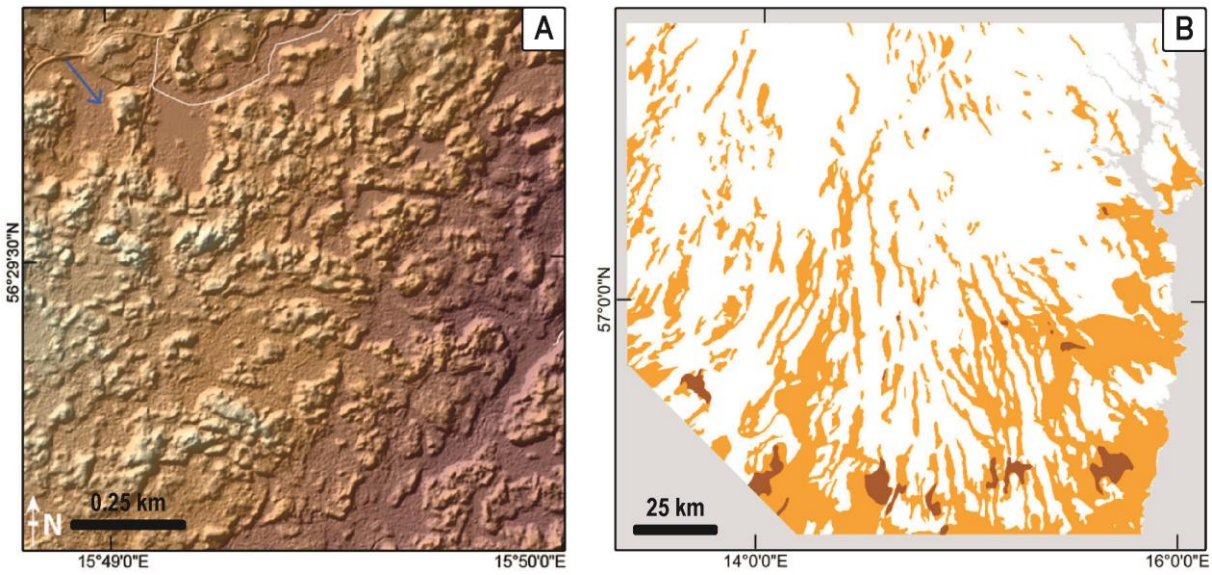

Figure 1.27. *(A). Disorganized irregular hills, referred to as hummocks. (B) Spatial distribution of hummock corridors (in orange) highlighting a radial pattern parallel to the ice flow direction of the south Sweden lobate termination of Fennoscandian Ice Sheet. Fields of ribbed bedforms (in brown) are also reported to be associated with hummock corridors (**Peterson et al., 2017**).*

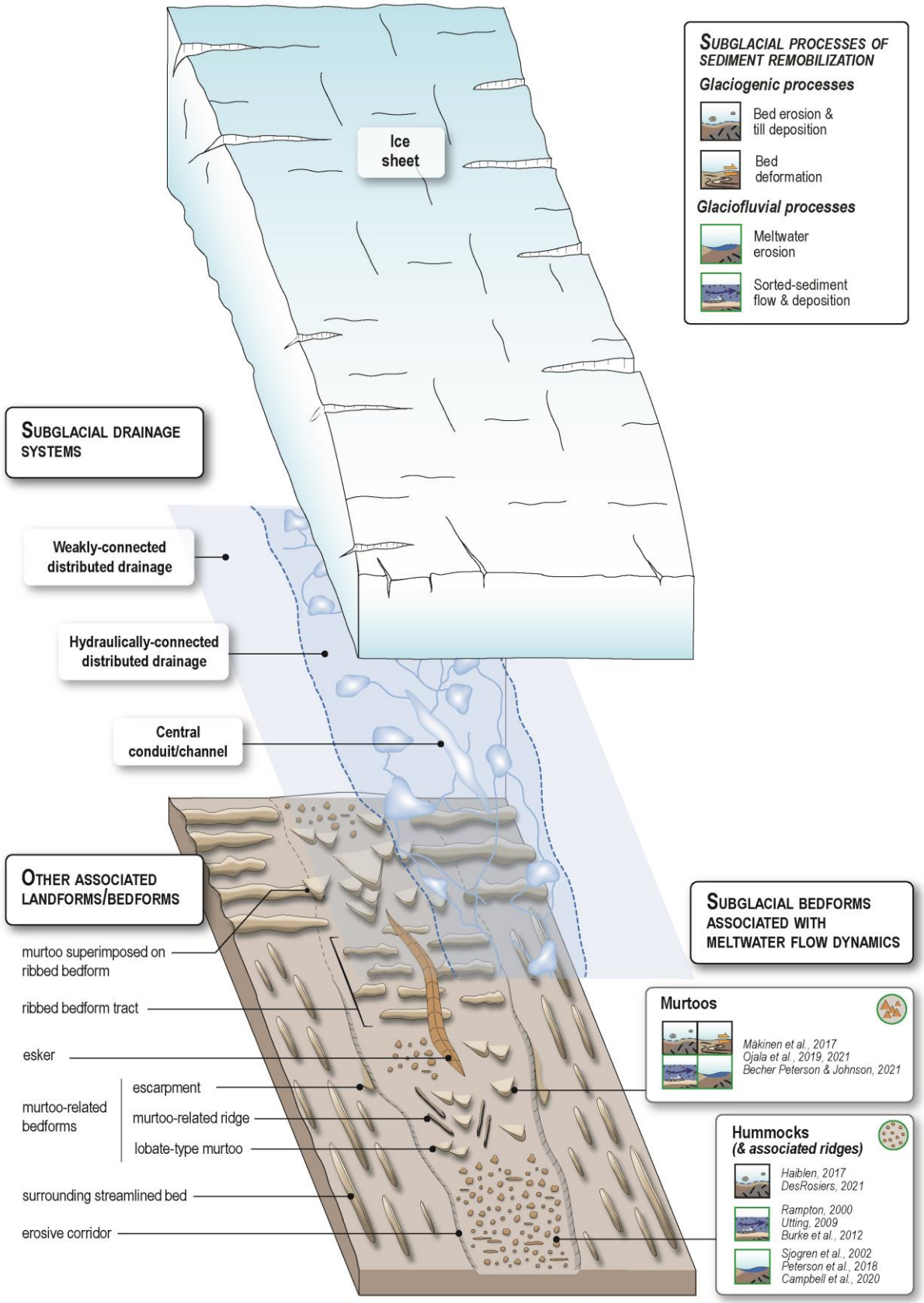

***Figure 1.28**. Assemblage of subglacial bedforms – murtoos, hummocks and associated bedforms – associated with the dynamics of meltwater flow in a typical context of subglacial meltwater route. Note that there is currently no distinction between hummocks and ridges formed by erosion or deposition, and no genetic relationship between murtoos and murtoo-related bedforms.*

d'érosion différentielle de lits sédimentaires formant, sous l'action de la circulation d'eau de fonte, des buttes résiduelles dont le sommet coïncide souvent avec la surface du lit sédimentaire environnant (***Sjogren et al., 2002 ; Peterson et al., 2018 ; Campbell et al., 2020***) (**Figure 1.28**).

Bedforms associés. Au sein des champs de hummocks, des rides sédimentaires transverses (i.e. ~80-90°) et obliques (i.e. < 80°) à la direction de déplacement de la glace sont également observées (***St-Onge, 1984; Utting et al., 2009; Burke et al., 2012; McMartin et al., 2015a,b; Sharpe et al., 2017; Peterson et al., 2018; Campbell et al., 2020***). Comme les hummocks, ces rides sédimentaires font en moyenne moins de 100 m de long et moins de 10 m d'amplitude et sont composées de tills sous-glaciaires ou de sédiments triés (essentiellement des graviers) (***Rampton, 2000; Burke et al., 2012***).

2.2. Murtoos et bedforms associés

Terminologie. Les murtoos ont été découverts en 2017 par des groupes de géologues suédois et finlandais grâce à l'acquisition de données Lidar Laser à très haute résolution (2 m). Ces bedforms de forme triangulaire ou en V pointant dans la direction de déplacement de la glace ont initialement été décrits comme des '*V-shaped hummocks'* en raison de leur découverte au sein de couloirs de hummocks (***Peterson et al., 2017***) – et comme des '*triangular-shaped landforms*' (***Mäkinen et al., 2017***). La première étude de caractérisation morphométrique de ces bedforms triangulaires est réalisée par ***Ojala et al. (2019)***. En raison de la description d'exemples typiques au niveau de la localité finlandaise de 'Murtoo', ces bedforms triangulaires sont alors nommés 'murtoos', nom qui sera majoritairement retenu dans les études ultérieures et au sein de ce manuscrit.

Morphométrie et composition. Les murtoos sont des bedforms triangulaires, ayant un axe de symétrie longitudinal parallèle à la direction de déplacement de la glace (**Figure 1.29A**). Les murtoos ont de petites dimensions – expliquant leur découverte tardive via l'analyse de MNT de très haute résolution – faisant en moyenne 40–100 m de long et de large et moins de 5 m d'amplitude. Le profil d'altitude de l'axe longitudinal des murtoos est caractérisé par une forte asymétrie avec un flanc amont long et peu pentu (4–5°) et un flanc aval court et très pentu (11°) (***Ojala et al., 2019***). Les murtoos sont composés de tills sous-glaciaires, présentant une fissilité fréquente, et d'intercalations de sédiments triés silto-sableux, présentant des traces de déformation principalement ductile et des évidences de liquéfaction (***Peterson Becher & Johnson, 2021; Ojala et al., 2021***).

Distribution spatiale. Des études cartographiques des paléo-lits glaciaires de la calotte Fennoscandinave ont montré que les murtoos sont regroupés en champs ou en corridors allongés parallèlement à la direction de déplacement de la glace ***(Peterson et al., 2017)***. Les champs de murtoos sont fréquemment associés spatialement aux corridors de hummocks, à des reliques de systèmes de drainage chenalisé (esker, chenaux) et à des ceintures morainiques marquant la position d'anciennes zones marginales de la calotte Fennoscandinave durant la période de déglaciation (**Figure 1.29B**) (***Ahokangas et al., 2021).*** Ces associations spatiales suggèrent que les murtoos sont associés à des routes de drainages d'eau de fonte, drainant d'importants débits notamment durant les périodes de retrait des calottes glaciaires (**Figures 1.18, 1.19**) *(**Peterson & Johnson, 2018; Ojala et al., 2019**).*

Formation. D'après leur géométrie, leur composition et leur association spatiale avec des témoins morphologiques de la circulation d'eau de fonte sous-glaciaire, les murtoos ont été interprétés comme résultant de la combinaison de processus (i) d'érosion et de dépôt par l'eau de fonte au cours de périodes de forts débits d'eau de fonte transitant le long de l'interface sous-glaciaire, (ii) de dépôt de tills sous-glaciaires et (iii) de déformation des sédiments saturés en eau par l'écoulement de la glace lors des périodes de recouplage (**Figure 1.28**) *(**Mäkinen et al., 2017; Ojala et al., 2019; Peterson Becher & Johnson, 2021; Ahokangas et al., 2021**).* La périodicité temporelle de ces épisodes de décharge d'eau de fonte est responsable de crues sous-glaciaires ('*subglacial floods*') dépassant la capacité de drainage des systèmes chenalisés ou des systèmes distribués hydrauliquement connectés (Chapitre I – Partie A §2.2.3), notamment le long des routes de drainage d'eau de fonte *(e.g., **Lewington et al., 2020; Mejía et al., 2021; Nanni et al., 2021**).* L'observation de champs de murtoos le long d'anciennes routes de drainage d'eau de fonte est ainsi interprétée comme le témoin morphologique de processus de remobilisation au sein de systèmes de drainage alternativement chenalisés ou distribués en fonction des débits de circulation d'eau de fonte basale *(**Mäkinen et al., 2017; Ojala et al., 2019, 2021; Peterson Becher & Johnson, 2021**).*

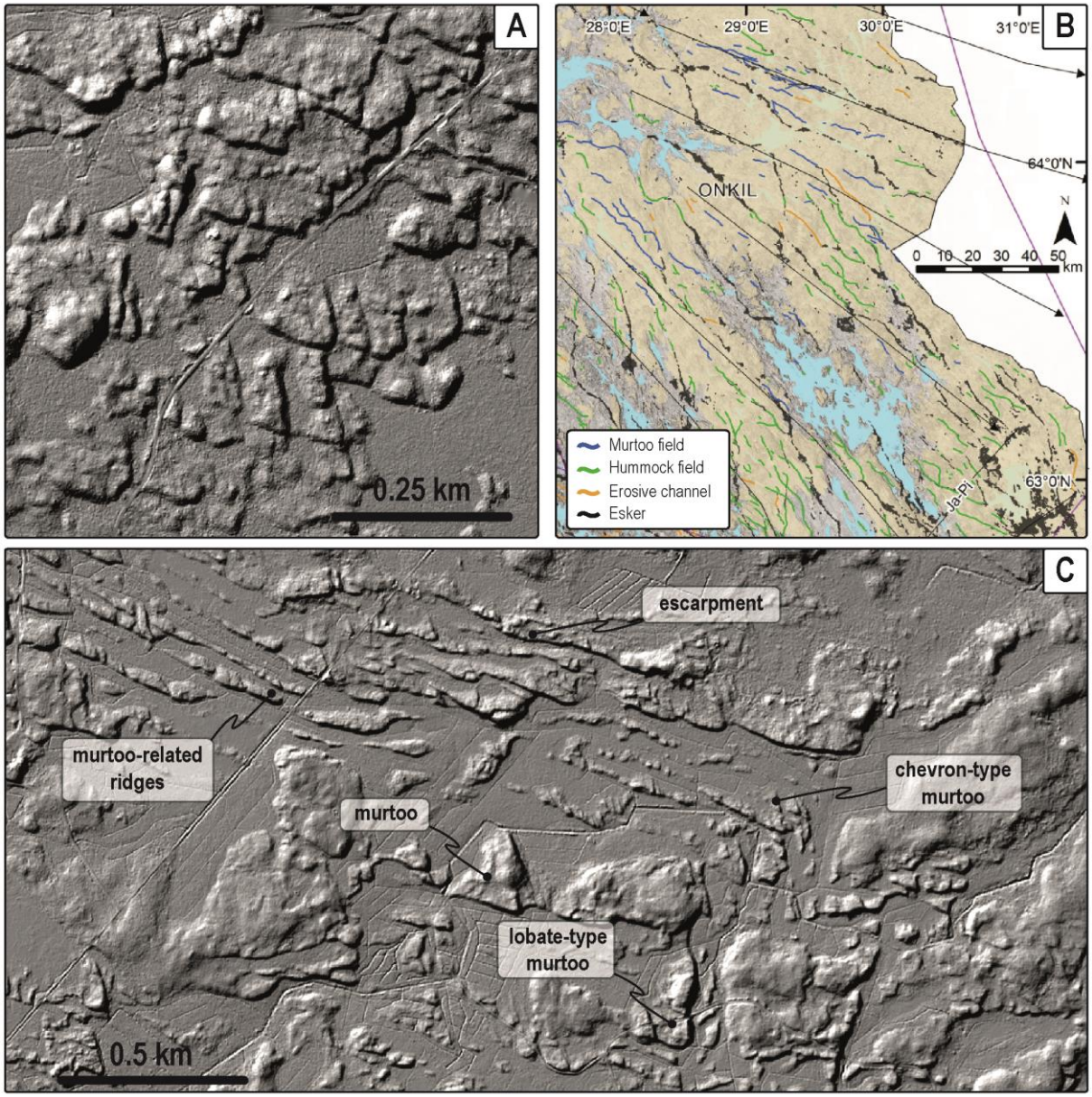

Figure 1.29. *(A) Triangular bedforms pointing toward the ice flow direction, referred to as murtoos (south Sweden – 56°54N, 15°24'E). (B) Spatial relationship between murtoo fields, hummock fields and morphological relics of channelized drainage system, suggesting that murtoos and hummocks form when subglacial meltwater routes are active (**Ahokangas et al., 2021**). (C) Examples of murtoo-related bedforms – such as lobate-type and chevron-type murtoos, murtoo-related ridges and escarpments – spatially associated with murtoos and sharing some of their morphological characteristics (central Finland - 63°23'N, 24°50'E).*

Bedforms associés. Les murtoos sont communément associés à des bedforms partageant partiellement leurs caractéristiques morphologiques et les mêmes compositions sédimentaires ('*murtoo-related bedforms*') (**Figure 1.29C**) (***Ojala et al., 2019, 2021, 2022 ; Ahokangas et al., 2021***). Certains bedforms, localisés au sein même des champs de murtoos, possèdent une forme lobée, de chevron ou sub-triangulaire, pointant dans la direction de déplacement de la glace et avec un profil longitudinal asymétrique caractéristique des murtoos. Ces bedforms associés aux murtoos – faisant en moyenne 75–200 m de long et de large et moins de 5 m d'amplitude – sont respectivement désignés comme des

'*lobate-type murtoos'*, '*chevron-type murtoos'* et '*polymorphous murtoo-related bedforms*' (***Ojala et al., 2021***). D'autres bedforms associés aux murtoos correspondent à des rides ('*murtoo-related ridges'*) et des escarpements ('*escarpments*') faisant 0.1–2 km de long, 10–150m de large et moins de 10 m d'amplitude. Ces rides et escarpements possèdent un profil longitudinal asymétrique et des orientations variables par rapport à la direction d'écoulement de l'eau de fonte. Alors que les rides apparaissent la plupart du temps au sein des champs de murtoos et des corridors d'eau de fonte sous-glaciaire, les escarpements sont quant à eux fréquemment localisés le long des bordures de ces champs et corridors (***Ojala et al., 2022***).

2.3. Autres bedforms et landforms associés

Bien que l'association des hummocks et murtoos avec un modèle de formation dominés par des processus glacio-fluviatiles soit en partie basée sur l'identification de sédiments triés dans leurs structures internes, elle est aussi intimement liée à leur relation spatiale avec des reliques morphologiques de systèmes de drainage chenalisé tels que :

- des couloirs érosifs larges d'un à quelques km incisés dans le lit sédimentaire sous-glaciaire (souvent recouvert de linéations en périphérie) dont les dimensions sont comparables à celles de vallées tunnels (e.g. ***Rampton, 2000; Campbell et al., 2020; Sharpe et al., 2021***). La base de ces corridors peut être dépourvue de bedforms, mais des hummocks y ont souvent été observés (***Utting et al., 2009 ; Peterson et al., 2018 ; Lewington et al., 2020***) (**Figure 1.30A**).

- des petits chenaux larges de quelques dizaines de mètres au maximum faisant moins de 10 m de profondeur sont fréquemment observés le long des flancs des murtoos, suggérant que leurs formes soient en partie façonnées par l'incision du substrat produite par l'activité de ces chenaux (***Mäkinen et al., 2017 ; Ojala et al., 2019***).

- des eskers observés au sein même des corridors de hummocks et de murtoos, ou dans des positions intermédiaires faisant la jonction entre plusieurs corridors (e.g., ***Sharpe et al., 2017; Peterson & Johnson, 2018 ; Lewington et al., 2020; Ahokangas et al., 2021***). Les eskers sont souvent observés en superposition sur les bedforms associés aux corridors d'eau de fonte, témoignant d'une mise en place tardive (***Lewington et al., 2020***).

Dans la littérature glaciaire, les ribbed bedforms sont essentiellement associés à la dynamique d'écoulement de la glace mais quelques exemples indiquent une possible relation avec la dynamique d'écoulement d'eau de fonte. Premièrement, certains murtoos ont été identifiés comme étant en superposition sur ou recoupant des ribbed bedforms (***Remmert & Kristiansson, 2018 ; Ojala et al., 2019 ; Ahokangas et al., 2021***) (**Figure 1.30B**). Deuxièmement, certains champs de ribbed bedforms prenant la forme de couloirs larges de 1–10 km, parallèles à la direction de déplacement de la glace et coïncidant avec la position d'eskers ('*ribbed bedform tracts*') (***Aylsworth & Shilts, 1989; Dunlop & Clark, 2006; Wagner, 2014; Trommelen et al., 2014***) ont été interprétés comme étant une empreinte morphologique d'anciens corridors d'eau de fonte sous-glaciaire (***Peterson et al., 2017 ; Lewington, 2020***) (**Figure 1.27B**).

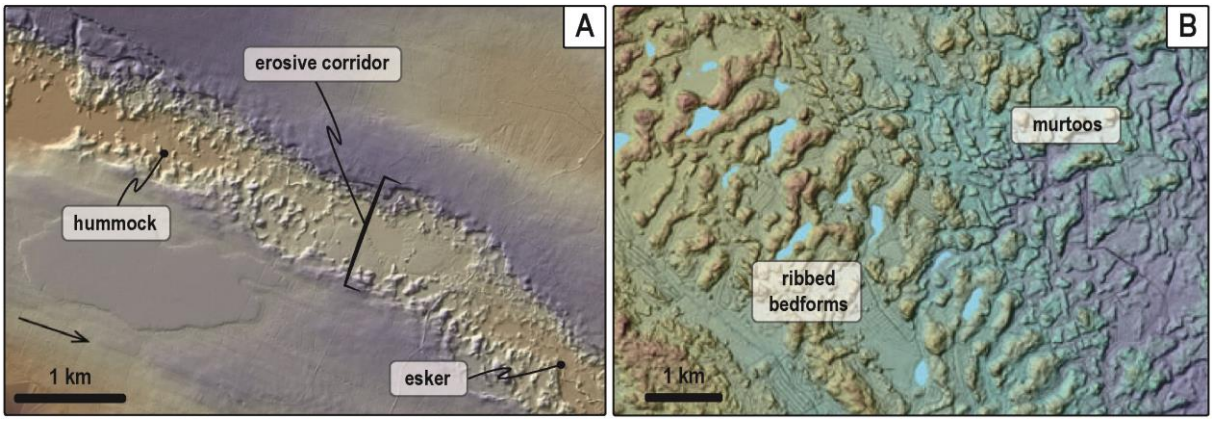

Figure 1.30. *(A) Hummock corridor incised in a streamlined till surface. Note the central position of an esker deposited on the bottom of the corridor (south Sweden Upland – 56°57'N, 14°7'E) (**Peterson & Johnson, 2018**). (B) Spatial association between ribbed bedforms and murtoos in central Finland (63°7'N, 25°E). Note the cross-cutting relationship suggesting murtoos developed later than ribbed bedforms (**Ojala et al., 2019**).*

3. Une continuité morphologique et génétique entre les bedforms sous-glaciaires ?

Bien que la géomorphologie glaciaire s'intéresse depuis près d'un siècle aux bedforms sous-glaciaires, la distribution spatiale et les processus de formation et d'évolution de ces bedforms sous-glaciaires demeurent mal contraints (**Figures 1.18, 1.19, 1.28**), notamment en raison de l'accès très récent à des données cartographiques de très haute résolution. Ces lacunes limitent la compréhension des relations entre la diversité morphologique des bedforms sous-glaciaires, la diversité des processus impliqués dans leur formation et les dynamiques d'écoulement de la glace et de l'eau de fonte. Certaines études ont tenté de proposer l'existence d'une continuité morphologique associée ou non à une continuité de processus afin d'expliquer la diversité des bedforms sous-glaciaires. Le résultat de ces études et les hypothèses qui en découlent sont synthétisés dans les paragraphes suivants.

3.1. Hypothèses d'un continuum de bedforms sous-glaciaires associés à la dynamique d'écoulement de la glace

Afin de comprendre les caractéristiques et l'évolution des bedforms sous-glaciaires de façon globale, en s'affranchissant des classifications classiques décrites dans le Chapitre I – Partie B §1, l'hypothèse d'un continuum morphologique dépendant de la dynamique d'écoulement de la glace a émergé de l'observation d'une continuité spatiale – d'amont en aval – entre des ribbed bedforms, des bedforms circulaires et des linéations (***Aario, 1977 ; Markgren & Lassila, 1980***). Cette hypothèse préliminaire, suggérant que les caractéristiques morphologiques, les distributions spatiales et la formation/évolution des différents types bedforms soient continues et non séparées par des frontières strictes, a débouché sur de nombreuses autres études considérant la potentielle continuité morphologique et génétique des bedforms sous-glaciaires (***Aario, 1977 ; Stokes et al., 2013 ; Ely et al., 2016 ; Sookhan et al., 2021***).

3.1.1. Un continuum morphologique entre les ribbed bedforms, les bedforms circulaires et les linéations

De nombreuses études ont mis en évidence l'existence de séquences spatiales d'évolution morphologique continue le long d'anciennes trajectoires de déplacement de la glace (i) entre des

linéations glaciaires de plus en plus allongées (i.e. drumlins à MSGLs) (***Rose, 1987 ; Ó Cofaigh et al., 2002; Greenwood & Clark, 2010 ; Stokes et al., 2013a ; Sookhan et al., 2021, 2022***), (ii) entre des ribbed bedforms et des bedforms circulaires (***Hattestrand, 1997 ; Dunlop & Clark, 2006 ; Greenwood & Clark, 2008***) et (iii) entre des ribbed bedforms et des drumlins (***Carl, 1978 ; Markgren & Lassila, 1980 ; Aylsworth & Shilts, 1989; Dyke et al., 1992; Knight et al., 1999 ; Sommerkorn, 2020***).

Afin de quantifier et de valider l'existence d'un continuum morphologique entre les ribbed bedforms, les bedforms circulaires et les linéations glaciaires, ***Ely et al. (2016)*** ont analysé la distribution des caractéristiques morphométriques (i.e. longueur, largeur et ratio d'élongation[10]) de près de 97 000 bedforms cartographiés en Scandinavie, Grande-Bretagne, Islande et au Canada. Ces auteurs ont notamment mis en évidence les points suivants (**Figure 1.31**) :

- Les caractéristiques morphométriques des drumlins et des MSGLs possèdent un taux de recouvrement de l'ordre de 75%, matérialisé par l'existence d'une même largeur moyenne, de l'ordre de 200 m, et le fort recouvrement entre la longueur maximale des drumlins et la longueur minimale des MSGLs ; à contrario les flutes sont des linéations et des bedforms morphologiquement distincts puisque qu'aucun recouvrement n'est observé avec les autres linéations.

- Les multiples sous-catégories de ribbed bedforms (i.e. '*ribbed moraines'* (***Hattestrand, 1997***), '*rogen moraines'* (***Shaw, 1979***), '*mega-ri*bs' (***Greenwood & Kleman, 2010***), '*traction ribs'* (***Stokes et al., 2016***)) – ne forment en réalité qu'un groupe continu de ribbed bedforms, dont la longueur moyenne est 3 fois plus grande que sa largeur moyenne.

- Bien que les bedforms circulaires aient des longueurs et largeurs globalement intermédiaires entre celles des ribbed bedforms et des linéations, l'analyse de la distribution de leurs caractéristiques morphométriques montre un recouvrement partiel avec celles des ribbed bedforms et des drumlins.

L'étude ***d'Ely et al. (2016)*** tend à démontrer qu'une catégorisation des bedforms sous-glaciaires associés à la dynamique d'écoulement de la glace basée sur des critères morphologiques est inutile,

[10] ***Ely et al. (2016)*** ont défini que le ratio d'élongation (dans la direction de déplacement de la glace) d'un bedform est défini comme le rapport entre l'axe 'a', mesuré parallèlement à la direction de déplacement, et l'axe 'b', mesuré perpendiculairement à la direction de déplacement. Considérant a-priori que les linéations sont parallèles et les ribbed bedforms perpendiculaires à la direction de déplacement de la glace, la longueur et la largeur des linéations correspondent respectivement à leurs axes 'a' et 'b', et, la longueur et la largeur des ribbed bedforms correspondent respectivement à leurs 'b' et 'a'. Le ratio d'élongation des linéations est donc compris entre 1 et + ∞ alors que celui des ribbed bedforms est compris entre 0 et 1.

puisque la distribution des caractéristiques morphométriques des bedforms suggère l'existence d'un continuum morphologique (**Figure 1.31**).

Cependant, bien qu'un continuum morphologique soit possible entre les ribbed bedforms, les bedforms circulaires, les drumlins et les MSGLs, une grande variété de bedforms sous-glaciaires de forme complexe et associés à ces bedforms communs n'est actuellement pas prise en compte dans ce continuum (Chapitre I - Partie B §1.1.4). De plus, puisque certains types de ribbed bedforms (i.e. '*traction ribs*') sont parfois obliques à la direction de déplacement de la glace, la méthode de mesure du ratio d'élongation proposée par ***Ely et al. (2016)*** n'est pas toujours adéquate. Enfin, les bedforms circulaires sont morphométriquement intermédiaires entre des ribbed bedforms et des drumlins, mais leur position dans ce continuum morphologique reste à définir.

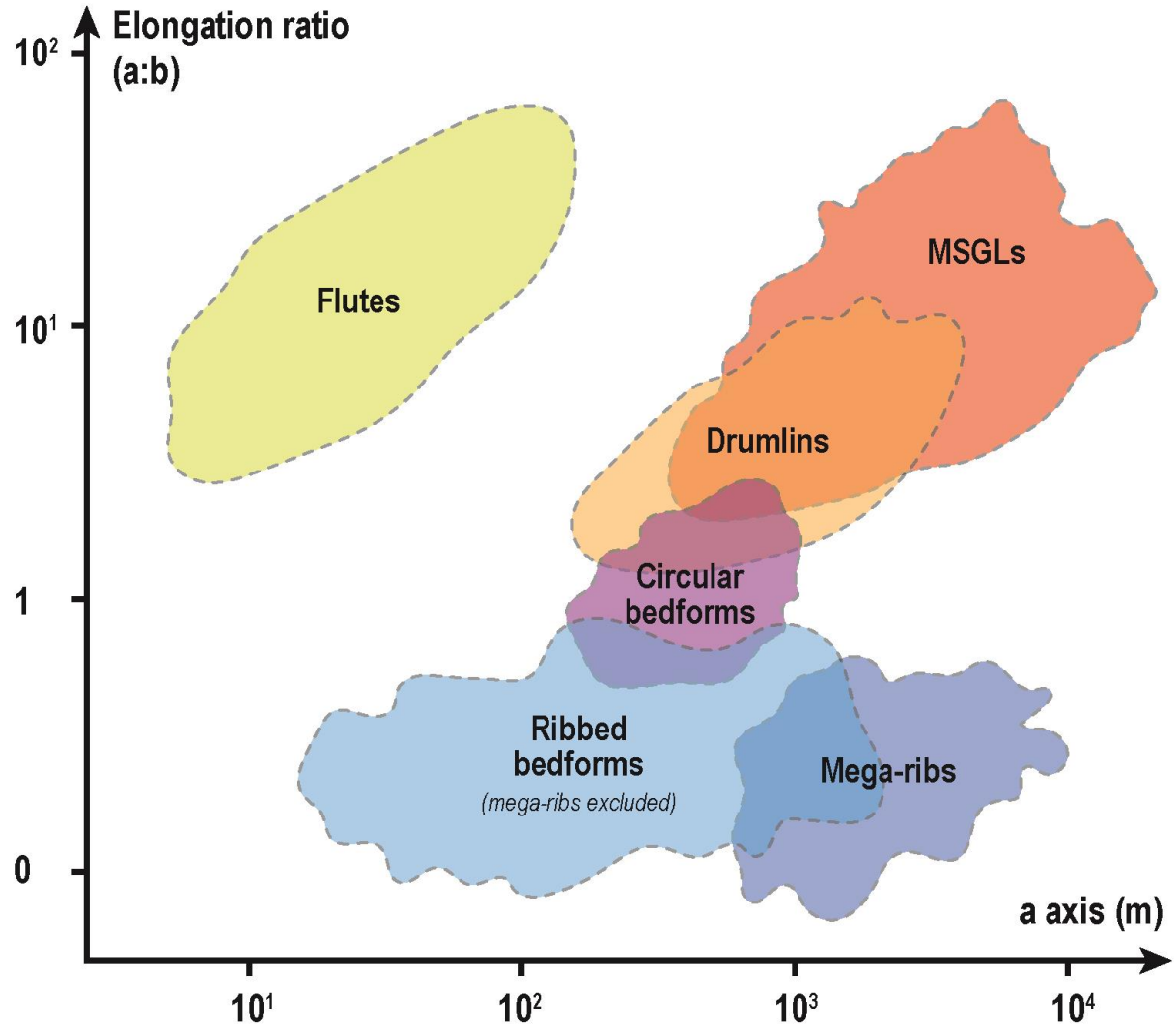

Figure 1.31. *Statistic distribution of a-axis (i.e. axis measured parallel to the ice flow direction) and elongation ratio of subglacial bedforms associated with ice flow dynamics (modified after* ***Ely et al., 2016****). Except flutes that correspond to a separate morphometric entity, all subglacial bedform categories overlap each over suggesting a morphometric continuum.*

3.1.2. Vers un modèle d'évolution contrôlé par la dynamique d'écoulement de la glace

- **Hypothèses de contrôle de l'évolution morphologique des bedforms**

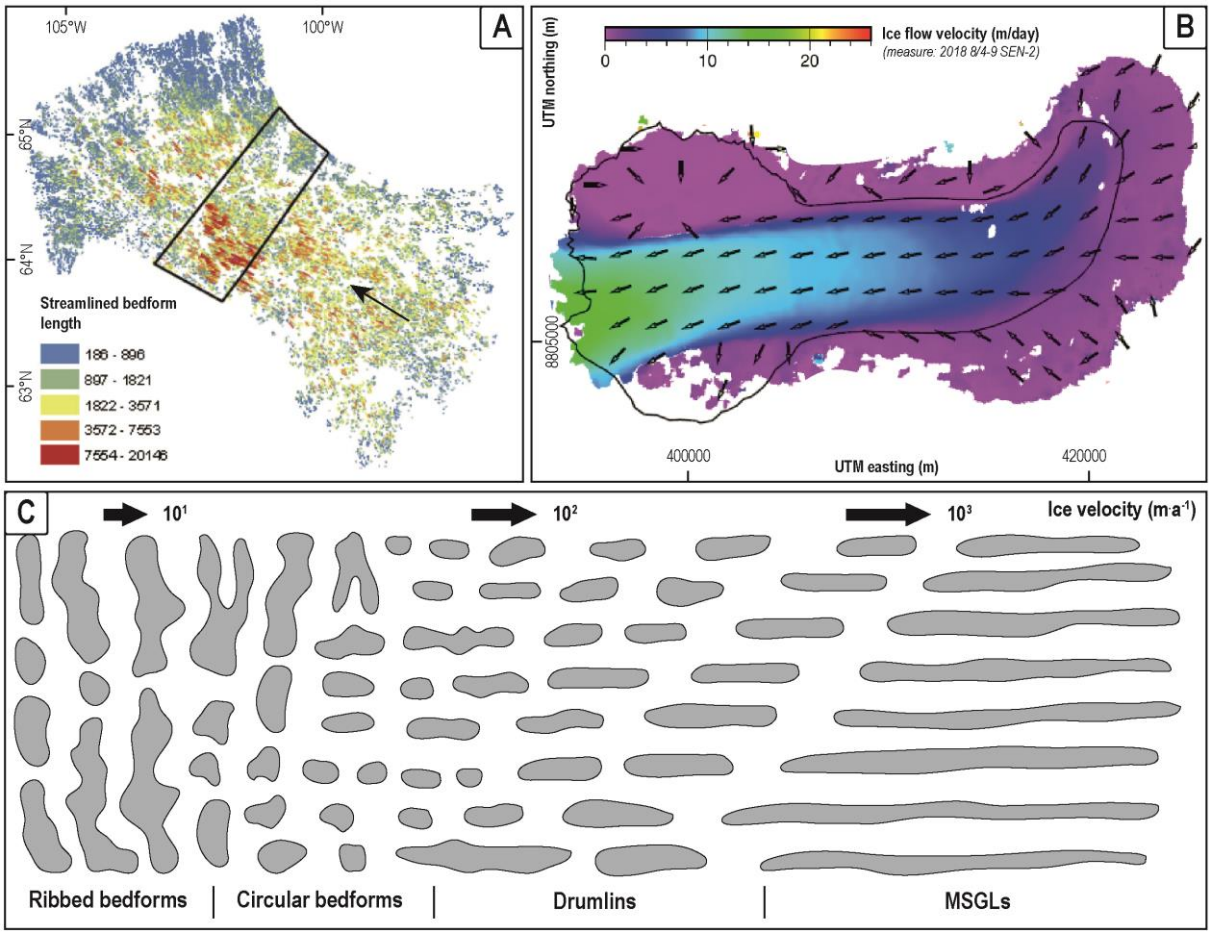

***Figure 1.32**. (A) Spatial evolution of streamlined bedform length in palaeo-Dubawnt Lake ice stream (Canada) (**Stokes et al., 2013**), mimicking (B) ice flow velocity patterns (i.e. lateral and longitudinal velocity gradients) of an modern ice stream on Vavilov Ice Cap (Russia) (**Zheng et al., 2019**). Those correlation have supported (C) a model of genetic continuum between ribbed, circular and streamlined bedforms depending on ice flow direction and velocity (**Stokes et al., 2013a**).*

Alors (i) qu'un continuum morphométrique a été mis en évidence entre les ribbed bedforms, les bedforms circulaires, les drumlins et les MSGLs et (ii) que les flutes possèdent un modèle de formation unanimement considéré comme à part, aucun consensus n'existe sur les modèles de formation et d'évolution des bedforms sous-glaciaires. Puisque de nombreuses séquences d'évolution de bedforms ont été observées le long d'anciens fleuves de glace mimant les gradients de vitesse observés au sein des fleuves de glace actuels (***Patterson, 1997; Sergienko & Hindmarsh, 2013; Zheng et al., 2019***) (**Figure 1.32A-B**), le continuum morphologique entre les ribbed bedforms et les linéations glaciaires a été interprété comme dépendant de la direction et de la vitesse d'écoulement de la glace (**Figure 1.32C**) (***Hart, 1999; Hättestrand & Kleman, 1999; Stokes & Clark, 2002a ; Briner, 2007; King et al., 2007;***

Stokes et al., 2013 ; Hillier et al., 2016 ; Hermanowski et al., 2019 ; Van Landeghem & Chiverrell, 2020 ; Sookhan et al., 2021, 2022). D'autres paramètres tels que les caractéristiques lithologiques des sédiments sous-glaciaires (***Aylsworth & Shilts, 1989; Wellner et al., 2001 ; Ó Cofaigh et al., 2002 ; Rattas & Piotrowski, 2003 ; Greenwood & Clark, 2010 ; McKenzie et al., 2022***), l'épaisseur du lit sédimentaire (***Kerr & Eyles, 2007 ; Barchyn et al., 2016***), la topographie du substrat (***Bouchard, 1989; Franke et al., 2020***), la durée d'activité de l'écoulement de la glace (***Boyce & Eyles, 1991 ; Zoet et al., 2021***) et la pression d'eau de fonte basale (***Shaw, 2002 ; Lewington et al., 2020***) ont également été proposés pour expliquer l'évolution des bedforms sous-glaciaires.

Bien qu'un certain consensus existe quant au fait que ces bedforms soient principalement associés à la dynamique de la glace et formés via des processus de remobilisation de sédiments essentiellement d'origine glaciogénique (e.g. ***Boutlon, 1987 ; Boyce & Eyles, 1991 ; Tulaczyk et al., 2001 ; Linden et al., 2008***), l'existence d'un unique modèle de formation et d'évolution des bedforms (i.e. continuum génétique) dépendant d'un ou plusieurs facteurs de contrôle glaciologique reste cependant largement débattue.

- **Notion d'équifinalité et d'équicausalité**

Le développement de modèles tentant d'unifier l'intégralité des bedforms associés à la dynamique d'écoulement de la glace doit tenir compte de la forte variabilité des caractéristiques des bedforms sous-glaciaires, notamment en termes de :

- morphométrie, bien qu'un continuum morphométrique existe entre les linéations, les ribbed bedforms et les bedforms circulaires (excluant d'autres bedforms morphologiquement plus complexes)
- composition interne, expliquant notamment les variabilités lithologiques (i.e. till sous-glaciaire et/ou substrat sédimentaire et/ou sédiments sableux/graveleux) et structurales (i.e. absence ou présence de déformation) au sein d'une même catégorie de bedforms
- distribution spatiale, impliquant des dynamiques d'écoulement de la glace distinctes.

Face à cette diversité de caractéristiques entre et au sein même des catégories de bedforms, deux concepts s'opposent à l'idée de concilier la diversité morphologique à la diversité des formation des bedforms sous-glaciaires : l'équifinalité et l'équicausalité (***Clark, 2010 ; Fowler, 2018 ; Möller & Dowling, 2018***).

L'équifinalité implique que de multiples processus peuvent être responsable de bedforms morphologiquement identiques, impliquant que chaque catégorie et sous-catégorie de bedforms sous-glaciaires peut être associée à une variété de processus de formation. Le principe d'équifinalité repose essentiellement sur la forte variabilité de compositions internes (i.e. lithologies et structures) observées au sein de bedforms possédant des caractéristiques morphologiques identiques (**Figure 1.33**) (***Möller & Dowling, 2018 ; Schomacker et al., 2018***). Par exemple, quatre modèles de formation ont été proposés pour expliquer la genèse de ribbed bedforms en Scandinavie : (i) la fracturation d'un lit sous-glaciaire gelé au niveau de zone d'extension dans l'écoulement de la glace (***Hattestrand & Kleman, 1999 ; Sarala, 2006***), (ii) le dépôt de till au sein de cavités marginales par fonte basale de glace stagnante (Åsnen-type ; ***Möller, 2010***), (iii) le remodelage et la déformation de bedforms préexistants (Rogen-type ; ***Möller, 2006***), (iv) la déformation de sédiments sous-glaciaires suivie du dépôt de sédiments triés par l'eau au sein de la cavité aval (Niemisel moraine ; ***Linden et al., 2008***).

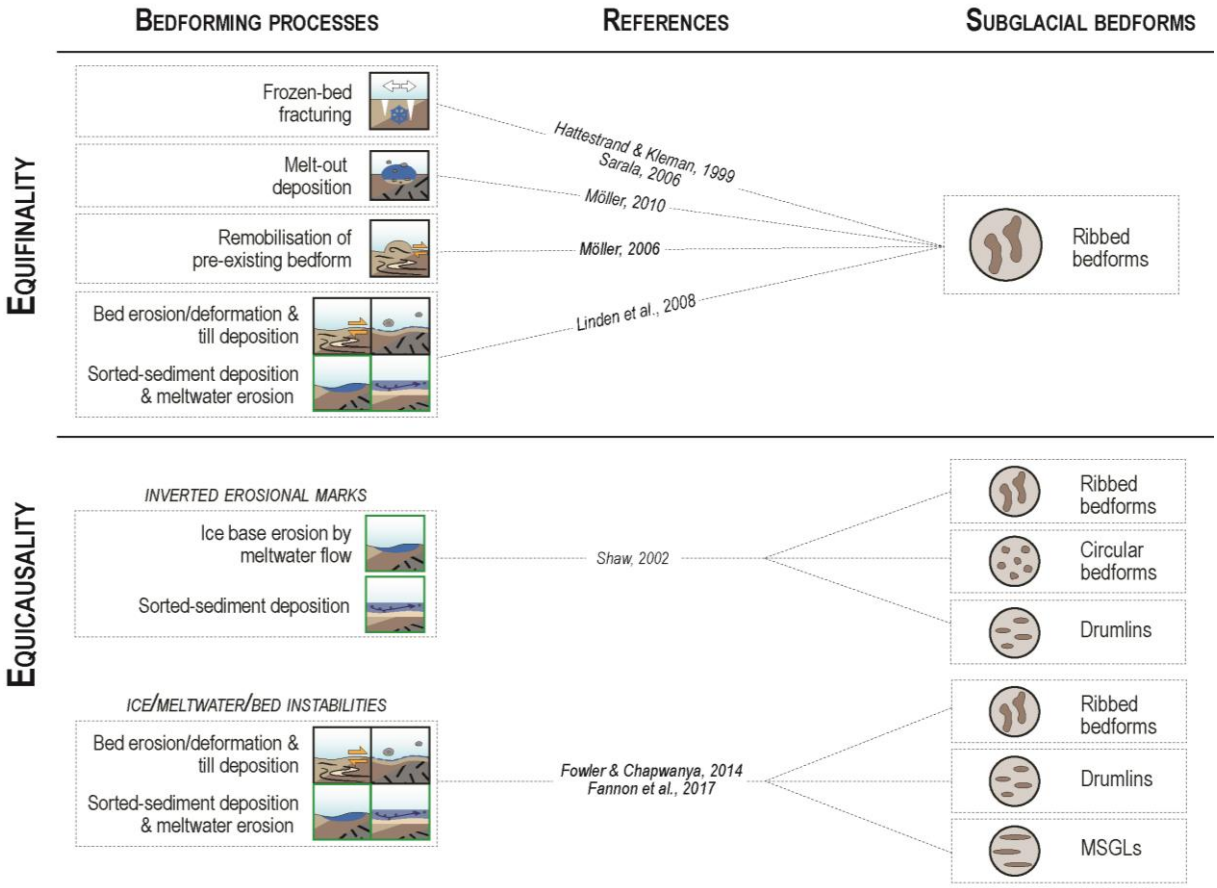

Figure 1.33*. Schematic illustration of the two philosophical schools regarding subglacial bedform formation. Equifinality suggests that distinct processes or combination of processes can result in bedforms with identical morphological characteristics but different internal composition (resulting from different processes of sediment remobilization). On the opposite, equicausality suggests a single process or a combination of processes can result in a variety of bedforms with different morphological characteristics.*

De l'autre côté, l'équicausalité propose qu'un unique assemblage de processus puisse être responsable de la formation des différents types de bedforms sous-glaciaires (e.g. ribbed bedforms, drumlins, MSGLs) dans leur diversité de forme, de distribution spatiale et de composition (**Figure 1.33**). Deux hypothèses d'équicausalité ont été proposées.

Le premier modèle suggère que des crues sous-glaciaires massives érodent la base de la glace et forment des cavités remplies par les sédiments d'origine fluvio-glaciaires érodés et transportés par l'eau de fonte, dont résulteraient les ribbed bedforms, les bedforms circulaires et les drumlins (***Shaw and Sharpe, 1987; Shaw et al., 1989; Fisher & Taylor, 2002***). Les principales faiblesses de cette hypothèse sont (i) la source supposée d'une telle quantité d'eau de fonte pour expliquer la formation de marques d'érosion de plus de 10m de hauteur et la présence homogène de bedforms sous-glaciaires le long des lits de paléo-fleuves de glace, et (ii) la démonstration de la relation entre ces bedforms et la dynamique d'écoulement de la glace sous les édifices glaciaires actuels (***Fowler, 2018***).

Le second modèle d'équicausalité, bien plus largement admis que le précédent dans la communauté des géomorphologues glaciaires, considère que les bedforms sous-glaciaires sont des bombements sédimentaires périodiques émergeant spontanément d'instabilités de l'écoulement de la glace et de l'eau de fonte sur un lit sédimentaire. Ce modèle est originellement basé sur l'interprétation que la formation de bedforms peut résulter de la déformation d'un till sous-glaciaire en réponse à l'écoulement de la glace sur un lit sédimentaire présentant des hétérogénéités spatiales de pression d'eau interstitielle, de régime thermique ou de lithologie (***Smalley & Unwin, 1968 ; Shaw, 1979 ; Bouchard, 1989 ; Kamb, 1991 ; Tulaczyk et al., 2000b ; Linden et al., 2008 ; Stokes et al., 2008***). Ce modèle, directement dépendant de la rhéologie d'un till sous-glaciaire en fonction des conditions glaciodynamiques et hydrologiques basales, a été conceptualisé mathématiquement avec la formation d'instabilités naturelles résultant du couplage entre un till viscoplastique érodable et déformable, l'écoulement de glace et l'écoulement d'eau (***Hindmarsh, 1998a,b ; Fowler, 2000 ; Schoof, 2007 ; Clark, 2010 ; Chapwanya et al., 2011 ; Stokes et al., 2013b***). Des modèles numériques ont ensuite permis de démontrer que les ribbed bedforms, les drumlins et les MSGLs forment une séquence d'évolution morphologique résultant de l'évolution d'instabilités dans un système glace / eau de fonte / sédiments dépendantes du temps ou des conditions basales, formant ainsi un continuum génétique (***Fowler & Chapwanya, 2014 ; Fannon et al., 2017***).

3.2. Vers une continuité morphologique et génétique pour les bedforms sous-glaciaires associés à la dynamique d'écoulement de l'eau de fonte ?

En raison de leurs faibles dimensions (< 100 m de large ; < 5-10 m d'amplitude), les bedforms sous-glaciaires associés à la dynamique d'écoulement de l'eau de fonte – murtoos, hummocks et bedforms associés – n'ont été découverts que tardivement (i.e. fin des années 2000) comparativement aux bedforms sous-glaciaires associés à la dynamique d'écoulement de la glace. En conséquence, seules quelques études ont permis de décrire les caractéristiques morphologiques de ces bedforms (***Ojala et al., 2019, 2021***) et aucune étude n'a actuellement mis en évidence l'existence d'un continuum morphologique ou génétique entre ces différents types de bedforms (Chapitre I - Partie B §2).

Pourtant des rides sédimentaires transverses et obliques, dont les gammes de dimensions recouvrent en partie celles des hummocks, ont été décrits comme spatialement associés aux hummocks (Chapitre I - Partie B §2.1). Comme pour les ribbed bedforms, les bedforms circulaires et les linéations glaciaires (Chapitre I - Partie B §3.1.1), ces associations spatiales et ces recouvrements des gammes de dimensions suggèrent que des seuils de dimensions permettant de catégoriser séparément les hummocks des rides sédimentaires soient difficilement définissables. Essentiellement constitués des sédiments triés sableux/graveleux d'origine fluvio-glaciaire et de tills sous-glaciaires, les rides sédimentaires et hummocks sont tous deux interprétés comme pouvant résulter de processus de dépôt ou d'érosion. Bien que ces bedforms aient fait l'objet de plusieurs études investiguant leur processus de formation, notamment dans des contextes de routes de drainage d'eau de fonte sous-glaciaire (e.g. ***Utting et al., 2009 ; Peterson et al., 2018 ; Lewington et al., 2020***), aucune étude n'a permis d'identifier l'existence de continuité morphologique ou génétique entre ces bedforms mais aussi avec d'autres bedforms sous-glaciaires associés à la dynamique d'écoulement de l'eau de fonte (e.g. murtoos) ou de la glace (e.g. ribbed bedforms, linéations).

Similairement, les murtoos et les bedforms associés – *'lobate-type murtoos', 'chevron-type murtoos', 'murtoos-related ridges*' et '*escarpments*' – possèdent de nombreuses caractéristiques morphologiques (e.g. forme sub-triangulaire, profil longitudinal asymétrique) et compositionnelles communes (Chapitre I - Partie B §2.2). Bien que toutes ces catégories de bedforms aient été décrites individuellement, aucune étude n'a intégré ces bedforms au sein d'une même base de données afin de

mettre en évidence un possible continuum morphologique. Très récemment, ***Ojala et al.*** (***2022***) ont démontré que la formation des rides et des escarpements associés spatialement aux murtoos résultait de processus fluvio-glaciaires, caractérisés par des phases répétées de dépôts de sédiments en suspension ou sous de faibles vitesses d'écoulement d'eau de fonte. Au sein des routes de drainage d'eau de fonte, ces bedforms sont situés dans une position intermédiaire et reflèteraient la transition entre (i) un système de cavités plus ou moins connectées, inefficace et distribué, caractérisé par des champs de murtoos en amont, et (ii) un système drainage chenalisé efficace plus en aval. Ces processus de formation et ces distributions spatiales sont corrélés à ceux des murtoos, mais l'existence d'une continuité morphologique entre les murtoos et *murtoo-related bedforms* pouvant suggérer une évolution dépendante de la dynamique d'écoulement d'eau de fonte n'a pas encore été démontrée.

Enfin, puisque l'activité des routes de drainage d'eau de fonte sont communément définie comme transitoire en raison des variabilités spatio-temporelles de production et de circulation d'eau de fonte (***Hubbard et al., 1995 ; Das et al., 2008 ; Andrews et al., 2014 ; Smith et al., 2021***), ces dernières sont caractérisées par une forte périodicité entre les périodes de (i) découplage dominées par la dynamique de circulation d'eau de fonte et les processus fluvio-glaciaires et de (ii) couplage dominées par la dynamique d'écoulement de la glace et les processus glaciogéniques (***Larsen et al., 2004 ; Piotrowski et al., 2006 ; Lesemann et al., 2010; Menzies & Ellwanger, 2011; Reinardy et al., 2011***). En revanche, aucune étude n'a actuellement mis en évidence d'éventuelles continuités morphologiques et/ou génétiques résultant de cette périodicité entre (i) des bedforms associés à la dynamique d'écoulement de l'eau de fonte et (ii) des bedforms associés à la dynamique d'écoulement de la glace.

Problématiques

Cet état de l'art a permis de faire émerger plusieurs problématiques qui seront développées dans ce travail de recherche. Ce travail explorera les caractéristiques morphologiques et les processus de formation afin d'étudier l'existence de continuums morphologiques et génétiques des bedforms sous-glaciaires. Cette approche sera menée pour l'intégralité des bedforms sous-glaciaires qu'ils soient associés à la dynamique d'écoulement de la glace ou à la dynamique d'écoulement de l'eau de fonte. Ces différentes problématiques structurent les chapitres suivants :

- **Chapitre II – Cartographie, modélisation analogique et analyse morphométrique des bedforms sous-glaciaires**

Problématiques

○ Comment tracer les bedforms sous-glaciaires afin d'explorer leurs caractéristiques morphologiques ?

○ Quels sont les apports de la modélisation analogique pour l'étude des variations temporelles des interactions glace-eau-sédiments, des processus de formation et de l'évolution morphologique des bedforms sous-glaciaire ?

○ Pourquoi la définition de nouveaux critères morphométriques est-elle nécessaire afin de caractériser les variabilités de forme et d'orientation de l'intégralité des bedforms sous-glaciaires ?

- **Chapitre III – Les bedforms associés à la dynamique de la glace : processus de formation et continuités morphologique et génétique**

Problématiques

○ L'existence de bedforms complexes remet-elle en question la relation présupposée entre la forme et l'orientation des bedforms et la direction de déplacement de la glace ?

○ Comment les variations de la dynamique d'écoulement de la glace au sein des calottes glaciaires permettent d'expliquer les variabilités de forme, d'orientation et de distribution spatiale des bedforms sous-glaciaires ?

○ Derrière la diversité de formes des bedforms sous-glaciaires associés à la dynamique d'écoulement de la glace, existe-t-il un continuum morphologique plus intégratif qu'actuellement proposé ? Par quels critères morphométriques est-il contraint ?

○ Existe-t-il un modèle d'évolution (i.e. continuum génétique) de bedforms sous-glaciaires dont la formation est attribuée à la dynamique d'écoulement de la glace ? Par quel(s) paramètre(s) glaciologique(s) est-il contraint ? Comment permet-il d'explorer les variabilités spatio-temporelles d'interactions glace-eau-sédiments et de reconstruire les environnements sous-glaciaires ?

- **Chapitre IV – Les bedforms associés à la dynamique de l'eau de fonte : processus de formation et continuités morphologique et génétique**

Problématiques

○ Dans quelle mesure le caractère transitoire des routes de drainage d'eau de fonte sous-glaciaires est à l'origine des variations de couplage/découplage glace-eau-sédiments et de processus de remobilisation sédimentaire sous-glaciaires ?

○ Comment cette diversité de processus de remobilisation sédimentaire permet d'expliquer la diversité de formes et de processus de formation des bedforms ?

○ Existe-t-il un ou plusieurs continuum(s) morphologique(s) intégrant la diversité de formes de bedforms formés le long des routes de drainage d'eau de fonte sous-glaciaires?

○ Leurs associations spatiales avec des bedforms associés à la dynamique d'écoulement de la glace (e.g. ribbed bedforms) témoignent-elles d'une relation génétique ?

○ Existe-t-il un ou plusieurs modèle(s) d'évolution de bedforms sous-glaciaires dont la formation est attribuée à la dynamique d'écoulement de l'eau de fonte ?

CHAPITRE II

METHODES : MODELISATION ANALOGIQUE, CARTOGRAPHIE ET ANALYSE MORPHOMETRIQUE DES BEDFORMS SOUS-GLACIAIRES

Introduction

Les interactions opérant à la base des calotte glaciaire entre la glace, l'eau de fonte et les sédiments sous-glaciaires contrôlent directement la dynamique d'écoulement des calottes glaciaires et les mécanismes de remobilisation de sédiments d'origine glaciogénique et fluvio-glaciaire qui sont responsable de la formation des bedforms sous-glaciaires (Chapitre I – Partie B). Plusieurs méthodes permettent d'explorer ces interactions.

Les données satellitaires (e.g. vitesses de déplacement et de déformation de la surface de la glace), géophysiques (e.g. données sismiques, radars et électriques pour l'imagerie la topographie du lit sous-glaciaire ou la détection d'eau de fonte basale) ou géochimiques (e.g. utilisation de traceurs pour le suivi de la circulation d'eau de fonte) sur des calottes glaciaires modernes sont les moyens les plus directs pour mettre en relation les dynamiques d'écoulement de glace et d'eau de fonte basale, les caractéristiques du lit sédimentaire et l'observation de bedforms sous-glaciaires. Cependant, les faibles échelles de temps et d'espace de ces observations combinées à la faible résolution de détection des bedforms sous-glaciaires ne permettent d'explorer ni les caractéristiques morphologique des bedforms ni la continuité spatio-temporelle des processus glaciogéniques et fluvio-glaciaires (e.g. ***King et al., 2009 ; Larter et al., 2009 ; Chandler et al., 2013 ; Sergienko & Hindmarsh, 2013 ; Smith et al., 2015 ; Nanni et al., 2021***).

Afin de pallier ces lacunes d'observations, l'étude des caractéristiques morphologiques et sédimentaires de paléo-bedforms sous-glaciaires observés le long du lit sédimentaire de calottes glaciaires aujourd'hui retirées permet, de façon indirecte, d'interpréter les processus de formation des bedforms et de remobilisation de sédiments, les interactions glace-eau-sédiments, les dynamiques d'écoulement de glace et d'eau de fonte et les caractéristiques du lit sédimentaire (e.g. ***Hättestrand & Kleman, 1999 ; Möller & Dowling, 2016 ; Stokes et al., 2016 ; Mäkinen et al., 2017 ; Peterson Becher & Johnson, 2021 ; Sookhan et al., 2022***). La disponibilité et la résolution croissante des données topographiques de surface, notamment au niveau de régions anciennement recouvertes par des calottes glaciaires permettent une description et une analyse morphologique précise des bedforms sous-glaciaires. En raison de leur caractère ubiquiste à la base des calottes, l'étude de leur diversité de formes

– dont le sculptage par les écoulements d'eau de fonte et de glace en font des témoins morphologiques directs des processus sous-glaciaires – permettent ainsi d'explorer les variations spatiales des interactions glace-eau-sédiments, bien que les variations temporelles restent difficiles à appréhender.

A partir de données naturelles, la modélisation permet aussi au travers la conception d'un modèle numérique (***Chapwanya et al., 2011; Fowler & Chapwanya, 2014 ; Barchyn et al., 2016 ; Fannon et al., 2017***) ou physique (***Paola et al., 2001 ; Corti et al., 2008, 2014 ; Lelandais et al., 2016, 2018***) d'établir une représentation simplifié des systèmes sous-glaciaires étudiés et ainsi de comprendre la nature des interactions glace-eau-sédiments. Lorsque les phénomènes physiques opérant au sein des systèmes naturels sont suffisamment simples et bien connus pour permettre une description mathématique complète, la modélisation numérique est parfaitement appropriée. Lorsque les systèmes naturels sont plus complexes, notamment pour les systèmes sous-glaciaires au sein desquels les phénomènes physiques sont régis par des interactions en la glace, l'eau et les sédiments possédant des rhéologies distinctes et complexes, cette description mathématique est parfois plus difficile. Les modèles analogiques représentent alors un moyen supplémentaire d'explorer les variations temporelles des interactions glace-eau-sédiments et de comprendre l'évolution morphologique des bedforms sous-glaciaires.

Au sein de ce Chapitre II, les données topographiques, les zones d'étude et les méthodes de cartographie des bedforms sous-glaciaires formés à la base de paléo-calottes glaciaire sont dans un premier temps présentées (Chapitre II §1). Dans un second temps, un rapide état sur l'apport de la modélisation analogique appliquée aux systèmes glaciaires est réalisé, avant que le modèle analogique et les méthodes de traitement des données expérimentales développés et utilisés durant cette thèse afin d'étudier la formation et l'évolution des bedforms sous-glaciaires ne soient présentés et discutés (Chapitre II §2). Enfin, une présentation des outils d'analyse morphométrique existants dans la littérature ainsi que de leurs limites est réalisée afin d'introduire le nouveau protocole d'analyse morphométrique développé durant cette thèse afin de comparer les formes de bedforms sous-glaciaires et expérimentaux (Chapitre II §3).

1. Cartographie des bedforms sous-glaciaires naturels

1.1. Données

Afin d'étudier les caractéristiques morphologiques, la distribution spatiale et le processus de formation des bedforms sous-glaciaires, j'ai cartographié de nombreux paléo-lits sous-glaciaires dans des zones de l'hémisphère nord recouvertes par des calottes glaciaires lors du Dernier Maximum Glaciaire (**Table 2.1**). Les zones d'étude ont été sélectionnées selon plusieurs critères :

- la présence de bedforms sous-glaciaires de formes variées et bien préservés, le long de paléo-lits glaciaires recouverts d'une couche de sédiments sous-glaciaires recouvrant le substrat rocheux
- la disponibilité de Modèles Numériques d'Elévations (MNE)[11] de haute résolution (résolution horizontale ≤ 25 m) permettant une cartographie précise des bedforms sous-glaciaires (**Table 2.2**)
- des contextes paléoglaciaires variés, tels que des fleuves de glace, des lobes, des dômes de glace ou des routes de circulation d'eau de fonte, permettant d'étudier des bedforms sous-glaciaires classiquement attribués à l'écoulement de la glace ou à celui de l'eau de fonte (**Figure 2.1**).

1.2. Méthode de cartographie

A partir de la compilation des MNEs dans un logiciel SIG, des cartes de reliefs ombrés illuminés de façon unidirectionnelle ('*unidirectional hillshaded DEM'*) et des cartes de reliefs résiduels ('*residual relief' ; **Hiller & Smith, 2008***) ont été produites pour chaque zone d'étude (**Figure 2.2A**). La réalisation d'une carte de relief résiduel à partir d'un DEM permet d'effectuer une séparation entre le relief régional et le relief local à une longueur d'onde donnée, et ainsi d'obtenir un modèle numérique de terrain normalisé n'indiquant que les amplitudes relatives des reliefs de courte longueur d'onde comme les bedforms sous-glaciaires (**Figure 2.2B**). Différentes cartes de reliefs résiduels ont été produites en considérant les variations de résolution horizontale des MNEs et des différences de longueurs d'onde de relief local pour chaque zone d'étude, en fonction de la largeur

[11] Un Modèle Numérique de Terrain (MNT) ('*Digital Terrain Model', DTM*) est une représentation de la topographie d'une surface construite à partir de données d'altitude de ce terrain, quand un Modèle Numérique d'Elévation (MNE) (*'Digital Elevation Model', DEM*) inclut également les élévations des bâtiments et de la canopée (le terme « Elévation » de MNE est en réalité un anglicisme du terme « Altitude »). Bien que des MNEs soient utilisés pour la cartographie des paléo-lits glaciaires, la résolution horizontale des sources de données (2-25m) et les dimensions des objets naturels cartographiés (souvent supérieures à plusieurs centaines de mètres) rendent négligeables l'impact de l'inclusion de la canopée et des bâtiments lorsque ces derniers ne sont pas filtrés.

Table 2.1. *Location of subglacial bedform mapping areas. All study areas have been covered by ice sheets during the Last Glacial Maximum (~20 ka BP). Locations of study areas are reported in* ***Figure 2.1****.*

	Location of study area	Glacial context	Number of bedforms (& crest lines)	Age of last glacial coverage (cal ka BP)	Reference	DEM Data set	Map
1	Amundsen Gulf Ice Stream (Nunavut, Canada)	Ice stream trunk & lateral shear margins	62	12.9	***Margold et al., 2018***	ArcticDEM	Article n° 1 Figs. 12a-b
2	Lowland Ice Dome (NE Ireland)	Ice dome to onset areas of ice streams	10 100	16	***Clark et al., 2012***	EU-DEM v1.0	Article n° 3 Fig. 4
3	Boyd Lake, Keewatin Ice Dome (NWT, Canada)	Ice dome & subglacial meltwater routes	3 400	8.9	***Margold et al., 2018***	ArcticDEM	Article n° 3 Fig. 5
4	Poorfish Lake, Keewatin Ice Dome (NWT, Canada)	Ice dome & subglacial meltwater routes	20 230	8.9	***Margold et al., 2018***	ArcticDEM	Annexe 1
5	Finnish Lake District Ice Lobe (Finland)	Ice dome trunk & subglacial meltwater routes	1 716	11	***Punkari, 1980***	NLSF DEM	Article n° 4 Fig. 4
6	Southern lobate termination of FIS (Sweden)	Ice lobe & subglacial meltwater routes	2 200	12.7	***Lundqvist & Wohlfarth, 2000***	Lantmäteriet DEM	Article n° 4 Figs. 5-6
7			3 292				
8	Central Alberta Ice Stream (Alberta, Canada)	Ice stream trunk, lateral shear margins & ice lobe	519	17	***Margold et al., 2018***	Alberta DEM	Article n° 1 Figs. 12e-h
9	Hay River Ice Stream (Alberta, Canada)	Ice stream trunk & lateral shear margins	78	12.9	***Margold et al., 2018***	Alberta DEM	Article n° 1 Figs. 12c-d
10	Naococane Lake, Labrador Ice Dome (NWT, Canada)	Ice dome & subglacial meltwater routes	3 875	7.8	***Margold et al., 2018***	MNEC DEM	Annexe 2

Table 2.2*. Acquisition method, location, horizontal resolution and source of Digital Elevation Models (DEMs) used in this study and mentioned in* ***Table 2.1****.*

DEM Data set	Acquisition method	Location	Horizontal resolution	Licence type	Source
Alberta DEM	Aeromagnetic survey	Alberta	15 m	Proprietary	Alberta Geological Survey
ArcticDEM	Optical stereo imagery	North Hemisphere (>60°N)	10 m	Open source	https://www.pgc.umn.edu/data/arcticdem/
EU-DEM v1.0	SRTM & ASTER GDEM	Europe	25 m	Open source	https://land.copernicus.eu/
NLSF DEM (filtrated canopy)	LiDAR	Finland	2 m	Open source	https://tiedostopalvelu.maanmittauslaitos.fi/tp/kartta?lang=en
MNEC DEM	SRTM	Canada	20 m	Open source	https://cartes.canada.ca/czs/index-fr.html
Lantmäteriet DEM (filtrated canopy)	LiDAR	Sweden	2 m	Open source	https://www.lantmateriet.se/sv/geodata/Geodataportalen/

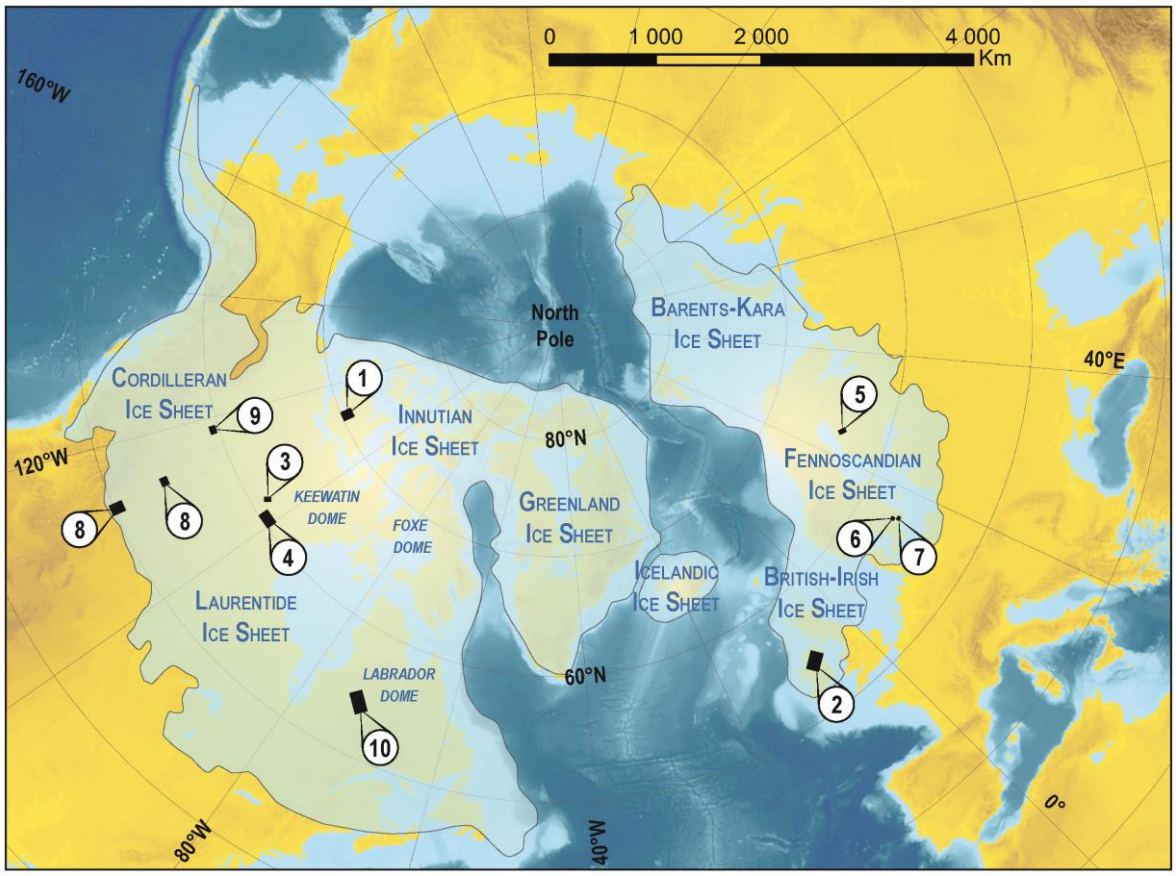

***Figure 2.1**. Location of study areas relative to the maximum extension of the northern hemisphere ice sheets during the Last Glacial Maximum (**Batchelor et al., 2019**).*

moyenne des bedforms sous-glaciaires. Pour les zones d'étude caractérisées par des bedforms dont la formation est principalement attribuée à la dynamique d'écoulement de l'eau de fonte sous-glaciaire (i.e. murtoos, hummocks ; dimensions : dizaines de mètres), la longueur d'onde du relief local du relief résiduel est d'une dizaine de mètres ; tandis que pour les zones d'étude caractérisés par des bedforms principalement associés à la dynamique d'écoulement de la glace (i.e. ribbed bedforms, linéations ; dimensions : centaines de mètres), la longueur d'onde du relief local du relief résiduel est d'une centaine de mètre (Chapitre I – Partie B), et (**Table 2.2**). Pour chaque zone d'étude, les contours et les lignes de crête des bedforms sous-glaciaires ont été digitalisés manuellement avec une tablette graphique via un outil de tracé à main levée. Les contours des bedforms ont été tracés à partir des lignes de rupture de pente du relief résiduel, et leurs lignes de crête ont été tracées à partir des maximums d'altitude du relief résiduel au sein de chaque contour (**Figure 2.2A**). Les bedforms attribués à la dynamique d'écoulement de la glace (i.e. ribbed bedforms, linéations, bedforms circulaires et autres bedforms associés) ont été digitalisés à une échelle de 1:10000^{e} ; tandis que les bedforms attribués à la dynamique d'écoulement de l'eau de fonte ont été digitalisés à une échelle de 1:5000^{e}.

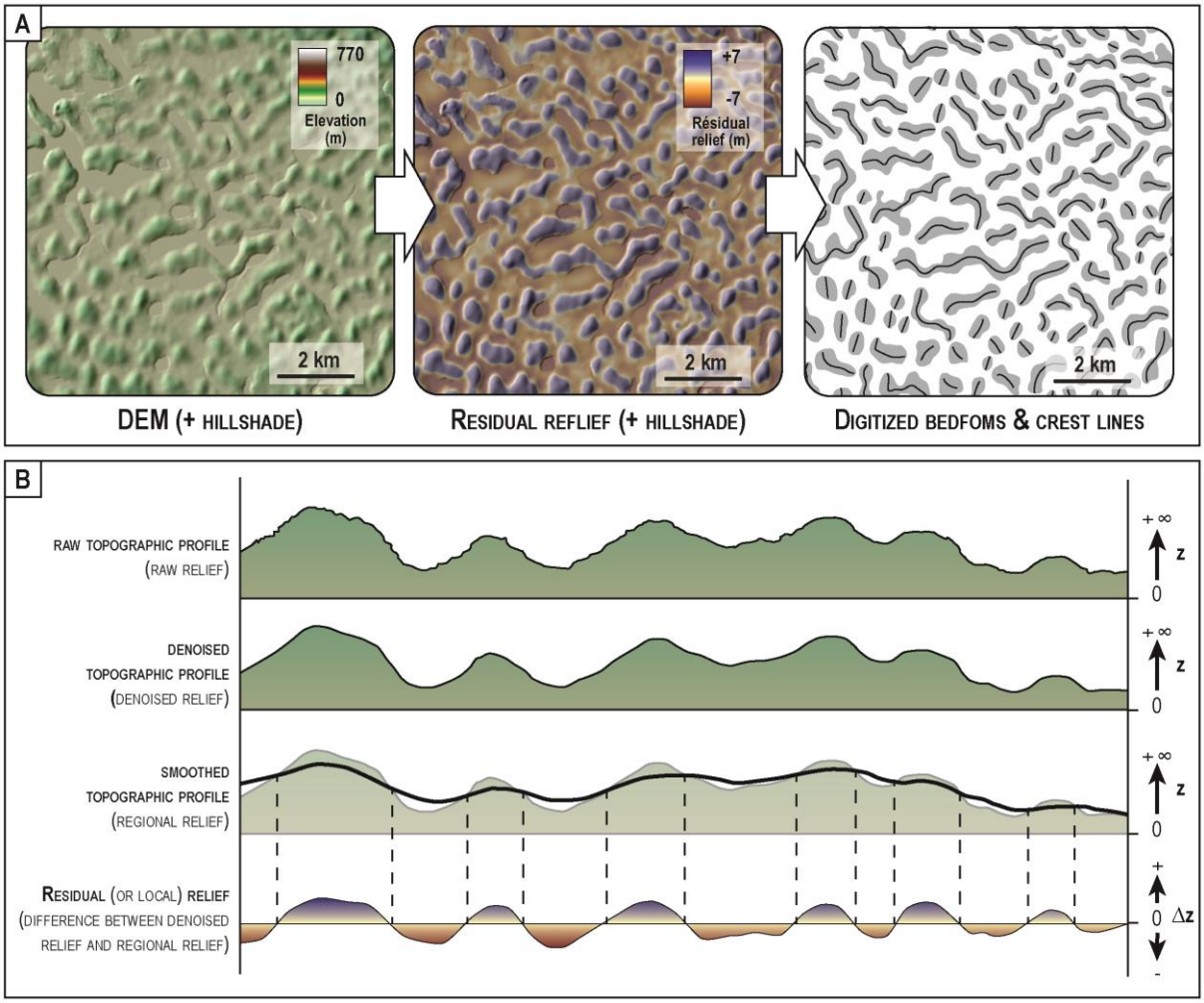

Figure 2.2. *(A) Using a digital elevation model (DEMs), a map of hillshaded residual relief is derived and is used to manually digitized bedform contours and crest lines. (B) Schematic illustration of residual relief computation from the difference between denoised topographic data (i.e. spatial moving average realized in a 3 pixel wide square) and the regional relief (i.e. spatial moving average whose the wavelength depends on the order of magnitude of bedform dimensions).*

2. Modélisation analogique des bedforms sous-glaciaires

2.1. Introduction

Afin d'explorer les conditions de formation des bedforms sous-glaciaires, des modèles mathématiques ont été établis à partir d'équations mécaniques régissant la dynamique d'écoulement de la glace, de l'eau de fonte et des sédiments et de grandeurs physiques mesurées dans les systèmes glaciaires naturels actuels (e.g. taux de cisaillement basal, production d'eau de fonte, épaisseur de déformation des lits sous-glaciaires, dimensions des bedforms et des calottes glaciaires) (***Hindmarsh, 1998a,b; Fowler, 2000; Schoof, 2007***). Le développement de modèles numériques basés sur ces modèles mathématiques a démontré que l'initiation d'instabilités à la suite de perturbations infinitésimales à la surface d'un lit sédimentaire déformable au comportement visqueux pouvait générer des bedforms périodiques en réponse à l'écoulement de la glace et de l'eau de fonte (Chapitre I – Partie B §3.1.2) (***Chapwanya et al., 2011; Fowler & Chapwanya, 2014 ; Fannon et al., 2017***). Cependant, la modélisation numérique ne permet pas actuellement d'aborder l'intégralité des processus de formation des bedforms sous-glaciaires puisque les équations régissant les interactions entre la glace, l'eau et les sédiments – ayant des caractéristiques rhéologiques (e.g. dépendance à la température et à la contrainte) et cinétiques (e.g. viscosité) qui peuvent différer de plusieurs ordres de grandeurs entre ces différents matériaux – sont difficiles à résoudre simultanément.

Au cours des deux dernières décennies, l'émergence de la modélisation analogique (ou expérimentale) appliquée aux systèmes glaciaires a permis d'explorer les dynamiques d'écoulement de l'eau de fonte sous-glaciaire et/ou de la glace. ***Catania & Paola (2001)*** ont été les premiers à démontrer que l'intérêt de la modélisation analogique pour l'étude de systèmes glaciaires complexes. Bien que simplificatrice et imparfaitement dimensionnée, la modélisation analogique permet d'explorer de multiples processus entre des matériaux dynamiques à des échelles de temps et d'espace très différentes. En modélisant l'écoulement d'eau sous pression au sein d'un lit sédimentaire érodable et non cohésif, confiné sous une plaque de verre, ***Catania & Paola (2001)*** ont mis en évidence l'impact d'un écoulement d'eau sous-pression sur la morphologie de systèmes de drainage en tresse.

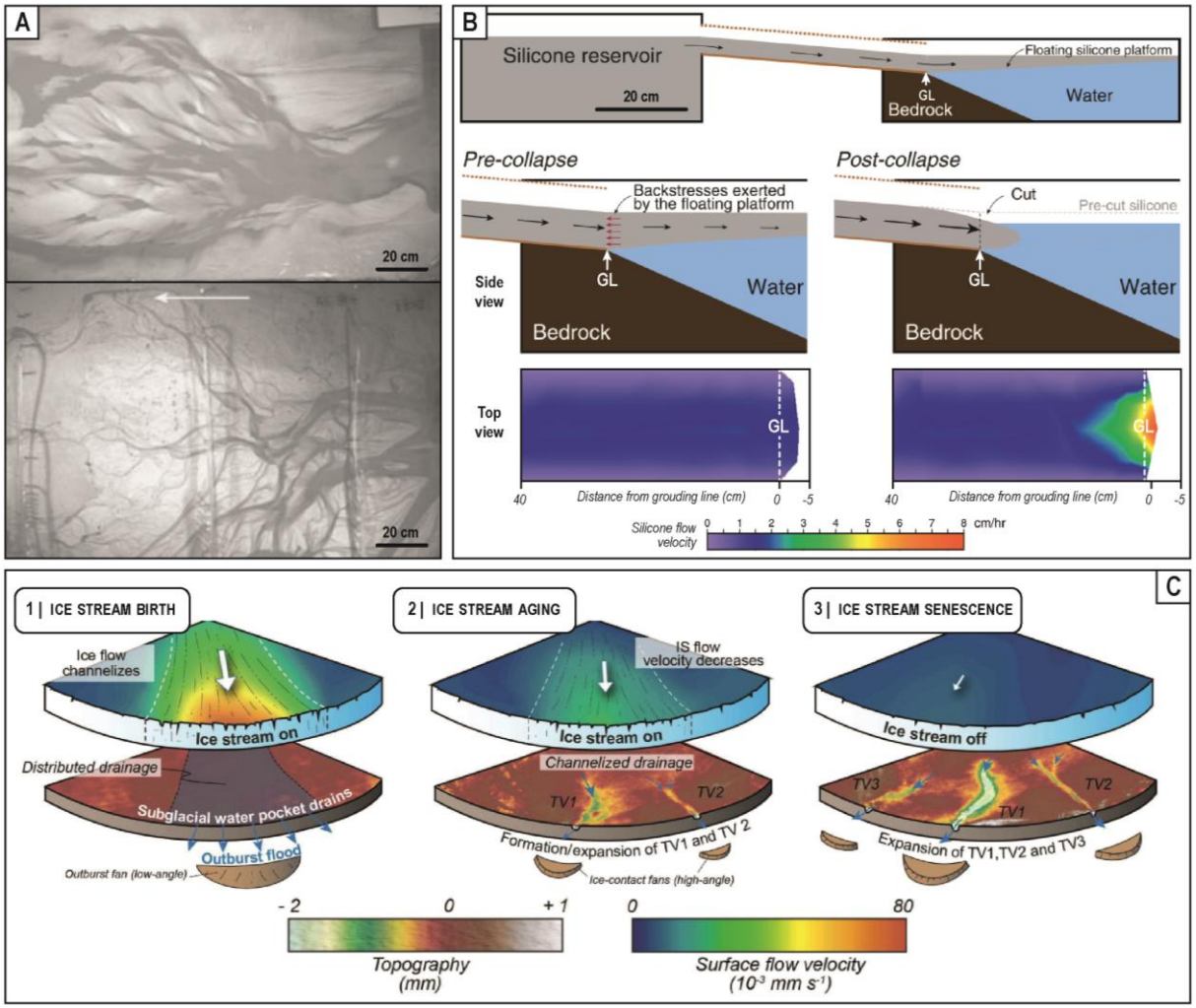

***Figure 2.3**. Some recent analog modelling works on (sub)glacial systems. (A) Channels formed in an erodible, non-cohesive bed under a transparent rigid lid, simulating subglacial water flow). Pressurised water flow produces higher braiding intensities (lower picture) than free-surface flow (upper picture) (**Catania & Paola, 2001**). (B) Simulation of ice stream acceleration as a response to the collapse of an ice shelf using a silicone platform floating on water (**Corti et al., 2014**). (C) Relationship between the life cycle of an ice stream and tunnel valley development inferred from a model simulating the water flow at the interface between a silicone cap and an erodible and permeable sand bed (**Lelandais et al., 2018**).*

L'écoulement confiné sous pression (analogue sous-glaciaire) produit des systèmes en tresses plus larges, avec une plus forte variabilité d'orientation par rapport à la direction d'écoulement, une courbure des chenaux plus importantes et des chenaux moins profonds et aux marges mieux définies que l'écoulement à surface libre (**Figure 2.3A**). En utilisant une gomme de silicone transparente comme matériau analogue de la glace, ***Corti et al. (2008, 2014)*** et ***Corti & Zoeli (2018)*** ont quant à eux étudié l'impact de la topographie du substrat et de la disparition d'une plateforme de glace sur la dynamique d'écoulement (i.e. vitesse et déformation) des glaciers de vallées et des fleuves de glace (**Figure 2.3B**).

Plus récemment, ***Lelandais et al. (2016, 2018)*** ont développé un modèle analogique permettant de simuler simultanément des processus sous-glaciaires de déformation, d'érosion, de transport et de

dépôt par l'écoulement de la glace et de l'eau de fonte sous-glaciaire. En injectant de l'eau au sein d'un lit sédimentaire érodable et non-cohésif recouvert d'une calotte de gomme de silicone, ils ont démontré que (i) la topographie du lit sous-glaciaire et la production d'eau de fonte contrôlaient la formation et la forme des vallées tunnels, et que (ii) le développement des vallées tunnels modulait la dynamique de formation et l'évolution des fleuves de glace (**Figure 2.3C**).

Cependant, aucune étude de modélisation analogique n'a jusqu'à présent exploré les processus de formation des bedforms sous-glaciaires. Sur la base du dispositif expérimental mis en place par Thomas Lelandais au cours de sa thèse (***Lelandais et al., 2016, 2018***), un nouveau dispositif dont les dimensions horizontales ont été agrandies (×3) pour permettre la simulation de bedforms a donc été développé (**Figure 2.4A**).

2.2. Modèle expérimental

Le dispositif expérimental est constitué d'un réceptacle carré en acier inoxydable large de 2 m et profond de 5 cm (**Figure 2.4B**). Le réceptacle est comblé par une couche de sable fin (h_S = 5 cm), de granulométrie médiane d_{50} = 100 µm, saturée en eau. La couche de sable fin, plane en surface et d'une densité ρ_{bulk} de 2000 kg/m^3, simule un lit sédimentaire sous-glaciaire meuble, poreux (porosité ϕ_S = 41%), perméable (perméabilité $K_S = 10^{-4}$ m/s), érodable et déformable (**Figure 2.4C**). Des grains de sable grossier (d_{50} = 1 mm) colorés en noir sont disséminés à la surface du lit sédimentaire afin de simuler de blocs sous-glaciaires et d'augmenter la rugosité du lit sédimentaire pour permettre la reconstruction de Modèles Numériques de Terrain (MNT) de la surface du lit sédimentaire par photogrammétrie. Une calotte circulaire de gomme de silicone (ρ_{sil} = 967 kg/m^3), visqueuse ($\eta_{sil} = 5 \times 10^4$ Pa/s) et transparente recouvre le lit sédimentaire et simule une calotte glaciaire. La gomme de silicone est déposée sur le lit sédimentaire sous la forme d'une boule de 13 kg, qui flue ensuite par écoulement gravitaire jusqu'à former une calotte circulaire de 90 cm de diamètre (r_{sil} = 90 cm) et de 3 cm d'épaisseur en son centre (h_{sil} = 3 cm). Des marqueurs UV d'1 mm de diamètre sont disposés à la surface de la calotte de silicone avec un espacement régulier de 5 cm afin de suivre le déplacement de la calotte de silicone.

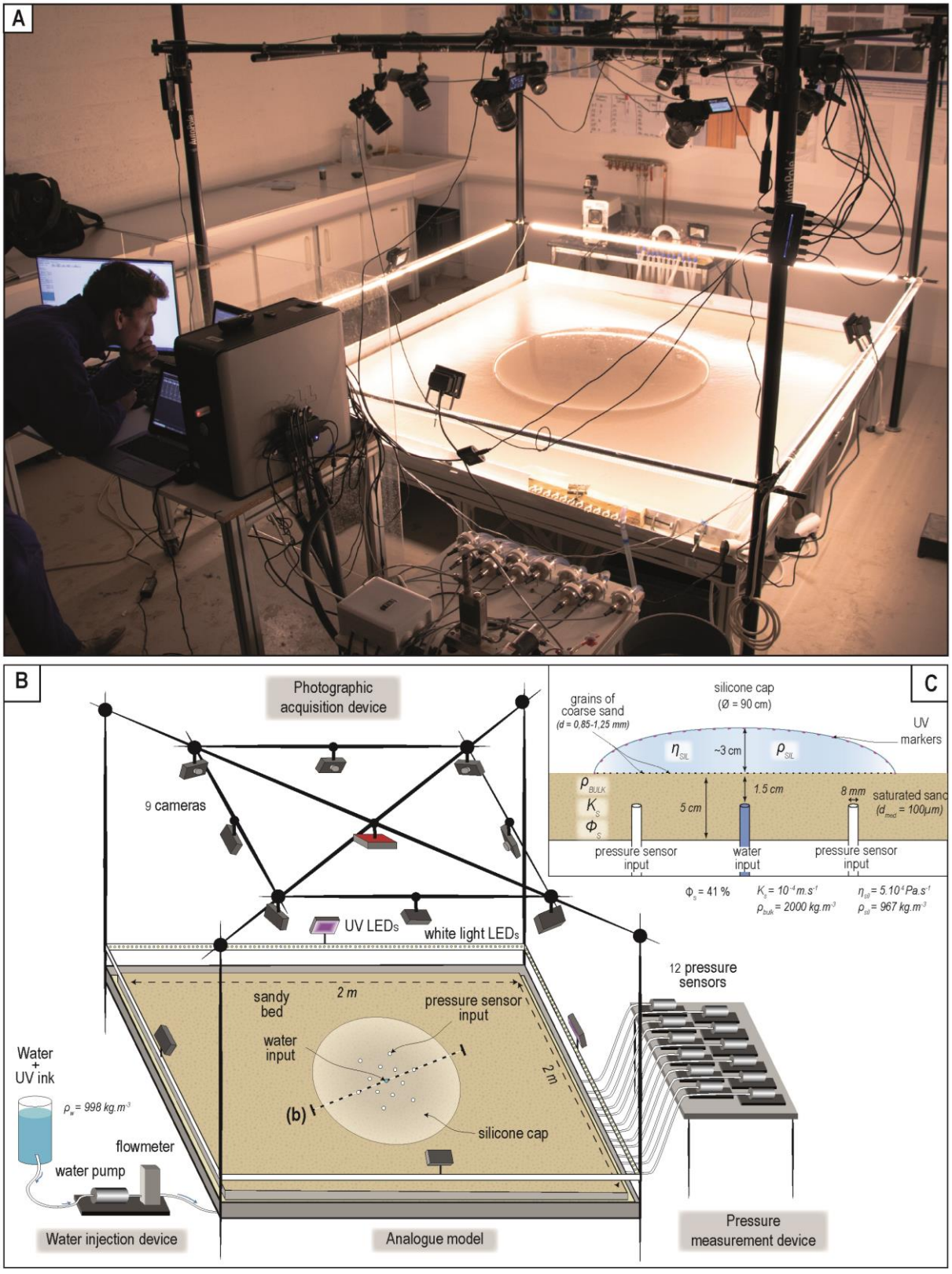

Figure 2.4. *(A) Photography of the experimental device used in this study. (B) Schematic representation of the experimental model and its monitoring apparatus. The flow of a transparent and viscous cap of silicone putty over a deformable and erodible bed made of water-saturated sand is triggered by the injection of a solution of water and UV ink through an injector located in the bed below the center of the silicone cap. The monitoring apparatus is composed of a lighting set-up, a photographic acquisition device and a pressure measurement device. (C) Transverse section of the model with the main physical parameters (**Vérité et al., 2021**).*

Une solution d'eau et d'encre UV (ρ_w = 998 kg/m^3) est injectée sous le centre de la calotte de silicone à l'aide d'un injecteur de 8 mm de diamètre (r_{inj} = 90 cm), situé à une profondeur h_{inj} = 1.5 cm sous la surface du lit sédimentaire afin de visualiser la trajectoire de l'écoulement d'eau à l'interface. L'injecteur est relié à une pompe équipée d'un débitmètre permettant de contrôler le débit d'injection entre la calotte de silicone et le lit sédimentaire. Le débit d'injection (Q en mL/min) imposé est calculé afin de permettre la reproduction (i) d'un écoulement poral au sein du lit sédimentaire et (ii) d'une circulation d'eau à l'interface entre la calotte de silicone et le lit sédimentaire lorsque la pression d'eau injectée (P_w) dépasse la pression exercée par la colonne de sable et la colonne de silicone au-dessus de l'injecteur (***Eq. 2.1***). Le débit d'injection Q est calculé d'après l'équation de Dupuit, approximant l'écoulement tridimensionnel en milieux poreux à un plan bidimensionnel, qui relie le débit d'injection au rayon de l'aquifère, à la pression d'eau et à la capacité d'écoulement dans l'aquifère (***Eq. 2.2***).

$$(\boldsymbol{Eq.2.1}) \qquad P_w = \left(\rho_{bulk} \times g \times h_{inj}\right) + \left(\rho_{sil} \times g \times h_{sil}\right)$$

$$(\boldsymbol{Eq.2.2}) \qquad Q = \frac{2\pi \times K \times h_S \times \left(\frac{P_w}{\rho_w \times g}\right)}{\ln\left(\frac{r_{sil}}{r_{inj}}\right)}$$

De ce fait la pression d'eau injectée P_w minimale afin de générer une circulation d'eau à l'interface entre la calotte de silicone et le lit sédimentaire est de 580 Pa, correspondant à un débit d'injection de 23.6 mL/min. Dans les expériences réalisées au cours de cette thèse, le débit d'injection minimale est ainsi de 25 mL/min.

2.3. Suivis des expériences et post-traitements des mesures

Le modèle expérimental est équipé d'un dispositif d'éclairage de LEDs diffusant, alternativement toutes les 15 secondes, de la lumière blanche et de la lumière ultraviolet (UV). Ce dispositif d'éclairage est couplé à un dispositif de captation photographique constitué de 9 appareils photo numériques synchronisés, qui permettent d'imager l'expérience en lumière blanche (**Figure 2.5A**) et en lumière UV (**Figure 2.5B**) de façon quasi-continue et ainsi de pouvoir suivre simultanément les dynamiques d'écoulement de la calotte de silicone et de l'eau le long de l'interface basale, ainsi que la formation et l'évolution des bedforms. La pression d'eau dans la porosité du lit sédimentaire est mesurée ponctuellement par 12 capteurs de pression, de 8 mm de diamètre, situés à 1.5 cm de profondeur sous la

surface du lit sédimentaire. Ces capteurs de pression sont répartis en deux cercles de 6 capteurs de 15 cm et 30 cm de rayons respectifs, centrés par rapport à l'injecteur d'eau (**Figure 2.5A**).

2.3.1. Imagerie et reconstructions photogrammétriques de la topographie du lit sédimentaire

Lors des phases d'éclairage en lumière blanche, les propriétés de transparence de la solution d'eau et d'encre UV et de la calotte de silicone permettent de visualiser puis de cartographier manuellement les bedforms à partir des photographies géoréférencées dans un logiciel SIG. Des MNTs de la topographie du lit sédimentaire sont également reconstruits par photogrammétrie avec le logiciel © *Agisoft Metashape,* selon la méthode développée par ***Lelandais et al. (2016)***, qui permet de traiter l'effet de réfraction induit par la silicone. La résolution horizontale des photographies (~ 10^{-1} mm) et la précision verticale (~ 2×10^{-1} mm) des MNTs reproduits par photogrammétrie permettent ainsi l'analyse morphométrique des structures de drainage et des bedforms qui se développent pendant l'expérience (**Figure 2.5C**) (Chapitre II - §3.2).

2.3.2. Circulation d'eau à l'interface entre la silicone et le lit sédimentaire

A partir des photographies prises en lumière UV, le caractère fluorescent de la solution d'eau et d'encre UV permet de visualiser puis de produire des cartes de distribution de l'eau qui circule le long de l'interface entre la calotte de silicone et le lit sédimentaire (**Figure 2.5B**). Le développement d'un protocole de traitement automatique d'images via le logiciel © *Photoshop* permet de quantifier l'intensité de la fluorescence, qui est ensuite convertie en épaisseur d'eau après calibration de à partir de MNTs de la surface du lit sédimentaire.

2.3.3. Vitesses de déplacement et de déformation de la surface de la calotte de silicone

L'analyse de la dynamique de la surface de la calotte de silicone se base sur la réalisation de cartes de vitesse de déplacement et de taux de déformation, à l'image des cartes réalisées pour les surfaces des glaciers et calottes glaciaires actuelles (***Colgan et al., 2016 ; Alley et al., 2018 ; Zheng et al., 2019 ; Jennings & Hambrey, 2021 ; Young et al., 2021***).

La réalisation de ces cartes consiste en cinq étapes successives : (i) extraction automatique sur les photographies de la position des marqueurs UV à différents stades de l'expérience (**Figure 2.6A**), (ii) calcul du vecteur déplacement horizontal de chaque marqueur UV entre deux stades successifs de

l'expérience (**Figure 2.6B**), (iii) calcul, à partir des vecteurs déplacements et par triangulation entre les marqueurs, de la déformation (longueurs et directions des axes de l'ellipse de déformation horizontale, magnitude du cisaillement horizontal) entre ces deux stades (**Figure 2.6C-E**), (iv) division des déplacements et des déformations obtenus par l'intervalle de temps entre les deux stades successifs, afin d'obtenir des vitesses de déplacement et des taux de déformation, et (v) création des cartes interpolées de vitesses de déplacement et de taux déformation (**Figure 2.6F**).

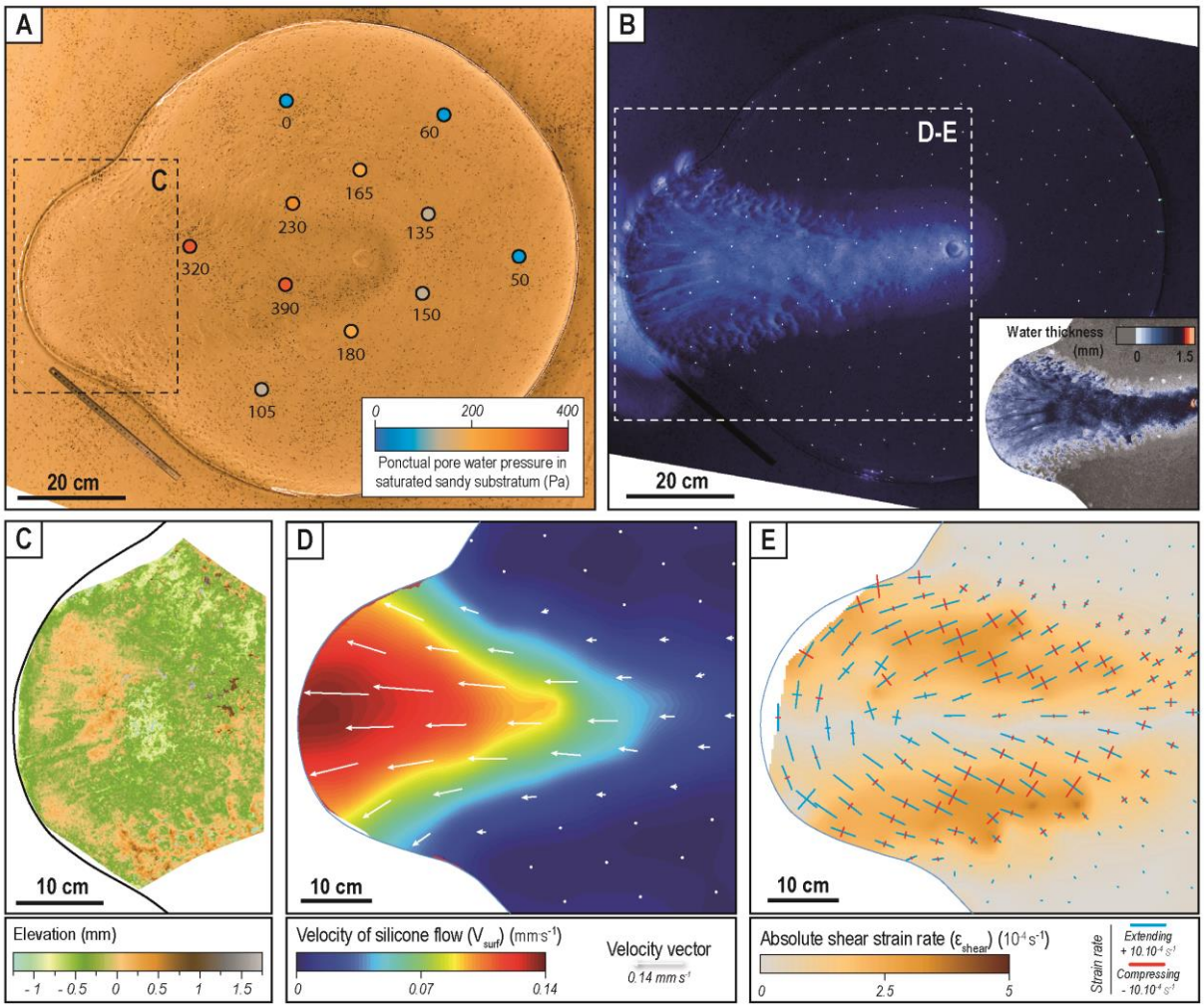

Figure 2.5. *Panel of data provided by the monitoring apparatus and numerical post-treatments. Surface views of the analog model in (A) white light and (B) UV light. In (A), colored circles indicates punctual values of pore water pressure measured in the sandy bed. In (B), the snapshot in the lower right corner shows a map of the water distribution and thickness along the basal interface calculated from the fluorescence calibration of the water and UV ink solution. (C) Digital Terrain Model (DTM) of the bed surface beneath the silicon cap reconstructed by a photogrammetric method. (D) Map of interpolated velocity of the silicone cap surface. (E) Map of interpolated absolute shear strain rate and orientation of the principal axes of the instantaneous strain ellipse. Axe lengths correspond to magnitudes of extending and compressing strain rates.*

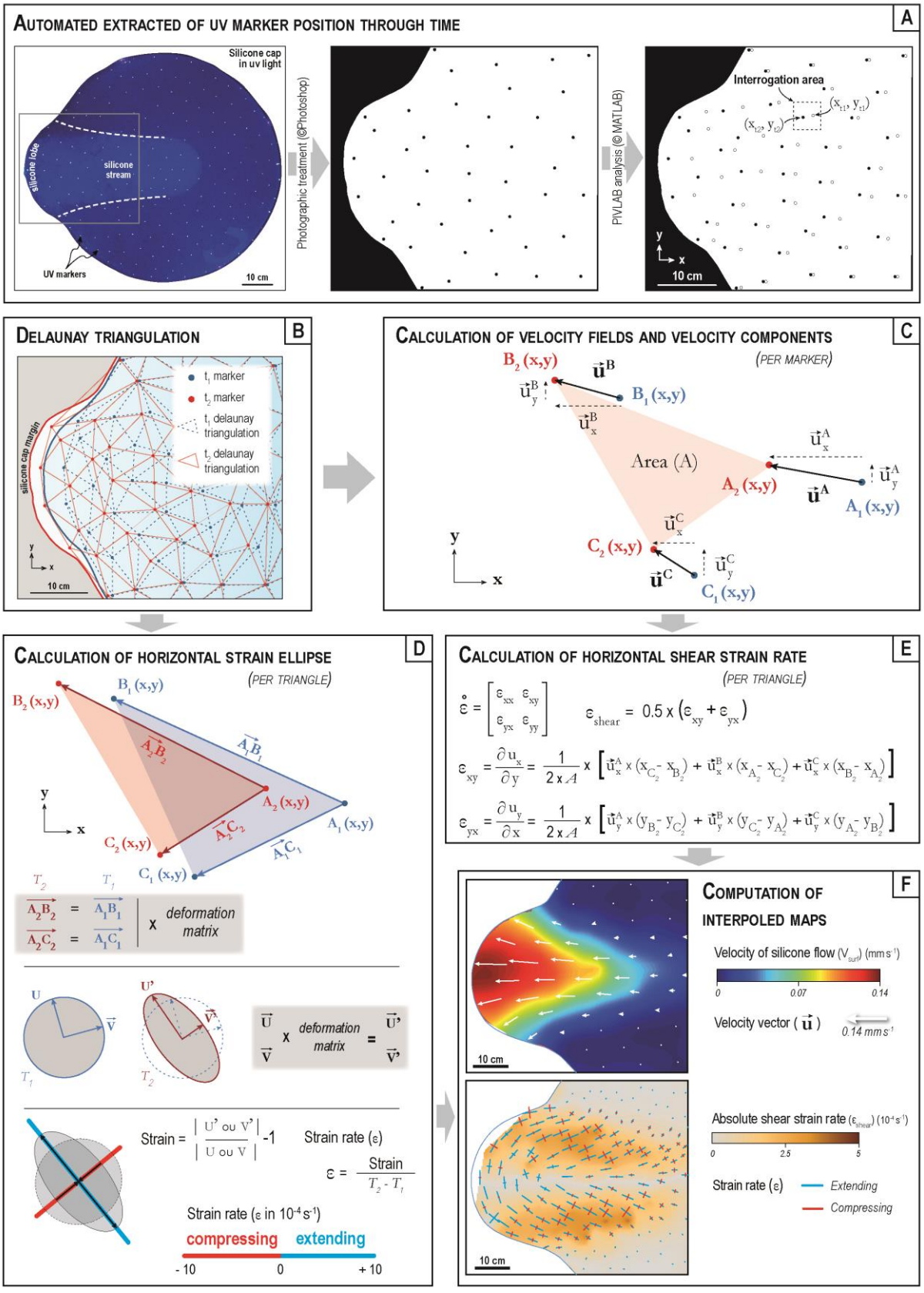

***Figure 2.6**. Processes of automated extraction of the position of UV markers through time using a PIV plugin in MATLAB, from which the velocity fields and the deformation dynamics of silicone cap surface are extracted.*

L'étape d'extraction automatique de la position des marqueurs UV au cours du temps est basée sur un protocole de traitement des images UV – développé durant cette thèse – et sur l'utilisation d'un module de vélocimétrie par image de particules ('*Particule Image Velocimetry', PIV*), nommé *PIVLab* et utilisable sur © *MATLAB* (***Thielicke & Sonntag, 2021***). Le protocole de traitement des images UV permet, à partir d'un seuillage de l'intensité de fluorescence puis d'une conversion de l'image en noir et blanc, d'obtenir des cartes de marqueurs (UV) pour chaque pas de temps (**Figure 2.6A**). La position de chaque marqueur dans un référentiel horizontal (x,y) est ensuite exportée depuis *PIVLab* afin d'être utilisée comme donnée en entrée dans le code © *MATLAB* développé pour ce travail.

A partir des positions de tous les marqueurs, une triangulation de Delaunay est réalisée pour deux instants t1 et t2 (**Figure 2.6B**), de manière à déterminer les vecteurs déplacements et les vecteurs vitesses de chaque marqueur entre ces deux instants (**Figure 2.6C**). À partir des équations classiques de la déformation homogène des matériaux, la déformation entre deux instants de chaque triangle – dont les trois sommets correspondent à trois marqueurs – est ainsi quantifiée par une matrice de déformation plane correspondant à une ellipse de déformation. La déformation horizontale de la surface de la silicone, ainsi calculée à partir des composantes en x et en y des vecteurs vitesses, est ensuite exprimée au travers de deux indicateurs : (i) la longueur et l'orientation des axes principaux de l'ellipse de déformation instantanée (raccourcissement : $\varepsilon_{compressing} < 0$; extension : $\varepsilon_{extending} > 0$) et (**Figure 2.6D**) (***Ramsay & Huber, 1987***), et (ii) la valeur absolue du taux de déformation cisaillante (ε_{shear}) (**Figure 2.6E**) (***Nye, 1959***). Les vitesses de déplacement et les taux de déformation sont ensuite calculés en prenant en compte l'intervalle de temps entre t1 et t2. Les données ponctuelles pour chaque marqueur (vitesse) et pour chaque triangle (taux de déformation) sont enfin interpolées sous forme de cartes, afin de représenter de façon continue la dynamique d'écoulement de la surface de la calotte de silicone (**Figure 2.6F**).

2.4. Dimensionnement et limites

2.4.1. Dimensionnement

Généralités sur le dimensionnement

La modélisation analogique vise à reproduire des phénomènes naturels en réduisant les échelles de temps et d'espace, et en choisissant des matériaux analogues dont les propriétés sont similaires à celles des systèmes naturels. Pour que cette modélisation analogique soit valide, il est théoriquement nécessaire qu'elle soit correctement dimensionnée par rapport à leur analogue naturel. ***Hubbert (1937)*** montre ainsi qu'une réduction des échelles de temps et d'espace implique, par les principes de similitude, une mise à l'échelle des rhéologies de matériaux. Ainsi, ***Hubbert (1937)*** proposa trois principes de similitude :

- la similitude géométrique, impliquant une préservation des rapports de dimensions et de forme entre les objets naturels et les objets expérimentaux
- la similitude cinématique, impliquant une proportionnalité des durées des processus expérimentaux par rapport aux processus naturels et donc une préservation des rapports de vitesses et d'accélération
- la similitude dynamique, impliquant que les rapports des forces exercées (e.g. forces visqueuses, de pression, inertielles et de gravité) sur des systèmes naturels et expérimentaux (similaires géométriquement et cinématiquement) soient constants. La définition des rapports entre ces forces régissant les systèmes étudiés et permettant de dimensionner les différentes grandeurs physiques impliquées fait apparaitre des nombres sans dimensions tels que les nombres de Froude, Reynolds ou Stokes.

Afin de définir le dimensionnement dynamique d'un modèle analogique, on utilise fréquemment les équations de la dynamique des fluides, de la mécanique des matériaux et de la chaleur. Dans le cas d'un modèle simulant un système sous-glaciaire avec deux fluides en mouvement (glace et eau) interagissant avec un matériau granulaire (sédiments), le nombre de grandeurs physiques à dimensionner est rapidement très important (e.g. vitesse, viscosité et masse volumique de la glace et de l'eau ; granulométrie et masse volumique des particules sédimentaires ; dimensions du système). Le nombre de gradeurs physiques à dimensionner, les limites en termes de matériaux et la méconnaissance de

certains processus opérant dans les systèmes naturels empêchent la plupart du temps un dimensionnement dynamique parfait.

Ainsi, la plupart des modèles analogiques s'attachent à ne conserver et simuler que certains aspects fondamentaux des systèmes naturels étudiés. De nombreuses travaux ayant étudiés les environnements sous-glaciaires ont notamment démontré que des modèles expérimentaux imparfaitement dimensionnés mais simulant des aspects fondamentaux, e.g. écoulements d'eau pressurisée dans un substrat lit sédimentaire poreux et érodable (***Catania & Paola, 2001***) ou à l'interface avec une couverture visqueuse (***Lelandais et al., 2016, 2018; Lelandais, 2019***), produisaient des objets morphologiques très semblables aux systèmes naturels. Cette similarité entre les objets morphologiques produits par les systèmes naturels et simulés par les systèmes expérimentaux – malgré un dimensionnement imparfait – s'explique par le principe d'efficacité déraisonnable ('*unreasonnable effectiveness*') défini par ***Paola et al. (2009)***. Ce principe démontre que les processus de transfert de matière opérant au sein des systèmes morpho-dynamiques naturels, tel que les environnements sous-glaciaires, agissent identiquement indépendamment de leur échelle d'observation. Ainsi ***Paola et al. (2009)*** proposent qu'une copie (i.e. modèle analogique) des processus opérant à petite échelle au sein d'un système naturel reproduise les processus opérant à grande échelle dans un système naturel. ***Paola et al. (2009)*** suggèrent donc de prendre de la distance avec le principe de dimensionnement dynamique, qui tend à limiter le développement de modèles analogiques étudiant les systèmes morpho-dynamiques naturels, au profit de modèles analogiques respectant l'origine et l'indépendance d'échelle des processus simulés.

Principes de dimensionnement du modèle expérimental

Les principes de dimensionnement du dispositif expérimental utilisé pour ce travail sont identiques à ceux du modèle développé et utilisé par ***Lelandais et al. (2016, 2018)***, dont les dimensions horizontales ont été agrandies (×3). Afin de reproduire la formation de bedforms, le modèle doit simuler et respecter des interactions mécaniques fondamentales entre un système hydrologique simplifié, un lit sédimentaire déformable et érodable, et une calotte visqueuse et imperméable. Ainsi, le modèle analogique reproduit les processus fondamentaux (ou processus primaires) de transfert de matières opérant dans les environnements sous-glaciaires (i.e. déformation,

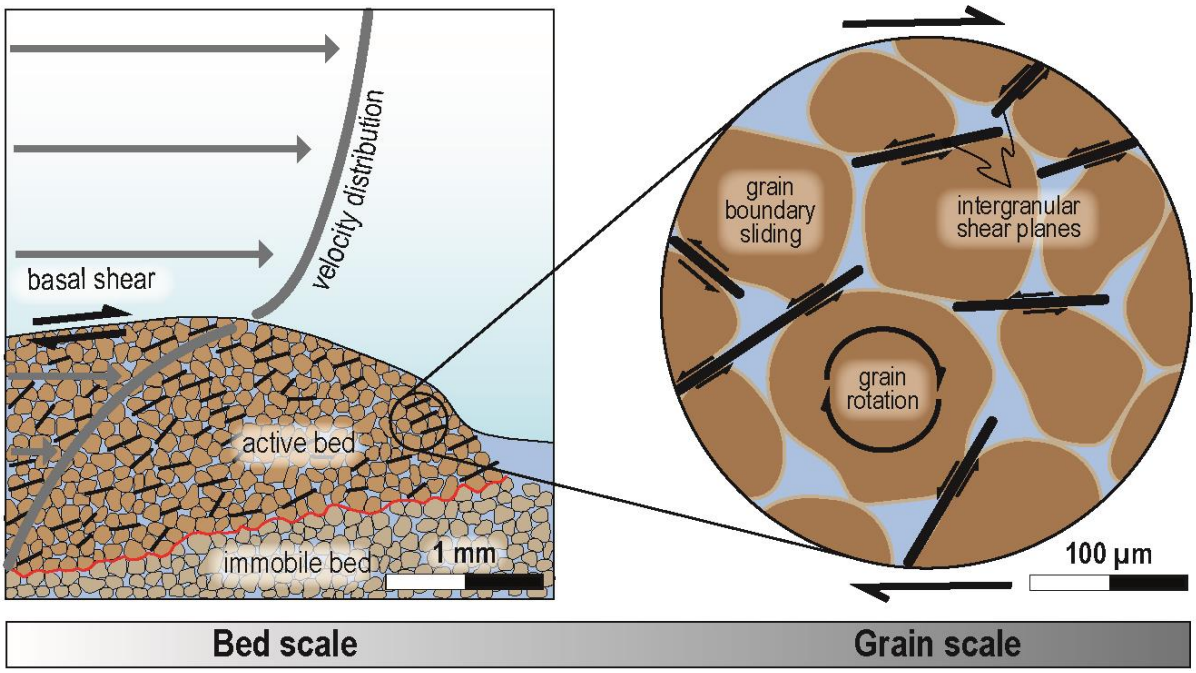

Figure 2.7. *Deformation of water-saturated and granular bed during silicone-bed coupling. The superficial portion of the bed (i.e. active bed) accommodate the basal shear stress generated by the overlying flow of silicone putty through boundary sliding of individual grains along inter-granular shear planes and individual grain rotations.*

érosion, transport et dépôt). Le lit sédimentaire constitué de grains de sable fin et saturé en eau est homogène et peut se déformer par localisation ou diffusion de la déformation via des plans de cisaillements intergranulaires (***Hamilton et al., 1968; Oda & Konishi, 1974; Owen, 1987 ; Bestmann & Prior, 2003***). Les écoulements de silicone produisent de la déformation interne au lit sédimentaire et du transport basal (i.e. transport sous-glaciaire) en raison du couplage entre la calotte de silicone et le lit sédimentaire (**Figure 2.7**). Les écoulements d'eau pressurisée, au sein de systèmes de drainage chenalisés et distribués, produisent des processus d'érosion, de transport et de dépôt de grains de sable en raison du couplage entre l'eau et le lit sédimentaire.

Le dimensionnement et le choix des matériaux du modèle analogique ayant été effectués afin de simuler et observer[12] ces processus fondamentaux, le dimensionnement dynamique classique n'est pas respecté. En effet malgré, la conservation des rapports de densité entre les systèmes glace-eau-sédiments et silicone-eau-sable, l'inégalité des rapports de forces visqueuses entre les systèmes naturels et expérimentaux est notamment assumée (voir Chapitre II - §2.4.2 pour plus de détails).

[12] La gomme de silicone est transparente permettant ainsi l'observation des processus de déformation, d'érosion, de transport et de dépôt le long de l'interface basale et possède une viscosité permettant l'initiation de déplacements significatifs à l'échelle d'une expérience de 60 minutes.

Un dimensionnement – dit à posteriori – a donc été réalisé et implique que les grandeurs physiques du modèle analogique régissant les processus fondamentaux énoncés ci-dessus soient définies de sorte que les ratios entre (1) la vitesse d'écoulement de la calotte et la vitesse d'incision des structures chenalisées sous-glaciaires (***Lelandais et al., 2016***) et (2) la longueur d'onde des bedforms et l'épaisseur de la calotte (***Vérité et al., 2021***) soient identiques dans la nature et dans le modèle analogique (**Table 2.3**) :

$$Ratio\ de\ dimensionnement\ n°1 : \frac{V_{cap\ margin}}{V_{incision}}$$

$$Ratio\ de\ dimensionnement\ n°2 : \frac{\lambda_{bedform}}{h_{cap}}$$

Où, $V_{cap\ margin}$ est la vitesse d'écoulement de la marge de la calotte (m/y), $V_{incision}$ est la vitesse d'incision des chenaux, $\lambda_{bedform}$ est la longueur d'onde entre les bedforms (de type ribbed bedforms) et h_{cap} est la hauteur de la calotte. Cette approche à postériori consiste ainsi à dimensionner le modèle expérimental en utilisant les grandeurs physiques contrôlant les interactions mécaniques de base entre un système hydrologique, un lit sédimentaire érodable et déformable et une calotte visqueuse responsables de la formation des bedforms sous-glaciaires, dans la nature comme dans l'expérience.

Table 2.3*. Compilation of physical dimensions from which are calculated ranges of values of scaling ratios.*

		Flow velocity of cap margins $V_{cap\ margin}$ **(m/y)**	**Incision rate of channels** $V_{incision}$ **(m/y)**	**Scaling ratio interval**	**References**
Scaling ratio n°1	Experimental	3.15×10^5 to 3.15×10^6	3.15×10^1 to 6.3×10^2	0.5 to 100	***Lelandais et al., 2016*** ***Lelandais, 2018***
	Natural	10^{-1} to 10^3	10^{-2} to 5×10^0	0.02 to 100000	
		Bedform wavelength $\lambda_{bedform}$ **(m)**	**Cap thickness** H_{cap} **(m)**	**Scaling ratio interval**	**References**
Scaling ratio n°2	Experimental	5×10^{-3} to 2.5×10^{-2}	5×10^{-3} to 2×10^{-2}	0.25 to 5	***Vérité et al., 2021***
	Natural	5×10^1 to 6×10^3	10^{-3} to 2×10^{-2}	0.02 to 12	***Dunlop & Clark, 2006*** ***Sergienko & Hindmarsh, 2013***

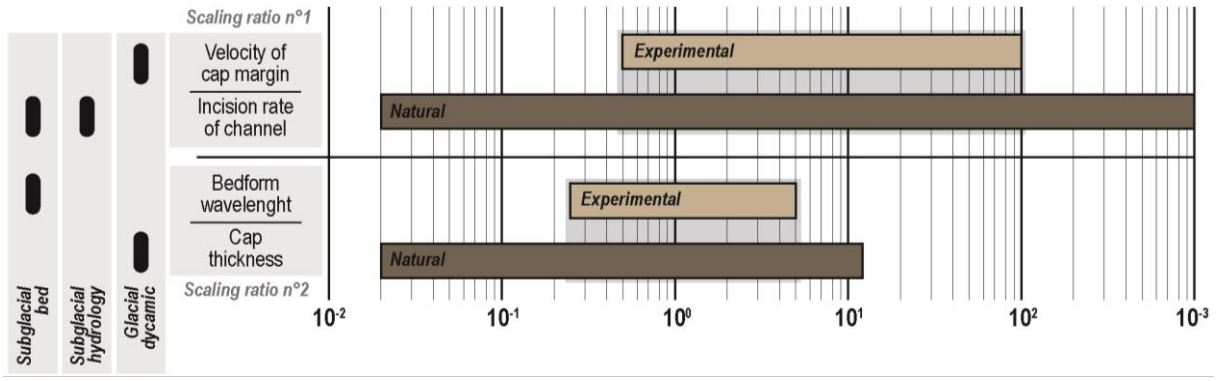

Figure 2.8. *Schematic representation of a-posteriori scaling principle of experimental model. The experimental device is scaled according to the scaling ratio n°1 and n°2 (**Table 2.3**) to take into account the intimate relationships between the glacial dynamics, subglacial hydrology and subglacial bed, from which derive subglacial landform development. Light-brown rectangles illustrate fields of validity for experimental scaling ratios, dark-brown rectangles illustrate fields of validity for natural scaling ratios and light-grey rectangles define the range of natural settings that are reproducible experimentally.*

2.4.2. Limites

Contrairement à la glace, la gomme de silicone est un fluide Newtonien, isotrope et imperméable. Dans les conditions expérimentales utilisées pour ce travail – entre 15 et 20°C et à pression atmosphérique – sa viscosité est indépendante de la température et de la pression, elle ne peut pas fondre et l'eau qui sature la lit sédimentaire ne peut pas congeler. Ainsi, (i) les processus naturels qui dépendent de la température dans les systèmes glaciaires, tels que la diminution de la viscosité de la glace quand la température augmente, la production interne d'eau de fonte, la fusion de la glace par cisaillement, la fonte ou la congélation du lit sédimentaire, et (ii) les transferts de matière entre la calotte et le substrat, ne sont pas reproduits dans le modèle analogique. Bien que les processus thermomécaniques soient fondamentaux dans les environnements sous-glaciaires et permettent notamment d'expliquer l'auto-organisation des fortes vitesses d'écoulement de la glace au sein des fleuves de glace (***Payne & Dongelmans, 1997 ; Hindmarsh, 2009***), ces derniers sont considérés comme secondaires et non reproduits dans le modèle analogique. En effet, l'une des conséquences des processus thermomécaniques (i.e. processus secondaires) au sein des environnements sous-glaciaires est de permettre ou non la production in-situ d'eau de fonte, induisant des variabilités spatio-temporelles de couplage/découplage glace-sédiments, de processus de transfert de sédiments et de vitesses d'écoulement de la glace (i.e. processus primaires). Dans le modèle, il est considéré que le système d'injection générant la circulation d'eau de fonte dans le lit sédimentaire et le long de l'interface basale

permet de simuler un système hydrologique sous-glaciaire simplifié reproduisant ces processus primaires malgré l'absence de processus thermomécaniques.

Alors que la dynamique d'écoulement de la glace dans la nature est fondamentalement modulée par un bilan de masse entre les processus d'accumulation et d'ablation (***Sudgen & John, 1976***), le volume de gomme de silicone reste constant durant une expérience et aucun de ces processus n'est reproduit. Comme mentionné ci-dessus, la dynamique de circulation d'eau le long de l'interface permet d'initier l'écoulement de la silicone au sein du modèle analogique, permettant de rendre négligeable l'impact de la non-reproduction des processus d'accumulation et d'ablation.

Dans les gammes de vitesses du modèle expérimental, le caractère Newtonien et isotrope de la gomme de silicone ne permet de reproduire ni les processus rhéofluidifiants, ni la déformation cassante qui peuvent se produire dans la glace (Chapitre I - Partie A §1.1).

Par conséquent, à gradients de contrainte équivalents, les gradients de vitesse reproduits par l'écoulement d'une calotte de silicone seront plus faibles que ceux produits par l'écoulement d'une calotte glaciaire. La capacité à localiser la déformation et à générer de forts gradients de vitesse est particulièrement importante au niveau des marges cisaillantes des fleuves de glace, où les forces de friction latérale (Chapitre I – Partie A §1.2.2) produites entre des glaces s'écoulant à de fortes (10^3 m/an) et de faibles vitesses (< 10^1 m/an) accommodent fréquemment plus de 50 % des forces motrices (***Echelmeyer et al., 1994; Raymond et al., 2001 ; Schoof, 2004***). Ainsi, la largeur des bandes de cisaillement bordant les couloirs d'écoulement rapide de la silicone sera surdimensionnée par rapport à la largeur des bandes des marges cisaillantes de fleuves de glace (**Figure 2.9**).

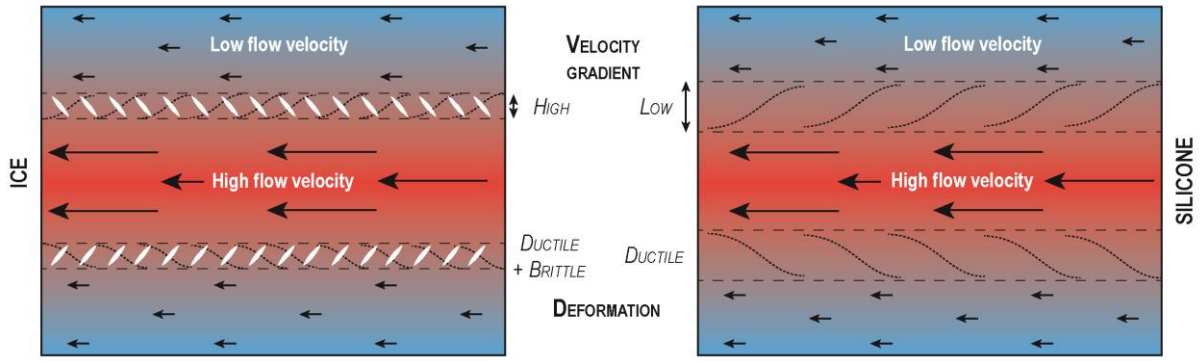

Figure 2.9. *Schematic representation of mechanical differences (i.e. velocity gradient and deformation type) between ice and silicone responsible for limitations in the experimental model. Unlike ice, the silicone putty used in the experimental model do not allow the reproduction of high velocity gradients and therefore narrow shear bands (delimited by black dotted lines) because of the lack of shear softening) and brittle deformation (i.e. crevasses in white lines), but only ductile deformation (i.e. undulating black lines).*

L'utilisation de l'eau pour la simulation de l'eau de fonte sous-glaciaire induit également une des limites majeures du dimensionnement puisque les rapports de viscosité entre les matériaux utilisés pour simuler la calotte – la glace dans la nature ($\eta_i = 10 \times 10^{13}$ Pa/s) et la silicone dans le modèle analogique ($\eta_{sil} = 5 \times 10^4$ Pa/s), et le fluide basal – l'eau dans les deux cas ($\eta_w = 1 \times 10^{-3}$ Pa/s) – ne sont pas identiques. Ainsi, puisque le fluide basal utilisé dans le modèle analogique est proportionnellement trop visqueux, les dimensions des structures de drainage chenalisées reproduites dans les expériences sont surdimensionnées par rapport à celles produites dans les systèmes naturels.

Le transport par charriage à la surface de la calotte de silicone (transport supra-glaciaire) ou par incorporation (transport intra-glaciaire) ne sont pas reproduits.

3. Analyse morphométrique des bedforms sous-glaciaires

Afin de pouvoir comparer les bedforms sous-glaciaires et les bedforms expérimentaux, le développement d'une nouvelle analyse morphométrique basée sur des paramètres de forme non-dimensionnés a pour but de :

- (i) confirmer la similitude morphologique entre les objets naturels et expérimentaux – le saut d'échelle entre leurs dimensions respectives – et ainsi démontrer la pertinence de l'utilisation du modèle analogique,
- (ii) suivre l'évolution morphologique des bedforms au cours du temps dans les expériences afin de reconstruire l'évolution morphologique des bedforms cartographiés dans la nature,
- (iii) déterminer les relations entre les caractéristiques morphologiques des bedforms et les dynamiques d'écoulement de la glace et de l'eau de fonte responsables de leur formation,
- (iv) caractériser la distribution statistique des formes des bedforms afin d'explorer la pertinence des classifications classiques basées sur des critères morphologiques.

3.1. État de l'art sur l'analyse morphométrique des bedforms

Les caractéristiques morphologiques des bedforms, qu'ils soient glaciaires, éoliens ou subaquatiques, sont particulièrement étudiées car elles permettent (i) dans les environnements actifs actuels, d'établir des relations entre la forme des bedforms et la dynamique d'écoulement du fluide (glace, vent ou eau), donc (ii) dans les paléo-environnements, de reconstruire la dynamique passée du fluide à partir de la forme des bedforms.

Ainsi, la compréhension des relations entre la dynamique des fluides et la dynamique d'évolution des bedforms s'effectue notamment au travers d'études morphométriques quantitatives fines. Ces études morphométriques s'attachent essentiellement à étudier les dimensions et l'organisation spatiale des bedforms, et plus rarement la forme de leur contour et de leur ligne de crête (**Table 2.4**).

Les bedforms sous-glaciaires sont classiquement catégorisés en fonction de leurs dimensions, de leur orientation par rapport à la direction de déplacement de la glace (i.e. communément décrite comme la direction d'écoulement) et de leur forme. Afin de quantifier la relation entre la forme d'un bedform et ses dimensions, ***Hollingworth (1931)*** défini le ratio 'longueur/largeur' ('*length/width'*, l/w)

Table 2.4. *Synthesis of morphometric parameters used to characterize quantitatively individual bedform dimensions, bedform field patterns and the shape of bedform contour and crest line, whether they are subglacial, aeolian or subaqueous. Note that the shape of bedform contours and crest lines are largely understudied.*

		BEDFORM DIMENSIONS									**BEDFORM FIELD PATTERNS**			**SHAPE OF BEDFORM CONTOURS**					**SHAPE OF CREST LINES**		
		Length	**Width**	**Elongation** or **Length : Width**	**Amplitude** or **Height**	**Height : Length** (or aspect ratio)	**Area**	**Perimeter**	**Volume**	**Slopes**	**Orientation**	**Wavelength** (or spacing)	**Density**	**Circularity**	**Compactness**	**Space filling**	**Shape factor**	**Asymmetry**	**Curvature / Sinuosity**	**Roundness)**	**Tip angle**
Glacial bedforms	***King, 1982***	●		●			●					●	●								
	Knight, 1997	●	●	●	●						●										
	Burgess, 2003						●	●				●		●	●		●				
	Dunlop & Clark, 2006	●	●		●							●									
	Clark et al., 2009	●	●	●																	
	Hess & Briner, 2009	●	●	●	●						●										
	Spagnolo et al., 2010	●	●													●		●			
	Stokes et al., 2013a	●	●	●								●						●			
	Spagnolo et al., 2014	●	●	●	●						●	●									
	Dowling et al., 2015	●	●	●	●		●				●										
	Yu et al., 2015				●		●		●												
	Ely et al., 2016	●	●	●																	
	Jorge & Brennand, 2017	●	●	●							●										
	Ojala et al., 2019	●	●		●		●			●											●
	Ojala et al., 2021	●	●		●					●											●
Aeolian bedforms	***Lancaster, 1988***				●							●									
	Dong et al., 2000	●	●		●		●		●		●										
	Bishop, 2001	●	●	●	●					●	●	●									
	Kleinhans et al, 2002	●			●				●			●									
	Ojeda et al., 2005						●			●											
	Kiss et al., 2009	●	●		●		●	●											●	●	
	Bullard et al., 2011				●				●												
	Zhang et al., 2012	●	●		●																
	du Pont et al., 2014				●						●	●									
	Vaz et al., 2015	●									●										
	Telfer et al., 2015				●							●									
	Hugenholtz & Barchyn, 2017	●	●	●	●							●									
	Cornwall et al., 2018	●								●			●								
	Day & Kocurek, 2018											●	●								
	Bhadra et al., 2019	●			●		●		●												
	Goudie et al., 2021		●		●								●								
Subaqueous bedforms	***Castello & Southard, 1981***	●			●																
	Amos & King, 1984	●			●													●			
	Ashley, 1990		●			●						●									
	Carling, 1999	●			●	●				●		●									
	Duffy, 2012	●			●						●							●			
	Normandeau et al., 2016				●					●		●						●			
	Schnyder et al., 2018		●		●					●	●	●						●			
	Venditti et al., 2019	●	●		●	●															
	Lu et al., 2021	●	●		●	●					●										
	Kola et al., 2021	●			●					●											

sur des drumlins, avant que de nombreuses autres études ne normalisent son utilisation (***Reed et al., 1962 ; Vernon, 1966 ; Embleton & King, 1968; Trenhaile, 1971***). Puisque l'axe long des drumlins a été interprété comme allongé parallèlement à la direction de déplacement de la glace (***Doornkamp & King, 1971; Mills, 1987; Rose, 1987***), le ratio 'l/w' représente le ratio d'élongation ('*elongation ratio*') pour les différentes catégories de linéations sous-glaciaires, i.e. drumlins, flutes et MSGLs (***Boyce and Eyles, 1991; Knight, 1997; O Cofaigh et al., 2002; Stokes and Clark, 2002; Briner, 2007; Clark et al., 2009; Dowling et al., 2015***). Le ratio 'l/w' a également été utilisé afin de différencier morphométriquement plusieurs sous-catégories de ribbed bedforms : '*ribbed/Rogen moraines*', '*mega-ribs*' et '*traction ribs*' (***Dunlop & Clark, 2006 ; Greenwood & Kleman, 2010 ; Stokes et al., 2016)***, qui – à la différence des linéations – sont décrits comme allongés perpendiculairement à la direction de déplacement de la glace (***Lundqvist et al., 1989***).

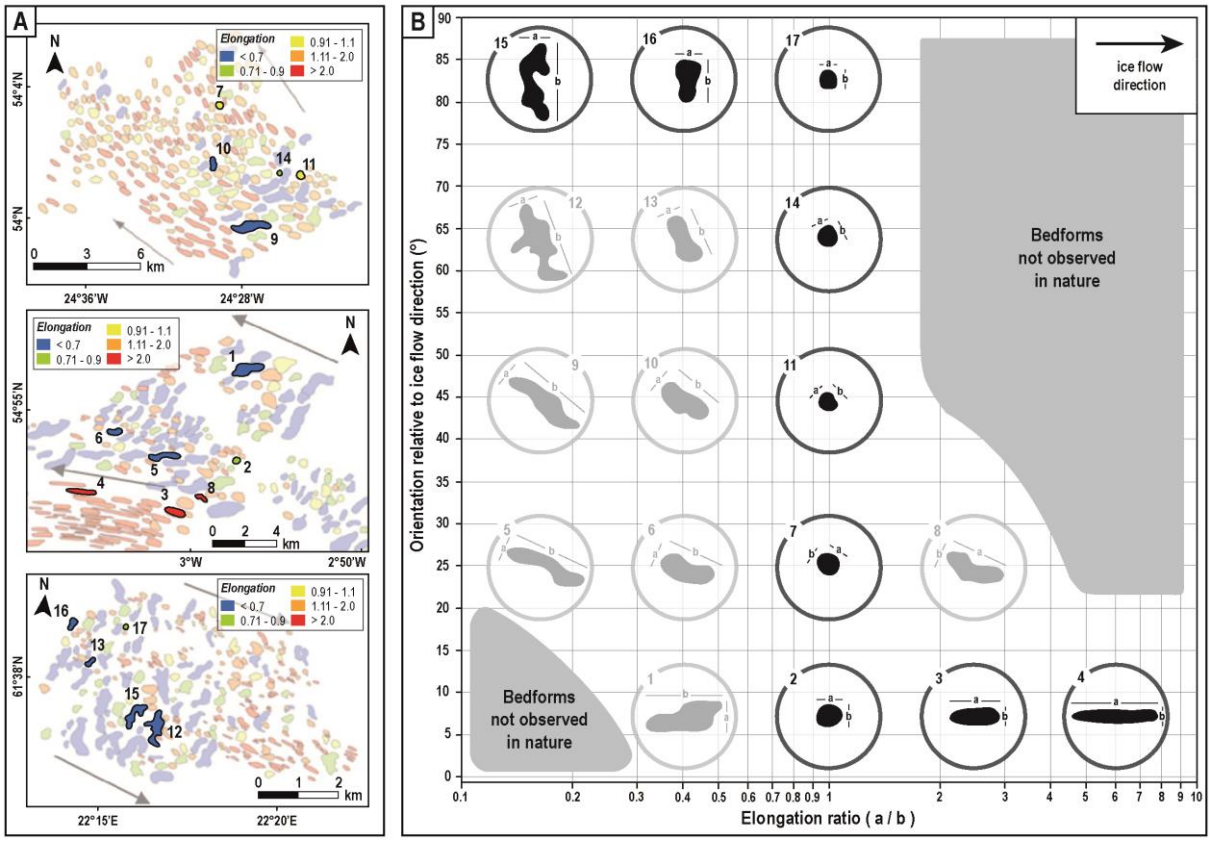

Figure 2.10. *(A) Contoured bedforms redrawn from* ***Ely et al. (2016 – Fig. 10)***. *Ribbed (a/b < 0.7), circular (a/b ~ 1) and streamlined bedforms (a/b > 2) have been defined by* ***Ely et al. (2016)*** *according to their elongation ratio. (B) Position of several bedforms extracted from Ely's maps in a graph displaying the bedform orientation relative to the local flow direction and the elongation ratio. Note that several bedforms mapped as ribbed bedforms (grey circles n°1, 5, 6, 9, 10, 12, 13) have a long axis that is not oriented at 90° to the direction and does not correspond to the true across-ice length as defined by* ***Ely et al. (2016)***. *Similarly, bedforms mapped as streamlined bedforms (grey circle n°8) are neither rectilinear nor parallel to the flow direction.*

Afin d'intégrer dans une unique étude morphométrique plusieurs catégories de bedforms ayant des orientations et des degrés d'allongement distincts par rapport à la direction de déplacement de la glace (i.e. ribbed bedforms, linéations, bedforms circulaires), ***Ely et al. (2016)*** ont redéfini le ratio d'élongation comme le rapport entre l'axe '*a*' ('*down-ice length*') et l'axe '*b*' ('*across-ice length*') du bedform, respectivement parallèle et transverse à la direction de déplacement de la glace. Ce ratio d'élongation '*a/b*' implique que l'orientation des bedforms par rapport à la direction de déplacement de la glace, parallèle ou transverse, soit ainsi connue ; ignorant ainsi la possibilité que les bedforms puissent être obliques. Dans le cadre de cette thèse, la réalisation d'une analyse complémentaire de certains bedforms cartographiés et étudiés par ***Ely et al. (2016)*** démontre que de nombreux bedforms ne peuvent pas être considérés comme transverses ou parallèles à la direction de déplacement de la glace, induisant un biais dans la caractérisation morphométrique des bedforms (**Figure 2.10**). En effet, dans leur étude, de nombreux bedforms considérés comme des ribbed bedforms (i.e. $a/b < 0.7$) – car ils ne correspondent ni à des bedforms circulaires ni à des linéations – ne sont en réalité pas purement transverse à la direction de déplacement de la glace (**Figure 2.10** – bedforms n°1, 5, 6, 9, 10, 12, 13). D'autres bedforms définis comme des linéations (i.e. $a/b > 2$) ne sont en réalité ni rectiligne ni parallèle à la direction de déplacement de la glace (**Figure 2.10** – bedform n°8).

Bien que certaines études (***Dunlop & Clark, 2006 ; Wagner, 2014***) aient démontré l'existence d'une forte variabilité de forme et de sinuosité au sein d'une seule et même classe de bedforms (Chapitre I – Partie B §1), aucun critère morphométrique courant la littérature glaciaire ne permet de définir quantitativement ces variabilités de forme de contours et de lignes de crête (**Table 2.4**). En effet, la longueur, la largeur et le ratio d'élongation ne permettent par exemple pas de distinguer la forme d'une ribbed moraine au contour ondulé de celle d'un drumlin de forme elliptique qui possèderait les mêmes rapports de dimensions (**Figure 2.11**). Sans en interpréter la signification en termes de dynamique d'écoulement de la glace, ***Burgess et al. (2003)*** sont les seuls à avoir étudié quantitativement la complexité de forme des ribbed bedforms à partir des paramètres de forme non-dimensionnés : la compacité ('*compactness*'), la circularité ('*circularity*') et le facteur de forme ('*shape factor'*)[13],

[13] Dans l'article de Burgess et al. (2003), avec A l'aire du bedform, P le périmètre du bedform et Pc le périmètre d'un cercle de même aire que le bedform :
- la compacité est définie comme $Compacité = P^2/(4 \times \pi \times A)$

antérieurement utilisés pour étudier la forme des bassins versants et des grains sédimentaires (***Folk, 1968 ; Moellering & Rayner, 1979***). Similairement, ***Spagnolo et al. (2010)*** et ***Stokes et al. (2013a)*** ont calculé l'asymétrie de drumlins et de MSGLs pour mettre en évidence les variations de forme du contour de ces bedforms.

Pour résumer, les paramètres de forme actuellement utilisés par les géomorphologues glaciaires – longueur, largeur et ratio d'élongation – ne permettent pas de quantifier la complexité des bedforms (sinuosité, orientation) dissimulant une partie du spectre de la variabilité morphologique des bedforms sous-glaciaires (**Figure 2.11**). En effet, ils ne rendent compte que des dimensions, des proportions et du degré d'allongement des bedforms sous-glaciaires, admettant des aprioris sur l'orientation des bedforms par rapport à la direction de déplacement de la glace (supposément transverse ou parallèle) et ignorant l'importance de leurs complexités et variabilités de forme. Afin de quantifier les variabilités de forme des contours, des lignes de crête et d'orientation des bedforms, d'autres critères morphométriques que ceux actuellement utilisés doivent être développés.

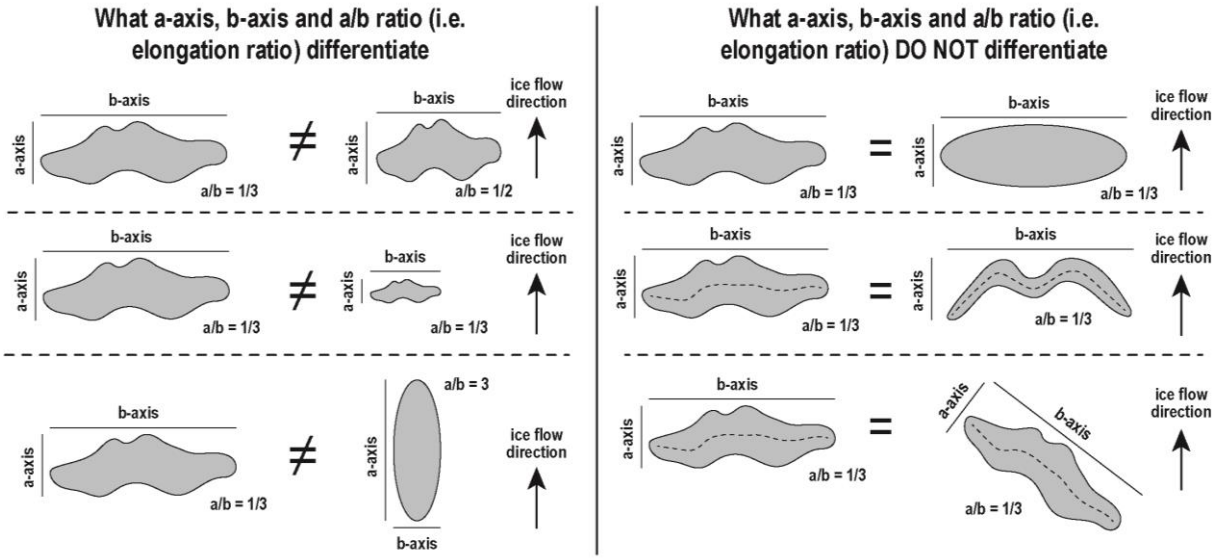

Figure 2.11. *Schematic illustration of utilities and limitations of morphometric parameters currently used in glacial geomorphology: a-axis (supposedly parallel to the ice flow direction), b-axis (supposedly transverse to the ice flow direction) and elongation ratio (a/b). These morphometric parameters do not allow to quantify variabilities in bedform and crest line shapes and in bedform orientations.*

- la circularité est définie comme $Circularité = (4 \times A)/P^2$
- l'indice de forme est défini comme $Indice\ de\ forme = (P/Pc)/100$

3.2. Protocole d'analyse morphométrique et nouveaux paramètres morphométriques

3.2.1. Extraction des grandeurs dimensionnées de base

A partir des contours de bedforms sous-glaciaires – expérimentaux et naturels – digitalisés manuellement sur le logiciel SIG © *ArcMap 10.8*, leurs périmètres (P), leurs aires (A) et leurs amplitudes sont automatiquement mesurés. En utilisant une boite à outils permettant de calculer des rectangles d'emprise minimale ('*Minimum Bounding Rectangle*'), les longueurs de l'axe long et de l'axe court ainsi que l'orientation de chaque bedform par rapport au Nord sont mesurées automatiquement. La longueur curviligne de chaque ligne de crête ('*curvilinear length*') et la distance entre ses deux extrémités ('*straight length*') sont également mesurées avec un rectangle d'emprise minimale (**Figure 2.12**). Une représentation schématique du protocole d'analyse morphométrique réalisé sous *ArcMap 10.*8 est proposée dans le Chapitre III – Partie B §3 – Supplementary Data 1.

3.2.2. Définition et calcul de nouveaux paramètres morphométriques

Afin de quantifier la variabilité des bedforms dans la forme de leurs contours et de leurs lignes de crête, dans leur orientation et dans leur allongement, qu'ils soient associés à la dynamique d'écoulement de la glace (e.g. ribbed bedforms, linéations, bedforms circulaires) ou de l'eau de fonte (e.g. hummocks, murtoos), trois paramètres de forme non-dimensionnés ont été développés pour cette étude : l'indice de circularité (I_{CIR}), l'indice de sinuosité (I_{SIN}) et l'indice d'élongation orientée (I_{OE}) (voir **Table 2.5**).

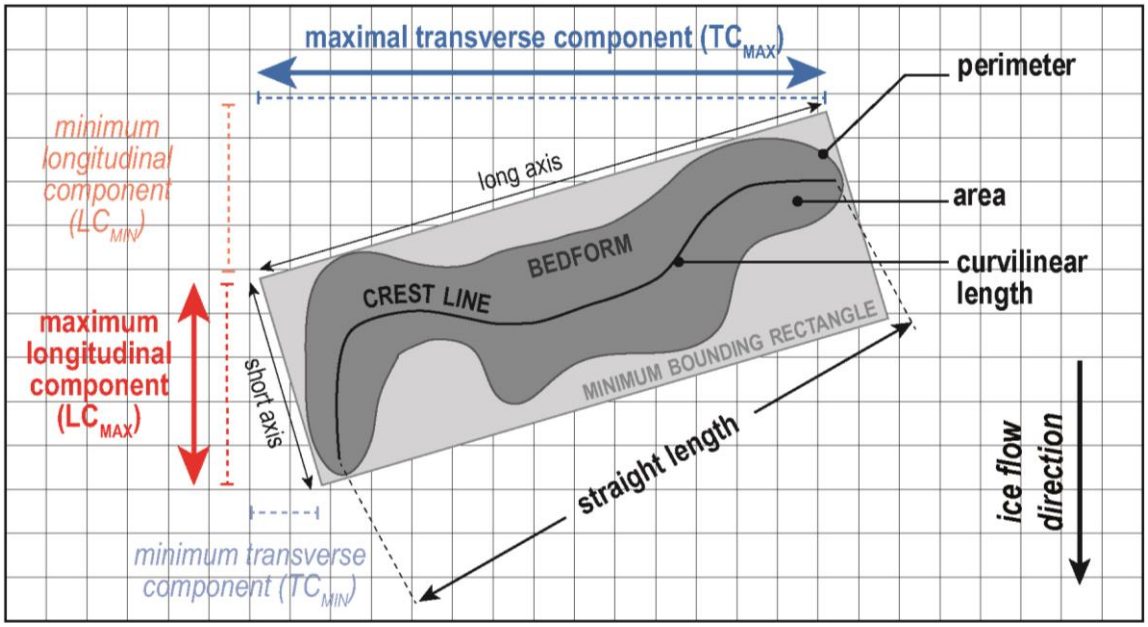

Figure 2.12. *Measured quantities for the calculation of dimensionless indexes: oriented elongation index, circularity index and sinuosity index (see formula in* ***Table 2.5****).*

***Table 2.5**. Description of morphometric indices used in this thesis.*

Shape indices	Formula	Signification	Range of values & Typical values
(A) Circularity index (I_{CIR})	$I_{CIR} = \frac{4 \times A \times \pi}{P^2}$	Compare the perimeter (P) of a contour of given area (A) with the perimeter of a circle of identical area (***Burgess et al., 2003***).	**I_{CIR} : [0 ; 1]** I_{CIR} = 0 : strongly non-circular contour I_{CIR} > 0.80 : highly circular contour I_{CIR} = 1 : perfectly circular contour
(B) Sinuosity index (I_{SIN})	$I_{SIN} = \frac{\frac{Curvilinear\ length}{Straight\ length} - 1}{\sqrt{5} - 1}$	Give the sinuosity ratio of the crestline (i.e. ratio between the curvilinear length of the crest line and its linear length; ***Schumm, 1963***), normalized to the sinuosity ratio of an equilateral triangle (√5) (***Vérité et al., 2022***).	**I_{SIN} : [0 ; +∞]** I_{SIN} = 0 : perfectly rectilinear crestline I_{SIN} < 0.10 : linear crestline I_{SIN} > 0.10 : sinuous crestline I_{SIN} = 1 : equilateral triangular crestline $I_{SIN} \rightarrow +\infty$: strongly sinuous crestline
(C) Orientated elongation index (I_{OE})	$I_{OE} = \log_{10}(\frac{LC_{MAX}}{TC_{MAX}})$	Define the ratio between the maximal longitudinal (i.e. along-ice flow; LC_{MAX}) and the maximal transverse (i.e. across-ice flow; TC_{MAX}) components of a bedforms, normalized to a logarithmic scale.	**I_{OE} : [-∞ ; +∞]** $I_{OE} \leq$ - 0.17 : $TC_{MAX} \geq 1.5 \times LC_{MAX}$ elongated transverse to the flow direction - 0.17 ≤ $I_{OE} \leq$ + 0.17 : $TC_{MAX} \sim LC_{MAX}$ elongated equally transverse and parallel to the flow direction $I_{OE} \geq$ + 0.17 : $LC_{MAX} \geq 1.5 \times TC_{MAX}$ elongated parallel to the flow direction $I_{OE} \geq$ + 0.60 : $LC_{MAX} \geq 4 \times TC_{MAX}$ strongly elongated parallel to the flow direction

Quantification de la forme du contour : indice de circularité (I_{CIR})

L'indice de circularité, dérivé du critère morphométrique non-dimensionné défini comme 'circulatory ratio' par ***Horton (1945)*** afin d'étudier la forme des bassins versants, permet de définir le degré de circularité du contour (matérialisé par son périmètre P) d'un bedform par rapport à un cercle de même aire A (**Table 2.5A**).

Quantification de la forme de la ligne de crête : indice de sinuosité (I_{SIN})

Pour chaque bedform, l'indice de sinuosité définit le degré de sinuosité de la ligne de crête à partir du rapport entre sa longueur curviligne ('*curvilinear length*') et la distance entre ses deux extrémités ('*straight length*'), tel que le rapport de sinuosité est classiquement défini pour les rivières. Dans cette étude, afin de calculer l'indice de sinuosité, ce ratio de sinuosité est normalisé par rapport au ratio de sinuosité d'un triangle équilatéral (i.e. ratio de la longueur cumulée de 2 cotés par rapport au 3ème coté, sinuosité = √5). Ce choix repose sur le fait que, parmi les différents bedforms sous-glaciaires inventoriés

dans le Chapitre I – Partie B, les bedforms sous-glaciaires dont la ligne de crête est qualitativement la plus sinueuse sont les murtoos, bedforms dont la forme est approximable à celle d'un triangle équilatéral. La normalisation du ratio de sinuosité permet également d'étaler les valeurs de l'indice de sinuosité en ayant comme référentiel la valeur 0, comme pour les deux autres paramètres de forme (**Table 2.5B**).

Quantification de l'allongement et de l'orientation : indice d'élongation orientée (I_{OE})

Afin de décrire la diversité de degré d'allongement et d'orientation des bedforms sous-glaciaires, l'indice d'élongation orientée (I_{OE}) a été défini pour des bedforms qui – à l'échelle d'une zone d'étude – sont supposément associés à une seule configuration d'écoulement de la glace, n'incluant donc pas superpositions de multiples phases d'écoulements (type '*time transgressive*'). En ne prenant comme unique a-priori que l'orientation des bedforms de type 'linéations', supposément parallèles à la direction de déplacement de la glace, l'échantillonnage de linéations glaciaires au sein d'une maille hexagonale de 25 km² permet par interpolation de reconstruire les trajectoires de déplacement de la glace à l'échelle d'une zone d'étude constituée d'une grande variété de bedforms sous-glaciaires (**Figure 2.13**). A partir de l'orientation de chaque bedform par rapport à la direction locale de déplacement, les composantes transverses (i.e. perpendiculaire à la direction de déplacement de la glace) et longitudinales (i.e. parallèle à la direction de déplacement de la glace) de son axe long et de son axe court sont calculées par trigonométrie (**Figure 2.12**). À partir du rapport entre les composantes transverses (TC_{MAX}) et longitudinales (LC_{MAX}) maximales, l'indice d'élongation orientée (I_{OE}) est calculé et permet de combiner les informations sur l'orientation et l'élongation des bedforms sous-glaciaires (**Table 2.5C**).

Ainsi, indépendamment de différences de dimensions, ces trois indices morphométriques non-dimensionnés permettent de différencier et de caractériser la forme du contour (I_{CIR}) et de la ligne de crête de chaque bedform (I_{SIN}), ainsi que son degré d'allongement transverse et/ou longitudinal modulé par son orientation (I_{OE}). L'indice d'élongation orientée (I_{OE}) permet notamment d'éviter tout biais généré par l'utilisation du ratio d'élongation a/b, en ne présupposant que de l'orientation des bedforms de type « linéations » par rapport à la direction de déplacement.

Ponctuellement et de façon non automatisée, des mesures de longueurs d'onde – mesurées de crêtes à crêtes entre chaque bedforms – et de pentes des flancs amont et aval des bedforms ont également été réalisées.

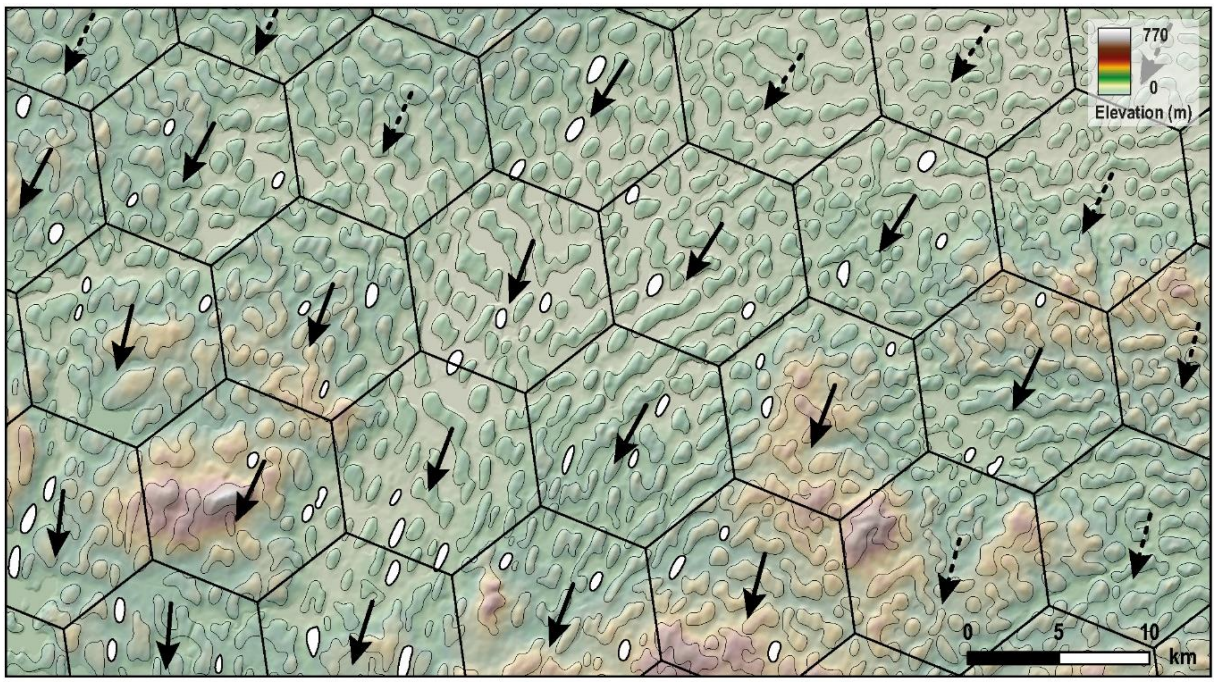

***Figure 2.13**. Reconstruction of local ice flow directions (solid black arrows) from samples of streamlined bedforms (white polygons) in a grid of 25-km² hexagons, based on the assumption that subglacial bedforms are associated to a unique configuration of ice flow trajectories. Where streamlined bedforms are absent, the average flow direction is extrapolated (dotted black arrows) from surrounding streamlined bedforms.*

CHAPITRE III

LES BEDFORMS ASSOCIES A LA DYNAMIQUE DE LA GLACE : PROCESSUS DE FORMATION ET CONTINUITES MORPHOLOGIQUE ET GENETIQUE

Introduction

Les possibilités d'observation de bedforms actifs sous les calottes glaciaires actuelles sont limitées dans l'espace et dans le temps ; cela rend difficile l'exploration directe des interactions entre leurs caractéristiques morphologiques, leurs processus de formation et l'écoulement de la glace (***O Cofaigh et al., 2002 ; King et al., 2007 ; Smith et al., 2007 ; Larter et al., 2009 ; Franke et al., 2020***). Pour chaque type de bedform sous-glaciaire (i.e. drumlins, MSGLs, ribbed bedforms, bedforms circulaires), des modèles de formation ont donc été développés à partir d'observations sédimentologiques, structurales et morphologiques sur les paléo-bedforms, interprétant une variabilité de dynamiques d'écoulement de glace (**Figure 1.19**). Sur la base de ces variabilités de dynamiques d'écoulement de la glace, la distribution spatiale et la diversité de forme des bedforms sous-glaciaires ont été utilisées pour proposer des modèles d'assemblages morphologiques ('*landform assemblages*') qui seraient caractéristiques de chaque type d'environnement sous-glaciaire (**Figure 1.18**). Les études sédimentologiques et les analyses morphométriques actuellement appliquées aux paléo-bedforms sous-glaciaires (Chapitre II - §3) permettent d'explorer leurs variabilités morphologiques et de discuter les processus à l'origine de leur formation ; cependant, elles restent insuffisantes pour établir le lien entre les variations spatio-temporelles de la dynamique d'écoulement de la glace, les interactions glace-eau-sédiments et l'évolution morphologique des bedforms.

Différents travaux de modélisation numérique ont permis d'identifier des grandeurs physiques (e.g. vitesse d'écoulement de la glace, épaisseur du lit sédimentaire, épaisseur du film d'eau basal, capacité de transport basal) mettant en relation la formation de ribbed bedforms, de drumlins et de MSGLs et les interactions entre la glace, l'eau et les sédiments sans explorer les variations spatio-temporelles de ces relations et l'évolution des caractéristiques morphométriques des bedforms sous-glaciaire (***Fowler & Chapwanya, 2014 ; Barchyn et al., 2016 ; Fannon et al., 2017 ; Fannon, 2020***). Des travaux de modélisation analogique ont quant à eux permis de quantifier certaines relations entre la dynamique des écoulements d'eau de fonte et la dynamique des fleuves de glace mais sans étudier le développement de bedforms sous glaciaires (***Lelandais et al., 2016, 2018 ; Lelandais, 2018***).

Récemment, en compilant et analysant près de 97 000 bedforms cartographiés en Scandinavie, en Grande-Bretagne, en Islande et au Canada, ***Ely et al.*** (***2016***) ont proposé l'existence d'un continuum morphométrique et spatial entre différents types de bedforms rectilignes et supposés a-priori transverses ou parallèles à la direction de déplacement de la glace : les ribbed bedforms, les bedforms circulaires, les drumlins et les MSGLs. Cette proposition est compatible avec l'hypothèse depuis longtemps émise sur l'existence d'un continuum d'évolution morphologique entre différents types de bedforms sous-glaciaires (e.g. ***Aario, 1977; Markgren & Lassila, 1980***) ; l'évolution de la géométrie des bedforms le long de ce continuum refléterait les variations de la vitesse d'écoulement de la glace (e.g. ***Boyce & Eyles, 1991; Hart, 1999; Hättestrand & Kleman, 1999; Stokes & Clark, 2002a; Briner, 2007; Stokes et al., 2013a; Zoet et al., 2021***). En revanche, de nombreux bedforms sous-glaciaires sinueux (i.e. complexes) et associés spatialement aux catégories de bedforms citées ci-dessus ne figurent pas dans ces compilations morphométriques. De plus, la possibilité que des bedforms puissent se développer de manière oblique par rapport à la direction de déplacement de la glace n'y est pas envisagée.

Les objectifs de ce Chapitre III sont donc (i) de déterminer si les bedforms sinueux peuvent être intégrés dans le continuum morphométrique proposé jusqu'à aujourd'hui, (ii) de tester l'hypothèse que des bedforms puissent se développer de manière oblique par rapport à la direction de déplacement de la glace et (iii) de déterminer si ce continuum morphométrique, enrichi par l'intégration de bedforms sinueux et obliques, peut être interprété comme un continuum génétique, c'est-à-dire intégré dans une théorie mécanique commune à l'ensemble des bedforms. Pour cela, je serai amené à discuter conjointement (i) les caractéristiques morphologiques des bedforms sous-glaciaires, (ii) les processus issus des interactions entre la glace, l'eau de fonte et les sédiments dont résultent ces bedforms et (iii) les variations spatio-temporelles de ces processus sous les calottes glaciaires. Ce chapitre se focalise sur les bedforms sous-glaciaires dont la formation est classiquement attribuée à la dynamique d'écoulement de la glace. Il s'organise en trois parties correspondant à trois articles scientifiques (un publié, un soumis et un en préparation).

- **Partie A. Processus de formation des ribbed bedforms : marqueurs de la déformation de la glace au sein des fleuves de glace (Article n°1)**

La première partie de ce chapitre étudie la relation entre la dynamique d'écoulement de la glace et les ribbed bedforms au travers de la comparaison entre bedforms expérimentaux et naturels. Cette étude met plus précisément en évidence les relations entre (i) les caractéristiques morphologiques des ribbed bedforms, (ii) les dynamiques d'écoulement et de déformation de la glace et des sédiments, notamment au niveau des marges latérales cisaillantes et des marges lobées des fleuves de glace, et (iii) les interactions glace-eau-sédiments responsables de la formation et de l'évolution des ribbed bedforms. J'y démontre en particulier que les ribbed bedforms se développent perpendiculairement à la direction de raccourcissement de la glace, qui peut être parallèle à sa direction de déplacement (sous les marges lobées), mais aussi oblique (sous les marges de cisaillement).

- **Partie B. Un continuum morphologique révélé derrière la diversité morphométrique des bedforms sous-glaciaires (Article n° 2)**

La seconde partie de ce chapitre explore les caractéristiques morphologiques de tous les bedforms sous-glaciaires associés à la dynamique d'écoulement de la glace via le développement d'une nouvelle approche d'analyse morphométrique, appliquée à 13 500 bedforms cartographiés le long de paléo-lits glaciaires des calottes Laurentide et Irlandaise. Cette seconde partie démontre l'existence d'un continuum morphologique et spatial entre (i) des bedforms circulaires, (ii) des ribbed bedforms linéaires, (iii) des linéations glaciaires (drumlins et MSGLs), et (iv) des bedforms sinueux de formes et d'orientations très variables. Ce continuum intègre la possibilité que certains bedforms puissent se développer de manière oblique par rapport à la direction de déplacement de la glace ; les bedforms sinueux y apparaissent comme des bedforms de transition, correspondant à un degré d'évolution intermédiaire, au sein d'un continuum d'évolution entre des ribbed bedforms et des linéations glaciaires.

- **Partie C. Un modèle d'évolution des bedforms contrôlé par les interactions glace-eau-sédiments et la déformation enregistrée dans les lits sédimentaires sous-glaciaires (Article n°3)**

La troisième partie de ce chapitre propose un nouveau modèle de continuum génétique entre les bedforms sous-glaciaires. A partir des résultats obtenus dans les Parties A & B et d'une compilation de ~250 000 bedforms sous-glaciaires cartographiés dans des environnements sous-glaciaires variés, cette partie explore les relations entre (i) le degré d'évolution des bedforms, (ii) la quantité et les directions de déformation accommodée par le lit sous-glaciaire, (iii) les interactions glace-eau-sédiments et (iv) les variations spatio-temporelles de vitesse d'écoulement de la glace, de déformabilité du lit sous-glaciaire et de circulations d'eau de fonte.

Partie A. Processus de formation des ribbed bedforms : marqueurs de la déformation de la glace au sein des fleuves de glace

Field of ribbed bedforms, Nunavut, Canada (© Google Earth – 60°34'N, 96°W)

1. Introduction

De précédentes études cartographiques et sédimentologiques réalisées sur des ribbed bedforms – terme regroupant ici les '*ribbed moraines',* les *'Rogen moraines'*, les '*mega-ribs*' et les '*traction ribs*' – observées le long de paléo-lits glaciaires ont mis en évidence une grande diversité de formes, de dimensions, de distribution spatiale et d'hypothèses de processus de formation (**Table 3.1**).

Malgré cette diversité d'hypothèses de formation – expliquée par la diversité de formes, de compositions sédimentaires et de contextes d'observation – un consensus tend à exister quant à leur association à l'écoulement de la glace. En effet, la déformation de sédiments sous-glaciaires en réponse à des contraintes cisaillantes basales générées sous de faibles vitesses de déplacement de la glace est souvent énoncée comme étant l'hypothèse de formation principale des ribbed bedforms (***Aylsworth &***

Table 3.1*. Synthesis of morphological characteristics, spatial distribution and formation hypotheses of ribbed bedforms (see Chapitre I – Partie 2 §1.2 for more details)*

● **MORPHOLOGICAL CHARACTERISTICS**					
Ribbed bedforms	***Length (l)***	***Width (w)***	***l/w***	***Height***	***Orientation***
○ *Ribbed/Rogen moraines (Dunlop & Clark, 2006)*	200-1000 m	100-400 m	2.5	10s m	Transverse
○ *Mega-ribs (Greenwood & Kleman, 2010)*	20-40 km	3-6 km	5.7	5-10 m	Transverse
○ *Traction ribs (Sergienko & Hindmarsh, 2013 ; Stokes et al., 2016)*	1-6 km	0.4-5 km	2.9	1-20 m	Transverse to oblique
● **SPATIAL DISTRIBUTION**					
○ Inner & slow-moving regions of ice sheets (ice dome)	*Aylsworth & Shilts (1989);Hättestrand & Kleman (1999); Greenwood & Kleman (2010); Stokes (2018)*				
○ Onset area of ice streams (transition cold-to-warm based ice)	*Bouchard (1989); Dyke et al.(1992); Hättestrand & Kleman (1999)*				
○ Sticky spots along ice stream trunks	*Dyke et al.(1992); Stokes & Clark (2003); Stokes et al. (2006, 2008) ; Stokes (2018)*				
○ Submarginal areas below stagnant ablation complexes	*Marich et al. (2005); Möller (2006, 2010)*				
● **HYPOTHESES OF FORMATION PROCESSES**					
○ Fracturation and extension of frozen beds along transitions from cold-to-warm based ice	*Hattestrand & Kleman (1999) ; Sarala (2006)*				
○ Melt-out deposition of sediment-rich and deformed ice layer	*Möller (2010)*				
○ Subglacial meltwater floods responsible for the formation of inverted erosional marks at the ice base, infilled by sediments	*Shaw (2002)*				
○ Deformation and erosion of subglacial sediments or pre-existing sedimentary mounds by the overriding flow of ice	*Shaw (1979) ; Bouchard (1989) ; Lundqvist (1989) ; Möller (2006); Stokes et al. (2008)*				
○ Deformation and erosion of subglacial sediments by the overriding flow of ice combined with erosion and deposition by glaciofluvial processes	*Linden et al. (2008) ; Fowler & Chapwanya (2014) ; Fannon et al. (2017)*				

Shilts, 1989; Dyke et al., 1992 ; Hättestrand & Kleman, 1999; Greenwood & Kleman, 2010; Stokes, 2018). Cependant, dans les reconstitutions paléoglaciaires classiques, la relation entre la géométrie des ribbed bedforms et les directions de déformation des sédiments et de la glace reste ambigüe, puisque les ribbed bedforms y sont généralement considérés comme simplement perpendiculaires à la direction de déplacement de la glace (***Dunlop & Clark, 2006 ; Trommelen et al., 2014***).

L'écoulement de la glace au sein des calottes glaciaires est largement contrôlé par la dynamique des fleuves de glace, qui sont associés à de fortes vitesses d'écoulement ('*ice streams*'). Bien que les ribbed bedforms soient communément associés à de faibles vitesses d'écoulement de la glace et ainsi généralement décrits comme des marqueurs des dômes de glace et des '*sticky spots'*, leur distribution spatiale à la base des calottes glaciaires – notamment aux niveaux des marges des fleuves de glace qui sont associés à de plus faibles vitesses d'écoulement – et leur processus de formation restent mal contraints. Alors qu'une grande variabilité de forme semble être observée au sein des ribbed bedforms, incluant notamment des *tractions ribs* dont les orientations sont considérées comme obliques par rapport à la direction de déplacement de la glace (***Stokes et al., 2016***), les relations entre leurs caractéristiques et évolutions morphologiques et la dynamique d'écoulement de la glace restent mal comprises.

Problématiques :

→ La grande variabilité morphologique des ribbed bedforms implique-t-elle nécessairement plusieurs processus de formation ? Quel(s) est (sont) ce(s) processus ?

→ Quelle est l'origine la diversité morphologique des ribbed bedforms ? Des ribbed bedforms peuvent-ils être oblique à la direction de déplacement de la glace ?

→ Par quoi est contrainte l'évolution morphologique des ribbed bedforms ?

→ Quelle est la distribution spatiale des ribbed bedforms sous les fleuves de glace ? Quelles sont les caractéristiques des systèmes de drainage associés ces environnements sous-glaciaires ?

2. Article n°1: Formation of ribbed bedforms below shear margins and lobes of palaeo-ice streams

Cette première partie fait donc l'objet d'un article publié dans la revue *The Cryosphere*.

The Cryosphere, 15, 2889–2916, 2021
https://doi.org/10.5194/tc-15-2889-2021

The Cryosphere Open Access EGU

Formation of ribbed bedforms below shear margins and lobes of palaeo-ice streams

Jean Vérité[1], Édouard Ravier[1], Olivier Bourgeois[2], Stéphane Pochat[2], Thomas Lelandais[1], Régis Mourgues[1], Christopher D. Clark[3], Paul Bessin[1], David Peigné[1], and Nigel Atkinson[4]

[1]Laboratoire de Planétologie et Géodynamique, UMR 6112, CNRS, Le Mans Université, Avenue Olivier Messiaen, 72085 Le Mans CEDEX 9, France
[2]Laboratoire de Planétologie et Géodynamique, UMR 6112, CNRS, Université de Nantes, 2 rue de la Houssinière, BP 92208, 44322 Nantes CEDEX 3, France
[3]Department of Geography, University of Sheffield, Sheffield, UK
[4]Alberta Geological Survey, 4th Floor Twin Atria Building, 4999-98 Ave., Edmonton, AB, T6B 2X3, Canada

Correspondence: Jean Vérité (jean.verite@univ-lemans.fr)

Received: 11 November 2020 – Discussion started: 21 November 2020
Revised: 28 May 2021 – Accepted: 3 June 2021 – Published: 28 June 2021

Abstract. Conceptual ice stream land systems derived from geomorphological and sedimentological observations provide constraints on ice–meltwater–till–bedrock interactions on palaeo-ice stream beds. Within these land systems, the spatial distribution and formation processes of ribbed bedforms remain unclear. We explore the conditions under which these bedforms may develop and their spatial organization with (i) an experimental model that reproduces the dynamics of ice streams and subglacial land systems and (ii) an analysis of the distribution of ribbed bedforms on selected examples of palaeo-ice stream beds of the Laurentide Ice Sheet. We find that a specific kind of ribbed bedform can develop subglacially through soft-bed deformation, where the ice flow undergoes lateral or longitudinal velocity gradients and the ice–bed interface is unlubricated; oblique ribbed bedforms develop beneath lateral shear margins, whereas transverse ribbed bedforms develop below frontal lobes. We infer that (i) ribbed bedforms strike orthogonally to the compressing axis of the horizontal strain ellipse of the ice surface and (ii) their development reveals distinctive types of subglacial drainage patterns: linked cavities below lateral shear margins and efficient meltwater channels below frontal lobes. These ribbed bedforms may act as convenient geomorphic markers to reconstruct lateral and frontal margins, constrain ice flow dynamics, and infer meltwater drainage characteristics of palaeo-ice streams.

1 Introduction

The dynamics of ice sheets is largely controlled by the activity of narrow corridors of fast-flowing ice, named ice streams (Paterson, 1994). In Antarctica, 10 % of the ice sheet is covered by ice streams and 90 % of the ice sheet is estimated to discharge through these corridors that flow at a few hundreds of $m\,yr^{-1}$ (Bamber et al., 2000). Studies on modern ice streams – through remote sensing, borehole observations and geophysical measurements – have improved our understanding of the influence of ice streams on the mass balance of ice sheets. Many investigations highlight the role of lateral shear margins and frontal lobes on the overall stress balance of ice streams and the importance of imparted drag, along with basal drag, in controlling flow speed and ice stream width and length (Engelhardt et al., 1990; Goldstein et al., 1993; Echelmeyer et al., 1994; Patterson, 1997; Tulaczyk et al., 2000; Raymond et al., 2001; Kyrke-Smith et al., 2014; Minchew and Joughin, 2020). A lack of knowledge remains however on the spatial and temporal evolution of basal conditions beneath ice streams (e.g. distribution of basal shear stresses, meltwater drainage patterns) and on the processes acting at the ice–bed interface during the formation of subglacial bedforms. This is because basal investigations into modern ice streams are restricted to punctual observations. Palaeoglaciology aims to fill this gap by using the geomorphological and sedimentological records of former ice

Published by Copernicus Publications on behalf of the European Geosciences Union.

stream beds. Based on this approach, conceptual models of ice stream land systems characterized by either synchronous or time-transgressive imprints have been developed (Dyke and Morris, 1988; Kleman and Borgström, 1996; Clark and Stokes, 2003).

Even though general models of ice stream land systems have now been established, the genesis of some landforms in these land systems remains under debate, notably its relation to ice dynamics and subglacial meltwater drainage. After mega-scale glacial lineations and drumlins, ribbed bedforms – subglacial periodic ridges that form transversely or obliquely to the ice flow direction – potentially represent some of the most conspicuous and ubiquitous landforms on palaeo-ice stream beds (Stokes, 2018). However, their distribution is not clearly accommodated in current ice stream land system models (Dyke et al., 1992; Stokes and Clark, 2001; Stokes et al., 2007). Their formation is attributed to (i) bed deformation (e.g. Boulton, 1987; Hättestrand and Kleman, 1999; Lindén et al., 2008), (ii) meltwater flow (e.g. Shaw, 2002), or (iii) a combination of these (e.g. Fowler and Chapwanya, 2014). The formation of ribbed bedforms by most of these mechanisms involves spatio-temporal variations in basal shear stress. Such variations are observed across lateral shear margins (Raymond et al., 2001) and frontal lobe margins (Patterson, 1997) of ice streams. These margins should therefore constitute preferential areas for the formation of ribbed bedforms. However, a possible relation between ribbed bedforms and ice stream margins has not been reported so far.

In the following sections, we present a thorough review of the literature on shape, size, spatial distribution and formation of ribbed bedforms, and then we provide new constraints on the formation and distribution of ribbed bedforms beneath ice stream margins. For that purpose, we developed an experimental model that reproduces the dynamics of ice stream margins together with the evolution of subglacial bedforms and meltwater drainage. From remotely sensed images and topographic data, we also mapped ribbed bedforms below lateral shear and frontal lobe margins of palaeo-ice streams of the Laurentide Ice Sheet (North America). By combining the experimental and geomorphological results, we propose an integrated model for the formation of ribbed bedforms associated with ice stream margins and discuss their palaeoglaciological implications for the mapping of palaeo-ice streams and the reconstruction of past subglacial hydrology and ice stream dynamics.

2 Ribbed bedforms in ice stream land systems

Glaciological, geomorphological and sedimentological studies on terrestrially terminating and marine-terminating ice streams have enabled the development of land system models (Fig. 1a; Dyke and Morris, 1988; Kleman and Borgström, 1996; Clark and Stokes, 2003) which are critical for reconstructing spatial and temporal variations in the distribution of palaeo-ice streams, as well as understanding their geomorphic imprints across the landscape (Denton and Hughes, 1981; Patterson, 1997; Winsborrow et al., 2004; Margold et al., 2015). The areas where the ice starts to form channels in the upstream part of ice streams (i.e. onset areas) are characterized by slow ice flow and a large spectrum of flow orientations due to the convergence of multiple tributaries. Ice is then incorporated within narrow and well-defined trunks with high flow velocities ($> 300\,\mathrm{m\,yr^{-1}}$; Clark and Stokes, 2003) and marked by swarms of streamlined bedforms parallel to the ice flow direction (Fig. 1; mega-scale glacial lineations, flutes, drumlins and mega-grooves; Menzies, 1979; Stokes and Clark, 2001, 2002a; Newton et al., 2018). Ice stream trunks are delimited by abrupt lateral shear margins, frequently underlined by continuous and linear shear moraines (Dyke and Morris, 1988; Dyke et al., 1992; Stokes and Clark, 2002b). Terminal zones of ice streams are characterized by either marine-based ice shelves and calving fronts or land-based marginal lobation (Stokes and Clark, 2001). At the margin of terrestrially terminating ice streams, belts of sediment ridges and mounds mimicking the lobe curvature can form in response to the ice lobe activity; stagnation produces hummocky moraines (e.g. Johnson and Clayton, 2003; Ebert and Kleman, 2004), advances produce push moraines, end moraines and overridden moraines (Totten, 1969; Boulton, 1986; Evans and Hiemstra, 2005), and retreats produce recessional moraines (Chandler et al., 2016) (Fig. 1).

Within this general model, the definition and genesis of ribbed bedforms remains unclear. Different types and shapes have been described; different theoretical models have been proposed for their formation; various interpretations exist for their timing and conditions of formation compared to ice and subglacial drainage dynamics, and their spatial distribution within glacial land systems is still debated.

2.1 Types and shapes

Ribbed bedforms are subglacial ridges of sediment, periodic, and transverse or oblique to the palaeo-ice flow (Fig. 1). We use the term "ribbed bedform" as a descriptive morphological term, without a genetic connotation, that embraces the following bedforms described in the literature: (i) Rogen moraines (Lundqvist, 1969), (ii) ribbed moraines (Hughes, 1964), (iii) mega-scale transverse bedforms (Greenwood and Kleman, 2010) and (iv) intermediate-sized bedforms interpreted as the topographic expression of traction ribs (Sergienko and Hindmarsh, 2013; Stokes et al., 2016).

Ribbed and Rogen moraines refer to sediment ridges originally described during the 1960s in North America and in the lake Rogen (Sweden), respectively. These bedforms exhibit a range of possible shapes and orientations, from transverse to oblique, relative to the palaeo-ice flow direction (Aylsworth and Shilts, 1989; Dunlop and Clark, 2006). They are hundreds of metres to a few kilometres in length, a few hundreds

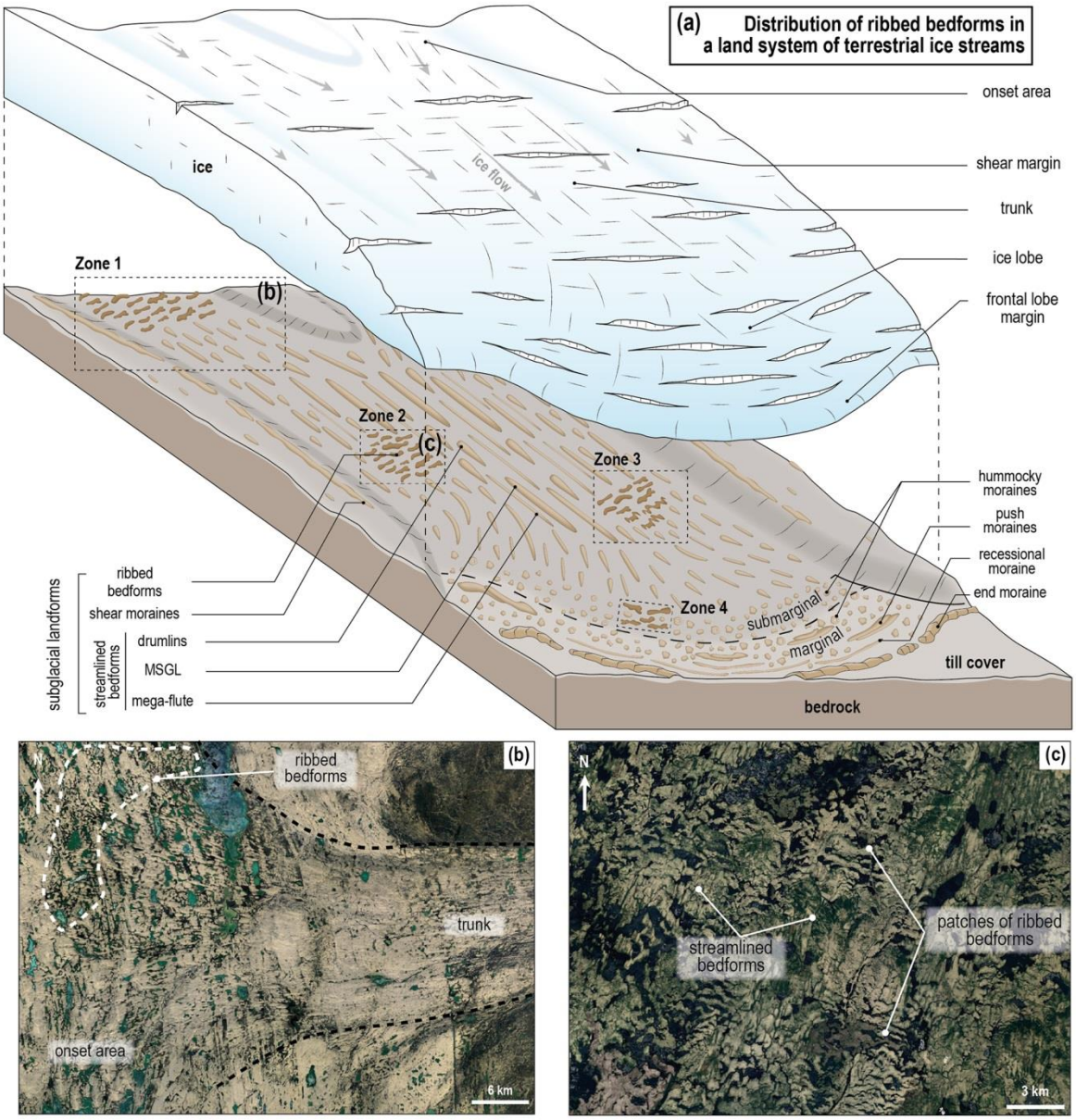

Figure 1. (a) Distribution of ribbed bedforms, as currently envisaged, in an "ideal" isochronous land system of terrestrial palaeo-ice streams (modified after Clark and Stokes, 2003). **(b)** Ribbed bedforms located in the cold-based onset area (Zone 1), upstream of the streamlined bedforms, recording the warm-based trunk of an ice stream (Fisher Lake, Prince of Wales Island, Canada). **(c)** Patches of ribbed bedforms with abrupt borders with surrounding streamlined bedforms (Zone 2; Lake Naococane, Canada). Also documented and shown in **(a)**, although not shown with specific examples, are progressive downstream transitions from ribbed bedforms to drumlins (Zone 3) and marginal relationships between hummocky and ribbed bedforms (Zone 4) (© Landsat/Copernicus – © Google Earth).

of metres in width ($l/w = 2.5$) and tens of metres in height, and their spacing is an order of magnitude lower than the ice thickness (Paterson, 1972; Dunlop and Clark, 2006).

Mega-scale transverse bedforms are 20 to 40 km in length, 3 to 6 km in width ($l/w = 5.7$) and 5 to 10 m in height (Greenwood and Kleman, 2010). They are depicted with a perpendicular orientation relative to the ice flow direction, and their spacing is an order of magnitude higher than the thickness of the overlying ice.

Intermediate-sized ribbed bedforms, interpreted as the morphological expression of traction ribs, are 1 to 6 km long, 0.4 to 2 km wide ($l/w = 2.9$) and 10 to 20 m high. They are believed to form perpendicularly (90°) to obliquely (20°) relative to the ice flow direction and below ice thicknesses equal to or an order of magnitude lower than their spacing (Sergienko and Hindmarsh, 2013; Stokes et al., 2016).

Crevasse-squeezed ridges also are subglacial periodic ridges oriented transversally or obliquely to the ice flow (Evans et al., 2015, 2016). However, their shapes and metrics differ from those of the bedforms described above and are therefore not considered ribbed bedforms here.

2.2 Spatial distribution in ice stream land systems

The palaeoglacial community agrees that some ribbed bedforms develop along rough ice–bed interfaces (frozen, unlubricated or associated with stiff beds) with high basal shear stresses under slow-flowing portions of ice sheets. Ribbed bedforms are thus believed to be ubiquitous from the inner, slow-moving regions of ice sheets (Aylsworth and Shilts, 1989; Dyke et al., 1992; Hättestrand and Kleman, 1999; Greenwood and Kleman, 2010; Stokes, 2018) up to the onset areas of ice streams at the transition between cold- and warm-based ice, where the ice flow velocity increases downstream (Fig. 1b – Zone 1; Bouchard, 1989; Dyke et al., 1992; Hättestrand and Kleman, 1999). They are thought to be less common in ice stream trunks, where they would occur only as isolated patches within a mosaic of sticky and slippery spots associated with streamlined bedforms (Fig. 1c – zones 2, 3; Cowan, 1968; Aylsworth and Shilts, 1989; Bouchard, 1989; Dyke et al., 1992; Stokes and Clark, 2003; Stokes et al., 2006a, 2008) and in submarginal areas, where they would be associated with hummocky moraines within stagnant ablation complexes (Fig. 1 – Zone 4; Marich et al., 2005; Möller, 2006, 2010). To summarize, within an isochronous glacial land system, ribbed bedforms are believed to form below large-scale portions of slow-flowing ice (ice domes and stagnant margins of ice sheets) and below localized patches of slow ice within fast-flowing ice streams (sticky spots). According to this model, they would develop contemporarily to streamlined bedforms, upstream (from ice domes to onset areas of ice streams), downstream (along marginal ablation complexes) or laterally (within sticky spots).

2.3 Theoretical models of formation

Theoretical models of formation invoke basal thermal conditions, meltwater flows or initial bed topography, to explain the shape and periodicity of ribbed bedforms. Four categories of formation processes have been proposed: (i) deformation or reshaping of pre-existing sedimentary mounds, such as former streamlined or marginal landforms, by overriding ice (Boulton, 1987; Lundqvist, 1989; Möller, 2006); (ii) fracturing and extension of frozen beds along transitions from warm-to-cold ice bases, where tensional stresses increase (Hättestrand and Kleman, 1999; Sarala, 2006); (iii) subglacial meltwater floods responsible for the formation of inverted erosional marks at the ice base, infilled by sediments (Shaw, 2002); and (iv) till deformation, in response to the flow of ice over bed heterogeneities resulting from variations in pore water pressure, the basal thermal regime and bed strength (Terzaghi, 1931; Shaw, 1979; Bouchard, 1989; Kamb, 1991; Tulaczyk et al., 2000; Lindén et al., 2008; Stokes et al., 2008). The last process is consistent with physically based mathematical models demonstrating that ribbed bedforms naturally arise from wavy instabilities in the combined flow of ice, basal meltwater and viscoplastic till (Hindmarsh, 1998a, b; Fowler, 2000; Schoof, 2007; Clark, 2010; Chapwanya et al., 2011; Sergienko and Hindmarsh, 2013; Fowler and Chapwanya, 2014; Fannon et al., 2017).

In conclusion, ribbed bedforms occur in a highly varied distribution within ice sheets and ice streams and multiple hypotheses have been proposed for their formation. A size and shape continuum has been suggested between ribbed, hummocky and streamlined bedforms, suggesting that these subglacial bedforms could form in response to the same governing processes modulated by either ice flow velocity or ice flow duration (Aario, 1977; Rose, 1987; Dunlop and Clark, 2006; Stokes et al., 2013b; Ely et al., 2016; Fannon et al., 2017). Moreover, ribbed bedforms are frequently overprinted by drumlins and embedded within polygenetic land systems, corresponding to multiphase stories, which complicate their interpretation (Cowan, 1968; Aylsworth and Shilts, 1989; Stokes et al., 2008). Previous studies emphasize the importance of ribbed bedforms in the reconstruction of basal shear stresses, ice–bed interactions, basal processes and ice dynamics (Dyke and Morris, 1988; Alley, 1993; Stokes et al., 2008, 2016).

3 Methods

3.1 Analogue modelling

The development of subglacial bedforms potentially involves four mass transfer processes – erosion, transport, deposition and deformation – that can occur simultaneously and interact beneath ice streams and four components – ice, water, till, and bedrock – that have complex and distinct rheolog-

ical behaviours (Paterson, 1994). To understand the formation of ribbed bedforms, numerical models have been developed using naturally occurring typical values for the physical properties of these components. In these models the growth of subglacial bedforms is based on (i) the development of along-flow instabilities which creates wave-like bedforms resulting from infinitesimal perturbations at the surface of a deformable till layer (Hindmarsh, 1998a, b; Fowler, 2000; Schoof, 2007; Chapwanya et al., 2011; Fowler and Chapwanya, 2014; Fannon et al., 2017) and (ii) till entrainment and deposition resulting from till flux (driven by bed deformation and the ice pressure gradient) and lee-side cavity deposition (Barchyn et al., 2016). Three-dimensional numerical modelling of bedforms remains a challenging enterprise. Their investigation is far from complete, mostly because the involved components show drastically distinct thermo-dependent and strain-rate-dependent rheologies and therefore temporal scales of activity (Paterson, 1994). To circumvent the challenge of numerically modelling these complex interactions, Lelandais et al. (2016, 2018) developed a laboratory-based model capable of simultaneously simulating ice flow, subglacial hydrology and subglacial erosion/transport/sedimentation/deformation. This model contributed to better constrain the link between subglacial meltwater drainage and the life cycle of ice streams, but subglacial bedforms were not included. We used the same approach with a new experimental setup, specifically designed to simulate the development of subglacial bedforms.

3.1.1 Experimental setup

The experimental device consists of a stainless-steel box, 5 cm high, 2 m × 2 m wide and surrounded by a gutter 5 cm in width (Fig. 2a). A 5 cm thick bed, composed of saturated fine sand (median grain size $d_{med} = 100\,\mu m$; density $\rho_{bulk} = 2000\,kg\,m^{-3}$; porosity $\Phi_s = 41\,\%$; permeability $K_s = 10^{-4}\,m\,s^{-1}$), fills the box to simulate a soft, porous, permeable and erodible subglacial bed (Fig. 2b). Grains of coloured coarse sand (grain size $d = 850$ to $1250\,\mu m$), representing bedrock blocks, are sprinkled over the flat surface of the bed. To simulate the ice sheet, a circular cap of viscous and transparent silicone putty (density $\rho_{sil} = 967\,kg\,m^{-3}$; viscosity $\eta_{sil} = 5 \times 10^4\,Pa\,s^{-1}$), 3 cm thick in its centre and 90 cm in diameter, covers the bed. We inject a solution of mixed water and UV ink (bulk density $\rho_w = 998\,kg\,m^{-3}$) through an injector located below the centre of the silicone cap in order to produce water flow beneath the silicone and highlight the flow pattern using UV light. The central injector, with a diameter of 8 mm, is placed 1.5 cm beneath the surface of the bed and connected to a water pump. The injection is regulated by a flow meter (discharge $Q = 0$–$50\,mL\,min^{-1}$) and is calculated to allow water circulation within the bed and along the silicone–bed interface, with a pressure of injected water exceeding the combined weights of the bed and silicone layers. Fifteen experiments, 60 min in duration, were performed with different injection scenarios: constant, binary and discontinuous (Table 1). Experimental scenarios were replicated at least three times in order to ensure the reproducibility of the experimental setup. The experimental device is scaled according to the principles described in Lelandais et al. (2016, 2018): to take into account the intimate links between glacial dynamics, subglacial hydrology and subglacial landform development, all physical quantities in the experiment are defined so that the dimensionless ratio between ice velocity and the incision rate of subglacial erosional landforms has similar values in the model and in nature. Lelandais et al. (2016, 2018) demonstrated that models based on this scaling ratio are able to reproduce landforms representative of subglacial systems.

3.1.2 Monitoring of experiments and post-processing of data

The experimental device is equipped with white-light LEDs and UV LEDs, alternating every 15 s during an experiment. An array of nine cameras acquires photographs (every 15 s) both in white light (all cameras) and in UV light (red camera only; Fig. 2a). The transparency of the injected water and the silicone cap in white light enables manual mapping of bedforms and reconstruction of digital elevation models (DEMs) of the bed surface from the white-light photographs, with a precision of ± 0.1 mm, through a photogrammetric method developed by Lelandais et al. (2016). The morphometric properties of bedforms and drainage features (Fig. S1 in the Supplement) are calculated from interpreted snapshots and DEMs. Maps of water distribution at the silicone–bed interface are derived from the UV photographs, thanks to the fluorescence of the injected water. An automatic treatment of these images and a calibration with DEMs of the sub-silicone bed allow fluorescence intensity to be converted into water thickness. The pore water pressure is punctually measured, 1.5 cm beneath the bed surface, with 12 pressure sensors (8 mm in diameter) distributed in two concentric circles, 15 and 30 cm in radius, respectively, and centred on the central water injector (Fig. 2a and b). The horizontal positions of UV markers, 1 mm in diameter and placed with an initial spacing of 5 cm on the silicone surface, are monitored with a time step of 90 s (Fig. 2b). Horizontal velocity (V_{surf}) and deformation maps for the surface of the silicone cap are then calculated and interpolated from the temporal record of the marker displacements. The horizontal deformation of the silicone cap surface is quantified with two indicators, (i) the strain rate and orientation of the principal axes of the instantaneous strain ellipse ($\varepsilon_{extending} > 0$ and $\varepsilon_{compressing} < 0$; Ramsay and Huber, 1987) and (ii) the absolute magnitude of the horizontal shear strain rate (ε_{shear}; Nye, 1959). Those indicators are computed for each triangle of a mesh, established by a Delaunay triangulation of all the UV markers (Fig. S2).

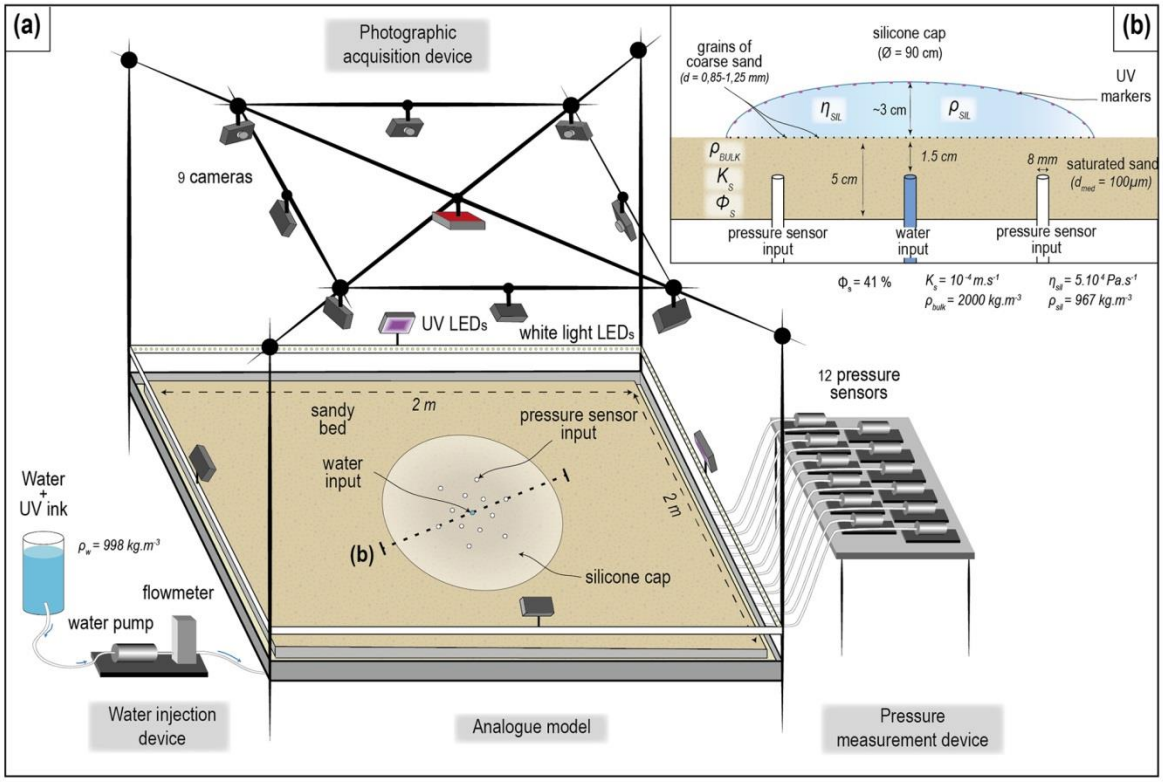

Figure 2. **(a)** Experimental model and monitoring apparatus. A cap, of transparent and viscous silicone putty, flows under its own weight above a bed composed of water-saturated sand. We inject coloured water into the bed, through an injector located below the centre of the silicone cap. We use a photographic acquisition device and pressure sensors to monitor the development of bedforms at the silicone–bed interface, the silicone flow velocity, the water flow and the water pressure. **(b)** Transverse section of the model with the experimental parameters.

3.1.3 Physics of silicone–water–bed interactions in the experiment

The model is designed to explore the basic mechanical interactions between a simplified water-routing system, a deformable and erodible sedimentary bed, and an impermeable viscous cover. The formation of sub-silicone bedforms in the experiments involves interactions between the silicone putty, the injected water and the sand bed. Compared with ice, the silicone putty is Newtonian, isotropic and impermeable. Under the experimental conditions (between 15–20 °C and at atmospheric pressure), its viscosity is nearly independent of temperature and the bed is constantly wet and saturated. Consequently, temperature-dependent processes (shear heating, heat softening, melting and freezing) and shear softening or shear hardening related to the non-Newtonian behaviour or the anisotropy of ice are not reproducible. Unlike ice, the Newtonian silicone putty is thus unable to localize viscous deformation when stress increases (in particular along lateral shear margins) or to produce fractures in the range of experimental flow velocities we can simulate. Consequently, spatial velocity gradients are expected to be smaller in the experiment than in nature, and the width of experimental lateral shear margins is overestimated compared to the width of experimental ice streams. The use of silicone putty also induces a major scaling limitation since the viscosity ratios between the cap materials, either ice or silicone putty, and the basal fluid, water in both cases, are different. The size of erosive channelized features produced in the analogue model is thus overestimated compared to the dimensions of experimental ice streams. Internal production of meltwater, complex spatial variations in subglacial hydrology, and lobe margin ablation and retreat are not reproducible either. The water-saturated sand bed is homogeneous and can deform by both localized and diffuse intergranular shearing; the flow of both water and silicone can thus produce both internal deformation of the bed and erosion, transport and deposition of grains at the bed–water or bed–silicone interface. The transport of sand grains through supra-silicone entrainment and incorporation into basal silicone are not simulated.

Table 1. Water injection scenarios and type of water drainage observed in each experiment.

Experiment number	Water injection scenario	Channelized drainage beneath lobes	
		Well-developed	Poorly developed
1	Constant 25 mL min^{-1} (60 min)	×	
2		×	
3		×	
4		×	
5		×	
6	Constant 37.5 mL min^{-1} (60 min)	×	
7			×
8		×	
9			×
10	Binary 25 mL min^{-1} (30 min) – 50 mL min^{-1} (30 min)	×	
11		×	
12		×	
13	Discontinuous 12.5 mL min^{-1} (15 min) – 25 mL min^{-1} (15 min) – 0 mL min^{-1} (15 min) – 25 mL min^{-1} (5 min) – 37.5 mL min^{-1} (5 min) – 50 mL min^{-1} (5 min)	×	
14			×
15		×	

The model, like all models, is not perfectly realistic since it reproduces neither a complete and scaled miniaturization of nature nor all subglacial physical processes. Previous physical experiments have reproduced subglacial channelized features (tunnel valleys) and marginal landforms (ice-contact fans and outburst fans) and have suggested a close relationship between the development of tunnel valleys and the stabilization of analogue ice streams (Lelandais et al., 2016, 2018). It turns out that experimental models, although imperfectly scaled, reproduce landforms visually conforming to subglacial landforms, emphasizing the "unreasonable effectiveness" of analogue modelling (Paola et al., 2009).

3.2 Mapping and morphometric analysis in palaeo-ice stream land systems

To identify, map and characterize ribbed bedforms associated with natural palaeo-ice stream margins, we compiled DEMs, hillshade maps and ice stream contours of the North American Laurentide Ice Sheet (Margold et al., 2015) in a geographic information system (GIS). Four distinct regions (Fig. 3), covering a few thousand square kilometres, overlapping the lateral shear and frontal lobe margins of three palaeo-ice stream beds were studied: (i) the Amundsen Gulf Ice Stream (21.8–12.9 ka cal BP), (ii) the Central Alberta Ice Stream (20.5–17 ka cal BP) and (iii) the Hay River Ice Stream (13.9–12.9 ka cal BP; Margold et al., 2018). We used a 15 m lidar bare-earth DEM supplied by the Alberta Geological Survey for the Central Alberta and Hay River ice streams and a 10 m digital surface model computed by optical stereo imagery (ArcticDEM; Porter et al., 2018) for the Amundsen Gulf Ice Stream. By means of breaks in slopes observed on hillshade maps, we digitized ribbed bedforms, streamlined bedforms indicative of predominant ice flow directions, and other landforms indicative of ice stream lateral and frontal margins at the scale of 1 : 50 000. The length (long axis), width (short axis) and orientation of ribbed bedforms compared to the ice flow direction were extracted using the "Minimum Bounding Geometry" tool in ArcGIS. The orientation values of ribbed bedforms and streamlined bedforms were compiled in rose diagrams for each selected region.

4 Results

4.1 Stream dynamics and development of ribbed bedforms in the experiment

Without obvious dependence on the injection scenarios, the experiments listed in Table 1 produced two types of streams and lobes related to two different types of water drainage networks beneath the silicone cap: (i) well-developed channelized drainage ($n = 12$ experiments) and (ii) poorly developed channelized drainage ($n = 3$ experiments). In the following section, we present the evolution of silicone stream dynamics and ribbed bedforms for one experiment representative of each kind: experiments 10 and 14, respectively (Table 1). In those two experiments, the water injection discharge was doubled in stage 3 ($Q = 50$ mL min^{-1}) compared to stages 1 and 2 ($Q = 25$ mL min^{-1}).

In both experiments, when water injection starts, a circular water pocket forms and grows along the silicone–bed interface until it reaches a diameter of 15 to 25 cm. This pocket migrates towards the margin of the silicone cap, as a continuous water film, until it suddenly drains outside the cap.

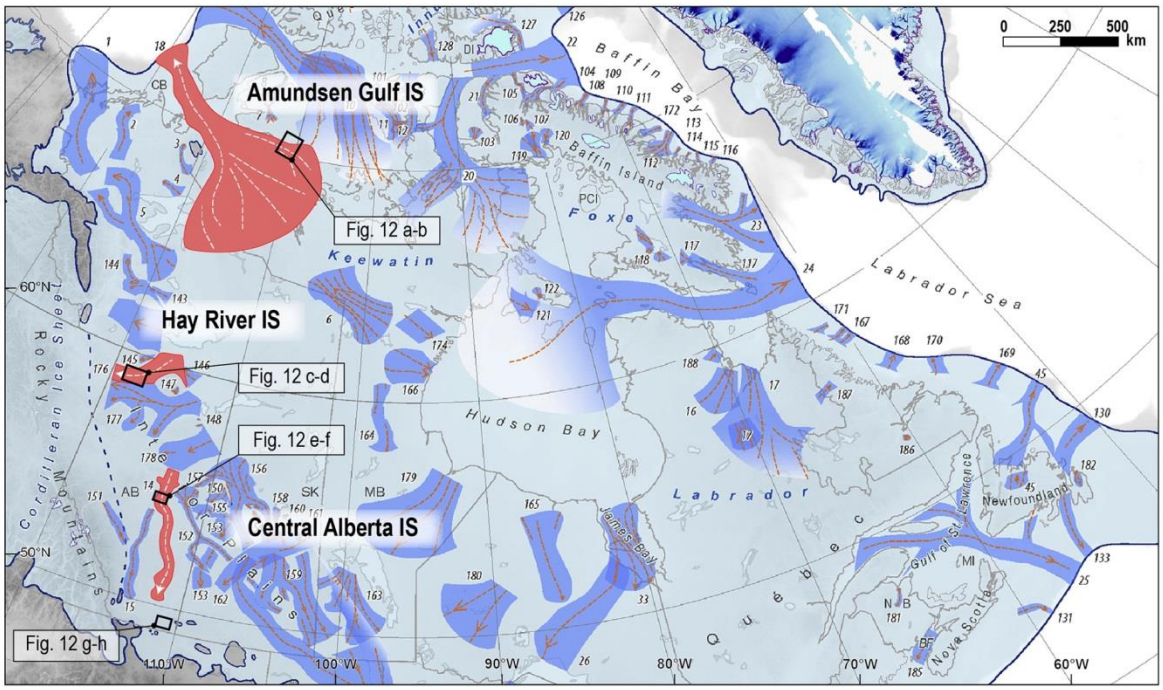

Figure 3. Extent of the North American Laurentide Ice Sheet during the Last Glacial Maximum with positions of known ice stream tracks (modified from Margold et al., 2018). The areas mapped in this study in three ice streams (Amundsen Gulf, Hay River and Central Alberta ice streams) are identified by black rectangles.

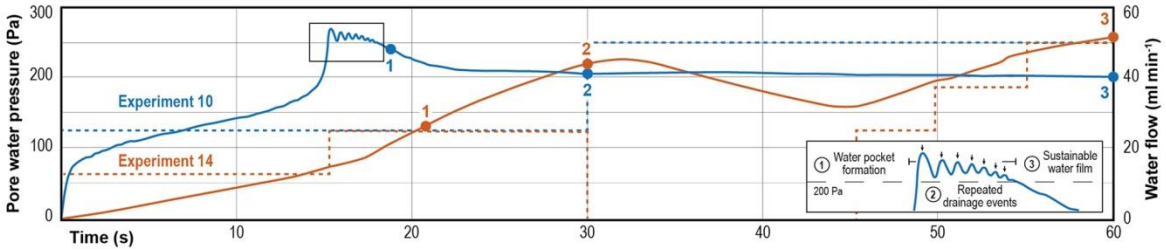

Figure 4. Evolution of pore water pressure (solid lines) measured in the trunk axis (see Fig. 5a for position) and water flow injected in the bed through the water injector (dotted lines), for experiments 10 and 14. Points numbered 1 to 3 correspond to stages described in Sect. 4.1, 4.2 and 4.3.

The presence and migration of the water pocket induces a local increase in silicone flow velocity (from $V_{surf} = 0.2 \times 10^{-2}$ mm s^{-1} to $V_{surf} = 10 \times 10^{-2}$ mm s^{-1}) forming a 20 cm wide stream that propagates from the margin towards the centre of the silicone cap. A lobe forms at the extremity of the fast-flowing corridor in response to this drainage and surge event. In Experiment 10, seven water pockets successively form and produce an equal number of drainage events and lobe advances; in Experiment 14, only one drainage event occurs (Fig. 4). The drainage events generate marginal deltas along the silicone margin, constituted by sand grains eroded from the bed during the migration of the water pocket. The sustainability of a water film at the silicone–bed interface, once the initial drainage event is over, contributes to maintaining a fast and durable silicone flow; the silicone stream switches on, and the silicone lobe keeps growing.

Landforms produced in the experiments are illustrated and annotated in Fig. 5: these include grooves, ribbed and hummocky bedforms beneath the streams and marginal deltas and pushed sediments in front of the lobes. The successive stages (Figs. 6–9) are described below in relation to (i) the stream evolution derived from surface measurements; (ii) the formation, evolution and morphometric characteristics of bedforms derived from photographs in white light and DEMs;

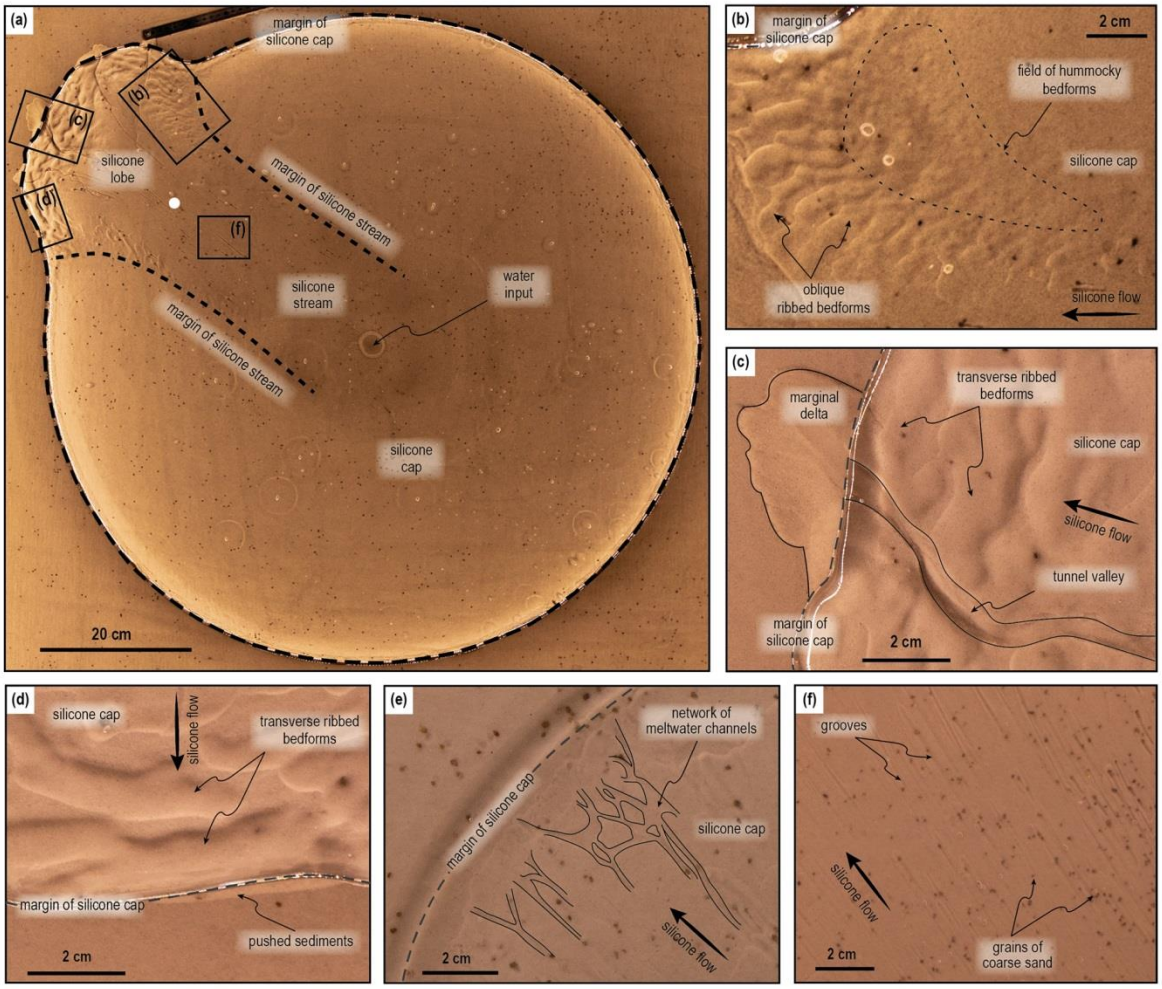

Figure 5. Illustration of bedform assemblages produced during the experiments. **(a)** Overall surface view of the silicone cap at the end of an experimental run, showing the distribution of bedforms beneath a stream/lobe system characterized by well-developed channelized drainage (Experiment 10). The white dot indicates the position of the pressure sensor where pore water pressure presented in Fig. 4 is measured. **(b)** Close-up on oblique ribbed and hummocky bedforms observed at the right lateral shear margin. **(c)** Transverse ribbed bedforms parallel to the lobe frontal margin and formed submarginally. Tunnel valley and associated marginal delta. **(d)** Transverse ribbed bedforms parallel to the lobe frontal margin and pushed marginal sediments bulldozed by the lobe margin. **(e)** Network of meltwater channels extending parallel and perpendicularly to the silicone flow (not located in panel **a**, because it was observed in Experiment 14, characterized by poorly developed channelized drainage). **(f)** Field of grooves inscribed in the bed and oriented parallel to silicone flow with embedded sand grains at the grooves' downstream extremities.

and (iii) the evolution of water drainage systems derived from UV photographs and DEMs.

4.1.1 Stage a – initiation of ribbed bedforms beneath incipient shear and lobe margins

The streams flow 10 to 20 times faster (Fig. 7a, $V_{\mathrm{surf}} = 0.08\,\mathrm{mm\,s^{-1}}$; Fig. 9a, $V_{\mathrm{surf}} = 0.17\,\mathrm{mm\,s^{-1}}$) than in the inter-stream areas ($V_{\mathrm{surf}} < 0.01\,\mathrm{mm\,s^{-1}}$), inducing velocity gradients across the lateral margins of the streams. The compressing strain rate of the strain ellipse and the shear strain rate are zero in the centre of the stream trunk and in the surrounding ice cap, while they are maximal along lateral margins of the streams where the velocity gradient is the highest (Figs. 7a and 9a; $\varepsilon_{\mathrm{compressing}} = -2.5 \times 10^{-4}\,\mathrm{s^{-1}}$; $\varepsilon_{\mathrm{shear}} = 3$ to $5 \times 10^{-4}\,\mathrm{s^{-1}}$). These patterns of high shear deformation define symmetrical bands on the silicone surface and resemble those of natural lateral shear margins (Echelmeyer et al., 1994; Raymond et al., 2001).

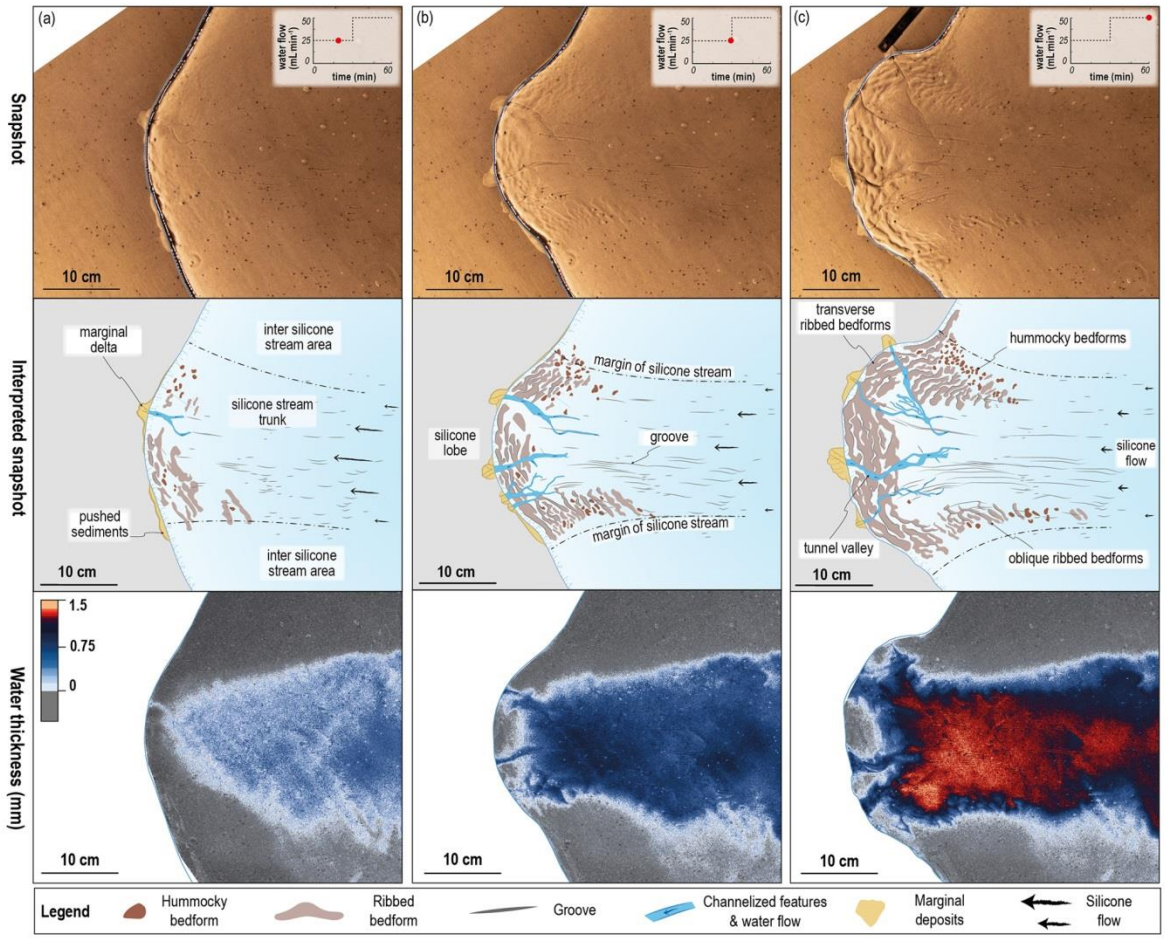

Figure 6. Temporal evolution (stages a, b and c) of the silicone stream and lobe system, for a typical experiment with a well-developed channelized drainage system (Experiment 10), illustrated with snapshots representative of the three main stages of development. The upper, intermediate and lower panels show, respectively, (i) white-light photographs of the surface of the model, (ii) interpretations of bedforms observed on the photographs and (iii) thickness (in mm) of the water film flowing beneath the silicone cap, derived from UV photographs.

In Experiment 10 (Fig. 7a), the stream velocity decreases from the centre ($V_{surf} = 0.08\,mm\,s^{-1}$) towards the frontal and lateral margins ($V_{surf} = 0.06\,mm\,s^{-1}$ and $V_{surf} = 0.04\,mm\,s^{-1}$, respectively), while the silicone–bed interfaces of these margins are dewatered (Fig. 7a; water thickness = 0). Beneath the lobe, meltwater channels, 50 to 70 mm in length and 4 to 8 mm in width, start to develop by regressive erosion from the margin and initiate channelization of the water flow (Figs. 6a and 8a). Sand grains washed away by bed erosion are transported within these incipient channels towards the marginal deltas (Figs. 5c and 6a). Radial growth and advance of the lobe over the marginal deltas form ridges of pushed sediments, 5 mm in width and 40 mm in length (Figs. 5d and 6a). Below the streams (Fig. 6a and 8a), some coarse sand grains are lodged in the base of the fast-flowing silicone and carve the bed to form sets of parallel grooves (1 mm wide, 10 to 20 mm long) highlighting the stream trunk and the direction of the silicone flow (Figs. 5f). Below frontal and lateral margins, fields of periodic ridges develop transversely to the ice flow, with undulating crests and an average wavelength of 8 mm (Figs. 6a and 8a). They are on average a few millimetres thick, 7 mm wide and 30 mm long, i.e. 4 times larger in length than in width. Their shapes (undulating crest, elongation ratio) and periodic spatial organization (Fig. 5b and d) resemble those of ribbed bedforms observed in glacial land systems. In the experiments, ribbed bedforms initiate perpendicularly (90°) to obliquely (60°) to the compressing axis of the instantaneous strain ellipse measured at the surface of the overlying silicone (Figs. 7a and 9a). Most of them form below the lobe margins perpendicularly to the silicone flow direction, and some scattered and isolated ones form below the lateral margins perpendicu-

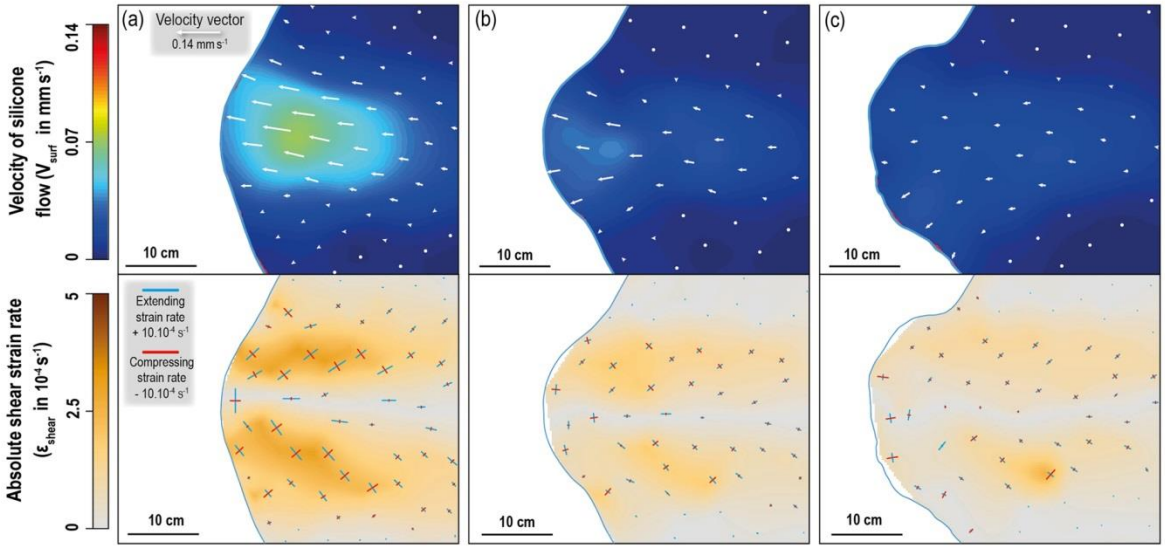

Figure 7. Temporal evolution (same stages a, b and c as in Fig. 6) of the silicone stream and lobe system, for a typical experiment with well-developed channelized drainage (Experiment 10). The upper and lower panels show (i) the velocity field of silicone flow (mm s^{-1}) and the velocity vector maps of the silicone cap upper surface and (ii) extrapolated maps of absolute shear strain rate (s^{-1}) and the orientation of the principal axes of the instantaneous strain ellipse whose length corresponds to either the extending or the compressing strain rate (ε in s^{-1}), respectively. Maps highlight the development of the fast-flowing corridor (i.e. silicone stream) surrounded by stagnant or very slow moving silicone (i.e. inter-stream area) and the formation of two symmetrical shear bands on both sides of the stream (i.e. the lateral shear margins).

larly (90°) to obliquely (45°) to the silicone flow. Other bedforms with circular to ovoid shapes (mounds) form in between the ribbed bedforms. These mounds are typically less than 0.1 mm high, 4 mm wide and 6 mm long, with an average spacing of 10 mm. Their long axes do not show a preferential orientation (Figs. 6a and 8a). The shape and spatial organization of these mounds (Fig. 5b) resemble those of some hummocky bedforms in glacial land systems.

4.1.2 Stage b – channelization of the drainage system below protruding lobes and evolution of ribbed bedforms

After 30 min, channelized drainage networks develop beneath the silicone lobe, draining water fed from the upstream water film towards the margin. The morphological evolution of these networks differs between both types of experiments, and we suggest it is a controlling influence on the distinctive evolution of stream dynamics from this point. From the previous stage, the incipient network of meltwater channels in Experiment 10 evolves into tunnel valleys – characterized by undulating long profiles with over-deepening and adverse slopes (Fig. 5c) – increasing in width (up to 1.2 cm), length (15 cm) and depth (0.07 cm), and marginal deltas continue to grow (Fig. 6b). Three individual tunnel valley systems, two slightly sinuous valleys with some tributaries and one anastomosed valley network, are observed (Fig. 6b). Simultaneously, the stream velocity decreases by half, resulting in a slowdown in the advance of the frontal lobe margin (Fig. 6b, 28 cm in width; Fig. 7b, $V_{surf} = 0.04\,mm\,s^{-1}$). Proportionally to the slowdown intensity, the lateral shear margins record a halving of the shear strain rate (Fig. 7b, $\varepsilon_{shear} = 1.25 \times 10^{-4}\,s^{-1}$) and strain ellipse deformation ($\varepsilon_{extending} = +2.5 \times 10^{-4}\,s^{-1}$; $\varepsilon_{compressing} = -1.3 \times 10^{-4}\,s^{-1}$).

In contrast to the above, in Experiment 14 the pre-existing meltwater channels remain shallow and keep a constant width but lengthen downstream in response to the migration of the lobe margin (Fig. 8b, 0.4 cm wide, 12 cm long, 0.04 cm deep). Meltwater channels are rectilinear with poorly developed tributaries and lack deltas at their downstream extremities (Fig. 5e). In parallel, the silicone streamflow maintains a high velocity, although a small deceleration occurs (Fig. 9b, $V_{surf} = 0.13\,mm\,s^{-1}$), sustaining lobe growth (36 cm in width). As a result, the lateral shear margins record a small decrease in the shear strain rate (Fig. 9b, $\varepsilon_{shear} = 3.5 \times 10^{-4}\,s^{-1}$) and a downstream-to-upstream decrease in the strain ellipse deformation ($\varepsilon_{extending} = +4.4 \times 10^{-4}\,s^{-1}$; $\varepsilon_{compressing} = -1.9 \times 10^{-4}\,s^{-1}$).

Within the trunk of both experiments, the orientation and direction of the grooves match the velocity vectors of the silicone flow. The grooves are restricted to the fast-flowing corridor and display lengths of up to 5 and 8 cm for experiments 10 and 14, respectively, and they tend to keep a con-

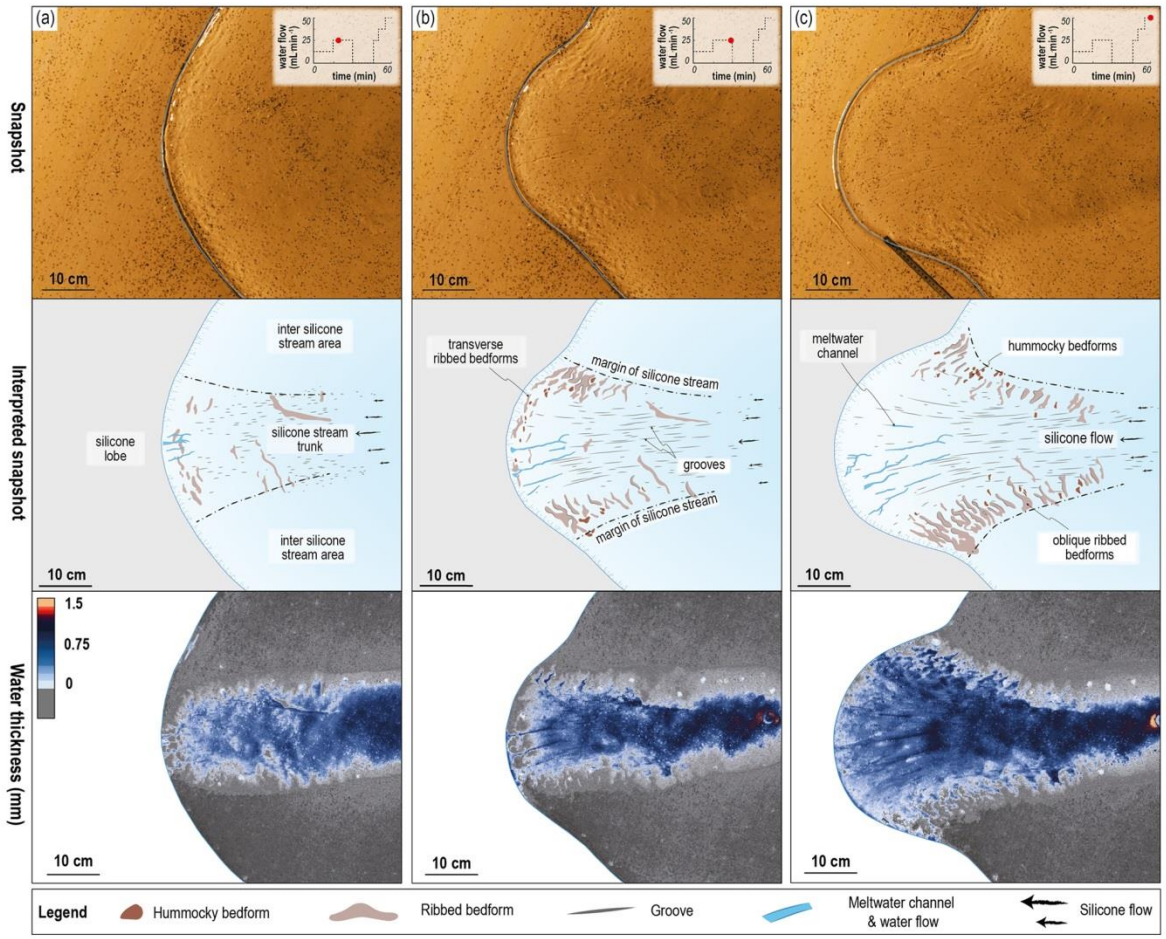

Figure 8. Temporal evolution (stages a, b and c) of the silicone stream and lobe system, for a typical experiment with poorly developed channelized drainage (Experiment 14). Same panels as in Fig. 6.

stant width of approximately 0.1 cm. Grooves remain rectilinear and parallel to the mean silicone displacement in the upstream part of the streams but diverge and curve in the downstream area following the fan-shaped pattern of silicone velocity vectors in the lobe (Figs. 6b and 8b). During this second stage, the ribbed bedforms keep growing but differ below lateral shear margins (i.e. lateral ribbed bedforms) and frontal lobes (i.e. submarginal ribbed bedforms). Below shear margins, new lateral ribbed bedforms with arcuate planforms progressively develop obliquely (45 to 60°) to silicone velocity vectors and perpendicularly to compressing axes of the horizontal strain ellipses. They first appear near the lobe and then develop towards the upstream area of the trunk borders. Pre-existing and newly formed lateral ribbed bedforms increase in length and width, parallel to the extending axes and perpendicularly to the compressing axes of the horizontal strain ellipse, respectively (Figs. 6b and 8b; 1 cm wide and 5 cm long). Their wavelength is typically 0.6 to 0.7 cm in Experiment 10 (Fig. 6b), while it is 1.0 to 1.5 cm in Experiment 14 (Fig. 8b). Beneath the lobe margin of Experiment 10, the water film ceases to exist in between the tunnel valleys (Fig. 6b). These water-free areas coincide with the growth of pre-existing submarginal ribbed bedforms and the formation of new ones parallel to the lobe margin and perpendicular to silicone velocity vectors and compressing axes (Fig. 7b). They develop below the lobe from (i) the initial sandy bed and (ii) the recycled marginal landforms (i.e. marginal deltas and pushed sediments). The development and the coalescence of these bedforms below the lobe tend to form a belt composed of broad, arcuate and transverse submarginal ribs (Fig. 6b; up to 1.6 cm in width, up to 8 cm in length and 1.1 cm in wavelength). In Experiment 14, characterized by smaller meltwater channels, only a few and scattered submarginal ribbed bedforms – most are inherited

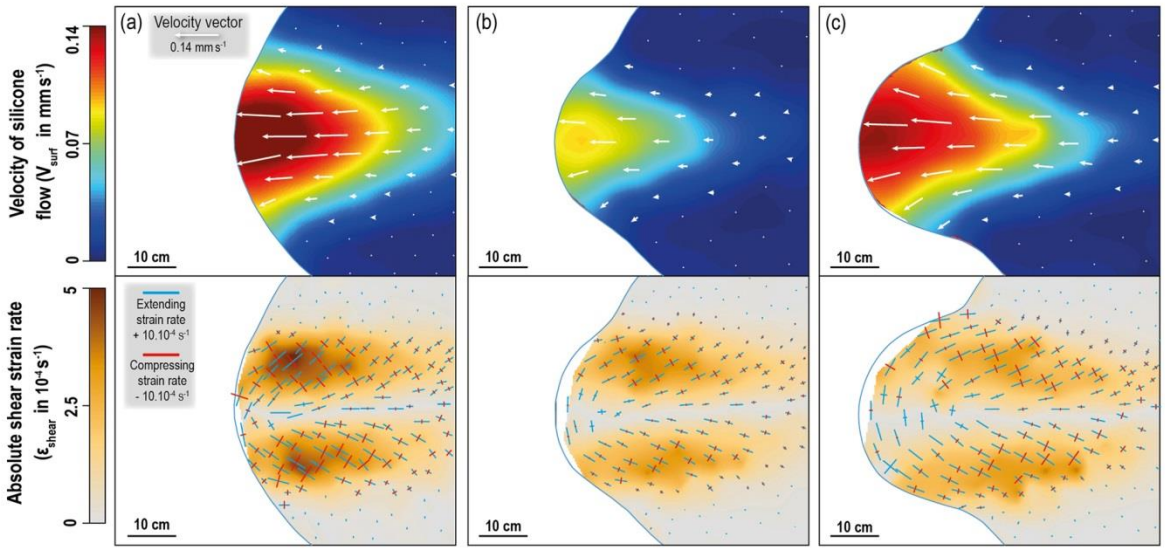

Figure 9. Temporal evolution (same stages a, b and c as in Fig. 8) of the surface behaviour of the silicone stream and lobe system, for a typical experiment with poorly developed channelized drainage (Experiment 14). Same panels as in Fig. 7.

from the previous stage, and a few are newly formed – of smaller dimensions appear (Fig. 8b; up to 0.8 cm in width and up to 4 cm in length). The population of mounds resembling hummocky bedforms keeps increasing (from 15 to 40 in Experiment 10 and from 0 to 17 in Experiment 14). Some mounds observed in the previous stage have evolved into ribbed bedforms, and new mounds form with constant dimensions (0.5 cm in width, 0.7 cm in length), especially in the bending zone between lobe borders and shear margins (Figs. 6b and 8b).

4.1.3 Stage c – morphological response to changes in drainage characteristics

After 60 min, the two experimental runs described here show distinctive drainage systems (well-developed vs. poorly developed), silicone streams dynamics and landform development histories.

Well-developed channelized drainage system (Experiment 10)

In response to the imposed increase in water discharge, tunnel valleys increase in number (from three to four) and in dimensions (up to 1.1 cm wide, up to 16 cm long and up to 0.10 cm deep) and keep ensuring the drainage of the distributed water film. Tunnel valleys continue to grow downstream, tracking the advance of the lobate margin, and they incise the belt of submarginally produced ribbed bedforms formed during the previous stage, as indicated by elevation profiles (Figs. 6c and 10a, d). The silicone flow velocity decreases along the stream axis; lobe growth slows down ($L_{\text{stream}} = 20$ cm; $V_{\text{surf}} = 0.02$ mm s^{-1}), and silicone thickness along the lobe margin stabilizes at between 5 and 15 mm. In response to this slowdown, the lateral velocity gradient decreases across the lateral stream margins, whose width becomes constant ($L_{\text{shear margin}} = 11$ cm). In these areas, the deformation of the strain ellipse ($\varepsilon_{\text{extending}} = +1.9 \times 10^{-4}$ s^{-1}; $\varepsilon_{\text{compressing}} = -1.0 \times 10^{-4}$ s^{-1}) and the shear strain rate ($\varepsilon_{\text{shear}} = 1 \times 10^{-4}$ s^{-1}) stabilize at low values (Fig. 7c). New and pre-existing submarginal ribbed bedforms form and grow perpendicularly to obliquely (70°) to the trunk axis and perpendicularly to compressing axes of the strain ellipses, respectively (Figs. 7c and 11c). Submarginal ribbed bedforms with oblique orientations correspond to bedforms that form and grow during the lobe spreading where the silicone velocity vectors deviate from the trunk axis orientation. Individual submarginal ribbed bedforms increase in dimensions and tend to evolve into a roughly coalescent belt that strike perpendicularly to compressing axes of the strain ellipses along the lobe margin (Figs. 7c and 10c; 1.4 cm in width, 4.2 cm in length and 0.1 cm in height), although they still display a regular wavelength, from 1.0 to 1.5 cm. New lateral ribbed bedforms form upstream below shear margins with orientations perpendicular to compressing axes of the strain ellipses Elevation profiles reveal they remain smaller in dimensions and display lower relief than their submarginal counterparts (Fig. 10e; 2.3 cm in length, 0.7 cm in width and up to 0.07 cm in height). Pre-existing and newly formed lateral ribbed bedforms are arranged in regular and oblique patterns, with a mean long-axis orientation of 45° to the trunk axis (Fig. 11c) and with a wavelength close to 0.7 cm (Fig. 6c). The grooves still increase in length but at a slower rate than during pre-

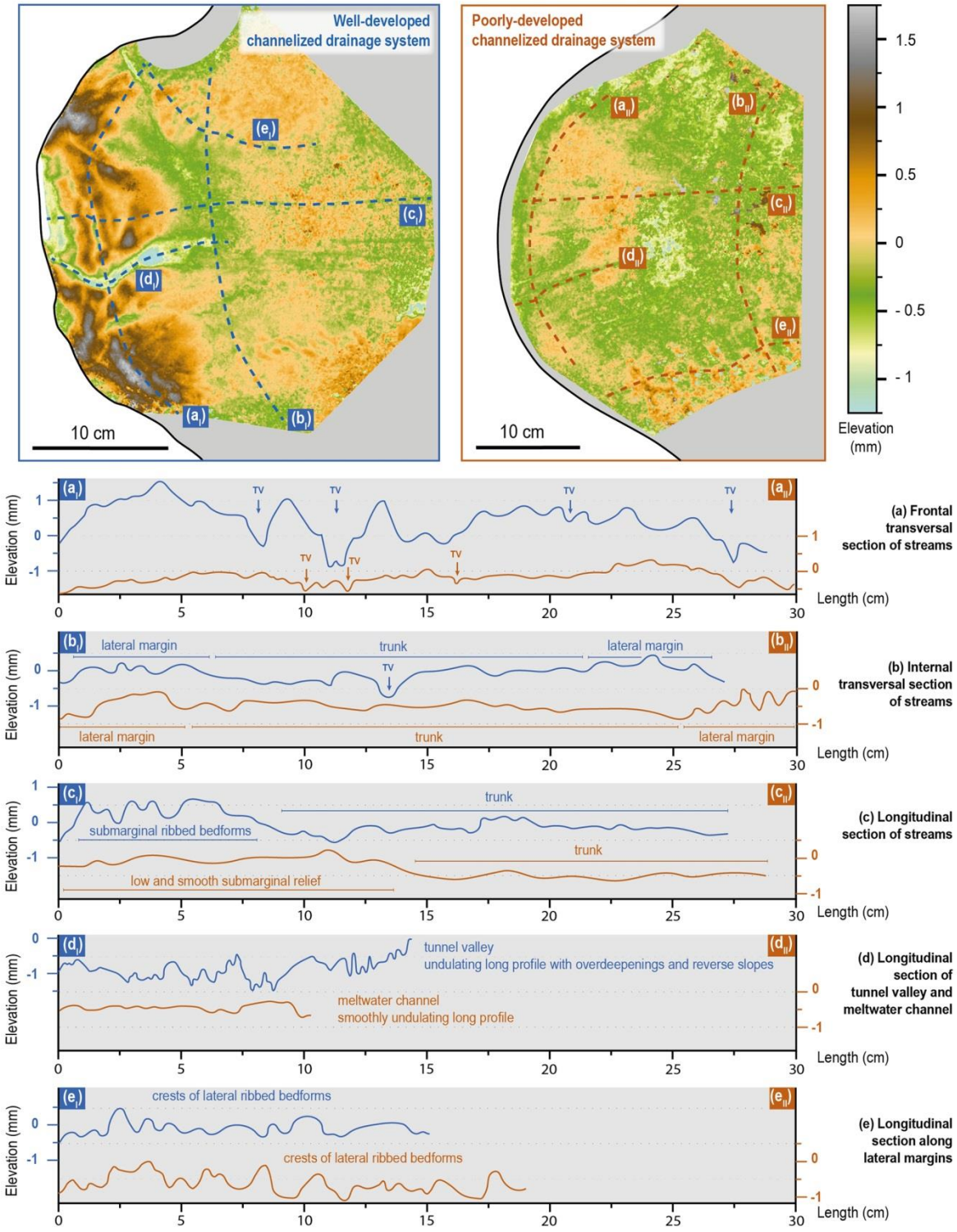

Figure 10. DEMs of the bed surface beneath the lobes of the silicone streams at the final stage of Experiment 10 (blue) and Experiment 14 (brown). Ten elevation profiles **(a–e)** within the lobes are drawn to compare the morphological imprint beneath the two types of stream.

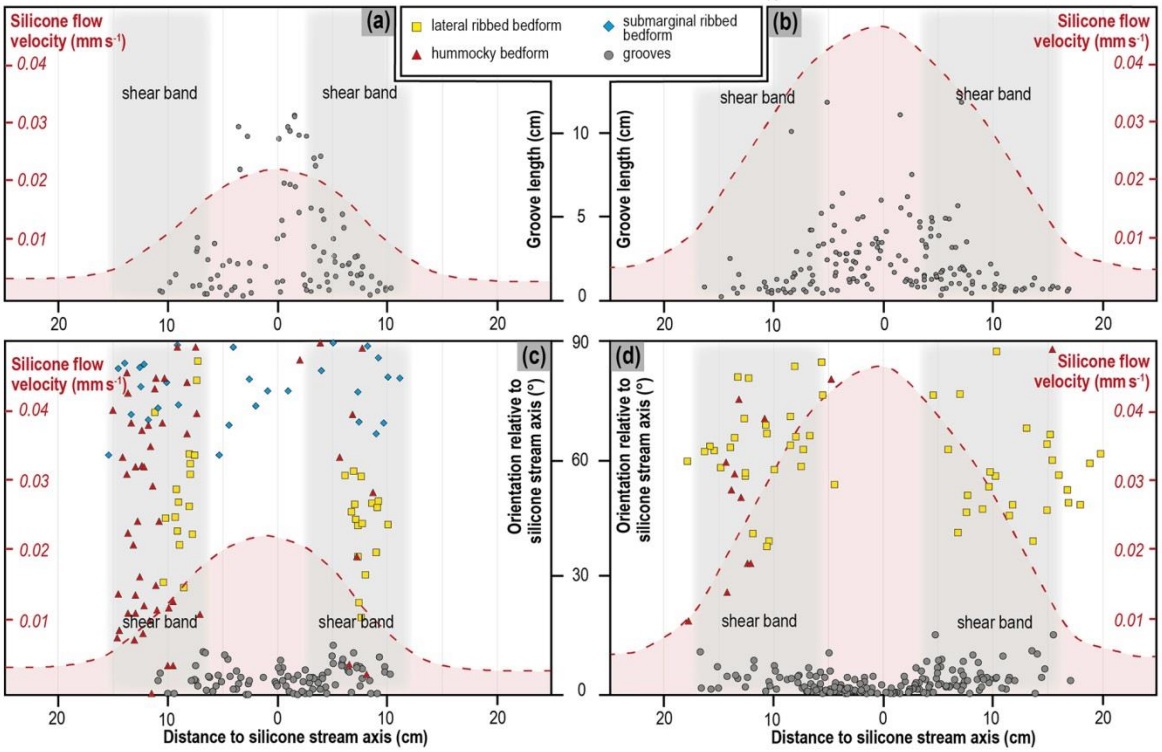

Figure 11. Morphometric properties of bedforms produced beneath each type of stream at the final stage of experiments 10 **(b, d)** and 14 **(a, c)** plotted according to the distance from the silicone stream central axis. **(a, b)** Relationship between groove length and silicone flow velocity ($\mathrm{mm\,s^{-1}}$). **(c, d)** Variation in orientation relative to silicone stream axis of each population of bedforms (lateral ribs, submarginal ribs, hummocky) compared to the silicone flow velocity and the shear band position (grey columns; defined as $\varepsilon_{\mathrm{shear}} > 0.5 \times 10^{-4}\,\mathrm{s^{-1}}$).

vious stages, although remaining subparallel (0–10°) to the silicone flow direction (Fig. 11c). The position and length of the grooves correlate with the time-averaged velocity profile measured across the silicone stream (Fig. 11a). Hummocky bedforms occur either sparsely between lateral ribbed bedforms or more densely in lobe corners. Their average length is 0.6 cm, and their average width is 0.4 cm (Fig. 6c).

Poorly developed channelized drainage system (Experiment 14)

In response to the imposed increase in water discharge, the sparse, shallow and narrow meltwater channels characterized by smoothly undulating long profiles (Fig. 10a and d; $n = 9$, up to 0.5 cm in width and up to 0.05 cm in depth) are not able to evacuate all the water transmitted to the bed. Thus, the distributed water film, hitherto constrained to the uppermost part of the stream, spreads down to the lobe (Fig. 8c). The stream velocity increases, and the lobe undergoes a surge (Fig. 9c; $V_{\mathrm{surf}} = 0.15\,\mathrm{mm\,s^{-1}}$). The high velocity gradient between the stream and the inter-stream area maintains a high rate of deformation of the silicone along the shear margins, with a strain ellipse rotation increasing downstream (α is up to 18°; $L_{\mathrm{R}} = 25\,\%$) and a maximal value of the shear strain rate localized along stream borders ($\varepsilon_{\mathrm{shear}} = 3 \times 10^{-4}\,\mathrm{s^{-1}}$). As the lobe advances, the stream thins and the silicone column is 20 mm thick along shear margins. The shear margins widen downstream, reaching a maximum width at the silicone cap margin within the lobe corners ($L_{\mathrm{shear\,band}}$ is up to 20 cm). Simultaneously with the downstream migration of the water film, the submarginal ribbed bedforms are eroded and evolve into a single shallow and smooth submarginal relief slightly higher than the trunk (Fig. 10c). Located beneath the shear margins, the lateral ribbed bedforms keep increasing in number (from 26 to 42) and in dimensions (Figs. 8c and 10e; 3.6 cm in length, 1.1 cm in width and up to 0.09 cm in height). New lateral ribbed bedforms form almost perpendicularly (70 to 90°) to compressing axes of the strain ellipses, while some pre-existing ones become progressively rotated because of the lobe spreading, resulting in the shift and rotation of the downstream part of the lateral shear margins. Lateral ribbed bedforms are characterized by subnormal to oblique long axes, deviating by 80 to 40° from the main trunk axis and with a mean orientation of 50° (Fig. 11d).

They are spaced with a wavelength of between 1.5 and 1.9 cm (Fig. 10e) and develop on both sides of a flat and grooved trunk (Fig. 10c). The corridors of lateral oblique ribbed bedforms thus constitute two bands of topographic highs below the shear margins (Fig. 10b).

The grooves are more elongated near the trunk axis where the highest flow velocities and the greatest cumulative displacement are recorded (Fig. 11b). Following the radial spreading of the silicone velocity vectors towards the lobate margin, the groove orientations curve and form a fan-shaped swarm (Fig. 8c). Groove orientations mostly remain subparallel to the local silicone flow, with a maximum deviation of 15° from the silicone flow direction (Fig. 11d). Sparse hummocky bedforms (width is 0.6 cm; length is 1.0 cm) occasionally occur within the corridors of lateral ribbed bedforms.

4.2 Palaeoglaciology – ribbed bedforms beneath ice stream margins

Palaeo-ice stream trunks of the Laurentide Ice Sheet – both with marine (Fig. 12a and b) and terrestrial (Fig. 12c–h) margins – are characterized by dense swarms of streamlined bedforms (e.g. mega-scale glacial lineations, drumlins), evidencing former ice flow directions. Several ice streams have been identified, mapped and described by others and were compiled by Margold et al. (2015). These streams were recognized through sharp transitions in streamlined bedform zonation, topographic borders, shear moraines and marginal bedforms. In total, we mapped 303 ribbed bedforms in four distinct areas on three palaeo-ice stream beds.

In the eastern branch of the marine-based Amundsen Gulf Ice Stream (AGIS), the trunk is characterized by streamlined bedforms delimited by two topographic borders. Two fields of ribbed bedforms ($n = 62$) elongated obliquely (mean orientation is 25 to 45°) to the streamlined bedforms occur along the lateral margins. The internal part (i.e. close to the trunk axis) of those two fields is partially overprinted by the streamlined bedforms observed along the trunk. The ribbed bedforms display elongated and arcuate shapes ($l/w = 4.2$; mean length is 4780 m; mean width is 1110 m) and a mean wavelength of 1450 m (Fig. 12a and b).

In the northern portion of the Hay River Ice Stream (HRIS), broad arcuate to rectangular ribbed bedforms ($n = 78$) strike obliquely to the streamlined bedforms of the trunk. The ridges are clustered in an elongated corridor located between the northern shear margin and the swarm of streamlined bedforms. The shear margin is marked by topographic borders, a sharp transition between a rough inter-ice-stream terrain and a smooth trunk covered by lineations, and linear ridges similar to shear moraines. The ribbed bedforms exhibit a mean orientation of 55° to streamlined bedforms and a mean wavelength of 460 m. Those ridges are shorter (1040 m in length and 360 m in width) and slightly less elongated ($l/w = 2.9$) than those of the AGIS (Fig. 12c and d).

In the upstream portion of the Central Alberta Ice Stream (CAIS), oblique and transverse ribbed bedforms ($n = 71$) are also recognized. Similarly to for the AGIS and HRIS, the ice stream trunk is characterized by topographic borders, a smoother bed than the surrounding landscape, a meltwater channel and a swarm of lineations. The ribbed bedforms located to the east of the meltwater channel are superimposed by lineations, while the oblique ribbed bedforms along the ice stream margins are apparently not overprinted by other structures. The ribbed bedforms display orientations ranging from 15 to 25° to streamlined bedforms for the slightly oblique set, while the transverse set displays orientations deviating by 85°. They are 2660 m in length and 690 m in width – thus displaying a mean elongation ratio of 3.8 – and have a mean wavelength of 685 m (Fig. 12e and f). The oblique ribbed bedforms are characterized by less arcuate and more elongated shapes than the transverse ones. Downstream and further south in the CAIS is a widespread belt of transverse ribbed bedforms ($n = 92$; mean orientation is 95°) overprinted with perpendicular lineations and cross-cut by large meltwater channels (width is 6 to 3.4 km). This belt presents a regular pattern of arcuate and coalescent ribbed bedforms (wavelength is 600 to 1200 m), paralleling a curved belt of fine, linear and almost continuous ridges – similar to recessional moraines – depicted further north. The mean length (4350 m), width (1350 m) and elongation ratio ($l/w = 3.0$) of the ribbed bedforms show that these ridges are longer and wider but less elongated than the oblique and transverse ridges upstream (Fig. 12g and h).

5 Discussion

5.1 Morphometric comparisons between experimental and natural ribbed bedforms

Our experiments and observations suggest that ribbed bedforms can develop in lateral corridors and submarginal belts displaying transverse or longitudinal ice velocity gradients, like shear margins and lobes of ice streams, respectively. They occur along the borders of swarms of elongated structures (Figs. 6, 8 and 12; i.e. lineations in nature and grooves in the experiments) that reveal fast-flowing trunks (Stokes and Clark, 2001; Clark and Stokes, 2003). Beneath the shear margins of the experimental ice streams, the lateral ribbed bedforms form perpendicularly to the compressing axis of the strain ellipse. Their mean long-axis orientation strikes at $\sim 45°$ to the trunk axis and to the boundaries of lateral shear margins (Fig. 10c and d), and they tend to gather in corridors elongated parallel to the flow direction. In the experiments, their elongation ratio of 3.3 (mean length is 3 cm; mean width is 0.9 cm) lies in between those of natural intermediate-sized ribbed bedforms considered the topographic expression of traction ribs and those of mega-scale transverse ridges, fitting a moderately elongated type of ribbed bedform. The

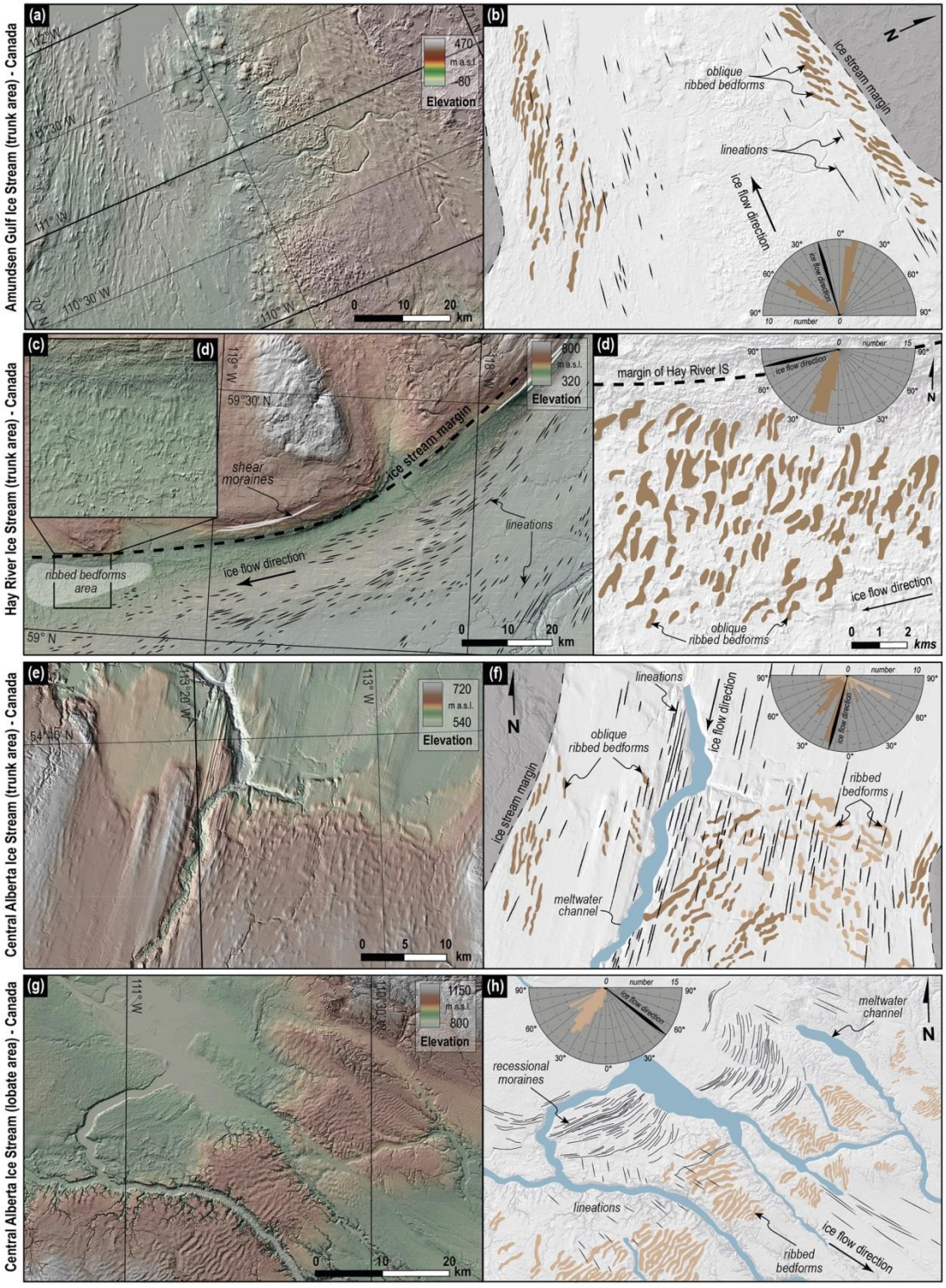

Figure 12. Manual mapping of ribbed bedforms, lineations and ice stream margins along different palaeo-ice stream tracks in Canada. Left panels show digital elevation models and hillshade maps using ArcticDEM database (Porter et al., 2018) and lidar data (Alberta Geological Survey). Right panels show our morphological interpretations and the rose diagrams compiling bedform orientations.

submarginal ribbed bedforms generated below lobe margins have a mean elongation ratio of 3.0 (mean length is 4.2 cm; mean width is 1.4 cm), and their long axis is almost perpendicular to both the local silicone flow and the local silicone compressing axis. Experimental lateral and submarginal ribbed bedforms display wavelengths ranging from 7 to 19 mm and from 10 to 15 mm, respectively. These wavelengths lie in between 0.4 and 1.5 times the overlying silicone thickness, suggesting that experimental ribbed bedforms tend to form with a spacing slightly lower than or equal to the silicone cap thickness, like intermediate-sized ribbed bedforms resembling traction rib patterns (Sergienko and Hindmarsh, 2013). Our observations of ribbed bedforms developing diagonally to the flow and perpendicularly to the silicone compressing axis in the physical experiments suggest that this might also occur in nature. Examples have been noted in the literature such as oblique ribbed bedforms resembling traction ribs in shape and pattern (Stokes et al., 2016), oblique ribbed moraines with superimposed drumlins (Greenwood and Clark, 2008), transverse asymmetrical drumlins (Shaw, 1983) and drumlins with "en echelon" arrangements (Clark et al., 2018). Along the shear margins of natural palaeo-ice stream beds, we mapped lateral ribbed bedforms whose long axes display oblique orientations (15 to 55°) to the ice flow direction along palaeo-shear margins (Fig. 12a–f), while they tend to display a transverse orientation ($\sim 90°$) close to lobe margins (Fig. 12g and h). The lateral ribbed bedforms have medium elongation ratios ($l/w = 2.9$–4.2) and display an arcuate shape and a regular pattern. Along the shear margins of the AGIS (Fig. 12a and b), the obliquity and the apparent overprinting of elongated bedforms were hitherto interpreted as converging and cross-cutting generations of streamlined bedforms (Winsborrow et al., 2004; Stokes et al., 2006b; De Angelis and Kleman, 2007) and mega-scale transverse ridges (Greenwood and Kleman, 2010) and thus as distinct flow sets arising from a change in flow direction over time. Given that the theory of a continuum in subglacial bedforms emerged in recent works (Stokes et al., 2013b; Fowler and Chapwanya et al., 2014; Barchyn et al., 2016; Ely et al., 2016; Fannon et al., 2017), it seems reasonable to propose that bedforms previously interpreted as drumlinized or overprinted ribbed bedforms could form an intermediate bedform between ribbed bedforms and drumlins. Indeed, our experiments demonstrate that streamlined bedforms juxtaposed to oblique ribbed bedforms could form simultaneously in response to the deformation of the strain ellipses, below a single flow set with lateral velocity gradients (Figs. 6–9). If it is common for ribbed bedforms to form diagonally to the ice flow and form under the same flow conditions as streamlined bedforms, then this needs careful consideration when using mapped bedforms to plot former ice flow directions such as in flow sets. Based on this hypothesis, we suggest that in the AGIS (Fig. 12a and b), these landforms were potentially generated in a single phase under unidirectional flow rather than in separate flow sets. An additional argument here is with regard to the elongation ratio obtained from the ridges mapped in this study ($l/w = 4.2$) and compared to the usual and much higher elongation ratio of mega-scale glacial lineations ($l/w = 8.7$; Stokes et al., 2013b). Similarly, even though they did not interpret their orientations, Greenwood and Kleman (2010) suggested that these oblique bedforms occurring along the lateral ice stream margins could correspond to mega-scale ribbed bedforms ($l/w = 5.7$).

Furthermore, Sergienko and Hindmarsh (2013) and Sergienko et al. (2014) deciphered rib-like patterns of high basal shear stress, driven by low hydraulic conductivity, beneath some modern ice streams (e.g. Pine Island Glacier or the Northeast Greenland Ice Stream). Because their orientation and formation may be controlled by the ice deformation directions and not directly by the ice flow directions, rib-like features show clear oblique orientations and symmetrical distribution below the shear margins with angles deviating from 20 to 70° from the ice flow direction (Fig. 13), comparably to the lateral ribbed bedforms depicted in the AGIS (Fig. 12a and b). Regarding the CAIS, the ridges mapped in the upstream (trunk) and downstream (lobe) areas (Fig. 12e–h) were previously interpreted as a type of ribbed bedform mimicking the pattern of traction ribs (Stokes et al., 2016) or overridden thrust masses (Evans et al., 2008, 2014; Atkinson et al., 2018). For both cases (i.e. trunk and lobe positions), we find the exceptional regularity in wavelength, form and scale between ridges to be suggestive of a common rather than entirely separate origin.

The comparison between experimental and natural ribbed bedforms occurring along ice stream margins is here limited to the mapping of already-identified margins of some palaeo-ice streams. Other natural examples can be found in the south of the Wollaston Peninsula, in the northeast of Ireland and in the southernmost sector of the Scandinavian Ice Sheet (Szuman et al., 2021). Despite those observations, the ribbed bedforms presented in this study certainly do not form or are preserved below all lateral shear margins and frontal lobes of palaeo-ice streams. Further investigation on a large sample of palaeo-ice stream beds is thus necessary to explore the conditions of preservation and formation of these characteristic ribbed bedforms along ice stream margins.

Considering their common spatial patterns, orientations, elongations, wavelength/cap thickness ratios and locations, we suggest that the ribbed bedforms (i) reproduced through experimental modelling and (ii) highlighted in our mapping within palaeo-ice stream beds are analogous. We also suggest that they represent ribbed bedforms with a medium elongation ratio like ribbed bedforms resembling traction rib patterns. Our suggestion of commonality between experimental and natural ribbed bedforms based on morphological characteristics is preliminary and has to be tested in view of basal interactions and formation processes.

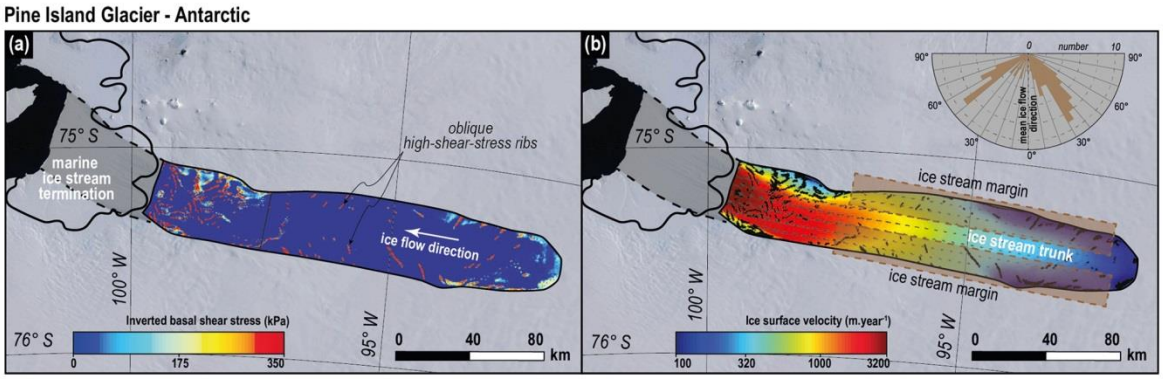

Figure 13. Maps of inverted **(a)** basal shear stress (kPa) beneath Pine Island Glacier and **(b)** ice-surface velocity (modified from Sergienko and Hindmarsh, 2013). Small and isolated areas of very high basal shear stress (red in panel **a** and black in panel **b**) referred to as "high-shear-stress ribs" are obliquely set to the main ice flow direction. The orientations of oblique ribs relative to the mean ice flow direction, located in the rectangular brown areas (along ice stream margins), are compiled in a rose diagram in **(b)** (© Landsat/Copernicus – © Google Earth).

5.2 Processes of ribbed bedform formation at ice stream margins

Our experimental results suggest that ribbed bedforms can form below shear and lobe margins of ice streams, areas experiencing high velocity gradients and transitions in basal water drainage (Echelmeyer et al., 1994; Patterson, 1997; Raymond et al., 2001). As observed in some of their natural counterparts, we experimentally demonstrated that shear margins can develop in response to sustained fast ice flow generated by surging events and lubrication of the silicone–bed interface (Dunse et al., 2015; Schellenberger et al., 2017; Lelandais et al., 2018; Sevestre et al., 2018; Zheng et al., 2019). In the light of these modelling results, we now propose a process of formation of experimental ribbed bedforms (Fig. 14) that takes into account their shape, the overlying cap dynamics and the basal water drainage. We then discuss the formation of experimental ribbed bedforms in the light of existing formation theories.

5.2.1 Formation processes of experimental ribbed bedforms

Bougamont et al. (2011) and Tulaczyk et al. (2000) proposed that the formation of a shear margin can be entirely controlled by the subglacial hydrology if the bed properties and the ice thickness remain constant. According to our experiments, we suggest a similar behaviour: the lateral transition between the widespread and pressurized water film (Fig. S3) in the trunk that induces silicone–bed decoupling and the dewatered outer area that induces silicone–bed coupling generate a stress balance disequilibrium (Fig. 15). In this configuration, the decrease in the basal drag in the trunk area induced by widespread decoupling has to be accommodated by an increase in lateral drag responsible for the formation of shear margins. Margin-parallel simple shear of the silicone occurs along the margins because this region accommodates a high lateral velocity gradient, conditioned by a transition in the basal water drainage (Fig. 15). The combination of silicone–bed coupling and moderate silicone flow velocity (compared to the stream and the outer-stream areas) generates a high basal shear stress along the basal interface and bed deformation below the shear margins. Considering the size of the ribbed bedforms (1 mm in height) and the mean grain size of the bed ($d_{med} = 100\,\mu m$), the deformation of the bed must be characterized at the granular scale. Boundary sliding of individual grains along intergranular shear planes and individual grain rotations can produce bulk deformation (Hamilton et al., 1968; Oda and Konishi, 1974; Owen, 1987; Bestmann and Prior, 2003). Thus, the basal shear stress may be accommodated by deformation resulting in the genesis of regularly spaced ribbed and hummocky bedforms (Fig. 14). The water film spreads between the incipient ribbed bedforms to form a linked-cavity system separated by ridges, whose crests remain coupled to the overlying silicone and keep accommodating basal shear stress. Because of the continuous deformation and flow by simple shear, the instantaneous strain ellipse in the silicone deforms and strain axes form at 45° to the shear margin boundaries while the amount of shear strain increases (Fig. 15). Given that lateral ribbed bedforms form beneath the shear margins where the silicone cap is coupled to the bed, their long axes strike at 45° to the flow direction.

Beneath lobe margins, the water film channelizes into a system of well-developed tunnel valleys resulting in basal coupling and high basal shear stress in interfluve areas (Fig. 15). This reduction in basal lubrication leads to a slowdown in margin advance, a stabilization of the ice lobe and a downstream increase in longitudinal compressive stress. Similarly to lateral ribbed bedforms, the high basal shear

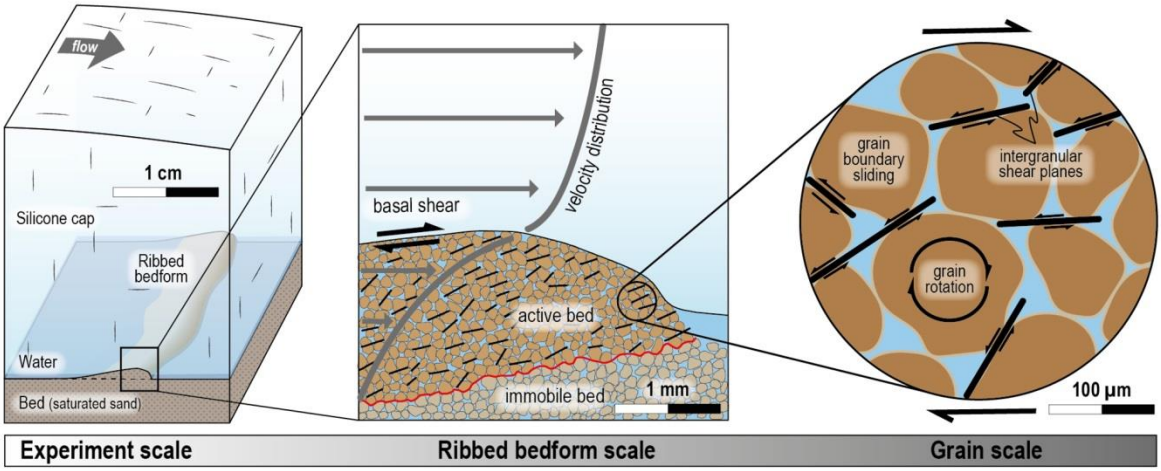

Figure 14. Model of experimental ribbed bedform formation. Deformation of a water-saturated and granular bed during silicone–bed coupling. The active bed (i.e. superficial portion of the bed accommodating the basal shear generated by the flow of silicone putty) is able to produce millimetre-thick bedforms through boundary sliding of individual grains along intergranular shear planes and individual grain rotations.

stress below lobe margins might be periodically accommodated by bed deformation. Once initiated, the submarginal ribbed bedforms continuously grow and elongate perpendicularly to the compressing axes of the strain ellipses (i.e. parallel to the lobe margin) and a linked-cavity system develops in between the set of coalescent submarginal ridges (Fig. 15). Belts of coalescent ribbed bedforms mirroring the shape of the lobe margin can also form subglacially in the distal part of the lobes. Similar coalescent ridges close to the lobe termination have been hitherto interpreted as landforms resulting from the bulldozing of marginal sediments or the subglacial remoulding of former marginal landforms as a result of lobe re-advances (e.g. glaciotectonic thrust masses, overridden moraines and push moraines; Totten, 1969; Boulton, 1986; Benn and Evans, 2010; Evans et al., 2014). We here propose an in situ and self-organized formation process for ribbed bedforms resulting from the shearing of the sedimentary bed (i.e. till layer or weak bedrock) beneath lobes.

5.2.2 Comparison between experimental bedform formation and current theories

The consistent wavelength of natural and experimental ribbed bedforms described in this paper and the bedforms' similarity in form, orientation, location and scale support a common model of formation.

Several theoretical models have been established for the development of subglacial bedforms. The large-scale subglacial meltwater flood hypothesis (Shaw, 2002) does not correspond to the process that occurs in our experiment since silicone flow, rather than water flow, is responsible for the bedforms' formation. Indeed, experimental ribbed bedforms only initiate in zones of silicone–bed coupling along the lateral margins of the flood path. Except for Shaw's theory, all theories of formation of subglacial ribbed bedforms are associated with a till or a sedimentary substratum being coupled to an overlying ice sheet that flows and either deforms or remoulds its bed. Even though the recycling of marginal landforms (i.e. marginal deltas and pushed sediments) during the silicone advance might be involved in the growth of submarginal ribbed bedforms in the experiment, the preexistence of ridges or mounds is not a prerequisite for their formation (Boulton, 1987; Lundqvist, 1989; Möller, 2006). Hättestrand and Kleman (1999) related the development of ribbed bedforms to transitions in the basal thermal regime and to the fracturing of a frozen bed. This cannot occur in our experiment because thermal and melting–freezing processes are not simulated.

Other hypotheses have sought specific mechanisms to explain the formation of ribbed bedforms that are related to neither meltwater flood nor pre-existing ridges or frozen bed. Some view ribbed bedforms as natural instabilities resulting from the coupled flow of ice, meltwater and deformable till and conditioned by spatial variations in effective pressure, the basal thermal regime and bed strength (Hindmarsh, 1998a, b; Fowler, 2000; Schoof, 2007; Dunlop et al., 2008; Chapwanya et al., 2011; Fowler and Chapwanya, 2014; Fannon et al., 2017). Others have suggested that bed deformation can form transverse bedforms through shearing and stacking of sediments, resulting from the flow of ice over the bed interface (Shaw, 1979; Aylsworth and Shilts, 1989; Bouchard, 1989; Lindén et al., 2008; Stokes et al., 2008). Both processes, regardless of the bed rheology, involve a deformable, flat and temperate bed whose deformation results from the

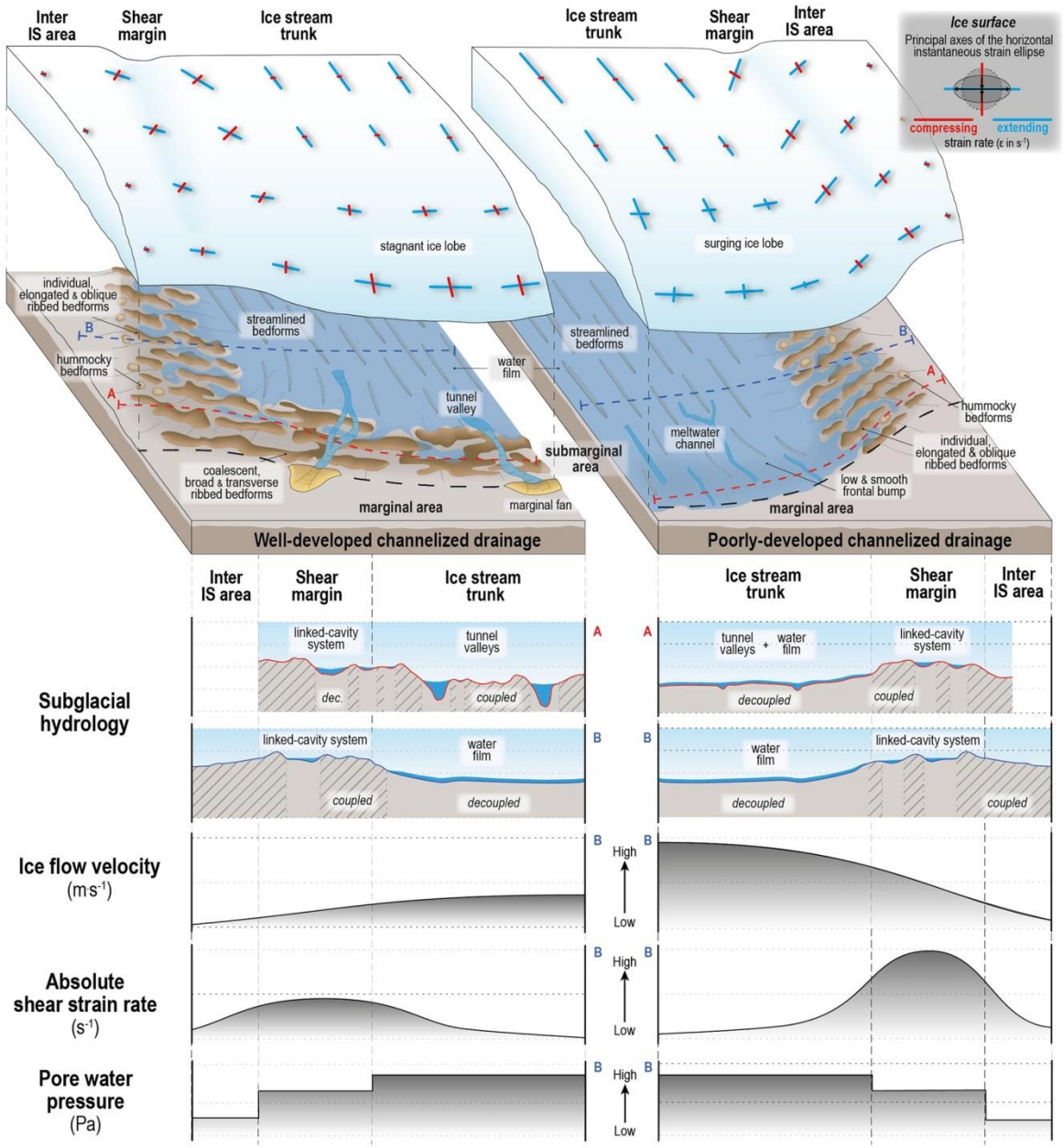

Figure 15. Conceptual model summarizing our observations and interpretations and the proposed role of hydrology, ice velocity and superficial ice strain in generating the observed landforms and their spatial distribution. This is for a terrestrial ice stream context characterized by either well-developed or poorly developed channelized drainage below the lobe frontal margin.

basal shear stress induced by the overlying ice. The high basal shear stress and the associated bed deformation are supposed to enable the formation of periodic subglacial ribbed bedforms transverse and oblique to the ice flow direction, either below modern ice streams (Sergienko and Hindmarsh, 2013; Sergienko et al., 2014) or along palaeo-ice stream beds (Stokes et al., 2016). The bed in our experimental model is flat and temperate and deforms under the action of the basal shear stress induced by the flow of the silicone putty. The model demonstrates that such periodic ribbed bedforms

could form below shear and lobe margins of streams. Consequently, the process responsible for the formation of experimental ribbed bedforms is very similar to the current theories that view natural ribbed bedforms as a product of till deformation under the effect of high shear stress along the basal interface (Fig. 14). However the technical limits of the experimental setup do not allow for these theories to be physically tested since we cannot estimate the water and effective pressure at the scale of a single ribbed bedform.

The contemporary development of ribbed bedforms and linked-cavity systems we observe in the experiments is consistent with the sedimentology work carried out by Lindén et al. (2008) relating the development of ribbed bedforms to the deposition of sediments into the lee-side cavity of moraine ridges. Shear heating within natural shear margins tends to produce high melting rates and subglacial water flow that could favour the development of water drainage systems (e.g. linked cavities, meltwater channels) in between ribbed bedforms (Perol et al., 2015; Perol and Rice, 2015). Hummocky bedforms, which have hitherto been considered mostly marginal landforms associated with ice stagnation and retreat (e.g. Johnson and Clayton, 2003), seem to exhibit a spatial association and a genetic proximity with the ribbed bedforms below the experimental shear margins. Some studies suggest that a morphological continuum between quasi-circular bedforms (i.e. hummocky shape) and ribbed bedforms exists below ice streams and ice sheets (Stokes et al., 2013b; Ely et al., 2016). It is thus appropriate to hypothesize a common origin for some hummocky bedforms coexisting with fields of ribbed bedforms (Fig. 15). They could be alternately interpreted as proto-ribbed bedforms in a continuum of subglacial bedforms inferred from the evolution of the basal shear stress intensity.

The experimental results provide an array of bedforms and contexts that can be used as analogues for ice stream land systems. Our work faithfully reproduces the distal/lobate part of ice streams since channelized features, marginal deltas and pushed sediments are observed. However, some key bedforms observed beneath natural ice streams are not reproduced in the experiment. The analogue model does not reproduce streamlined bedforms that resemble drumlins or mega-scale glacial lineations (MSGLs). If the process that forms experimental ribbed bedforms is identical to those of current till deformation theories, which form both ribbed and streamlined bedforms, our experimental model should allow the formation of drumlins and MSGLs. Streamlined bedforms, as opposed to ribbed bedforms, are mostly explained as formed beneath corridors of high ice flow velocity (Clark, 1993; Stokes and Clark, 1999; Stokes et al., 2013a). In our experiments, we inferred that ribbed bedforms form where the silicone–bed interface is coupled and where silicone flows 10 times faster than the surrounding stagnant silicone cap. By comparison, the trunks of silicone streams – where silicone flows the fastest and ribbed bedforms do not form – exhibit velocities up to 30 times faster than the surrounding silicone cap. As the only way to trigger an experimental silicone stream is to initiate decoupling above a pressurized water film, the basal interface of the silicone stream is entirely decoupled, therefore providing an explanation for the lack of drumlins and MSGL in our experiments. Where the silicone–bed interface is coupled, which is one of the conditions key to forming streamlined bedforms (Boulton, 1987; Hindmarsh et al., 1998a, b; Cofaigh et al., 2005; Fannon et al., 2017), the maximum silicone flow velocity we experimentally reproduce is equal to the silicone flow velocity where ribbed bedforms form; thus it is probably insufficient to initiate streamlined bedforms. Indeed, the presumed velocities that enable drumlin and MSGL formation in nature are 10 or 100 times faster than where ribbed bedforms form, respectively (Stokes et al., 2013b). Furthermore, the low viscosity of the silicone putty and its potential high rates of creep closure prevent the formation of water-free cavities, crevasses and Nye channels and the downstream propagation of basal ice roughness that have sometimes been proposed as prerequisites for the formation of drumlins, MSGLs and shear moraines (Bluemle et al., 1993; Punkari, 1997; Tulaczyk et al., 2001; Clark et al., 2003; Smith et al., 2007).

5.3 Ribbed bedforms in ice stream land systems

5.3.1 Implications for reconstructing the spatial organization of ice streams

Ribbed bedforms are ubiquitous and conspicuous features covering extensive areas of former ice sheet beds (Aylsworth and Shilts, 1989; Hättestrand and Kleman, 1999; Souček et al., 2015; Stokes, 2018). Their occurrence along palaeo-ice stream beds and their relation with the dynamics of fast-flowing ice corridors have however been little discussed since their formation has mostly been attributed to slow ice flow. Ribbed bedforms have been described so far mostly in isolated patches in trunks (Stokes et al., 2008) or in large fields in the onset zone of ice streams (Dyke et al., 1992) and more rarely in corridors (e.g. ribbons track; Dunlop and Clark, 2006; Trommelen et al., 2014) or belts (Greenwood and Kleman, 2010; Stokes et al., 2016) like the ones we mapped in DEMs and on remotely sensed images or identified in the experiments. The coexistence of ribbed bedform patches (i.e. sticky spots) within swarms of streamlined bedforms and alternating corridors of ribbed and streamlined bedforms below ice streams has previously been reported. Ribbed bedforms coexisting with streamlined bedforms have been associated with velocity gradients resulting from the spatial and temporal variations in the distribution of slippery and sticky portions of the bed (Shaw, 1979; Bouchard, 1989; Lindén et al., 2008; Stokes et al., 2008, 2016; Trommelen et al., 2014). By combining experimental and natural observations, we demonstrate that velocity gradients at the ice stream and lobe scale could be identified through specific patterns of ribbed bedform distribution. We therefore hypothesize they

could constitute additional morphological markers contributing to the identification of shear and lobe margins (Fig. 14).

These results could have new implications for the identification of palaeo-ice streams. An important point, if our conclusions hold, is that parallel ridge sequences mirroring the shape of lobate margins might be subglacially produced ribbed bedforms rather than proglacial thrust tectonic ridges, placing the ice margin in a different location in an ensuing reconstruction. Topographic borders and shear moraines are usually used to define the position of palaeo-shear margins (Dyke and Morris, 1988; Dyke et al., 1992; Stokes and Clark, 2002b). Corridors of oblique and regularly spaced ribbed bedforms could be used as an additional proxy for the reconstruction of shear margin positions, notably when shear moraines are not observed or when ice streams are not controlled by the topography. In addition, multiple activations, migrations or retreats of ice streams imply the superimposition of several generations of bedforms that makes ice stream beds a complex palimpsest to decipher (e.g. Clark, 1999). Indeed, the belts of marginal bedforms mimicking the morphology of palaeo-ice lobes and swarms of streamlined bedforms characterizing the position of palaeo-trunks are commonly modified through bed erosion, deformation and overprinting, thus altering partially to fully the initial land systems. In the light of our results, the interpretation of some fields of ribbed bedform forming successive corridors (parallel to ice flow) or belts (perpendicular to ice flow) deserves reconsideration. Depending on the orientation of the ribbed bedform long axes relative to the direction of streamlined bedforms, as well as on the elongation ratio and the spacing between individual bedforms, the corridors and belts of ribbed bedforms could indicate lateral and/or frontal migrations of palaeo-ice stream positions through time. Thus, this study provides additional mapping criteria to constrain the temporal migration of previously identified palaeo-ice streams (e.g. CAIS; Fig. 12e and f). It is important to note that depending on their size, corridors of ribbed bedforms could also illustrate transverse velocity gradients within ice streams, potentially across ice bands flowing at distinct velocities due to variations in basal stick-slip conditions and subglacial roughness.

This hypothesis needs to be tested through the identification of corridors and belts of ribbed bedforms in order to establish if they could correlate with hitherto non-recognized palaeo-ice stream margins. If this hypothesis is validated, ribbed bedforms with specific shapes and orientations could potentially help identify new palaeo-ice streams through the identification of their margins, particularly when features such as MSGL are poorly preserved or absent.

5.3.2 Implications for ice stream dynamics and subglacial hydrology

Our experimental model does not reproduce thermo-mechanical feedbacks within the ice, which have been suggested as the first mechanisms responsible for the self-organization of ice streams (Payne and Dongelmans, 1997; Hindmarsh, 2009). Despite this lack of thermally based mechanisms, streams initiate in the model as a result of interactions with the basal hydrology as suggested by Winsborrow et al. (2010) and Kyrke-Smith et al. (2014). The combination of analogue modelling – which demonstrates that ribbed bedforms can form through the interaction of silicone flow, water flow and bed deformation – and ice stream bed mapping has allowed us to establish a link between bedform development, ice stream dynamics, and the evolution of spatially and temporally efficient drainage systems (Fig. 14). The efficiency of the subglacial drainage system is estimated by the capacity of channelized features (e.g. tunnel valleys and meltwater channels) to accommodate the meltwater discharge (Moon et al., 2014). Therefore, when considering the relationships between the distribution of subglacial water, the development of channelized features and the development of ribbed bedforms below experimental lobes, we suggest that the presence or absence of submarginal ribbed bedforms along lobate margins might reveal the type and efficiency of meltwater drainage below marginal lobes of terrestrially terminating ice streams (Raymond, 1987; Patterson, 1997; Kim et al., 2016). For instance, well-developed channelization facilitates subglacial drainage by concentrating meltwater flow into tunnel valleys and induces an overall increase in basal drag beneath the lobe due to water pressure reduction, widespread ice–bed coupling and elevated basal shear stress. The increase in basal drag, highlighted by the development of submarginal ribbed bedforms, is responsible for ice stream slowdown and stabilization of the marginal lobe. This configuration should be associated with the formation of well-developed end moraines (Fig. 14) because the margin experiences a standstill over time. Conversely, poorly developed channelization characterized by shallow and narrow meltwater channels reveals the incapacity of the subglacial drainage system to evacuate all the meltwater efficiently. This configuration is more likely characterized by higher water pressure, widespread ice–bed decoupling and distributed drainage that promote basal sliding and inhibit the formation of ribbed bedforms in sub-marginal environments. The inefficient drainage might favour the storage of meltwater up-ice during periods of increased melting that is episodically delivered to the margin through outburst floods. We suggest that outburst flood events and basal sliding could alter the dynamics of ice streams and trigger surging of ice lobes. The absence of submarginal ribbed bedforms and a poorly developed drainage system should therefore be associated with typical surge diagnostic features dominated by compressional structures (Fig. 14). Glaciotectonic thrust masses and crevasse-squeezed ridges have notably been observed in southeast Alberta and linked to the dynamics of surging lobes during melting and retreat of the Laurentide Ice Sheet (Evans et al., 2020).

6 Conclusion

Despite the ubiquitous and extensive nature of subglacially produced ribbed bedforms beneath former ice sheets (variously called Rogen moraines, ribbed moraines, ribbed bedforms, mega-scale transverse ridges), their significance in ice stream land systems and their formation processes remain poorly understood. Providing new constraints on the formation, evolution and distribution of ribbed bedforms is therefore critical to characterizing ice–bed interactions beneath key zones of ice streams and reconstructing past glacial dynamics. Based on experimental modelling and geomorphological mapping of natural ice stream beds, we suggest that ribbed bedforms are produced subglacially beneath ice streams margins where the soft bed is coupled to the ice and subject to high basal shear stresses that result from abrupt lateral and longitudinal variations in subglacial drainage characteristics and ice flow velocity. We suggest that these ribbed bedforms develop both (i) in narrow corridors parallel to lineations and (ii) in broad belts parallel to and upstream of marginal landforms. The former (i.e. lateral ribbed bedforms) can be used to highlight the position of ice stream shear margins. These ribbed bedforms are regularly spaced, slightly arcuate and moderately elongated ($l/w = 3$ to 4). Due to the specific stress and strain configuration, lateral ribbed bedforms developing beneath shear margins of ice streams should present higher elongation ratios than the classic ribbed/Rogen moraines that occur outside ice stream contexts. In our experiments the long axis of ribbed bedforms develops perpendicularly to the compressing axis of the strain ellipse and at 45° to the shear margin boundary. This oblique relationship has implications for those reconstructing palaeo-ice flow directions (flow sets) from bedforms, where misinterpretation could be made using the usual assumption of ribs forming orthogonally to the flow. Rather than reflecting the flow direction, we demonstrate that the ribbed bedforms are compressional structures whose orientation depends on the orientation of strain axes. The latter (i.e. submarginal ribbed bedforms) form larger belts of coalescent and broad ribbed bedforms characterized by arcuate crests arranged orthogonally to the compressing axis. They are interpreted as the morphological imprints of ice lobe positions, but unlike the usual belt of marginal landforms hitherto described in the literature and interpreted as proglacial glaciotectonic structures, this type of ribbed bedform initiates and develops subglacially from the basal shearing of a flat subglacial bed. Its preferential development in interfluve areas between meltwater channels implies that its formation is enhanced in zones of channelized and efficient drainage where extensive areas of ice–bed coupling exist due to the decrease in subglacial water pressure. We therefore suggest that those two types of ribbed bedforms (i.e. lateral and submarginal) result from the same deformation process of the underlying soft bed.

These results provide new criteria for palaeoglaciological reconstructions of ice streams to help identify lateral shear and frontal lobes and provide insights into ice–bed interactions, ice dynamics and subglacial hydrology. Whether the process of ribbed bedforms discussed here in the context of ice streams and lobes is relevant and applicable more widely to the full population of ribbed/Rogen moraines found extensively across many ice sheet beds is still an open question.

Code availability. The code for the DEM reconstruction of experimental beds is available from the corresponding author of Lelandais et al. (2016). The code for the calculation of the horizontal deformation of the silicone cap is available under https://github.com/JeanVerite/Verite_et_al_2021 (last access: 23 June 2021) (GNU General Public License v2.0).

Data availability. All datasets used in this paper are available from the corresponding author on request.

Supplement. The supplement related to this article is available online at: https://doi.org/10.5194/tc-15-2889-2021-supplement.

Author contributions. ER conceived this research project with contributions by OB, SP and CDC and gathered funding. RM developed the experimental lab and contributed to the computation of strains in the experiments. TL, DP, ER and RM designed the experimental device. JV and ER conducted the experiments. JV post-treated the experiments, carried out the palaeoglaciological mapping and wrote the first draft of the paper. All authors contributed to the interpretations of the results and to the proofreading of the paper.

Competing interests. The authors declare that they have no conflict of interest.

Disclaimer. Publisher's note: Copernicus Publications remains neutral with regard to jurisdictional claims in published maps and institutional affiliations.

Acknowledgements. This study is part of the Ice-Collapse project (The dynamics of ice sheet collapse in deglaciation periods) funded by the French Agence Nationale de la Recherche through grant ANR-18-CE01-0009. This project has benefited from the PALGLAC team of researchers and received funding from the European Research Council (ERC) under the European Union's Horizon 2020 research and innovation programme (grant agreement no. 787263).

Financial support. This research has been supported by the Agence Nationale de la Recherche (grant no. ANR-18-CE01-0009) and the European Research Council, H2020 (PALGLAC grant no. 787263).

Review statement. This paper was edited by Delphine Lannuzel and reviewed by Richard C. A. Hindmarsh and Martin Ross.

References

Aario, R.: Classification and terminology of morainic landforms in Finland, Boreas, 6, 87–100, https://doi.org/10.1111/j.1502-3885.1977.tb00338.x, 1977.

Alley, R. B.: In search of ice-stream sticky spots, J. Glaciol., 39, 447–454, https://doi.org/10.3189/s0022143000016336, 1993.

Atkinson, N., Utting, D. J., and Pawley, S. M.: An Update to the Glacial Landforms Map of Alberta, in: Alberta Geological Survey, 735, https://doi.org/10.13140/RG.2.2.20500.40320, 2018.

Aylsworth, J. M. and Shilts, W. W.: Bedforms of the Keewatin Ice Sheet, Canada, Sed. Geol., 62, 407–428, https://doi.org/10.1016/0037-0738(89)90129-2, 1989.

Bamber, J. L., Vaughan, D. G., and Joughin, I.: Widespread complex flow in the interior of the antarctic ice sheet, Science, 287, 1248–1250, https://doi.org/10.1126/science.287.5456.1248, 2000.

Barchyn, T. E., Dowling, T. P. F., Stokes, C. R., and Hugenholtz, C. H.: Subglacial bed form morphology controlled by ice speed and sediment thickness, Geophys. Res. Lett., 43, 7572–7580, https://doi.org/10.1002/2016GL069558, 2016.

Benn, D. I. and Evans, D. J. A.: Glaciers and Glaciation, 2nd edn., Hodder Education, London, 802 pp., 2010.

Bestmann, M. and Prior, D. J.: Intragranular dynamic recrystallization in naturally deformed calcite marble: Diffusion accommodated grain boundary sliding as a result of subgrain rotation recrystallization, J. Struct. Geol., 25, 1597–1613, https://doi.org/10.1016/S0191-8141(03)00006-3, 2003.

Bluemle, J. P., Lord, M. L., and Hunke, N. T.: Exceptionnaly long, narrow drumlins formed in subglacial cavities, North Dakota, Boreas, 22, 15–24, https://doi.org/10.4135/9781544354453.n41, 1993.

Bouchard, M. A.: Subglacial landforms and deposits in central and northern Québec, Canada, with emphasis on Rogen moraines. Sedimentary Geology, 62, 293–308, https://doi.org/10.1016/0037-0738(89)90120-6, 1989.

Bougamont, M., Price, S. F., Christoffersen, P., and Payne, A. J.: Dynamic patterns of ice stream flow in a 3-D higher-order ice sheetmodel with plastic bed and simplified hydrology, J. Geophys. Res., 116, 1–13, https://doi.org/10.1029/2011JF002025, 2011.

Boulton, G. S.: Push-moraines and glacier-contact fans in marine and terrestrial environments, Sedimentology, 33, 677–698, https://doi.org/10.1111/j.1365-3091.1986.tb01969.x, 1986.

Boulton, G. S.: A theory of drumlin formation by subglacial sediment, in: Drumlin Symposium, edited by: Rose, J. and Menzies, J., Balkema, Rotterdam, 25–80, 1987.

Chandler, B. M. P., Evans, D. J. A., and Roberts, D. H.: Characteristics of recessional moraines at a temperate glacier in SE Iceland: Insights into patterns, rates and drivers of glacier retreat, Quaternary Sci. Rev., 135, 171–205, https://doi.org/10.1016/j.quascirev.2016.01.025, 2016.

Chapwanya, M., Clark, C. D., and Fowler, A. C.: Numerical computations of a theoretical model of ribbed moraine formation, Earth Surf. Proc. Land., 36, 1105–1112, https://doi.org/10.1002/esp.2138, 2011.

Clark, C. D.: Mega-scale glacial lineations and cross-cutting ice-flow landforms, Earth Surf. Proc. Land., 18, 1–29, https://doi.org/10.1002/esp.3290180102, 1993.

Clark, C. D.: Glaciodynamic context of subglacial bedform generation and preservation, Ann. Glaciol., 28, 23–32, https://doi.org/10.3189/172756499781821832, 1999.

Clark, C. D.: Emergent drumlins and their clones: from till dilatancy to flow instabilities, J. Glaciol., 56, 1011–1025, https://doi.org/10.3189/002214311796406068, 2010.

Clark, C. D. and Stokes, C. R.: Palaeo-ice stream landsystem, in: Glacial Landsystems, edited by: Evans, D. J. A., 204–227, Edward Arnold, London, 2003.

Clark, C. D., Tulaczyk, S. M., Stokes, C. R., and Canals, M.: A groove-ploughing theory for the production of mega-scale glacial lineations, and implications for ice-stream mechanics, J. Glaciol., 49, 240–256, https://doi.org/10.3189/172756503781830719, 2003.

Clark, C. D., Ely, J. C., Spagnolo, M., Hahn, U., Hughes, A. L., and Stokes, C. R.: Spatial organization of drumlins, Earth Surf. Proc. Land., 43, 499–513, https://doi.org/10.1002/esp.4192, 2018.

Cofaigh, C. O., Dowdeswell, J. A., Allen, C. S., Hiemstra, J. F., Pudsey, C. J., Evans, J., and Evans, D. J. A.: Flow dynamics and till genesis associated with a marine-based Antarctic palaeo-ice stream, Quaternary Sci. Rev., 24, 709–740, https://doi.org/10.1016/j.quascirev.2004.10.006, 2005.

Cowan, W. R.: Ribbed moraine: Till-fabric analysis and origin, Can. J. Earth Sci., 5, 1145–1159, https://doi.org/10.1139/e68-112, 1968.

De Angelis, H. and Kleman, J.: Palaeo-ice streams in the Foxe/Baffin sector of the Laurentide Ice Sheet, Quaternary Sci. Rev., 26, 1313–1331, https://doi.org/10.1016/j.quascirev.2007.02.010, 2007.

Denton, G. H. and Hughes, T. J. (Eds.): The last great ice sheets, vol. 1, Wiley-Interscience, New York, 1981.

Dunlop, P. and Clark, C. D.: The morphological characteristics of ribbed moraine, Quaternary Sci. Rev., 25, 1668–1691, https://doi.org/10.1016/j.quascirev.2006.01.002, 2006.

Dunlop, P., Clark, C. D., and Hindmarsh, R. C.: Bed ribbing instability explanation: testing a numerical model of ribbed moraine formation arising from coupled flow of ice and subglacial sediment, J. Geophys. Res.-Earth Surf., 113, https://doi.org/10.1029/2007JF000954, 2008.

Dunse, T., Schellenberger, T., Hagen, J. O., Kääb, A., Schuler, T. V., and Reijmer, C. H.: Glacier-surge mechanisms promoted by a hydro-thermodynamic feedback to summer melt, The Cryosphere, 9, 197–215, https://doi.org/10.5194/tc-9-197-2015, 2015.

Dyke, A. S. and Morris, T. F.: Drumlin fields, dispersal trains and ice streams in Arctic Canada, Canadian Geographer/Le Géographe Canadien, 32, 86–90, https://doi.org/10.1111/j.1541-0064.1988.tb00860.x, 1988.

Dyke, A. S., Morris, T. F., Green, D. E. C., and England, J.: Quaternary geology of Prince of Wales Island, Arctic Canada, in: Memoir, Geol. Surv. Canada, 433, 142, https://doi.org/10.4095/134058, 1992.

Ebert, K. and Kleman, J.: Circular moraine features on the Varanger Peninsula, northern Norway, and their possible relation to polythermal ice sheet coverage, Geomorphology, 62, 159–168, https://doi.org/10.1016/j.geomorph.2004.02.009, 2004.

Echelmeyer, K. A., Harrison, W. D., Larsen, C., and Mitchell, J. E.: The role of the margins in the dynamics of an active ice stream, J. Glaciol., 40, 527–538, https://doi.org/10.3189/S0022143000012417, 1994.

Ely, J. C., Clark, C. D., Spagnolo, M., Stokes, C. R., Greenwood, S. L., Hughes, A. L. C., Dunlop, P., and Hess, D.: Do subglacial bedforms comprise a size and shape continuum?, Geomorphology, 257, 108–119, https://doi.org/10.1016/j.geomorph.2016.01.001, 2016.

Engelhardt, H., Humphrey, N., Kamb, B., and Fahnestock, M.: Physical conditions at the base of a fast moving Antarctic ice stream, Science, 248, 57–59, https://doi.org/10.1126/science.248.4951.57, 1990.

Evans, D. J. A. and Hiemstra, J. F.: Till deposition by glacier submarginal, incremental thickening, Earth Surf. Proc. Land., 30, 1633–1662, https://doi.org/10.1002/esp.1224, 2005.

Evans, D. J. A., Clark, C. D., and Rea, B. R.: Landform and sediment imprints of fast glacier flow in the southwest Laurentide Ice Sheet, J. Quaternary Sci., 23, 249–272, https://doi.org/10.1002/jqs.1141, 2008.

Evans, D. J. A., Young, N. J. P., and Cofaigh, C. O.: Glacial geomorphology of terrestrial-terminating fast flow lobes/ice stream margins in the southwest Laurentide Ice Sheet, Geomorphology, 204, 86–113, https://doi.org/10.1016/j.geomorph.2013.07.031, 2014.

Evans, D. J. A., Ewertowski, M., and Orton, C.: Fláajökull (north lobe), Iceland: active temperate piedmont lobe glacial landsystem, J. Maps, 12, 777–789, https://doi.org/10.1080/17445647.2015.1073185, 2015.

Evans, D. J., Storrar, R. D., and Rea, B. R.: Crevasse-squeeze ridge corridors: diagnostic features of late-stage palaeo-ice stream activity, Geomorphology, 258, 40–50, https://doi.org/10.1016/j.geomorph.2016.01.017, 2016.

Evans, D. J. A., Atkinson, N., and Phillips, E.: Glacial geomorphology of the Neutral Hills Uplands, southeast Alberta, Canada: The process-form imprints of dynamic ice streams and surging ice lobes, Geomorphology, 350, 106910, https://doi.org/10.1016/j.geomorph.2019.106910, 2020.

Fannon, J. S., Fowler, A. C., and Moyles, I. R.: Numerical simulations of drumlin formation, P. Roy. Soc. A, 473, 20170220, https://doi.org/10.1098/rspa.2017.0220, 2017.

Fowler, A. C.: An instability mechanism for drumlin formation, Geological Society Special Publication, 176, 307–319, https://doi.org/10.1144/GSL.SP.2000.176.01.23, 2000.

Fowler, A. C. and Chapwanya, M.: An instability theory for the formation of ribbed moraine, drumlins and megascale glacial lineations, P. Roy. Soc. A, 470, 20140185, https://doi.org/10.1098/rspa.2014.0185, 2014.

Goldstein, R., Engelhardt, H. F., Kamb, B., and Frolich, R.: Satellite Radar lnterferometry for Monitoring lce-sheet Motion: application to Antarctic Ice Stream, Science, 262, 1525–1530, https://doi.org/10.1126/science.262.5139.1525, 1993.

Greenwood, S. L. and Clark, C. D.: Subglacial bedforms of the Irish ice sheet, J. Maps, 4, 332–357, https://doi.org/10.4113/jom.2008.1030, 2008.

Greenwood, S. L. and Kleman, J.: Glacial landforms of extreme size in the Keewatin sector of the Laurentide Ice Sheet, Quaternary Sci. Rev., 29, 1894–1910, https://doi.org/10.1016/j.quascirev.2010.04.010, 2010.

Hamilton, N., Owens, W. H., and Rees, A. I.: Laboratory experiments on the production of grain orientation in shearing sand, J. Geol., 76, 465–472, https://doi.org/10.1086/627344, 1968.

Hättestrand, C. and Kleman, J.: Ribbed moraine formation, Quaternary Sci. Rev., 18, 43–61, https://doi.org/10.1016/S0277-3791(97)00094-2, 1999.

Hindmarsh, R. C. A.: Drumlinization and drumlin-forming instabilities: Viscous till mechanisms, J. Glaciol., 44, 293–314, https://doi.org/10.1017/S002214300000263X, 1998a.

Hindmarsh, R. C. A.: The stability of a viscous till sheet coupled with ice flow, considered at wavelengths less than the ice thickness, J. Glaciol., 44, 285–292, https://doi.org/10.1017/S0022143000002628, 1998b.

Hindmarsh, R. C. A.: Consistent generation of ice-streams via thermo-viscous instabilities modulated by membrane stresses, Geophys. Res. Lett., 36, 1–6, https://doi.org/10.1029/2008GL036877, 2009.

Hughes, O.: Surficial geology, Nichicun-Kaniapiskau map-area, Quebec, 1964.

Johnson, M. D. and Clayton, L.: Supraglacial landsystems in lowland terrain, in: Glacial Landsystems, edited by: Evans, D. J. A., 228–258, Edward Arnold, London, 2003.

Kamb, B.: Rheological nonlinearity and flow instability in the deforming bed mechanism of ice stream motion, J. Geophys. Res., 96, 16585–16595, https://doi.org/10.1029/91jb00946, 1991.

Kim, B.-H., Lee, C.-K., Seo, K.-W., Lee, W. S., and Scambos, T.: Active subglacial lakes and channelized water flow beneath the Kamb Ice Stream, The Cryosphere, 10, 2971–2980, https://doi.org/10.5194/tc-10-2971-2016, 2016.

Kleman, J. and Borgström, I.: Reconstruction of palaeo-ice sheets: The use of geomorphological data, Earth Surf. Proc. Land., 21, 893–909, https://doi.org/10.1002/(SICI)1096-9837(199610)21:10<893::AID-ESP620>3.0.CO;2-U, 1996.

Kyrke-Smith, T. M., Katz, R. F., and Fowler, A. C.: Subglacial hydrology and the formation of ice streams, P. R. Soc. A, 470, 20130494, https://doi.org/10.1098/rspa.2013.0494, 2014

Lelandais, T., Mourgues, R., Ravier, É., Pochat, S., Strzerzynski, P., and Bourgeois, O.: Experimental modeling of pressurized subglacial water flow: Implications for tunnel valley formation, J. Geophys. Res.-Earth Surf., 121, 2022–2041, https://doi.org/10.1002/2016JF003957, 2016.

Lelandais, T., Ravier, É., Pochat, S., Bourgeois, O., Clark, C., Mourgues, R., and Strzerzynski, P.: Modelled subglacial floods and tunnel valleys control the life cycle of transitory ice streams, The Cryosphere, 12, 2759–2772, https://doi.org/10.5194/tc-12-2759-2018, 2018.

Lindén, M., Möller, P., and Adrielsson, L.: Ribbed moraine formed by subglacial folding, thrust stacking and lee-side cavity infill, Boreas, 37, 102–131, https://doi.org/10.1111/j.1502-3885.2007.00002.x, 2008.

Lundqvist, J.: Problems of the so-called Ribbed moraines, Sverige Geologiske Undersökning, Series C, 648, 1969.

Lundqvist, J.: Rogen (ribbed) moraine-identification and possible origin, Sed. Geol., 62, 281–292, https://doi.org/10.1016/0037-0738(89)90119-X, 1989.

Margold, M., Stokes, C. R., and Clark, C. D.: Ice streams in the Laurentide Ice Sheet: Identification, characteristics and comparison to modern ice sheets, Earth-Sci. Rev., 143, 117–146, https://doi.org/10.1016/j.earscirev.2015.01.011, 2015.

Margold, M., Stokes, C. R., and Clark, C. D.: Reconciling records of ice streaming and ice margin retreat to produce a palaeogeographic reconstruction of the deglaciation of the Laurentide Ice Sheet, Quaternary Sci. Rev., 189, 1–30, https://doi.org/10.1016/j.quascirev.2018.03.013, 2018.

Marich, A., Batterson, M., and Bell, T.: The Morphology and Sedimentological Analyses of Rogen Moraines, Central Avalon Peninsula, Newfoundland, Curr. Res., 5, 1–14, 2005.

Menzies, J.: A review of the literature on the formation and location of drumlins, Earth-Sci. Rev., 14, 315–359, https://doi.org/10.1016/0012-8252(79)90093-X, 1979.

Minchew, B. and Joughin, I.: Toward a universal glacier slip law, Science, 368, 29–30, https://doi.org/10.1126/science.abb3566, 2020.

Möller, P.: Rogen moraine: An example of glacial reshaping of pre-existing landforms, Quaternary Sci. Rev., 25, 362–389, https://doi.org/10.1016/j.quascirev.2005.01.011, 2006.

Möller, P.: Melt-out till and ribbed moraine formation, a case study from south Sweden, Sed. Geol., 232, 161–180, https://doi.org/10.1016/j.sedgeo.2009.11.003, 2010.

Moon, T., Joughin, I., Smith, B., Van Den Broeke, M. R., Van De Berg, W. J., Noël, B., and Usher, M.: Distinct patterns of seasonal Greenland glacier velocity, Geophys. Res. Lett., 41, 7209–7216, https://doi.org/10.1002/2014GL061836, 2014.

Newton, M., Evans, D. J. A., Roberts, D. H., and Stokes, C. R.: Bedrock mega-grooves in glaciated terrain: A review, Earth-Sci. Rev., 185, 57–79, https://doi.org/10.1016/j.earscirev.2018.03.007, 2018.

Nye, J. F.: The motion of ice sheets and glaciers, J. Glaciol., 3, 493–507, https://doi.org/10.3189/s002214300001724x, 1959.

Oda, M. and Konishi, J.: Microscopic deformation mechanism of granular material in simple shear, Soil and Foundations, 14, 25–38. https://doi.org/10.3208/sandf1972.14.4_25, 1974.

Owen, G.: Deformation processes in unconsolidated sands, Geological Society Special Publication, 29, 11–24, https://doi.org/10.1144/GSL.SP.1987.029.01.02, 1987.

Paola, C., Straub, K., Mohrig, D., and Reinhardt, L.: The "unreasonable effectiveness" of stratigraphic and geomorphic experiments, Earth-Sci. Rev., 97, 1–43, https://doi.org/10.1016/j.earscirev.2009.05.003, 2009.

Paterson, W. S. B.: Laurentide ice sheet: estimated volumes during late Wisconsin, Rev. Geophys., 10, 885–917, https://doi.org/10.1029/RG010i004p00885, 1972

Paterson, W. S. B.: The Physics of Glaciers, 3rd edn., Pergamon, UK, Oxford, 1994.

Patterson, C. J.: Southern Laurentide ice lobes were created by ice streams: Des Moines Lobe in Minnesota, USA, Sed. Geol., 111, 249–261, https://doi.org/10.1016/S0037-0738(97)00018-3, 1997.

Payne, A. J. and Dongelmans, P. W.: Self-organization in the thermomechanical flow of ice sheets, J. Geophys. Res.-Sol. Ea., 102, 12219–12233. https://doi.org/10.1029/97jb00513, 1997.

Perol, T. and Rice, J. R.: Shear heating and weakening of the margins of West Antarctic ice streams, May, 3406–3413, https://doi.org/10.1002/2015GL063638, 2015.

Perol, T., Rice, J. R., Platt, J. D., and Suckale, J.: Subglacial hydrology and ice stream margin locations Special Section, J. Geophys. Res.-Earth Surf., 120, 1352–1368, https://doi.org/10.1002/2015JF003542, 2015.

Porter, C., Morin, P., Howat, I., Noh, M.-J., Bates, B., Peterman, K., Keesey, S., Schlenk, M., Gardiner, J., Tomko, K., Willis, M., Kelleher, C., Cloutier, M., Husby, E., Foga, S., Nakamura, H., Platson, M., Wethington, M., Willamson, C., Bauer, G., Enos, J., Arnold, G., Kramer, W., Becker, P., Doshi, A., D'Souza, C., Cummens, P., Laurier, F., and Bojensen, M.: ArcticDEM, Harvard Dataverse, V1, https://doi.org/10.7910/DVN/OHHUKH, 2018.

Punkari, M.: Glacial and glaciofluvial deposits in the interlobate areas of the Scandinavian Ice Sheet, Quaternary Sci. Rev., 16, 741–753, https://doi.org/10.1016/S0277-3791(97)00020-6, 1997.

Ramsay, J. and Huber, M.: The techniques of modern structural geology: Folds and fractures, Elsevier Science, Academic press, 1987.

Raymond, C. F.: How Do Glaciers Surge? A Review, J. Geophys. Res., 92, 9121–9134, https://doi.org/10.1029/JB092iB09p09121,1987.

Raymond, C. F., Echelmeyer, K. A., Whillans, I. M., and Doake, C. S. M.: Ice stream shear margins, Antarct. Res. Ser., 77, 137–155, https://doi.org/10.1029/AR077p0137, 2001.

Rose, J.: Drumlins as part of a glacier bedform continuum, in: Drumlin symposium, Balkema, Rotterdam, https://doi.org/10.1111/jawr.2010.46.issue-5, 1987.

Sarala, P.: Ribbed moraine stratigraphy and formation in southern Finnish Lapland, J. Quaternary Sci., 21, 387–398, https://doi.org/10.1002/jqs.995, 2006.

Schellenberger, T., Dunse, T., Kääb, A., Schuler, T. V., Hagen, J. O., and Reijmer, C. H.: Multi-year surface velocities and sea-level rise contribution of the Basin-3 and Basin-2 surges, Austfonna, Svalbard, The Cryosphere Discuss. [preprint], https://doi.org/10.5194/tc-2017-5, 2017.

Schoof, C.: Pressure-dependent viscosity and interfacial instability in coupled ice-sediment flow, J. Fluid Mech., 570, 227–252, https://doi.org/10.1017/S0022112006002874, 2007.

Sergienko, O. V. and Hindmarsh, R. C. A.: Regular patterns in frictional resistance of ice-stream beds seen by surface data inversion, Science, 342, 1086–1089, https://doi.org/10.1126/science.1243903, 2013.

Sergienko, O. V., Creyts, T. T., and Hindmarsh, R. C. A.: Similarity of organized patterns in driving and basal stresses of Antarctic and Greenland ice sheets beneath extensive areas of basal sliding, Geophys. Res. Lett., 41, 3925–3932, https://doi.org/10.1002/2014GL059976, 2014.

Sevestre, H., Benn, D. I., Luckman, A., Nuth, C., Kohler, J., Lindbäck, K., and Pettersson, R.: Tidewater Glacier Surges Initiated at the Terminus, J. Geophys. Res.-Earth Surf., 123, 1035–1051, https://doi.org/10.1029/2017JF004358, 2018.

Shaw, J.: Genesis of the Sveg tills and Rogen moraines of central Sweden: a model of basal melt out, Boreas, 8, 409–426, https://doi.org/10.1111/j.1502-3885.1979.tb00437.x, 1979.

Shaw, J.: Drumlin formation related to inverted meltwater erosional marks, J. Glaciol., 29, 461–479, https://doi.org/10.1017/S0022143000030367, 1983.

Shaw, J.: The meltwater hypothesis for subglacial bedforms, Quaternary Int., 90, 5–22, https://doi.org/10.1016/S1040-6182(01)00089-1, 2002.

Smith, A. M., Murray, T., Nicholls, K. W., Makinson, K., Adalgeirsdóttir, G., Behar, A. E., and Vaughan, D. G.: Rapid erosion, drumlin formation, and changing hydrology

beneath an Antarctic ice stream, Geology, 35, 127–130, https://doi.org/10.1130/G23036A.1, 2007.

Souček, O., Bourgeois, O., Pochat, S., and Guidat, T.: A 3 Ga old polythermal ice sheet in Isidis Planitia, Mars: Dynamics and thermal regime inferred from numerical modeling, Earth Planet. Sc. Lett., 426, 176–190, https://doi.org/10.1016/j.epsl.2015.06.038, 2015.

Stokes, C. R.: Geomorphology under ice streams: Moving from form to process, Earth Surf. Proc. Land., 43, 85–123, https://doi.org/10.1002/esp.4259, 2018.

Stokes, C. R. and Clark, C. D.: Geomorphological criteria for identifying Pleistocene ice streams, Ann. Glaciol., 28, 67–74, https://doi.org/10.3189/172756499781821625, 1999.

Stokes, C. R. and Clark, C. D.: Palaeo-ice streams, Quaternary Sci. Rev., 20, 1437–1457, https://doi.org/10.1016/S0277-3791(01)00003-8, 2001.

Stokes, C. R. and Clark, C. D.: Are long subglacial bedforms indicative of fast ice flow?, Boreas, 31, 239–249, https://doi.org/10.1111/j.1502-3885.2002.tb01070.x, 2002a.

Stokes, C. R. and Clark, C. D.: Ice stream shear margin moraines, Earth Surf. Proc. Land., 27, 547–558, https://doi.org/10.1002/esp.326, 2002b.

Stokes, C. R. and Clark, C. D.: The Dubawnt Lake palaeo-ice stream: evidence for dynamic ice sheet behaviour on the Canadian Shield and insights regarding the controls on ice-stream location and vigour. Boreas, 32, 263–279, https://doi.org/10.1080/03009480310001155, 2003.

Stokes, C. R., Clark, C. D., Lian, O. B., and Tulaczyk, S.: Geomorphological map of ribbed moraines on the Dubawnt Lake Palaeo-Ice Stream bed: A signature of ice stream shut-down?, J. Maps, 2, 1–9, https://doi.org/10.4113/jom.2006.43, 2006a.

Stokes, C. R., Clark, C. D., and Winsborrow, C. M.: Subglacial bedform evidence for a major palaeo-ice stream and its retreat phases in Amundsen Gulf, Canadian Arctic Archipelago, J. Quaternary Sci., 21, 399–412, https://doi.org/10.1002/jqs.991, 2006b.

Stokes, C. R., Clark, C. D., Lian, O. B., and Tulaczyk, S.: Ice stream sticky spots: A review of their identification and influence beneath contemporary and palaeo-ice streams, Earth-Sci. Rev., 81, 217–249, https://doi.org/10.1016/j.earscirev.2007.01.002, 2007.

Stokes, C. R., Lian, O. B., Tulaczyk, S., and Clark, C. D.: Superimposition of ribbed moraines on a palaeo-ice-stream bed: implications for ice stream dynamics and shutdown, Earth Surf. Proc. Land., 33, 593–609, https://doi.org/10.1002/esp.1671, 2008.

Stokes, C. R., Fowler, A. C., Clark, C. D., Hindmarsh, R. C., and Spagnolo, M.: The instability theory of drumlin formation and its explanation of their varied composition and internal structure, Quaternary Sci. Rev., 62, 77–96, https://doi.org/10.1016/j.quascirev.2012.11.011, 2013a.

Stokes, C. R., Spagnolo, M., Clark, C. D., Ó Cofaigh, C., Lian, O. B., and Dunstone, R. B.: Formation of mega-scale glacial lineations on the Dubawnt Lake Ice Stream bed: 1. size, shape and spacing from a large remote sensing dataset, Quaternary Sci. Rev., 77, 190–209, https://doi.org/10.1016/j.quascirev.2013.06.003, 2013b.

Stokes, C. R., Margold, M., and Creyts, T. T.: Ribbed bedforms on palaeo-ice stream beds resemble regular patterns of basal shear stress ("traction ribs") inferred from modern ice streams, J. Glaciol., 62, 696–713, https://doi.org/10.1017/jog.2016.63, 2016.

Szuman, I., Kalita, J. Z., Ewertowski, M. W., Clark, C. D., and Livingstone, S. J.: Dynamics of the last Scandinavian Ice Sheet's southernmost sector revealed by the pattern of ice streams, Boreas, https://doi.org/10.1111/bor.12512, 2021.

Terzaghi, C.: The Static Rigidity of Plastic Clays, J. Rheology, 2, 253–262, https://doi.org/10.1122/1.2116377, 1931.

Totten, S. M.: Overridden Recessional Moraines of North-Central Ohio, GSA Bull., 80, 1931–1946, https://doi.org/10.1130/0016-7606(1969)80[1931:ORMONO]2.0.CO;2, 1969.

Trommelen, M. S., Ross, M., and Ismail, A.: Ribbed moraines in northern Manitoba, Canada: Characteristics and preservation as part of a subglacial bed mosaic near the core regions of ice sheets, Quaternary Sci. Rev., 87, 135–155, https://doi.org/10.1016/j.quascirev.2014.01.010, 2014.

Tulaczyk, S. M., Kamb, W. B., and Engelhardt, H. F.: Basal mechanics of Ice Stream B, West Antarctica 2. Undrained plastic bed model, J. Geophys. Res., 105, 483–494, https://doi.org/10.1029/1999JB900328, 2000.

Tulaczyk, S. M., Scherer, R. P., and Clark, C. D.: A ploughing model for the origin of weak tills beneath ice streams: A qualitative treatment, Quaternary Int., 86, 59–70, https://doi.org/10.1016/S1040-6182(01)00050-7, 2001.

Winsborrow, M. C. M., Clark, C. D., and Stokes, C. R.: Ice streams of the Laurentide Ice Sheet, Geographie Physique et Quaternaire, 58, 269–280, https://doi.org/10.7202/013142ar, 2004.

Winsborrow, M. C. M., Clark, C. D., and Stokes, C. R.: What controls the location of ice streams?, Earth-Sci. Rev., 103, 45–59, https://doi.org/10.1016/j.earscirev.2010.07.003, 2010.

Zheng, W., Pritchard, M. E., Willis, M. J., and Stearns, L. A.: The Possible Transition From Glacial Surge to Ice Stream on Vavilov Ice Cap, Geophys. Res. Lett., 46, 13892–13902. https://doi.org/10.1029/2019GL084948, 2019.

3. Figures et résultats supplémentaires

3.1. Figures supplémentaires de l'Article n°1

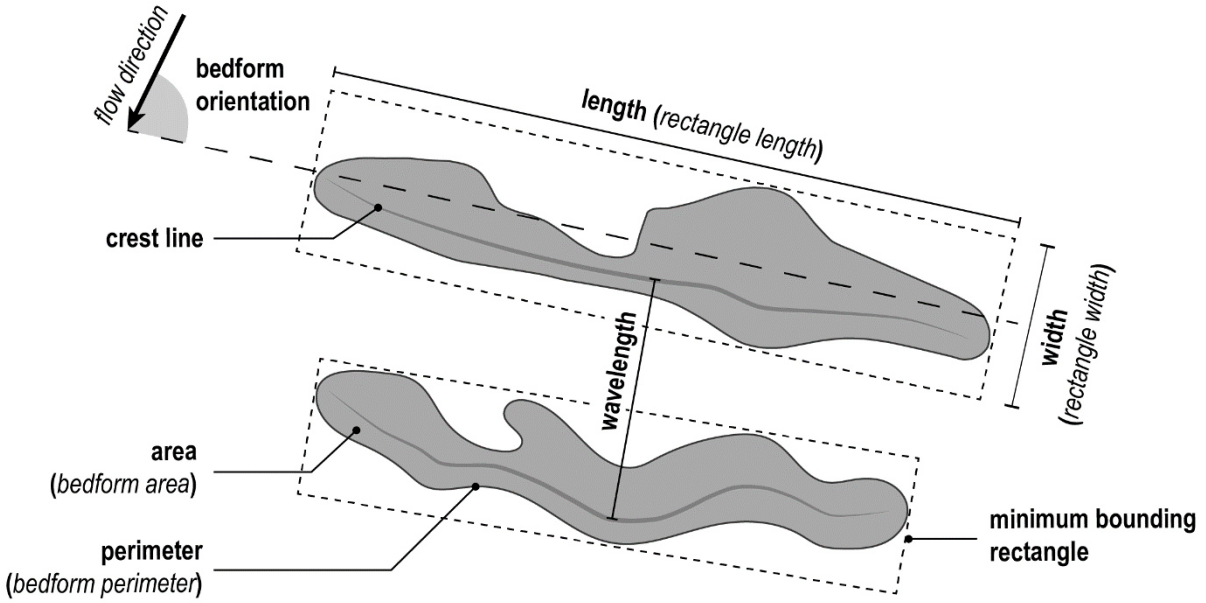

***Figure S1**: Scheme illustrating the method of the "minimum bounding rectangle" and the parameter used to characterize the morphology on natural and analogue bedforms*

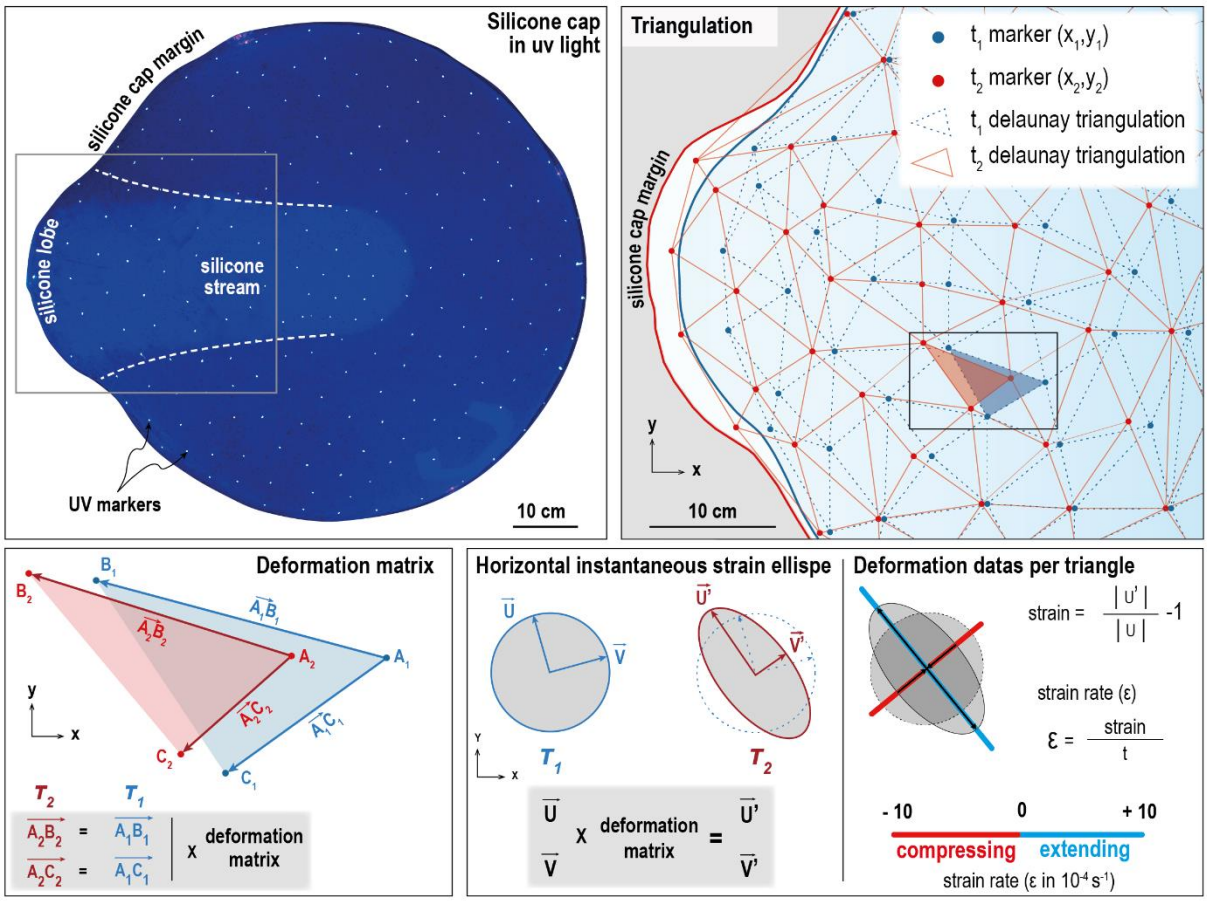

***Figure S2**: Procedure of triangulation from UV markers used for computation of 2D-horizontal strain ellipse*

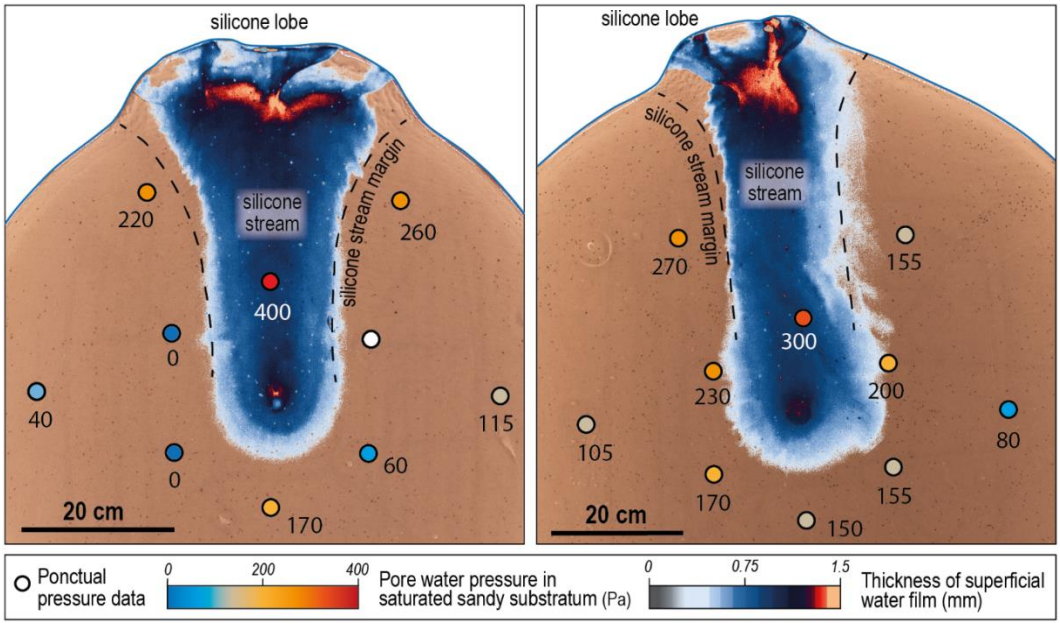

***Figure S3**: Example of the spatial distribution of the pore-water pressure (Pa) within the silicon stream bed during active silicone streaming. Pore-water pressures in the bed below the silicone streams exceed the maximal weight of the silicone layer (285 Pa), resulting is silicone-bed decoupling.*

3.2. Résultats complémentaires de l'Article n°1

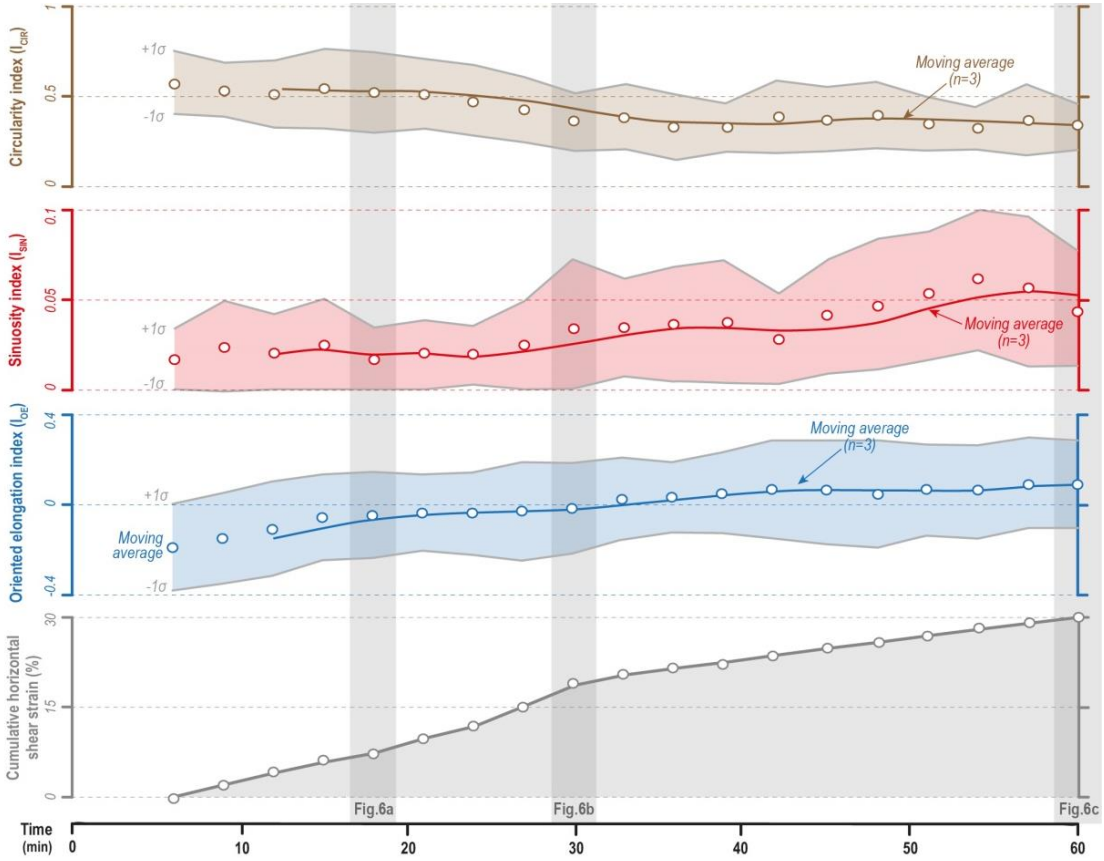

***Supplementary Figure 1**: Morphometric evolution (circularity I_{CIR}, sinuosity I_{SIN} and oriented elongation I_{OE} indices) of experimental subglacial bedforms formed along the coupled silicone-bed interface right below shear margins of silicone streams, whose snapshot are presented in Fig. 6 of Article n°1. Experimental bedforms - with an initial appearance of circular/hummocky ribbed bedforms or linear and elongated ribbed bedforms - are decreasingly circular (I_{CIR}), and increasingly sinuous (I_{SIN}) and elongated parallel (I_{OE}) to the silicone flow direction as the horizontal shear strain undergone by the silicone cap increases.*

Partie B. Un continuum morphologique révélé derrière la diversité morphométrique des bedforms sous-glaciaires

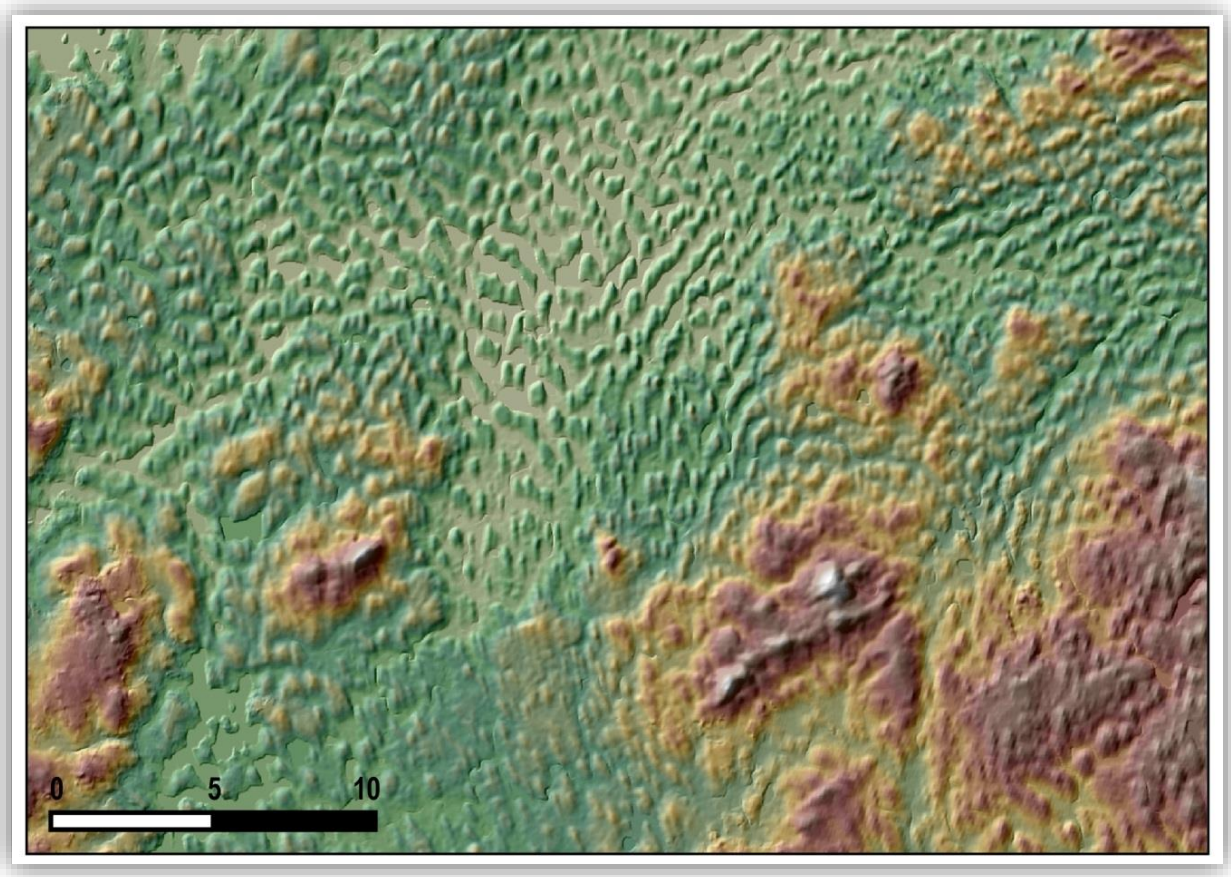

Spatial transition between a field of ribbed bedforms and a field of drumlins, North-East Ireland (© EU DEM – 54°N, 7°30'W)

1. Introduction

Les géomorphologues glaciaires ont depuis la fin du 19ème siècle classé les bedforms sous-glaciaires en fonction de leurs formes, dimensions et orientations supposées par rapport à la direction de déplacement de la glace, comme suit : les linéations glaciaires *('streamlined bedforms'*), les ribbed bedforms et les bedforms circulaires (**Table 3.2**) (Chapitre I - Partie B §1).

En plus de ces classes de bedforms sous-glaciaires, d'autres bedforms de forme plus complexe ont été identifiés comme des sous-classes spécifiques de ribbed bedforms ou de drumlins mais n'ont jamais pu être précisément décrits par les paramètres morphométriques actuellement utilisés dans la littérature glaciaire (Chapitre II - §3). Afin d'expliquer leurs formes complexes, celles-ci sont donc couramment interprétées comme résultant de la superposition ou du recoupement de plusieurs générations de bedforms de forme simple (i.e. ribbed bedforms et linéations glaciaires) (***Knight et al., 1999; Dunlop & Clark, 2006; De Angelis & Kleman, 2007; Greenwood & Clark, 2009***), avec lesquels ils sont géographiquement associés (***Carl, 1978 ; Markgren & Lassila, 1980***). Ainsi, les bedforms complexes sont typiquement interprétés comme des marqueurs de changements de trajectoires et de configurations d'écoulement des calottes glaciaires et des fleuves de glace (***Clark et al., 1993; Stokes et al., 2006a;***

Table 3.2. *Synthesis of morphological characteristics of subglacial bedforms whose the formation is predominantly attributed to the dynamics of ice flow (see Chapitre I – Partie B §1.2 for more details)*

SUBGLACIAL BEDFORM	MAIN MORPHOLOGICAL CHARACTERISTICS	REFERENCES
Streamlined bedforms → Drumlins → MSGLs → Flutes	- Linear and elongated parallel relative to the ice flow direction - Subclasses differentiation based on their elongation ratio	***Menzies, 1979*** ***Clark, 1993*** ***Shaw, 2000***
Ribbed bedforms → Ribbed/Rogen moraines → Mega-ribs → Traction ribs	- Linear to undulated bedform elongated transverse (80-90°) to the ice flow direction - Subclasses differentiation based on their width, lengths and amplitudes	***Dunlop & Clark, 2006*** ***Greenwood & Kleman, 2010*** ***Stokes et al., 2016***
Circular bedforms	- Sub-circular forms without preferential orientation relative to the ice flow direction	***Greenwood & Clark, 2008***
Complex bedforms → Ribbed bedform-related → *'drumlinized'* → *'Blattnick'* → *'blocky-angular'* → *'jagged-type'* → *'extensional'* → *'barchan-shaped'* → Drumlin-related → *'transverse/asymmetrical'* → *'crescentic/parabolic'* → *'channeled'*	- Complex and sinuous shape - Neither transverse nor parallel to the ice flow direction	***Carl, 1978*** ***Markgren & Lassila, 1980*** ***Lundqvist, 1981*** ***Shaw, 1983*** ***Smalley & Warburton, 1994*** ***Knight, 1997*** ***Dunlop & Clark, 2006*** ***Wagner, 2014*** ***Eyles et al., 2016*** ***Sookhan et al., 2021***

Brown et al., 2011), de l'évolution de la vitesse d'écoulement ou du régime thermique basal au cours du temps (***Stokes et al., 2006b, 2008***). De récents travaux de modélisation analogique (Chapitre III – Partie A §2) (***Vérité et al., 2021***) et de géomorphologie glaciaire (***Sookhan et al., 2021, 2022***) ont cependant suggérés que des bedforms complexes, sinueux et/ou obliques, pouvaient se former sous la même direction de déplacement de la glace que des ribbed bedforms et des linéations glaciaires. En revanche, aucune étude n'a intégré la diversité morphologique et la distribution spatiale de l'ensemble des bedforms sous-glaciaires.

L'hypothèse d'un continuum de bedforms sous-glaciaires associés à la dynamique d'écoulement de la glace a cependant émergé de l'observation d'une continuité spatiale (***Aario, 1977; Dyke et al., 1992 ; Sookhan et al., 2022***) et morphométrique (***Rose, 1987 ; Stokes et al., 2013a ; Ely et al., 2016***) entre les ribbed bedforms, les bedforms circulaires et les linéations glaciaires. Alors que ce continuum de bedforms est caractérisé par le ratio d'élongation des bedforms (Chapitre I - Partie B §3.1.1), ne prenant ainsi pas en compte les bedforms complexes, l'origine du changement d'orientation entre des bedforms transverses et des bedforms parallèles ou perpendiculaires à la direction d'écoulement de la glace reste mal comprise.

Problématiques :

→ Les nouveaux critères morphométriques développés durant cette thèse permettent-ils de caractériser la diversité de formes des bedforms sous-glaciaires (i.e. ribbed bedforms, bedforms circulaires, linéations glaciaires et bedforms complexes) ?

→ Les bedforms complexes résultent-ils nécessairement de plusieurs phases d'écoulement de la glace ? Existe-t-il un continuum morphologique plus large qu'initialement décrit incluant également les bedforms complexes ? Par quels critères morphométriques ce continuum est-il contraint ?

2. Article n°2: New metrics reveal the evolutionary continuum behind the morphological diversity of subglacial bedforms

Cette deuxième partie fait l'objet d'un article soumis dans la revue *Geomorphology*.

New metrics reveal the evolutionary continuum behind the morphological diversity of subglacial bedforms

Jean Vérité[1], Édouard Ravier[1], Olivier Bourgeois[2], Paul Bessin[1], Stéphane Pochat[2]

[1] Laboratoire de Planétologie et Géosciences, UMR 6112, CNRS, Le Mans Université, Avenue Olivier Messiaen, 72085 Le Mans CEDEX 9, France
[2] Laboratoire de Planétologie et Géosciences, UMR 6112, CNRS, Nantes Université, 2 rue de la Houssinière, BP 92208, 44322 Nantes CEDEX 3, France

Abstract

Understanding the formation of subglacial bedforms is primordial to constrain ice-meltwater-bed interactions and the dynamics of past and present ice sheets. However, the difficulty to observe active subglacial bedforms below present-day ice sheets implies that their formation and evolution are essentially deduced from the inversion of morphological and sedimentological data from palaeo-subglacial bedforms. In this study, the morphological characteristics of subglacial bedforms are explored with a new approach based on the combination of three dimensionless morphometric indices i.e., circularity, sinuosity and oriented elongation. We measure the spatial distribution of these indices on an unpublished database composed of ~13 500 digitized bedforms taken from two selected portions of the Irish Ice Sheet and Laurentide Ice Sheet beds considering that (1) all subglacial bedforms in each region were formed under a single ice flow configuration and (2) the bedforms may have developed either orthogonal, parallel, or oblique to ice displacement directions. Our results reveal a morphometric and spatial continuum between (i) linear ribbed bedforms, (ii) circular bedforms, (iii) streamlined bedforms and (iv) sinuous bedforms with various orientations and shapes. In this continuum, ribbed bedforms of various lengths and shapes - ranging from circular to elongated flow-transverse forms - are incipient bedforms that can evolve into transitional sinuous ribbed bedforms, then into predominantly flow-parallel sinuous bedforms, which progressively realign to form streamlined bedforms. Considering the glaciological contexts of selected study areas, this continuum may provide new geomorphic criteria to constrain spatial variations in subglacial conditions (e.g. ice flow velocity, bedrock characteristics, meltwater pressure).

1. Introduction

Glacial geomorphologists have historically classified subglacial bedforms in different classes, based on their differences in shapes, dimensions and orientations in relation to a presupposed direction of ice displacement (i.e. ice flow direction). Linear ridges supposedly parallel to the ice flow direction have been called streamlined bedforms and include drumlins (***Hill, 1973; Menzies, 1979***), flutes (***Shaw et al., 2000; Eyles, 2012***), and mega-scale glacial lineations (MSGLs; ***Clark, 1993; Canals et al., 2000***) by order of increasing elongation ratios. Periodic ridges supposedly orthogonal to the ice flow direction have been defined as ribbed bedforms (***Stokes et al., 2016; Vérité et al., 2021***), and include bedforms that have been variously called ribbed moraines (***Cowan, 1968; Hättestrand, 1997***), Rogen moraines (***Lundqvist, 1969; Shaw, 1979***) and mega-ribs (***Greenwood and Kleman, 2010***) depending on their sizes and locations of first description. Sub-circular mounds without a determinable orientation have been referred to as circular bedforms (***Knight et al., 1999; Greenwood & Clark, 2008***), mammillary hills (***Aario, 1977***), ovoid forms (***Smith & Wise, 2007***) or hummocky ribbed bedforms (***Hättestrand, 1997; Dunlop & Clark, 2006; Möller & Dowling, 2015***).

Although these different morphological classes have sometimes been attributed to different subglacial formation processes, the alternative hypothesis that they may be part of a same morphometric, and perhaps genetic, continuum has emerged from the observation of spatial and morphometric transitions between ribbed and streamlined bedforms (**Fig. 1**) (***Carl, 1978; Aylsworth & Shilts, 1989; Dyke et al., 1992; Knight et al., 1999; Fannon et al., 2017; Sommerkorn, 2020***), between circular and ribbed bedforms (***Hättestrand, 1997; Dunlop and Clark, 2006; Greenwood & Clark, 2008; Vérité et al., 2022***), between different types of streamlined bedforms (e.g. ***Rose, 1987; Clark et al., 2009; Stokes et al., 2013; Sookhan et al., 2021, 2022***), and between circular, ribbed and streamlined bedforms *(**Aario, 1977; Markgren & Lassila, 1980; Ely et al., 2016**).*

Several additional classes were also proposed to describe more specific or more complex bedforms, such as smoothsided/drumlinized ribbed moraines (**Fig. 1b**) (***Carl, 1978; Lundqvist, 1981; Dunlop & Clark, 2006***), Blattnick moraines (**Fig. 1c**) (***Markgren & Lassila, 1980***), transverse/asymmetrical drumlins (**Fig. 1d**) (***Shaw, 1983; Boulton, 1987; Knight, 1997***), crescentic/parabolic ridges and drumlins (**Fig. 1e**) (***Boulton, 1987; Lundqvist, 1989; Smalley & Warburton, 1994; Maclachlan &***

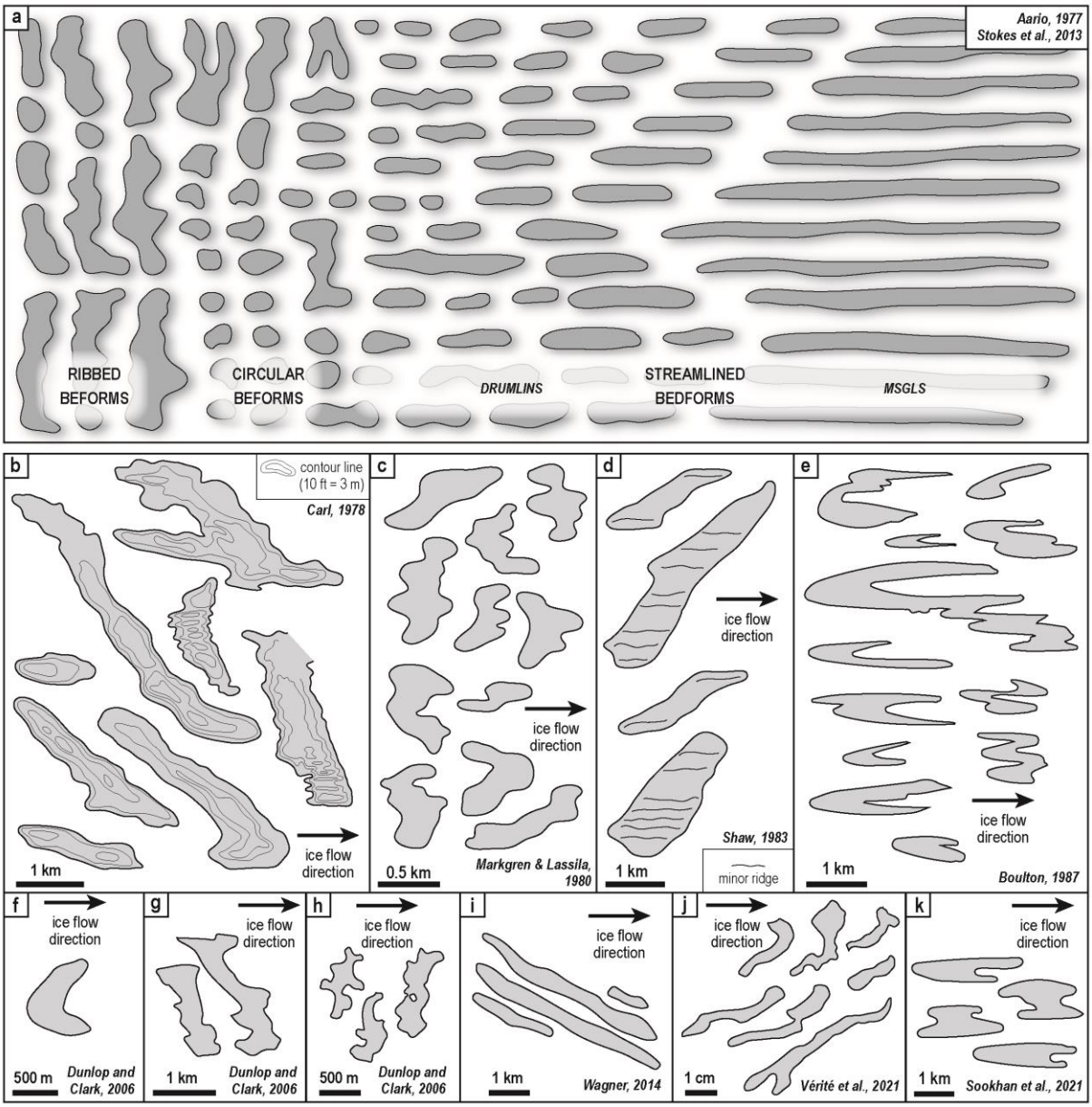

Figure 1. *(a) Schematic representation, as currently envisioned, of the subglacial bedform continuum between ribbed, circular and streamlined bedforms (drumlins and MSGLs) (after* ***Aario, 1977*** *and* ***Stokes et al., 2013****). (b) to (j) Examples of complex subglacial bedforms commonly associated with fields of ribbed and streamlined bedforms but excluded from the existing subglacial bedform continuum models. They are referred to as (b) smoothsided/drumlinized ribbed moraines (****Carl, 1978****), (c) Blattnick moraines (****Markgren & Lassila, 1980****), (d) transverse/asymmetrical drumlins (****Shaw, 1983****), (e) parabolic drumlins (****Boulton, 1987*** *for mapping ;* ***Eyles et al., 2016*** *for denomination), (f) barchan-shaped, (g) blocky angular and (h) jagged-type ribbed moraines (****Dunlop & Clark, 2006****), (i) extensional ribbed moraines (****Wagner, 2014****), (j) oblique ribbed bedforms (****Vérité et al., 2021****) and (k) channeled drumlins (****Sookhan et al., 2021****).*

Eyles, 2013; Eyles et al., 2016), barchan-shaped (**Fig. 1f**), blocky angular (**Fig. 1g**) and jagged-type ribbed moraines (**Fig. 1h**) (***Dunlop & Clark, 2006***), extensional ribbed moraines (**Fig. 1i**) (***Wagner, 2014***), oblique ribbed bedforms (**Fig. 1j**) (***Vérité et al., 2021***) and channeled drumlins (**Fig. 1k**) (***Sookhan et al., 2021***) among others. Since most of these complex bedforms are sinuous and/or have apparently no clear orientation relative to the local ice flow direction, they do not fit with usual bedform

classes and have therefore been excluded from most of the existing models of subglacial bedform continuum. Complex bedforms have frequently been interpreted as resulting from the remolding of simple bedforms or the superimposition/ crosscutting of several generations of bedforms (***Knight et al., 1999; Dunlop & Clark, 2006; De Angelis & Kleman, 2007; Greenwood & Clark, 2009***), in response to changes in ice flow direction (***Clark et al., 1993; Stokes et al., 2006a; Brown et al., 2011***) or velocity (***Stokes et al., 2006b, 2008***).

A demonstration that all subglacial bedform classes, including simple and complex ones, may or may not be part of a same spatial, morphometric, and perhaps evolutionary, continuum is missing. Previous attempts were based on two main preliminary assumptions: (1) simple elongated bedforms may be classified a-priori as either parallel or orthogonal to ice flow direction; (2) complex (oblique and/or sinuous) bedforms cannot form under constant ice flow directions. Physical modeling (**Fig. 1j**) (***Vérité et al., 2021***) and glacial geomorphology (**Fig. 1k**) (***Sookhan et al., 2021***) however recently demonstrated that both oblique and/or complex ribbed and streamlined bedforms can develop under constant ice flow directions. Therefore, we perform here a systematic morphometric analysis, devoid of a-priori classification, of ~13 500 subglacial bedforms mapped in selected portions of the Irish and Laurentide Ice Sheet beds. We quantify the complexity and variability of subglacial bedform shapes in these regions with three dimensionless morphometric parameters and a spatial analysis of subglacial bedform distribution. We propose that all subglacial bedforms stand along an overall morphometric and spatial continuum that correspond to an evolutionary continuum.

2. Data and method

2.1. Study areas

The two study areas are selected for (i) their great diversity of subglacial bedforms and (ii) the occurrence of complex forms at the spatial transitions between fields of ribbed and streamlined bedforms (**Fig. 2**). The first study area (11300-km²) is located in northeastern Ireland, where a layer of subglacial till, commonly more than 15 m thick and deposited below the Irish Ice Sheet (IIS) during the last Midlantian glaciation, covers the Paleozoic sedimentary bedrock (***McConnell & Gatley, 2006***). Large-scale streamlined bedform tracts that have been interpreted as corridors of fast ice flow (***Stokes & Clark, 1999; Greenwood & Clark, 2009a***) possibly ice streams (***Synge & Stephens, 1960***) are reported south

of the northern ice divide of the Lowland Ice Dome between 19 and 16 ka BP (***Clark et al., 2012***) and downstream from ribbed and circular bedform fields (***Dunlop & Clark, 2006; Greenwood & Clark, 2008***). Based on frequent apparent superimposition and crosscutting relationships between bedforms over the study area, the geomorphological record has been interpreted as a superimposition of several configuration of ice-sheet flow trajectories (***Greenwood & Clark, 2009a,b***).

The second study area (2100-km²) is located west of the Hudson Bay in northern Canada, between Firedrake Lake and Boyd Lake (**Fig. 2**). The area was covered by the Keewatin Ice Dome of the Laurentide Ice Sheet (LIS) during the last Wisconsinian glaciation and the surficial geology is characterized by a 10 m thick (at most) layer of subglacial till deposited over the Canadian Precambrian bedrock (***Shilts et al., 1979***; ***Dyke et al., 1989***). Ribbed and streamlined bedform tracts laterally alternate, radiating outwards from the Keewatin ice divide (***Shilts et al., 1987; Aylsworth and Shilts, 1989***) and paralleling meltwater corridors described in the Keewatin area by ***Storrar et al. (2013)*** and ***Lewington et al., (2019, 2020).***

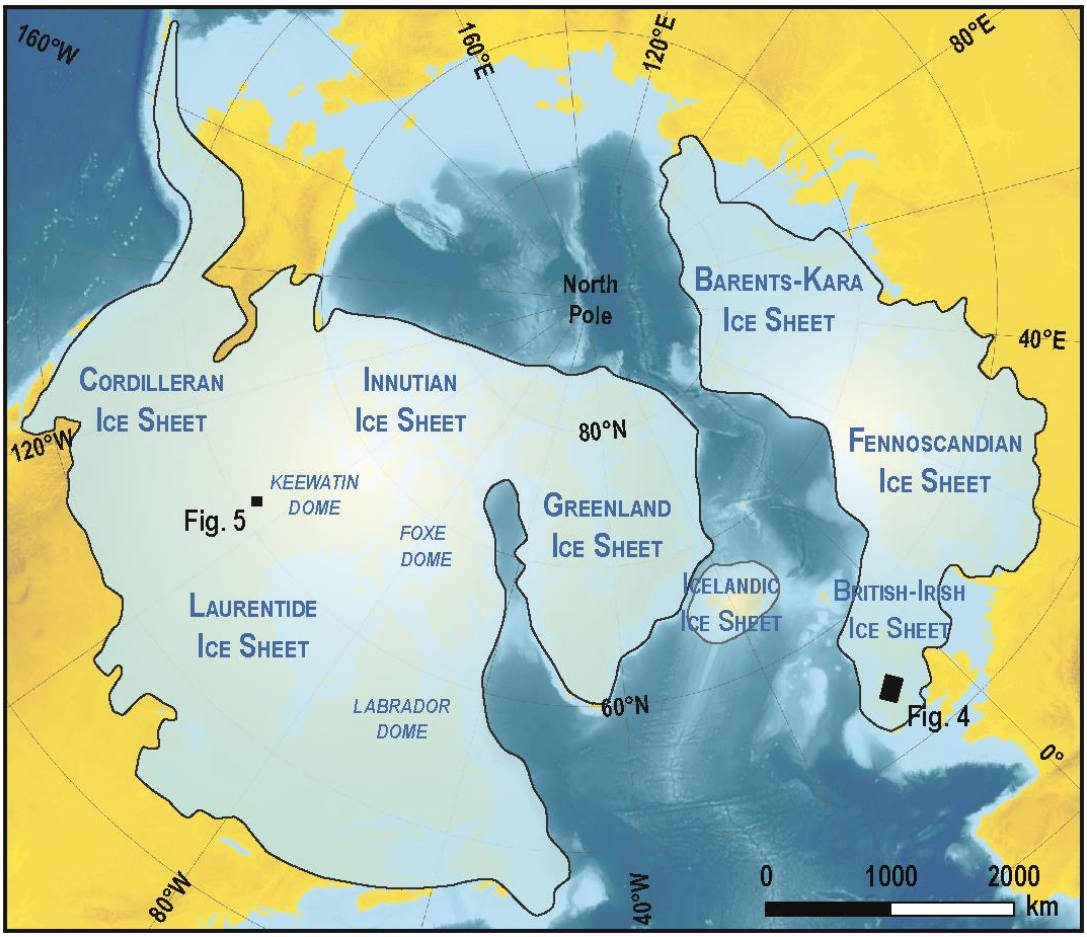

Figure 2. *Location of study areas relative to the maximum extension of the northern hemisphere ice sheets during the Last Glacial Maximum (**Batchelor et al., 2019**).*

2.2. Data sources and processing

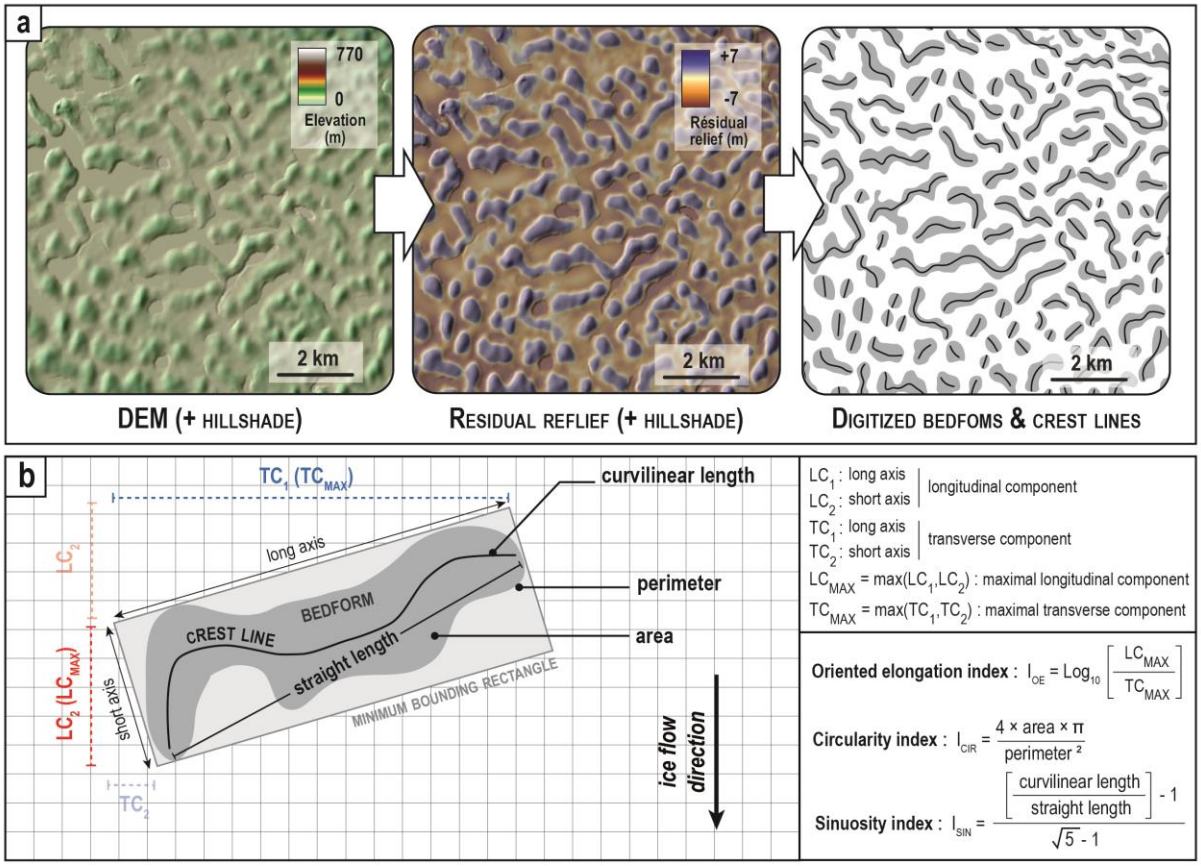

***Figure 3**. (a) Hillshaded residual relief derived from a digital elevation model and from which bedform contours and crest lines are manually digitized. (b) Measured quantities for the calculation of dimensionless indexes: oriented elongation index (I_{OE}), circularity index (I_{CIR}) and sinuosity index (I_{SIN}).*

We conducted high-resolution (1:10 000) mapping from open-data DEMs of the LIS bed in Canada (10-m DEMs; ArcticDEM, https://www.pgc.umn.edu/data/arcticdem/, ***Porter et al., 2018***) and IIS bed in Ireland (25-m DEMs; EU-DEM v1.1, https://land.copernicus.eu/). From these DEMs, we derived and superimposed hillshade maps and residual relief maps (***Hiller & Smith, 2008***) with a Geographic Information System (GIS) software (**Fig. 3a**). Break values of hillshaded residual relief data were delineated manually to produce bedform contours whereas lines of maximum elevation were delineated within each contoured bedform to draw its crest line (**Fig. 3a**).

2.3. Morphometric analysis

2.3.1. Current morphometric techniques on subglacial bedforms

Subglacial bedform shapes are classically characterized by their dimensions, orientations relative to the supposed ice flow direction, and degrees of elongation. ***Hollingworth (1931)*** used the 'length/width' ratio (l/w) on drumlins, which has been latter referred to as the 'elongation ratio' because

drumlins are assumed to be elongated parallel to ice flow directions (e.g. ***Doornkamp and King, 1971; Mills, 1987; Rose, 1987***). Latter, the elongation ratio was abundantly used to distinguish different types of streamlined bedforms such as flutes, drumlins, mega-flutes, mega-drumlins, lineations and MSGLs (***Boyce and Eyles, 1991; Knight, 1997; O Cofaigh et al., 2002; Stokes & Clark, 2002a; Briner, 2007; Clark et al., 2009; Dowling et al., 2015***). The 'l/w' ratio has also been used to characterize the shape and dimensions of different sub-classes of ribbed bedforms, such as ribbed/Rogen moraines (***Dunlop & Clark, 2006***), mega-ribs (***Greenwood & Kleman, 2010***) and traction ribs (***Stokes et al., 2016***), for which, unlike drumlins, the length was measured perpendicular to the ice flow direction. In an attempt to integrate ribbed, circular and streamlined bedforms in a unique morphometric dataset, ***Ely et al. (2016)*** redefined the elongation ratio as the down-ice length of bedforms (i.e. the length of streamlined bedforms and the width of ribbed bedforms) divided by their across-ice length (i.e. conversely). Bedforms were thus assumed a-priori to be either orthogonal or parallel to ice displacement directions and the possibility that they may be oblique to ice displacement was ignored.

Using the equations provided by ***Folk (1968)*** and ***Moellering & Rayner (1979)*** who respectively studied the shapes of sedimentary grains and catchment areas, ***Burgess et al. (2003)*** computed three dimensionless shape parameters (compactness, circularity, and shape factor) on subglacial bedforms from their perimeters and areas to study the complex and contorted shapes of hummocky and Rogen moraines in Canada. Recently, ***Vérité et al. (2022)*** calculated the sinuosity index of bedform crest lines to demonstrate a morphometric continuum between ribbed bedforms and murtoos. Although dimensionless shape parameters used by ***Burgess et al. (2003)*** and ***Vérité et al. (2022)*** (i.e. compactness, circularity, shape factor, sinuosity) better describe the complexity of subglacial bedform contours and crest lines than dimensioned morphometric parameters commonly in the geomorphological literature (i.e. length, width, elongation ratio), they do not allow to characterize their orientation with respect to ice flow.

2.3.2 Definition of morphometric indexes

Using the same method as ***Vérité et al. (2022)***, we measure the perimeters and areas of bedform contours and the curvilinear and rectilinear lengths of bedform crest lines (**Fig. 3b**). In order to characterize the complex shapes of bedform contours and crestlines, we use these dimensioned shape

parameters to calculate their circularity (I_{CIR}) (**Table 1.A**) and sinuosity (I_{SIN}) (**Table 1.B**) indices respectively. The maximal height (h_{MAX}), defined as the amplitude, is also measured for each bedform. We complement this morphometric protocol to describe the diversity of elongation and orientation of subglacial bedforms relative to the ice flow direction (**Supplementary Data 1**). We assume that all bedforms were formed under constant ice flow trajectories. We use streamlined bedforms as a proxy for reconstructing local ice flow directions. To do so, we derive the average orientation of the long-axis of streamlined bedforms, sampled in a 25-km² hexagonal grid, to build the resulting vectors of ice flow direction in each hexagonal grid and to attribute a local ice flow direction to each bedforms located in the hexagonal grid. In area where streamlined bedforms were absent, we extrapolate ice flow directions from adjacent areas, with a method based on the principle of nearest neighborhood (**Figs. 4-5**). Since the orientation of the long-axis of streamlined bedforms highly varies spatially, the nearest neighborhood in a hexagonal grid more convenient than in a rectangular grid (***Birch et al., 2007***). The hexagonal grid area is chosen to guaranty the presence of a minimum of 10 subglacial bedforms in each cell.

Table 1. *Description of dimensionless morphometric indices.*

Shape indices	Formula	Signification	Range of values & typical values
(A) Circularity index (I_{CIR})	$I_{CIR} = \frac{4 \times A \times \pi}{P^2}$	Compares the perimeter (P) of a contour of a given area (A) with the perimeter of a circle of an identical area (***Burgess et al., 2003***).	**I_{CIR} : [0 ; 1]** $I_{CIR} = 0$: strongly non-circular contour $I_{CIR} > 0.80$: highly circular contour $I_{CIR} = 1$: perfectly circular contour
(B) Sinuosity index (I_{SIN})	$I_{SIN} = \frac{\frac{Curvilinear\ length}{Straight\ length} - 1}{\sqrt{5} - 1}$	Measures the sinuosity of the crestline (i.e. ratio between the curvilinear length of the crest line and its straight length; ***Schumm, 1963***), normalized to the sinuosity of an equilateral triangle (√5) (***Vérité et al., 2022***).	**I_{SIN} : [0 ; +∞]** $I_{SIN} = 0$: perfectly rectilinear crestline $I_{SIN} < 0.10$: linear crestline $I_{SIN} > 0.10$: sinuous crestline $I_{SIN} = 1$: equilateral triangular crestline $I_{SIN} \rightarrow +\infty$: strongly sinuous crestline
(C) Orientated elongation index (I_{OE})	$I_{OE} = \log_{10}(\frac{LC_{MAX}}{TC_{MAX}})$	Measures the ratio between the maximal longitudinal (i.e. along-ice flow; LC_{MAX}) and the maximal transverse (i.e. across-ice flow; TC_{MAX}) components of a bedforms, expressed on a logarithmic scale.	**I_{OE} : [-∞ ; +∞]** $I_{OE} \leq -0.17$: $TC_{MAX} \geq 1.5 \times LC_{MAX}$ elongated transverse to the flow direction $-0.17 \leq I_{OE} \leq +0.17$: $TC_{MAX} \sim LC_{MAX}$ elongated equally transverse and parallel to the flow direction $I_{OE} \geq +0.17$: $LC_{MAX} \geq 1.5 \times TC_{MAX}$ elongated parallel to the flow direction $I_{OE} \geq +0.60$: $LC_{MAX} \geq 4 \times TC_{MAX}$ strongly elongated parallel to the flow direction

To allow the possibility that bedforms can be oblique to the ice flow directions and to quantify this obliquity, we develop a new morphometric parameter called "oriented elongation ratio", computed from transverse (i.e. across-ice flow) and longitudinal (i.e. along-ice flow) components for each bedform (**Fig. 3b**). Using minimum bounding rectangles, we automatically measure the lengths of transverse and longitudinal components for the long axis (i.e. TC_1 and LC_1) and the short axis (i.e. TC_2 and LC_2) of each bedform (**Fig. 3b**). From the ratio between the maximal transverse (TC_{MAX}) and maximal longitudinal components (LC_{MAX}), we compute the "oriented elongation index" (I_{OE}) (**Table 1.C**), which integrates both orientation and elongation of bedforms (**Supplementary Data 2**).

3. Results

3.1. A morphometric continuum of subglacial bedforms

The results of our morphometric measurements in northeastern Ireland (n = 10100; **Fig. 4a**) and in northern Canada (n = 3400; **Fig. 5a**) have been compiled in a single dataset (**Table 2**). First of all, there is no cluster or gap but a continuum in the distribution of bedform morphometric values (**Fig. 6**). This continuum shows a wide diversity of bedform shapes ranging from circular to either flow-transverse or flow-parallel bedforms with linear crest lines. It includes complex bedforms, with sinuous crest lines and variable orientations relative to local ice flow directions. For the convenience of description, and by reference to usual classes of subglacial bedforms, we divide this bedform diversity in four classes with no morphometric gaps in between.

(1) Bedforms with highly circular contours ($I_{CIR} \geq 0.80$), similar maximal longitudinal (LC_{MAX}) and maximal transverse components (TC_{MAX}), no preferential elongation with respect to the flow direction ($-0.17 \leq I_{OE} \leq 0.17$) and linear crest lines ($I_{SIN} < 0.10$), were classified as circular bedforms. On average, these bedforms have constant diameters of 340 m and amplitudes close to 10 m (**Table 2**).

(2) Bedforms with a linear crest line ($I_{SIN} < 0.10$; average $I_{SIN} = 0.04$), a slightly undulating contour and a TC_{MAX} at least 1.5 times larger and in average 2.2 times larger than their LC_{MAX} (i.e. $I_{OE} < -0.17$; average $I_{OE} = -0.32$) were classified as linear ribbed bedforms since they share all characteristics defined by ***Dunlop and Clark (2006)*** (**Table 2**). These bedforms have a homogeneous maximal longitudinal component ($LC_{MAX} \sim$ 400-500 m) and an average amplitude of 12.3 m. The absence of point clusters among linear ribbed bedforms, potentially materializing sub-classes, and the progressive decrease in I_{OE}

as the TC_{MAX} increases and I_{CIR} decreases (**Fig. 6**) are consistent with the hypothesis of a morphometric continuity among linear ribbed bedforms, as suggested by ***Hättestrand (1997), Dunlop and Clark (2006), Möller and Dowling (2015)*** and ***Vérité et al. (2021, 2022)***.

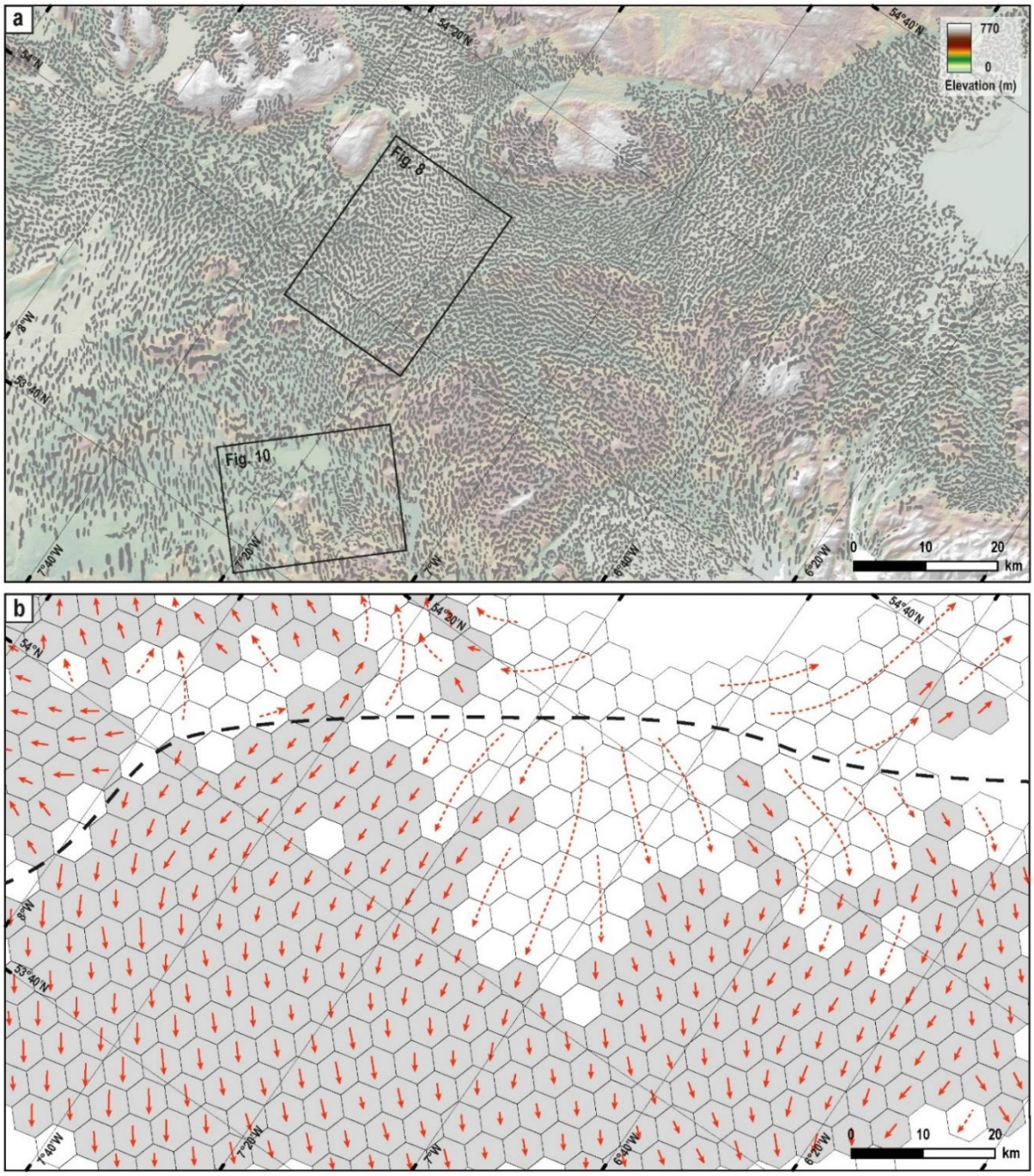

Figure 4. *(a) Hillshaded DEM and interpretative map with digitized bedforms of a portion of the Irish Ice Sheet bed in northern east Ireland. (b) Reconstruction of local ice flow directions (solid red lines) from sampled glacial lineations in a grid of 25-km² hexagons based on the assumption that the formation of streamlined bedforms is associated to a unique configuration of ice flow trajectories. Where streamlined bedforms are absent (white hexagons), the average flow direction is extrapolated (dotted red lines) from surrounding glacial lineations (grey hexagons). The ice divide (black stippled line) revealed by diverging flowsets is consistent with ice sheet reconstructions from* ***Greenwood and Clark (2009a,b)***.

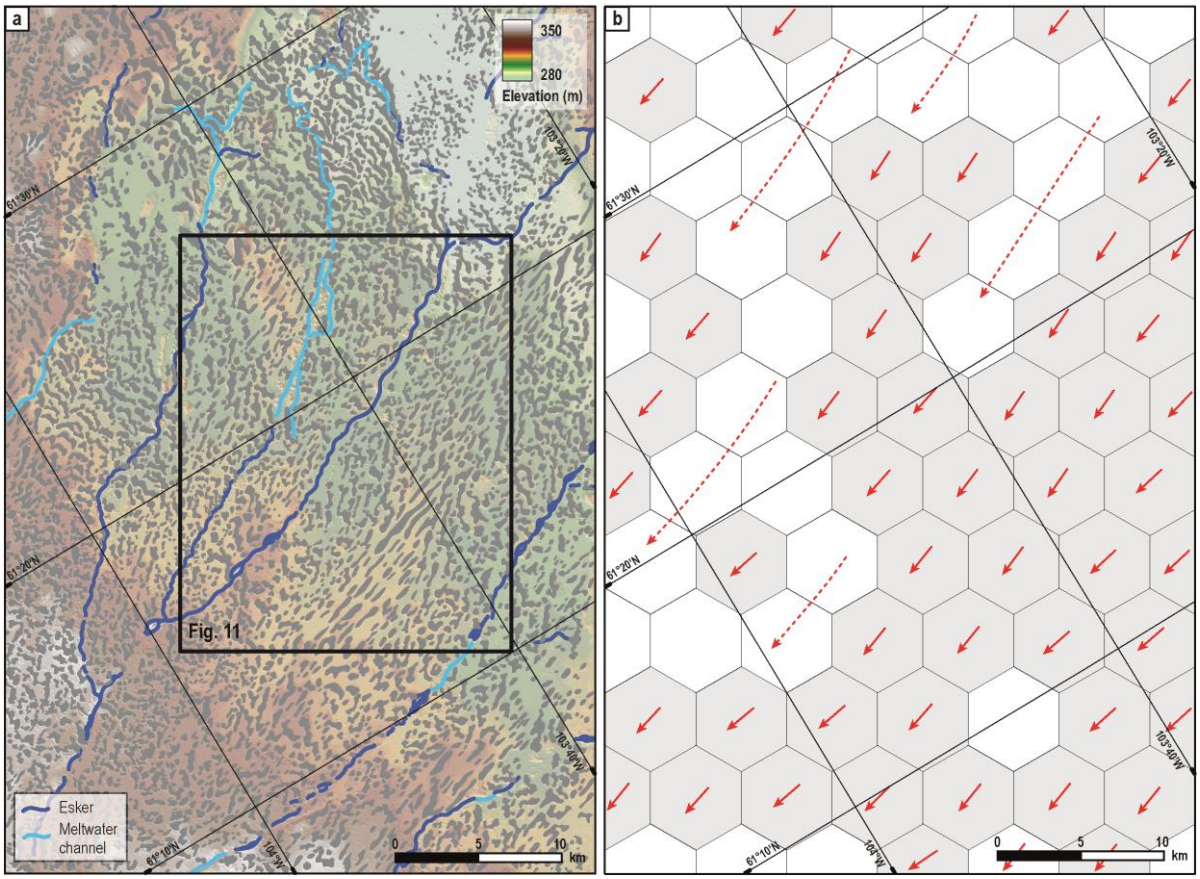

***Figure 5**. (a) Hillshaded DEM and contours of digitized bedforms for a portion of the Laurentide Ice Sheet bed in northern Canada, between Firedrake Lake and Boyd Lake. (b) Reconstruction of local ice flow directions in a grid of 25-km² hexagons with the same method as described in **Fig. 4**. Ice flow was directed toward the southwest.*

***Table 2**. Classification of subglacial bedforms mapped in this study and their morphological characteristics: oriented elongation index (I_{OE}), sinuosity index (I_{SIN}), circularity index (I_{CIR}), maximal transverse component (TC_{MAX}), maximal longitudinal component (LC_{MAX}) and amplitude (h_{MAX}). Arbitrary thresholds between classes are highlighted in grey and defined in **Table 1**.*

				I_{OE}	I_{SIN}	I_{CIR}	TC_{MAX} (m)	LC_{MAX} (m)	h_{MAX} (m)
(1) Circular bedforms		n = 2256	*min*	-0.17	0	0.80	98	103	0.7
			average (± σ)	0.02 ± 0.10	0.01 ± 0.02	0.92 ± 0.05	336 ± 122	347 ± 124	10.5 ± 5.7
			max	0.17	0.10	1	965	899	32.5
(2) Linear ribbed bedforms		n = 1996	*min*	-0.87	0	0.11	143	94	1.0
			average (± σ)	-0.32 ± 0.11	0.04 ± 0.03	0.57 ± 0.19	1011 ± 630	453 ± 230	12.3 ± 5.9
			max	-0.17	0.10	0.93	4936	2147	31.0
(3) Streamlined bedforms	***(a) Low elongated*** ($I_{OE} \leq 0.60$) *(Drumlins)*	n = 2827	*min*	0.17	0	0.20	63	151	0.1
			average (± σ)	0.38 ± 0.11	0.01 ± 0.02	0.70 ± 0.13	283 ± 127	697 ± 376	9.1 ± 5.8
			max	0.60	0.10	0.93	1428	3369	48.5
	(b) Highly elongated ($I_{OE} > 0.6$) *(MSGLs)*	n = 396	*min*	0.60	0	0.15	84	360	0.4
			average (± σ)	0.68 ± 0.07	0.01 ± 0.01	0.41 ± 0.08	312 ± 126	1534 ± 767	7.2 ± 5.2
			max	1.08	0.10	0.55	862	6461	38.1
(4) Sinuous bedforms	**(a) Sinuous ribbed bedforms**	n = 2701	*min*	-0.67	0.10	0.09	127	107	0.6
			average (± σ)	-0.19 ± 0.12	0.23 ± 0.21	0.46 ± 0.17	1105 ± 594	685 ± 312	11.7 ± 5.5
			max	0	1.51	0.90	4549	2668	41.8
	(b) Sinuous and predominantly flow-parallel bedforms	n = 3290	*min*	0	0.10	0.13	71	144	0.6
			average (± σ)	0.22 ± 0.13	0.17 ± 0.24	0.54 ± 0.19	564 ± 326	929 ± 536	11.2 ± 6.0
			max	0.68	1.79	0.98	2418	4994	58.9

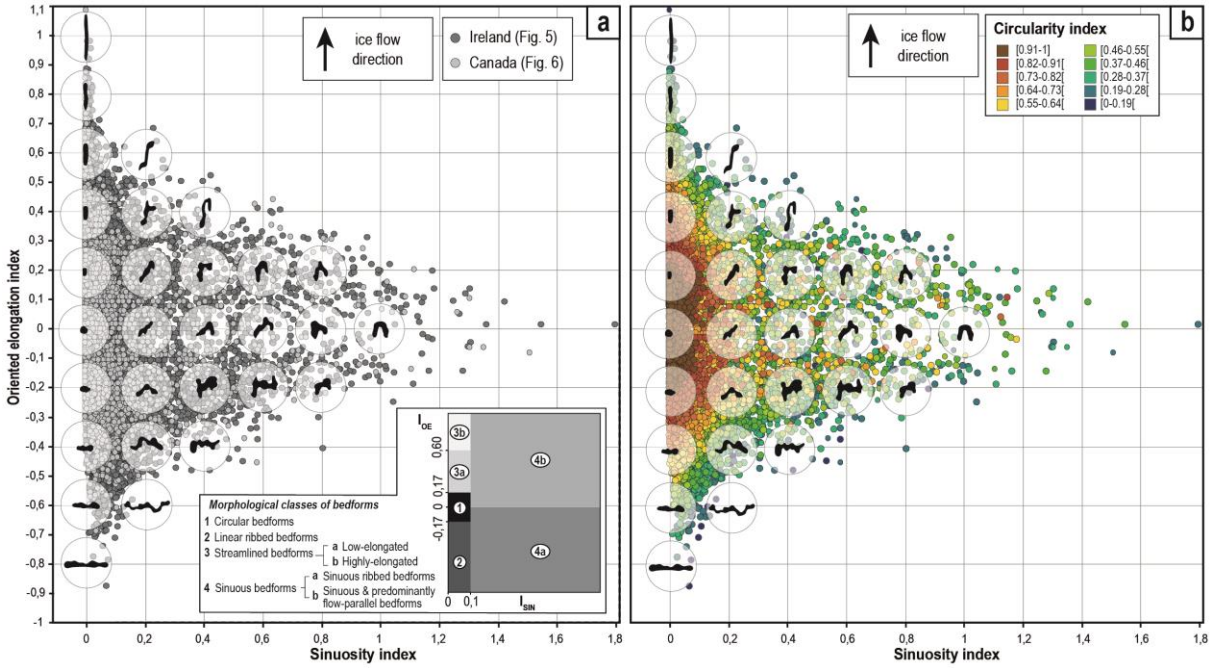

Figure 6. *Plots of oriented elongation (I_{OE}) and sinuosity indexes (I_{SIN}). (a) Irish (dark grey dots) and Canadian bedforms (light grey dots). Selected bedform contours picked up from the database are shown at each node of the grid to illustrate how I_{SIN} and I_{OE} reflect their shapes. Morphological classes of bedforms defined by arbitrary thresholds (**Table 2**) are schematized in the bottom right corner. (b) Dot color refers to the circularity index (I_{CIR}) value of bedforms, reflecting its relation with both I_{OE} and I_{SIN}. Bedforms with high circularity values ($I_{CIR} \geq 0.80$) have similar maximal longitudinal (LC_{MAX}) and maximal transverse components (TC_{MAX}) ($-0.17 \leq I_{OE} \leq 0.17$) and a low-to-null I_{SIN} ($I_{SIN} < 0.10$).*

(3) Bedforms with a linear crest line ($I_{SIN} < 0.10$; average $I_{SIN} = 0.01$) and a LC_{MAX} at least 1.5 times larger than their TC_{MAX} (i.e. $I_{OE} > 0.17$) were classified as flow-parallel bedforms (**Table 2**). These bedforms have an ovoid shape and have an increasing LC_{MAX} and a decreasing I_{CIR} as their I_{OE} increases (**Fig. 6**). Among linear flow-parallel bedforms, we observe higher amplitudes (average $h_{MAX} = 9.1$ m) for low-elongated bedforms ($0.17 \leq I_{OE} < 0.60$) than for highly-elongated bedforms (average $h_{MAX} = 7.2$; $0.60 < I_{OE} < 1.08$). These bedforms correspond to typical streamlined bedforms, classically subdivided in drumlins and MSGLs depending if they are respectively low- ($I_{OE} < 0.60$) or highly-elongated ($I_{OE} > 0.60$) (i.e. elongation ratio > 4; ***Ely et al., 2016***).

(4) Other bedforms, representing 44% of the morphometric cluster, are neither parallel nor transverse to the ice flow direction and have more sinuous crest lines than ribbed and streamlined bedforms (**Table 2**; **Fig. 6**).

(a) Sinuous ($I_{SIN} \geq 0.10$) and predominantly flow-transverse bedforms ($I_{OE} < 0$) are morphologically related to linear ribbed bedforms: they share a mainly transverse orientation relative to the ice flow direction (i.e. $TC_{MAX} > LC_{MAX}$) (**Fig. 6**) and have a similar TC_{MAX} (average $TC_{MAX} = 1105$ m) (**Table**

2). However, they differ from linear ribbed bedforms by their higher LC_{MAX}, similar to those of low-elongated streamlined bedforms (average LC_{MAX} = 685 m), and their increase of crest line sinuosity (average I_{SIN} = 0.23) (**Table 2; Fig. 8**). In average, their I_{SIN} is increasingly high as their I_{OE} increases and tends to 0, and their I_{CIR} decreases as their I_{SIN} increases (**Fig. 6**). These bedforms are on average 11.7 m in amplitude. Examples of sinuous predominantly flow-transverse bedforms have usually been reported as ribbed moraines although their sinuous appearance and their shape complexity have led some authors to create sub-categories of ribbed bedforms with new descriptive terms, such as Blattnick moraines (***Markgren and Lassila, 1980***), drumlinized/smoothsided ribbed moraines (***Carl, 1978; Lundqvist, 1981; Dunlop and Clark, 2006***), blocky angular or jagged-type ribbed moraines (***Dunlop & Clark, 2006***) (**Fig. 1**). Considering their morphological similarities with linear ribbed bedforms but also their higher degree of complexity, we refer to these sinuous predominantly flow-transverse bedforms as sinuous ribbed bedforms.

(b) When the LC_{MAX} exceeds the TC_{MAX}, sinuous bedforms are predominantly parallel to the ice flow direction ($I_{OE} \geq 0$; average I_{SIN} = 0.17) (**Table 1**). In average, their I_{SIN} decreases as their I_{OE} increases and their I_{CIR} decreases as their I_{SIN} increases (**Fig. 6**). Their TC_{MAX} is half of the linear and sinuous ribbed bedforms ones (average TC_{MAX} = 564 m) while their LC_{MAX} overlaps those of streamlined bedforms (average LC_{MAX} = 929 m). These bedforms display lower amplitude than sinuous and predominantly flow-transverse bedforms (average h_{MAX} = 11.2 m). Although sinuous and predominantly flow-parallel bedforms are more similar to streamlined bedforms than ribbed bedforms, their TC_{MAX} are on average two times longer and their crest line sinuosity twenty times higher than those of streamlined bedforms (**Table 2**). Some are highly sinuous with a U-shape, resembling bedforms referred in the literature to as crescentic/parabolic drumlins (***Boulton, 1987; Lundqvist, 1989; Warburton, 1994; Maclachlan and Eyles, 2013; Eyles et al., 2016***), barchan-shaped ribbed moraines (***Dunlop and Clark, 2006***) or channeled drumlins (***Sookhan et al., 2021***); while others are slightly sinuous, oblique to the flow direction and similar to bedforms described in the literature as oblique ribbed bedforms (***Vérité et al., 2021***), extensional ribbed moraines (***Wagner, 2014***), transverse/asymmetrical drumlins (***Shaw, 1983; Boulton, 1987***; ***Knight, 1997***) or drumlinized moraines (***Carl, 1978; Brown et al., 2011***) (**Fig. 1**).

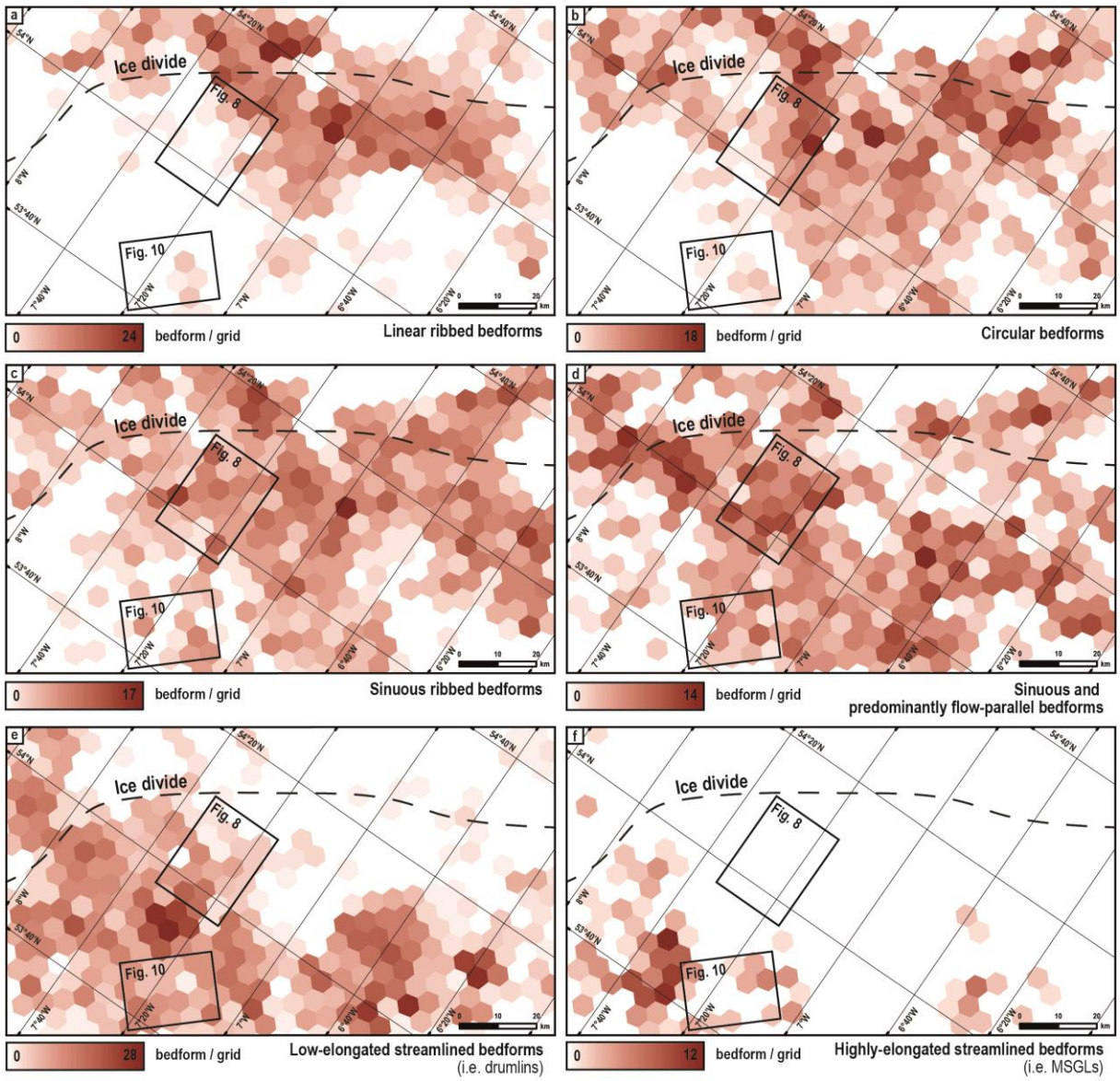

Figure 7. *Density maps of the different classes of bedforms observed along the IIS bed in north-eastern Ireland. Ribbed and circular bedforms have a similar spatial extent and occur up-ice of streamlined bedforms, while sinuous bedforms (i.e. sinuous ribbed bedforms and predominantly flow-parallel sinuous bedforms) gather in an intermediate position between ribbed and streamlined bedforms.*

3.2. Spatial distribution of subglacial bedform morphometrics

To investigate whether the morphometric continuum described in Section 3.1 is supported by a spatial continuum, we describe now the distribution of bedform shapes in the two study areas (**Figs. 7-11**).

Ireland

In the central part of the Irish study area, linear ribbed bedforms gather in a 70-km long and 30-km wide field lying along the ice divide (**Fig. 7a**). To the southwest, streamlined bedforms predominate and gather in a 60-km long and 40-km wide field (**Figs. 7e-f**).

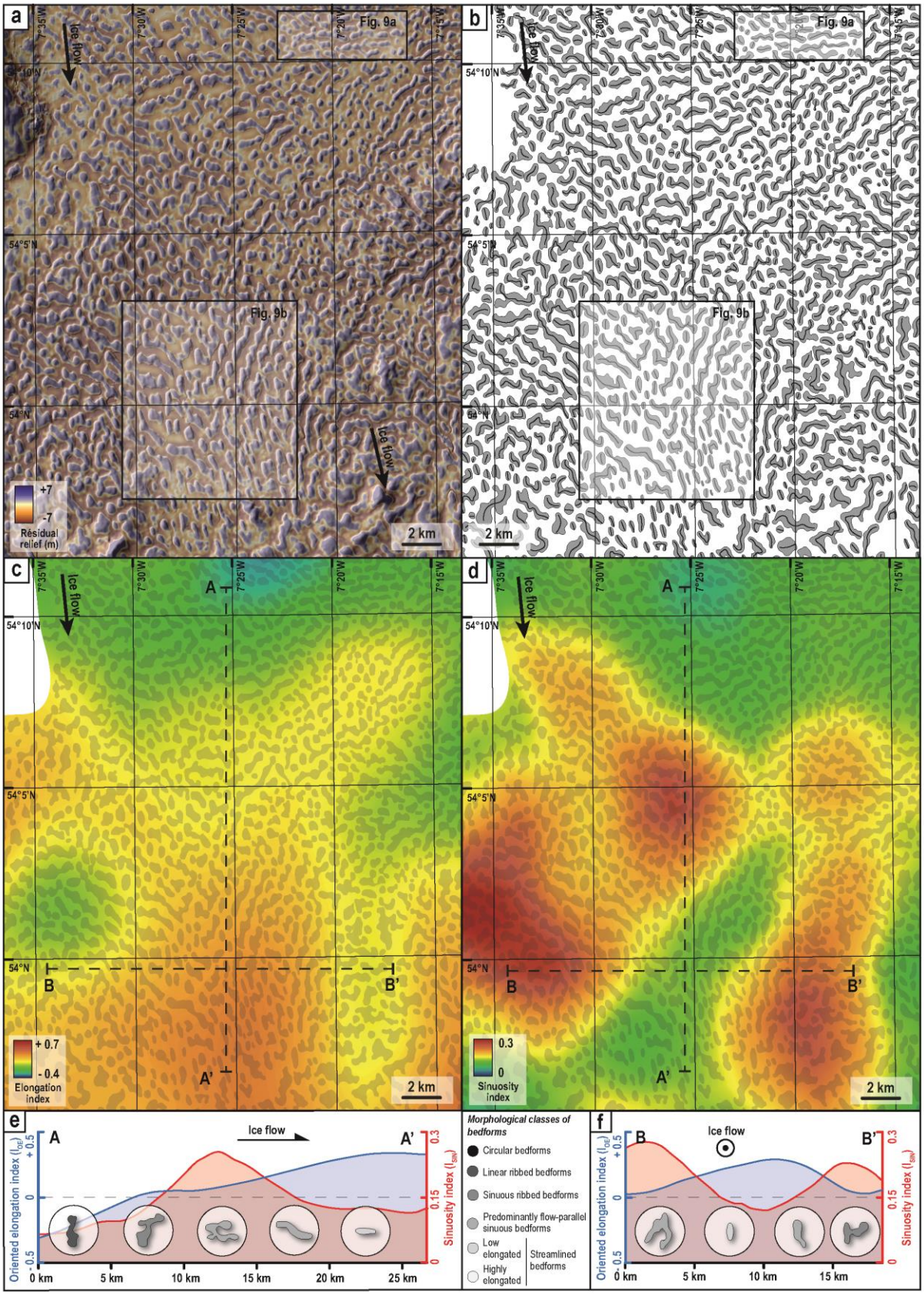

Figure 8. *(a) Hillshaded residual relief and (b) interpretative map with digitized bedforms and crest lines of the central part of the Irish study area (cf. location on* ***Fig. 4****). (c) Interpolated maps of oriented elongation index (I_{OE}) and (d) sinuosity index (I_{SIN}). Longitudinal (e) and transverse (f) profiles, crossing the spatial transition between linear ribbed bedforms in the northern part and streamlined bedforms in the southern part, highlight the progressive spatial evolution of bedform morphometry.*

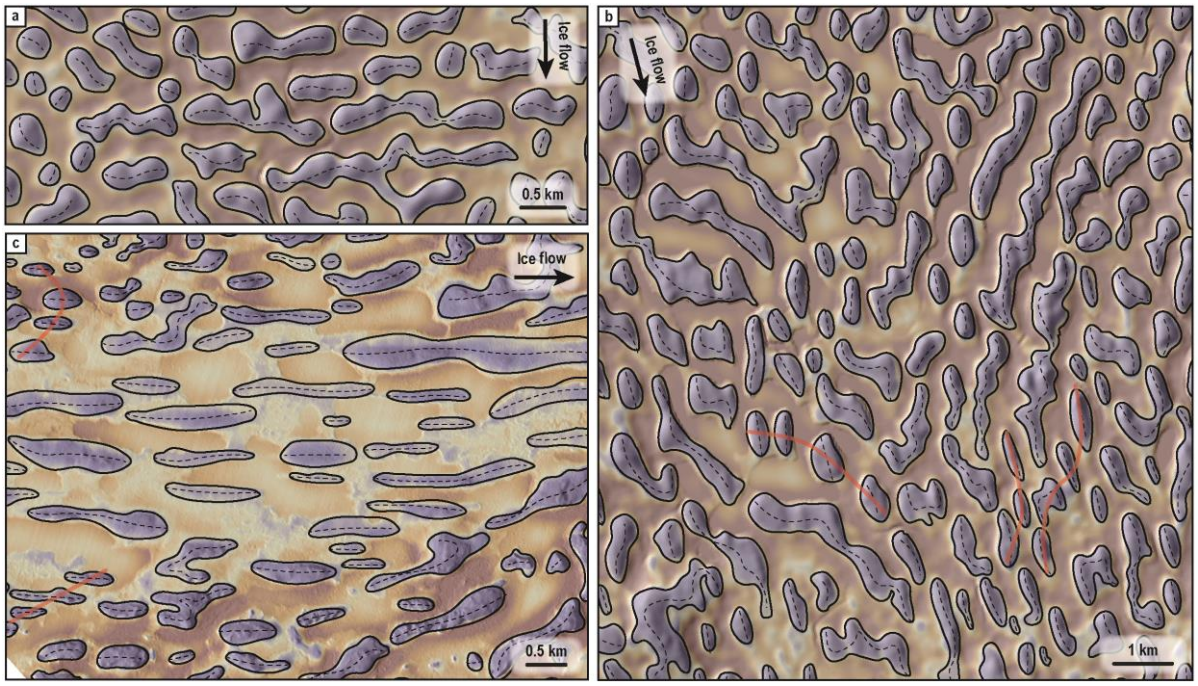

***Figure 9**. (a) Circular bedforms are scattered within a field of linear ribbed bedforms. (b) Sinuous bedforms with symmetric oblique orientations relative to the ice flow direction form an "opening gate" pattern. Down-ice of oblique bedforms, streamlined bedforms are aligned following the same oblique orientation forming an 'en-echelon' pattern (red lines). (c) Within a streamlined bedform tract elongated parallel to the ice flow direction, highly-elongated streamlined bedforms are laterally bounded by low-elongated streamlined bedforms, highlighting a progressive lateral diminution of I_{OE}. Some of these low-elongated streamlined bedforms, associated down-ice with sinuous bedforms with oblique orientation relative to the ice flow direction, exhibit an "en-echelon" pattern (red lines).*

The transition between ribbed and streamlined bedforms is gradual and characterized by an increase in sinuosity index (I_{SIN}) of bedform crest lines (**Figs. 8a-b**). Within this transitional field of bedforms, another transition towards the southwest is observed between sinuous ribbed bedforms (**Fig. 7c**), whose spatial distribution has a high degree of overlap with those of linear ribbed bedforms, and sinuous predominantly flow-parallel bedforms (**Fig. 7d**), whose spatial distribution has a high degree of overlap with those of low-elongated streamlined bedforms. Along a longitudinal profile through this transition zone (**Fig. 8e**), a progressive increase in the oriented elongation index (I_{OE}) occurs from linear ribbed bedforms to streamlined bedforms via sinuous ribbed bedforms with increasing I_{SIN} then sinuous predominantly flow-parallel bedforms with decreasing I_{SIN}. A symmetrical trend emerges from the lateral borders to the center of a transverse profile through the same zone (**Fig. 9f**): the I_{OE} increases from negative to positive values, through intermediate sinuous bedforms with I_{OE} close to zero and either high I_{SIN} or oblique orientations relative to the ice flow direction. Sinuous bedforms with an oblique orientation relative to the local ice flow direction are located on both sides of the center of the profile, forming an "opening gate" pattern (**Fig. 9b**). Down-ice, streamlined bedforms are aligned following the

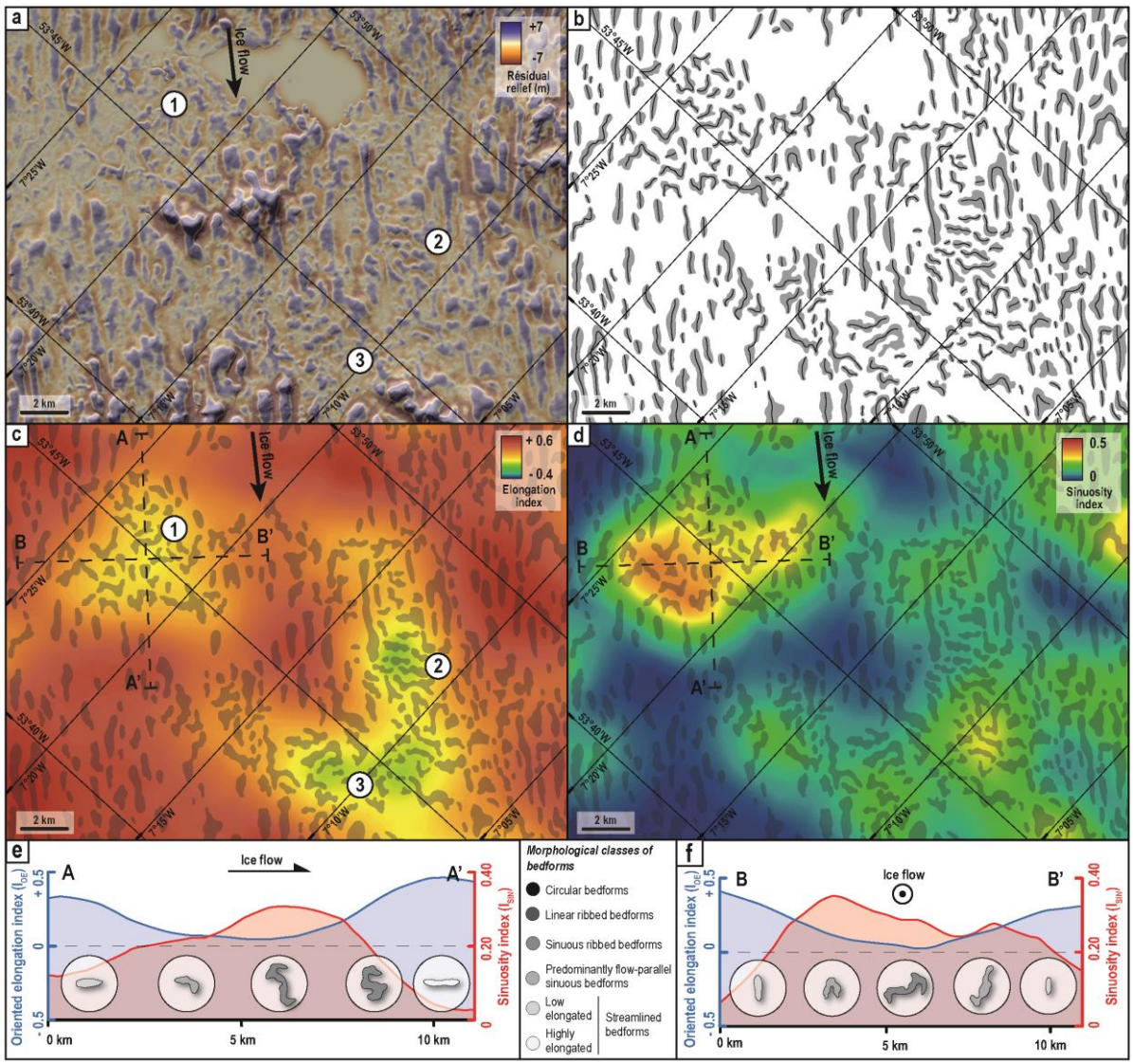

Figure 10. *(a) Hillshaded residual relief and (b) interpretative map with digitized bedforms and crest lines of the southwest part of the Irish study area. (c) Interpolated maps of oriented elongation index (I_{OE}) and (d) sinuosity index (I_{SIN}). Interpolated maps highlight the existence of spots (1, 2 and 3) of linear to sinuous ribbed bedforms surrounded by streamlined bedforms. Longitudinal (e) and transverse (f) profiles highlight that sinuous ribbed bedforms populating the spot n°1 have lower I_{OE} and higher I_{SIN} than the surrounding streamlined bedforms.*

same oblique orientation forming an "en-echelon" pattern (**Fig. 9b**). South of the study area, the progressive increase in I_{OE} highlights that streamlined bedforms are increasingly elongated, ranging from typical drumlins to MSGLs dimensions (**Figs. 7e-f**). Circular bedforms are scattered within the field of linear ribbed bedforms but are absent within the field of streamlined bedforms (**Fig. 7b, 9a**).

In the southwest part of the Irish study area, linear and sinuous ribbed bedforms (**Figs. 7a, c; 10**) occur within a sub-circular spot (1), approximately 3-km in diameter, surrounded by a field of streamlined bedforms (**Figs. 7e-f; 10**). Along both longitudinal (**Fig. 10e**) and transverse (**Fig. 10f**) profiles, morphometric indexes show striking symmetrical trends in bedform evolution: streamlined bedforms, predominantly flow-parallel sinuous bedforms and sinuous ribbed bedforms respectively

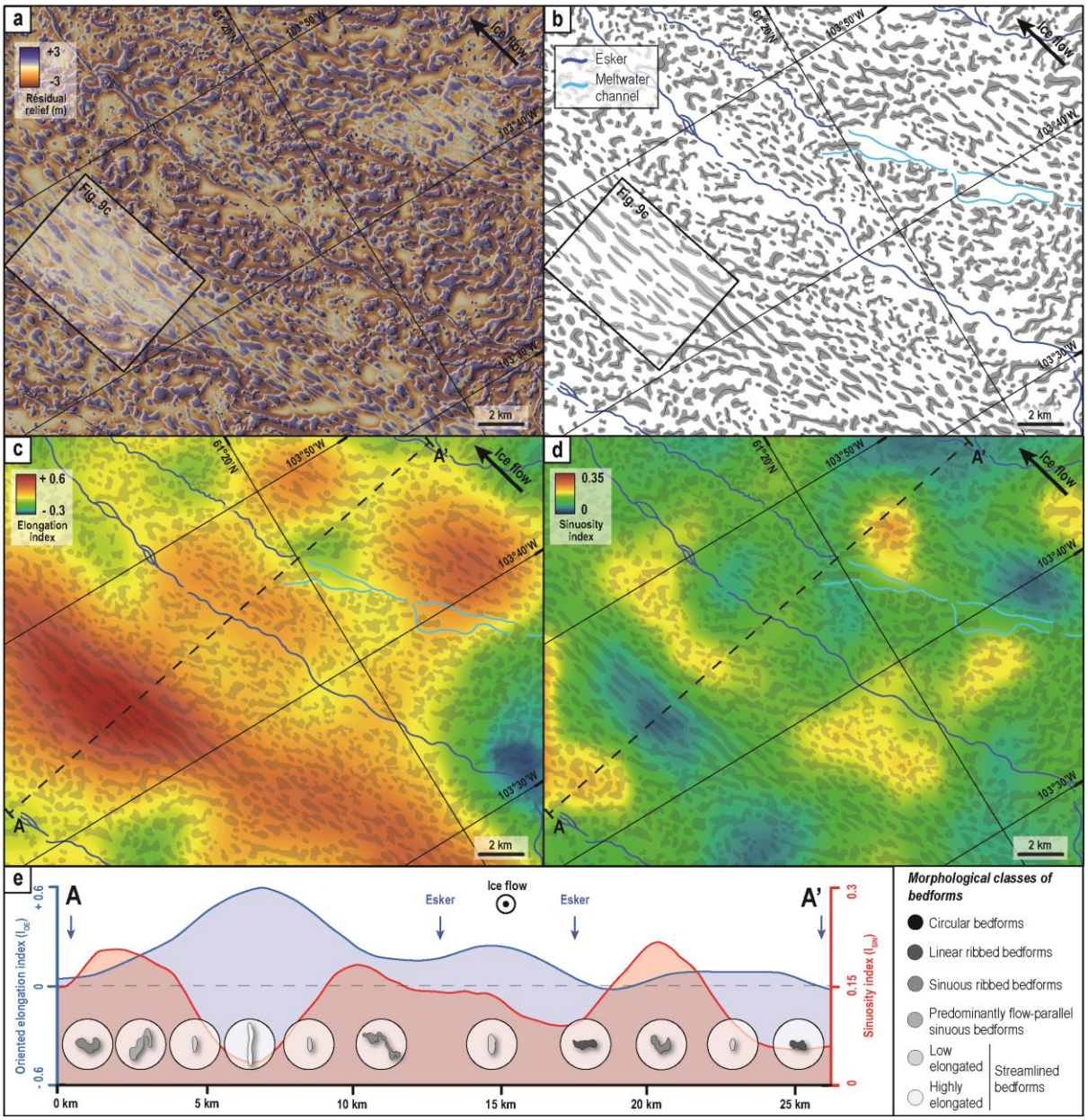

Figure 11. *(a) Hillshaded residual relief and (b) interpretative map with digitized bedforms and crest lines of the central part of the Canadian study area. (c) Interpolated maps of oriented elongation index and (d) sinuosity index. Ribbed bedform tracts with low oriented elongation values and crossed by eskers laterally alternate with streamlined bedform tracts characterized by high oriented elongation values. Note that sinuous bedforms occur at the transition between ribbed and streamlined bedform tracts.*

occur from the borders to the core of the circular spot. Other spots (2 & 3) with similar morphometric evolutions are observed within the field of streamlined bedforms and are all associated with topographic highs (**Fig. 10a**).

Canada

This site is characterized by alternating tracts of streamlined and ribbed bedforms (**Figs. 5, 11**). These tracts are about 4 km wide and several tens of kilometers long; they are elongated parallel to the local ice flow direction and meltwater drainage features (eskers and meltwater channels). Along a profile

transverse to these tracts (**Fig. 11e**), tracts of ribbed bedforms characterized by low values of I_{OE} and linear to low sinuous crest lines correlate with the position of drainage features (i.e. eskers and channels). Streamlined bedforms characterized by a high I_{OE} and linear crest lines are located in between drainage features. Laterally, sinuous ribbed bedforms and predominantly flow-parallel sinuous bedforms occur at the transition between linear ribbed bedform and streamlined bedform tracts. Some of these sinuous bedforms exhibit an obliquity to the local ice flow direction on both tract sides (**Fig. 11c**). Along the transverse profile (**Fig. 11e**), a 4 kilometers-wide corridor of streamlined bedforms with maximal I_{OE} in the core of the corridor is bounded by streamlined bedforms with lower I_{OE}, whose some of them exhibit an "en-echelon" pattern (**Fig. 10c**). The spatial evolution of I_{OE} highlights there is no break in the distribution of streamlined bedforms morphometrics when increasing the I_{OE} (**Fig. 11a**), which is materialized by an increasing LC_{MAX} with a constant TC_{MAX} of 300 m (**Fig. 6a**). This evolution demonstrates the morphometric and spatial continuity between drumlins and MSGLs.

4. Discussion

The morphometric approach developed in this study, based on dimensionless parameters allowing the possibility that bedforms can be sinuous and oblique to the ice flow directions, reveals that all the analyzed bedforms can be integrated in a morphometric continuum. Bedform classes defined for descriptive convenience have in fact no bounds and can be differentiated only on the basis of arbitrary thresholds (**Table 2; Fig. 6**). Scatterplots (**Fig. 6**) and spatial transects (**Figs. 7-11**) demonstrate a continuum between: (i) circular bedforms, (ii) linear ribbed bedforms, (iii) low- to highly-elongated streamlined bedforms, respectively corresponding to typical drumlins and MSGLs, and (iv) a variety of morphologically intermediate sinuous bedforms which were hitherto interpreted as superimposed or multiphased bedforms.

4.1. A unifying sequence of bedform evolution

Based on the morphometric (**Fig. 6**) and spatial (**Figs. 7-11**) continuum of subglacial bedform shapes, we explore how the variations of the dimensionless morphometric parameters could help deciphering the subglacial bedform evolution in a time and space grid. Keeping in mind the initial assumption that the formation of all bedforms is associated with constant ice flow trajectories, we suggest that ribbed bedforms with linear crest lines are the first bedforms to form, then become more

sinuous and more elongated in the ice flow direction as they evolve. As the sinuosity index of their crest line (I_{SIN}) increases, we suggest that they then evolve into predominantly flow-parallel bedforms, until progressively paralleling the local ice flow direction to form streamlined bedforms with increasing oriented elongated index (I_{OE}) (**Figs. 12-13**).

Three major assumptions are required to reconstruct the chronological frame of this bedform evolution: (1) ribbed bedforms, ranging from circular to linear forms, are incipient bedforms and their I_{OE} is independent of their degree of bedform evolution; (2) sinuous bedforms are transitional bedforms between ribbed and streamlined bedforms along a sequence of increasing degree of bedform evolution; (3) streamlined bedforms arise from the fragmentation of transitional sinuous bedforms and their I_{OE} increases as their degree of bedform evolution increases. We translate these assumptions into an equation in order to characterize the degree of bedform evolution by a quantitative parameter derived from the combination of morphometric parameters (**Fig. 12**). This quantitative parameter is defined by the following equation:

$$Degree\ of\ bedform\ evolution = \left(\frac{\pi}{2} + \tan^{-1}\left(\frac{I_{OE}}{I_{SIN}}\right)\right) \times (I_{OE} + 1)$$

represents our interpretation of the degree of bedform evolution (equation details presented in **Supplementary Data 3**). These three assumptions and the bedform evolution sequence are hereafter discussed.

4.1.1. Ribbed bedforms with various elongation come first

Circular bedforms are circular forms of ribbed bedforms

Along the ordinate axis of the scatter plot in **Fig. 6,** circular bedforms are intermediate bedform among the range of bedforms displaying linear crestlines (i.e. $I_{SIN} < 0.10$). This morphometric continuity is reflected (i) by their I_{OE}, which is intermediate between those of linear ribbed bedforms and streamlined bedforms, and (ii) their average diameter, which is similar to the average TC_{MAX} of streamlined bedforms and to the average LC_{MAX} of linear ribbed bedforms (**Table 2**). The morphometric continuity between linear ribbed, circular and streamlined bedforms corroborates the size and shape bedform continuum proposed by ***Ely et al. (2016)***. However, although circular bedforms are scattered within an area overlapping the highest linear ribbed bedforms density (**Figs. 7a-b**), circular bedforms

are absent in the area where streamlined bedforms are abundant and do not particularly gather at the transition between ribbed and streamlined bedforms (**Figs. 7, 10**). Those spatial distributions contradict interpretations that circular bedforms are transitional forms between ribbed and streamlined bedforms (***Aario, 1977; Ely et al., 2016***). Considering the spatial relationship between subglacial bedforms, we suggest to insert circular bedforms in a morphometric and spatial continuum of ribbed bedforms ranging from circular to linear forms. In agreement with previous observations reported by ***Hättestrand (1997)***, ***Greenwood and Clark (2008)***, ***Möller and Dowling (2015)*** and ***Vérité et al. (2021, 2022),*** we therefore consider circular forms as circular ribbed bedforms.

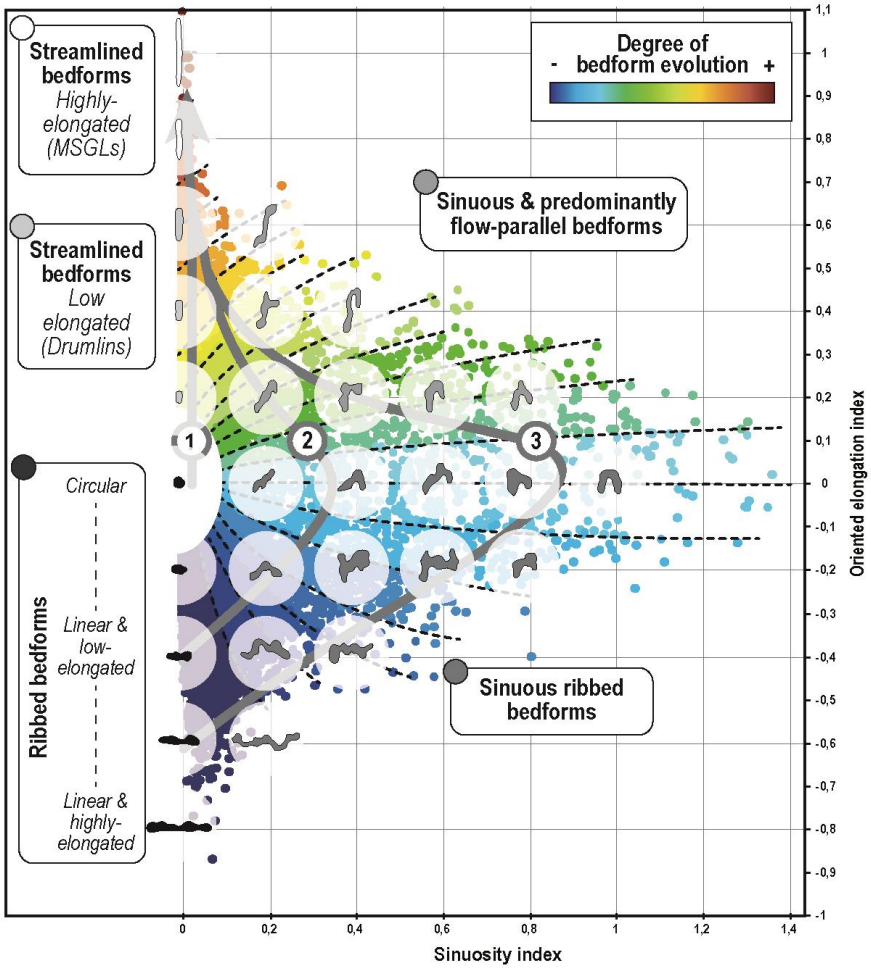

Figure 12*. Degree of subglacial bedform evolution (from dark blue for the lower degree of evolution to red for the higher one) based on the evolution of oriented elongation (I_{OE}) and sinuosity (I_{SIN}) indices along natural sections. Dotted black lines are graduations of the colored scale materializing the degree of bedform evolution. Bold grey arrows are three examples of evolutionary sequences described hereafter and schematically represented in* ***Fig. 13****. We suggest that ribbed bedforms with linear crest lines correspond to incipient bedforms, independently of their random I_{OE}, from circular forms (I_{OE} ~ 0) to elongated flow-transverse forms ($I_{OE} \rightarrow - \infty$). Depending on their initial I_{OE}, circular ribbed bedforms evolve into streamlined bedforms through an increase I_{OE} without sinuous transitional forms (evolution sequence n°1); while elongated ribbed bedforms evolve into increasingly sinuous transitional bedforms (i.e. first sinuous ribbed bedforms then sinuous and predominantly flow-parallel bedforms) as they are initially highly-elongated, before fragmenting to form streamlined bedforms with an increasing I_{OE} (evolution sequences n°2 and 3). Note that the degree of bedform evolution is not calculated for circular ribbed bedforms (white zone) since the equation is not applicable (see the text for more details).*

Ribbed bedforms are incipient bedforms

Numerical models simulating the formation of subglacial bedforms demonstrate that ribbed bedforms with linear crest lines are the first bedforms to form, and constitute incipient bedforms in evolutionary sequences (***Chapwanya et al., 2011; Barchyn et al., 2016; Fannon et al., 2017***). Numerical models also demonstrated that circular bedforms can emerge from the random dislocation of ribbed bedforms without any increases of their width and sinuosity during the early stages of evolutionary sequences, constituting incipient bedforms just as ribbed bedforms (***Fannon, 2020 p.139-140***). Similarly, physical simulations demonstrated the synchronous formation of ribbed bedforms with various values of their maximal transverse components and various shapes, ranging from circular to highly-elongated forms (***Vérité et al., 2021, 2022***). Considering (i) these modeling observations and (ii) the high overlap between the spatial distribution of circular ribbed bedforms (**Fig. 7b**) and linear ribbed bedforms with variable elongation (**Fig. 7a**), we interpret that incipient ribbed bedforms arise with a random maximal transverse component. Corroborating works from ***Hättestrand (1997)*** and ***Möller and Dowling (2015)*** interpreting a continuum of ribbed bedforms from circular to transverse and elongated forms as resulting from a single process, we propose that ribbed bedforms with linear crest lines correspond to the first stage of subglacial bedform evolution whatever their size and shape (**Fig. 13a**).

4.1.2. Ribbed bedforms evolve into sinuous transitional bedforms

According to the initial size and shape of the ribbed bedform and to the later stages of bedform transformation, an infinite number of trajectories of bedform evolution can be followed (**Fig. 12; three of them are represented**), leading to variations in the metrics of bedform sequences (**Fig. 13**). Taking the evolution sequence n° 2 and 3, we suggest that elongated ribbed bedforms, characterized by a linear crest line when they initially form, become increasingly sinuous (with increasing I_{OE}) as their degree of evolution increases and as they are initially highly-elongated (**Fig. 12**). Numerical simulations of subglacial bedforms demonstrated that, whatever the glaciological and hydrological conditions simulated, ribbed bedforms become increasingly stretched toward the ice flow direction, sinuous and oblique as they evolve before dislocating into streamlined bedforms (Supplementary materials of ***Fannon et al. 2017; Fannon, 2020 p.139***). Those numerical simulations, supporting our model of bedform evolution, correlate with recent physical modeling works describing increasingly sinuous and

oblique ribbed bedform through experimental run (***Vérité et al., 2021, 2022***). These works support the hypothesis - postulated from scatterplots (**Fig. 6**) and morphometrical transects through bedform fields (**Figs. 7-11**) - that sinuous ribbed bedforms and predominantly flow-parallel sinuous bedforms are transitional bedforms resulting from the evolution of linear ribbed bedforms (**Figs. 13b-c**).

However, if the initial ribbed bedforms tend to display a more circular shape (**Figs. 12-13; evolution sequence n°1**), they will evolve into increasingly elongated streamlined bedforms without transitional sinuous bedforms. Considering the uncertain computation of the orientation relative to the ice flow direction of highly circular bedform ($I_{CIR} > 0.80$), for which the ratio between the two elongation components is lower than 1.5, the equation calculating the degree of bedform evolution – which is strongly function of the oriented elongated index – is not applicable for circular ribbed bedforms (**Fig. 12**). Considering the uncertain computation of the orientation relative to the ice flow direction of highly

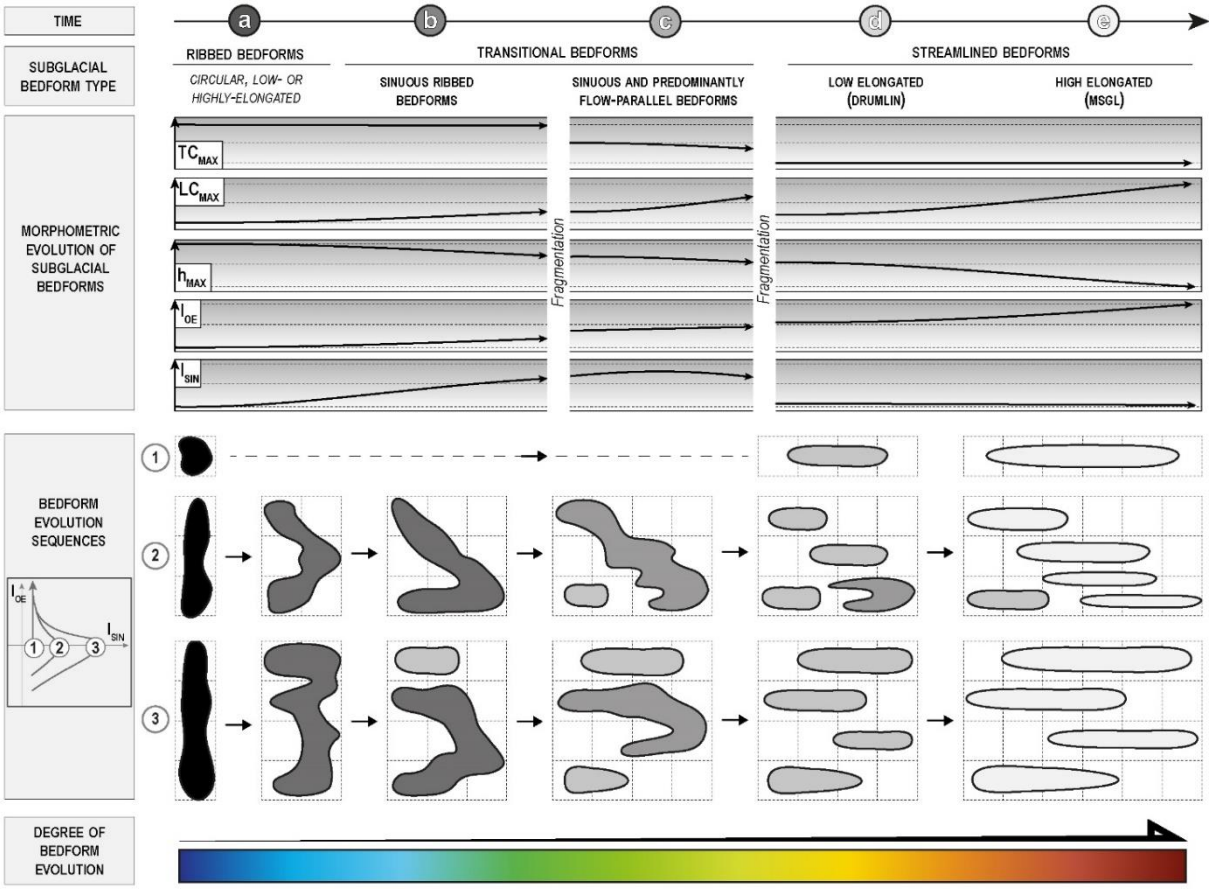

Figure 13. *Model of morphological evolution of subglacial bedforms, derived from the morphometric and spatial continuum observed in our study. Subglacial bedforms initiate as linear ribbed bedforms, and progressively evolve through complex transitional bedforms with variable sinuosities and orientations, towards increasingly elongated streamlined bedforms. The degree of bedform evolution, defined from the combination of their I_{OE} and I_{SIN}, is a quantitative measure of this progressive evolution. Three examples of bedform evolutionary sequences are proposed (see* ***Fig. 12****) depending on the initial I_{OE} of the ribbed bedform.*

circular bedform (I_{CIR} > 0.80) whose the ratio between their two elongation components is inferior 1.5, the equation calculating the degree of bedform evolution – which is strongly function of the oriented elongated index – is not applicable for circular bedforms whose circular ribbed bedforms are taking part (**Fig. 12**).

4.1.3. Streamlined bedforms arise from sinuous transitional bedform fragmentation and are increasingly elongated as they evolve

In Ireland and Canada, sinuous oblique bedforms and "en-echelon" drumlins – examples of which have been independently mentioned in the literature (***Shaw, 1983; Stokes et al., 2016; Clark et al., 2018***) – are observed along transition zones between ribbed and streamlined bedforms (**Figs. 9b-c**). Similar examples of sinuous oblique bedforms fragmenting into streamlined bedforms with en-echelon patterns have been numerically simulated by ***Fannon et al. (2017)*** and ***Fannon (2020; p.139)***, suggesting that streamlined bedforms derive from the fragmentation of sinuous, sometimes oblique bedforms (**Fig. 12**; evolution sequence n°2 and 3). Our results strongly support these observations and simulations. On average, the maximal transverse components (TC_{MAX}) of transitional bedforms and streamlined bedforms are respectively half and a quarter the TC_{MAX} measured for ribbed bedforms (**Table 2**) (**Fig. 13**). The evolution of the maximal longitudinal component (LC_{MAX}) is anti-correlated with both TC_{MAX} and amplitudes (h_{MAX}) illustrating the progressive elongation (parallel to the ice flow direction) and thinning of bedforms (**Fig. 13**). The process of bedform evolution leading to inversion of the dominant component (i.e., TC_{MAX} towards LC_{MAX}) is concomitant with an increase in bedform sinuosity. The fragmentation of sinuous bedforms in response to sustained stretching subdivides the bedforms into multiple smaller and less sinuous entities (**Figs. 13c-d**).

The fragmentation first leads to the formation of distinct and individualized low-elongated and flow-parallel bedforms we consider as being proto-drumlins (***Clark et al., 2009***). **Figure 6** shows there is no break in the distribution of streamlined bedforms morphometrics when increasing the $I_{OE,}$ demonstrating continuity between drumlins and MSGLs. In Ireland and Canada, this continuity is also spatial as increasing I_{OE} gradients – which is materialized by an increasing LC_{MAX} with a constant TC_{MAX} (~300 m) – occur parallel (i.e. in the down-ice direction; **Figs. 8c, 9b**) or transverse to the local ice flow direction (**Figs. 9c, 11c**). In addition to several studies highlighting the spatial (***Aario, 1977; Boyce and***

Eyles, 1991; Hart, 1999; Stokes and Clark, 2002; Briner, 2007; Sookhan et al., 2021) and morphometric (***Rose, 1987***; ***Clark et al., 2009***; ***Stokes et al., 2013; Ely et al., 2016)*** continuity between drumlins and MSGLs, we quantitatively demonstrate that the intensity of streamlined bedform elongation parallel to the ice flow direction illustrates their degree of evolution (**Figs. 12, 13d-e**).

4.2. Glaciodynamics significance of the bedform evolution degree

The sequences of bedform evolution have sometimes been interpreted as spatial variations in the duration of ice streaming process (***Boyce and Eyles, 1991; Zoet et al., 2021***), bed lithology (***Aylsworth and Shilts, 1989; Wellner et al., 2001; O Cofaigh et al., 2002; Greenwood and Clark, 2010; McKenzie et al., 2022***), bed topography (***Bouchard, 1989; Franke et al., 2020***), bed thickness (***Kerr & Eyles, 2007 ; Barchyn et al., 2016***) or meltwater pressure (***Shaw, 2002***; ***Livingstone et al., in press***). In most cases, they have been interpreted as spatial variations in ice flow velocity from the onset area to the ice stream core (***Dyke et al., 1992; King et al., 2007***) and even along or across the ice stream itself (***Aario, 1977; Hart, 1999; Briner, 2007; Stokes et al., 2013; Hillier et al., 2016; Hermanowski et al., 2019; Van Landeghem & Chiverrell, 2020; Sookhan et al., 2021, 2022***).

In Ireland, streamlined bedform tracts – several 10s of kilometers long and wide – have been interpreted as palaeo-corridors of fast ice flow (***Synge and Stephens, 1960; Stokes and Clark, 1999; Greenwood and Clark, 2009a***), which probably correspond to palaeo-ice streams draining the Lowland Ice Dome between 20 and 17 ka BP (***Clark et al., 2022***). Morphometric and spatial analysis conducted in Ireland suggest that the bedform distribution reveals longitudinal and lateral gradients of bedform evolution relative to the ice flow direction (**Figs. 7-8**), certainly recording ice flow velocity pattern along an across an ice stream. Indeed, the transition between slow ice near the ice dome (i.e. onset area) and at ice stream margins (i.e. shear margins) to fast ice in the ice stream core is respectively recorded through transitions between ribbed, sinuous and streamlined bedforms (**Fig. 9b**). Our model, encompassing the degree of bedform evolution in a spatio-temporal continuum, is convincing as it manages to explain transitions in ice flow velocity classically monitored in modern ice streams (***Sergienko & Hindmarsh, 2013; Zheng et al., 2019***).

Small fields of linear to sinuous ribbed bedforms contained within streamlined bedform tracts in Ireland (**Fig. 10**) indicate abrupt and very localized changes in the degree of bedform evolution. We

interpret this local anomaly in bedform evolution as the morphological expression of slow ice patches within fast-flowing ice corridor, as it has commonly been reported for ice stream sticky spots (***Alley, 1993).*** We notice that palaeo-sticky spots have mainly been recognized through the superposition of ribbed bedforms on top of streamlined bedforms (***Stokes et al., 2006, 2007, 2016***). There is no cross-cutting relationships or superposition in the sticky spots revealed in Ireland, instead we suggest that streamlined bedforms and ribbed bedforms are synchronous and that patches of bedform of lower evolution reveal sustained sticky conditions related to nearby bedrock topographic highs.

In Canada, previous studies suggest that the position of the study area below the Keewatin Ice Dome intersects meltwater corridors that developed below the retreating Laurentide Ice Sheet (***Storrar et al., 2013; Lewington et al., 2020***). Moreover, ***Lewington (2020)*** suggested that corridors of ribbed bedforms below the Keewatin – which were identified alternating with corridors of drumlins by ***Aylsworth & Shilts (1989)*** – correspond to potential geomorphic markers of meltwater corridors. This suggests that the lateral variations in bedform morphologies observed across well-defined meltwater drainage features indicate the influence of meltwater pressure variations on the degree of bedform evolution (**Fig. 11**).

Assuming the model bedform continuum is correct, the spatial diversity of bedform shapes, dimensions and orientation observed in Ireland and Canada indicates various degree of bedform evolution relative to spatial variations in subglacial conditions (e.g. ice flow velocity, bedrock characteristics, meltwater pressure) considering constant ice-flow trajectories. Given that complex and neither parallel or transverse bedforms (e.g. sinuous transitional bedforms in this study) have mainly been interpreted as bedform superimposition and/or crosscutting relationships recording several changing ice flow directions, the integration of these bedforms into a single continuum model could help revising the number of ice-sheet flow trajectories currently envisaged in Ireland (***Greenwood et al., 2009***) or in Canada (***Winsborrow et al., 2004; De Angelis & Kleman, 2007***).

5. Conclusion

Combined mapping and morphometric analysis of 13 500 subglacial bedforms enabled the morphological evolution of subglacial bedforms to be explored.

First, a new morphometric approach – based on the computation of the circularity (I_{CIR}), sinuosity (I_{SIN}) and oriented elongation (I_{OE}) of subglacial bedforms – reveals a morphometric and spatial continuum between ribbed bedforms (i.e. circular to elongated, flow-transverse and linear forms), streamlined bedforms (i.e. drumlins and MSGLs) and sinuous bedforms with various shapes and orientations (i.e. sinuous ribbed bedforms and predominantly flow-parallel sinuous bedforms). Complex, oblique and sinuous bedforms, which have been excluded from most existing models of subglacial continuum and commonly interpreted as resulting from the remolding/superimposition of more simple and younger bedforms, are part of this continuum and can form under the same ice flow trajectory as ribbed and streamlined bedforms.

Second, we interpreted this morphological and spatial continuum as the expression of evolutionary sequences between a diversity of ribbed bedforms, ranging from circular to linear transverse, and streamlined bedforms. Intermediate sinuous bedforms, recording the progressive realignment and elongation in the ice flow direction, are indeed transitional bedforms that result from the stretching of linear ribbed bedforms and fragment into several streamlined bedforms. The degree of bedform evolution along these evolutionary sequences can be quantified by a morphometric parameter based on the oriented elongation index and the sinuosity index.

The spatial relationships between bedform evolutionary sequences reported in Ireland and Canada and their assumed glaciological contexts (e.g. ice flow velocity, meltwater pressure, bed topography and lithology) suggest the degree of bedform evolution could be used to (1) explore factors controlling subglacial bedform formation and evolution and (2) reconstruct the past glacial dynamics with an unprecedented accuracy. This work opens up new perspectives to bridge the gap between subglacial bedforms morphology, subglacial processes and ice dynamics. Further work is needed to explore the genetic significance of this morphometric continuum and bring palaeoglaciological reconstructions to the next level.

References

Aario, R. (1977). Classification and terminology of morainic landforms in Finland. Boreas, 6(2), 87-100.

Allen, J. R. L. (1968). The nature and origin of bed-form hierarchies. Sedimentology, 10(3), 161-182.

Aylsworth, J. M., & Shilts, W. W. (1989). Bedforms of the Keewatin ice sheet, Canada. Sedimentary Geology, 62(2-4), 407-428.

Barchyn, T. E., Dowling, T. P., Stokes, C. R., & Hugenholtz, C. H. (2016). Subglacial bed form morphology controlled by ice speed and sediment thickness. Geophysical Research Letters, 43(14), 7572-7580.

Birch, C. P., Oom, S. P., & Beecham, J. A. (2007). Rectangular and hexagonal grids used for observation, experiment and simulation in ecology. Ecological modelling, 206(3-4), 347-359.

Boulton, G. S. 1987. A theory of drumlin formation by subglacial sediment deformation. In: Menzies, J. & Rose, J. (eds) Drumlin Symposium. Balkema, Rotterdam, 25-80.

Boyce, J. I., & Eyles, N. (1991). Drumlins carved by deforming till streams below the Laurentide ice sheet. Geology, 19(8), 787-790.

Briner, J. P. (2007). Supporting evidence from the New York drumlin field that elongate subglacial bedforms indicate fast ice flow. Boreas, 36(2), 143-147.

Brown, V. H., Stokes, C. R., & O'Cofaigh, C. (2011). The glacial geomorphology of the north-west sector of the Laurentide Ice Sheet. Journal of Maps, 7(1), 409-428.

Burgess, D. O., Shaw, J., & Eyton, J. R. (2003). Morphometric comparisons between Rogen terrain and hummocky terrain. Physical Geography, 24(4), 319-336.

Canals, M., Urgeles, R., & Calafat, A. M. (2000). Deep sea-floor evidence of past ice streams off the Antarctic Peninsula. Geology, 28(1), 31-34.

Carl, J. D. (1978). Ribbed moraine–drumlin transition belt, St. Lawrence Valley, New York. Geology, 6(9), 562-566.

Carling, P. A. (1999). Subaqueous gravel dunes. Journal of Sedimentary Research, 69(3), 534-545.

Chapwanya, M., Clark, C. D., & Fowler, A. C. (2011). Numerical computations of a theoretical model of ribbed moraine formation. Earth Surface Processes and Landforms, 36(8), 1105-1112.

Clark, C. D. (1993). Mega-scale glacial lineations and cross-cutting ice-flow landforms. Earth surface processes and landforms, 18(1), 1-29.

Clark, C. D., Hughes, A. L., Greenwood, S. L., Spagnolo, M., & Ng, F. S. (2009). Size and shape characteristics of drumlins, derived from a large sample, and associated scaling laws. Quaternary Science Reviews, 28(7-8), 677-692.

Clark, C. D., Hughes, A. L., Greenwood, S. L., Jordan, C., & Sejrup, H. P. (2012). Pattern and timing of retreat of the last British-Irish Ice Sheet. Quaternary Science Reviews, 44, 112-146.

Clark, C. D., Ely, J. C., Spagnolo, M., Hahn, U., Hughes, A. L., & Stokes, C. R. (2018). Spatial organization of drumlins. Earth Surface Processes and Landforms, 43(2), 499-513.

Clark, C. D., Ely, J. C., Hindmarsh, R. C., Bradley, S., Ignéczi, A., Fabel, D., ... & Wilson, P. (2022). Growth and retreat of the last British–Irish Ice Sheet, 31 000 to 15 000 years ago: the BRITICE-CHRONO reconstruction. Boreas.

Courrech du Pont, S., Narteau, C., & Gao, X. (2014). Two modes for dune orientation. Geology, 42(9), 743-746.

Cowan, W. R. (1968). Ribbed moraine: till-fabric analysis and origin. Canadian Journal of Earth Sciences, 5(5), 1145-1159.

De Angelis, H., & Kleman, J. (2007). Palaeo-ice streams in the Foxe/Baffin sector of the Laurentide Ice Sheet. Quaternary Science Reviews, 26(9-10), 1313-1331.

Doornkamp, J. C., & King, C. A. (1971). Numerical analysis in geomorphology: an introduction. Hodder Education.

Dowling, T. P., Spagnolo, M., & Möller, P. (2015). Morphometry and core type of streamlined bedforms in southern Sweden from high resolution LiDAR. Geomorphology, 236, 54-63.

Dunlop, P., & Clark, C. D. (2006). The morphological characteristics of ribbed moraine. Quaternary Science Reviews, 25(13-14), 1668-1691.

Dyke, A. S., Vincent, J. S., Andrews, J. T., Dredge, L. A., & Cowan, W. R. (1989). The Laurentide Ice Sheet and an introduction to the Quaternary geology of the Canadian Shield.

Dyke, A. S., Morris, T. F., Green, D. E., & England, J. (1992). Quaternary geology of Prince of Wales island, arctic Canada.

Ely, J. C., Clark, C. D., Spagnolo, M., Stokes, C. R., Greenwood, S. L., Hughes, A. L., ... & Hess, D. (2016). Do subglacial bedforms comprise a size and shape continuum?. Geomorphology, 257, 108-119.

Eyles, N. (2012). Rock drumlins and megaflutes of the Niagara Escarpment, Ontario, Canada: a hard bed landform assemblage cut by the Saginaw–Huron Ice Stream. Quaternary Science Reviews, 55, 34-49.

Eyles, N., Putkinen, N., Sookhan, S., & Arbelaez-Moreno, L. (2016). Erosional origin of drumlins and megaridges. Sedimentary Geology, 338, 2-23.

Fannon, J. S., Fowler, A. C., & Moyles, I. R. (2017). Numerical simulations of drumlin formation. Proceedings of the Royal Society A: Mathematical, Physical and Engineering Sciences, 473(2204), 20170220.

Folk, R. L. (1968). Petrology of sedimentary rocks: Hemphill's. Austin, Texas, 170, 85.

Franke, S., Jansen, D., Binder, T., Dörr, N., Helm, V., Paden, J., ... & Eisen, O. (2020). Bed topography and subglacial landforms in the onset region of the Northeast Greenland Ice Stream. Annals of Glaciology, 61(81), 143-153.

Greenwood, S. L. (2008). A palaeo-glaciological reconstruction of the last Irish Ice Sheet (Doctoral dissertation, University of Sheffield).

Greenwood, S. L., & Clark, C. D. (2008). Subglacial bedforms of the Irish ice sheet. Journal of Maps, 4(1), 332-357.

Greenwood, S. L., & Clark, C. D. (2009a). Reconstructing the last Irish Ice Sheet 1: changing flow geometries and ice flow dynamics deciphered from the glacial landform record. Quaternary Science Reviews, 28(27-28), 3085-3100.

Greenwood, S. L., & Clark, C. D. (2009b). Reconstructing the last Irish Ice Sheet 2: a geomorphologically-driven model of ice sheet growth, retreat and dynamics. Quaternary Science Reviews, 28(27-28), 3101-3123.

Greenwood, S. L., & Kleman, J. (2010). Glacial landforms of extreme size in the Keewatin sector of the Laurentide Ice Sheet. Quaternary Science Reviews, 29(15-16), 1894-1910.

Hart, J. K. (1999). Identifying fast ice flow from landform assemblages in the geological record: a discussion. Annals of Glaciology, 28, 59-66.

Hättestrand, C. (1997). Ribbed moraines in Sweden—distribution pattern and palaeoglaciological implications. Sedimentary Geology, 111(1-4), 41-56.

Hermanowski, P., Piotrowski, J. A., & Szuman, I. (2019). An erosional origin for drumlins of NW Poland. Earth Surface Processes and Landforms, 44(10), 2030-2050.

Hill, A. R. (1973). The distribution of drumlins in County Down, Ireland. Annals of the Association of American Geographers, 63(2), 226-240.

Hiller, J. K., & Smith, M. (2008). Residual relief separation: digital elevation model enhancement for geomorphological mapping. Earth Surface Processes and Landforms, 33(14), 2266-2276.

Hillier, J. K., Benediktsson, Í. Ö., Dowling, T. P. F., & Schomacker, A. (2018). Production and preservation of the smallest drumlins. GFF, 140(2), 136-152.

Hollingworth, S. E. (1931). The glaciation of western Edenside and adjoining areas and the drumlins of Edenside and the Solway basin. Quarterly Journal of the Geological Society, 87(1-4), 281-359.

Jackson, R. G. (1975). Hierarchical attributes and a unifying model of bed forms composed of cohesionless material and produced by shearing flow. Geological Society of America Bulletin, 86(11), 1523-1533.

Kerr, M., & Eyles, N. (2007). Origin of drumlins on the floor of Lake Ontario and in upper New York State. Sedimentary Geology, 193(1-4), 7-20.

King, E. C., Woodward, J., & Smith, A. M. (2007). Seismic and radar observations of subglacial bed forms beneath the onset zone of Rutford Ice Stream, Antarctica. Journal of Glaciology, 53(183), 665-672.

Knight, J. (1997). Morphological and morphometric analyses of drumlin bedforms in the Omagh Basin, north central Ireland. Geografiska Annaler: Series A, Physical Geography, 79(4), 255-266.

Knight, J., Stephen, G. M., & McCabe, A. M. (1999). Landform modification by palaeo-ice streams in east-central Ireland. Annals of Glaciology, 28, 161-167.

Kocurek, G., & Day, M. (2018). What is preserved in the aeolian rock record? A Jurassic Entrada Sandstone case study at the Utah–Arizona border. Sedimentology, 65(4), 1301-1321.

Lancaster, N. (1988). Development of linear dunes in the southwestern Kalahari, southern Africa. Journal of arid environments, 14(3), 233-244.

Lancaster, N. (2013). Geomorphology of desert dunes. Routledge.

Larter, R. D., Graham, A. G., Gohl, K., Kuhn, G., Hillenbrand, C. D., Smith, J. A., ... & Schenke, H. W. (2009). Subglacial bedforms reveal complex basal regime in a zone of paleo–ice stream convergence, Amundsen Sea embayment, West Antarctica. Geology, 37(5), 411-414.

Lewington, E. L., Livingstone, S. J., Clark, C. D., Sole, A. J., & Storrar, R. D. (2020). A model for interaction between conduits and surrounding hydraulically connected distributed drainage based on geomorphological evidence from Keewatin, Canada. The Cryosphere, 14(9), 2949-2976.

Lewington, E. L. M. (2020). New insights into subglacial meltwater drainage pathways from the ArcticDEM (Doctoral dissertation, University of Sheffield).

Lundqvist, J. (1969). Problems of the so-called Rogen moraine (pp. 1-32). Svensk reproduktions AB (distr.).

Lundqvist, J. (1981). Moraine morphology: terminological remarks and regional aspects. Geografiska Annaler: Series A, Physical Geography, 63(3-4), 127-138.

Lundqvist, J. (1989). Rogen (ribbed) moraine—identification and possible origin. Sedimentary Geology, 62(2-4), 281-292.

Maclachlan, J. C., & Eyles, C. H. (2013). Quantitative geomorphological analysis of drumlins in the Peterborough drumlin field, Ontario, Canada. Geografiska Annaler: Series A, Physical Geography, 95(2), 125-144.

Markgren, M., & Lassila, M. (1980). Problems of moraine morphology: Rogen moraine and Blattnick moraine. Boreas, 9(4), 271-274.

McConnell, B., and Gatley, S. (2006). Bedrock geological map of Ireland, 1:500,000 scale : derived from the Geological Survey of Ireland 1:100,000 bedrock map series and the Geological Survey of Northern Ireland 1:250,000 Geological map of Northern Ireland. Geological Survey of Ireland.

McKenzie, M. A., Simkins, L. M., Principato, S. M., & Munevar Garcia, S. (2022). Streamlined subglacial bedform sensitivity to bed characteristics across the deglaciated Northern Hemisphere. Earth Surface Processes and Landforms.

Menzies, J. (1979). A review of the literature on the formation and location of drumlins. Earth-Science Reviews, 14(4), 315-359.

Mills, H. H. (1987). Morphometry of drumlins in the northeastern and north-central USA. In Drumlin symposium (pp. 131-147).

Möller, P., & Dowling, T. P. (2015). The importance of thermal boundary transitions on glacial geomorphology; mapping of ribbed/hummocky moraine and streamlined terrain from LiDAR, over Småland, South Sweden. Gff, 137(4), 252-283.

Moellering, H., & Rayner, J. N. (1979). Measurement of shape in geography and cartography. Reports of the Numerical Cartography Laboratory, Ohio State University, NSF Report# SOC77-11318.

Ó Cofaigh, C., Pudsey, C. J., Dowdeswell, J. A., & Morris, P. (2002). Evolution of subglacial bedforms along a paleo-ice stream, Antarctic Peninsula continental shelf. Geophysical Research Letters, 29(8), 41-1.

Porter, C., Morin, P., Howat, I., Noh, M.J., Bates, B., Peterman, K., Keesey, S., Schlenk, M., Gardiner, J., Tomko, K., Willis, M., 2018. Arctic DEM, Harvard DataVerse, vol. 1. Polar Geospatial Center, University of Minnesota, St. Paul, Minnesota, USA.

Rose, J. (1987). "Drumlins as part of a glacier bedform continuum". In Drumlin Symposium, Edited by: Menzies, J. and Rose, J. 103–116. Rotterdam: A.A. Balkema.

Schumm, S. A. (1963). Sinuosity of alluvial rivers on the Great Plains. Geological Society of America Bulletin, 74(9), 1089-1100.

Sergienko, O. V., & Hindmarsh, R. C. (2013). Regular patterns in frictional resistance of ice-stream beds seen by surface data inversion. Science, 342(6162), 1086-1089.

Shaw, J. (1979). Genesis of the Sveg tills and Rogen moraines of central Sweden: a model of basal melt out. Boreas, 8(4), 409-426.

Shaw, J. (1983). Drumlin formation related to inverted melt-water erosional marks. Journal of Glaciology, 29(103), 461-479.

Shaw, J., Faragini, D. M., Kvill, D. R., & Rains, R. B. (2000). The Athabasca fluting field, Alberta, Canada: implications for the formation of large-scale fluting (erosional lineations). Quaternary Science Reviews, 19(10), 959-980.

Shilts, W. W., Cunningham, C. M., & Kaszycki, C. A. (1979). Keewatin Ice Sheet—Re-evaluation of the traditional concept of the Laurentide Ice Sheet. Geology, 7(11), 537-541.

Shilts, W. W., Aylsworth, J. M., Kaszycki, C. A., & Klassen, R. A. (1987). Canadian shield. In Geomorphic Systems of North America (Vol. 2, pp. 119-161). Geological Society of America Boulder, Colorado.

Smalley, I., & Warburton, J. (1994). The shape of drumlins, their distribution in drumlin fields, and the nature of the sub-ice shaping forces. Sedimentary geology, 91(1-4), 241-252.

Smith, A. M., Murray, T., Nicholls, K. W., Makinson, K., Aðalgeirsdóttir, G., Behar, A. E., & Vaughan, D. G. (2007). Rapid erosion, drumlin formation, and changing hydrology beneath an Antarctic ice stream. Geology, 35(2), 127-130.

Smith, M. J., & Wise, S. M. (2007). Problems of bias in mapping linear landforms from satellite imagery. International Journal of Applied Earth Observation and Geoinformation, 9(1), 65-78.

Sommerkorn, J. (2020). Distribution of ribbed moraines and their connection to subglacial water-in the Oppland region of Norway (Master's thesis).

Sookhan, S., Eyles, N., Bukhari, S., & Paulen, R. C. (2021). LiDAR-based quantitative assessment of drumlin to mega-scale glacial lineation continuums and flow of the paleo Seneca-Cayuga paleo-ice stream. Quaternary Science Reviews, 263, 107003.

Sookhan, S., Eyles, N., & Bukhari, S. (2022). Drumlins and mega-scale glacial lineations as a continuum of subglacial shear marks: A LiDAR based morphometric study of streamlined surfaces on the bed of a Canadian paleo-ice stream. Quaternary Science Reviews, 292, 107679.

Stokes, C. R., & Clark, C. D. (1999). Geomorphological criteria for identifying Pleistocene ice streams. Annals of glaciology, 28, 67-74.

Stokes, C. R., & Clark, C. D. (2002). Are long subglacial bedforms indicative of fast ice flow?. Boreas, 31(3), 239-249.

Stokes, C. R., Clark, C. D., & Winsborrow, M. C. M. (2006). Subglacial bedform evidence for a major palaeo-ice stream and its retreat phases in Amundsen Gulf, Canadian Arctic Archipelago. Journal of Quaternary Science: Published for the Quaternary Research Association, 21(4), 399-412.

Stokes, C. R., Lian, O. B., Tulaczyk, S., & Clark, C. D. (2008). Superimposition of ribbed moraines on a palaeo-ice-stream bed: implications for ice stream dynamics and shutdown. Earth Surface Processes and Landforms: The Journal of the British Geomorphological Research Group, 33(4), 593-609.

Stokes, C. R., Spagnolo, M., Clark, C. D., Cofaigh, C. Ó., Lian, O. B., & Dunstone, R. B. (2013). Formation of mega-scale glacial lineations on the Dubawnt Lake Ice Stream bed: 1. size, shape and spacing from a large remote sensing dataset. Quaternary Science Reviews, 77, 190-209.

Stokes, C. R., Margold, M., & Creyts, T. T. (2016). Ribbed bedforms on palaeo-ice stream beds resemble regular patterns of basal shear stress ('traction ribs') inferred from modern ice streams. Journal of Glaciology, 62(234), 696-713.

Storrar, R. D., Stokes, C. R., & Evans, D. J. (2013). A map of large Canadian eskers from Landsat satellite imagery. Journal of maps, 9(3), 456-473.

Stow, D. A., Hernández-Molina, F. J., Llave, E., Sayago-Gil, M., Díaz del Río, V., & Branson, A. (2009). Bedform-velocity matrix: the estimation of bottom current velocity from bedform observations. Geology, 37(4), 327-330.

Synge, F. M., & Stephens, N. (1960). The Quaternary period in Ireland—an assessment, 1960. Irish Geography, 4(2), 121-130.

Van Landeghem, K. J., & Chiverrell, R. C. (2020). Bed erosion during fast ice streaming regulated the retreat dynamics of the Irish Sea Ice Stream. Quaternary Science Reviews, 245, 106526.

Venditti, J. G., Nittrouer, J. A., Allison, M. A., Humphries, R. P., & Church, M. (2019). Supply-limited bedform patterns and scaling downstream of a gravel–sand transition. Sedimentology, 66(6), 2538-2556.

Vérité, J., Ravier, É., Bourgeois, O., Pochat, S., Lelandais, T., Mourgues, R., ... & Atkinson, N. (2021). Formation of ribbed bedforms below shear margins and lobes of palaeo-ice streams. The Cryosphere, 15(6), 2889-2916.

Vérité, J., Ravier, É., Bourgeois, O., Bessin, P., Livingstone, S. J., Clark, C. D., ... & Mourgues, R. (2022). Formation of murtoos by repeated flooding of ribbed bedforms along subglacial meltwater corridors. Geomorphology, 408, 108248.

Wagner, K. (2014). Ribbed moraines and subglacial geomorphological signatures of interior-sector palaeo-ice sheet dynamics.

Wellner, J. S., Lowe, A. L., Shipp, S. S., & Anderson, J. B. (2001). Distribution of glacial geomorphic features on the Antarctic continental shelf and correlation with substrate: implications for ice behavior. Journal of Glaciology, 47(158), 397-411.

Winsborrow, M., Clark, C., & Stokes, C. (2004). Ice streams of the Laurentide ice sheet. Géographie physique et Quaternaire, 58(2-3), 269-280.

Zheng, W., Pritchard, M. E., Willis, M. J., & Stearns, L. A. (2019). The possible transition from glacial surge to ice stream on Vavilov Ice Cap. Geophysical Research Letters, 46(23), 13892-13902.

Zoet, L. K., Rawling III, J. E., Woodard, J. B., Barrette, N., & Mickelson, D. M. (2021). Factors that contribute to the elongation of drumlins beneath the Green Bay Lobe, Laurentide Ice Sheet. Earth Surface Processes and Landforms, 46(13), 2540-2550.

3. Figures supplémentaires

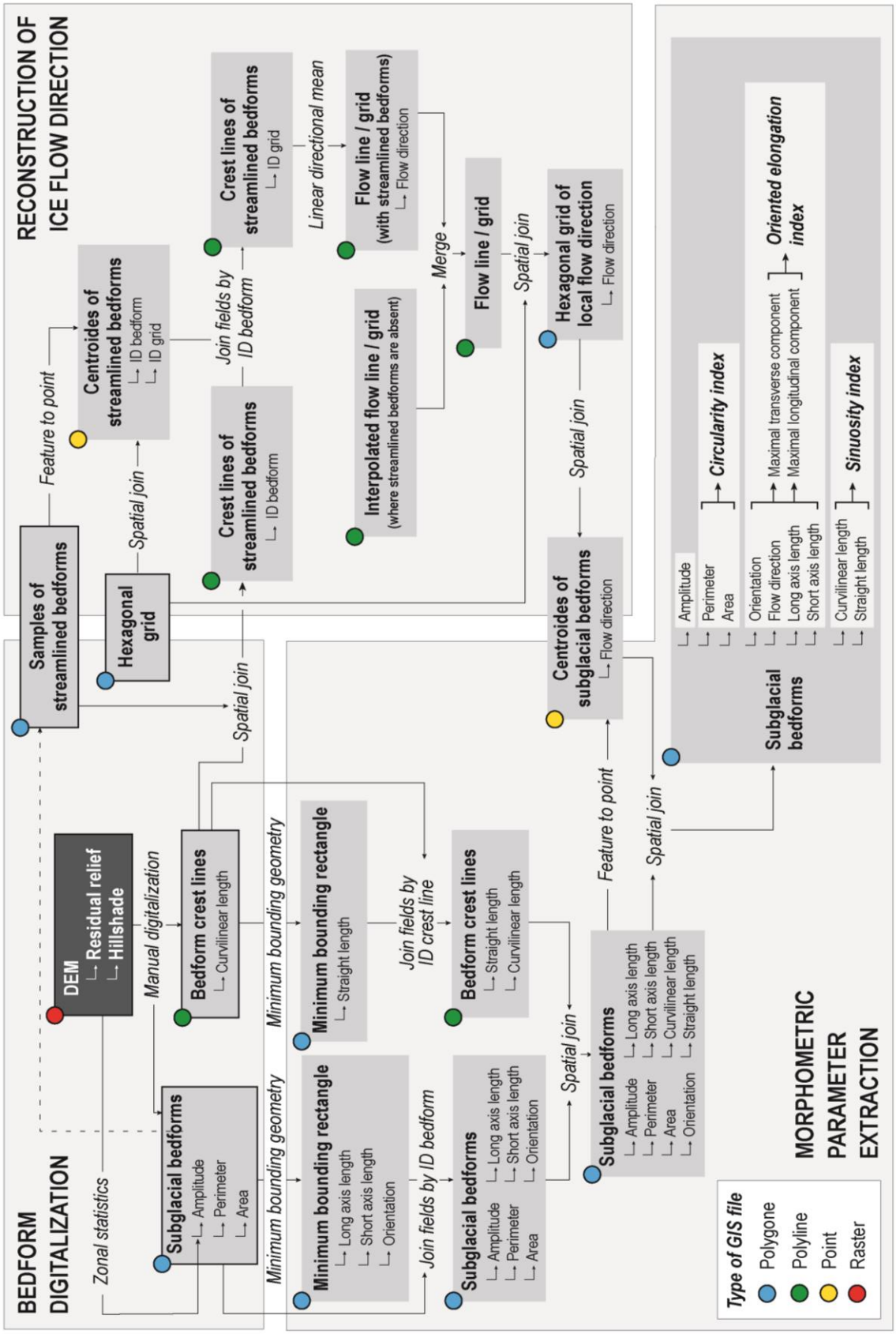

Supplementary Data 1. *Schematic representation of the GIS protocol allowing the reconstruction of ice flow direction and the extraction of morphometric parameters of manually digitized subglacial bedforms from Digital Elevation Models (DEMs).*

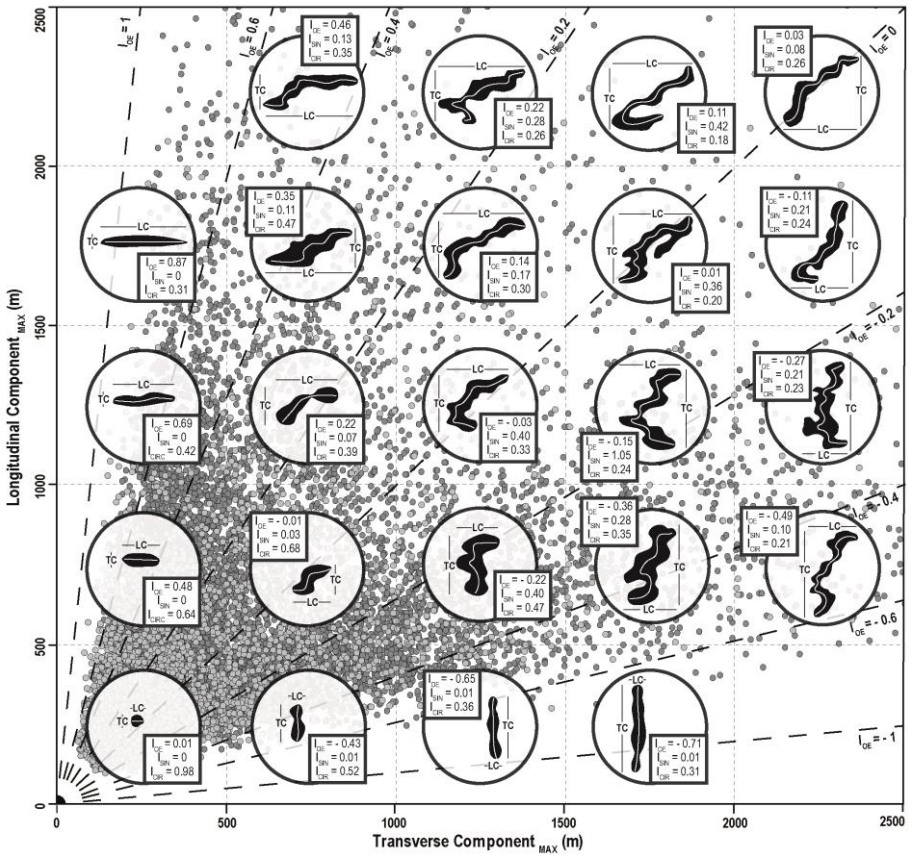

Supplementary Data 2. *Values of morphometric indexes (I_{OE}, I_{SIN} and I_{CIR}) used to characterize bedform shapes, plotted as a function of their maximal transverse and longitudinal components (TC_{MAX}, LC_{MAX}), with selected bedform. Irish and Canadian bedforms are plotted as dark and light grey dots, respectively. The oriented elongation index (I_{OE}, dashed lines) of a bedform is computed as a combination of its maximal transverse (TC_{MAX}) and maximal longitudinal (LC_{MAX}) components: as such, it reflects both its degree of elongation and its orientation relative to ice flow direction. Large subglacial bedforms, for which at least one component exceeds 2500 m, are scarce in the study areas, and therefore not plotted.*

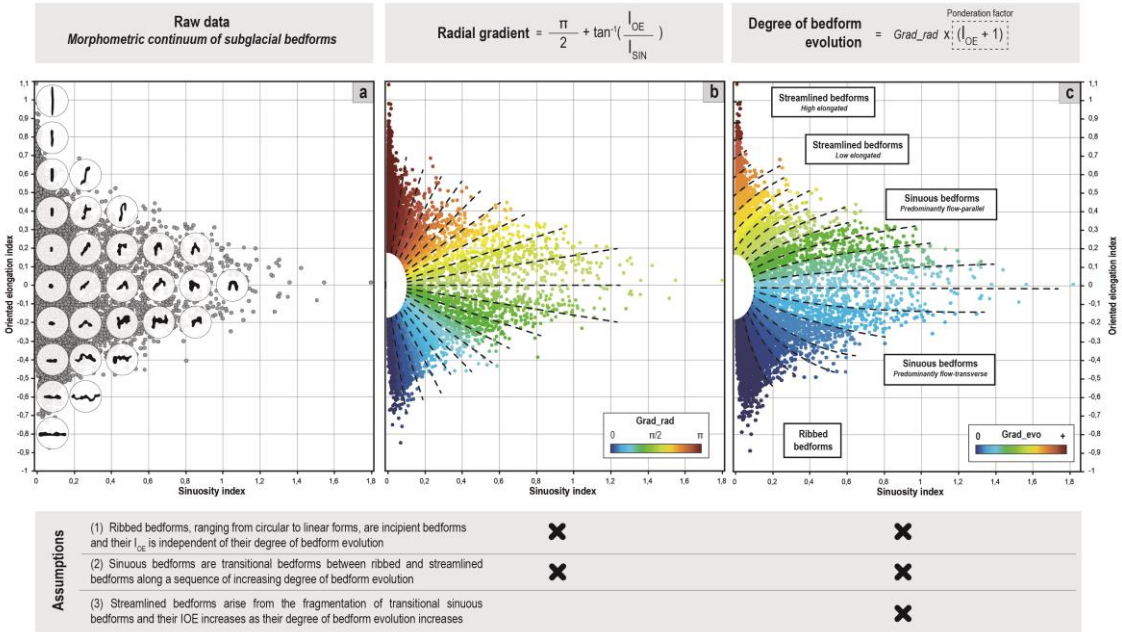

Supplementary Data 3. *Illustrations and equations of the degree of subglacial bedform evolution (i.e. evolution gradient) built from a non-linear relationship between the oriented elongation and the sinuosity indexes in order to fit with the three fundamental assumptions of the morphological sequence.*

Partie C. Un modèle d'évolution des bedforms contrôlé par les interactions glace-eau-sédiments et la déformation enregistrée dans les lits sédimentaires sous-glaciaires

---

Field of crevasse squeeze ridges: the orientations and patterns of which are controlled by the direction of deformation along ice lobe, Eyjabakkajökull, Vatnajökull Ice Sheet, Iceland (2021) (personal photograph).

1. Introduction

Les bedforms sous-glaciaires, de par leur variabilité de forme (i.e. ribbed bedforms, bedforms circulaires, bedforms sinueux, linéations glaciaires), sont des témoins des conditions et des interactions entre la glace, l'eau et les sédiments à la base des calottes glaciaires. Les bedforms sous-glaciaires sont ainsi interprétés comme des marqueurs morphologiques des trajectoires de déplacement de la glace (***Hattestrand & Kleman, 1999; Stokes & Clark, 2002a ; Benediktsson et al., 2016***). Les observations géophysiques et satellitaires sur et sous les calottes glaciaires actuelles permettent localement et ponctuellement d'établir des relations directes entre certains types de bedforms sous-glaciaires et la dynamique d'écoulement de la glace (***King et al., 2009; Larter et al., 2009; Smith et al., 2015***). Cependant, elles ne permettent d'explorer ni l'évolution morphologique des bedforms sous-glaciaires ni les facteurs et processus glaciogéniques contrôlant cette évolution au sein d'un possible continuum morphologique (***Aario, 1977; Stokes et al., 2013; Ely et al., 2016***).

Pour pallier ces lacunes d'observations, les géomorphologues glaciaires étudient les variabilités spatiales des caractéristiques morphologiques des paléo-bedforms sous-glaciaires et leurs relations avec d'autres landforms glaciaires (e.g. reliques de systèmes de drainage, édifices morainiques). Les variabilités spatiales permettent notamment de reconstituer les dynamiques d'écoulement des calottes glaciaires (***Clark et al., 2012; Margold et al., 2015; Benediktsson et al., 2022***). L'observation de séquence d'évolution entre différentes catégories de linéations glaciaires (***Rose, 1987; Ó Cofaigh et al., 2002; Briner, 2007; Greenwood & Clark, 2010; Stokes et al., 2013 ; Sookhan et al., 2021; McKenzie et al., 2022***), ou entre des ribbed bedforms, des bedforms circulaires et des linéations glaciaires (***Aario, 1977; Aylsworth & Shilts, 1989; Knight et al., 1999; Hättestrand & Kleman, 1999; Ely et al., 2016 ; Fannon et al., 2017***) ont permis d'identifier que la dynamique d'écoulement de la glace (i.e. vitesse et durée), la dynamique d'écoulement de l'eau de fonte et les caractéristiques du substrat sous-glaciaire (i.e. lithologie, épaisseur, topographie) étaient de possibles facteurs de contrôle d'un continuum génétique entre les ribbed bedforms, les bedforms circulaires et les linéations glaciaires (**Table 3.3**).

Cependant, des bedforms complexes observés le long des paléo-lits glaciaires mais interprétés comme résultant du remodelage et/ou de la superposition de plusieurs générations de ribbed bedforms et linéations glaciaires ne sont pas inclus dans ces modèles de continuum génétique (***Clark et al., 1993 ;***

Knight et al., 1999; Dunlop & Clark, 2006; Stokes et al., 2006a; Brown et al., 2011). Or, l'analyse des indices d'élongation orientée, de sinuosité et de circularité d'une grande diversité de bedforms sous-glaciaires (Chapitre III – Partie B §2) a démontré l'existence d'un continuum morphologique au sein duquel les bedforms complexes résultent de l'étirement, de la fragmentation et de la réorientation des ribbed bedforms en des linéations glaciaires de plus en plus allongées. La nature et l'évolution du/des processus responsable(s) de ces séquences d'évolution morphologique nouvellement décrites n'ont pas encore été explorées.

Table 3.3. *Synthesis of glaciological controlling factors proposed for the subglacial bedform continuum between ribbed and streamlined bedforms.*

	Shaw, 1983	*Bouchard, 1989*	*Boyce & Eyles, 1991*	*Hart, 1999*	*Hättestrand & Kleman, 1999*	*Wellner et al., 2001*	*O Cofaigh et al., 2002*	*Stokes & Clark, 2002a*	*Briner, 2007*	*Kerr & Eyles, 2007*	*Hess & Briner, 2009*	*Greenwood & Clark, 2010*	*Stokes et al., 2013*	*Barchyn et al., 2016*	*Fannon et al., 2017*	*Franke et al., 2020*	*Lewington et al., 2020*	*Sookhan et al., 2021*	*Zoet et al., 2021*	*McKenzie et al., 2022*
ICE FLOW VELOCITY				●	●			●	●				●					●		
BED LITHOLOGY						●	●					●								●
BED THICKNESS										●				●						
BASAL TOPOGRAPHY		●									●					●				
ICE FLOW DURATION			●												●				●	
MELTWATER FLOW	●																●			

Problématiques :

→ Au sein des séquences d'évolution morphologique nouvellement décrites dans le Chapitre III – Partie B §2, comment les volumes des bedforms sous-glaciaires issus de l'étirement et de la fragmentation des ribbed bedforms nous permettent-ils d'explorer l'origine du/des processus contrôlant leur évolution ?

→ Comment les directions et la quantité de déformation accumulée au sein de la glace permettent-elles d'expliquer la formation de bedforms complexes et le degré d'évolution des bedforms ?

→ Comment la relation entre les caractéristiques morphologiques des bedforms et la quantité de déformation enregistrée dans les lits sédimentaires permet d'explorer les évolutions spatio-temporelles d'interactions glace-eau-sédiments et d'améliorer la qualité des reconstitutions paléoglaciologiques ?

2. Article n°3: Ice-meltwater-bed interactions control directions and quantity of bed deformation and subglacial bedform evolution

Cette troisième partie fait l'objet d'un article qui sera soumis prochainement à *Nature Communications*.

Ice-meltwater-bed interactions control directions and quantity of bed deformation and subglacial bedform evolution

Jean Vérité[1], Édouard Ravier[1], Olivier Bourgeois[2], Paul Bessin[1], Stéphane Pochat[2], Régis Mourgues[1]

[1] Laboratoire de Planétologie et Géosciences, UMR 6112, CNRS, Le Mans Université, Avenue Olivier Messiaen, 72085 Le Mans CEDEX 9, France
[2] Laboratoire de Planétologie et Géosciences, UMR 6112, CNRS, Nantes Université, 2 rue de la Houssinière, BP 92208, 44322 Nantes CEDEX 3, France

Target journal: Nature Communications

Abstract

While they probably represent the most relevant proxies for reconstructing ice-meltwater-bed interactions and ice sheet dynamics, the formation and evolution of subglacial bedforms is nowadays made difficult by the inability to monitor active bedforming processes at high temporal and spatial resolutions. Based on an unprecedented data compilation (~250 000 bedforms) and new morphometric indices we revisit the theory and significance of the subglacial bedform continuum to propose a new model correlating the degree of bedform evolution with the quantity and direction of deformation accommodated by the subglacial bed. We build high-resolution maps of subglacial bed deformation to explore the complex ice-meltwater-bed interactions and unravel the role of ice flow velocity, bed deformability and meltwater routes in bedforming processes. The model and method we propose contribute to perform field-based palaeoglaciological reconstructions with unprecedented resolution.

Introduction

The ubiquitous distribution and the diversity of subglacial bedforms – from ribbed bedforms (i.e. flow-transverse and undulating) ***(Hättestrand & Kleman, 1999; Dunlop & Clark, 2006)*** to streamlined bedforms (i.e. flow-parallel and linear; drumlins and Mega-Scale Glacial Lineations, MSGLs) ***(Rose, 1987; Clark, 1993)*** – along deglaciated terrains must reveal something about the nature and geography of ice-meltwater-bed interactions. Subglacial bedforms are the unique relics of these interactions regulating ice flow dynamics ***(Hess & Briner, 2009; Larter et al., 2009; Benediktsson et al., 2022)***, especially for timescales ***(Menzies, 1989; Clark, 1993; Stokes et al., 2016)*** stretching beyond the yearly

monitoring of modern ice masses (***King et al., 2009; Smith et al., 2015***). Therefore, tracing their morphological evolution and formation mechanisms is a critical challenge to reconstruct the spatial and temporal dynamics of ice sheet over longer timespans (***Stokes et al., 2006, 2008; Greenwood & Clark, 2009; Benediktsson et al., 2022***) and to provide new constraints for ice sheet modelling.

To circumvent the challenging monitoring of active subglacial bedforms below modern ice sheets, glacial geomorphologists investigate the bedforms morphometry along palaeo-ice sheet beds to interpret spatial and/or temporal changes in palaeoglaciological conditions. A bedform continuum between increasingly elongated streamlined bedforms (***Rose, 1987; Ó Cofaigh et al., 2002; Greenwood & Clark, 2010; Sookhan et al., 2021; McKenzie et al., 2022***) or between ribbed, circular and streamlined bedforms (***Aario, 1977; Aylsworth & Shilts, 1989; Knight et al., 1999; Ely et al., 2016***) have commonly been interpreted as a proxy for increasing ice speeds and changing flow trajectories (***Hart, 1999; Hättestrand & Kleman, 1999; Stokes & Clark, 2002a; Briner, 2007; Stokes et al., 2013***) (**Fig. 1a**). Bed properties (***Wellner et al., 2001; Ó Cofaigh et al., 2002; Greenwood & Clark, 2010; McKenzie et al., 2022***), bed thickness (***Kerr & Eyles, 2007; Barchyn et al., 2016***), basal topography (***Bouchard, 1989; Hess & Briner, 2009; Franke et al., 2020***), duration of ice streaming processes (***Boyce & Eyles, 1991; Zoet et al., 2021***) and subglacial meltwater flow (***Shaw, 1983; Lewington et al., 2020; Vérité et al., 2022***) have also been invoked to explain the variability and continuity of subglacial bedform metrics.

Many other subglacial bedforms associated with fields of ribbed and streamlined bedforms (***Carl, 1978; Markgren & Lassila, 1980; Boulton, 1987; Dunlop & Clark, 2006; Sookhan et al., 2021; Vérité et al., 2021***), not perfectly fitting the morphological classes historically defined due to complex shapes and orientations, are not included in most models of subglacial bedform continuum (***Aario, 1977; Stokes et al., 2013; Ely et al., 2016***). Using new morphometric indices and assuming that complex and apparently composite bedforms are not necessarily correlated with more than one ice flow trajectory (***Boulton, 1987; Clark, 1993; Stokes et al., 2006***), a recent work has demonstrated that complex and sinuous bedforms correspond to transitional forms along a subglacial bedform continuum between ribbed and streamlined bedforms (**Fig. 1b**) (***Vérité et al., submitted***). The genetic meaning of this subglacial bedform continuum and the mechanisms driving the continuous bedform evolution are however still poorly-constrained.

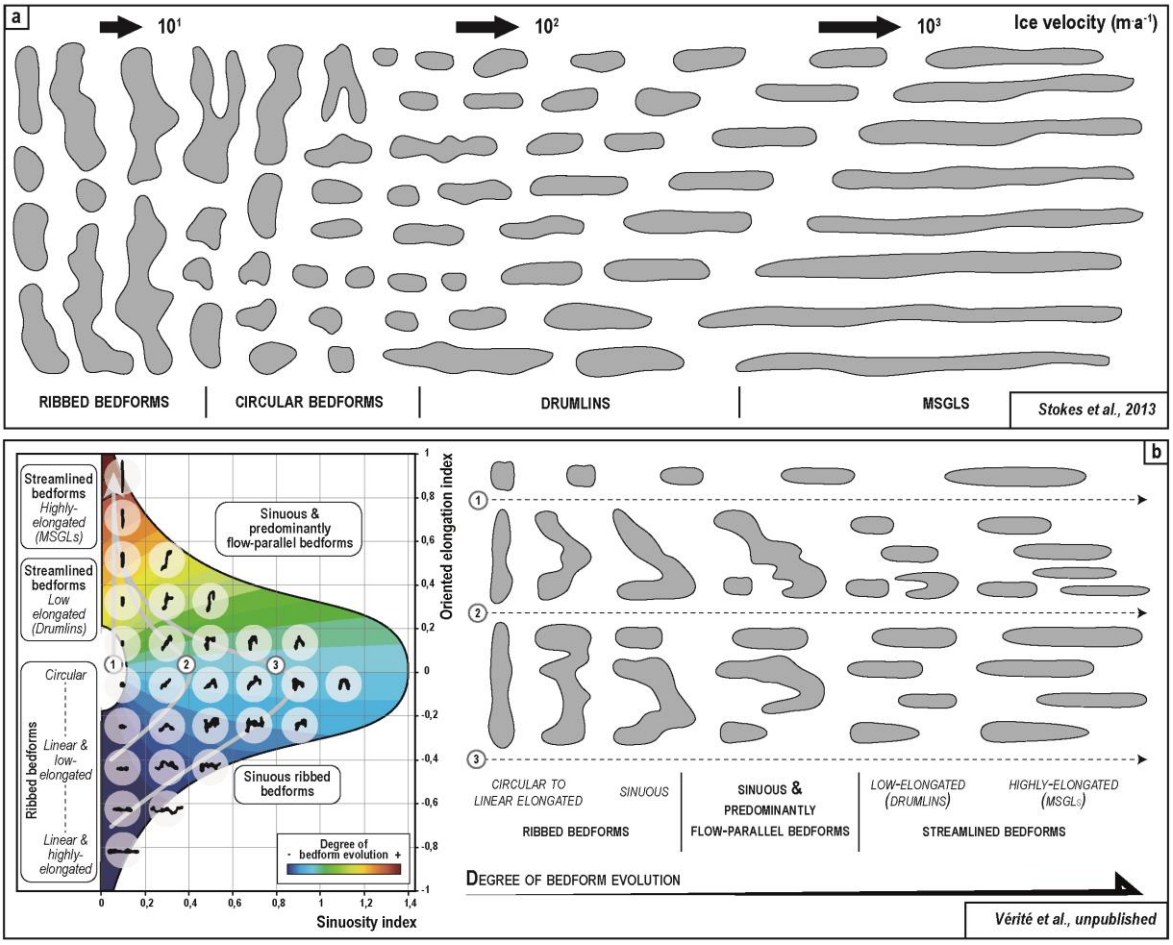

***Figure 1**. (a) Schematic representation of the subglacial bedform evolution from ribbed to streamlined bedforms (i.e. drumlins and MSGLs) reflecting increasing ice flow velocity. This model considers that intermediate circular bedforms result from the fragmentation of ribbed bedforms as they are stretched parallel to the ice flow direction when the ice flow velocity increases (**Aario, 1977; Stokes et al., 2013**). (b) A new model of subglacial bedform evolution between ribbed, transitional bedforms (i.e. sinuous ribbed bedforms and predominantly flow-parallel sinuous bedforms) and streamlined bedforms, through (Vérité et al., submitted). This model is based on the integration of all subglacial bedforms, including those with sinuous shapes and complex orientations, and considers circular bedforms as circular forms of ribbed bedforms. The degree of bedform evolution is represented by a quantitative parameter (i.e. colored scale) function of the crest line sinuosity (I_{SIN}, sinuosity index) and the bedform oriented elongation (I_{OE}, oriented elongation index) making the assumptions that linear ribbed bedforms – whatever their elongation – as incipient bedforms and streamlined bedforms are as evolved as they are elongated. Several examples of evolutionary sequences (i.e. light grey arrow; evolutionary sequences n°1, n°2 and n°3) exist depending on the initial shape and elongation of ribbed bedforms.*

Based on an unprecedented bedform data compilation from literature and unpublished mapping (~250 000 bedforms) we highlight the remarkable evolution of subglacial bedform volumes along a continuum unifying ribbed bedforms, sinuous and complex bedforms and streamlined bedforms. In the lights of numerical and experimental modelling of subglacial bedform formation and surface data inversion in Antarctica, we explore the hypothesis of a unifying genetic continuum, where the degree of bedform evolution is controlled by a gradient of cumulative deformation accommodated by the subglacial bed. This gradient of cumulative deformation reflects different ice-meltwater-bed interactions that will contribute to make a significant step forward into palaeoglaciological reconstructions.

Results

Morphometry of subglacial bedforms

Our dataset (**Table 1**), collected from previous studies (***Supplementary Table 1***) and additional mapping (***Supplementary Table 2***), comprises the largest ever-published compilation in number and morphometric diversity of subglacial bedforms (n = 250 583).

It reveals that sub-circular ribbed bedforms, without any preferential orientation relative to the ice flow direction (average oriented elongation index I_{OE} = 0.01), display on average similar maximal transverse (TC_{MAX}) and longitudinal (LC_{MAX}) components of 300 m, an amplitude of 9.0 m and a volume of 0.8 × 10^6 m^3 (**Table 1a**); while elongated ribbed bedforms, which are defined as periodic and predominantly flow-transverse ridges (I_{OE} < 0), display on average a TC_{MAX} of 800 m, an amplitude of 10.3 m and a volume of 3.1 × 10^6 m^3 (**Table 1b-c**). Depending if they have a linear (sinuosity index I_{SIN} < 0.10; average I_{SIN} = 0.04) or sinuous crest line (I_{SIN} > 0.10; average I_{SIN} = 0.19), elongated ribbed bedforms have a LC_{MAX} respectively 2.5 and 1.5 times than their TC_{MAX}.

Predominantly flow-parallel (I_{OE} > 0; average I_{OE} = 0.20) and sinuous (I_{SIN} > 0.10; mean I_{SIN} = 0.17) bedforms (***Vérité et al., submitted***), whose complexities have not been integrated in previous classifications, have on average slightly lower TC_{MAX} (565 m), amplitudes (9.1 m) and volumes (2.0 × 10^6 m^3), but two times longer LC_{MAX} (706 m) compared with elongated ribbed bedforms (**Table 1d**). The dataset also reveals that drumlins, which are defined as linear (I_{SIN} < 0.10; mean I_{SIN} = 0.01) and low-elongated streamlined bedforms (I_{OE} < 0.60; average I_{OE} = 0.47) (***Ely et al., 2016***), have on average a LC_{MAX} (673 m) three times longer than their TC_{MAX} (224 m). Compared with elongated ribbed bedforms and predominantly flow-parallel sinuous bedforms, drumlins display on average a three to four times smaller TC_{MAX}, intermediate amplitude (7.0 m) and a three times smaller volume (0.9 × 10^6 m^3); while they have similar TC_{MAX} and volumes with circular ribbed bedforms (**Table 1e**). Linear (I_{SIN} < 0.10; mean I_{SIN} = 0.01) and highly-elongated streamlined bedforms (I_{OE} ≥ 0.60), referred to as MSGLs (***Ely et al., 2016***), have on average I_{OE} (0.87) and LC_{MAX} (1207 m) two times superior to drumlins, with a slightly lower TC_{MAX} (160 m). Conversely, the average amplitude of MSGLs (4.4 m) is two times inferior to drumlins and 2.5 times inferior to elongated ribbed bedforms and predominantly flow-parallel sinuous bedforms. The mean volume of MSGLs is similar to those of drumlins and

circular, three to four times inferior to those of elongated ribbed bedforms and two times inferior to those predominantly flow-parallel sinuous bedforms (**Table 1e**).

***Table 1**. Morphometric characteristics (average ± 1 σ) of subglacial bedforms populating the morphological continuum from ribbed bedforms to streamlined bedforms.*

n_{TOTAL} = 250583		Bedform description	TC_{MAX} (m)	LC_{MAX} (m)	I_{OE}	I_{SIN}	Amplitude (m)	Volume ($\times 10^6$ m^3)
Ribbed bedforms (n = 102110)	**(a) Sub-circular** 	Sub-circular bedforms with linear crest lines	292 ± 111 (*n = 7418*)	306 ± 118 (*n = 7418*)	0.02 ± 0.11 (*n = 7418*)	0.01 ± 0.02 (*n = 7418*)	9.0 ± 2.8 (*n = 5042*)	0.8 ± 0.5 (*n = 7418*)
	(b) Elongated & linear 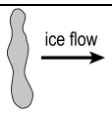	Bedforms elongated transverse to the flow direction with linear crest lines	803 ± 558 (*n = 4358*)	345 ± 210 (*n = 4358*)	-0.35 ± 0.12 (*n = 4358*)	0.04 ± 0.03 (*n = 4358*)	10.3 ± 3.7 (*n = 16553*)	3.1 ± 2.6 (*n = 92333*)
	(c) Elongated & sinuous 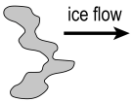	Bedforms elongated predominantly transverse to the flow direction with sinuous crest lines	781 ± 514 (*n = 8772*)	472 ± 283 (*n = 8772*)	-0.20 ± 0.12 (*n = 8772*)	0.19 ± 0.19 (*n = 8772*)		
(d) Predominantly flow-parallel & sinuous bedforms (n = 7116) 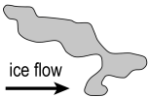		Bedforms elongated predominantly parallel to the flow direction with sinuous crest lines	565 ± 282 (*n = 7116*)	706 ± 467 (*n = 7116*)	0.20 ± 0.12 (*n = 7116*)	0.17 ± 0.22 (*n = 7116*)	9.1 ± 5.3 (*n = 7116*)	2.0 ± 2.2 (*n = 7116*)
Streamlined bedforms (n = 1141357)	**(e) Low-elongated (Drumlins) (n = 86059)** 	Bedforms low-elongated parallel to the flow direction with linear crest lines	224 ± 39 (*n = 61674*)	673 ± 180 (*n = 85884*)	0.46 ± 0.08 (*n = 61674*)	0.01 ± 0.01 (*n = 7534*)	7.0 ± 1.1 (*n = 39853*)	0.9 ± 0.4 (*n = 86059*)
	(f) Highly-elongated (MSGLs) (n = 55298) 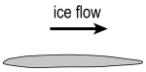	Bedforms highly-elongated parallel to the flow direction with linear crest lines	160 ± 31 (*n = 37804*)	1207 ± 413 (*n = 54985*)	0.87 ± 0.05 (*n = 37804*)	0.01 ± 0.01 (*n = 832*)	4.4 ± 1.3 (*n = 3000*)	0.8 ± 0.5 (*n = 55298*)

250 583 subglacial bedforms are compiled from previous studies (Supplementary Table 1) and 33384 are additional contributions (Supplementary Table 2). The database compiles bedforms from diverse locations, either onshore and offshore (Supplementary Fig. 1). TC_{MAX} and LC_{MAX} are the elongation components of the bedform that are respectively measured transverse and parallel to the ice flow direction. I_{OE} is the oriented elongation index that corresponds to the ratio between LC_{MAX} and TC_{MAX} expressed as a logarithmic function. The sinuosity index of subglacial bedform (I_{SIN}) is calculated using the curvilinear and rectilinear lengths of bedform crest line; theoretical I_{SIN} values range from 0 (i.e. rectilinear crest lines) to +∞ (i.e. highly-sinuous crest lines). Amplitude of subglacial bedforms correspond to their maximal height. Volumes are calculated using metrics compiled on bedforms from the literature (i.e. length, width, amplitude) and this study (i.e. area, amplitude). See Methods summary for more details.

Considering the bedform continuum represented in **Fig. 1b**, morphometric characteristics reveal that subglacial bedforms record progressive increases in LC_{MAX} and I_{OE} as the amplitude decreases during their gradual evolution (**Table 1**). Depending on the initial shape of ribbed bedforms – elongated and linear (high TC_{MAX}) or circular (low TC_{MAX}) – two evolutionary sequences are observed. From elongated ribbed bedforms, first linear then sinuous, to predominantly flow-parallel sinuous bedforms, we notice slightly decreasing TC_{MAX} and volumes – whose magnitude of the decreases correspond

respectively to the TC_{MAX} and the volume of an average streamlined bedform – while the I_{SIN} keeps increasing. The database suggests that streamlined bedforms result from the fragmentation of these increasingly sinuous bedforms (***Knight et al., 1999; Vérité et al., submitted***). Indeed, drumlins display TC_{MAX} and volumes three to four times lower than elongated and sinuous ribbed bedforms and two times lower than predominantly flow-parallel sinuous bedforms. This indicates that initial elongated and linear ribbed bedforms lead to the formation of three to four drumlins on average during their progressive fragmentation and reorientation parallel to the local ice flow direction. Stretching of drumlins leads to MSGLs with increasing LC_{MAX}, decreasing amplitudes but almost constant volumes. This trend also correlates the evolution of an initial circular ribbed bedform into a streamlined bedform, purely by stretching and without fragmentation (***Vérité et al., submitted***), since the database shows increasing LC_{MAX}, decreasing amplitudes and almost constant TC_{MAX} and volumes.

Orientation of subglacial bedforms relative to ice strain axes

Studies suggest that subglacial bedforms are emergent and periodic bumps arising from a subglacial deforming bed in response to the basal shear stress generated by the coupled flow of ice and sediment (***Smalley & Unwin, 1968; Boulton, 1987; Linden et al., 2008; Clark, 2010; Fowler & Chapwanya, 2014; Fannon et al., 2017***). Based on previous works investigating the origin of periodic bedforms and patterns of high basal shear stress along subglacial beds (***Sergienko & Hindmarsh, 2013; Vérité et al., 2021)***, we explore the relationship between bedform morphology, bedforming processes and ice dynamics (*see Methods for details*) (**Fig. 2**). Regular patterns of high basal shear stress, referred to as subglacial high shear stress ribs, have been detected beneath regions of Antarctica exhibiting pronounced flow velocity gradients and high shear strain rates of ice surface (**Fig. 2a**). Although the topography of potentially related bedforms must be too subtle to be detected beneath thick ice, ribbed bedforms exhibiting similar patterns in Canada have been suggested to be the topographic expression of these subglacial shear stress patterns (***Stokes et al., 2016***). Ribbed bedforms with regular wavelengths have been reproduced experimentally right below silicone surface zones characterized by flow velocity gradients and high shear strain rates, implying that such bedforms develop by deformation when ice-related shear is transmitted to the bed (***Vérité et al., 2021)*** (**Fig. 2b**).

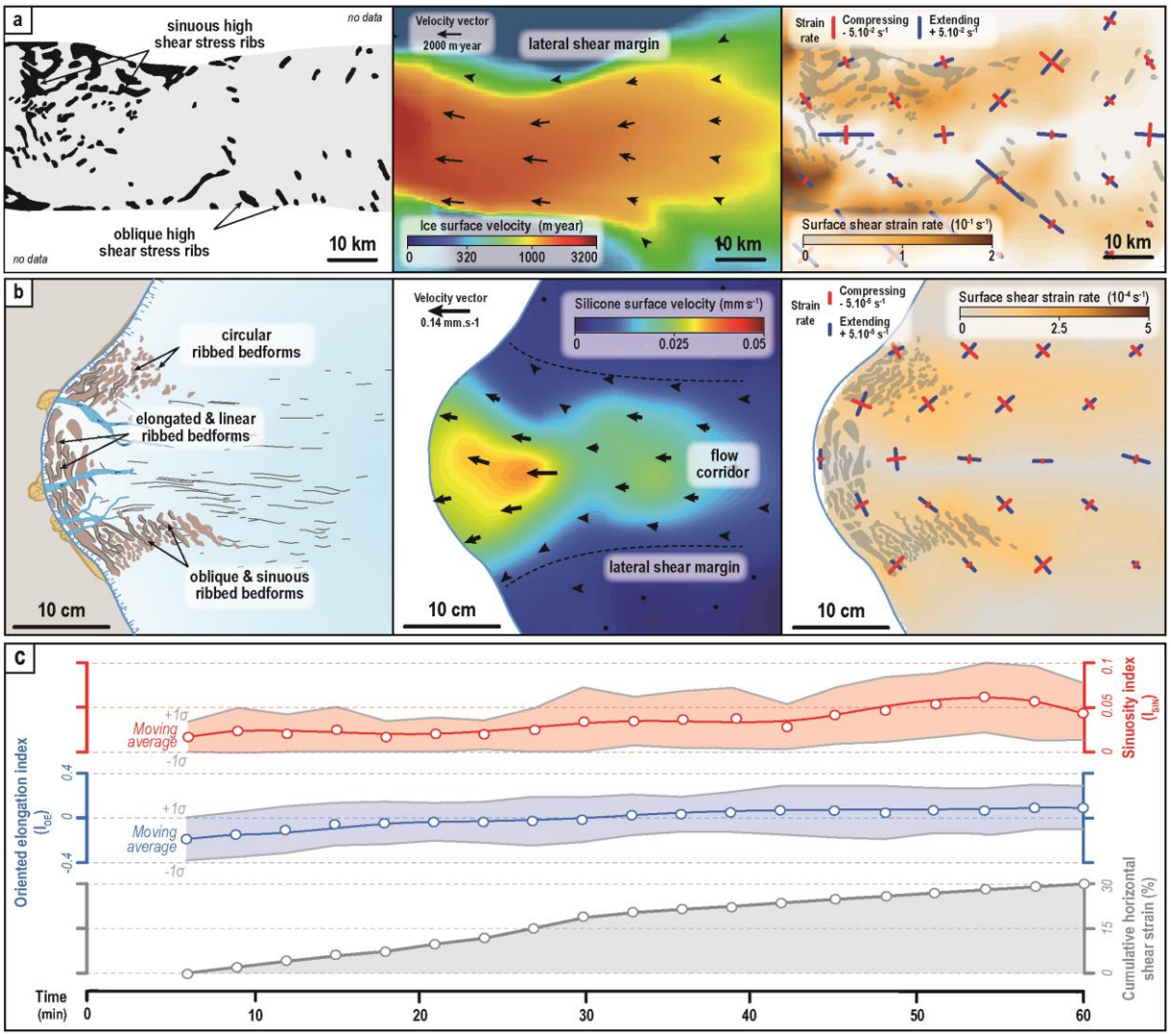

Figure 2. *Maps of periodic deformational features recorded in the bed beneath the (a) Pine Island Glacier (Antarctica) (**Sergienko & Hindmarsh, 2013**) and an (b) experimental silicone glacier (**Vérité et al., 2021**) (i.e. left panel), surface velocity (i.e. central panel) and surface deformation (i.e. right panel). The orientation of natural (i.e. high shear stress ribs) and experimental periodic deformational features (i.e. sub-silicone ribbed bedforms) seems to correlate with the orientation of surficial strain axes rather than the orientation of ice velocity vectors. (c) Morphometric evolution (oriented elongated index I_{OE} and sinuosity index I_{SIN}) of experimental bedforms formed along the coupled silicone-bed interface below shear margins as the cumulative horizontal shear strain of silicone surface increases (**Vérité et al., 2021**).*

We also highlight that the long-axis orientation of high shear stress ribs and experimental ribbed bedforms observed below regions exhibiting flow velocity gradients and high shear strain rates of ice/silicone surface – which are supposedly responsible for lateral gradients of basal shear stress – are mostly oblique to the orientation of flow velocity vectors (**Fig. 1a-b**). This obliquity questions the assumed transverse or parallel relationship between subglacial bedforms and ice flow direction (***Greenwood & Clark, 2009; Stokes et al., 2013; Ely et al., 2016***). Instead, the orientation of experimental bedforms correlates with the orientation of strain axes since their long-axis are mostly parallel to the semi-long axis of the horizontal strain ellipse of ice/silicone surface. Beneath lateral shear

margins of natural and experimental glaciers, ribbed bedforms, high shear stress ribs and semi-long axes of strain ellipses all strike at ~45° to the flow velocity vectors measured in surface, mimicking the orientation and shape of some complex and sinuous subglacial bedforms compiled in this study (**Fig. 1b; Table 1c-d**) (e.g. sinuous ribbed bedforms and predominantly flow-parallel bedforms). Where the semi-short axes are parallel to the velocity vectors and both highlight downstream decreasing velocity and compressive deformation regime, bedforms set perpendicular to the flow direction and display linear forms. In this case, deformational features resemble linear ribbed bedforms characterized by a transverse orientation relative to the flow direction (**Fig. 1b; Table 1b**).

Beneath lateral shear margins of experimental glaciers, a morphometric analysis also demonstrates that ribbed bedforms form initially with flow-transverse orientated (average I_{OE} = -0.2) and linear crest lines (average I_{SIN} = 0.02). As the cumulative horizontal shear strain of silicone surface increases and generates increasing bed deformation along coupled basal interfaces (***Vérité et al., 2021)***, ribbed bedforms are increasingly stretched parallel to the flow direction, giving them an oblique orientation (average I_{OE} = + 0.1), and sinuous (average I_{SIN} = 0.06), evolving into predominantly flow-parallel and sinuous bedforms (**Fig. 2c**).

In summary, natural and experimental data reveal that regions of ice sheets recording flow velocity gradients are characterized by high shear strain rates and strain ellipses with oblique long-axes relative to the ice flow direction. In these regions, the direction and shape of subglacial bedforms mimics the orientation of strain axes rather than flow velocity vectors, while the magnitudes of bedform stretching parallel to the flow direction and bedform sinuosity appear to be controlled by the increase in cumulative ice deformation as it is transmitted to the bed.

Discussion

The remarkable evolution of bedforms shape and orientation along the subglacial bedform continuum (**Table 1**) and the intricate relation between ice deformation and subglacial bedform morphometry (**Fig. 2**) provide a unique opportunity to explore the existence of a common genetic process unifying the wide range of subglacial bedform forms (**Fig. 1b**).

The equicausality hypothesis for subglacial bedform formation

The variability in morphological and sedimentological characteristics as well as the diverse geographical and glaciological frames invoked for subglacial bedforms development have naturally led to multiple bedforming models where erosion, deposition or deformation processes governed by ice (***Boulton, 1987; Boyce & Eyles, 1991; Tulaczyk et al., 2001***), meltwater (***Shaw, 1983***) or a combination of both (***Linden et al., 2008; Fowler & Chapwanya, 2014; Fannon et al., 2017; Vérité et al., 2022***) have been proposed. The hypotheses of bedform formation can be gathered into two different philosophical viewpoints: equifinality and equicausality (***Clark, 2010; Möller & Dowling, 2018; Fowler, 2018***).

Equifinality implies that different sedimentological composition and multiple sedimentary units, respectively interpreted to reflect various bedforming processes and multi-stages bedform growth, can characterize subglacial bedforms with identical shapes. Equifinality has for example contributed to multiply the number of terms given for describing ribbed bedform morphologies (Rogen-type, Åsnen-type and Niemisel-type moraines; ***Markgren & Lassila, 1980; Linden et al., 2008; Möller & Dowling, 2018***) based on the number of associated models. However, different compositions and architecture do not necessarily imply different processes of formation for the three following reasons: (1) the sediment type remolded during bedforming processes does not necessarily influence the final bedform shape (***Boulton, 1987; Stokes et al., 2016***); (2) the bedforming processes may not affect all the sedimentary units since the maximum penetration depth of basal shear stress is much thinner than bedform heights (***Engelhardt, 1998; Dowdeswell et al., 2004***) and (3) instability models generate ribbing instabilities whatever the nature of the sedimentary material (***Fannon et al., 2017; Fowler, 2018***).

Equicausality instead proposes that a single process of formation can be responsible for the development of a variety of subglacial bedform morphologies. The most widely accepted equicausality hypothesis proposes that subglacial bedforms are periodic and self-organized bumps naturally arising from instabilities in the coupled flow of ice and meltwater over a sedimentary bed, resulting in sediment deformation and fluvial transport (***Smalley & Unwin, 1968; Clark, 2010***). This hypothesis has mathematically been conceptualized (***Hindmarsh, 1998; Fowler, 2000; Schoof, 2007***) and numerically demonstrated (***Fowler & Chapwanya, 2014; Fannon et al., 2017***), producing morphological sequences

of bedform depending on timespans or changes in basal conditions (i.e. water film thickness, bed load transport, till diffusion).

A fundamental question is whether the morphological continuum of subglacial bedforms unrevealed from our massive data compilation and a previous study (***Vérité et al., submitted***) could help deciding whether equicausality or equifinality control the formation of subglacial bedforms. We interpret spatial evolutionary sequences between ribbed, transitional sinuous and streamlined bedforms with no jumps in size and shape (***Aario, 1977; Carl, 1978; Markgren & Lassila, 1980; Ely et al., 2016; Vérité et al., submitted***) (**Fig. 1**) as indicative of bedform equicausality reflecting gradual subglacial sediment remobilization and molding arising from subglacial instabilities. Time-transgressive processes related to cross-cutting ice flow directions and/or changing subglacial bed conditions might rework subglacial bedforms through overprinting and superimposition (***Stokes et al., 2008; Ross et al., 2009; Benediktsson et al., 2022***) and create complex morphologies that is not fitting anymore the spatial evolutionary sequence described in **Fig. 1b**. Our data suggest however that transitional bedforms, although complex (i.e., sinuous and variable orientations), are part of a bedform continuum that is governed by the degree of bedform evolution under a single ice flow trajectory.

Subglacial bedform evolution records cumulative bed deformation

Based on (i) this new subglacial bedform database (**Table 1**), (ii) the relationships deciphered between the temporal evolution of subglacial bedform morphometry, strain ellipsoid axes and cumulative deformation in the ice (**Fig. 2**) and (iii) the hypothesis of an equicausality theory driven by bed instabilities, we propose a new unifying model explaining the genetic evolution between ribbed, transitional and streamlined bedforms (***Vérité et al., submitted***). We propose to withdraw from the binary vision considering subglacial bedforms a-priori as either transverse or parallel to the flow direction (***Aario et al., 1977; Stokes et al., 2013; Ely et al., 2016***) to instead consider the degree of subglacial bedform evolution (i.e. orientation and shape) as proxies recording the cumulative bed deformation in response to the subsimple shear (i.e. combination of pure strain and simple shear) generated by the overlying ice flow. In a ductile deforming/flowing material (i.e. soft sedimentary bed) in response to high stresses and at a scale (i.e. macroscopic) at which deformation can be considered as continuous, deformation in three dimensions is described as the change in shape of sphere or ellipsoid

(***Ramsay and Huber, 1987***). Changes in shape and orientation of the ellipsoid describe the strain, and is therefore referred to as strain ellipsoid. Considering the apparent relationship between subglacial bedform morphometry and ice deformation along ice/bed coupling areas, we hypothesize here that the morphological evolution of bedforms reflects the evolution of strain ellipsoids in the subglacial bed (**Fig. 3**).

Whatever their dimensions, an elongated and flow-transverse ribbed bedform ($I_{OE} < 0$) characterized by a linear crest line ($I_{SIN} \sim 0$) is the initial bedform resulting from incipient, linear and transverse subglacial instabilities generated under low cumulative bed deformation (**Fig. 2**) (**Fig. 3a**). This is consistent with studies describing ribbed bedforms as preferentially populating the ice dome and onset area of ice streams, where the low ice flow velocity at the basal interface generates low basal shear stress and low bed deformation (***Aylsworth & Shilts, 1989; Hättestrand & Kleman, 1999; Linden et al., 2008***). Initial ribbed bedforms therefore represent an initial deformable sedimentary volume, materialized by an initial ellipsoid as elongated as ribbed bedform is elongated. As the cumulative deformation related to ice-bed coupling and bed shearing by the overlying ice flow increases, flow-parallel extension and vertical shortening of initial ellipsoids result in plan strain, with neither extension nor shortening along the flow-transverse direction. This is responsible for the stretching (i.e. increasing strain) and migration (i.e. increasing translation) of the initial ribbed bedform in the ice flow direction, as well as a vertical thinning. The initial ribbed bedform thus record a progressive shape transformation materialized by the increases of its maximal longitudinal component (LC_{MAX}) and crestline sinuosity (I_{SIN}), the decrease of its amplitude, while its maximal transverse component (TC_{MAX}) and volume remains constant (**Table 1**; **Fig. 3b**). Typically, the points of maximum elevation of these ribbed bedforms will constitute cores that preferentially focus deformation (***Boulton, 1987; Clark, 2010***) and record the maximum strain and translation rates leading to the development of several major shear planes along sinuous ribbed bedforms.

At this stage, if the quantity of bed deformation increases homogeneously over the bedform, the resulting transitional bedforms are sinuous and remains predominantly transverse to the flow direction, i.e. sinuous ribbed bedforms. Local lateral variations in cumulative bed deformation could however trigger bedform-scale gradient in stretching and/or migration rates. The resulting offsets by active shear

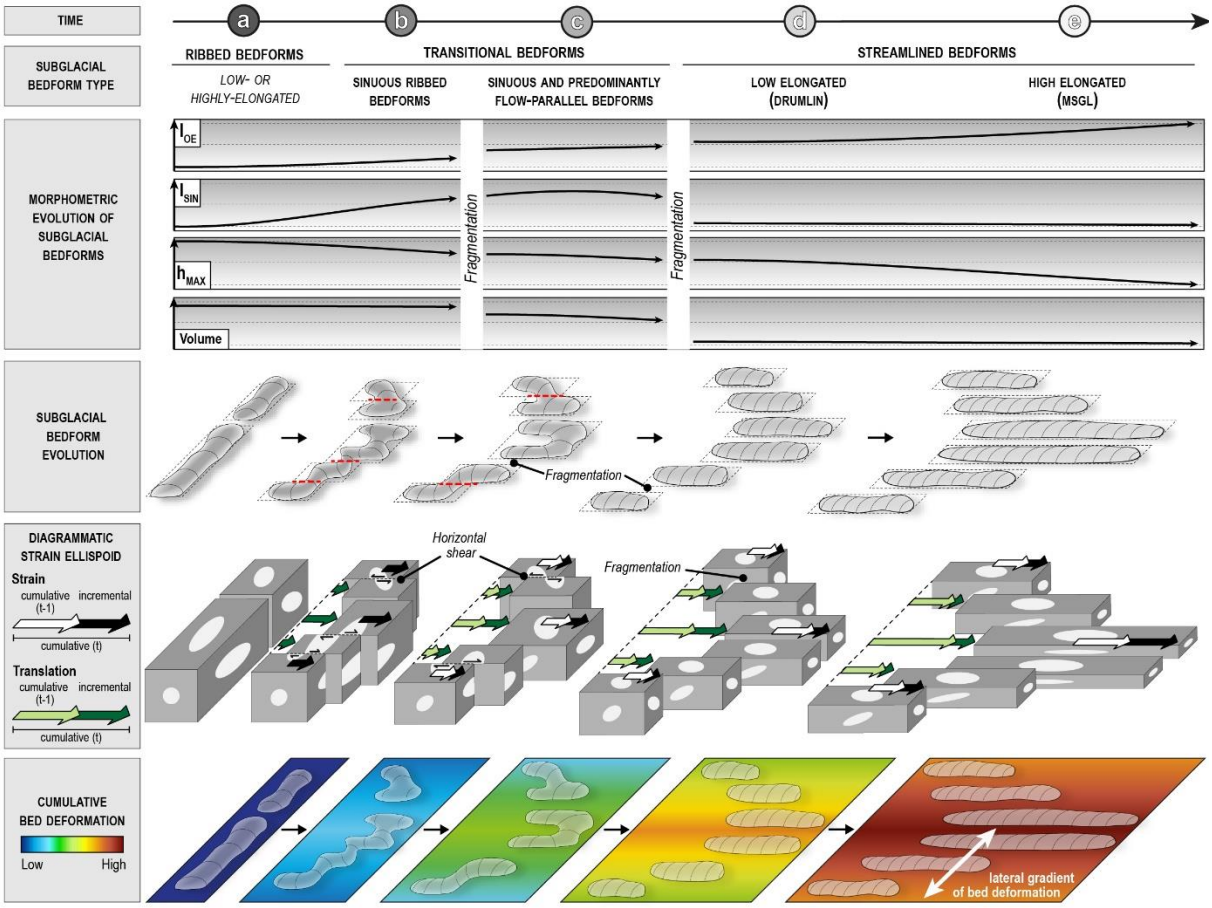

***Figure 3**. Conceptual model for the morphological evolution of subglacial bedforms depending on the cumulative bed deformation, based on the morphometric and spatial continuum observed in our study. Subglacial bedforms progressively evolved between (a) linear ribbed bedforms, (b) sinuous ribbed bedforms, (c) sinuous and predominantly flow-parallel bedforms, and (d-e) increasingly elongated streamlined bedforms (i.e. drumlins, MSGLs). Assuming that the morphological evolution of bedforms reflects the evolution of strain ellipsoids in the subglacial bed in response to subsimple shear (i.e. combination of pure strain and simple shear) generated by the overlying ice flow, bedforms recording lateral gradient of deformation are neither parallel nor transverse to the ice flow direction. This illustrates that the shape and orientation of bedforms is controlled by the basal deformation rather by ice flow velocity/direction. Shear planes (dotted red lines), developing along the bedform as cumulative strain and translation increase, constitute weakness zones favoring bedform fragmentation.*

planes produce oblique transitional bedforms in response to their progressive realignment with the long axis of the rotating strain ellipsoid (**Fig. 3c**). The influence of bed deformation gradients on bedform obliquity is indeed supported by the observation of oblique bedforms and high shear stress ribs below the shear margins of natural (***Sergienko & Hindmarsh, 2013***) and experimental (***Vérité et al., 2021***) ice streams (**Fig. 2**).

As the processes flow-parallel extension and vertical shortening of strain ellipsoid – respectively responsible for bedform stretching and migration and bedform thinning – follows the continuous increases in the cumulative bed deformation, transitional bedforms start fragmenting at their lowest elevations along major shear planes to form individualized low-elongated streamlined bedforms

corresponding to drumlins (**Figs. 3d**). Drumlins often display en-echelon patterns inherited from shear planes development within ribbed to transitional bedforms; this pattern is even more pronounced when fragmentation processes affect oblique transitional bedforms (***Aario, 1977; Carl, 1978; Patterson & Hooke, 1995; Clark et al., 2018***).

When the cumulative deformation accommodated by the bed is maximal, streamlined bedforms become increasingly elongated in the flow direction, reaching the typical dimensions of MSGLs. Estimations of bedform volume indicate that transition from drumlins to MSGLs operate at almost constant volume due to compensation of lengthening by thinning (**Table 1**; **Figs. 3d-e**). This is consistent with studies interpreting streamlined bedforms, from drumlins to MSGLs as typical geomorphological markers of ice corridors characterized by increasingly high flow velocity (***Stokes & Clark, 2002a; Sookhan et al., 2021***), basal shear stress and cumulative bed deformation (***Boulton, 1987; Stokes et al., 2008; King et al., 2009***). During this progressive shape transformation governed by the cumulative bed deformation and its directions (**Fig. 3**), we assume that the concentration of subglacial meltwater flow in between subglacial bedforms – developing lee-side cavities and streams – is a potential side process participating to the shaping and the fragmentation of ribbed bedforms (***Linden et al., 2008; Fannon et al., 2017***) and streamlined bedforms (***Fowler, 2009, 2010, 2018; Fannon et al., 2017***), without causing substantial changes in their volumes.

The missing link between transverse and longitudinal bedforms mainly relies on the hypothesis of subglacial bedform fragmentation during increasing cumulative bed deformation. It is based on the assumption of an overall volume preservation during the evolution of a single linear ribbed bedform into several streamlined bedforms (i.e. three to four). This hypothesis relies on (1) the common spatial association of ribbed bedforms, transitional bedforms and en-echelon streamlined bedforms (***Carl, 1978; Markgren & Lassila, 1980; Vérité et al., submitted***), (2) the incompressible nature of subglacial till at the micro-scale (***Tulaczyk et al., 2001***) and (3) by the joint evolution of both maximal transverse and longitudinal components with bedform amplitudes (**Table 1**). Subglacial till is often considered as a viscous deformable material at the macroscopic scale enabling instability development (***Hindmarsh, 1998***), however it remains non-viscous at the microscopic scale (i.e. intergranular shear planes) implying that bed deformation should not alter the initial volume of sediment contained in bedforms throughout

its evolution (***Fowler, 2018***). Till dilatancy can slightly increase the volume of bedforms (***Smalley and Unwin, 1968***) although we consider this volume change negligible. Considering the averaged volumes of ~250 000 subglacial bedforms, we make the assumption that at each stage of evolution (**Fig. 3**), the cumulative volumes of bedforms resulting from the evolution and fragmentation of an initial ribbed bedform remains constant. We demonstrate that the transformation of linear ribbed bedforms into sinuous ribbed bedforms operates at constant volumes. However, the fragmentation phases of (i) a sinuous ribbed bedform produce on average one predominantly flow-parallel sinuous bedform and one streamlined bedforms, then (ii) predominantly flow-parallel sinuous bedform produce on average two to three streamlined bedforms that will keep elongating (under constant volumes) as cumulative bed deformation increases (**Table 1**). Considering an initial ribbed bedform with a sub-circular, the transformation into streamlined bedform operates at constant volume and maximal transverse component, without fragmentation and sinuous transitional bedforms (**Supplementary Fig. 2**).

Revisited glaciodynamics significance of the subglacial bedform spectrum

Examples of morphological evolutionary sequences associated with a single ice flow configuration have been variously interpreted in the glacial literature as spatial variations in ice flow velocity (***Dyke et al., 1992; Hart et al., 1999; Briner et al., 2007; King et al., 2009; Stokes et al., 2013; Sookhan et al., 2021***), bed properties (***Aylsworth & Shilts, 1989; Wellner et al., 2001; O Cofaigh et al., 2002; Greenwood & Clark, 2010***), meltwater pressure (***Menzies, 1989; Vérité et al., 2022***) or duration of ice streaming (***Boyce & Eyles, 1991***). Instead, we propose a unifying model interpreting the degree of subglacial bedform evolution (**Fig. 1b**) as a proxy for reconstructing the cumulative subglacial bed deformation we intend to connect with the nature and temporality of ice-meltwater-bed interactions.

At the ice sheet scale, large-scale topography, thermo-mechanical feedbacks within ice and basal hydrological variations are the main mechanisms responsible for variations in ice flow velocity and the self-organization of corridors of high ice flow velocity, referred to as ice streams (***Hindmarsh, 2009; Winsborrow et al., 2010***). When ice streams operate, fast-flowing ice corridor generate high basal shear stress and high cumulative bed deformation favorable to the formation of highly-elongated streamlined bedforms (***Aario, 1977; Hart et al., 1999; Briner et al., 2007; Stokes et al., 2013***), whereas lower ice flow velocities upstream or outside the corridors generate lower basal shear stress and less cumulative

bed deformation, favorable to the formation of ribbed bedforms (***Dyke et al., 1992; Hättestrand & Kleman, 1999***). Transitions between low- and high-flow velocities (onset areas and shear margins of ice streams) covers a broad spectrum of cumulative bed deformation and associated bedforms from low (ribbed bedforms), intermediate (transitional bedforms) to high (streamlined bedforms) degree of evolution (**Fig. 4a**). Longitudinal increase in ice velocity gradients from the onset area to the ice stream core is associated with longitudinal gradients of cumulative bed deformation that favors the formation of increasingly elongated bedforms with decreasing amplitudes (***Dyke et al., 1992; King et al., 2007***). On the opposite, lateral velocity gradients across the ice stream margins favor shear deformation regime and lateral gradients in cumulative bed deformation recorded through the rotation of bedforms relative to the local flow direction (oblique transitional bedforms) (**Figs. 2**, **3c**) (***Vérité et al., 2021***).

Variations in bed properties are also susceptible to modify ice-bed interactions and produce geographical variations in cumulative bed deformation. If a deformable subglacial sediment layer at the ice stream bed favors fast ice flow velocity at regional-scale by enhanced basal slipping, local variations in basal conditions associated with altered bed properties (stiffer bed) and subglacial hydrology (low pore water pressure, frozen conditions) or topographic highs may inhibit basal slipping and generate patches of reduced basal shear stress, referred to as sticky spots (***Alley, 1993; Smith et al., 2015***). Such patches produce radial gradient of cumulative bed deformation that is preserved through abrupt and multi-directional transition between ribbed, transitional and streamlined bedforms as we move away from the sticky spot core (**Figs. 4b, 5c**). This is totally consistent with morphological criteria suggested in the literature to identify palaeo-sticky spots such as MSGLs transitioning into shorter drumlins around exposed bedrock (***Clark & Stokes, 2001; Stokes et al., 2007***), deflected ribbed moraines around topographic highs (***Greenwood & Clark, 2009***) (i.e. oblique transitional bedforms) and mosaic of ribbed moraines superimposed on or surrounded by streamlined bedforms (***Dunlop & Clark, 2006; Stokes et al., 2008***) (**Fig. 4b**). The ability of a subglacial sedimentary bed to support pervasive deformation, promote basal slipping and bedforming processes is also strongly dependent on the substratum lithology as it controls the thickness and stiffness of the subglacial sedimentary bed and thus the quantity of deformation it can accumulate (***Aylsworth & Shilts, 1989; Clark & Stokes, 2001; Wellner et al., 2001; Ó Cofaigh et al., 2002***). The formation of MSGLs (high cumulative deformation) is thought to be

promoted where till derived from carbonated bedrock is softer and more deformable while till derived from sandstone and crystalline bedrock is stiffer resulting in the predominance of ribbed bedforms and drumlins (lower cumulative deformation) (***Greenwood & Clark, 2010***).

Setting constant bed properties and ice flow velocities, we can also consider the role of subglacial hydrology in generating gradient of cumulative bed deformation and remarkable transition in bedform morphologies (***Sergienko & Hindmarsh, 2013; Vérité et al., 2022; Livingstone et al., submitted***). Looking at the spatial evolution of bedform morphologies across meltwater corridors, we can establish the relation between bed deformation, meltwater drainage pathways and transition in bedform assemblages. Changes in hydraulic connectivity and water pressure across subglacial meltwater routes, whose central axis is commonly highlighted by eskers (**Fig. 4c**), result in lateral variations in the degree of ice-bed coupling (***Lewington et al., 2020***). Along zone of high hydraulic connectivity where the coupling between the bed and the ice base is considered minimal, cumulative bed deformation is low and the development of ribbed bedforms predominate (**Fig. 4c**). Toward the meltwater route margins ice-bed decoupling is becoming more scattered and intermittent laterally, increasing the cumulative deformation accommodated by the bed and favoring the formation of transitional bedforms. In response to this deformation gradient, shear deformation and bedform rotation generate oblique transitional bedforms at the meltwater corridor margins (***Vérité et al., submitted***). In between meltwater routes, the concentration of streamlined bedforms indicates higher cumulative deformation related to the decrease in hydraulic connectivity and more persistent ice-bed coupling. The decrease of hydraulic connectivity away from the meltwater routes is gradual as the streamlined bedforms become increasingly elongated as the distance to the meltwater corridor axis increases (**Fig. 4c**) (***Vérité et al., submitted; Livingstone et al., submitted***).

Finally, the last factor controlling the cumulative deformation accommodated by the subglacial bed is the duration of the deformation process generated by ice flow and related basal shear stresses (***Boyce & Eyles, 1991; Zoet et al., 2021***). Considering continuous coupling between the ice and a deformable bed, deformation accumulated through time will control the degree of bedform evolution. Ribbed bedforms would develop in response to shorter periods of ice-bed coupling while transitional, drumlins and MSGLs will respectively develop as the duration of coupling will increase. The duration effect on

bedform assemblages is difficult to estimate however as changing glaciological conditions (e.g. ice flow velocity, meltwater pressure, bed characteristics) will conceal the effect of time on bedform evolution. This implies that bedforms with a similar degree of evolution could indeed indicate different duration of coupling as geographical variations in bed deformability and/or ice flow velocity will obscure the temporal primary signal.

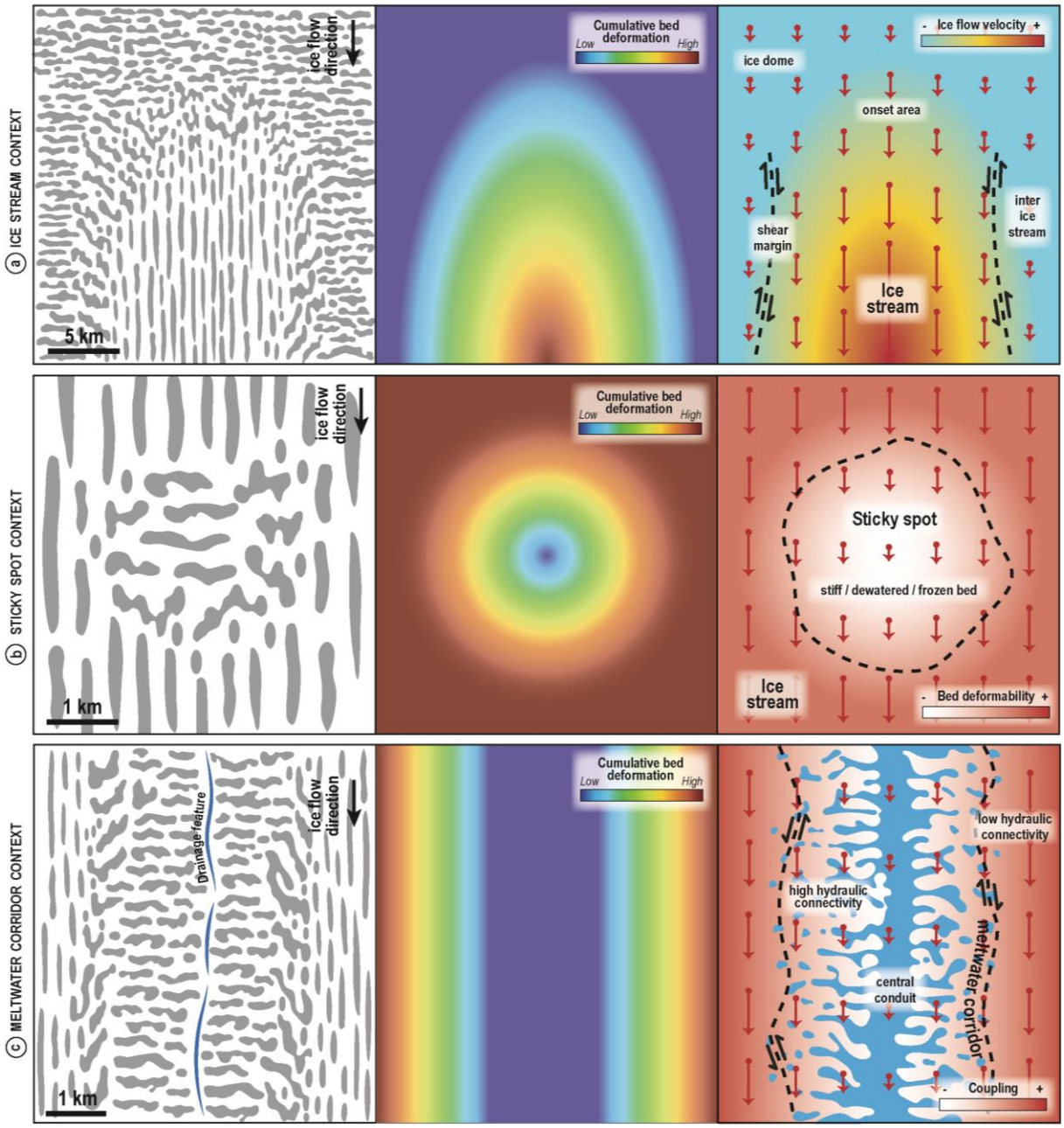

Figure 4. *Conceptual model illustrating the relation between three subglacial bedform assemblages (left panel), the cumulative bed deformation (central panel) and the associated glaciodynamics interpretations (right panel) in three distinct configurations: (a) ice streams, (b) sticky spots and (c) meltwater routes. Note that in the right panel, bed deformation is schematized by elongation rates (red arrows) and shear rates (black arrow).*

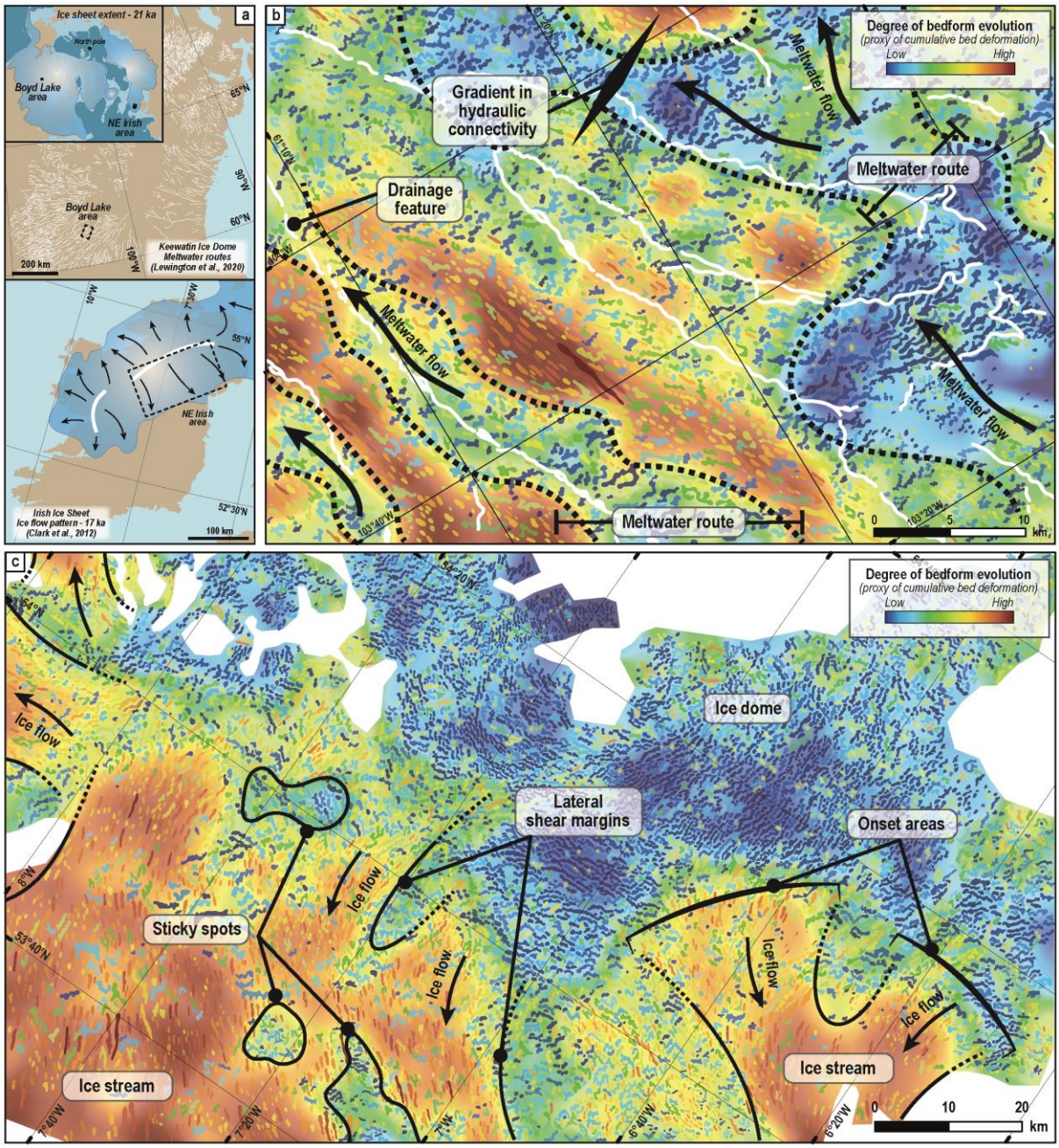

Figure 5. *(a) Location of study areas and associated interpolated maps of degree of bedform evolution along sections of (b) the Keewatin Ice Dome (Boyd Lake, Canada) characterized by meltwater routes (eskers in white lines) (**Lewington et al., 2020**) and (c) the Irish Ice Sheet (NE Ireland) characterized by fast-flowing corridors during its retreat at 17ka BP (supposed ice flow directions in black arrows) (**Clark et al., 2012**). Interpolation maps derives from the degree of bedform evolution are calculated using subglacial bedform metrics (I_{SIN} and I_{OE}) (**Fig. 1b**) (**Vérité et al., submitted**), which is considered as a proxy of a degree of cumulative bed deformation (**Fig. 3**). Spatial variations of the degree of bedform evolution reflect longitudinal and lateral variations in cumulative bed deformation that allow the identification and reconstruction of (b) meltwater routing systems and (c) palaeo-ice streams with unprecedented resolutions.*

Towards high-resolution palaeoglaciological reconstructions

The degree of bedform evolution (***Vérité et al., submitted***) (**Fig. 1b**), which has been shown to reflect the evolution of cumulative bed deformation and mirror ice-meltwater-bed interactions, is a new proxy to perform palaeoglaciological reconstructions with unprecedented accuracy. We therefore

propose that interpolations of the bedform evolution degree, which is function of the oriented elongation (I_{OE}) and sinuosity (I_{SIN}) indices of each subglacial bedform (***Vérité et al., submitted***) (**Fig. 1b**), could provide a unique opportunity to reconstruct spatial variations in subglacial bed deformation along palaeo-ice sheet beds (**Fig. 5**). We performed these interpolations over palaeo-subglacial beds in Canada (**Fig. 5b**) and Ireland (**Fig. 5c**) where thousands of bedforms, whose morphological characteristics spread over the full range of existing subglacial bedform classes ***(Supplementary Table 2)***, display clear and gradual transitions between ribbed and streamlined bedforms.

Interpolated maps reveal the spatial distribution of past glacial features with a remarkable resolution such as (i) ice streams and their upstream and lateral boundaries (i.e. onset area and lateral shear margins), (ii) sticky spots and (iii) subglacial meltwater routes. Interpolation maps notably highlight the typical fan shape of onset areas (***Dyke et al., 1992***) where converging flow sets of low-elongated streamlined bedforms record ice flow trajectories converging toward the ice stream trunk, where cumulative bed deformation and degree of bedform evolution are maximal (***King et al., 2007; Larter et al., 2009***) (**Fig. 5c**). Maps also confirm the existence of numerous sticky spots populated by ribbed and transitional bedforms, corresponding to low-evolved bedforms and low cumulative bed deformation (**Fig. 5c**). Although the downstream portion of ice stream bedform assemblages is not preserved upland in the northeastern part of the Irish Ice Sheet, we do observe that sticky spots occur in the onset area suggesting that heterogeneous slippery bed properties could have conditioned the acceleration of ice towards the ice stream trunk (***Wellner et al., 2001; O Cofaigh et al., 2002***).

Interpolated maps also highlight the lateral transitions in the degree of bedform evolution beneath a selected area of the Keewatin dome where meltwater corridors have been mapped (***Lewington et al., 2020***) allowing the location and dimension of meltwater routes to be refined (**Fig. 5b**). We further suggest that the degree of bedform evolution mirrors the degree of spatial connectivity of the subglacial hydrological system. High connectivity results in more widespread decoupling, lower cumulative bed deformation and a lower degree of bedform evolution (i.e., predominant ribbed bedforms) while progressive decrease in hydrological connectivity away from the main corridor axis will increase the duration of coupling and thus the cumulative bed deformation (i.e., transitional to streamlined bedforms) (**Fig. 5b**).

We report the first morphometric-based model unifying the diversity of subglacial bedforms through a gradient of cumulative bed deformation rather than ice flow velocity. Based on this model, we provide an innovative method for the identification of local, regional and ice-sheet scale variations in ice-meltwater-bed interactions, which enable high-resolution reconstruction of palaeo-ice streams, sticky spots and meltwater routes positions. The large-scale application of this method through modern data mining processes could help reconstructing palaeo-ice sheet dynamics with an unprecedented accuracy and calibrating ice sheet models.

Methods

Morphometric analysis.

A database of 250583 subglacial bedforms was compiled from previous studies (***Supp. Table 1***; n = 217199) and additional mapping (***Supp. Table 2***; n = 33384) from both onshore and offshore locations (***Supp. Fig. 1***).

Subglacial bedforms selected from the literature only concern purely-constructive sedimentary lineations classified as MSGLs and drumlins (i.e. avoiding flutes, rock drumlins, obstacle drumlins, bedrock lineations or crag and tails features) and ribbed bedforms. Mapped areas have been selected from studies dating from the mid-1990s to today to ensure a mapping resolution higher than 30m using digital elevation models (DEMs), aerial and satellite. Finally, we only selected cartographic and morphometric studies whose number and mean metrics of bedforms were available to computed weighted means of their length, width and amplitude. Mean areas were calculated for each bedform categories considering the shape of MSGLs, drumlins and ribbed bedforms can be approximated to the shape of an ellipse.

Regarding subglacial bedforms additionally mapped and analysed in this study, we compiled open-source DEMs from Canada (https://www.pgc.umn.edu/data/arcticdem/) and Ireland (https://land.copernicus.eu/), which are respectively provided at 10-meter and 25-m spatial resolution, in a Geographic Information System software. Hillshade maps and residual relief maps were generated from DEMs and used to manually digitized subglacial bedforms at high resolution (1:10 000) using

break of slope of hillshaded residual relief data. Crest lines of each bedforms were manually delineated and bedform amplitudes were automatically calculated from the maximum crest elevation within each polygons. For each bedform, area, dimensionless morphometric indices (i.e. oriented elongation (I_{OE}) and sinuosity indices (I_{SIN})), maximal transverse (TC_{MAX}) and longitudinal (LC_{MAX}) components were calculated using the protocol we built in an earlier work (***Vérité et al., submitted***). Volumes were estimated using average areas and amplitudes of bedforms from the literature (***Supp. Table 1***) and analyzed in this study (***Supp. Table 2***).

In order to compile morphometric statistics from the literature and this study in a single table, we assume that the length and the width of streamlined bedforms are suitable approximations of their LC_{MAX} and TC_{MAX} respectively by considering that drumlins and MSGLs are strictly defined as rectilinear bedforms parallel to the ice flow direction. Regarding ribbed bedforms, whose examples from the literature have been categorized as such whether they are transverse or predominantly flow-transverse and rectilinear or sinuous, morphometric statistics derived the literature and this study cannot be mutually averaged except for their amplitudes, areas and volumes.

Deriving horizontal strain ellipses.

To produce the maps of horizontal strain ellipses in **Fig. 2**, we extracted u and v component of velocity vectors from the experimental (i.e. silicone sheet) (***Vérité et al., 2021***) and Pine Island Glacier, Antarctica (https://nsidc.org/data/nsidc-0525/). The horizontal deformation of the glacier surface is calculated from using Delaunay Triangulation and classic equations of instantaneous deformation and is quantified by two indicators: (i) the instantaneous strain ellipse illustrating the orientation and the rate of compression/extension of the principal axes, and (ii) the absolute magnitude of the horizontal shear strain rate. Maps of surficial horizontal deformation are compared with periodic deformational patterns observed at the bed of silicone (i.e. experimental ribbed bedforms) (***Vérité et al., 2021***) and ice (i.e. subglacial high shear stress ribs) (***Sergienko & Hindmarsh, 2013***) sheet.

References

Aario, R. Classification and terminology of morainic landforms in Finland. Boreas 6, 87–100 (1977).

Alley, R. B. In search of ice-stream sticky spots. J. Glaciol. 39, 447–454 (1993).

Aylsworth, J. M. & Shilts, W. W. Bedforms of the Keewatin Ice Sheet, Canada. Sediment. Geol. 62, 407–428 (1989).

Barchyn, T. E., Dowling, T. P. F., Stokes, C. R. & Hugenholtz, C. H. Subglacial bed form morphology controlled by ice speed and sediment thickness. Geophys. Res. Lett. 43, 7572–7580 (2016).

Benediktsson, Í. Ö., Aradóttir, N., Ingólfsson, Ó. & Brynjólfsson, S. Cross-cutting palaeo-ice streams in NE-Iceland reveal shifting Iceland Ice Sheet dynamics. Geomorphology 396, 108009 (2022).

Bouchard, M. A. Subglacial landforms and deposits in central and northern Québec, Canada, with emphasis on Rogen moraines. Sediment. Geol. 62, 293–308 (1989).

Boulton, G. S. A theory of drumlin formation by subglacial sediment deformation. Drumlin symposium. Manchester, 1985 25–80 (1987).

Boyce, J. I. & Eyles, N. Drumlins carved by deforming till streams below the Laurentide Ice Sheet. Geology 19, 787–790 (1991).

Briner, J. P. Supporting evidence from the New York drumlin field that elongate subglacial bedforms indicate fast ice flow. Boreas 36, 143–147 (2007).

Carl, J. D. Ribbed moraine-drumlin transition belt, St. Lawrence Valley, New York. Geology 6, 562–566 (1978).

Clark, C. D. Mega-scale glacial lineations and cross-cutting ice-flow landforms. Earth Surf. Process. Landforms 18, 1–29 (1993).

Clark, C. D. & Stokes, C. R. Extent and basal characteristics of the M'Clintock Channel Ice Stream. Quat. Int. 86, 81–101 (2001).

Clark, C. D. Emergent drumlins and their clones: From till dilatancy to flow instabilities. J. Glaciol. 56, 1011–1025 (2010).

Clark, C. D., Hughes, A. L. C., Greenwood, S. L., Jordan, C. & Sejrup, H. P. Pattern and timing of retreat of the last British-Irish Ice Sheet. Quat. Sci. Rev. 44, 112–146 (2012).

Clark, C. D. et al. Spatial organization of drumlins. Earth Surf. Process. Landforms 43, 499–513 (2018).

Dowdeswell, J. A., Ó Cofaigh, C. & Pudsey, C. J. Continental slope morphology and sedimentary processes at the mouth of an Antarctic palaeo-ice stream. Mar. Geol. 204, 203–214 (2004).

Dunlop, P. & Clark, C. D. The morphological characteristics of ribbed moraine. Quat. Sci. Rev. 25, 1668–1691 (2006).

Dyke, A. S., Morris, T. F., Green, D. E. C. & England, J. Quaternary geology of Prince of Wales Island, Arctic Canada. Memoir - Geological Survey of Canada vol. 433 (1992).

Ely, J. C. et al. Do subglacial bedforms comprise a size and shape continuum? Geomorphology 257, 108–119 (2016).Greenwood, S. L. & Clark, C. D. Reconstructing the last Irish Ice Sheet 1: changing flow geometries and ice flow dynamics deciphered from the glacial landform record. Quat. Sci. Rev. 28, 3085–3100 (2009).

Engelhardt, H. Basal sliding of Ice Stream B, West Antarctica. J. Glaciol. 44, 223–230 (1998).

Fannon, J. S., Fowler, A. C. & Moyles, I. R. Numerical simulations of drumlin formation. Proc. R. Soc. A Math. Phys. Eng. Sci. 473, (2017).

Fowler, A. C. An instability mechanism for drumlin formation. Geol. Soc. Spec. Publ. 176, 307–319 (2000).

Fowler, A. C. Instability modelling of drumlin formation incorporating lee-side cavity growth. Proc. R. Soc. A Math. Phys. Eng. Sci. 465, 2681–2702 (2009).

Fowler, A. C. The formation of subglacial streams and mega-scale glacial lineations. Proc. R. Soc. A Math. Phys. Eng. Sci. 466, 3181–3201 (2010).

Fowler, A. C. & Chapwanya, M. An instability theory for the formation of ribbed moraine, drumlins and mega-scale glacial lineations. Proc. R. Soc. A Math. Phys. Eng. Sci. 470, (2014).

Fowler, A. C. The philosopher in the kitchen: the role of mathematical modelling in explaining drumlin formation. Gff 140, 93–105 (2018).

Franke, S. et al. Bed topography and subglacial landforms in the onset region of the Northeast Greenland Ice Stream. Ann. Glaciol. 1–11 (2020)

Greenwood, S. L. & Clark, C. D. The sensitivity of subglacial bedform size and distribution to substrate lithological control. Sediment. Geol. 232, 130–144 (2010).

Hättestrand, C. & Kleman, J. Ribbed moraine formation. Quat. Sci. Rev. 18, 43–61 (1999).

Hart, J. K. Identifying fast ice flow from landform assemblages in the geological record: A discussion. Ann. Glaciol. 28, 59–66 (1999).

Hess, D. P. & Briner, J. P. Geospatial analysis of controls on subglacial bedform morphometry in the New York Drumlin Field - Implications for Laurentide Ice Sheet dynamics. Earth Surf. Process. Landforms 34, 1126–1135 (2009).

Hindmarsh, R. C. A. The stability of a viscous till sheet coupled with ice flow, considered at wavelengths less than the ice thickness. J. Glaciol. 44, 285–292 (1998).

Hindmarsh, R. C. A. Consistent generation of ice-streams via thermo-viscous instabilities modulated by membrane stresses. Geophys. Res. Lett. 36, 1–6 (2009).

Kerr, M. & Eyles, N. Origin of drumlins on the floor of Lake Ontario and in upper New York State. Sediment. Geol. 193, 7–20 (2007).

King, E. C., Woodward, J. & Smith, A. M. Seismic and radar observations of subglacial bed forms beneath the onset zone of Rutford Ice Stream, Antarctica. J. Glaciol. 53, 665–672 (2007).

King, E. C., Hindmarsh, R. C. A. & Stokes, C. R. Formation of mega-scale glacial lineations observed beneath a West Antarctic ice stream. Nat. Geosci. 2, 585–588 (2009).

Knight, J., Mccarron, S. G. & Mccabe, A. M. Landform modification by palaeo-ice streams in east-central Ireland. Ann. Glaciol. 28, 161–167 (1999).

Larter, R. D. et al. Subglacial bedforms reveal complex basal regime in a zone of paleo-ice stream convergence, Amundsen Sea embayment, West Antarctica. Geology 37, 411–414 (2009).

Lewington, E. L. M., Livingstone, S. J., Clark, C. D., Sole, A. J. & Storrar, R. D. A model for interaction between conduits and surrounding hydraulically connected distributed drainage based on geomorphological evidence from Keewatin, Canada. Cryosphere 14, 2949–2976 (2020).

Lindén, M., Möller, P. & Adrielsson, L. Ribbed moraine formed by subglacial folding, thrust stacking and lee-side cavity infill. Boreas 37, 102–131 (2008).

Livingstone, S. J. et al. Diversity of landforms in subglacial meltwater corridors and a potential unifying explanation. Earth Surf. Process. Landforms 1–46.

Markgren, M. & Lassila, M. Problems of moraine morphology: Rogen moraine and Blattnick moraine. Boreas 9, 271–274 (1980).

McKenzie, M. A., Simkins, L. M., Principato, S. M. & Munevar Garcia, S. Streamlined subglacial bedform sensitivity to bed characteristics across the deglaciated Northern Hemisphere. Earth Surf. Process. Landforms 2341–2356 (2022)

Menzies, J. Subglacial hydraulic conditions and their possible impact upon subglacial bed formation. Sediment. Geol. 62, 125–150 (1989).

Möller, P. & Dowling, T. P. F. Equifinality in glacial geomorphology: instability theory examined via ribbed moraine and drumlins in Sweden. Gff 140, 106–135 (2018).

Ó Cofaigh, C., Pudsey, C. J., Dowdeswell, J. A. & Morris, P. Evolution of subglacial bedforms along a paleo-ice stream, Antarctic Peninsula continental shelf. Geophys. Res. Lett. 29, 41-1-41–4 (2002).

Ramsay, J. & Huber, M. The techniques of modern structural geology: Folds and fractures. (1987).

Rose, J. Drumlins as part of a glacier bedform continuum. Drumlin symposium (Balkema, Rotterdam, 1987).

Ross, M., Campbell, J. E., Parent, M. & Adams, R. S. Palaeo-ice streams and the subglacial landscape mosaic of the North American mid-continental prairies. Boreas 38, 421–439 (2009).

Schoof, C. Pressure-dependent viscosity and interfacial instability in coupled ice-sediment flow. J. Fluid Mech. 570, 227–252 (2007).

Patterson, C. & Hooke, R. Physical environlent of drumlin formation. J. Glaciol. 41, (1995).

Sergienko, O. V. & Hindmarsh, R. C. A. Regular Patterns in Frictional Resistance of Ice-Stream Beds Seen by Surface Data Inversion. Science (80-.). 342, 1086–1089 (2013).

Shaw, J. Drumlin formation related to inverted melt-water erosional marks. J. Glaciol. 29, 461–479 (1983).

Smalley, I. J. & Unwin, D. J. The Formation and Shape of Drumlins and their Distribution and Orientation in Drumlin Fields. J. Glaciol. 7, 377–390 (1968).

Smith, E. C., Smith, A. M., White, R. S., Brisbourne, A. M. & Pritchard, H. D. Mapping the ice-bed interface characteristics of Rutford Ice Stream, West Antarctica, using microseismicity. J. Geophys. Res. Earth Surf. 120, 1881–1894 (2015).

Sookhan, S., Eyles, N., Bukhari, S. & Paulen, R. C. LiDAR-based quantitative assessment of drumlin to mega-scale glacial lineation continuums and flow of the paleo Seneca-Cayuga paleo-ice stream. Quat. Sci. Rev. 263, 107003 (2021).

Stokes, C. R. & Clark, C. D. Are long subglacial bedforms indicative of fast ice flow? Boreas 31, 239–249 (2002).

Stokes, C. R., Clark, C. D. & Winsborrow, C. M. Subglacial bedform evidence for a major palaeo-ice stream and its retreat phases in Amundsen Gulf, Canadian Arctic Archipelago. J. Quat. Sci. 21, 399–412 (2006).

Stokes, C. R., Clark, C. D., Lian, O. B. & Tulaczyk, S. Ice stream sticky spots: A review of their identification and influence beneath contemporary and palaeo-ice streams. Earth-Science Rev. 81, 217–249 (2007).

Stokes, C. R., Lian, O. B., Tulaczyk, S. & Clark, C. D. Superimposition of ribbed moraines on a palaeo-ice-stream bed: implications for ice stream dynamics and shutdown. Earth Surf. Process. Landforms 33, 593–609 (2008).

Stokes, C. R. et al. Formation of mega-scale glacial lineations on the Dubawnt Lake Ice Stream bed: 1. size, shape and spacing from a large remote sensing dataset. Quat. Sci. Rev. 77, 190–209 (2013).

Stokes, C. R., Margold, M. & Creyts, T. T. Ribbed bedforms on palaeo-ice stream beds resemble regular patterns of basal shear stress ('traction ribs') inferred from modern ice streams. J. Glaciol. 62, 696–713 (2016).

Tulaczyk, S. Ice sliding over weak, fine-grained tills: Dependence of ice-till interactions on till granulometry. Spec. Pap. Geol. Soc. Am. 159–178 (1999)

Tulaczyk, S. M., Scherer, R. P. & Clark, C. D. A ploughing model for the origin of weak tills beneath ice streams: A qualitative treatment. Quat. Int. 86, 59–70 (2001).

Vérité, J. et al. Formation of ribbed bedforms below shear margins and lobes of palaeo-ice streams. Cryosphere 15, 2889–2916 (2021).

Vérité, J. et al. Formation of murtoos by repeated flooding of ribbed bedforms along subglacial meltwater corridors. Geomorphology 408, 108248 (2022).

Vérité, J., Ravier, É., Bourgeois, O., Bessin, P. & Pochat, S. A new morphometric approach revealing the morphological diversity and evolution of subglacial bedforms. 1–29.

Wellner, J. S., Lowe, A. L., Shipp, S. S. & Anderson, J. B. Distribution of glacial geomorphic features on the Antarctic continental shelf and correlation with substrate: Implications for ice behavior. J. Glaciol. 47, 397–411 (2001).

Winsborrow, M. C. M., Clark, C. D. & Stokes, C. R. What controls the location of ice streams? Earth-Science Rev. 103, 45–59 (2010).

Zoet, L. K., Rawling, J. E., Woodard, J. B., Barrette, N. & Mickelson, D. M. Factors that contribute to the elongation of drumlins beneath the Green Bay Lobe, Laurentide Ice Sheet. Earth Surf. Process. Landforms 46, 2540–2550 (2021).

3. Données et figures supplémentaires

***Supplementary Table 1**. Compilation of subglacial bedforms from the literature with mean values length, width and amplitude (n = 217199). Volumes are estimated considering weighted means of each metrics and average ellipsoidal shape.*

	Ref.	Location	n	Length (m)	Width (m)	Amplitude (m)	Mean I_{OE} (approx.)	Estimated volume (x 10^6 m^3)
Highly-elongated streamlined bedforms (MSGLs) ***(n = 54466)***	1	Antarctica	313			3		
	2	Antarctica	200	982				
	3	Norway	650	2200				
	4	Antarctica; Norway; Canada (*NWT & Alberta*)	3068 *(1929) (1697)*	2750	270	4		
	5	Canada (*Quebec, NWT, Nunavut, Alberta*)	31668	1102	150		0.88	0.63
	6	USA (*Minnesota*)	158	3107	209	8.2		
	7	Canada (*Saskatchewan*)	15192	1040				
	8	USA (*WA, NY, PA*); Canada (*Nunnavut*); Iceland; Norway; Sweden	3217	1269	173			
		Mean (± 1σ)		**1206 (± 415) (approx. LC_{MAX})**	**159 (± 27) (approx. TC_{MAX})**	**4.2 (± 1.2)**		
Low-elongated streamlined bedforms (Drumlins) ***(n = 78525)***	9	Poland	517	138	51	4.2		
	10	N Ireland	1562	420	250			
	11	Denmark	161	1111				
	12	Ireland	24049	678				
	13	Britain	37043	601	209			
	14	Scotland	175			9.3		
	15	Britain	*(25848 from n°13)*			7.1	0.48	0.85
	16	Iceland (*Mulajokull*)	155	206	86	7.7		
	6	USA (*Minnesota*)	5624	728	267	6.7		
	17	Iceland	797	719	185			
	8	USA (*WA, NY, PA*); Canada (*Nunnavut*); Iceland; Norway; Sweden	8442	1147	275			
		Mean (± 1σ)		**687 (± 176) (approx. LC_{MAX})**	**226 (± 34) (approx. TC_{MAX})**	**7.0 (± 0.4)**		
Ribbed bedforms ***(n = 81832)***	18	N Ireland; Canada (*Quebec*); Sweden	800			17		
	19	Canada (*Nunavut*)	733	9512	1474	15		
	20	Britain	1829	920	400			
	21	Canada (*Nunavut*)	45879 *(200)*	652	319	29		
	5	Canada; Ireland; USA (NY); Sweden	18384	701	197			
	22	Canada (*Alberta, Saskatchewan*)	1478 *(85)*	2973	700	15		2.55
	23	Sweden	1286	484	166	9.9		
	24	Iceland (*East*)	241	112	66	6.4		
	25	Iceland (*North East*)	78	157	51	3.6		
	26	Canada (*Alberta, Victoria Island*)	307	3190	919			
	27	Sweden; Finland	2692	229	87			
	28	Russia (*Kola Peninsula*)	8125	1258	397			
		Mean (± 1σ)		**857 (± 918)**	**281 (± 216)**	**13.5 (± 7.0)**		
Circular ribbed bedforms ***(n = 2376)***	5	Ireland	1955	417	409			
	27	Sweden; Finland	232	82	64			
	28	Russia (*Kola Peninsula*)	189	641	493			
		Mean (± 1σ)		**402 (± 121)**	**382 (± 107)**			

***Supplementary Table 2**. Compilation of subglacial bedforms morphometrically mapped and analyzed in this study*

Total bedforms : 33654		**n**	**I_{OE} (±σ)**		**I_{SIN} (±σ)**		**TC_{MAX} (m) (±σ)**		**LC_{MAX} (m) (±σ)**		**Amplitude (m) (±σ)**		**Area ($\times 10^5$ m^2)**		**Volume ($\times 10^6$ m^3)**
Streamlined bedforms - *High elongated (MSGLs)* *(n = 832)*	Northeast Ireland	309	0.67	± 0.07	0.01	± 0.01	335	± 117	1624	± 735	5.1	± 4.7	4.31	± 3.20	1.08
	Canada (Boyd Lake)	83	0.7	± 0.08	0	± 0.01	216	± 91	1146	± 739	2.7	± 2.3	2.01	± 2.25	
	Canada (Poorfish Lake)	440	0.7	± 0.09	0.01	± 0.01	183	± 82	929	± 448	3.1	± 2.8	1.32	± 1.03	
	Mean	**832**	**0.69**	**± 0.08**	**0.01**	**± 0.01**	**244**	**± 124**	**1215**	**± 689**	**3.8**	**± 4.1**	**2.52**	**± 2.64**	
Streamlined bedforms - *Low elongated (Drumlins)* *(n = 7534)*	Northeast Ireland	2570	0.37	± 0.11	0.01	± 0.01	310	± 116	746	± 344	10.2	± 5.8	1.91	± 1.37	0.75
	Canada (Boyd Lake)	857	0.35	± 0.11	0.01	± 0.02	194	± 92	445	± 249	4.8	± 3.5	0.75	± 0.74	
	Canada (Poorfish Lake)	4107	0.36	± 0.11	0.01	± 0.02	173	± 84	407	± 245	5.6	± 3.9	0.61	± 0.64	
	Mean	**7534**	**0.36**	**± 0.11**	**0.01**	**± 0.01**	**218**	**± 117**	**525**	**± 337**	**7.1**	**± 5.1**	**1.05**	**± 1.23**	
Sinuous and predominantly flow-parallel bedforms *(n = 7116)*	Northeast Ireland	1869	0.21	± 0.13	0.22	± 0.25	696	± 314	1146	± 562	13.4	± 5.9	4.74	± 3.09	1.97
	Canada (Boyd Lake)	772	0.19	± 0.11	0.18	± 0.23	466	± 286	716	± 432	6.5	± 3.2	2.04	± 1.82	
	Canada (Poorfish Lake)	4475	0.19	± 0.12	0.18	± 0.21	345	± 199	542	± 323	7.5	± 4.1	1.22	± 1.11	
	Mean	**7116**	**0.2**	**± 0.12**	**0.17**	**± 0.22**	**565**	**± 282**	**706**	**± 467**	**9.1**	**± 5.3**	**2.16**	**± 2.33**	
Sinuous ribbed bedforms *(n = 8772)*	Northeast Ireland	1929	-0.2	± 0.13	0.24	± 0.21	1224	± 595	753	± 312	13.1	± 5.2	5.34	± 3.50	2.30
	Canada (Boyd Lake)	947	-0.19	± 0.11	0.18	± 0.19	801	± 496	501	± 270	6.5	± 2.9	2.46	± 2.06	
	Canada (Poorfish Lake)	5896	-0.21	± 0.12	0.17	± 0.18	632	± 393	374	± 204	7.9	± 3.4	1.45	± 1.29	
	Mean	**8772**	**-0.2**	**± 0.12**	**0.19**	**± 0.19**	**781**	**± 514**	**472**	**± 283**	**9.5**	**± 5.1**	**2.42**	**± 2.61**	
Linear ribbed bedforms *(n = 4358)*	Northeast Ireland	1588	-0.32	± 0.14	0.04	± 0.03	1066	± 634	484	± 233	14.2	± 5.7	3.51	± 2.83	2.03
	Canada (Boyd Lake)	248	-0.34	± 0.11	0.04	± 0.03	821	± 560	349	± 176	7.4	± 3	2.03	± 2.03	
	Canada (Poorfish Lake)	2522	-0.36	± 0.12	0.04	± 0.03	637	± 425	261	± 146	8.4	± 4	1.22	± 1.32	
	Mean	**4358**	**-0.35**	**± 0.12**	**0.04**	**± 0.03**	**803**	**± 558**	**345**	**± 210**	**9.7**	**± 4.8**	**2.09**	**± 2.31**	
Circular ribbed bedforms *(n = 4358)*	Northeast Ireland	1815	0.01	± 0.11	0.01	± 0.02	361	± 116	371	± 121	12.8	± 6.5	1.32	± 0.74	0.65
	Canada (Boyd Lake)	441	0.03	± 0.10	0.01	± 0.02	231	± 83	248	± 83	6.2	± 3.2	0.57	± 0.38	
	Canada (Poorfish Lake)	2786	0.02	± 0.11	0.01	± 0.02	181	± 73	190	± 77	7.0	± 4.1	0.35	± 0.26	
	Mean	**5042**	**0.02**	**± 0.11**	**0.01**	**± 0.02**	**250**	**± 125**	**261**	**± 128**	**9.1**	**± 5.9**	**0.72**	**± 0.67**	

Note that 13428 bedforms in Northeast Ireland and Boyd Lake areas have been mapped by Vérité et al. (in prep.). Mean values of dimensionless morphometric indices (i.e. oriented elongation, I_{OE} and sinuosity indices, I_{SIN}), maximal transverse (TC_{MAX}) and longitudinal components (LC_{MAX}), amplitude and area are presented with their standard deviation. Volumes of each bedforms categories were estimated considering mean areas and amplitude.

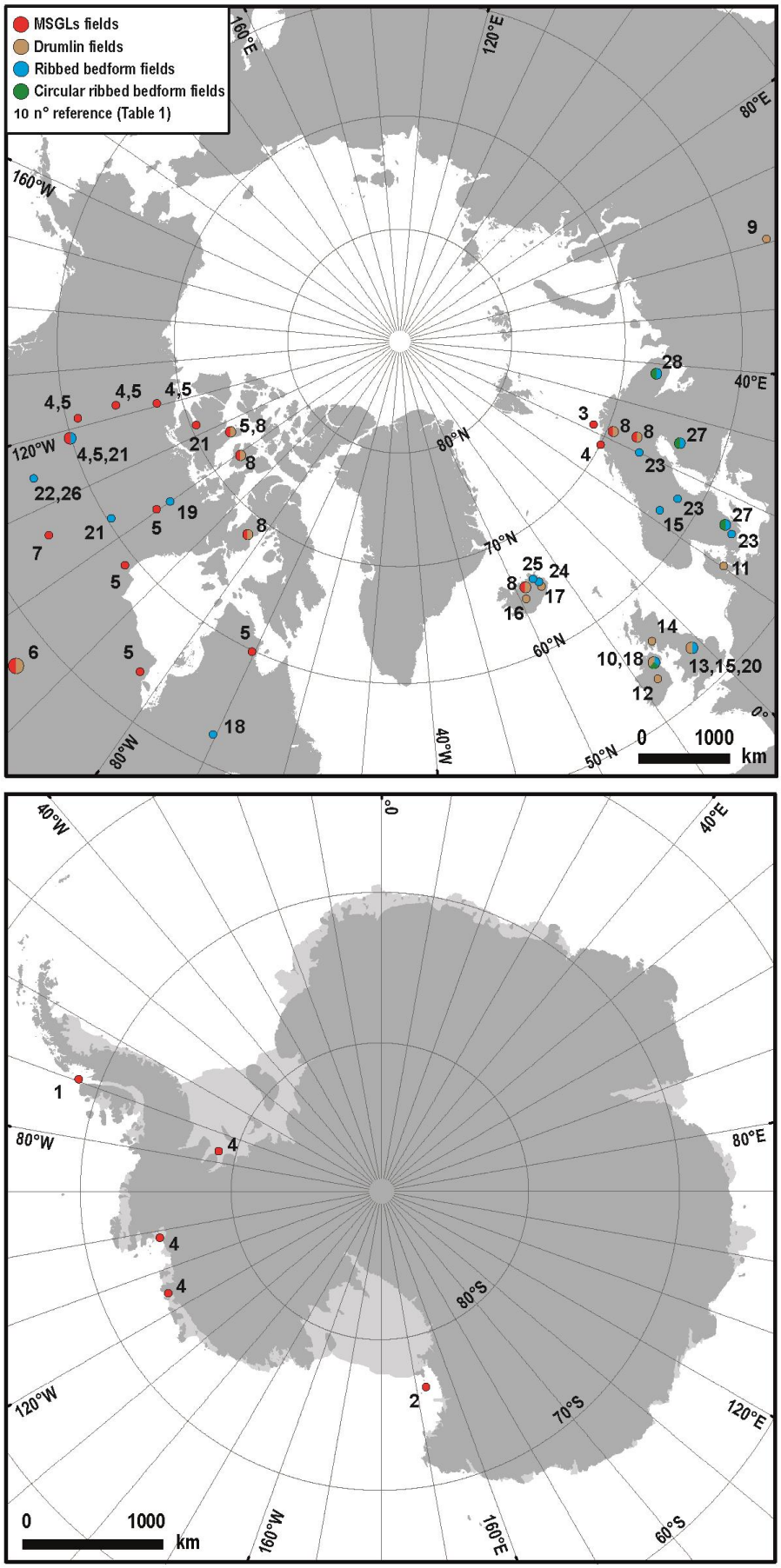

***Supplementary Figure 1**. Location of subglacial bedforms compiled in Supplementary Table 1.*

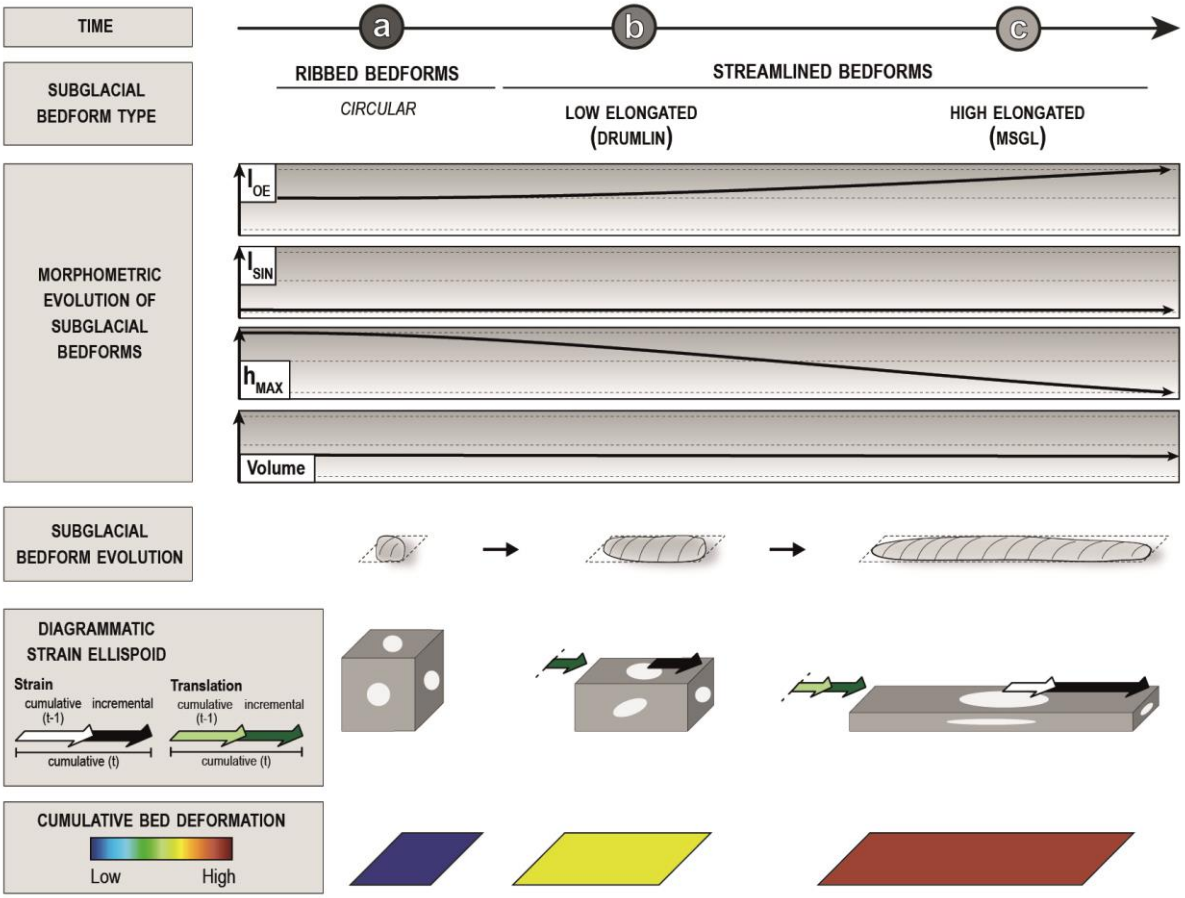

Supplementary Figure 2. *Conceptual model for the morphological evolution of a circular ribbed bedforms depending on the cumulative bed deformation, based on the morphometric and spatial continuum observed in our study. This model is built assuming that the morphological evolution of bedforms reflects the evolution of strain ellipsoids in the subglacial bed in response to subsimple shear (i.e. combination of pure strain and simple shear) generated by the overlying ice flow.*

Supplementary references

1. Ó Cofaigh, C. et al. Flow dynamics and till genesis associated with a marine-based Antarctic palaeo-ice stream. Quaternary Science Reviews vol. 24 (2005).

2. Greenwood, S. L., Gyllencreutz, R., Jakobsson, M. & Anderson, J. B. Ice-flow switching and East/West Antarctic Ice Sheet roles in glaciation of the western Ross Sea. Bull. Geol. Soc. Am. 124, 1736–1749 (2012).

3. Winsborrow, M. C. M., Stokes, C. R. & Andreassen, K. Ice-stream flow switching during deglaciation of the southwestern Barents Sea. Bull. Geol. Soc. Am. 124, 275–290 (2012).

4. Spagnolo, M. et al. Size, shape and spatial arrangement of mega-scale glacial lineations from a large and diverse dataset. Earth Surf. Process. Landforms 39, 1432–1448 (2014).

5. Ely, J. C. et al. Do subglacial bedforms comprise a size and shape continuum? Geomorphology 257, 108–119 (2016).

6. Sookhan, S., Eyles, N., & Putkinen, N. LiDAR-based volume assessment of the origin of the Wadena drumlin field, Minnesota, USA. Sedimentary Geology, 338, 72-83. (2016).

7. Norris, S. L., Margold, M. & Froese, D. G. Glacial landforms of northwest saskatchewan. J. Maps 13, 600–607 (2017).

8. McKenzie, M. A., Simkins, L. M., Principato, S. M., & Munevar Garcia, S. Streamlined subglacial bedform sensitivity to bed characteristics across the deglaciated Northern Hemisphere. Earth Surface Processes and Landforms (2022).

9. Wysota, W. Morphology, internal composition and origin of drumlins in the southeastern part of the Chelmno-Dobrzyń Lakeland, North Poland. Sediment. Geol. 91, 345–364 (1994).

10. Knight, J. Morphological and morphometric analyses of drumlin bedforms in the Omagh Basin, north central Ireland. Geogr. Ann. Ser. A Phys. Geogr. 79, 255–266 (1997).

11. Jørgensen, F. & Piotrowski, J. Signature of the Baltic Ice Stream on Funen Island, Denmark during the Weichselian glaciation. Boreas 32, 242–255 (2003).

12. Greenwood, S. L. & Clark, C. D. Subglacial bedforms of the Irish ice sheet. J. Maps 4, 332–357 (2008).

13. Clark, C. D., Hughes, A. L. C., Greenwood, S. L., Spagnolo, M. & Ng, F. S. L. Size and shape characteristics of drumlins, derived from a large sample, and associated scaling laws. Quat. Sci. Rev. 28, 677–692 (2009).

14. Smith, M. J., Rose, J. & Gousie, M. B. The Cookie Cutter: A method for obtaining a quantitative 3D description of glacial bedforms. Geomorphology 108, 209–218 (2009).

15. Spagnolo, M., Clark, C. D. & Hughes, A. L. C. Drumlin relief. Geomorphology 153–154, 179–191 (2012).

16. Benediktsson, Í. Ö. et al. Progressive formation of modern drumlins at Múlajökull, Iceland: stratigraphical and morphological evidence. Boreas 45, 567–583 (2016).

17. Benediktsson, Í. Ö., Aradóttir, N., Ingólfsson, Ó., & Brynjólfsson, S. Cross-cutting palaeo-ice streams in NE-Iceland reveal shifting Iceland Ice Sheet dynamics. Geomorphology, 396, 108009 (2022).

18. Dunlop, P. & Clark, C. D. The morphological characteristics of ribbed moraine. Quat. Sci. Rev. 25, 1668–1691 (2006).

19. Greenwood, S. L., & Kleman, J. Glacial landforms of extreme size in the Keewatin sector of the Laurentide Ice Sheet. Quaternary Science Reviews, 29(15-16), 1894-1910 (2010).

20. Hughes, A. L. C., Clark, C. D. & Jordan, C. J. Subglacial bedforms of the last British Ice sheet. J. Maps 6, 543–563 (2010).

21. Wagner, K. Ribbed moraines and subglacial geomorphological signatures of interior-sector palaeo-ice sheet dynamics. (2014).

22. Stokes, C. R., Margold, M. & Creyts, T. T. Ribbed bedforms on palaeo-ice stream beds resemble regular patterns of basal shear stress ('traction ribs') inferred from modern ice streams. J. Glaciol. 62, 696–713 (2016).

23. Möller, P. & Dowling, T. P. F. Equifinality in glacial geomorphology: instability theory examined via ribbed moraine and drumlins in Sweden. Gff 140, 106–135 (2018).

24. Helgadóttir, E. G. Ribbed moraines in the Vopnafjörður region, Iceland. (Master degree dissertation) (2020).

25. Benjamínsdóttir, M. M. Ribbed moraine ridges in Bakkaflói, NE Iceland – morphometry, sedimentology and formation (Master degree dissertation) (2021).

26. Vérité, J. et al. Formation of ribbed bedforms below shear margins and lobes of palaeo-ice streams. Cryosphere 15, 2889–2916 (2021).

27. Vérité, J. et al. Formation of murtoos by repeated flooding of ribbed bedforms along subglacial meltwater corridors. Geomorphology 408 (2022).

28. Boyes, B. M., Pearce, D. M., & Linch, L. D. Glacial geomorphology of the Kola Peninsula and Russian Lapland. Journal of Maps, 17(2), 497-515 (2021).

Synthèse des principaux résultats

Partie A. Processus de formation des ribbed bedforms : marqueurs de la dynamique d'écoulement et de déformation de la glace au sein des fleuves de glace

→ ***La grande variabilité morphologique des ribbed bedforms implique-t-elle nécessairement plusieurs processus de formation ? Quel(s) est (sont) ce(s) processus ?***

Les expériences de modélisation analogique ont démontré que des ribbed bedforms de formes et d'orientation diverses peuvent se former par un unique processus gouverné par la déformation d'un lit sédimentaire accommodant les contraintes cisaillantes basales ('*basal shear stress*' ; τ_b) générées par l'écoulement de la glace.

→ ***Quelle est l'origine la diversité morphologique des ribbed bedforms ? Des ribbed bedforms peuvent-ils être obliques à la direction de déplacement de la glace ?***

Les ribbed bedforms sont des bedforms sous-glaciaires compressifs perpendiculaires aux axes de raccourcissement des ellipses de déformation à la surface de la glace. En considérant que ces axes de déformation sont les mêmes à la base de la base et sont transmis au lit sédimentaire par couplage, l'orientation des ribbed bedforms est ainsi contrôlée par les directions de déformation au sein du lit sédimentaire et n'est donc pas nécessairement transverse (~80-90°) à la direction de déplacement de la glace. Les ribbed bedforms peuvent être perpendiculaires à la direction de déplacement de la glace lorsque la glace enregistre des contraintes longitudinales compressives ('*compressive longitudinal stress*' ; $\Delta\sigma_{com}$), comme par exemple sous les lobes frontaux des courants de glace ; ils peuvent aussi être obliques (< 80°) lorsque la glace enregistre des contraintes de cisaillantes latérales ('*lateral shear stress'* ; τ_l), comme le long des marges de cisaillement des fleuves de glace.

Des bedforms sous-glaciaires obliques par rapport à la direction de déplacement de la glace – morphologiquement similaires aux '*drumlinized ribbed bedforms*' (***Carl, 1978 ; Dunlop & Clark, 2006***), '*transverse/asymetrical drumlins*' (***Shaw, 1983 ; Knight, 1997***) ou '*extensional ribbed bedforms*' (***Wagner, 2014***) – ne résultent donc pas nécessairement de plusieurs phases ou directions d'écoulement.

→ ***Par quoi est contrainte l'évolution morphologique des ribbed bedforms ?***

L'évolution morphologique des ribbed bedforms est dépendante de la quantité de déformation cumulée enregistrée par le till et transmise par couplage depuis la glace. Cette évolution morphologique est notamment contrôlée par des gradients de déformation cumulée générés par des contraintes cisaillantes latérales ou des contraintes longitudinales compressives.

→ ***Quelle est la distribution spatiale des ribbed bedforms sous les fleuves de glace ? Quelles sont les caractéristiques des systèmes de drainage associés à ces environnements sous-glaciaires ?***

Les ribbed bedforms peuvent être des marqueurs morphologiques des déformations à l'interface glace-sédiments générés par des contraintes cisaillantes latérales ou des contraintes longitudinales compressives, caractérisant typiquement les marges latérales cisaillantes des fleuves de glace ou les marges lobées des fleuves de glace.

L'observation de ribbed bedforms le long de paléo-marges de lobes glaciaires (e.g. associées à des ceintures morainiques) permet de de discuter la nature du réseau hydrologique sous-glaciaire. En effet, le développement d'un système de drainage chenalisé efficace favorise un couplage généralisé, des faibles vitesses d'écoulement de la glace et la formation de ribbed bedforms. Des lobes sous lesquels se développent des systèmes de drainage faiblement efficaces favorisent quant à eux un découplage généralisé et des vitesses d'écoulement de glace élevées mais sont en revanche défavorables à la formation de ribbed bedforms.

Partie B. Un nouveau modèle de continuum morphologique révélé par la diversité morphométrique des bedforms sous-glaciaires

→ ***Les nouveaux critères morphométriques développés durant cette thèse permettent-ils de caractériser la diversité de formes des bedforms sous-glaciaires (i.e. ribbed bedforms, bedforms circulaires, linéations glaciaires et bedforms complexes) ?***

La nouvelle approche de caractérisation morphométrique d'un bedform – prenant en compte les degrés de circularité de son contour ('circularity index' I_{CIR}), de sinuosité de sa ligne de crête ('sinuosity index' I_{SIN}) et le rapport de ses composantes d'allongement parallèle et transverse à la direction de

déplacement de la glace ('oriented elongation index' I_{OE}) – permet de caractériser l'intégralité de la diversité morphologique des bedforms sous-glaciaires, notamment des bedforms complexes.

→ Les bedforms complexes résultent-ils nécessairement de plusieurs phases d'écoulement de la glace ? Existe-t-il un continuum morphologique plus large qu'initialement décrit incluant également les bedforms complexes ? Par quels critères morphométriques ce continuum est-il contraint ?

Les bedforms sous-glaciaires sinueux (i.e. complexes) – d'orientation ni purement transverse ni purement parallèle à la direction d'écoulement de la glace – ne résultent pas nécessairement de plusieurs phases d'écoulement de la glace et peuvent se former sous la même configuration d'écoulement que des linéations glaciaires ou des ribbed bedforms transverses.

L'observation d'une continuité morphométrique et spatiale entre les différents types de bedforms sous-glaciaires révèle un continuum morphologique entre (i) des ribbed bedforms de forme circulaire à transverse, (ii) des bedforms sinueux (i.e. complexes) et (iii) des linéations glaciaires de plus en plus allongées (i.e. drumlins puis MSGLs). Au sein de ce continuum, les bedforms sinueux sont interprétés comme des bedforms de transition enregistrant le changement d'orientation et l'étirement parallèle à la direction de déplacement de la glace le long d'une séquence d'évolution entre des ribbed bedforms transverses et des linéations glaciaires.

Considérant la séquence d'évolution des bedforms sous-glaciaire interprétée, le « degré d'évolution d'un bedform » peut être défini par un paramètre quantitatif dérivé directement de ses caractéristiques morphologiques : l'indice d'élongation orientée I_{OE} et l'indice de sinuosité I_{SIN}. L'observation de séquences d'évolution de bedforms sous-glaciaires au sein de différents contextes paléoglaciologiques (i.e. fleuves de glace, routes de drainage de l'eau de fonte) suggère par ailleurs que l'étude des variations spatiales du degré d'évolution des bedforms sous-glaciaires pourrait permettre d'explorer les facteurs contrôlant la formation et l'évolution morphologique des bedforms dans les environnements sous-glaciaires.

Partie C. Un modèle d'évolution des bedforms contrôlé par les interactions glace-eau-sédiments et la déformation enregistrée dans les lits sédimentaires sous-glaciaires

→Au sein du continuum entre les ribbed bedforms (subcirculaires à allongés), les bedforms sinueux et les linéations glaciaires, comment les volumes des bedforms sous-glaciaires nous permettent-ils d'explorer la signification génétique du processus d'étirement et de fragmentation ?

A partir d'une compilation de ~250 000 bedforms sous-glaciaires, vaste en termes de diversité morphologique, les volumes moyens de bedforms au sein du continuum morphologique révèlent qu'un ribbed bedform transverse peut évoluer en moyenne en un à deux bedforms sinueux, dont la fragmentation peut produire en moyenne trois à quatre linéations glaciaires.

→ Comment les directions et la quantité de déformation accumulée au sein de la glace permettent-elles d'expliquer la formation de bedforms complexes et le degré d'évolution des bedforms ?

Les relations entre la continuité morphologique des bedforms et la déformation mesurée en surface et à la base des calottes glaciaires suggèrent un modèle de continuum génétique gouverné par la direction et la quantité des déformations enregistrées par un lit sédimentaire meuble en réponse à l'écoulement cisaillant de la glace sus-jacente. Dans ce modèle de continuum, le « degré d'évolution d'un bedform » est interprété comme le résultat d'une direction et d'une quantité et de déformation cumulée du till plutôt que d'une direction, d'une quantité ou d'une vitesse de déplacement de la glace.

→ Comment la relation entre les caractéristiques morphologiques des bedforms et la quantité de déformation enregistrée dans les lits sédimentaires permet d'explorer les évolutions spatio-temporelles d'interactions glace-eau-sédiments et d'améliorer la qualité des reconstitutions paléoglaciologiques ?

A partir de ce modèle de continuum génétique, une méthode mettant en relation le « degré d'évolution d'un bedform » – paramètre quantitatif basé uniquement sur ses caractéristiques morphologiques – et la quantité de déformation cumulée est proposée pour reconstruire les variations spatiales d'interactions entre la glace, l'eau et les sédiments, à l'échelle locale, régionale ou d'une calotte glaciaire. Cette méthode de reconstruction des interactions glace-eau-sédiments permet ainsi de reconstruire avec plus de précision la position et la géométrie des paléo-fleuves de glace, des '*sticky-spots*' et des routes de drainage d'eau de fonte sous-glaciaire.

CHAPITRE IV

LES BEDFORMS ASSOCIES A LA DYNAMIQUE DE L'EAU DE FONTE : PROCESSUS DE FORMATION ET CONTINUITES MORPHOLOGIQUE ET GENETIQUE

Introduction

La dynamique de circulation d'eau de fonte au sein des systèmes de drainage sous-glaciaires contrôlent directement la dynamique d'écoulement de la glace (***Anandakrishnan & Alley, 1997; Bartholomew et al., 2010; Andrews et al., 2014; Williams et al., 2020; Smith et al., 2021***) ainsi que les processus de remobilisation sédimentaire d'origine fluvio-glaciaire tels que l'érosion (***Cowton et al., 2012; Overeem et al., 2017; Alley et al., 2019; Cook et al., 2020***) et le dépôt de sédiments (***Simkins et al., 2016; Bendixen et al., 2017***). Les études sur les calottes glaciaires actuelles, notamment au Groenland, permettent d'explorer la dynamique des systèmes de drainage sous-glaciaire sur des échelles de temps journalières à saisonnières et sur des échelles spatiales locales au travers de traceurs (colorants, GPS) ou de données géophysiques (e.g. radar, sismique) (***Chandler et al., 2013, 2021; Davison et al., 2020; Nanni et al., 2021***). En revanche, ces études ne permettent pas d'étudier ni cette dynamique sur de plus grandes échelles de temps et d'espace, ni d'explorer la nature des processus sous-glaciaires résultant de multiples interactions entre la glace, l'eau et le substrat sédimentaire.

Les processus de remobilisation de sédiments par l'eau de fonte sont interprétés comme étant à l'origine d'une grande variété de bedforms (e.g. hummocks, murtoos) et de landforms (e.g. eskers, chenaux sous-glaciaires, vallées tunnel) préférentiellement préservés et observables le long de paléo-routes de drainage d'eau de fonte sous-glaciaires, dont les reliques morphologiques sont appelées « corridors d'eau de fonte sous-glaciaires » (subglacial meltwater corridors). Comprendre les processus de formation, l'évolution morphologique et la distribution spatiale de ces bedforms et landforms est un moyen indirect d'étudier la dynamique de circulation d'eau de fonte sous-glaciaire et les interactions entre la glace, l'eau de fonte et les sédiments. La cartographie et l'étude des caractéristiques sédimentaires et morphologiques de ces bedforms permet ainsi d'étudier la dynamique hydrologique sous-glaciaire sur des échelles de temps (> 100-1000 ans) et d'espace (de l'échelle régionale à l'échelle d'une calotte glaciaire) dépassant celles du monitoring des systèmes de drainage actuels et d'espace (***Greenwood et al., 2016 ; Davison et al., 2019***) (Chapitre I – Partie B §2).

Cependant, à la différence des bedforms sous-glaciaires associés à la dynamique d'écoulement de la glace dont les dimensions sont supérieurs à plusieurs 100^{nes} de mètres et dont l'identification remonte

à la fin du 19ème siècle, les premières traces sédimentaires et morphologiques de ces corridors d'eau de fonte n'ont été découvertes qu'à la fin du 20ème siècle (***St-Onge, 1984 ; Rampton, 2000***). En raison de leurs faibles dimensions (< 100 m de large et < 5-10 m d'amplitude) et de l'émergence récente de données topographiques de haute résolution, les premiers travaux de cartographie et d'étude morphologique des hummocks (***Utting et al., 2009*** ; ***Peterson & Johnson, 2018***) et des murtoos (***Mäkinen et al., 2017 ; Peterson et al., 2017***) n'ont qu'une dizaine d'années et leurs modèles de formation sont encore débattus.

Tandis que certaines études ont démontrés la diversité des caractéristiques morphologiques notamment au sein des murtoos et '*murtoo-related bedforms*' (***Peterson et al., 2017 ; Ojala et al., 2021 ; Ahokangas et al., 2021***), d'autres études focalisées sur leurs compositions sédimentaires suggèrent des processus de formation communs régis par l'érosion, le dépôt et la déformation des sédiments (***Peterson Becher & Johnson, 2021 ; Ojala et al., 2022***). Cependant, aucune étude n'a démontré l'existence d'une continuité morphologique et/ou génétique entre cette diversité de bedforms dont la formation est attribuée à la dynamique d'écoulement de l'eau de fonte.

Par ailleurs, le caractère transitoire et la forte variabilité spatio-temporelle de l'activité des routes de drainage sous-glaciaire (***Hubbard et al., 1995 ; Das et al., 2008 ; Andrews et al., 2014 ; Lewington et al., 2020 ; Smith et al., 2021***) suggèrent une périodicité entre des périodes dominées par les processus de remobilisation d'origine glaciogénique (routes de drainage peu actives ; couplage glace-sédiments dominant) et des périodes dominées par les processus de remobilisation d'origine fluvio-glaciaires (routes de drainage actives ; découplage glace sédiments). Certaines études ont également mis en évidence des relations spatiales entre différents types de bedforms associés respectivement à la dynamique d'écoulement de l'eau de fonte (hummocks / murtoos) et de la glace (ribbed bedforms / linéations glaciaires) le long ou en périphérie des routes de drainage sous-glaciaires (e.g. ***Peterson et al., 2017 ; Ojala et al., 2019 ; Ahokangas et al., 2021)***. Cependant, aucune d'elles n'a proposé de signification génétique à ces relations spatiales ou n'a étudié l'impact de la périodicité des apports d'eau de fonte au sein des routes de drainage sur la dynamique de formation et d'évolution morphologique des bedforms.

L'objectif de ce chapitre est donc d'étudier conjointement (i) les caractéristiques morphologiques des bedforms observés au sein des corridors d'eau de fonte sous-glaciaire, (ii) leur distribution spatiale et leur association spatiale avec d'autres bedforms sous-glaciaires associés à la dynamique d'écoulement de la glace, et (iii) la nature et la variabilité spatio-temporelle des interactions glace-eau-sédiments responsables de leur formation. Ce chapitre s'organise en deux parties correspondant à deux articles : un publié et un soumis.

- **Partie A. Formation des murtoos par inondation répétée de ribbed bedforms le long des routes de drainage d'eau de fonte sous-glaciaire mise en évidence par un continuum morphométrique et génétique**

Au travers d'expériences de modélisation expérimentale et de la cartographie haute-résolution de paléo-routes de drainage en Scandinavie, la première partie de ce chapitre explore les processus de formation des murtoos le long des routes de drainage sous-glaciaires qui se mettent en place au sein de champs de ribbed bedforms. Un continuum morphométrique et génétique entre les murtoos, leurs bedforms associés ('*murtoo-related bedforms*') et les ribbed bedforms a été mis en évidence expérimentalement et dans la nature. Ce continuum a permis d'établir un modèle reliant (i) les dynamiques d'écoulement de l'eau de fonte et de couplage/découplage entre la glace et son substrat, (ii) la périodicité des processus de remobilisation d'origine glaciogénique et fluvio-glaciaire, et (iii) l'évolution des caractéristiques morphologiques des bedforms remobilisés et formés le long des routes de drainage sous-glaciaires.

- **Partie B. Un modèle d'évolution des bedforms observés le long des corridors d'eau de fonte sous-glaciaires basé sur les variations de couplage glace-eau-sédiments**

La deuxième partie de ce chapitre explore la diversité morphologique des bedforms observés le long des corridors d'eau de fonte sous-glaciaire de manière la plus exhaustive possible. A partir de la compilation de données satellites, aériennes et de terrain observés le long d'une multitude de corridors d'eau de fonte sous-glaciaires en Scandinavie et au Canada, ces travaux essayent de proposer un modèle génétique commun à l'ensemble de ces formes. Ce modèle relie (i) la diversité morphologique des

bedforms et landforms (i.e. hummocks, rides, murtoos, ribbed bedforms, linéations glaciaires, esker et chenaux) observés le long des corridors d'eau de fonte, et (ii) la dynamique des routes de drainage sous-glaciaire qui sont caractérisées par une périodicité du débit d'écoulement, de connectivité hydraulique et de processus de remobilisation de sédiments (couplage : glaciogénique ; découplage : fluvio-glaciaire).

Partie A. Formation des murtoos par inondation répétée de ribbed bedforms le long des routes de drainage d'eau de fonte sous-glaciaire mise en évidence par un continuum morphométrique et génétique.

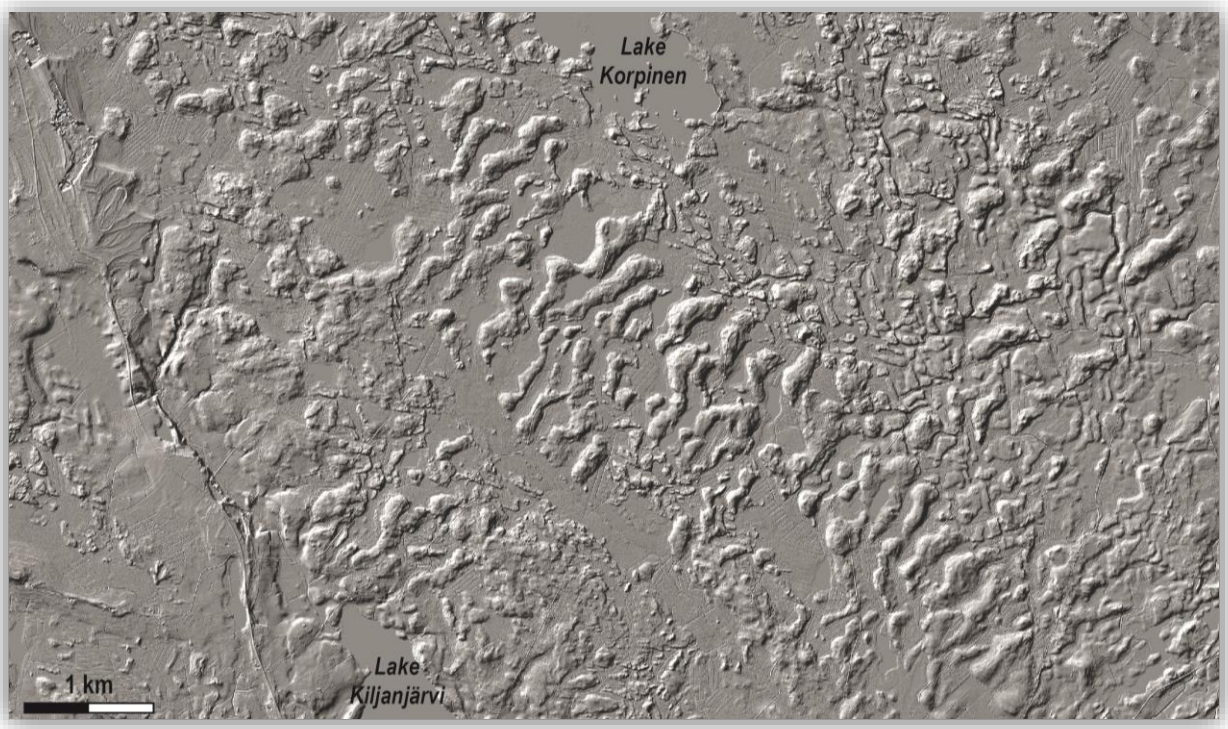

Field of murtoos and murtoo-related bedforms, associated with a field of ribbed bedforms, eskers and channels, Finland (63°39'N – 24°56'E).

1. Introduction

En Scandinavie, des études récentes ont mis en évidence l'existence de bedforms de forme triangulaire pointant dans la direction de déplacement de la glace et les ont nommés 'murtoos', en référence à leur localité de découverte en Finlande (***Mäkinen et al., 2017 ; Peterson et al., 2017***). Leur association spatiale avec des hummocks et des systèmes hydrologiques chenalisés (eskers et chenaux) (***Ojala et al., 2019 ; Ahokangas et al., 2021***) et leur composition sédimentaire (***Mäkinen et al., 2017 ; Peterson Becher & Johnson, 2021***) suggèrent que les murtoos sont formés par l'action combinée de l'érosion et du dépôt par l'eau de fonte suivi par des épisodes de déformation syn-sédimentaires (**Table 4.1**). Leur regroupement en champs le long de corridors d'eau de fonte sous-glaciaires et en amont de ceintures morainiques formés durant le retrait de la calotte Fennoscandinave a permis de relier leur formation à des drainages épisodiques de larges volumes d'eau de fonte au sein de routes de drainage sous-glaciaires (***Ojala et al., 2019 ; Peterson Becher & Johnson, 2021***). Le long des corridors d'eau de fonte sous-glaciaires, les murtoos sont associés à une variabilité de bedforms morphologiquement proches ('*murtoo-related bedforms*'), même si aucune continuité morphologique ou génétique n'a jusqu'à présent été identifiée.

Table 4.1. *Synthesis of morphological characteristics, spatial distribution, landform associations and formation hypotheses of murtoos (see Chapitre I – Partie B §2.2 for more details)*

Morphological characteristics	→ Triangular bedforms, 30 to 200 m long and wide → Longitudinal axis of symmetry parallel to the ice displacement direction with a tip pointing downstream → Asymmetric longitudinal profile (i.e. sharp and steep downstream edges)	***Mäkinen et al., 2017*** ***Peterson et al., 2017*** ***Ojala et al., 2019***
Spatial distribution	→ Gathered in corridors parallel to former ice displacement directions → Along subglacial meltwater corridors → Up-ice of morainic complexes formed during ice sheet retreats	***Ojala et al., 2019*** ***Ahokangas et al., 2021***
Associated bedforms and landforms	→ Murtoo-related bedforms (lobate-type and chevron-type murtoos, murtoo-related ridges and escarpments) : partially sharing some of morphological characteristics of murtoos → Hummocks and small-scale ridges → Eskers and channels → Ribbed bedforms (crosscut by murtoos)	***Peterson et al., 2017*** ***Ahokangas et al., 2021*** ***Ojala et al., 2019, 2021, 2022***
Formation processes	→ Combination of erosion, deposition and deformation of water saturated subglacial traction till and sorted-sediments when a large amount of meltwater is delivered to the bed	***Mäkinen et al., 2017*** ***Peterson Becher & Johnson, 2021***

Hormis les '*murtoo-related bedforms*', certains champs de murtoos cartographiés en Scandinavie ont également montrés une association spatiale et des relations de recoupement avec des champs de ribbed bedforms ; bedforms dont les hypothèses de formation invoquent essentiellement des contraintes cisaillantes basales générées sous de faibles vitesses d'écoulement de la glace et reliées à de faibles volumes d'eau de fonte sous-glaciaires (Chapitre I – Partie B §1.2). Malgré cette association spatiale et probablement en raison de ces hypothèses de formation a-priori incompatibles, aucune relation génétique n'a été identifiée entre les murtoos et les ribbed bedforms.

Enfin, malgré quelques études récentes portant sur le processus de formation des murtoos, les relations entre les caractéristiques morphologiques, les mécanismes de formation des murtoos et l'activité transitoire des routes de drainage d'eau de fonte sous-glaciaire restent mal comprises.

Problématiques :

→ Quelle est la nature de l'association spatiale entre les murtoos, la variété de bedforms morphologiquement proches ('murtoo-related bedforms') et les ribbed bedforms ? Suggère-t-elle l'existence d'une relation génétique entre ces bedforms au sein des routes de drainage d'eau de fonte sous-glaciaire ?

→ Comment la périodicité de l'écoulement d'eau de fonte et des processus de couplage/découplage module-t-elle les caractéristiques morphologiques et les processus de formation des murtoos au sein des routes de drainage ?

→ En quoi ces processus font des murtoos et autres bedforms associés ('murtoo-related bedforms') des marqueurs de la dynamique d'écoulement de l'eau de fonte à la base des calottes glaciaires ?

2. Article n°4: Formation of murtoos by repeated flooding of ribbed bedforms along subglacial meltwater corridors

Cette première partie fait donc l'objet d'un article publié dans la revue *Geomorphology*.

Geomorphology 408 (2022) 108248

Contents lists available at ScienceDirect

Geomorphology

journal homepage: www.journals.elsevier.com/geomorphology

Formation of murtoos by repeated flooding of ribbed bedforms along subglacial meltwater corridors

Jean Vérité [a,*], Édouard Ravier [a], Olivier Bourgeois [b], Paul Bessin [a], Stephen J. Livingstone [c], Christopher D. Clark [c], Stéphane Pochat [b], Régis Mourgues [a]

[a] Laboratoire de Planétologie et Géosciences, UMR 6112, CNRS, Le Mans Université, Avenue Olivier Messiaen, 72085 Le Mans CEDEX 9, France
[b] Laboratoire de Planétologie et Géosciences, UMR 6112, CNRS, Nantes Université, 2 rue de la Houssinière, BP 92208, 44322 Nantes CEDEX 3, France
[c] Department of Geography, University of Sheffield, Sheffield, UK

ARTICLE INFO

Keywords:
Glacial geomorphology
Analog modeling
Subglacial hydrology
Subglacial bedforms
Scandinavia

ABSTRACT

Fluctuations in meltwater discharge below modern glaciers and ice sheets due to diurnal, seasonal and long-term temperature variations are modulated by complex interactions between subglacial drainage, basal processes and bedform development. The bed of palaeo-ice sheets contains a variety of bedforms recording these modulations and provides an open window into the subglacial environment. Through the morphometric analysis of natural and experimental bedforms, respectively mapped along Scandinavian meltwater corridors and produced in a physical model simulating transitory subglacial water flow, we observe a morphological and genetic bedform continuum corresponding to the progressive transformation of ribbed bedforms into murtoos. Two alternating drainage configurations, related to repeated subglacial flooding events, are involved in this transformation: (i) significant meltwater discharge, high hydraulic connectivity and ice-bed decoupling during flooding events lead to hydraulic alteration of ribbed bedforms by erosion, sediment deposition and channel incision, while (ii) limited meltwater flow, low hydraulic connectivity and ice-bed recoupling that follow flooding events lead to their deformational reshaping into murtoos. The degree of transformation of ribbed bedforms into murtoos can be quantified by combining two dimensionless morphometric parameters (circularity and sinuosity) and provides a convenient proxy to constrain magnitudes, durations and/or frequencies of subglacial floods in palaeo-meltwater corridors.

1. Introduction

The reconstruction of subglacial hydrological systems and routes is critical for inferring basal thermal regimes (Kleman and Hättestrand, 1999; Irvine-Fynn et al., 2011; Smith-Johnsen et al., 2020), meltwater discharge fluctuations (Moon et al., 2014; Simkins et al., 2017; O'Connor et al., 2020), flow dynamics (Iken and Bindschadler, 1986; Anandakrishnan and Alley, 1997; Bell et al., 2007; Schroeder et al., 2013; Williams et al., 2020) and frontal ablation (Slater et al., 2015; Fried et al., 2019) of ice masses. Palaeoglaciology can help reconstruct past subglacial hydrological systems from the geomorphological imprints left behind by palaeo-ice sheets to understand their evolution and dynamics during deglaciation (St-Onge, 1984; Cofaigh, 1996; Rampton, 2000; Utting et al., 2009; Storrar and Livingstone, 2017; Lewington et al., 2019; Ojala et al., 2019; Coughlan et al., 2020) and extrapolate these findings to contemporary ice sheets. New high-resolution (<5 m) Digital Elevation Models (DEMs) based on aerial LiDAR data enable the glacial geomorphological records to be more accurately deciphered through revised mapping, identification of previously unrecognized landforms and more accurate morphometric analyses.

Recent studies conducted in Scandinavia unraveled hitherto unidentified subglacial bedforms characterized by a triangular shape. These bedforms, referred to as murtoos (Ojala et al., 2019; Peterson Becher and Johnson, 2021) or triangle-type murtoos (Ojala et al., 2021), were initially called 'V-shaped hummocks' (Peterson et al., 2017) and 'triangular-shaped landforms' (Mäkinen et al., 2017). In plan view, murtoos are triangles with a longitudinal axis of symmetry parallel to the ice flow direction and a tip pointing downstream. Murtoos are 30 to 200 m long and wide, less than 5 m high and have asymmetric longitudinal profiles with sharp and steep downstream edges (Ojala et al., 2019). They are composed of subglacial traction till interbedded with lenses of sorted sandy sediments, both showing deformation related to

* Corresponding author.
E-mail address: jean.verite@univ-lemans.fr (J. Vérité).

https://doi.org/10.1016/j.geomorph.2022.108248
Received 30 November 2021; Received in revised form 5 April 2022; Accepted 5 April 2022
Available online 9 April 2022

shearing and liquefaction processes (Peterson Becher and Johnson, 2021; Ojala et al., 2021). Within single subglacial bedform fields, murtoos are commonly associated with bedforms that partially share some of their characteristics, such as a lobate or irregular/asymmetric triangular shape and asymmetric longitudinal profiles: these have been referred to as murtoo-related landforms by Ojala et al. (2021).

Previous geomorphological mapping on the bed of the former Scandinavian Ice Sheet (SIS) demonstrated that murtoos are frequently gathered in fields or corridors parallel to the former ice flow directions. Murtoo fields commonly occur in close association with eskers along hummock tracts, which are characterized by a rough texture contrasting with the surrounding streamlined glacial bed (Peterson et al., 2017; Ahokangas et al., 2021). Hummock tracts are a few kilometers wide and several to tens of kilometers long and are interpreted as routes that drained pulses of meltwater flow beneath decaying ice sheets (Peterson and Johnson, 2018). These routes were first observed as 'glaciofluvial corridors' in Canada (St-Onge, 1984; Utting et al., 2009), and were more recently referred to as 'meltwater corridors' (Lewington et al., 2019, 2020; Ojala et al., 2019; Sharpe et al., 2021), a term that we use in the article.

Murtoos have been interpreted to form by a combination of erosion, deposition and deformation of water-saturated sediments and subglacial till when large volumes of meltwater are delivered to warm subglacial beds (Mäkinen et al., 2017; Ojala et al., 2019; Peterson Becher and Johnson, 2021; Ahokangas et al., 2021). These periodic meltwater inputs are likely to cause flooding events overwhelming channelized or hydraulically connected distributed drainage systems along meltwater corridors (e.g., Lewington et al., 2020; Mejía et al., 2021; Nanni et al., 2021). Murtoo fields, forming parts of longer and wider meltwater routes, have been interpreted to represent small-scale transitional drainage systems between alternating channelized and distributed regimes, controlled by variations in the amount of meltwater (Mäkinen et al., 2017; Ojala et al., 2019, 2021; Peterson Becher and Johnson, 2021).

In Scandinavia, some murtoo fields are spatially associated with ribbed bedforms (Fig. 1), which have been referred to as 'ribbed moraines' (Hughes, 1964; Lundqvist, 1969, 1989; Hättestrand and Kleman, 1999; Möller and Dowling, 2015), with crosscutting relationships suggesting murtoos postdate the formation of the ribbed bedforms (Ojala et al., 2019; Ahokangas et al., 2021). The terms 'Rogen moraine,' 'Åsnen moraine,' and 'Niemisal moraine' refer to special forms of ribbed moraines in the Lake Rogen area (Lundqvist, 1969, 1989), southern Småland, Sweden (Möller and Dowling, 2015), and in northeastern Sweden (Lindén et al., 2008). Ribbed bedforms are subglacially-produced ridges transverse to the ice flow direction (Dunlop and Clark, 2006). They are primarily thought to result from subglacial shear and bed deformation, but the context and primary driving mechanism varies between localized areas of ice-bed recoupling associated with spatial variations in water drainage and ice flow velocity under warm-based ice (Shaw, 1979; Boulton, 1987; Lindén et al., 2008; Fowler and Chapwanya, 2014; Vérité et al., 2021); or at the transition between cold-based and warm-based ice (Hättestrand and Kleman, 1999). Except for the hypothesis of Shaw (2002), who invokes large-scale subglacial meltwater floods, the formation of ribbed bedforms has most commonly been related to low meltwater flow. Although spatial associations between ribbed bedforms and murtoos have been observed, a possible genetic relationship between them has not been reported yet.

Over the last decade, the emergence of numerical (Fowler and Chapwanya, 2014; Fannon et al., 2017) and experimental (Lelandais et al., 2016, 2018; Vérité et al., 2021) models have enabled the exploration of relationships between genesis and evolution of subglacial bedforms and drainage features, and ice flow dynamics and meltwater flow at the ice-bed interface. The experimental model initiated by Lelandais et al. (2016, 2018) and further developed by Vérité et al. (2021) notably contributed to better understand the link between the development of meltwater channels and ribbed bedforms and the dynamics of ice lobes and ice streams. However, neither numerical nor experimental models have simulated the formation of murtoos.

In this study, we explore the relationship between the dynamics of subglacial hydrological systems and the formation of murtoos when they are associated with ribbed bedforms. For that purpose, we mapped bedforms using selected portions of LiDAR DEMs along Scandinavian meltwater corridors. Based on the definition of new dimensionless morphometric criteria, we compared these natural bedforms with experimental bedforms produced in an analog model, identical to that used by Vérité et al. (2021). From this comparison, we derive a model for the formation of murtoos and discuss the implications for the reconstruction of meltwater corridors.

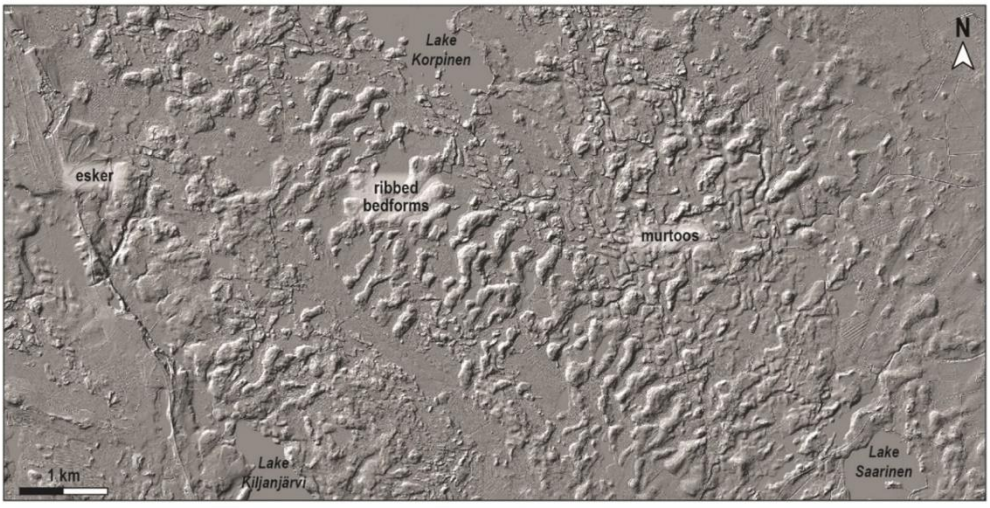

Fig. 1. A spatial association between murtoos and ribbed bedforms. The field is located north of Lake Kiljanjärvi, W Finland (63°39′12″N – 24°56′41″E). Ice flow was directed toward the southeast. Ribbed bedforms (undulating ridges striking SW-NE) dominate the landscape but are interrupted in places (notably downstream from Lake Korpinen) by murtoos (downstream pointing triangular hills).

2. Morphometric characterization of subglacial bedforms in Scandinavian meltwater corridors

2.1. Study areas

The study areas are located on the crystalline Fennoscandian Shield (Koistinen et al., 2001) covered by a layer of subglacial sediments less than 10 m thick and deposited during the Late Weichselian glaciation. The SIS covered Scandinavia entirely and extended to northern continental Europe during the Last Glacial Maximum (LGM) (22 ka BP; Hughes et al., 2016; Stroeven et al., 2016 for ages), before progressively retreating over Scandinavia between 17 and 9 ka BP (Fig. 2a). Within the central part of the SIS, both in Sweden and Finland, hummock tracts and murtoo fields occur in places characterized by rapid SIS retreat corresponding to warmer periods during which the meltwater flow increased ('Bølling-Allerød interstadial', 14.7–13 ka BP and 'early Holocene warming', 11.7–9 ka BP) (Peterson and Johnson, 2018; Ojala et al., 2019).

The selected study areas are located along hummock tracts, interpreted as meltwater corridors, where murtoo fields are locally associated with ribbed bedforms (Fig. 2). In Sweden, the study areas are located in the southern Swedish highland, south of the Middle Swedish end moraines (12.7 ka BP) related to the southern lobate termination of the SIS (Fig. 2b; Lundqvist and Wohlfarth, 2000). The study area in Finland lies in the trunk of the Finnish Lake District Ice Lobe, northwest of the Salpausselkä end moraine zone (12.7 ka BP) and the Central Finland Ice Marginal Formation (11 ka BP; Punkari, 1980).

2.2. Method

2.2.1. Data sources and processing

We conducted high-resolution (1:5000 to 1:10,000) mapping from open-data LiDAR-based DEMs available on the online databases of the Geological Survey of Finland (http://gtkdata.gtk.fi/maankamara/) and the Swedish Mapping, Cadastral and Land Registration Authority (https://www.lantmateriet.se/sv/). From these 2-m LiDAR DEMs, we derived hillshade maps and residual relief maps (Hiller and Smith, 2008) with Geographic Information System (GIS) software.

2.2.2. Bedform delineation and morphometric analysis

Break values of hillshade and residual relief data were delineated manually to produce bedform contours, for which perimeters (P) and areas (A) were measured (Fig. 3a). Lengths of transverse (i.e. transverse to the local ice flow direction), and longitudinal (i.e. parallel to the local ice flow direction) axes were measured using minimum bounding rectangles. Local ice flow directions were determined using streamlined bedforms observed within or in the vicinity of the mapped area. We also drew bedform crest lines by delineating lines of maximum elevation within each contour. Curvilinear and straight lengths of bedform crest lines were measured, using minimum bounding rectangles. The slopes of downstream and upstream edges of bedforms, the wavelength between bedform crest lines and the tip angle of sub-triangular and triangular bedforms were also measured.

From these measurements, we computed three dimensionless morphometric indices that describe bedform differences in shape independently of their differences in size: elongation (Eq. (1)), circularity index (Eq. (2), modified from Burgess et al., 2003) and sinuosity index (Eq. (3)). Theoretical elongation values range from 0 (for contours strongly elongated parallel to ice flow) to $+\infty$ (for contours strongly elongated orthogonal to ice flow), and a value of 1 corresponds to an isotropic contour. Theoretical circularity index values range from 0 (for strongly non-circular contours) to 1 (for perfectly circular contours). Theoretical sinuosity index values range from 0 (for perfectly straight crestlines) to $+\infty$ (for strongly sinuous crestlines), and a value of 1 corresponds to an equilateral triangular crestline.

$$Elongation\ (El) = \text{Transverse axis}/\text{Longitudinal axis} \tag{1}$$

$$Circularity\ index\ (I_{circ}) = (4\pi A)/P2 \tag{2}$$

$$Sinuosity\ index\ (\mathrm{I_{sin}}) = ((\text{Curvilinear length}/\text{Straight length}) - 1)\Big/\left(\sqrt{5} - 1\right) \tag{3}$$

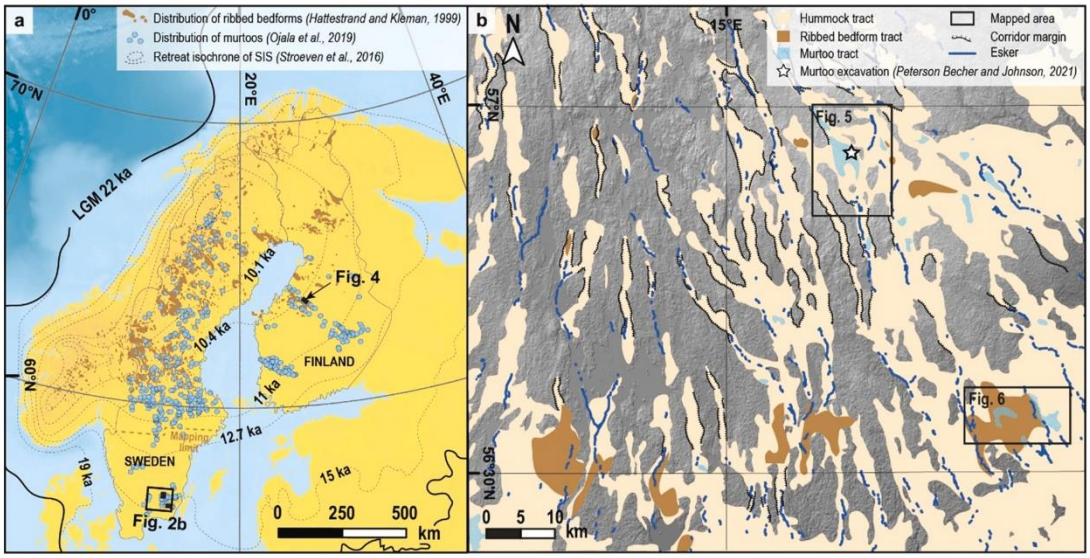

Fig. 2. (a) Overview map of northern Europe with selected retreat isochrones of the Scandinavian Ice Sheet (Stroeven et al., 2016), distributions of murtoo fields (Ojala et al., 2019) and ribbed bedform fields (Hättestrand and Kleman, 1999) in Scandinavia. Black boxes indicate locations of mapped areas. (b) Hillshaded DEM and glacial geomorphological map of the South Swedish uplands illustrating the spatial relationships between eskers, hummock tracts, ribbed bedform tracts and murtoo tracts (modified after Peterson et al., 2017). The white star indicates the location of a murtoo excavated by Peterson Becher and Johnson (2021).

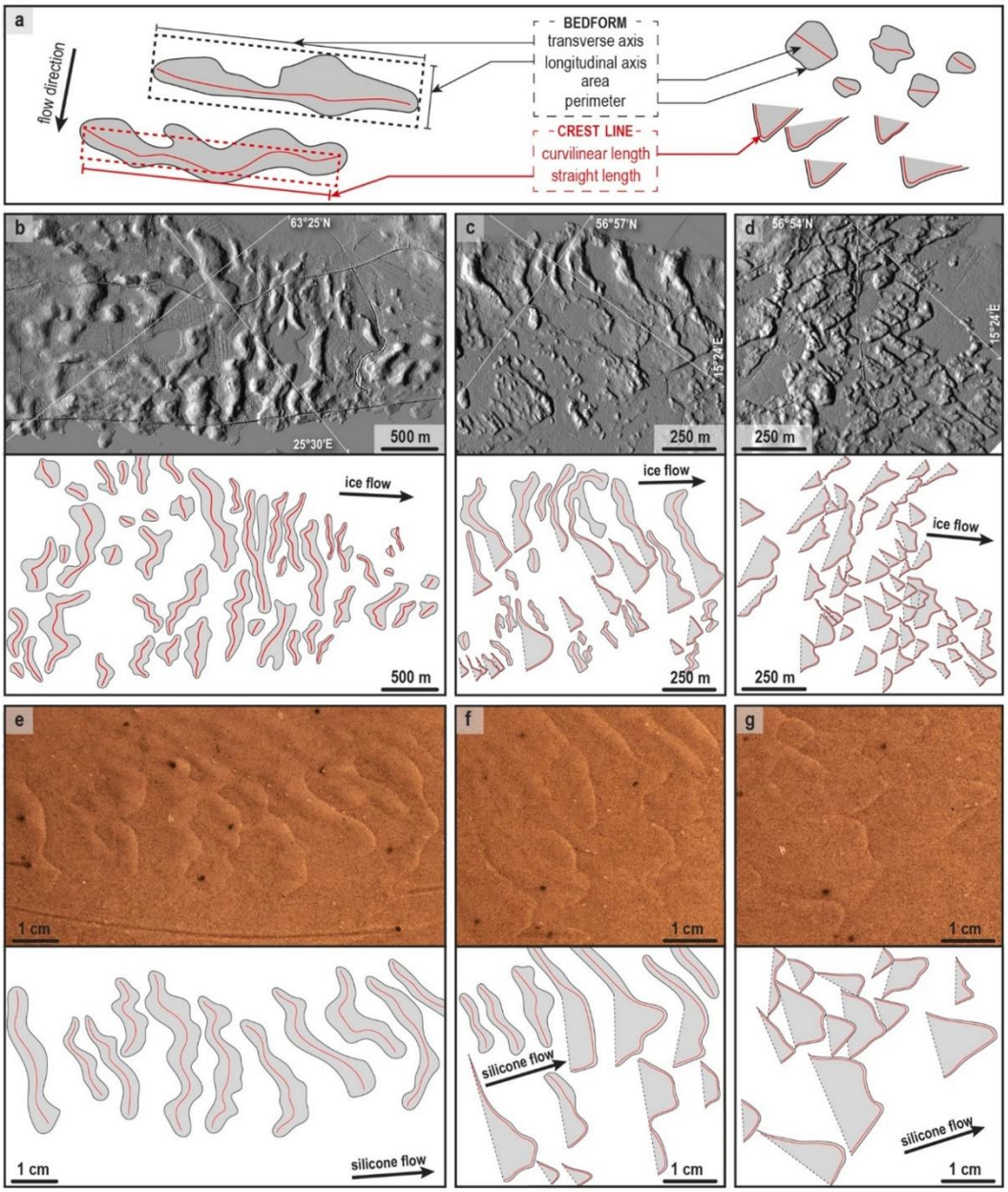

Fig. 3. Typical examples of natural (from Finland and Sweden) and experimental bedforms (see Section 3 for experimental description), and our mapping of their morphology as grey polygons with red crest lines. Note the differences in scale. (a) Measurement method of dimensioned morphometric parameters on bedforms and crest lines, which are used for the calculation of the dimensionless indices: elongation, circularity index and sinuosity index. (b) and (e) Natural and experimental ribbed bedforms. (c) and (f) Examples of bedforms spatially-associated with ribbed bedforms and murtoos that display intermediate morphological properties between those of ribbed bedforms and murtoos. These bedforms are named intermediate bedforms. (d) and (g) Fields of natural and experimental murtoos and intermediate bedforms.

2.3. Results: subglacial bedforms along Scandinavian meltwater corridors

2.3.1. Bedform morphometry: a morphometric continuum between ribbed bedforms and murtoos

In the selected study areas, the total number of bedforms identified is 7208 (Figs. 4–6). Their morphological characteristics are remarkably similar within and between each area, and were therefore compiled in a single database (Figs. 7–8). There are no gaps or jumps in the distribution of their morphometric characteristics (Fig. 8): all analyzed bedforms stand along a morphometric continuum between three end members, which we schematically portray in the left-hand column of Fig. 7 and in Fig. 8. The 1st end member corresponds to sub-circular

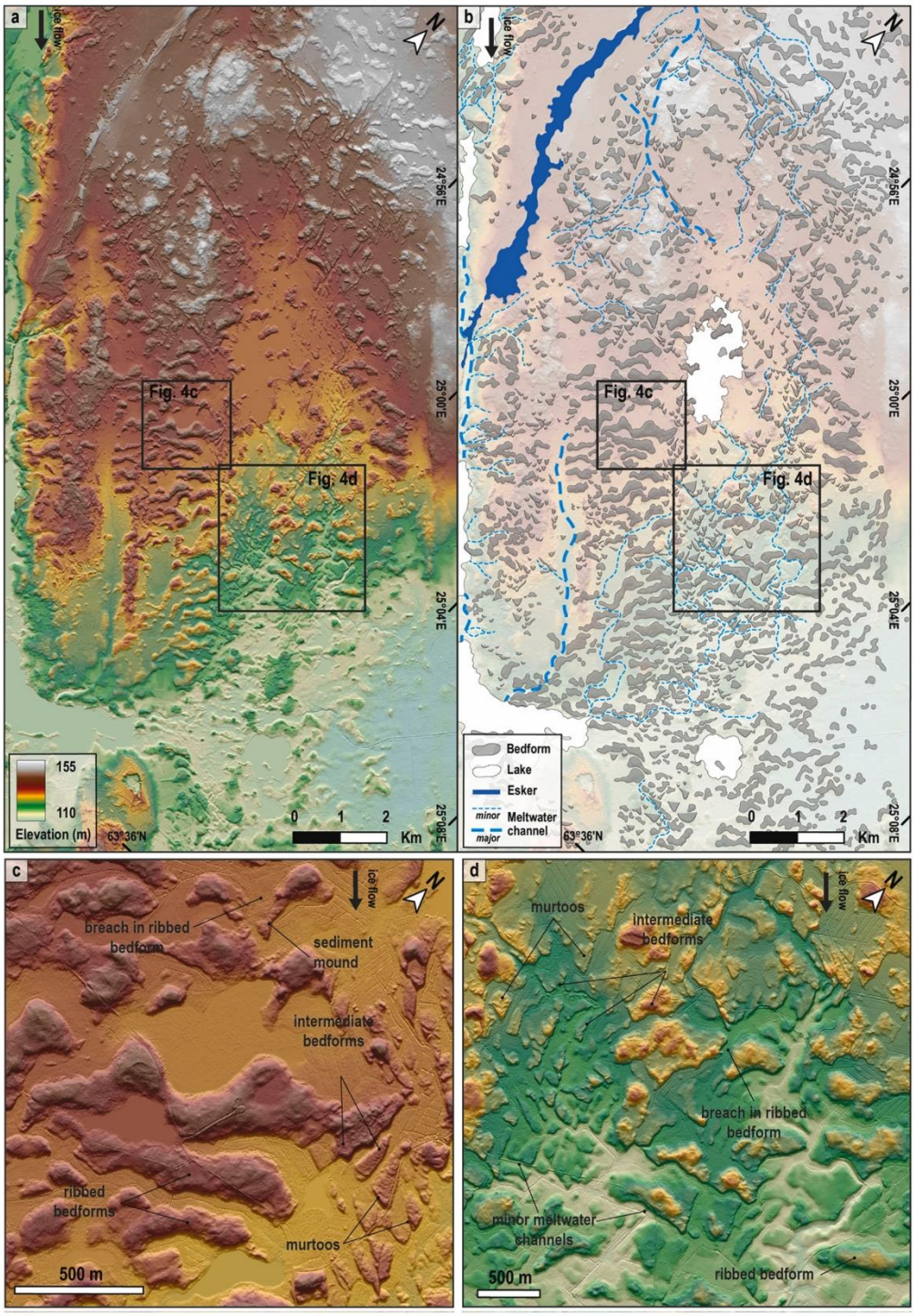

Fig. 4. (a) LiDAR DEM and (b) interpretative morphological map with digitized bedforms of a portion of the Finnish Lake District Ice Lobe. (c) and (d) Murtoos occur in close spatial association with ribbed bedforms. Some ribbed bedforms located close to murtoo fields are breached forming sediment mounds in front of their downstream edges. Other bedforms – which we named intermediate bedforms – are spatially associated with ribbed bedforms and murtoos, and characterized by intermediate morphological properties to these two types of bedform. (d) Murtoos and intermediate bedforms are gathered into corridors, often at slightly lower elevations compared with surrounding terrain of ribbed bedforms, and sometimes form a chevron-like geometrical pattern associated with minor meltwater channels.

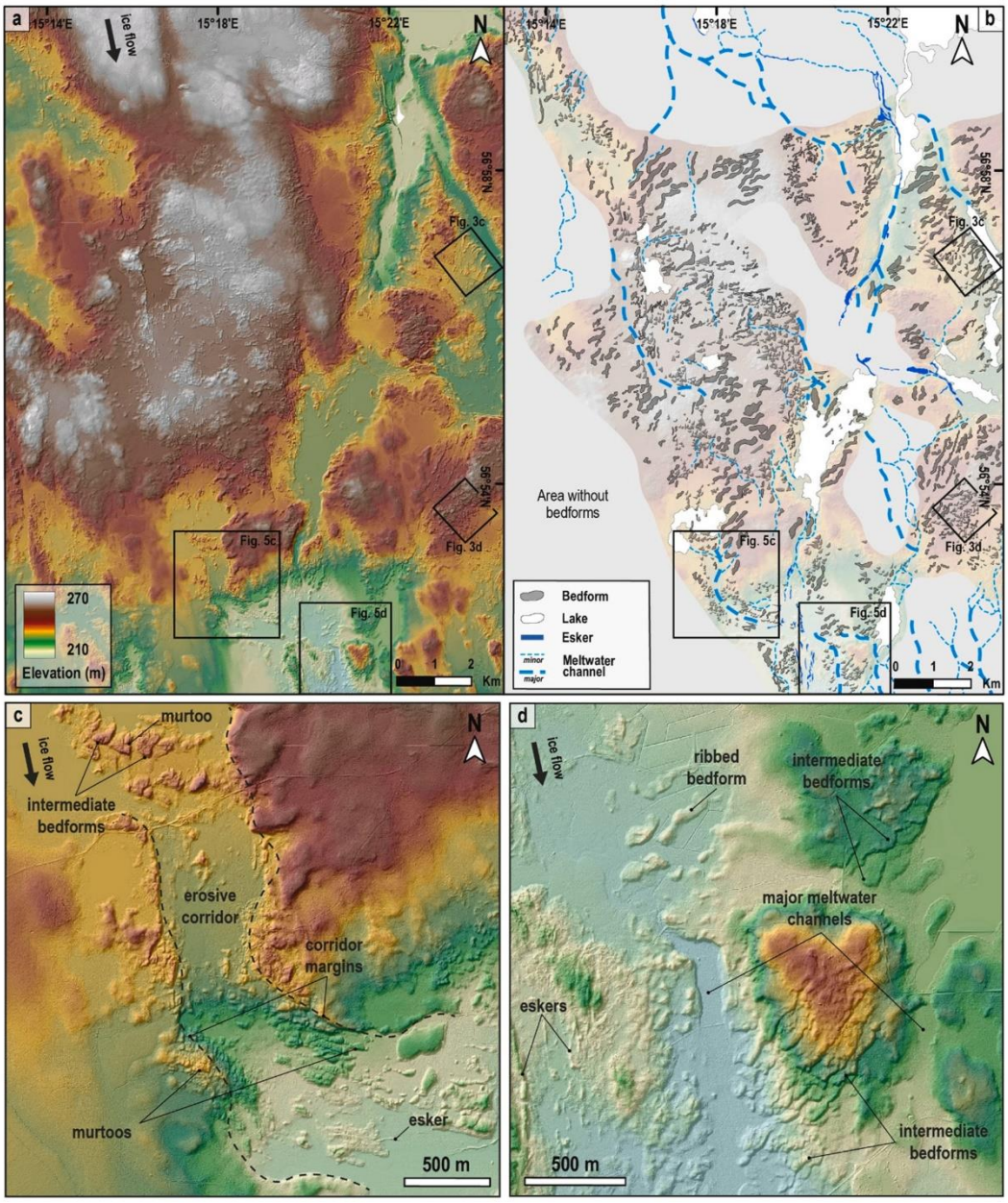

Fig. 5. (a) LiDAR DEM and (b) interpretative morphological map with digitized bedforms of a northern portion of the south Sweden Ice Lobe. (c) and (d) Murtoos frequently occur within erosive corridors delimited by sharp margins. In the same field, murtoos are associated with a variety of intermediate bedforms. Major meltwater channels and eskers commonly have a central position in the corridors and are surrounded by ribbed bedforms, murtoos and intermediate bedforms.

bedforms without any preferential orientation showing a circularity index of 1, a sinuosity index close to 0 and an elongation ratio of 1. The 2nd end member corresponds to slightly undulating to linear bedforms transverse to the local ice flow direction with a circularity index close to 0.2, a sinuosity index close to 0.1 and an elongation ratio of up to 10. The 3rd end member is composed of bedforms displaying an equilateral triangular shape with a circularity index close to 0.8, a sinuosity index of 1 and an elongation ratio of 1.

Between the 1st and 2nd end members lies a category corresponding to regularly-spaced bedforms (λ = ~200–300 m), mostly transverse to the ice flow direction, with an undulating to linear crest line: we refer to these as ribbed bedforms since they have all the characteristics described by Dunlop and Clark (2006) (Fig. 3b). Their longitudinal profile is almost symmetrical; in most cases the downstream edge (median slope value = 8.3°) is slightly steeper than the upstream edge (median slope value = 6.5°). Ribbed bedforms are typically 10 m high, 110–275 m long, and 50–110 m wide. Close to the 1st end member, ribbed bedforms are slightly elongated (El < 2), non-sinuous (I_{sin} <

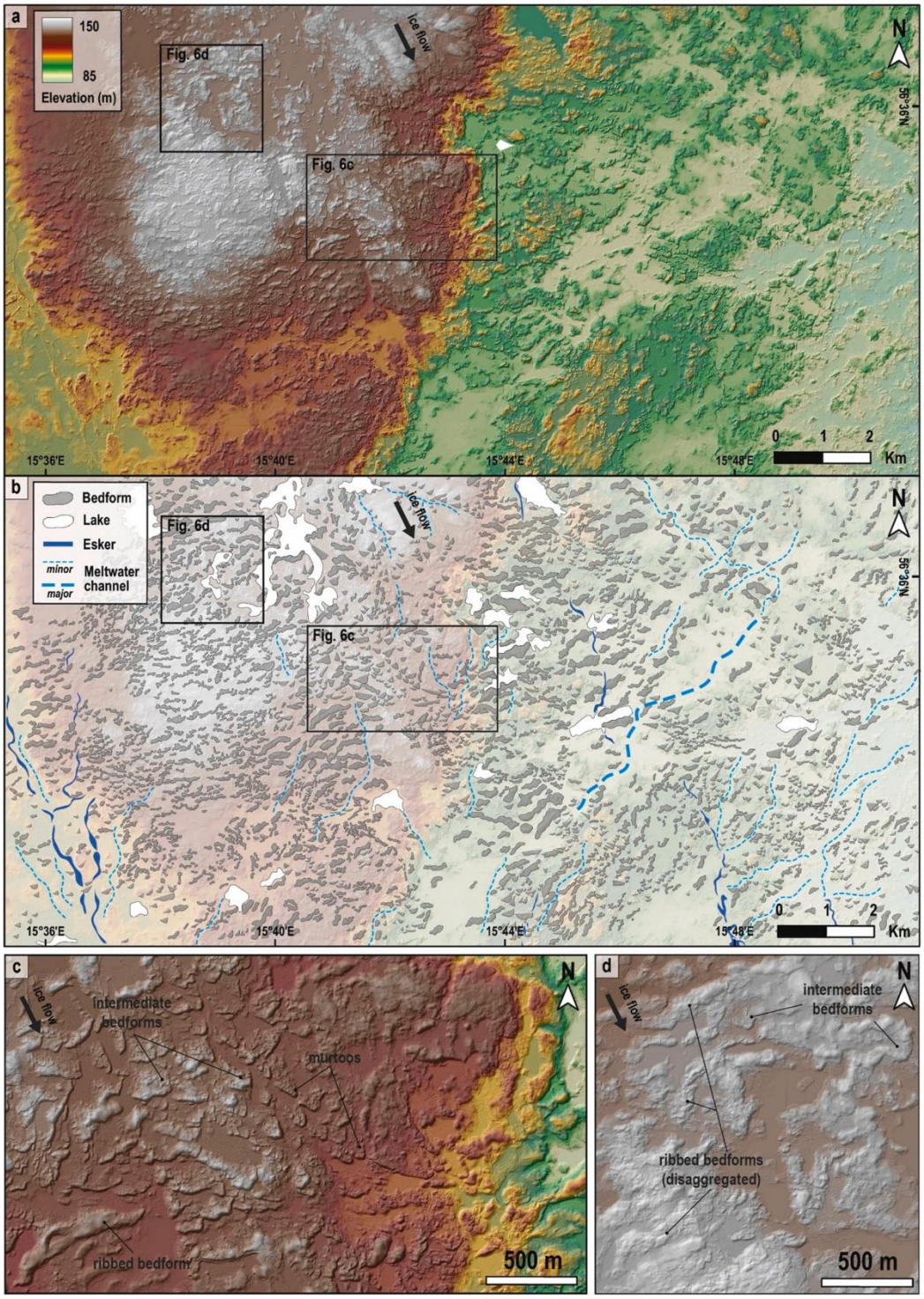

Fig. 6. (a) LiDAR DEM and (b) interpretative morphological map with digitized bedforms of a southern portion of the south Sweden Ice Lobe. (c) Murtoos, intermediate bedforms and ribbed bedforms form a morphological transition from the center toward the lateral margin of the murtoo field. (d) Some ribbed bedforms display a disaggregated appearance and are spatially associated with murtoos and intermediate bedforms.

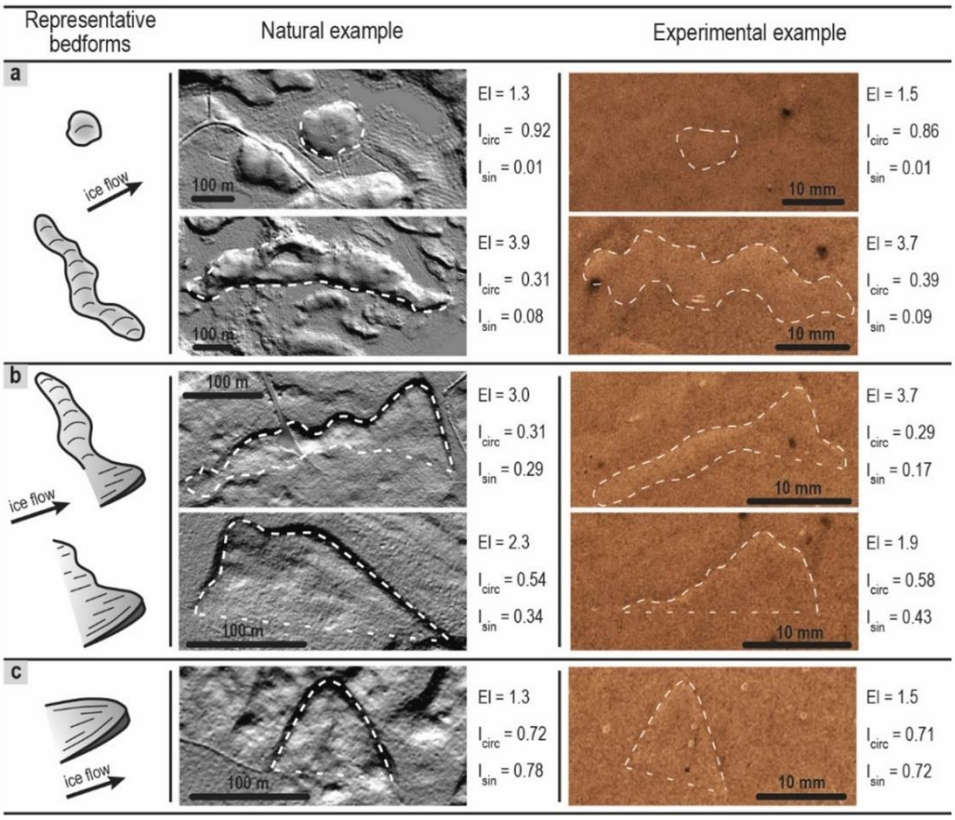

Fig. 7. Morphological appearance and morphometric characteristics of typical natural and experimental (a) ribbed bedforms, (b) intermediate bedforms and (c) murtoos.

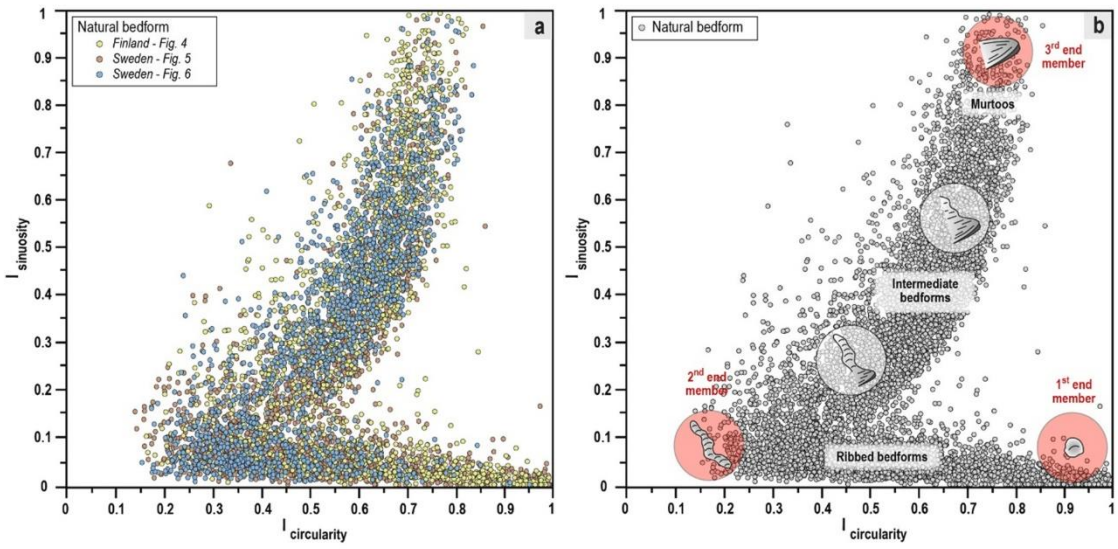

Fig. 8. Morphometry of natural bedforms in the Swedish and Finnish study areas. A morphological continuum is observed between three end members (red circles): a continuum of ribbed bedforms with variable circularity (and elongation) and low sinuosity between the 1st and 2nd end members, and a continuum between ribbed bedforms (low circularity and low sinuosity) and murtoos (high circularity and high sinuosity), with a panel of morphologically intermediate bedforms, between the 2nd and 3rd end members.

0.05) and highly circular ($I_{circ} > 0.6$); while they are more elongated (El > 2), slightly more sinuous ($0.05 < I_{sin} < 0.15$) and less circular ($I_{circ} < 0.6$) close to the 2nd end member. Some ribbed bedforms have experienced morphological transformations that result from their disaggregation (Fig. 6d) or breaching (Fig. 4c), sometimes splitting initial ribbed bedforms in two parts or more.

Between the 2nd and 3rd end members, bedforms present morphometric characteristics intermediate between ribbed bedforms and triangular-shaped bedforms and are therefore referred to as intermediate bedforms (Figs. 3c, 7c, 8b). Some intermediate bedforms are morphometrically close to ribbed bedforms: they have one or several parts that display a symmetric longitudinal profile and an arcuate crest line transverse to the ice flow direction (i.e. ribbed bedforms), while other parts, cross-cutting or overlapping the latter, show a lobate to triangular form pointing in the downstream direction with an asymmetric longitudinal profile (Figs. 4c, 5d). Other bedforms show an overall lobate to irregular triangular shape with a tip pointing in the downstream direction and an opening angle ranging between 70 and 110°. Close to the 3rd end member, we observe regular triangular forms in plan view that are typically 65–120 m long and 40–80 m wide, representing typical morphological values of murtoos measured by Ojala et al. (2019, 2021) (Fig. 3d). Like murtoos, the triangle tip generally points in the direction of the local ice flow direction, determined through surrounding lineations, and its angle ranges from 56 to 72°, corresponding to the average form of an equilateral triangle (Figs. 4c–d, 6c). The longitudinal axis is almost the bisector of the tip angle and its topographic profile is asymmetric; the downstream edge (mean value = 12°) is steeper than the upstream edge (mean value = 4°). On average, intermediate bedforms are slightly elongated transverse to the ice flow direction ($1 < El < 1.5$), circular ($0.6 < I_{circ} < 0.8$) and very sinuous ($I_{sin} > 0.7$) (Figs. 7c, 8b). The 3rd end member corresponds to typical murtoos and the intermediate bedforms between ribbed bedforms and murtoos typically correspond to lobate-type murtoos, murtoo-related ridges and to murtoos cross-cutting ribbed bedforms described by Ojala et al. (2019, 2021).

The elongation, sinuosity index and circularity index of the bedforms mapped in the study areas show the existence of a morphometric continuum between three end members: (1) circular bedforms, (2) linear to undulating transverse bedforms, and (3) triangular bedforms pointing in the ice flow direction. The first branch of the morphometric continuum, between the 1st and 2nd end members, illustrates a continuum of ribbed bedforms from circular to transverse and elongated forms. Greenwood and Clark (2008) and Ely et al. (2016) integrated circular bedforms – also referred to as hummocky-ribbed bedforms (Hättestrand, 1997; Dunlop and Clark, 2006; Möller and Dowling, 2015) – in a unique bedform assemblage intimately associated with ribbed bedforms and demonstrated the existence of a morphometric continuum. Hättestrand (1997) and Möller and Dowling (2015) have previously emphasized that this morphometric continuum corresponds to a genetic continuum related to the development of ribbed bedforms. Therefore, this branch of the morphometric continuum will not be much further discussed here. The second branch, between the 2nd and 3rd end members, illustrates a previously unknown continuum between ribbed bedforms, murtoos and a variety of morphologically intermediate bedforms.

2.3.2. Spatial distribution of bedforms and their relationship with meltwater corridors

In the mapped areas, where murtoos are observed in spatial association with ribbed bedforms, murtoos and intermediate bedforms gather in fields that are 0.5–2 km wide and 1–4 km long on average and develop parallel to the ice flow direction, preferentially in flat or low-relief areas. Within these fields, bedforms frequently overlap each other in the downstream direction and exhibit chevron-like patterns (Fig. 4d), while others are isolated. Fields of murtoos appear adjacent to or within fields of ribbed bedforms, and in most cases the lateral boundaries between these fields are diffuse and difficult to define (Figs. 5d, 6c–d). However, murtoos commonly appear in the core of the fields while the concentration of intermediate bedforms gradually increases toward the field margins (Fig. 6c). Boundaries between murtoo fields and ribbed bedform fields are typically defined by bedforms related to breaching, disaggregation, transformation of ribbed bedforms forming an array of intermediate bedforms (Figs. 4c–d, 6d).

Edges of murtoos and intermediate bedforms are often delineated by minor meltwater channels – up to 50 m wide and several hundreds of meters long – forming braided systems (Fig. 4d) that connect with major meltwater channels few hundreds of meters wide and several kilometers long (Fig. 5d). These major meltwater channels frequently cross murtoo fields and are generally orientated parallel to the field margins and to the local ice flow direction. In some places, murtoo fields are delimited by sharp margins related to large erosive meltwater corridors (Fig. 5c). Other drainage features are depositional and correspond to eskers in association with murtoos (Fig. 5d). Eskers frequently connect with meltwater channels (Figs. 5b, 6b) and intersect or overlap murtoos and intermediate bedforms (Fig. 5c). These observations show that fields of murtoos and intermediate bedforms are intimately associated with both erosional and depositional drainage features at different scales, while these drainage features are not apparent along adjacent fields of ribbed bedforms.

3. Experimental modeling of subglacial bedforms development along meltwater corridors

We explored experimentally the hypotheses (i) that the spatial relationships described in Section 2.3.2 reflect that murtoo formation involves flooding events along meltwater corridors as suggested by Mäkinen et al. (2017), Ojala et al. (2019) and Peterson Becher and Johnson (2021), and (ii) that the morphometric continuum between ribbed bedforms and murtoos described in Section 2.3.1 reflects a genetic continuum. For that purpose, we used an experimental model able to simulate flooding events (Lelandais et al., 2018) and ribbed bedform development (Vérité et al., 2021).

3.1. Methods: analog modeling

The experimental model consists of a square box, 2 × 2 m wide and 5 cm high. The box is filled with a 5 cm thick sand layer (median grain size d_{med} = 100 μm) that simulates a flat, deformable, erodible, porous and permeable subglacial bed (Fig. 9a) (Evans et al., 2006). The bed is saturated and compacted to ensure homogeneous values for its density (ρ_{bulk} = 2000 kg·m^{-3}), porosity (ϕ_S = 41%) and permeability (Ks = 10^{-4} m·s^{-1}). The ice cap is modeled with a circular layer of viscous and transparent silicone putty (density ρ_{sil} = 967 kg·m^{-3}, viscosity η_{sil} = 5.10^4 Pa·s^{-1}) covering the bed (Fig. 9b). Ultraviolet (UV) markers, 1 mm in diameter, are placed with an initial spacing of 5 cm on the surface of the silicon surface. The subglacial hydrological system is simulated by the injection of a solution of water and UV ink (bulk density ρ_w = 998 kg·m^{-3}) through an injector located below the center of the silicone cap. The injector is 8 mm in diameter and placed at a depth of 1.5 cm below the bed surface. The water injection is regulated by a flowmeter (discharge Q = 0–100 ml·min^{-1}) and is calculated to allow water flow within the bed and at the silicone-bed interface when water pressure exceeds the combined weight of the bed and silicone layers. Isolated values of the pore water pressure are measured with twelve pressure sensors placed at a depth of 1.5 cm below the bed surface and distributed concentrically at 15 and 30 cm from the central injector (Fig. 9c). The photographic set-up and the lighting device, which is composed of white light and UV LEDs that alternate every 15 s, enable simultaneous monitoring of landform development, water distribution and silicone cap dynamics. In UV light, the water distribution along the silicone-bed interface is interpreted through the fluorescence of the injected solution and the positions of UV markers are tracked with a time step of 90 s in order to build interpolated maps of the horizontal velocity (V_{surf}) of the

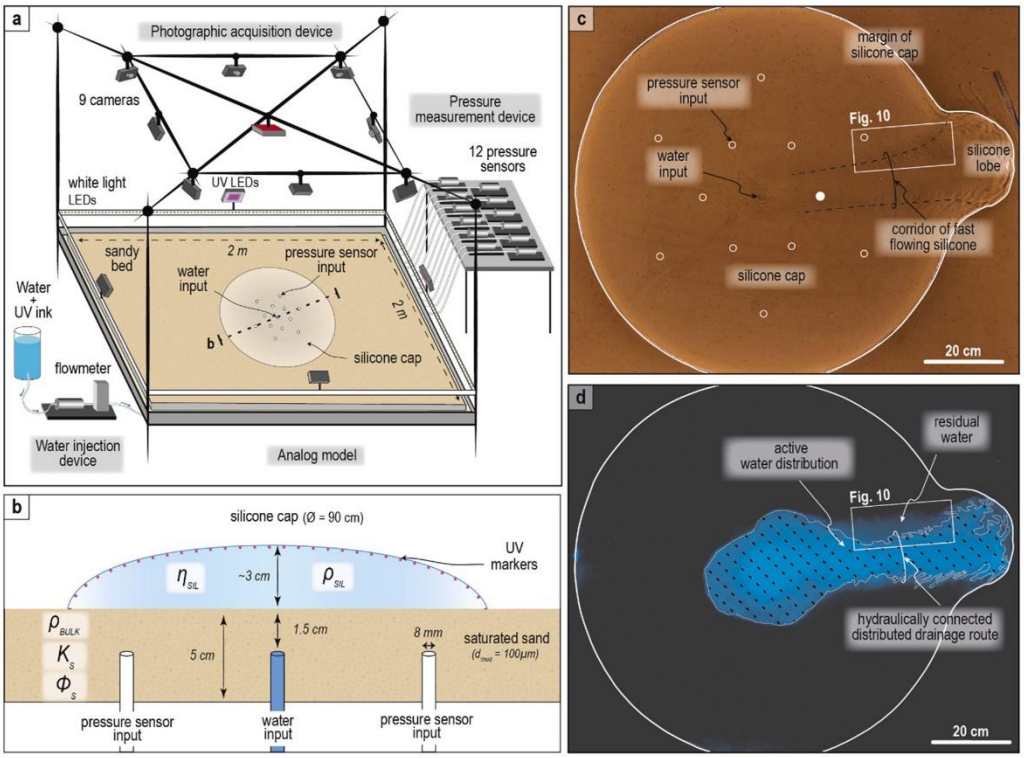

Fig. 9. (a) Experimental model, monitoring apparatus and (b) cross-section of the experimental model with the main physical parameters involved (modified after Vérité et al., 2021). The flow of a transparent and viscous cap of silicone putty over a deformable and erodible bed made of water-saturated sand is triggered by the injection of a solution of water and UV ink through an injector located in the bed below the center of the silicone cap. The monitoring apparatus is composed of a lighting set-up, a photographic acquisition device and a pressure measurement device. Surface view of the analog model in (c) white light and (d) UV light. Filled white circle indicates position of pressure sensor input used to produce the plot of pore water pressure in Fig. 10. (d) Distribution of water along the silicone-bed interface (stippled area) revealed by the fluorescence of the solution of water and UV ink. Variations in fluorescence intensity indicate if water flow is active or not (i.e. residual water).

silicone cap surface (Fig. 9d). In white light, the transparency of the injected solution and the silicone enables manual mapping of bedform contours and crest lines with a horizontal precision of ±0.1 mm (Figs. 3e–g, 9c). The morphological analysis described in Section 2.2.2 for natural bedforms is applied to experimental bedforms presented in the following section.

The model is designed to simulate the basic physical interactions between an ice cap, a subglacial hydrological system and a sedimentary bed. The bed is composed of wet sand that enables internal deformation by localized and diffuse intergranular shearing, bed-load transport and deposition of grains by flow of water and silicone. The scaling of the experimental model is defined so that the dimensionless ratios between (i) the lobe margin velocity and the incision rate of water channels, and (ii) the bedform wavelength and the cap thickness have similar values in the model and in nature. Limitations stem from the experimental conditions (15–20 °C and atmospheric pressure) and rheological properties of the silicone putty (Newtonian viscosity independent of temperature, isotropic and impermeable) that differ from those of ice. The wet and water-saturated sedimentary bed does not allow the reproduction of cold-based subglacial conditions. Temperature-dependent and stress-dependent processes – as heat and shear softening, shear heating and brittle deformation – characterizing glacier ice are not reproducible by the silicone cap. Self-production of meltwater by supraglacial melting, the spatial complexity of basal hydrological systems and ablation processes are not reproducible either (further details regarding scaling and limitations of the experimental model are discussed in Lelandais et al., 2016 and Vérité et al., 2021). Although the experimental model is not a complete and perfectly scaled miniaturization of nature, the landforms obtained experimentally are remarkably similar in appearance to their natural counterparts (Fig. 3). These findings strongly accord with the notion of "unreasonable effectiveness" of experimental modeling as articulated by Paola et al. (2009).

In order to explore the formation of murtoos along meltwater corridors experiencing large, episodic influxes of meltwater, we performed experiments with water discharge scenarios producing repeated flooding events (Supplementary data 1). The water injection scenario aims to produce a dynamic hydrological system and can be divided in two main periods. The first period (t = 0–90 min) is characterized by continuous water flow (Q = 25 ml·min^{-1}), while the second period (t = 90–145 min) is characterized by discontinued water flow with alternating quiescent and re-injection phases producing three flooding events (Fig. 10). The water flow is doubled during the first and the second re-injection phases (i.e. flooding events #1 and #2; Q = 50 ml·min^{-1}) compared to the first period, and quadrupled during the third re-injection phase (i.e. flooding event #3; Q = 100 ml·min^{-1}). The experiments were duplicated to check their reproducibility.

3.2. Results: progressive transformation of ribbed bedforms into murtoos during repeated flooding events

As soon as the water injection starts below the silicone cap, which is flowing under its own weight (V_{surf} = 0.2 × 10^{-2} mm·s^{-1}), a circular

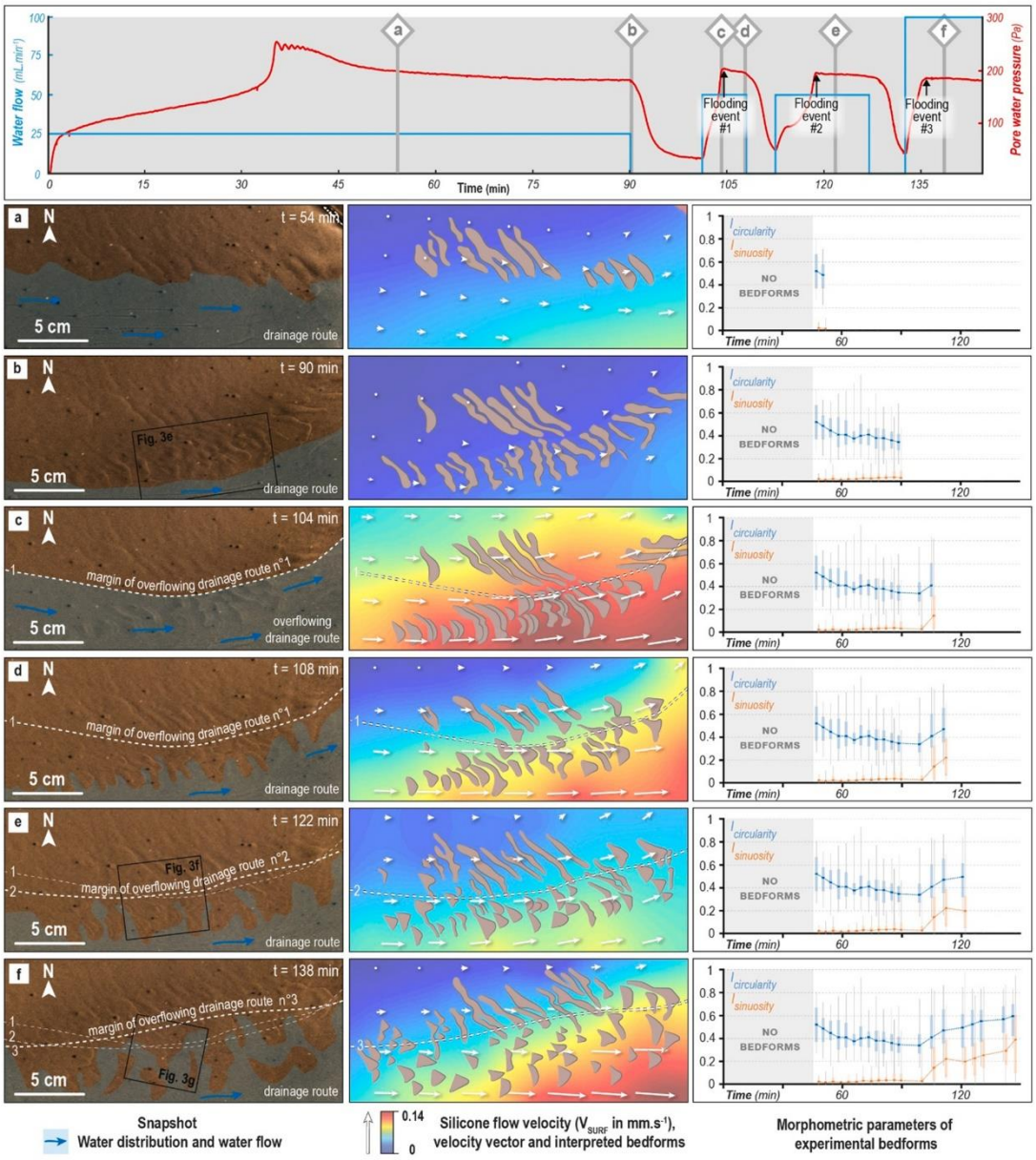

Fig. 10. Temporal evolution (*Stages a*, *b*, *c*, *d*, *e* and *f*) of the water drainage, the silicone flow dynamics and the bedform morphometry for an experiment comprising steady water input and then repeated flooding events (header graph). Upper graph shows evolution of water flow injected to the bed (blue line) and pore water pressure (red line) measured below the stream and close to the water injection. Labels (a) to (f) correspond to stages described in Section 3.2.

water pocket forms along the silicone-bed interface below the center of the cap. As the water pocket grows, reaching 25 to 30 cm in width, the pore water pressure increases below the water pocket. When the pore water pressure exceeds ~190 Pa, the water pocket migrates toward the margin of the silicone cap – forming a temporary hydraulically connected distributed drainage route (Lelandais et al., 2018; Lewington et al., 2020) – and finally drains outside the cap. From t = 35 min to t = 41 min, eight water pockets successively migrate and drain. Each drainage route produces a temporary corridor of fast-flowing silicone ($V_{surf} = 12 \times 10^{-2}$ mm·s^{-1}) forming a lobe at its front. After the pulsed drainage phase with repeated drainage events (t = 42 min), a persistent hydraulically connected distributed drainage route develops along the silicone-bed interface. Sustained and focused drainage triggers the formation of a persistent corridor of fast-flowing silicone and enhances the growth rate of the lobe. Beneath the lobe, the drainage route locally channelizes resulting in the formation of two drainage channels. The drainage route is widespread below the corridor of fast flowing silicone but some areas remain dewatered in the periphery of the drainage channels and outside the drainage route. Hereafter, we detail in six stages the evolution of basal hydrology, silicone flow velocity and

bedform morphometry along one of the dewatered areas located in the northern periphery of the drainage route (Fig. 9c–d).

3.2.1. Stage a (Fig. 10a)

As a result of water channelization below the lobe, the silicone cap starts to stabilize at low flow velocity above the drainage route (t = 54 min; V_{surf} = 5–6 × 10^{-2} mm·s^{-1}). Contemporaneously, north of the drainage route, a field of subsilicone bedforms develop transverse to the silicone flow (number of bedforms, n = 12). The bedforms comprise periodic ridges with a regular wavelength (median λ = 0.9 cm), a linear crest line (median I_{sin} = 0.01) and an ovoid to slightly elongated shape (median El = 2.2; median I_{circ} = 0.52). The shape and the periodic pattern of these subsilicone bedforms are equivalent to those of ribbed bedforms (Fig. 7a) experimentally reproduced by Vérité et al. (2021).

3.2.2. Stage b (Fig. 10b)

At the very end of the first period, when water flow is still low and continuous (t = 90 min; Q = 25 ml·min^{-1}), and as a result of the sustained channelization below the lobe, the flow velocity of the silicone cap is low and stable (V_{surf} = 2–3.5 × 10^{-2} mm·s^{-1}) over the narrowing drainage route. North of the drainage route, where the silicone-bed interface is coupled, newly-formed (n = 14) and previously-formed periodic bedforms (n = 12) display a slightly arcuate crest line, symmetrical upstream and downstream edge slopes, a regular wavelength (median λ = 0.9 cm) and an orientation transverse to the silicone flow direction. Just before the start of the flooding events, the bedforms are more elongated (median El = 4.4), less circular (median I_{circ} = 0.34), and slightly more sinuous (median I_{sin} = 0.04) than in *Stage a*, resulting in bedforms similar in appearance to ribbed bedforms (Figs. 3e, 7a).

3.2.3. Stage c (Fig. 10c)

After a 10 min period with no water injection during which the silicone cap stops flowing (V_{surf} = 0.2 × 10^{-2} mm·s^{-1}), a new injection phase starts at t = 100 min (Q = 50 ml·min^{-1}). A new water pocket forms along the silicone-bed interface below the center of the cap. The water pocket grows as the pore water pressure increases until it exceeds ~190 P at t = 104 min, at which point it migrates, overflows the pre-existing drainage route – flooding the majority of existing ribbed bedforms and increasing the flow velocity of the overlying silicone (V_{surf} = 14 × 10^{-2} mm·s^{-1}) – and finally drains outside the cap, producing flooding event #1 and lobe growth. Along the overflowing drainage route, erosion and deposition of sand grains by water flow are responsible for the formation of breaches fragmenting bedforms and sand deposition at the downstream foot of flooded or partially flooded ribbed bedforms. Compared with *Stage b*, the bedforms (n = 36) become, on average, more sinuous (median I_{sin} = 0.15), more circular (median I_{circ} = 0.41) but less elongate (median El = 3.7), preserving, in most cases, bedforms similar in appearance to sinuous ribbed bedforms. Existing ribbed bedforms outside the overflow route do not experience any shape modification.

3.2.4. Stages d to f (Fig. 10d–f)

After flooding events #1 (t = 104 min), #2 (t = 119 min) and #3 (t = 132 min), which follow a scenario similar to *Stage c*, the drainage route narrows and returns to its initial state: a hydraulically connected distributed drainage route with local areas of silicone-bed coupling. Corridors of fast flowing silicone that developed above the overflowing drainage route during repeated flooding events maintain high velocity (V_{surf} = 6–11 × 10^{-2} mm·s^{-1}). Along former overflowing drainage routes, where the silicone-bed interface is coupled, crest lines of previously flooded bedforms are stretched in the silicone flow direction and bedforms with an initial ribbed appearance (*Stage b*) record a progressive shape transformation that we describe hereafter.

After flooding event #1 (Fig. 10d), one or several parts of some ribbed bedform crest lines are stretched in the silicone flow direction: some parts display lobate crest lines and steep downstream edges, while other parts preserve a ribbed appearance with a linear to arcuate crest line transverse to the flow direction (Fig. 3f). Other bedforms and adjacent (formed during flooding events) stretched in the silicone flow direction produced lobate crest lines pointing downstream and steep downstream edges (Fig. 7b), similar to lobate-type murtoos described by Ojala et al. (2021). At this stage, experimental bedforms are on average more sinuous (median I_{sin} = 0.22), more circular (median I_{circ} = 0.46) and less elongated (median El = 3.4) compared to *Stage c* (Figs. 10d, 11). Bedforms located north of the margin of the overflowing drainage route #1 are not reshaped and preserve a ribbed appearance.

After flooding event #2 (Fig. 10e), bedforms continue to be partially to entirely stretched in the silicone flow direction, preserving steep downstream edges, inducing a continuous evolution from lobate to sub-triangular crest lines and typically dividing them in two smaller bedforms (Fig. 7b). Some minor transverse ridges exhibiting smaller dimensions (1.5 cm long, 0.3 cm wide) than non-flooded ribbed bedforms (5 cm long, 0.6 cm wide) are observed in place of stretched bedforms, suggesting they result from their fragmentation during the flood. After two flooding events, the bedforms are, on average, as sinuous (median I_{sin} = 0.21), more circular (median I_{circ} = 0.50) and less elongate (median El = 3.1) than those that experienced just one flood (Figs. 10e, 11).

After flooding event #3 (Fig. 10f), as a result of the continuous stretching of bedforms along the drainage route, bedforms are almost all characterized by a triangular shape with (i) a tip angle that points downstream and typically lies in between 55 and 75°, and (ii) steep downstream edges, suggesting an asymmetric longitudinal profile. These triangular bedforms sometimes overlap each other, exhibiting a chevron-like pattern (Fig. 3f). Their shape and spatial organization resemble those of murtoos described in Scandinavian glacial landsystems (Ojala et al., 2019) (Figs. 3d, 7c). Some ribbed bedforms with a partial lobate shape still occur along the margin of overflowing drainage route #3 (Figs. 3f, 7b). After three flooding events, bedforms are very sinuous (median I_{sin} = 0.40), with higher circularity (median I_{circ} = 0.60) and lower elongation (median El = 2.5) values compared with *Stages d* and *e* (Fig. 11).

To summarize, the repetition of flooding events and intermediate quiescent periods in response to fluctuating water flows triggers an increase in fragmentation and stretching of experimental ribbed bedforms, which successively evolve into transitional forms – such as ribbed bedforms with lobate parts, lobate and sub-triangular bedforms – in a process that finally produces murtoos. This evolution supports the hypothesis that the morphometric continuum described in Section 2.3.1 corresponds to a progressive increase in circularity and sinuosity of ribbed bedforms during successive flooding events (Fig. 11).

4. Discussion

4.1. A continuum between ribbed bedforms and murtoos along meltwater corridors: expression of flooding events

4.1.1. Morphometric comparison of experimental and natural bedforms

Experimental ribbed bedforms display an intermediate elongation (3–5) lying in between natural ribbed bedforms (elongation = 2.9; Stokes et al., 2016) and mega-scale transverse bedforms (elongation = 5.7; Greenwood and Kleman, 2010). Natural ribbed bedforms mapped in this study display lower elongation (2–3) than their experimental counterparts but correlate with the typical elongation of ribbed moraines mapped by Dunlop and Clark (2006; elongation = 2.5). The circularity (0.2–1) and sinuosity (0–0.1) of ribbed bedforms have similar values for natural and experimental forms (Fig. 7a). Morphometric data illustrate that experimental and natural murtoos both display high sinuosity (Fig. 7c; 0.7–1), high circularity (0.65–0.75) and low elongation values (1.3–1.7), which contrast sharply with the range of values characterizing ribbed bedforms (Fig. 7a).

Some transitional experimental bedforms, related to gradual transformation of ribbed bedforms into murtoos, are morphologically similar

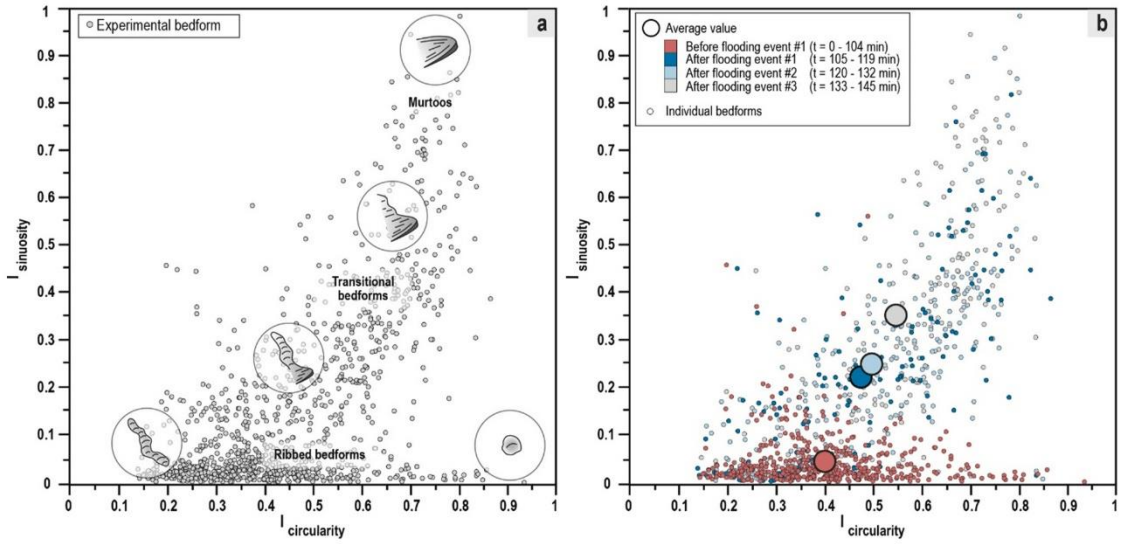

Fig. 11. Morphometric plot of experimental bedforms produced and modified under steady water flow input and then during three flooding events of varying durations and magnitudes. A morphometric continuum appears through time and with water input, with no gaps between ribbed bedforms, through transitional bedforms and into murtoos.

to some natural bedforms spatially associated with and morphologically intermediate between ribbed bedforms and murtoos in Scandinavia (Figs. 7b, 8, 11). Both natural and experimental bedforms show modified ribbed bedforms with lobate parts, or a lobate to sub-triangular shape (Fig. 3c, f). They commonly arise on the border of murtoo fields (Figs. 4c, 10d) and display sinuosity (0.2–0.7) and circularity (0.3–0.7) values intermediate between those of ribbed bedforms and murtoos (Fig. 7b). These bedforms have been either excluded from previous morphological studies since they only share some characteristics with murtoos (Mäkinen et al., 2017; Ojala et al., 2019), or for some of them, recently classified as murtoo-related ridges and lobate-type murtoos (Ojala et al., 2021). Considering the morphometric similarities between experimental and natural bedforms, these bedforms are therefore both referred to as transitional bedforms with morphological characteristics intermediate between ribbed bedforms and murtoos.

The morphometric comparison of natural and experimental ribbed bedforms, transitional bedforms and murtoos is here limited to three areas located in Finland and Sweden in which all these bedforms coexist. However, even though a correlation in the spatial distribution of ribbed bedforms and murtoos has been observed in several instances (Fig. 2a; Hättestrand and Kleman, 1999; Ojala et al., 2019), they do not always coexist along SIS beds (Peterson et al., 2017; Ahokangas et al., 2021). Further investigations of palaeo-glacial beds, in Scandinavia and North America (i.e. Laurentide Ice Sheet), are necessary to explore the spatial and genetic relationships between these bedforms, notably along meltwater corridors.

4.1.2. Origin of bedform continuum

The spatial association of murtoos with ribbed bedforms (Peterson et al., 2017; Mäkinen et al., 2017) and transitional bedforms including, overprinted ribbed bedforms (Ojala et al., 2019) and murtoo-related landforms (Ojala et al., 2021) has been reported along meltwater corridors in southern SIS areas. While no clear genetic relationships between these different bedforms have been established so far (Mäkinen et al., 2017; Ojala et al., 2019), we suggest that they form part of a same morphological and genetic continuum, with some implied commonality of processes. The distribution of values for elongation, sinuosity index and circularity index of both natural and experimental bedforms (Figs. 8, 11) indeed reveals a morphometric continuum between ribbed bedforms, transitional bedforms and murtoos. From the evolution of experimental bedforms, we reveal a genetic continuum between 'ribbed bedform' and 'murtoo' end members, which is materialized by the progressive remobilization of ribbed bedforms into partially remobilized ribbed bedforms (i.e., ribbed bedform with lobate parts), proto murtoos (i.e., lobate to sub-triangular bedform) and murtoos in an environment characterized by transient flooding events (Fig. 12a). Based on morphometrics and interpolation of the degree of remobilization (i.e., the magnitude of reshaping) of each experimental bedform at distinct stages, our experiments suggest that the degree of ribbed bedform remobilization depends on the number of (i) subsilicone floods and (ii) silicone-bed recoupling episodes experienced by any single bedform (Fig. 13).

Given the bedform continuum observed in nature is morphometrically identical to that observed in the experiments (Figs. 8, 11), we suggest that the processes responsible for the progressive transformation of ribbed bedforms into transitional forms and then into murtoos in the experiments are similar in nature (Fig. 12b). Indeed, as demonstrated in Vérité et al. (2021), the processes responsible for the formation of experimental ribbed bedforms are compatible with processes stated to explain the formation of natural ribbed bedforms despite the differences in bedform dimensions, scale of deformation processes and materials (cf. Section 3.1). In our experiments, some processes such as small-scale channelization and hydrofracturing are not simulated due to insufficient water pressure and homogeneous bed grain size. However, hydrological variations and processes of stretching, erosion and sedimentation are reproduced and responsible for the formation of transitional forms and murtoos, which correlates with processes already described by Mäkinen et al. (2017), Ojala et al. (2019) and Peterson Becher and Johnson (2021). Ribbed bedforms are part of this morphometric and genetic continuum only as a starting point representing an initial deformable and erodible sedimentary body later remobilized during flooding and recoupling. Thus, we suggest that the formation of murtoos through the continuous remobilization of ribbed bedforms along Scandinavian meltwater routes depends on the repetition of flooding events. These interpretations have strong implications for deciphering the physical mechanisms operating at the basal interface

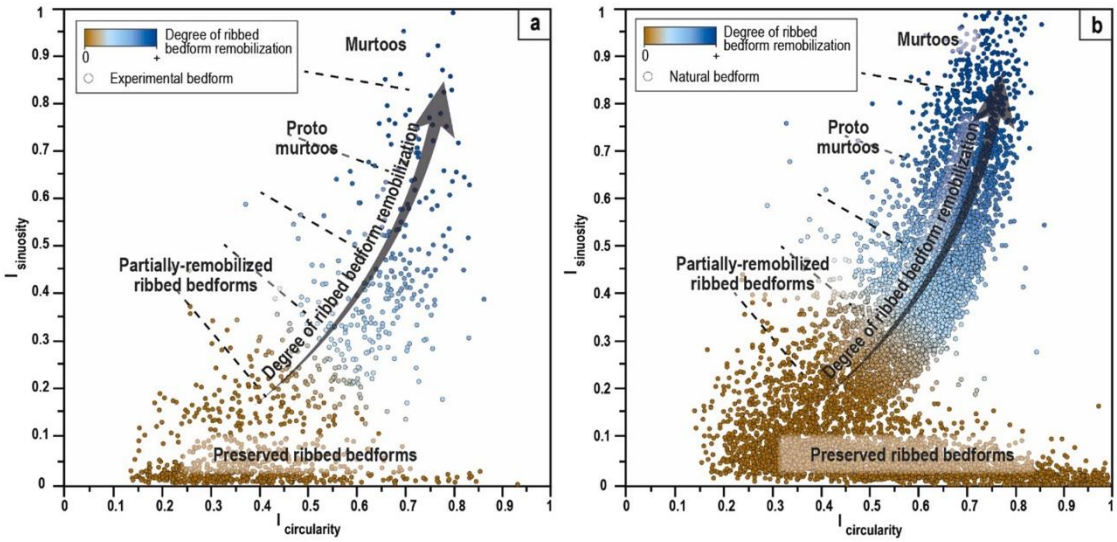

Fig. 12. Degree of experimental (a) and natural (b) ribbed bedform remobilization based on the continued increase in circularity and sinuosity indexes from typical ribbed bedforms to typical murtoos during repetitive flooding events.

and the meltwater drainage configurations during the formation of murtoos.

4.2. A model for the transformation of ribbed bedforms into murtoos along meltwater corridors

Based on the experimental observations, the mapping of Scandinavian ice sheet beds, the bedform continuum depicted in experiments and nature and the current knowledge regarding the sedimentology of murtoos (Peterson Becher and Johnson, 2021), we propose a model for the formation of murtoos along meltwater corridors.

4.2.1. Formation of ribbed bedforms (Fig. 14a)

A low and constant meltwater discharge at the bed is associated with the development of hydraulically poorly connected distributed drainage routes beneath warm-based ice (Greenwood et al., 2016), forming a mosaic of coupling and decoupling zones that can change and migrate through time. Subglacial drainage channels can possibly develop close to the ice sheet margin, where thinner ice inhibits creep closure and hydraulic gradients are steeper. In areas of ice-bed coupling, where the bed undergoes high basal shear stresses, periodic bedforms arise from the deformation of a flat bed (composed of subglacial traction till) sheared by the overlying ice (Lindén et al., 2008; Fowler and Chapwanya, 2014; Fannon et al., 2017; Vérité et al., 2021). Depending on their degree of development, the array of bedforms produced is distributed along a morphological continuum ranging from slightly elongated (i.e. circular) to elongated (i.e. slightly circular) ribbed bedforms (Fig. 12). Ribbed bedforms keep growing in dimensions by bed deformation as long as the meltwater flow is low and the ice sheet remains coupled to the crest lines of bedforms (Fig. 10a–b). Ribbed bedforms could be a prerequisite for the initiation of some murtoo fields, and this phase of ribbed bedform formation could occur anytime before the first flooding event.

4.2.2. Erosion and breaching of ribbed bedforms during flooding events (Fig. 14b)

Increase in the water discharge delivered to the bed of modern glaciers and ice sheets can occur in response to diurnal, seasonal and long-term thermic fluctuations, and to supraglacial or subglacial lake drainages, producing subglacial floods (Hubbard et al., 1995; Andrews et al., 2014; Rada and Schoof, 2018; Nanni et al., 2021; Smith et al., 2021). During subglacial floods (Fig. 10c), the preexisting hydraulically poorly connected distributed drainage route overflows and widens the drainage routeway to form a km-wide hydraulically-connected meltwater corridor (Lewington et al., 2020; Mejía et al., 2021). The incapacity of drainage channels to accommodate the sudden increase in water discharge results in widespread ice-bed decoupling, triggering a temporary increase in ice flow velocity and possible surges (Kamb, 1987; Dunse et al., 2015; Zheng et al., 2019). Ribbed bedforms are flooded leading to the erosion of their stoss-sides and locally to their sudden breaching (Fig. 4c). Erosion, transport and sorting of tills by meltwater are responsible for the re-deposition of sediments on the lee-side toe of ribbed bedforms (Figs. 4c, 10c). The erosion of ribbed bedforms is evidenced by their occasional disaggregated appearance, irregularities on their crest lines, their fragmentation related to breaching and their gentler stoss-side slopes (Fig. 6d).

4.2.3. Stretching of ribbed bedforms during reorganization of meltwater drainage (Fig. 14c)

When the flooding event ceases and as the subglacial drainage reorganizes, the basal meltwater pressure decreases and the ice flow velocity starts to decrease but remains higher than the initial conditions. The km-scale hydraulically well-connected drainage route is envisioned to be characterized by a series of minor meltwater channels (Fig. 4d), incising the bed in between bedforms and draining meltwater toward a major and sustained conduit (Lewington et al., 2020; Mejía et al., 2021). Within this hydraulically well-connected distributed drainage route, the fast-flowing ice recouples to the top of eroded ribbed bedforms and mounds of re-deposited sediments (Fig. 10d), transmitting high basal shear stresses to the bed accommodated by soft-bed deformation (Vérité et al., 2021). Depending on irregularities along their crest line and the subsequent degree of ice-bed coupling, the ice partially or entirely stretches ribbed bedforms and mounds of re-deposited sediments, forming partially remobilized ribbed bedforms and proto murtoos. The transformation produces more sinuous, more circular and less elongated, bedforms, which display steeper edges and develop a lobate tip pointing downstream. Where the ice recouples with the bed, lenses of water-sorted sediments are incorporated into the matrix of subglacial

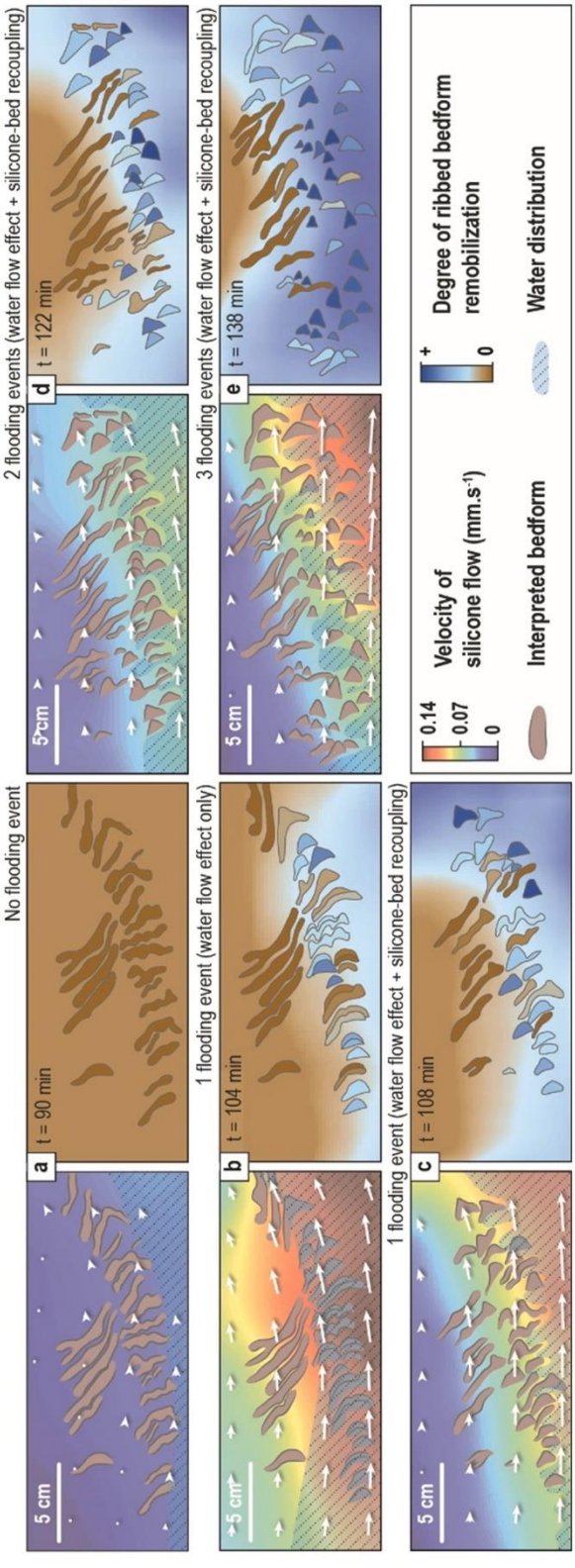

Fig. 13. Relationship between the degree of ribbed bedform remobilization (based on the sinuosity and circularity indexes of bedforms; on the right hand side of each panel), the silicone cap dynamics and the subsilicone hydrological system (on the left hand side) for experimental stages presented in Fig. 10.

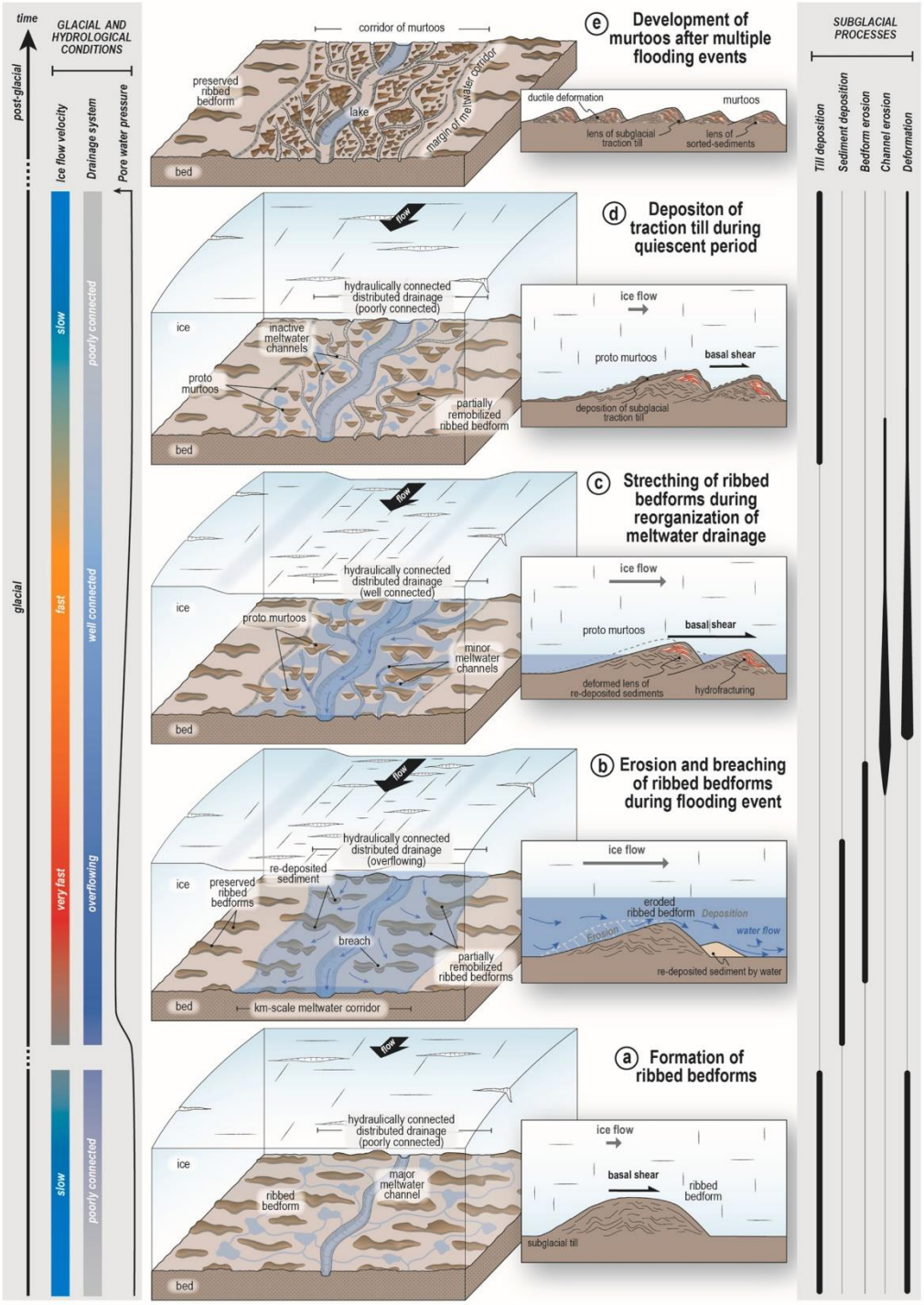

Fig. 14. Conceptual model for the formation of murtoos by repeated flooding of ribbed bedforms along subglacial meltwater corridors, based on our natural observations, experimental results, and sedimentological observations from Peterson Becher and Johnson (2021).

traction till, mainly through soft deformation processes. This correlates with the sedimentological observations in murtoo excavations by Peterson Becher and Johnson (2021) that show evidence of deformed silt-sand sediments in a till matrix. As the water pressure builds up in confined water-saturated bed, hydrofracturing develops along lithological interfaces between sorted sediments and subglacial traction till (Peterson Becher and Johnson, 2021).

4.2.4. Deposition of traction till during quiescent periods (Fig. 14d)

As the water discharge progressively decreases and channelization becomes more efficient along the hydraulically connected distributed drainage route, widespread ice-bed recoupling occurs, thus reducing the ice flow velocity (Andrews et al., 2014; Mejía et al., 2021; Smith et al., 2021). The meltwater drainage system, basal conditions and ice flow velocity returns to conditions that prevailed before the flooding event. In response to recoupling, a layer of subglacial traction till sustaining ductile bed deformation can accumulate on top of partially remobilized ribbed bedforms and proto murtoos (Peterson Becher and Johnson, 2021). Bedforms along the drainage route undergo little further shape transformation during this stage, probably because basal shear stress transmitted to the bed has decreased in response to a reduction in ice flow velocity.

4.2.5. Development of murtoos after multiple flooding events (Fig. 14e)

The ice sheet demise is associated with the production of large volumes of meltwater that is typically delivered to the bed and transferred subglacially through recurrent episodes of storage and drainage of supra/subglacial lakes (Greenwood et al., 2016). Variations in the meltwater discharge and possible flooding can also occur in response to shorter term temperature fluctuations (i.e., diurnal or seasonal) (Dunse et al., 2015; Smith et al., 2021). Whatever the frequency of meltwater discharge perturbations, the subglacial bed undergoes multiple alternations between (i) floods characterized by overflow of channels and/or the formation of hydraulically connected distributed drainage routes (Fig. 14b) and (ii) quiescent periods characterized by a return to hydraulically poorly connected distributed drainage (Fig. 14c–d). Repeated flooding and recoupling result in the progressive fragmentation, reshaping and stretching of ribbed bedforms along meltwater corridors, forming partially remobilized ribbed bedforms, proto murtoos and finally murtoos (Fig. 12). Apart from progressive bedform reshaping, Peterson Becher and Johnson (2021) demonstrated that repeated flooding and recoupling phases are recorded in the sedimentary core of murtoos where lenses of sorted-sediment are interbebbed with layers of subglacial traction till, both ductily deformed and hydrofractured. Through experimental modeling, we confirm conclusions based on geomorphological and sedimentological investigations by Mäkinen et al. (2017), Peterson et al. (2017), Ojala et al. (2019) and Peterson Becher and Johnson (2021) that murtoos most likely form within a subglacial environment characterized by a transient distributed drainage system focused in meltwater corridors.

Although the presence of ribbed bedforms is a pre-requisite for the formation of murtoos in this model, murtoo fields do not always co-occur with ribbed bedforms along SIS beds (Peterson et al., 2017; Ahokangas et al., 2021); this suggests murtoos may not necessarily form from the transformation of ribbed bedforms. Based on morphological characteristics and trench excavations, murtoos have been interpreted to form through alternating deformation of saturated-diamicton and the erosion and deposition of water-sorted sediments (Mäkinen et al., 2017; Peterson Becher and Johnson, 2021). These previous interpretations and the frequent absence of ribbed bedforms around murtoo fields might imply that any sedimentary mound, not necessarily a ribbed bedform, could be deformed and stretched to form murtoos. However, it is not known whether murtoos could develop from a flat subglacial bed. Although the proportion of murtoos mapped in association with ribbed bedforms appears to be minor, the multiphase character of the SIS and the tendency to overprint or erase older landforms makes it difficult to determine the true degree of their association. Ribbed bedforms are interpreted to form essentially under low ice flow velocity and basal meltwater flow (Shaw, 1979; Boulton, 1987; Hättestrand and Kleman, 1999; Lindén et al., 2008; Fowler and Chapwanya, 2014; Vérité et al., 2021). Murtoo and hummock tracts are interpreted to form during periods of deglaciation when the amount of subglacial meltwater flow increases (Peterson and Johnson, 2018; Ojala et al., 2019, 2021). As subglacial bedforms tend to be overprinted over time and ribbed bedforms tend to be remobilized into murtoos, we hypothesize that the "ribbed bedform" signal could be totally overprinted, thus underestimating the proportion of this murtoo/ribbed bedform spatial relationship.

4.3. Implications for the reconstruction of meltwater corridors

Using combined modeling and palaeo-glacial mapping, we demonstrate that reshaping of ribbed bedforms is linked to repeated changes in subglacial water flow implying that bedforms analysis can be used to better constrain the subglacial hydrological pattern.

Swedish and Finnish murtoos and proto murtoos analyzed in this study gather into elongated corridors (a few kilometer wide and several kilometers long on average) parallel to the ice flow direction within fields of ribbed bedforms. Murtoo fields are also intimately associated with either narrow (up to 50 m wide) or large (few hundreds of meters wide) meltwater channels, supporting a spatial association with meltwater corridors (Mäkinen et al., 2017; Peterson and Johnson, 2018; Ojala et al., 2021; Ahokangas et al., 2021). Along meltwater corridors, we also observe that major and minor meltwater channels seem to develop prior and contemporaneously to murtoos while eskers appear to form contemporaneously to or after murtoos (Figs. 5b, 6). Based on the transitory hydrological conditions experimentally simulated, the position of murtoo fields relative to SIS end moraine belts confirm they formed along meltwater corridors in relation to long-term perturbations in meltwater discharge during the Bølling-Allerød (14.7 ka) and the early Holocene warmings (11.7 ka) when the margins of the southern Swedish SIS termination and Finnish Lake District Ice Lobe respectively retreated (Punkari, 1980; Lundqvist, 1986; Hughes et al., 2016; Stroeven et al., 2016). These inferences imply that murtoos and the transitional forms located along meltwater corridors are attributed to deglaciation, since they are absent along the LGM margin of the SIS, and formed ubiquitously under ice streams, lobes or any front of the ice sheet. This timing relative to the formation of murtoo fields in Scandinavia is in agreement with previous conclusions made by Ojala et al. (2019) and Peterson Becher and Johnson (2021). Similarly to Peterson Becher and Johnson (2021) and Ojala et al. (2019), we demonstrate that the formation of murtoo fields and meltwater corridors is associated with periodic high meltwater discharge events. This periodicity, possibly related to diurnal, seasonal or long-term thermic fluctuations and the rapid drainage of supraglacially or subglacially stored water, is responsible for the variations in hydraulic connectivity of distributed drainage routes (Lewington et al., 2020; Ahokangas et al., 2021; Mejía et al., 2021), resulting in alternating quiescent periods and flooding events. Observations of minor meltwater channels developing along the edges of murtoos and proto murtoos, indicate that the chevron-like pattern of murtoos fields influences the geometry of the drainage system along meltwater corridors, which is neither purely distributed nor purely channelized as mentioned by Mäkinen et al. (2017) (Figs. 4d, 13c).

The morphological continuum observed along meltwater corridors suggests the progressive remobilization of ribbed bedforms into partially remobilized ribbed bedforms, proto murtoos and murtoos depends on the number (and probably the magnitude and duration) of flooding events experienced by ribbed bedforms (Fig. 12). Even though some murtoo fields strongly correlate with erosive corridors characterized by well-defined margins (Fig. 5c), the location of murtoo fields does not seem to be controlled by bed topography (Figs. 4–6) implying that

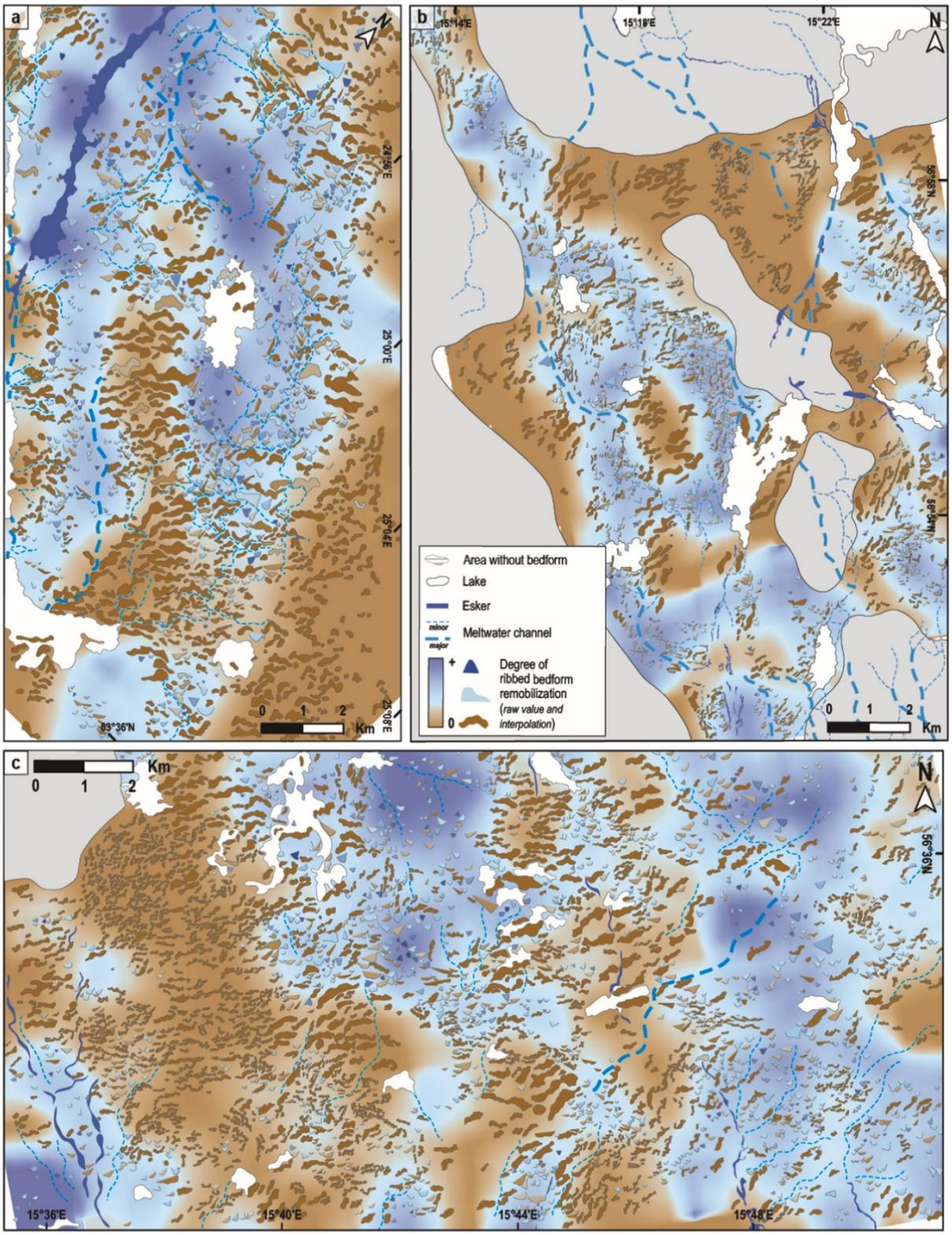

Fig. 15. Interpolation maps of the degree of natural ribbed bedform remobilization, based on the sinuosity index and circularity index values of bedforms along Finnish (a) and Swedish zones (b and c).

drainage routes during successive floods are potentially subject to lateral migration. We suggest that the borders of the hydraulically connected distributed drainage routes vary depending on the migration of the meltwater flood and water discharge (Rada and Schoof, 2018).

The number of flooding events that temporarily submerged each bedform along a single meltwater corridor can vary spatially, suggesting that bedforms can experience different stages of morphological evolution according to their positions. Considering the morphometry of experimental bedforms as a proxy for the number of floods recorded along meltwater corridors (Figs. 12–13), interpolation of the degree of

remobilization (i.e., degree of reshaping) of each bedform mapped in Scandinavia provides a proxy for (i) the position of meltwater corridors and (ii) the recurrence of floods along a single meltwater corridor (Fig. 14). Interpolation maps of the degree of ribbed bedform remobilization also highlight that meltwater corridors are locally slightly more sinuous (from 1.2 to 1.5) compared with the linearity of the ice flow direction (Fig. 14), even though they are relatively linear on the scale of an ice sheet (Peterson et al., 2017; Lewington et al., 2020). Meltwater corridors drawn by the interpolation of the degree of ribbed bedform remobilization are up to 10 km wide, display meandering to anastomosing patterns and longitudinally extend over at least several tens of kilometers across the entire study areas. These meltwater corridors, corresponding to fields of murtoos, proto murtoos and partially remobilized ribbed bedforms, are wider and longer than meltwater corridors reconstructed from murtoo fields only (Ojala et al., 2019, 2021; Ahokangas et al., 2021), revealing more continuous and more widespread meltwater drainage paths than expected (Fig. 15).

5. Conclusion

The combined mapping and modeling approaches in this study enabled the relationship between the evolution of subglacial bedforms and the dynamics of meltwater corridors to be explored. First, we revealed a morphological continuum between ribbed bedforms, transitional forms (i.e. partially remobilized ribbed bedforms and proto murtoos) and murtoos using new dimensionless morphometric parameters (circularity and sinuosity indexes). We demonstrated that bedforms, which have been variously described as ribbed bedforms cross-cut by murtoos (Ojala et al., 2019), murtoo-related bedforms and lobate murtoos (Ojala et al., 2021), are indeed transitional forms included in a continuous process of murtoo formation from the reshaping of preexisting ribbed bedforms. Second, we interpreted this bedform continuum as the expression of progressive remobilization of ribbed bedforms into murtoos, depending on the recurrence of flooding events that triggers repeated and transitory reorganization of the subglacial hydrological system along meltwater corridors. This dynamic subglacial water system includes alternating phases of (i) significant meltwater discharge, high hydraulic connectivity and ice-bed decoupling (leading to bedform erosion and sediment deposition) and (ii) limited meltwater flow, low hydraulic connectivity and ice-bed recoupling (leading to bedform stretching/deformation). The composite processes (erosion, deposition, deformation) recorded through this morphometric and genetic continuum contribute to better constrain the distribution, evolution and dynamics of meltwater corridors, which are critical for understanding the evolution of past and present day subglacial hydrological configurations and processes over centennial to millennial time-scales and spatially over 100 s of km.

Supplementary data to this article can be found online at https://doi.org/10.1016/j.geomorph.2022.108248.

Data availability

All datasets used in this paper are available from the corresponding author on request.

Declaration of competing interest

The authors declare that they have no conflict of interest.

Acknowledgment

This study is part of the Ice-Collapse project (The dynamics of ice sheet collapse in deglaciation periods) funded by the French Agence Nationale de la Recherche through grant ANR-18-CE01-0009. This project has benefited from the PALGLAC team of researchers and received funding from the European Research Council (ERC) to Chris Clark under the European Union's Horizon 2020 - Research and Innovation Framework Programme (grant agreement no. 787263). We thank Mark Johnson and Ivar Benediktsson for their constructive comments that helped to improve the manuscript.

References

Ahokangas, E., Ojala, A.E., Tuunainen, A., Valkama, M., Palmu, J.P., Kajuutti, K., Mäkinen, J., 2021. The distribution of glacial meltwater routes and associated murtoo fields in Finland. Geomorphology 389, 107854.
Anandakrishnan, S., Alley, R.B., 1997. Stagnation of ice stream C, West Antarctica by water piracy. Geophys. Res. Lett. 24 (3), 265–268.
Andrews, L.C., Catania, G.A., Hoffman, M.J., Gulley, J.D., Lüthi, M.P., Ryser, C., Hawley, R.L., Neumann, T.A., 2014. Direct observations of evolving subglacial drainage beneath the Greenland Ice Sheet. Nature 514 (7520), 80–83.
Bell, R.E., Studinger, M., Shuman, C.A., Fahnestock, M.A., Joughin, I., 2007. Large subglacial lakes in East Antarctica at the onset of fast-flowing ice streams. Nature 445 (7130), 904–907.
Boulton, G.S., 1987. A theory of drumlin formation by subglacial sediment deformation. In: Menzies, In J., Rose, J. (Eds.), Drumlin Symposium. Balkema, Rotterdam, pp. 28–80.
Burgess, D.O., Shaw, J., Eyton, J.R., 2003. Morphometric comparisons between Rogen terrain and hummocky terrain. Phys. Geogr. 24 (4), 319–336.
Cofaigh, C.Ó., 1996. Tunnel valley genesis. Prog. Phys. Geogr. 20 (1), 1–19.
Coughlan, M., Tóth, Z., Van Landeghem, K.J., Mccarron, S., Wheeler, A.J., 2020. Formational history of the Wicklow Trough: a marine-transgressed tunnel valley revealing ice flow velocity and retreat rates for the largest ice stream draining the late-Devensian British-Irish Ice Sheet. J. Quat. Sci. 35 (7), 907–919.
Dunlop, P., Clark, C.D., 2006. The morphological characteristics of ribbed moraine. Quat. Sci. Rev. 25 (13–14), 1668–1691.
Dunse, T., Schellenberger, T., Hagen, J.O., Kääb, A., Schuler, T.V., Reijmer, C.H., 2015. Glacier-surge mechanisms promoted by a hydro-thermodynamic feedback to summer melt. Cryosphere 9 (1), 197–215.
Ely, J.C., Clark, C.D., Spagnolo, M., Stokes, C.R., Greenwood, S.L., Hughes, A.L., Hess, D., 2016. Do subglacial bedforms comprise a size and shape continuum? Geomorphology 257, 108–119.
Evans, D.J.A., Phillips, E.R., Hiemstra, J.F., Auton, C.A., 2006. Subglacial till: formation, sedimentary characteristics and classification. Earth Sci. Rev. 78 (1–2), 115–176.
Fannon, J.S., Fowler, A.C., Moyles, I.R., 2017. Numerical simulations of drumlin formation. Proc. R. Soc. London, Ser. A 473 (2204), 20170220.
Fowler, A.C., Chapwanya, M., 2014. An instability theory for the formation of ribbed moraine, drumlins and mega-scale glacial lineations. Proc. R. Soc. London, Ser. A 470 (2171), 20140185.
Fried, M.J., Carroll, D., Catania, G.A., Sutherland, D.A., Stearns, L.A., Shroyer, E.L., Nash, J.D., 2019. Distinct frontal ablation processes drive heterogeneous submarine terminus morphology. Geophys. Res. Lett. 46 (21), 12083–12091.
Greenwood, S.L., Clark, C.D., 2008. Subglacial bedforms of the Irish ice sheet. J. Maps 4 (1), 332–357.
Greenwood, S.L., Kleman, J., 2010. Glacial landforms of extreme size in the Keewatin sector of the Laurentide Ice Sheet. Quat. Sci. Rev. 29 (15–16), 1894–1910.
Greenwood, S.L., Clason, C.C., Helanow, C., Margold, M., 2016. Theoretical, contemporary observational and palaeo-perspectives on ice sheet hydrology: processes and products. Earth Sci. Rev. 155, 1–27.
Hättestrand, C., 1997. Ribbed moraines in Sweden—distribution pattern and palaeoglaciological implications. Sediment. Geol. 111 (1–4), 41–56.
Hättestrand, C., Kleman, J., 1999. Ribbed moraine formation. Quat. Sci. Rev. 18 (1), 43–61.
Hiller, J.K., Smith, M., 2008. Residual relief separation: digital elevation model enhancement for geomorphological mapping. Earth Surf. Process. Landf. 33 (14), 2266–2276.
Hubbard, B.P., Sharp, M.J., Willis, I.C., Nielsen, M., Smart, C.C., 1995. Borehole water-level variations and the structure of the subglacial hydrological system of Haut Glacier d'Arolla, Valais, Switzerland. J. Glaciol. 41 (139), 572–583.
Hughes, O.L., 1964. Surficial geology, Nichicun-Kaniapiskau map area, Quebec. Geol. Surv. Can. Bull. 106, 18 pp.
Hughes, A.L., Gyllencreutz, R., Lohne, Ø.S., Mangerud, J., Svendsen, J.I., 2016. The last Eurasian ice sheets–a chronological database and time-slice reconstruction, DATED-1. Boreas 45 (1), 1–45.
Iken, A., Bindschadler, R.A., 1986. Combined measurements of subglacial water pressure and surface velocity of Findelengletscher, Switzerland: conclusions about drainage system and sliding mechanism. J. Glaciol. 32 (110), 101–119.
Irvine-Fynn, T.D., Hodson, A.J., Moorman, B.J., Vatne, G., Hubbard, A.L., 2011. Polythermal glacier hydrology: a review. Rev. Geophys. 49 (4).
Kamb, B., 1987. Glacier surge mechanism based on linked cavity configuration of the basal water conduit system. J. Geophys. Res. Solid Earth 92 (B9), 9083–9100.
Kleman, J., Hättestrand, C., 1999. Frozen-bed Fennoscandian and Laurentide ice sheets during the last Glacial Maximum. Nature 402 (6757), 63–66.
Koistinen, T., Stephens, M.B., Bogatchev, V., Nordgulen, Ø., Wennerström, M., Korhonen, J., 2001. Geological map of the Fennoscandian Shield 1: 2 000 000. Espoo: Geological Survey of Finland, Trondheim: Geological Survey of Norway, Uppsala: Geological Survey of Sweden, Moscow: Ministry of Natural Resources of Russia.

Lelandais, T., Mourgues, R., Ravier, É., Pochat, S., Strzerzynski, P., Bourgeois, O., 2016. Experimental modeling of pressurized subglacial water flow: implications for tunnel valley formation. J. Geophys. Res. Earth Surf. 121 (11), 2022–2041.
Lelandais, T., Ravier, É., Pochat, S., Bourgeois, O., Clark, C., Mourgues, R., Strzerzynski, P., 2018. Modelled subglacial floods and tunnel valleys control the life cycle of transitory ice streams. Cryosphere 12 (8), 2759–2772.
Lewington, E.L., Livingstone, S.J., Sole, A.J., Clark, C.D., Ng, F.S., 2019. An automated method for mapping geomorphological expressions of former subglacial meltwater pathways (hummock corridors) from high resolution digital elevation data. Geomorphology 339, 70–86.
Lewington, E.L., Livingstone, S.J., Clark, C.D., Sole, A.J., Storrar, R.D., 2020. A model for interaction between conduits and surrounding hydraulically connected distributed drainage based on geomorphological evidence from Keewatin, Canada. Cryosphere 14 (9), 2949–2976.
Lindén, M., Möller, P., Adrielsson, L., 2008. Ribbed moraine formed by subglacial folding, thrust stacking and lee-side cavity infill. Boreas 37 (1), 102–131.
Lundqvist, J., 1969. In: Problems of the So-called Rogen Moraine. Svensk reproduktions AB (distr.), pp. 1–32.
Lundqvist, J., 1986. Late Weichselian glaciation and deglaciation in Scandinavia. Quat. Sci. Rev. 5, 269–292.
Lundqvist, J., 1989. Rogen (ribbed) moraine—identification and possible origin. Sediment. Geol. 62 (2–4), 281–292.
Lundqvist, J., Wohlfarth, B., 2000. Timing and east–west correlation of south swedish ice marginal lines during the late Weichselian. Quat. Sci. Rev. 20 (10), 1127–1148.
Mäkinen, J., Kajuutti, K., Palmu, J.P., Ojala, A., Ahokangas, E., 2017. Triangular-shaped landforms reveal subglacial drainage routes in SW Finland. Quat. Sci. Rev. 164, 37–53.
Mejía, J.Z., Gulley, J.D., Trunz, C., Covington, M.D., Bartholomaus, T.C., Xie, S., Dixon, T., 2021. Isolated cavities dominate Greenland Ice Sheet dynamic response to lake drainage. Geophys. Res. Lett. 48 (19), e2021GL094762.
Möller, P., Dowling, T.P., 2015. The importance of thermal boundary transitions on glacial geomorphology; mapping of ribbed/hummocky moraine and streamlined terrain from LiDAR, over Småland, South Sweden. Gff 137 (4), 252–283.
Moon, T., Joughin, I., Smith, B., Van Den Broeke, M.R., Van De Berg, W.J., Noël, B., Usher, M., 2014. Distinct patterns of seasonal Greenland glacier velocity. Geophys. Res. Lett. 41 (20), 7209–7216.
Nanni, U., Gimbert, F., Roux, P., Lecointre, A., 2021. Observing the subglacial hydrology network and its dynamics with a dense seismic array. Proc. Natl. Acad. Sci. 118 (28).
Ojala, A.E., Peterson, G., Mäkinen, J., Johnson, M.D., Kajuutti, K., Palmu, J.P., Ahokangas, E., Öhrling, C., 2019. Ice-sheet scale distribution and morphometry of triangular-shaped hummocks (murtoos): a subglacial landform produced during rapid retreat of the Scandinavian Ice Sheet. Ann. Glaciol. 60 (80), 115–126.
O'connor, J.E., Baker, V.R., Waitt, R.B., Smith, L.N., Cannon, C.M., George, D.L., Denlinger, R.P., 2020. The Missoula and Bonneville floods—a review of ice-age megafloods in the Columbia River basin. Earth Sci. Rev. 208, 103181.
Ojala, A.E., Mäkinen, J., Ahokangas, E., Kajuutti, K., Valkama, M., Tuunainen, A., Palmu, J.P., 2021. Diversity of murtoos and murtoo-related subglacial landforms in the finnish area of the Fennoscandian Ice Sheet. Boreas 50 (4), 1095–1115.
Paola, C., Straub, K., Mohrig, D., Reinhardt, L., 2009. The "unreasonable effectiveness" of stratigraphic and geomorphic experiments. Earth Sci. Rev. 97 (1–4), 1–43.
Peterson, G., Johnson, M.D., 2018. Hummock corridors in the south-central sector of the Fennoscandian ice sheet, morphometry and pattern. Earth Surf. Process. Landf. 43 (4), 919–929.
Peterson, G., Johnson, M.D., Smith, C.A., 2017. Glacial geomorphology of the south Swedish uplands–focus on the spatial distribution of hummock tracts. J. Maps 13 (2), 534–544.
Peterson Becher, G.P., Johnson, M.D., 2021. Sedimentology and internal structure of murtoos-V-shaped landforms indicative of a dynamic subglacial hydrological system. Geomorphology 380, 107644.
Punkari, M., 1980. The ice lobes of the scandinavian ice sheet during the deglaciation in Finland. Boreas 9 (4), 307–310.
Rada, C., Schoof, C., 2018. Channelized, distributed, and disconnected: subglacial drainage under a valley glacier in the Yukon. Cryosphere 12 (8), 2609–2636.
Rampton, V.N., 2000. Large-scale effects of subglacial meltwater flow in the southern Slave Province, Northwest Territories, Canada. Can. J. Earth Sci. 37 (1), 81–93.
Schroeder, D.M., Blankenship, D.D., Young, D.A., 2013. Evidence for a water system transition beneath Thwaites Glacier, West Antarctica. Proc. Natl. Acad. Sci. 110 (30), 12225–12228.
Sharpe, D.R., Lesemann, J.E., Knight, R.D., Kjarsgaard, B.A., 2021. Regional stagnation of the western Keewatin ice sheet and the significance of meltwater corridors and eskers, northern Canada. Can. J. Earth Sci. 99 (999), 1–22.
Shaw, J., 1979. Genesis of the Sveg tills and Rogen moraines of Central Sweden: a model of basal melt out. Boreas 8 (4), 409–426.
Shaw, J., 2002. The meltwater hypothesis for subglacial bedforms. Quat. Int. 90 (1), 5–22.
Simkins, L.M., Anderson, J.B., Greenwood, S.L., Gonnermann, H.M., Prothro, L.O., Halberstadt, A.R.W., DeConto, R.M., 2017. Anatomy of a meltwater drainage system beneath the ancestral East Antarctic ice sheet. Nat. Geosci. 10 (9), 691–697.
Slater, D.A., Nienow, P.W., Cowton, T.R., Goldberg, D.N., Sole, A.J., 2015. Effect of near-terminus subglacial hydrology on tidewater glacier submarine melt rates. Geophys. Res. Lett. 42 (8), 2861–2868.
Smith, L.C., Andrews, L.C., Pitcher, L.H., Overstreet, B.T., Rennermalm, Å.K., Cooper, M. G., Cooley, S.W., Ryan, J.C., Miège, C., Kershner, C., Simpson, C.E., 2021. Supraglacial river forcing of subglacial water storage and diurnal ice sheet motion. Geophys. Res. Lett. 48 (7), e2020GL091418.
Smith-Johnsen, S., Fleurian, B.D., Schlegel, N., Seroussi, H., Nisancioglu, K., 2020. Exceptionally high heat flux needed to sustain the Northeast Greenland Ice Stream. Cryosphere 14 (3), 841–854.
St-Onge, D.A., 1984. Surficial deposits of the Redrock Lake area, District of Mackenzie. In: Current Research, Part A; Geological Survey of Canada, Paper, pp. 271–276.
Stokes, C.R., Margold, M., Creyts, T.T., 2016. Ribbed bedforms on palaeo-ice stream beds resemble regular patterns of basal shear stress ('traction ribs') inferred from modern ice streams. J. Glaciol. 62 (234), 696–713.
Storrar, R.D., Livingstone, S.J., 2017. Glacial geomorphology of the northern Kivalliq region, Nunavut, Canada, with an emphasis on meltwater drainage systems. J. Maps 13 (2), 153–164.
Stroeven, A.P., Hättestrand, C., Kleman, J., Heyman, J., Fabel, D., Fredin, O., Goodfellow, B.W., Harbor, J.M., Jansen, J.D., Olsen, L., Caffee, M.W., 2016. Deglaciation of fennoscandia. Quat. Sci. Rev. 147, 91–121.
Utting, D.J., Ward, B.C., Little, E.C., 2009. Genesis of hummocks in glaciofluvial corridors near the Keewatin Ice Divide, Canada. Boreas 38 (3), 471–481.
Vérité, J., Ravier, É., Bourgeois, O., Pochat, S., Lelandais, T., Mourgues, R., Clark, C.D., Bessin, P., Peigné, D., Atkinson, N., 2021. Formation of ribbed bedforms below shear margins and lobes of palaeo-ice streams. Cryosphere 15 (6), 2889–2916.
Williams, J.J., Gourmelen, N., Nienow, P., 2020. Dynamic response of the Greenland ice sheet to recent cooling. Sci. Rep. 10 (1), 1–11.
Zheng, W., Pritchard, M.E., Willis, M.J., Stearns, L.A., 2019. The possible transition from glacial surge to ice stream on Vavilov ice cap. Geophys. Res. Lett. 46 (23), 13892–13902.

Partie B. Un modèle d'évolution des bedforms observés le long des corridors d'eau de fonte sous-glaciaires basé sur les variations de couplage glace-eau-sédiments

---

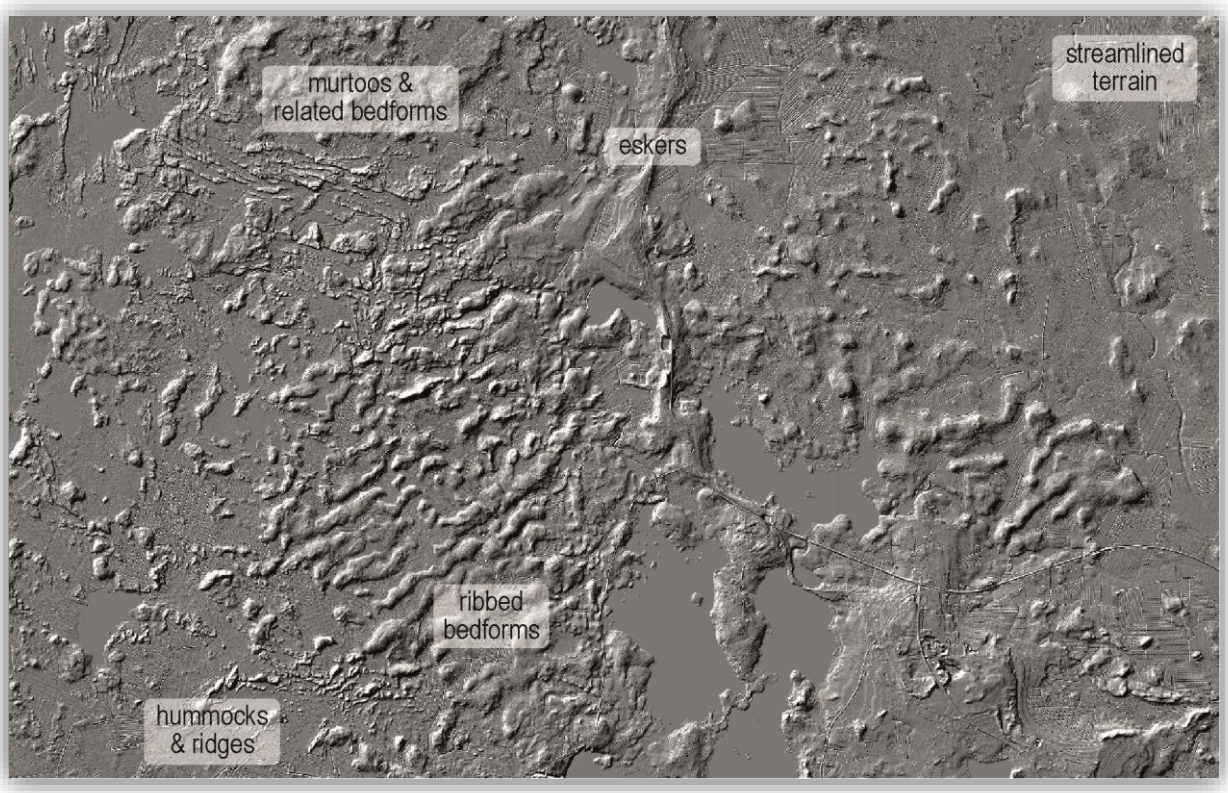

Diversity of subglacial bedforms and landforms found in relationships along subglacial meltwater corridors, Finland (24°55'N – 63°23'E)

1. Introduction

Par opposition aux eskers et chenaux sous-glaciaires largement observés le long des paléo-lits glaciaires et matérialisant d'anciennes entités de drainage chenalisées, les corridors d'eau de fonte sous-glaciaires ('*subglacial meltwater corridors'*) constituent les reliques de paléo-systèmes de drainage sous-glaciaires composites (chenalisés et distribués) et de plus grande échelle (e.g. ***St Onge, 1984 ; Rampton, 2000 ; Utting et al., 2009 ; Ahokangas et al., 2021***). La distribution de ces corridors – mesurant plusieurs 100^{nes}-1000^{s} m de large et jusqu'à plusieurs 100^{nes} de km de long – est corrélée avec la position de réseaux d'esker, formant des motifs radiaux divergeant depuis les paléo-dômes de glace (e.g. ***Peterson et al., 2017 ; Lewington et al., 2020 ; Dewald et al., 2022***).

Dans la littérature, ces corridors d'eau de fonte sous-glaciaires ont été interprétés comme les reliques morphologiques de routes de drainage hydrauliquement connectées. Les types de systèmes de drainage (chenaux, conduits, cavités, films d'eau et écoulement poral) constituant ces routes ainsi que les processus de remobilisation de sédiments (érosion, dépôt, déformation) sont contrôlés par les variations de spatio-temporelles de pression d'eau basale (e.g. ***Rada & Schoof, 2018 ; Davison et al., 2019 ; Lewington et al., 2020***), notamment en raison des variations diurnes à saisonnières de l'apport d'eau de fonte d'origine supra-glaciaire (***Hubbard et al., 1995 ; Andrews et al., 2014 ; Smith et al., 2021***).

Ces corridors d'eau de fonte sous-glaciaires ont été historiquement décrits grâce à l'identification de hummocks (***St-Onge, 1984; Ward, 1997; Rampton, 2000; Utting et al., 2009; Dahlgren, 2013; Haiblen, 2017***) puis de murtoos (***Mäkinen et al., 2017; Peterson et al., 2017; Ojala et al., 2019, 2021; Ahokangas et al., 2021; Becher Peterson & Johnson, 2021***) (Chapitre I – Partie B §2). En revanche, une variété d'autres bedforms ont depuis été décrits comme associés aux hummocks (i.e. petites rides sédimentaires transverses ou obliques) (e.g. ***St-Onge, 1984 ; Rampton, 2000***) et aux murtoos (i.e. murtoos lobées ou en chevron, escarpements et rides sédimentaires obliques) (e.g. ***Ojala et al., 2021***). Des corridors de ribbed bedforms associés à des eskers et observés en amont ou en aval de corridors de hummocks ont également été associés à ces corridors d'eau de fonte sous-glaciaires (***Lewington, 2020***).

Le Chapitre IV – Partie A a permis de démontrer l'existence d'un continuum morphologique et génétique expliquant la diversité de forme, la formation et l'évolution des '*murtoo-related bedforms*' et

des murtoos par la répétition de cycles de couplage/découplage contrôlé par les fluctuations de la circulation d'eau de fonte le long des routes de drainage sous-glaciaires. Cependant, aucune étude n'a à ce jour mis en relation la diversité de formes et de processus de formation de l'intégralité des bedforms et landforms observés le long de ces routes de drainage.

Problématiques :

→ Quelle diversité d'assemblages morphologiques existe-t-il le long des corridors d'eau de fonte sous-glaciaire ?

→ Comment ces différents assemblages morphologiques permettent-ils de caractériser les processus de remobilisation de sédiments, les interactions glace-eau-sédiments et les variations de circulation d'eau de fonte de fonte le long des routes de drainage sous-glaciaires ?

→ Est-il possible de construire un modèle d'évolution (i.e. continuum génétique) permettant de relier la diversité morphologique observé le long des corridors d'eau de fonte à la dynamique spatio-temporelle d'écoulement de l'eau de fonte au sein des routes de drainage ?

2. Article n°5: Variable ice-water-sediment coupling provides unifying explanation for diverse landforms in subglacial meltwater corridors

Cette deuxième partie fait donc l'objet d'un article soumis à la revue *Earth Surface Processes and Landforms*.

Cet article a été réalisé en collaboration avec d'autres chercheurs de l'Université de Sheffield (UK) et du Service Géologique du Canada, dont Stephen J. Livingston qui est l'auteur principal de l'article. J'ai collaboré à cet article en tant que 2nd auteur en participant à (1) l'identification et la description des bedforms et landforms, (2) la production des figures, (3) la conceptualisation du modèle de continuum génétique et (4) l'apport de contributions et de corrections lors de l'écriture de l'article.

Variable ice-water-sediment coupling provides unifying explanation for diverse landforms in subglacial meltwater corridors

Livingstone, S.J.[1], Vérité, J.[2], Ravier, E.[2], McMartin, I.[3], Campbell, J.[3], Lewington, E.L.M.[1], Dewald, N.[1], Clark, C.D.[1], Sole, A.J.[1], Storrar, R.D.[4]

[1] Department of Geography, University of Sheffield, Sheffield, UK
[2] Laboratoire de Planétologie et Géosciences, UMR 6112, CNRS, Le Mans Université, Avenue Olivier Messiaen, 72 085 Le Mans CEDEX 9, France
[3] Geological Survey of Canada, Natural Resources Canada, Ottawa, ON, Canada
[4] Department of the Natural and Built Environment, Sheffield Hallam University, Sheffield, UK

Corresponding author email: s.j.livingstone@sheffield.ac.uk

Keywords: subglacial meltwater corridors; subglacial hydrology; meltwater channels; subglacial bedforms; eskers

Abstract

Subglacial meltwater landforms found on the beds of former ice sheets allow the properties of meltwater drainage to be reconstructed, informing our understanding of modern day subglacial hydrological processes. In northern Canada and Fennoscandia, subglacial meltwater landforms are organised into continental-scale networks, often comprising broad (100s to 1000s m wide) corridors incorporating a diverse range of depositional and erosional landforms. We combine high-resolution (2 m) digital elevation models and field-based observations to describe the diverse morphologies of subglacial meltwater landform assemblages (tracts) within these corridors. This includes tracts of hummocks and ridges, murtoos, ribs and streamlined bedforms, and eskers and channels, which together are interpreted to reflect time-transgressive formation in response to variations in ice-water-sediment coupling. Specifically, we suggest that meltwater tends to organise down subglacial meltwater corridors (SMC), which represent the hydraulically-connected parts of the subglacial drainage system that undergo large variations in meltwater input, effective pressure and drainage efficiency. When the hydraulic capacity of the subglacial drainage system is overwhelmed, flooding the bed, fluvial erosion and deposition will dominate in the SMC, resulting in tracts of hummocks and ridges produced by fragmentation of underlying bedforms, creating geometric patterns, and downstream deposition of the sediment in basal cavities and crevasses. Re-coupling of ice with the bed when melt supply decreases facilitates deformation, transforming existing landforms and producing new bedforms concomitant with the wider subglacial bedform imprint. Switches in the relative importance of ice-water-sediment

coupling in response to fluctuating meltwater supply explains a continuum of morphologies associated with the formation, transformation and fragmentation of bedforms, including the formation of murtoos and subglacial bedform tracts. Eskers are interpreted to record the final phase of deposition in a conduit close to or at the ice margin.

1. Introduction

The configuration and evolution of meltwater drainage under ice sheets is a key control on ice flow (***Anandakrishnan & Alley, 1997; Bartholomew et al., 2010; Andrews et al., 2014; Williams et al., 2020; Smith et al., 2021***), erosion (***Cowton et al., 2012; Overeem et al., 2017; Alley et al., 2019; Cook et al., 2020***), sedimentation (***Simkins et al., 2016; Bendixen et al., 2017***) and frontal ablation at water-terminating margins (***Jenkins et al., 2011; Fried et al., 2015; Slater et al., 2015; Bunce et al., 2020***). Understanding how subglacial drainage systems evolve under changing climate conditions is therefore paramount to studies trying to model the future of present-day ice sheets, climate and the Earth's system as a whole. However, direct observations of the subglacial drainage system under present-day ice sheets remain challenging for obvious reasons. Meltwater landforms preserved in glaciated landscapes allow the properties of subglacial meltwater drainage to be reconstructed, typically over centennial to millennial time-scales and spatially over hundreds of kilometres. They therefore have enormous potential for informing our understanding of modern day subglacial hydrological configurations and processes (***Greenwood et al., 2016***).

One of the most obvious geomorphological expressions of former subglacial drainage systems are subglacial meltwater corridors (SMC). SMC, also termed hummock corridors, glaciofluvial corridors and washed zones, are hundreds of metres to several kilometres wide and up to hundreds of kilometres long tracts with diverse forms ranging from incised till and rock surfaces to subglacial and glaciofluvial landforms ***(St-Onge, 1984; Dredge et al., 1985; Ward et al., 1997; Rampton, 2000; Utting et al., 2009; Burke et al., 2012; Kerr et al., 2014a, b; McMartin et al., 2015a, 2021; Sharpe et al., 2017, 2021; Storrar & Livingstone, 2017; Peterson et al., 2017, 2018; Peterson & Johnson, 2018; Ojala et al., 2019; Lewington et al., 2019, 2020; Campbell et al., 2020; Ahokangas et al., 2021; Vérité et al., 2022***). Corridors can cut down into the bed (sediment and/or bedrock) forming negative expressions or can

form positive-relief features comprising tracts of glaciofluvial sediments (***Lewington et al., 2020***), with the latter more common in areas of thin sediment cover (***Peterson et al., 2017; Peterson & Johnson, 2018***). Holistic mapping of meltwater traces from high resolution (1-2 m) digital elevation models (e.g., ArcticDEM) has revealed SMC to be widespread beneath the former Laurentide and Fennoscandian ice sheets (**Fig. 1**) (***Peterson et al., 2017; Lewington et al., 2020; McMartin et al., 2021; Ahokangas et al., 2021; Dewald et al. 2022***). The large-scale distribution of SMC largely mirrors and extends that of eskers forming networks roughly parallel to ice flow that radiate out from former ice divides (**Fig. 1**).

The formation of SMC has been attributed to subglacial meltwater drainage (e.g., ***Rampton, 2000; Utting et al., 2009; Burke et al., 2012***). Building on earlier work, ***Lewington et al. (2020)*** propose that meltwater corridors are the imprint of hydraulically-connected distributed subglacial drainage (***Iken & Bindschadler, 1986; Andrews et al., 2014; Rada and Schoof, 2018; Davison et al., 2019***), with the style of drainage and resultant geomorphic processes (erosion and/or deposition) driven by spatial and temporal variations in basal water pressure (see also ***Ojala et al., 2021***). A variant of this hypothesis is that the corridors represent focused synchronous drainage following a sheet flood from a subglacial water body (***Sharpe et al., 2017, 2021***).

SMC are typically identified and mapped from their rough, 'hummocky' texture that distinguishes them from intervening smoother till sheets and glacially-produced ice flow bedforms (e.g., ***Utting et al., 2009; Peterson & Johnson, 2018; Lewington et al., 2019***). However, this definition encompasses a wide range of depositional and erosional landforms identified from detailed morphological and sediment studies, including hummocks of various shapes and sizes, ridges, gravel bars, eskers and scoured bedrock (***St-Onge, 1984; Rampton, 2000; Utting et al., 2009; Haiblen, 2017; Peterson & Johnson, 2018; Sharpe et al., 2017, 2021***). SMC have also been associated with murtoos and murtoo-related bedforms (***Mäkinen et al., 2017; Peterson et al., 2017; Ojala et al., 2019, 2021; Ahokangas et al., 2021; Becher Peterson & Johnson, 2021; Vérité et al., 2022***) and subglacial bedforms such as ribbed moraine tracts (***Peterson et al., 2017; Lewington, 2020***). A diversity of processes (e.g., water erosion and deposition, crevasse fills) and water flow conditions (distributed drainage vs. channelised) have been invoked to explain the manifold SMC landform 'types'. Despite this variety, recent studies

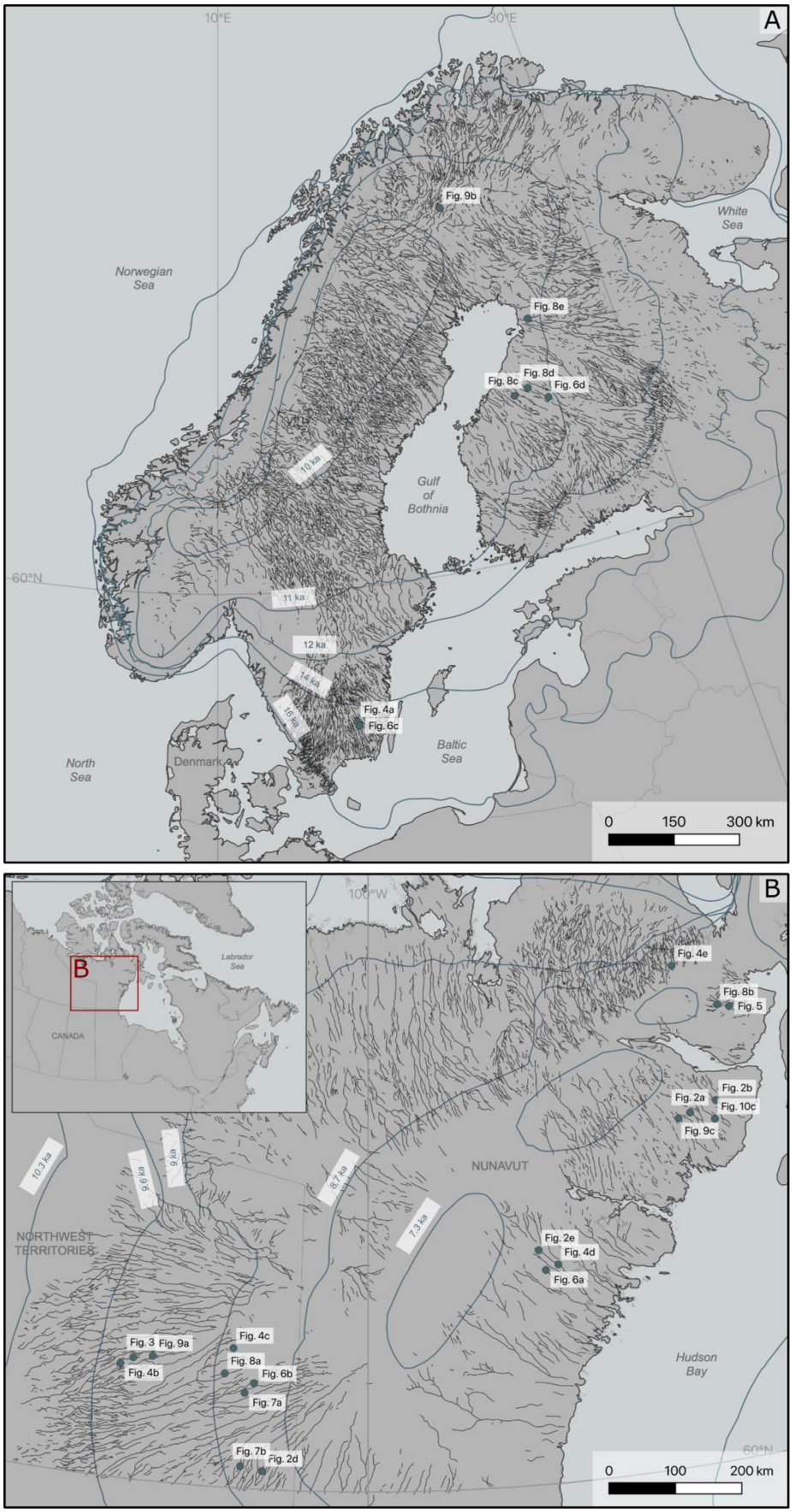

Figure 1. *Mapped subglacial meltwater traces (corridors and eskers – dark grey lines) and locations of Figures 2-10 in (A) Fennoscandia (**Dewald et al., 2022**) and (B) Keewatin, Canada (**Lewington et al., 2020**). Selected ice-margin positions from **Hughes et al. (2016**) (A, most credible) and **Dalton et al. (2020**) (B).*

have suggested a morphological continuum of some forms occurred in SMC (e.g., from ribbed bedforms, through murtoo- related bedforms to murtoos - ***Ojala et al., 2021; Vérité et al., 2022***). In this paper we review key aspects of the existing literature and use selected high-resolution digital elevation models (DEMs) in northern Canada and Fennoscandia to show the association of landforms, which lead us to erect a conceptual model of changing ice-water-sediment interactions to explain the diversity of landforms found in and around subglacial meltwater corridors. In doing so we are able to unify seemingly contradictory interpretations of landform genesis spanning across glacial, fluvial and deformational processes.

2. Previous work on subglacial meltwater corridor landforms and sediments

A variety of landforms have been reported within SMC: hummocks, transverse and oblique ridges, ribbed moraine, murtoos, channels, sculpted bedrock and eskers. SMC were first identified by the presence of glaciofluvial sediments and fields of hummocks and ridges (***St-Onge, 1984; Ward, 1997; Rampton, 2000***). Hummocks are commonly identified within both Canadian and Fennoscandian SMC, often forming tracts of irregular topography (e.g., hummock corridors – ***Peterson et al., 2017***). Their composition, shape, size (10s to 100s metres) and relief (1 to 10s metres) vary considerably (e.g., ***Utting et al., 2009; Dahlgren, 2013; Haiblen, 2017; Peterson & Johnson, 2018; Lewington et al., 2019***). Hummocks consist of glaciofluvial sand and gravel material, sandy diamicton and older glacially reworked or eroded sediments (***Utting et al., 2009; Dahlgren, 2013; Haiblen, 2017; Peterson et al., 2018; McMartin et al., 2015a; Campbell et al., 2020***). The formation of hummocks has been associated with deposition of glaciofluvial sediments within sub-ice cavities during periods of high meltwater discharge (***Utting et al., 2009***), rapid deposition of sandy diamicton by hyperconcentrated flows in sub-ice cavities following meltwater erosion of till (***Haiblen, 2017; DesRosiers, 2021***) and erosion of existing sediments during subglacial meltwater corridor formation (***Sjogren et al., 2002; Peterson et al., 2018; Campbell et al. 2020***). In the latter interpretation hummock tops are often concordant with the surrounding till plain consistent with them being erosional remnants of a former surface (***Peterson et al., 2018***).

Small-scale transverse and oblique ridges have been described in northern Canada and Fennoscandia (***St-Onge, 1984; Rampton, 2000; Utting et al., 2009; Burke et al., 2012; McMartin et al., 2015a,b; Sharpe et al., 2017; Peterson et al., 2018; Campbell et al., 2020***). Transverse ridges up to 8 m high and 100 m wide and composed of gravel have been interpreted as dunes deposited during large flood events (***Rampton, 2000; Burke et al., 2012a***), while smaller diamictic or gravelly transverse ridges 1-5 m high, 10-30 m wide and 10-80 m long have been interpreted as crevasse fills (***St-Onge, 1984***).

Larger transverse ridges, typically hundreds of metres long and wide and metres to tens of metres relief, identified as ribbed moraine, are widespread in Fennoscandia and Canada and typically form broad fields (often greater than several hundred km^2) not associated with SMC. However, some ribbed moraines are organised into ice-flow aligned tracts hundreds of metres to several kilometres wide that are typically characterised by closely spaced and relatively small features (***Aylsworth & Shilts, 1989; Dunlop & Clark, 2006; Wagner, 2014; Trommelen et al., 2014***). In both Fennoscandia (***Peterson et al., 2017***) and northern Canada (***Lewington, 2020***) these narrow tracts have been associated with SMC. Murtoos have recently been discovered in Fennoscandia (***Mäkinen et al., 2017; Peterson et al., 2017; Ojala et al., 2019, 2021***) and often appear along SMC (e.g., ***Ahokangas et al., 2021; Vérité et al., 2022***). Murtoos are triangular shaped bedforms that are typically 30-200 m in length, 30-200 m wide and with a relief of <5 m. (***Ojala et al., 2019, 2021***). Their tip points in the direction of ice flow and they have an asymmetric long-profile characterised by a shorter and steeper down-ice slope (***Ojala et al., 2021***). Murtoos are composed of sandy diamicton and sorted sediment (***Mäkinen et al., 2017; Becher Peterson & Johnson, 2021; Ojala et al., 2022***). There is also a range of murtoo-related subglacial bedforms, including parallel to oblique ridges and escarpments and proto murtoos (i.e., lobate to sub-triangular murtoos), which share overlapping morphological characteristics, contain similar sediments and co-occur in swarms suggesting formation in a common environment (***Ojala et al., 2021***). Ridges and escarpments (hereafter referred together as ridges) are up to a few km long, 10-100 m wide and <5 m high, with a characteristic asymmetrical cross-profile (***Ojala et al., 2021***). Ridges often display a high degree of local parallel conformity and tend to be orientated along the direction of meltwater drainage. Formation of murtoos and their related bedforms is thought to be subglacial, primarily via till deposition and sedimentation from meltwater undergoing fluctuations in water pressure, with the steeper down-ice

slope subsequently sculpted by meltwater (***Mäkinen et al., 2017; Ojala et al., 2019, 2021; Becher Peterson & Johnson, 2021***). Ductile deformation, hydrofracturing, liquefaction structures, and strong fabrics also indicate that sediments were deformed by overlying ice (***Becher Peterson & Johnson, 2021***). Physical modelling and digital mapping in Fennoscandia have strengthened the hypothesis of murtoo formation by progressive reshaping of ribbed moraines by multiple flooding events along SMC causing repeated ice-bed decoupling (erosion, sedimentation) and recoupling (deformation) (***Vérité et al., 2022***).

Meltwater flow along SMC has exposed and scoured bedrock producing apparent depressions (potholes), plunge pools and inverted plunge pools (downflow edges defined by steep slopes and their up-flow sides relatively unconfined) in some areas of western Keewatin (***Rampton, 2000; Sharpe et al., 2021***), or leaving boulder lags on both till and bedrock surfaces in erosional corridors throughout Keewatin (e.g., ***Rampton, 2000; Campbell et al., 2020; Sharpe et al., 2021***). Some of these erosional corridors are deeply incised, with sparse or limited evidence of the landform signature described above (except for eskers), and are more similar in size and shape to tunnel valleys/channels, and may thus share a common genesis (***Peterson & Johnson, 2018; Lewington et al., 2020***). These deeper incised SMC are more common in areas of thicker sediments (***Peterson & Johnson, 2018***).

Eskers and other associated glaciofluvial deposits (e.g., outwash fans) primarily occur along SMC or in-between corridor segments, suggesting they are part of the same drainage network (e.g., ***Johnson et al., 2017; Sharpe et al., 2017; Lewington et al., 2020; Ahokangas et al., 2021***). However, superimposition of esker on other subglacial meltwater corridor landforms and their varying lateral position across and sometimes out of corridors suggests they represent a separate, later stage of deposition (***Lewington et al., 2020***).

3. Data and Methods

Guided by previous large-scale SMC mapping in Keewatin, Canada and Fennoscandia (***Lewington et al., 2020; McMartin et al., 2021; Vérité et al., 2022; Dewald et al., 2022***), our approach was to describe landforms found within corridors and to investigate their associations and transitions with each other, and subglacial bedforms outside the corridors that might be impacted by variations in meltwater drainage

(e.g., ribbed moraines and glacial lineations). This involved landforms description and interpretation from selective sites across Keewatin, Canada and Fennoscandia (**Fig. 1**) to capture the full range of meltwater corridor landforms and arrangements. High-resolution DEMs, including national 2-m LiDAR datasets in Sweden (https://www.lantmateriet.se) and Finland (https://www.maanmittauslaitos.fi/en) and the 2-m ArcticDEM mosaic v7 (https://www.pgc.umn.edu/data/arcticdem) in Canada, were used to identify and describe subglacial bedforms and meltwater landforms. Landform visualisation was carried out using hillshaded DEMs in QGIS, illuminated from two orthogonal directions (45° and 315°) to alleviate the issue of azimuth bias (e.g., ***Smith & Clark, 2005***), a sun angle of 40-45° and a range of vertical exaggerations. Morphological studies were supplemented with field observations and mapping in Keewatin. We also used additional field studies demonstrating glacial sediment variations between and within SMC (e.g., ***Haiblen, 2017; Peterson et al., 2017, 2018; Becher Peterson & Johnson, 2021***).

4. Subglacial Meltwater Corridor (SMC) tracts

In the following section, we describe the morphology and patterning of a range of distinct SMC landform assemblages (tracts) and channelised subglacial meltwater landforms (eskers and channels) that together contribute to the reconstruction of a wider palaeo-subglacial meltwater drainage network (***Lewington et al., 2020; Dewald et al., 2022***). This includes tracts of hummocks and ridges, murtoos, ribbed moraines and streamlined bedforms.

4.1 Hummock tracts

Hummock tracts (**Figs. 2-4**), typically 1-2 km but up to ~5 km wide, occur in SMC cut down into the bed and also on top of bedforms and other meltwater landforms producing positive meltwater corridors, although this is qualitatively rarer, particularly in Fennoscandia.

Hummock tracts typically produce chaotic and irregular hummock and ridge topographies commonly capped by angular to sub-angular boulders, which form an ablation cover (Fig. 3), and often connect or contain eskers (e.g., ***Haiblen, 2017; Peterson et al., 2017, 2018***). The hummocks are typically 10s m wide and <5 m high and can co-occur with small-scale transverse, straight to sinuous ridges that are

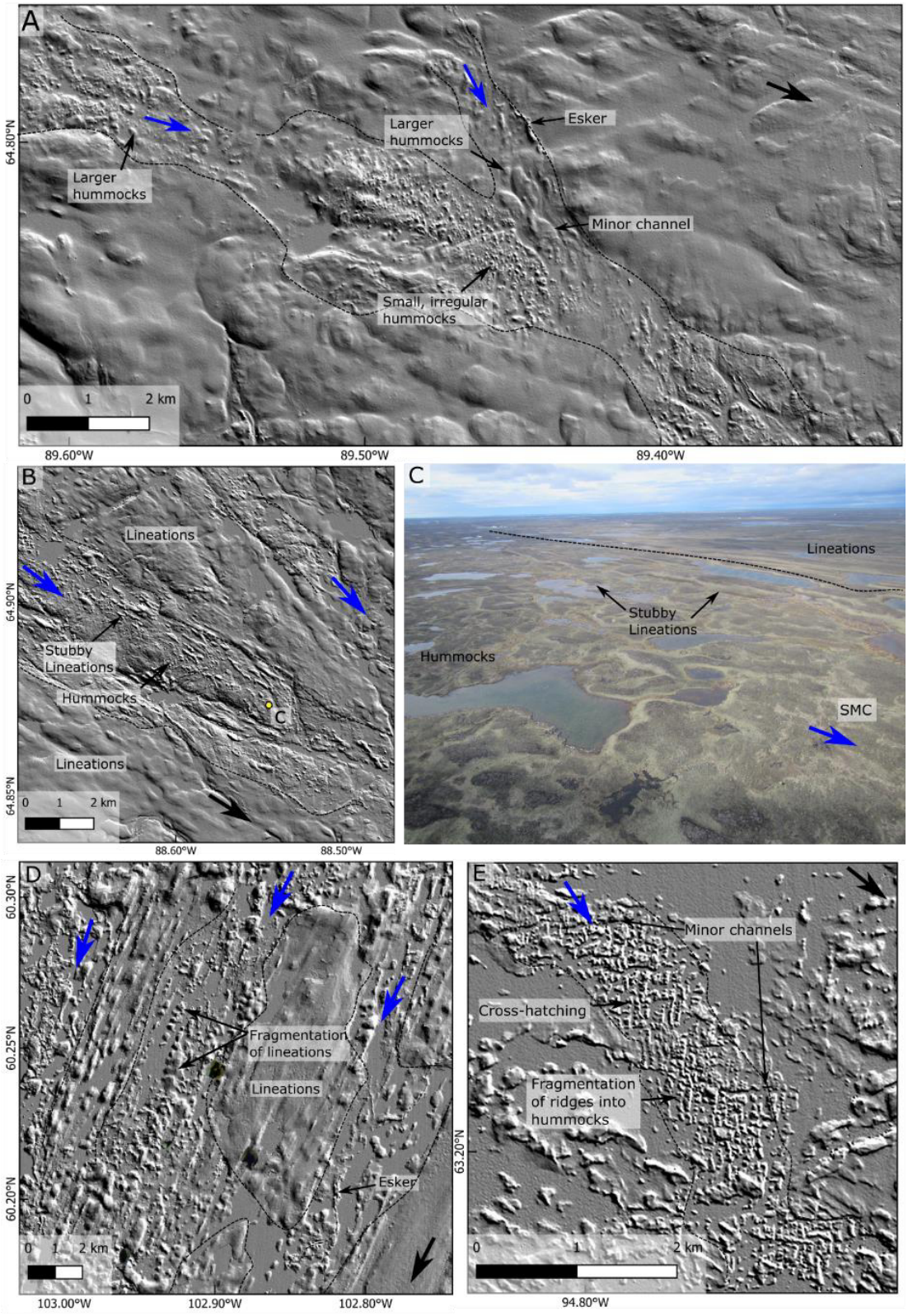

Figure 2. Examples of hummocks and small-scale transverse/oblique ridges found within SMC in Keewatin*. **A**. Small depositional hummocks of sandy diamicton forming an irregular pattern in the ESE corridor and larger, more subdued hummocks. **B**. SMC displaying a transition from hummocks (inside) to fluted hummocks, short streamlined bedforms and large streamlined bedforms (outside) along the boundary of corridor. **C**. Field photograph from the air looking to the North into the boundary of the corridor in **B**. **D**. Partial fragmentation of lineations into longitudinally aligned hummocks. **E**. Fragmentation of obliquely orientated small-scale ridges into hummocks. In places there is evidence for minor channels cutting between features, and organisation into a cross-hatched pattern. SMC edges are annotated with black dashed lines, blue arrows show drainage directions and black arrows indicates ice flow directions.*

more elongated perpendicular to local ice flow direction (up to 1 km long) but of similar width and height (**Figs. 2E, 3, 4B**). The ridges and hummocks often appear to form a landform continuum. These small-scale hummocks and transverse ridges are predominantly confined to the central portion of the corridors (**Figs. 2A, 4B**). Based on morphology, some ridges appear to be the amalgamation of multiple hummocks while others appear as singular ridges superimposed on the hummocks. They are generally asymmetrical ridges with steeper lee-side slopes. We observe lateral transitions at some corridor boundaries from hummocks to fluted hummocks, short streamlined bedforms and large streamlined bedforms, concordant with the regional ice-flow direction (**Fig. 2B, C**).

Internally hummocks and ridges commonly consist of a sandy diamicton (**Fig. 3C**) and/or poorly sorted pebbly sand to bouldery gravel and stratified sediments (e.g., ***Utting et al., 2009; Haiblen, 2017; Campbell et al., 2020***) (**Fig. 3E**). Although compositionally similar, the diamicton is generally coarser-grained and less compact than the surrounding till sheet (***DesRosiers, 2021***). Except possibly near corridor margins, there is no truncation with finer-grained regional till observed as deep as 1 m (***McMartin et al., 2015a***). However, where stratified sediments overlie or underlie diamictons, the contacts are sharp and sometimes erosive (e.g., ***Haiblen, 2017***; **Fig. 3E**). It is also common in northern Canada for flat to low relief ridges to be composed of the same regional till.

We also observe hummocks and ridges arranged in sets with different orientations in respect to assumed meltwater flow. Some are transverse (**Fig. 4B**), some longitudinal (**Fig. 4D**), some oblique and others arranged in a cross-hatched pattern (**Figs. 2E**). Transverse hummock patterns are aligned with small-scale (10s metres up to ~150 m wide and metres high) ridges and ribbed tracts (see Section 4.3), longitudinal hummock patterns are parallel to surrounding lineations (**Figs. 2B, 4D**), while cross-hatched and oblique hummock and ridge patterns are sometimes related to murtoos (see Section 4.2) and residual topography (**Fig. 4D**). The maximum size of these aligned hummocks and ridges seems to be controlled by the related bedform, reaching up to ~400 m wide and 10s m high for hummocks and ridges associated with lineations, ribbed moraines and murtoos. Where associated with murtoos, ribbed moraines and lineations there is often a gradation in size, making clear delineations difficult. "Fish-scale" hummock arrangements are not common within SMC but can occur (**Fig. 5**). First noted in the vicinity of Wager Bay, Keewatin, these hummocks are low relief (2-4 m high), possibly

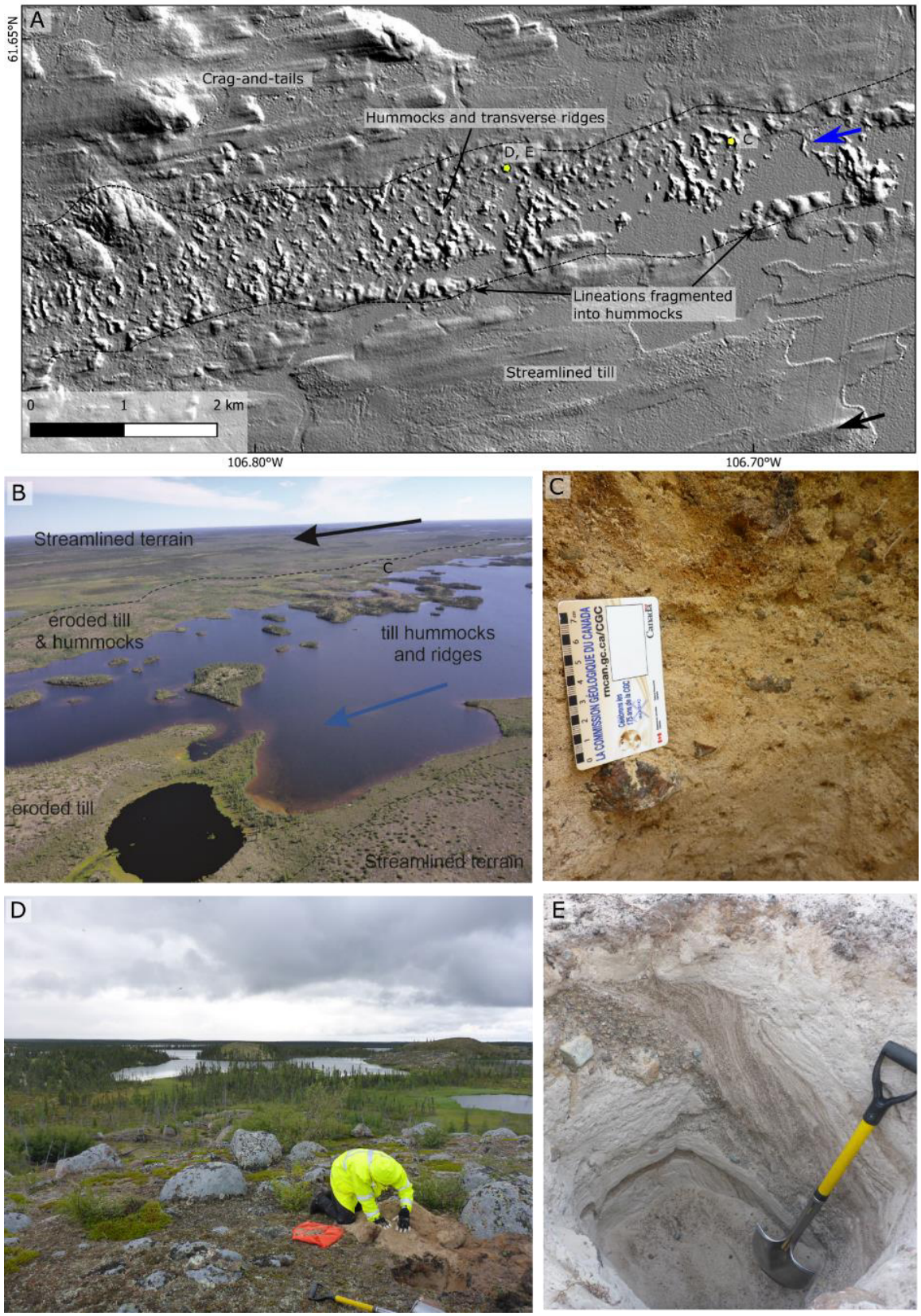

Figure 3. Hummock tract within a WSW trending SMC in SW Keewatin. *The hummocks and transverse ridges overly eroded till near the margins, which is organised into longitudinal hummocks (fragmented lineations: A and B). A. ArcticDEM of the corridor; B. Aerial view of the corridor shown on A. C. Section view in a hummock ridge showing massive sandy diamicton. D. View across the ridges capped by angular to sub-angular boulders. E. Section view in a small hummock in the same corridor showing less common stratified sand and gravel with diamicton inclusions.*

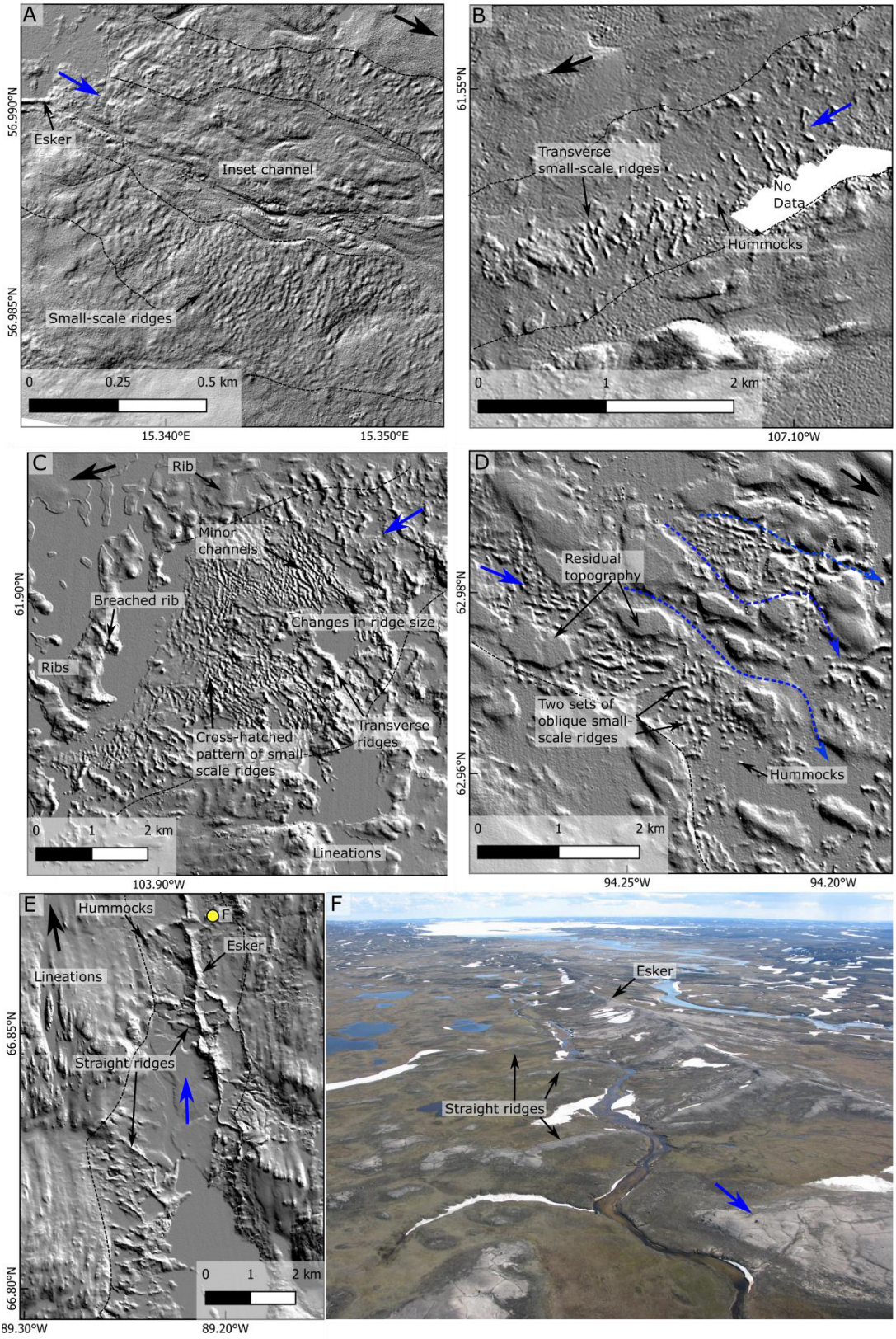

***Figure 4**. **Varied small-scale transverse and obliquely orientated ridge patterns found within subglacial meltwater corridors in Sweden (A) and Canada (B-F)**. A. Very subdued (1 m high and about 10-20 m wide) transverse ridges in SMC either side of an inset channel. B. Sinuous ~3–10 m high and ~10–20 m wide transverse ridges interspersed with hummocks in a SW flowing subglacial meltwater corridor system in SW Keewatin. C and D. Cross-hatched ridge patterns with evidence of minor channels (dashed blue lines in D) and residual topography. E. Straight ridges leading into an esker complex. F. Field photograph of E, showing up to 1 km long straight ridges leading into the esker. SMC edges are annotated with a black dashed line, blue arrows show drainage direction and bold black arrows indicate ice flow direction.*

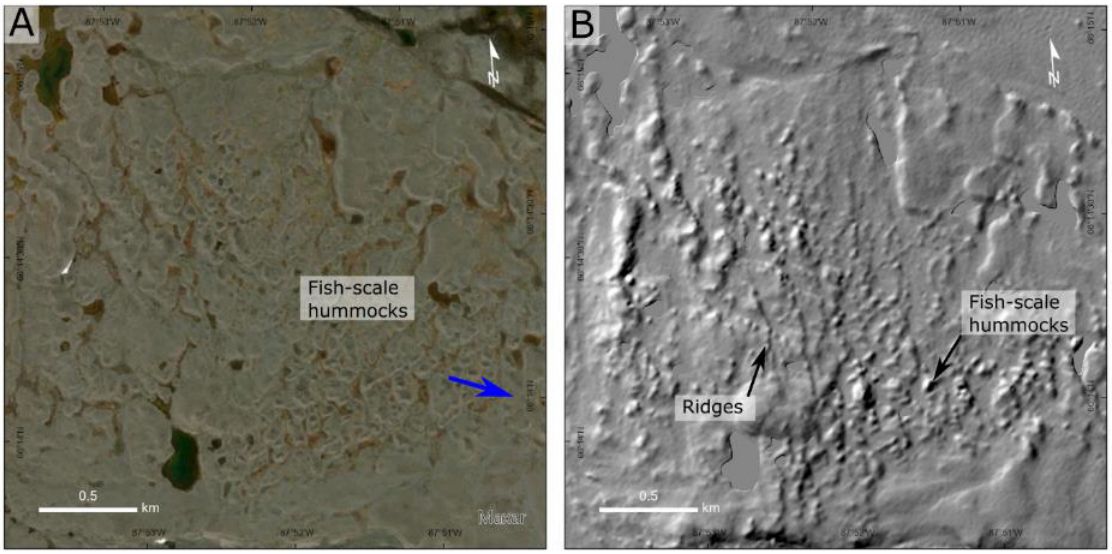

***Figure 5. Low relief fish-scale hummocks**. **A**. SPOT ESRI World Imagery showing the overlapping fish-scale pattern. **B**. The fish-scale pattern is not as evident on the 2m ArcticDEM hillshade but does reveal that the hummocks are superimposed on ridges. Meltwater flow is obliquely to the right (blue arrow).*

overlapping mounds resembling a fish-scale pattern. They appear to have an erosional "till" core with a low-relief ring of sorted sediments. These fish-scale hummocks are superimposed on subtle transverse till ridges in some locations, and the long axis of the hummocks is locally orthogonal to the SMC axis.

4.2. Murtoo tracts

Murtoos and associated murtoo-related bedforms tend to concentrate along tracts that clearly delineate SMC (***Ahokangas et al., 2021, Vérité et al., 2022***). These tracts are roughly parallel to the local ice flow direction and are 0.5 to 5 km wide and tens of km long. Although murtoos and associated murtoos-related bedforms have been previously identified in Fennoscandia, we establish that, although rarer, murtoos and related ridges also occur in northern Canada in association with SMC (**Figs. 6A, B**). The wide range of bedforms in murtoo tracts show common lateral and downstream transitions associated with the progressive modification of ribbed moraines along corridors (see also Section 4.3). Murtoo-related ridges share overlapping morphologies with the small-scale ridges described in Section 4.1 (e.g., **Fig. 6B**). Where murtoos co-occur with ridges, the latter are primarily orientated in the same direction as one of the downstream pointing murtoo sides (**Figs. 6A, C, D**). In some cases, the ridge trends into a murtoo at its downstream end (**Fig. 6D**). Together, murtoos and associated ridges and hummocks can form a chevron-like pattern, similar to cross-hatched patterns observed in hummock tracts (e.g., **Figs. 6A, D**).

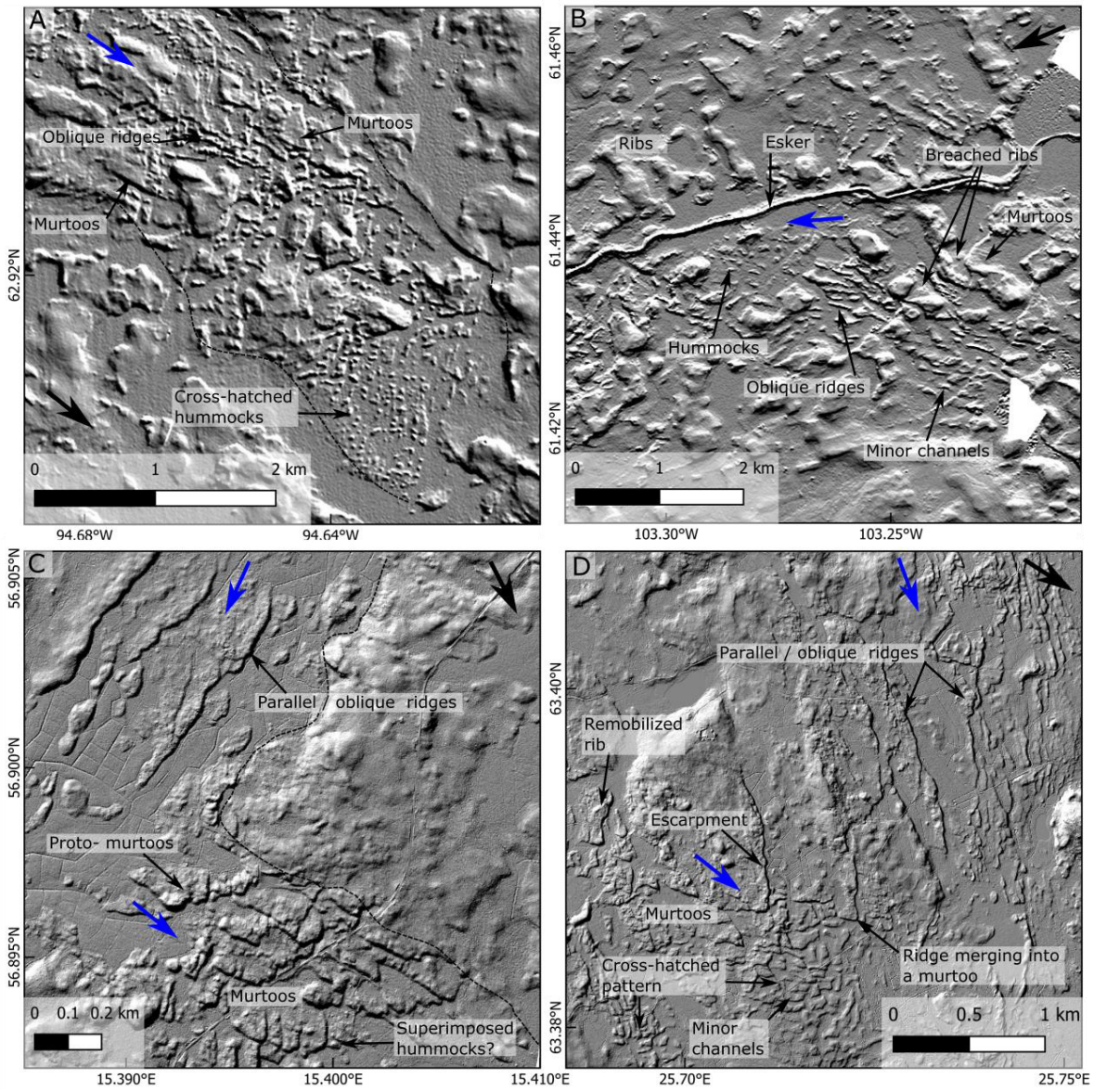

***Figure 6. Details of murtoos and murtoo-related ridges in Canada (A, B), Sweden (C) and Finland (D)**. **A**. Murtoos and associated oblique ridges in E Keewatin. Downstream of the murtoos are hummocks arranged in a cross-hatched pattern. **B.** Murtoos, ridges and hummocks in SW Keewatin. Note the associated ribs, which have been breached and fragmented. **C** and **D**. Murtoos and parallel ridges, with the ridges associated with a connecting meltwater corridor. The ridges in **A-D** all have a similar orientation to one side of the murtoos and in **C-D** exhibit the same direction of asymmetry (i.e., steep slope on the downstream side), and in **D** there is evidence of transitions between the two (i.e., a ridge with a 'v' shape at the downstream end). Meltwater corridor edges are annotated with a black dashed line, blue arrows show drainage direction and bold black arrows indicate ice flow direction.*

4.3. Ribbed tracts

In Keewatin and Fennoscandia, we observe ribbed tracts composed of up to 100s m wide transverse ribs. The tracts are up to ~5 km wide, with some up to 20 km wide in central Finland, and typically separated by smooth and/or streamlined terrain (**Fig. 7**). This includes at least 40 ice-flow parallel ribbed tracts in SW Keewatin (see also ***Wagner, 2014; Lewington, 2020***), which coincide with broader fields of ribbed moraines (**Fig. 7A**). The ribs are typically wider than the small-scale

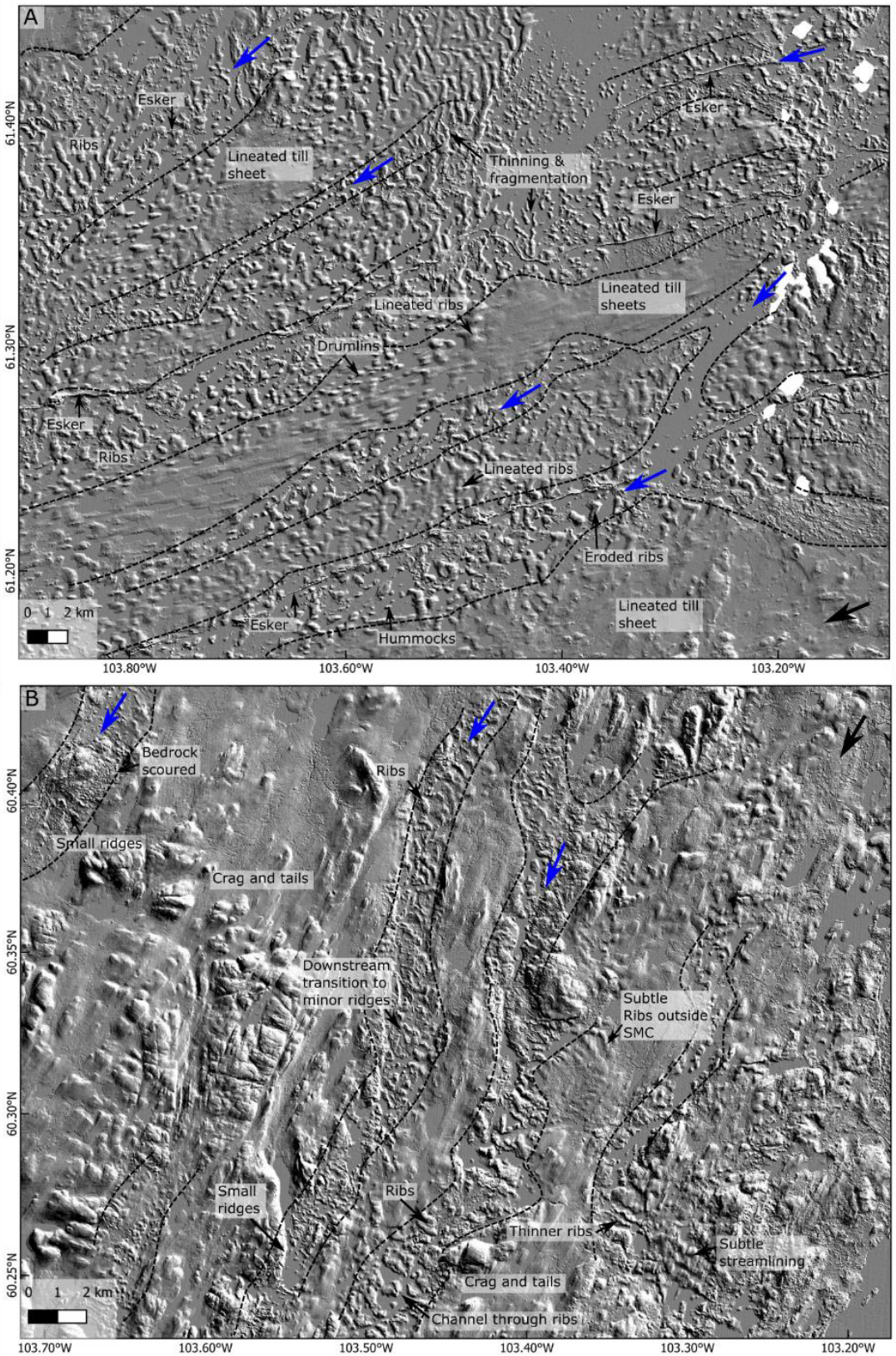

***Figure 7. Large-scale pattern of ribbed tracts in Canada. A**. Alternations between streamlined terrain / till sheets and rougher ribbed tracts, which include partially remobilised and eroded ribs. The ribs can often be traced outside the corridors where they are often streamlined and larger. **B.** Narrow ribbed tracts showing ribbed moraines that have been partially streamlined in places in the direction of ice-flow, consistent with the orientation of lineations outside of the corridors. There is also evidence of longitudinal transitions from clear ribbed moraine into small-scale ridges. Note that ribs are wider (100s m) than the small-scale ridges (10s m) in **Figs. 3 and 4**. SMC edges are annotated with a black dashed line, blue arrows show drainage direction and bold black arrows indicate ice flow direction.*

ridges described in Section 4.1 (100s m vs 10s m, respectively) and mimic the general shape and orientation of ribbed moraine outside the corridors, sometimes producing tracts of ribs trending obliquely to the meltwater corridor they are contained within. We also observe 100s m wide ribbed tracts not associated with regional ribbed moraines (e.g., **Fig. 7B**). In both cases the ribbed tracts are identified based on their spatial correlation with other subglacial meltwater tracts (i.e., form a network) and eskers. The ribs in the tracts typically show evidence of remobilisation and erosion, including lateral and longitudinal transitions into hummocks and smaller-scale transverse ridges (hummock tracts) (**Figs. 8A, E**), reshaping of ribs and/ or transformation into proto murtoos and murtoos (murtoo tracts) (**Figs. 8C, D**). This often manifests as thinning and reshaping of ribs into smaller-scale ridges and hummocks laterally into the corridors and is followed by channel-induced breaching and fragmentation into hummocks (e.g., **Fig. 8A**). Visually, ribs are often more prominent towards the corridor edges (**Figs. 8B, E**). Other evidence of rib remobilisation includes streamlining, although this is rare and often limited to stubby lineations (up to about 200 m long) (**Fig. 7B**).

4.4. Streamlined tracts

SMC are typically devoid of streamlined bedforms (drumlins, crag-and-tails and lineations) making them easy to distinguish from the smooth streamlined terrain commonly surrounding them (**Fig. 3A**). However, we also identified several examples in northern Canada and Sweden (**Fig. 9**) where streamlining occurs in tracts of a few kilometres' width and which contain landforms typical of SMC, including eskers, channels, hummocks and scoured bedrock. The streamlined features exhibit variations in morphology over short distances across flow, with those within the corridor characteristically shorter (typically 10^2 m long vs 10^3 m outside SMC) but better defined than those outside the corridor, which are smoother and more subdued. In western Keewatin (**Fig. 9A**) the streamlined tract connects downstream with another partially streamlined SMC. The streamlined tracts are negative features (i.e., erosional) and the orientation of lineations and drumlins within them mimics the wider geomorphic signature of palaeo-ice flow. Although this is broadly parallel to the orientation of the SMC oblique streamlining patterns manifest where the corridors change direction (**Fig. 9B**).

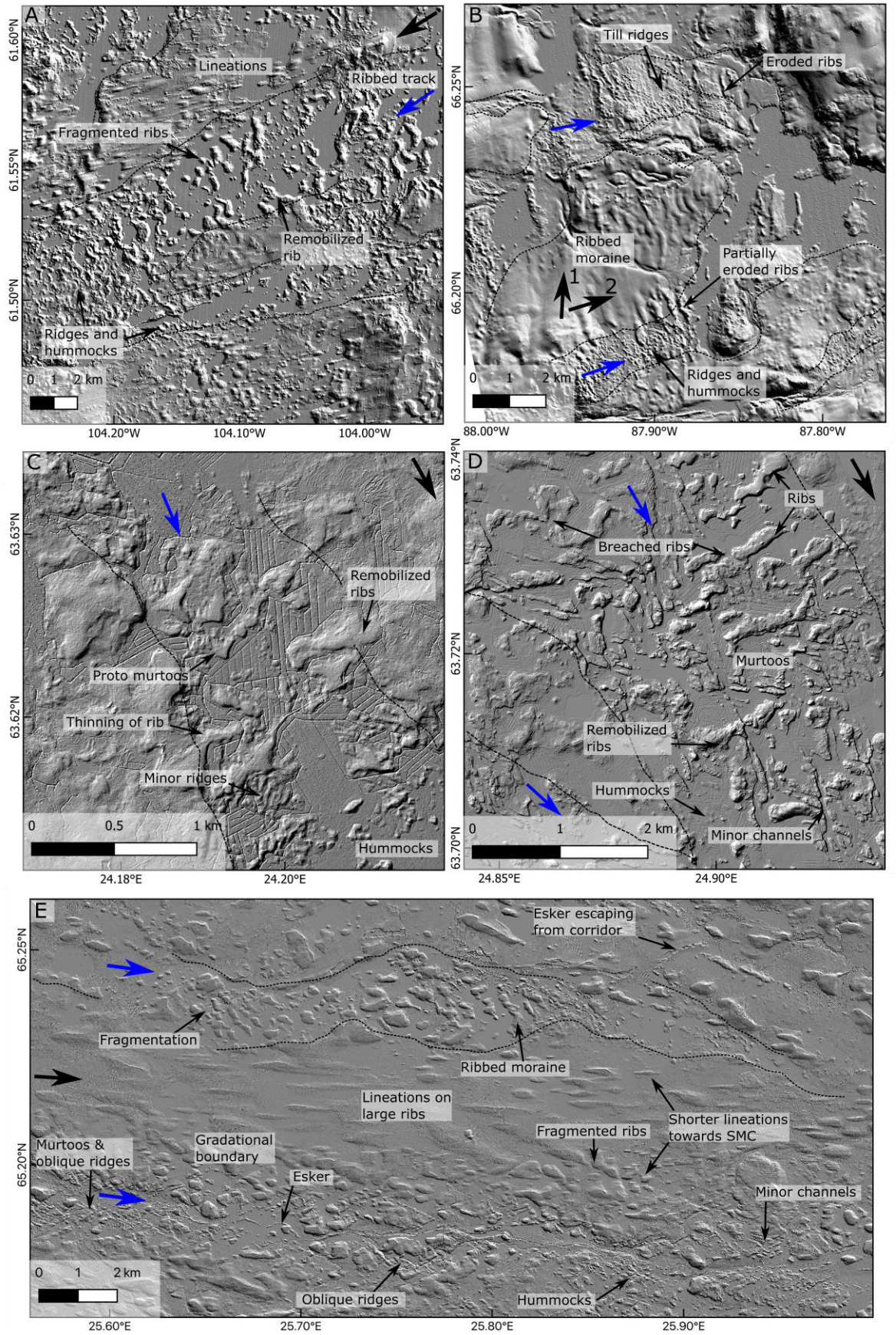

Figure 8. Relationships between ribs and other landforms in SMC. A. *Ribbed tract surrounded by streamlined terrain. Note that streamlined ribbed moraines outside the corridors become thinner and more sinuous into the corridor (remobilised) and become fragmented. Also note longitudinal downstream transition from remobilised ribs into smaller ridges and hummocks.* ***B****. The relationship between ribs, eroded ribs and late-stage depositional*

hummocks and small-scale ridges. The latter are confined to the centre of the corridors. Ribbed moraine and subglacial meltwater corridors are related to late east-flowing ice (arrow 2), which cross-cut the earlier main ice flow to the north (arrow 1). ***C****. Thinning and partial remobilization of ribs into murtoos within a SMC.* ***D****. Downstream transition from ribs into murtoos and hummocks. Note, the minor channels that have breached the ribs and sculpted the murtoos.* ***E****. Lineations are superimposed on ribs that can be traced downstream into the lower of the two meltwater corridors. The ribs have been dissected by minor channels and fragmented and remobilised into hummocks and murtoos respectively. Lineations tend to shorten towards the two SMC, and the lower corridor has a gradational boundary suggesting contemporaneous formation. Note, the esker escaping out of the upper SMC, possibly indicative of a separation in time of esker deposition and corridor formation. SMC edges are annotated with a black dashed line, blue arrows show drainage direction and bold black arrows indicate ice flow direction. A-B are from Canada and C-E from Finland.*

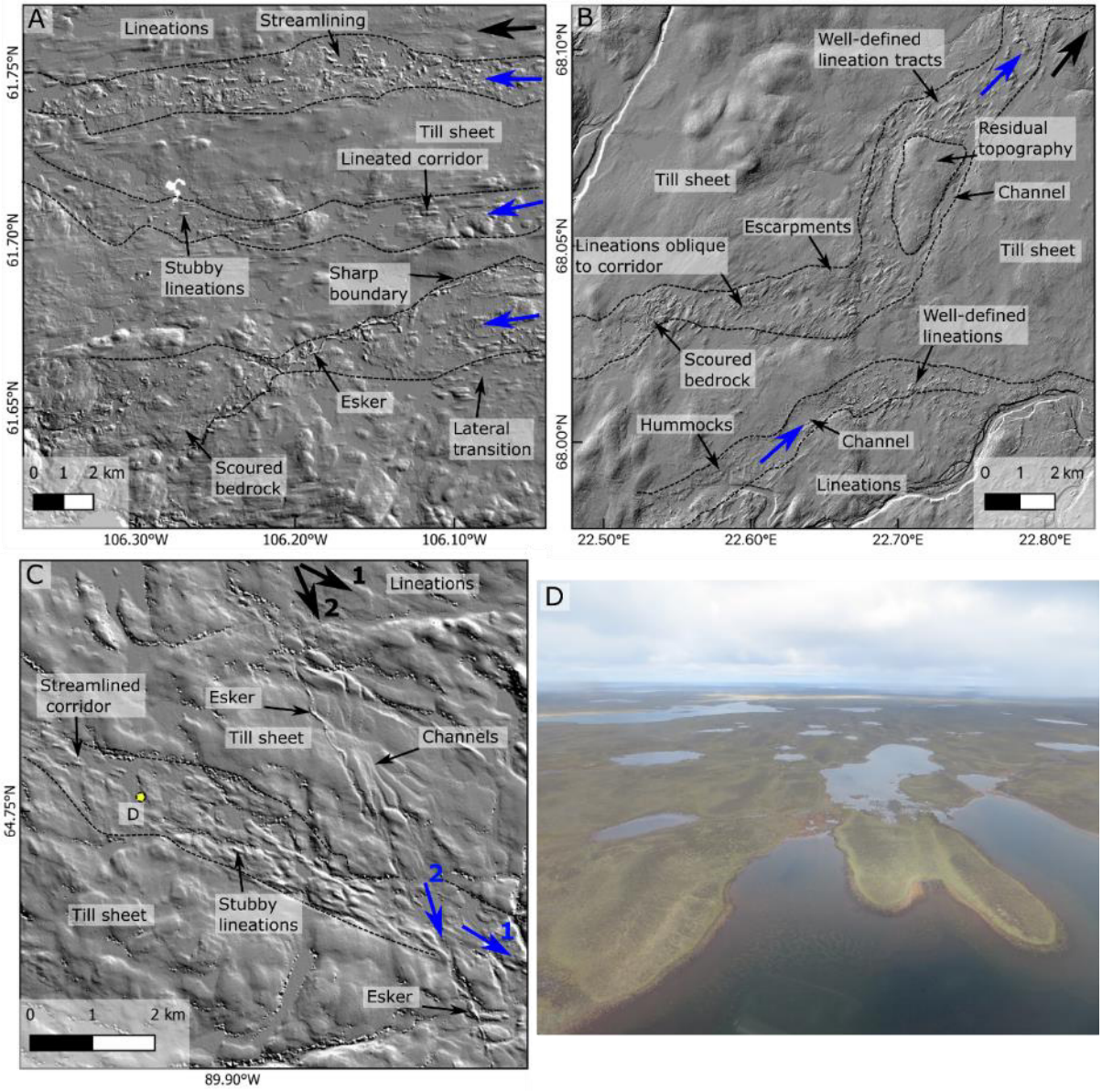

Figure 9. Streamlined tracts in Canada (A, C, D) and Sweden (B). *Streamlined tracts in SMC are associated with other meltwater landforms (e.g., scoured bedrock, channels and hummocks). Streamlined features in the tracts tend to be stubbier but more clearly defined than those outside the corridors suggesting coupling might co-exist with meltwater flow in between lineations. In* ***A****, note how some edges are clearly defined while others show a lateral transition in streamlining size/elongation towards the corridor. In* ***C****, south of Wager Bay note the later streamlined features, eskers and channels (blue arrow 2) cross-cutting to the SSE.* ***D****: Oblique air photograph of the streamlined features in the corridor illustrated in* ***C****. SMC edges are annotated with a black dashed line, blue arrows show drainage direction and bold black arrows indicate ice flow direction (numbers indicate relative timing).*

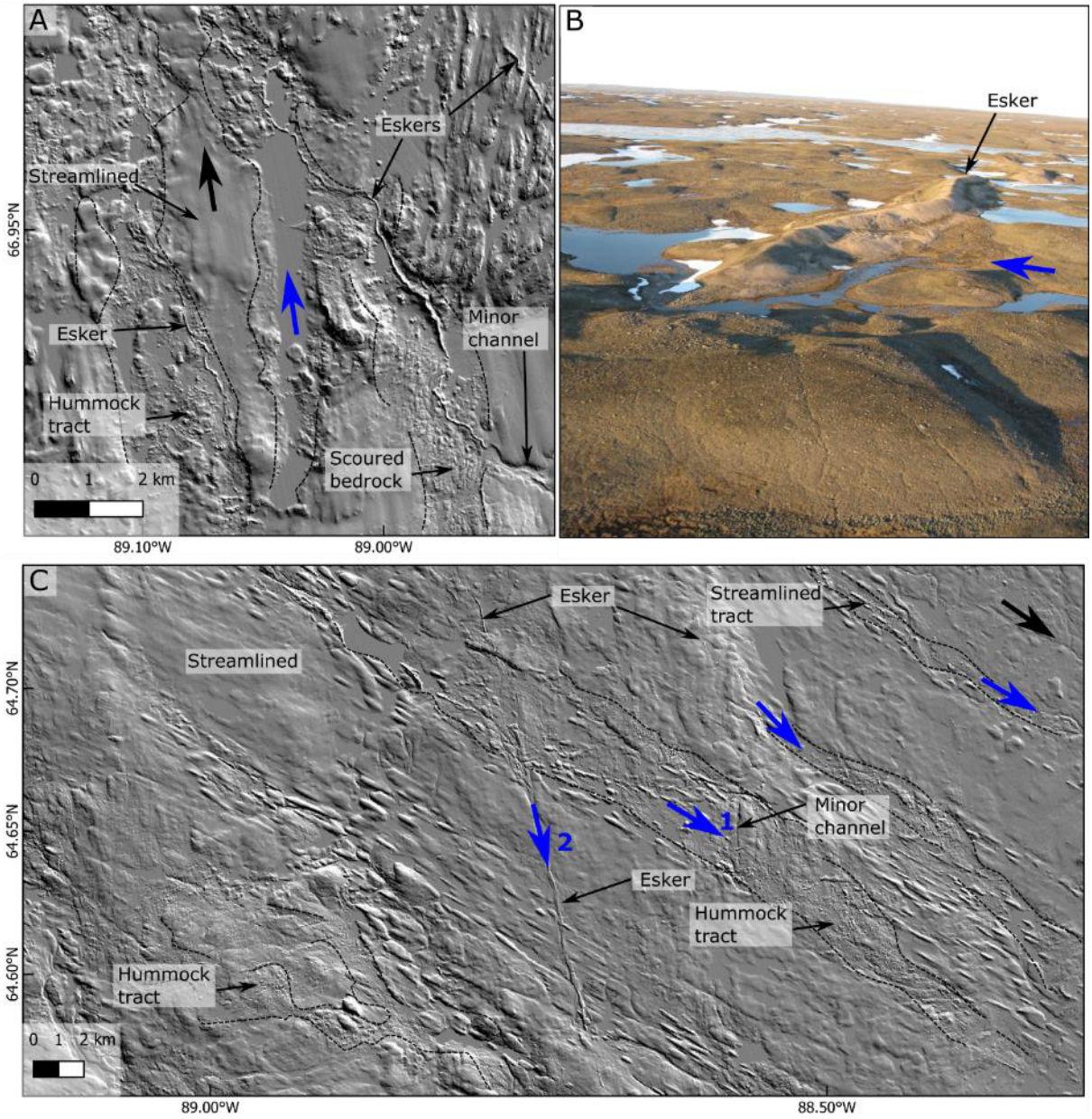

Figure 10: Spatial relationship of eskers and SMC. A. *Depositional corridors north of Wager Bay with eskers misaligned with the central axis of the corridor (left) and trending into another corridor at an oblique angle (right).* ***B.*** *A small discordant esker north of Wager Bay, deposited on top of corridor landforms, representing late-stage meltwater drainage within a restricted conduit associated with the corridor system.* ***C****. Late SSE-trending eskers and associated subglacial meltwater channels (blue arrow 2) cross-cutting prominent SE-trending ice flow and meltwater corridors (blue arrow 1) south of Wager Bay. SMC edges are annotated with a black dashed line, blue arrows show drainage direction and bold black arrows indicate ice flow direction (numbers indicate relative timing).*

4.5. Channelised drainage landforms associated with corridors

4.5.1. Eskers

Large (typically kilometres to tens of kilometres long) esker systems are often either contained or partially contained within SMC, or link SMC, but not all SMC contain an esker (see also ***Lewington et al., 2020; McMartin et al., 2021***). Where eskers do occur, they are often misaligned with the central

axis of the corridor (**Fig. 10A**), and esker-channel networks can also cross-cut corridors at oblique orientations (**Figs. 9C, 10B, C**). Eskers are frequently superimposed on landforms or exposed bedrock found in SMC.

4.5.2. Minor channels

Minor channels, tens to hundreds of metres wide and hundreds of meters long are often found to breach ribbed moraine and ridges, and form along the flanks of murtoos (**Figs. 4C, 6B**). These channels are not always parallel to the main SMC. Complex channel networks are possibly responsible for the formation of some hummocks (**Fig. 4D**) and multiple orientated sets of ridges resulting from the fragmentation of pre-existing landforms (cross-hatched pattern) (**Fig. 2E**) or, at a larger scale, residual topography between channels (**Figs. 4D, 9B**). Larger (up to ~1 km) inset channels that follow the main drainage axis are also occasionally observed to cut through the original SMC (**Fig. 4A**), connect esker segments, or form overflows from one corridor to the next.

5. Interpretation

5.1. Depositional hummock tracts

Evidence for meltwater deposition within SMC includes eskers, hummocks (including with the ring component of "fish-scale" arrangement) and small-scale transverse ridges (see also: ***Utting et al., 2009; Haiblen, 2017***).

Depositional hummocks, which vary in morphology and composition, often form a chaotic pattern mixed with small depositional ridges. Sandy diamicton samples in depositional hummocks commonly display lower percentages of silt and clay than the till samples outside the corridors, suggesting these hummocks were not eroded from the surrounding till sheet, but that some winnowing occurred during meltwater erosion of till upflow and rapid deposition (***Haiblen, 2017; DesRosiers, 2021***). The intermingling with hummocks comprised of diamicton and/or stratified sediments also suggests meltwater erosion of till upflow, ice-held debris and rapid deposition. In some locations, the hummocks are streamlined, suggesting syn- or post depositional deformation during ice bed re-coupling (***Haiblen. 2017***).

Depositional small-scale transverse ridges appear to form a landform continuum from the hummocks. The surface composition of ridges is predominantly a sandy diamicton similar to the hummocks. Their association with the depositional hummocks suggests they are syn- and post-depositional. We interpret the depositional hummocks and small-scale transverse ridges within SMC to predominantly reflect conditions associated with large magnitude drainage event(s), capable of incorporating and then rapidly depositing large volumes of reworked till in basal ice cavities and crevasses (e.g., hyperconcentrated flows) (see also: ***Utting et al., 2009; Haiblen, 2017; DesRosiers, 2021***), and in rare cases forming mega-dunes (***Rampton, 2000***). Megadunes and the rings on fish-scale hummocks likely represent late-stage deposition during waning flood flows that extended across much of the corridor width. ***Utting et al. (2009)*** and ***DesRosiers (2021)*** suggested that depositional ridges and hummocks, respectively, formed where meltwater flow eroded cavities at irregularities in subglacial conduits, providing accommodation space for rapid sedimentation. For the transverse depositional ridges, we suggest that accommodation space could also be controlled by basal crevasses (see also ***St-Onge, 1984***) formed by hydrofracture during flood events, consistent with the interpretation of transverse ridges of similar dimensions in Svalbard as crevasse-fill ridges (***Evans et al., 2022***).

The depositional hummocks and small-scale ridges tend to form hummocky tracts in the centre of the corridors superimposed on eroded till or bedrock surfaces, with erosional till hummocks and remnants near the margins of the corridors (***Campbell et al., 2020***). This lateral transition suggests deposition in a narrower corridor under different flow conditions. The superimposition of hummocks and ridges on top of eroded till or bedrock indicates that deposition typically post-dates erosion and thus occurs closer to but not at the ice margin. These observations are consistent with increased drainage efficiency (i.e., channelisation) near to ice-margins leading to concentration of drainage along a narrower lateral extent (e.g., ***Rada & Schoof, 2018; Nanni et al., 2021***). The relatively thinner ice near to the margins would also have reduced the impact of subglacial conduit closure, facilitating prolonged waning stage flow (***Roberts, 2005***) and thus complex deposition (***Burke et al., 2012a***). An alternative scenario is that deposition occurred in a narrower zone during waning water flows as drainage efficiency reduced and the ice began to recouple to the bed.

5.2. Erosional hummock tracts and geometric patterning

Meltwater erosion must be a significant process in producing the largely negative topography of SMC, which are often characterised by exposed and scoured bedrock, boulder lags, marginal escarpment and eroded till ridges. We interpret the geometric arrangements (e.g., transverse, longitudinal, cross-hatched) of hummocks and small-scale till ridges we observe (see also **Figs. 6A, 8B**) as eroded roots of subglacial bedforms (***Peterson & Johnson, 2018; Ojala et al., 2021***), which are known to exhibit regularity in spacing and spatial organisation (***Clark et al., 2018***). Minor channels incised along the edges of murtoos, breaching of small-scale ridges and ribs and larger networks of multiple channels separated by residual topography support this inference. Transverse and longitudinal arrangements of hummocks can be explained by the erosion of ribs, small-scale ridges and lineations, while more complex geometric patterns including cross-hatching (e.g., hummocks and small-scale ridges) could arise from fragmentation of murtoos. Fragmentation of underlying subglacial bedforms suggests meltwater drainage occurred after their formation. More generally, geometric patterns and multiple channels separated by residual topography are analogous to small (cm) and large-scale (m) patterns seen on beaches and river beds (e.g., ***Morton, 1968; Allen, 1982***). Simple laboratory experiments suggest these natural bedform patterns can be generated by erosion of sediment in a shallow, draining water layer (***Daerr et al., 2003***).

5.3. Murtoo tracts

Fields of murtoos and murtoo-related bedforms are suggested to form when a significant amount of meltwater was delivered to the ice bed and enlarged subglacial conduits and cavities became filled with sandy diamicton under high-pressure conditions (***Mäkinen et al., 2017; 2019; Ojala et al., 2022***). Following ***Vérité et al. (2022)*** we interpret the high concentration of murtoos along well-defined tracts as the morphological expression of meltwater corridors when pre-existing bedforms have been flooded. Examples from Fennoscandia are composed of a variety of bedforms linked within a single morphological and genetic continuum originating from the progressive reshaping of preexisting ribbed moraine fields (***Vérité et al. 2022***). Hence, other murtoo tracts in northern Canada and Fennoscandia are here associated with reshaping of pre-existing sediments by a combination of glaciofluvial erosion (minor channels associated with murtoos; **Fig. 6D**) and glacial deformation during periods of ice-bed

recoupling. This dynamic concept invokes alternating phases of (i) significant meltwater discharge, high hydraulic connectivity and ice-bed decoupling (leading to bedform erosion and sediment deposition) and (ii) limited meltwater flow, low hydraulic connectivity and ice-bed recoupling (leading to bedform stretching/deformation). This explanation is consistent with the orientation of murtoos in the direction of ice flow (***Ojala et al., 2019***), the overlapping morphological properties of their different forms including ridges (***Ojala et al., 2021; Vérité et al., 2022***) and sedimentological characteristics such as strong fabrics and ductile deformation structures (***Becher Peterson & Johnson, 2021***).

5.4. Ribbed and streamlined tracts

It is unlikely that the ribbed and streamlined tracts were formed directly by meltwater flow down the corridors as their orientation mimics the broader geomorphic signature of regional palaeo-ice flow rather than the more varied drainage axes of the corridors. In addition, ribbed tracts can often be traced laterally beyond the bounds of subglacial meltwater corridors and streamlining occasionally becomes less elongate towards the corridor. The oblique orientation of subglacial bedform tracts along stretches of some SMC is also difficult to reconcile with a broader sheet flood collapsing into narrower corridors (e.g., ***Fisher & Shaw, 2002; Shaw, 2002; Sharpe et al., 2021***).

The occurrence of subglacial bedforms in narrow tracts along SMC therefore suggests that when regional-scale bedforms were generated the process was sensitive to substrate conditions (e.g. granulometry, strength, drainage properties), which were different along the SMC in comparison to the surroundings. This sensitivity produced ribs or lineations of different size and wavelength to those outside the corridors and a mismatch to the surroundings. This interpretation is consistent with bedforming theories where spatially variable drainage at the bed acts as an important control on subglacial bedform genesis, development and preservation (***Hindmarsh, 1998a, b, c; Boulton et al., 2001; Schoof, 2007; Dunlop et al., 2008; Fowler and Chapwanya, 2014; Fannon et al., 2017; Vérité et al., 2021***).

As ribbed tracts are often bounded by streamlined ribbed moraines, the simplest interpretation is that ribbed moraines initially formed over a wide area, with subsequent streamlining inhibited or reduced in SMC allowing the ribs to be (partially) preserved as tracts along them. The visual gradation to less elongate streamlined features towards some SMC (see also ***Lewington, 2020***) and the occurrence of

predominantly short (<200 m) lineations in corridors supports the idea that streamlining and SMC formation can be contemporaneous. This is consistent with theory that greater sediment deformation, and thus streamlining, will occur in regions of low effective pressure (i.e., high water pressure in the till) where the ice and bed are coupled (e.g., ***Hindmarsh, 1998a; Schoof, 2007; Fowler and Chapwanya, 2014***); conditions that are characteristically found outside SMC in the hydraulically isolated or weakly connected drainage system (e.g., ***Wright et al., 2016; Rada & Schoof, 2018***). Conversely, sediment deformation is likely reduced along hydraulically connected drainage routes (SMC) where repeated ice-bed decoupling limits the amount of cumulative deformation (e.g., ***Piotrowski & Kraus, 1997; Iverson et al., 2007***), the till layer is thinned or removed by meltwater erosion (***Alley, 1997, 2019; Rampton, 2000; Swift et al., 2005; Lewington et al., 2020***) and efficient drainage causes sediment dewatering (***Sole et al., 2013; Bougamont et al., 2014; Hoffman et al., 2016***).

An alternative or possible additional hypothesis is that ribs formed contemporaneously with the SMC, preferentially forming tracts along them due to differences in cumulative bed deformation inside and outside the corridors, or have formed by a different process to ribbed moraine. This could apply to locations where ribs are restricted to SMC or where the ribbed tracts are morphologically different to surrounding ribbed moraine fields (see ***Dunlop & Clark, 2006***). In such a scenario the ribbed tracts might represent lower cumulative deformation compared to outside the corridor where lineations form, assuming that theories gathering ribbed and streamlined bedforms in a single continuum (***Ely et al., 2016***) are primarily controlled by a gradient of deformation accommodated by the subglacial bed through time.

The observation of generally short bedforms in streamlined tracts is consistent with reduced growth while their higher relief could reflect higher effective pressures in the till due to more efficient drainage (***Rattas & Piotrowski, 2003***) and perhaps also the influence of increased meltwater erosion along SMC. This explanation indicates that ice-bed coupling and deformation might co-exist with meltwater flow in-between lineations (e.g., ***Fannon et al., 2017***). Alternatively, the subglacial meltwater corridor could have formed first, with meltwater erosion resulting in less sediment substrate available to deform, hence resulting in smaller streamlined bedforms (including streamlined hummocks) compared to adjacent regions. In both models, the initial bedforms could have been ribbed moraines that were subsequently

streamlined, with lower deformation rates in corridors (due to the impact of fluctuating water pressure and/ or bed conditions), or a field of streamlined features that underwent differential cumulative deformation within and outside corridors.

5.5. Eskers

Eskers and associated outwash fans are superimposed on top of other corridor landforms or directly on bedrock and are therefore interpreted to record the final phase of deposition in a subglacial conduit close to or at the ice margin (e.g., ***Mäkinen, 2003; Hewitt & Creyts, 2019; Lewington et al., 2020; Livingstone et al., 2020***). Within northern Canada and Fennoscandia, we identify narrow esker-channel networks that cross-cut corridors at oblique orientations. These cross-cutting relationships, along with eskers that trend out of SMC indicate a separation in time, sometimes associated with a switch in ice sheet geometry during retreat, and thus that SMC likely formed up-ice from the margin. These narrow esker-channel networks also support the idea that SMC generally narrow towards the ice margin as drainage becomes concentrated in efficient conduits.

6. Discussion

6.1. A potential unifying model for the formation of SMC landforms

Based on the above observations, any potential unifying model to explain the diversity of SMC landforms must account for subglacial deposition, erosion and deformation processes. Below, we outline how SMC could respond to the interplay between these subglacial processes and pre-existing morphologies, building on the significant legacy of field and remote observations (e.g., ***St-Onge, 1984; Dredge et al., 1985; Ward et al., 1997; Rampton, 2000; Utting et al., 2009; McMartin et al., 2015a, 2019, 2021; Campbell et al., 2016; 2020; Haiblen, 2017; Peterson et al., 2017, 2018; Peterson & Johnson, 2018; Ojala et al., 2019, 2021, 2022; Lewington et al., 2019, 2020; Ahokangas et al., 2021; DesRosiers, 2021***), recent physical modelling (e.g., ***Vérité et al., 2022***) and modern observations of ice sheet hydrological processes (see ***Davison et al., 2019*** for a review).

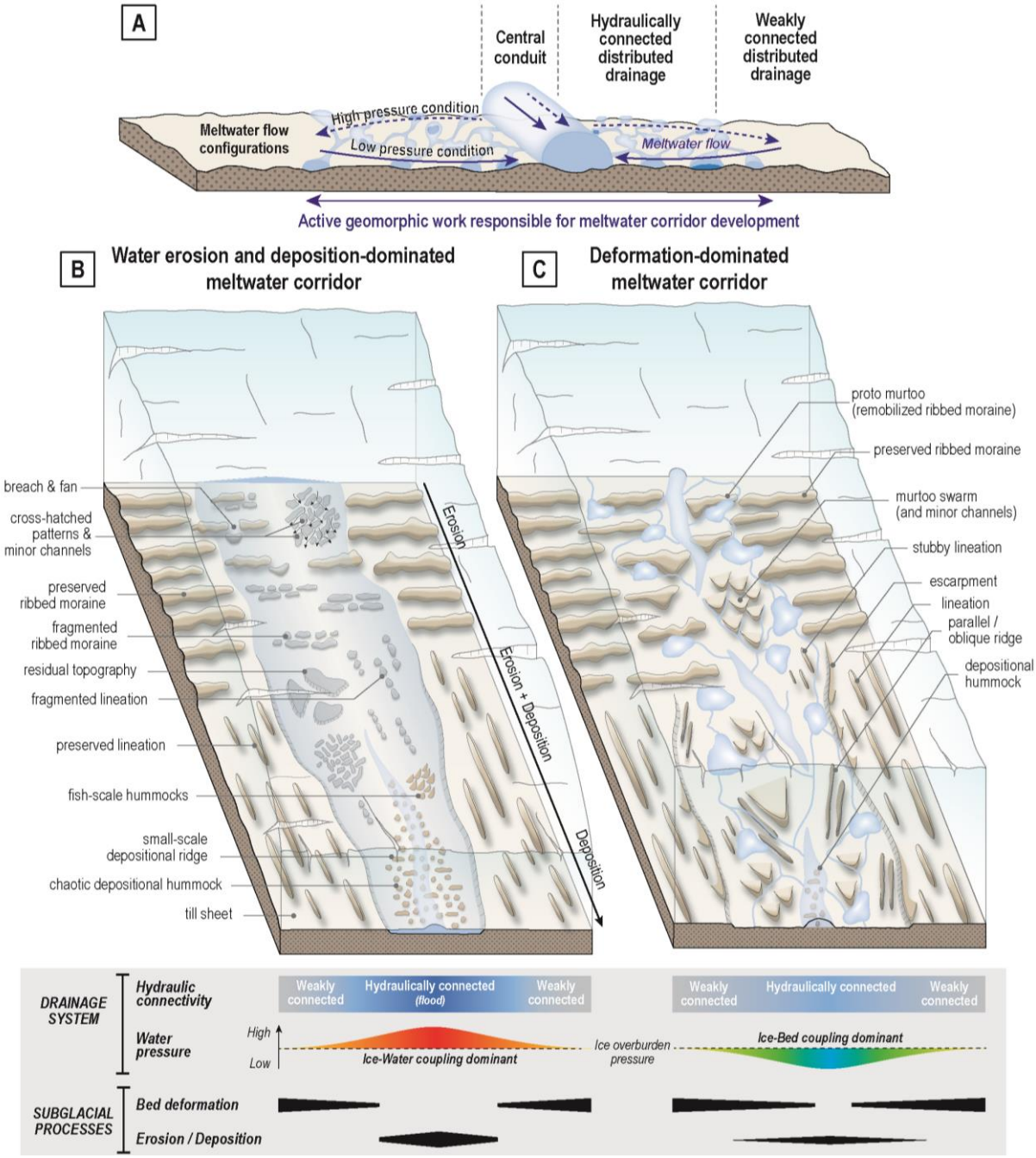

Figure 11. A general theory for SMC formation. A. *SMC are the morphological expression of the hydraulically well-connected parts of the subglacial drainage system, which undergo large variations in meltwater input, effective pressure and drainage efficiency. Based on the width of corridors the hydraulically well-connected drainage system is inferred to be hundreds of metres to several kilometres wide.* ***B*** *represents a snapshot of SMC processes and landforms produced when a large and rapid meltwater input overwhelms the drainage capacity (flood) resulting in active water flow, erosion and deposition over a large lateral extent within the corridor. This is conceptualised as a bankfull flood, but could also comprise other or additional drainage configurations.* ***C*** *represents a snapshot of SMC processes and landforms produced when effective pressure increases and the ice recouples with the bed resulting in deformation of existing bedforms. The black bars in the legend indicate extent (length) and magnitude (width) of bed deformation and erosion/ deposition at the bed. Note, B-C could be tens of kilometres length. The size of example landforms is not to scale.*

The general premise of our model is that away from ice-divide zones meltwater tends to organise down hundreds of metres to several kilometres wide SMC characterised by high hydraulic connectivity (at least seasonally) (**Fig. 11A**) (***Andrews et al., 2014; Tedstone et al., 2014; Hoffman et al., 2016; Davison et al., 2019; Nanni et al., 2021***). Close to the ice margin the hydraulically-connected drainage system likely contains a central conduit (e.g., ***Chandler et al., 2021; Nanni et al., 2021***) while further upstream, thicker ice, fewer surface melt inputs and lower hydraulic gradients are more likely to maintain multiple smaller conduits (e.g., ***Vore et al. 2019***). Surface meltwater inputs that overwhelm the hydraulic capacity of the subglacial drainage system (i.e., a flood event) produce rapid (hours to days) spikes in water pressure (***Iken & Bindschadler, 1986; Hubbard et al., 1995; Das et al., 2008; Bougamont et al., 2014***). Over the course of a melt season, increased drainage hydraulic efficiency leads to higher effective pressures concentrated along narrower SMC (e.g., ***Rada & Schoof, 2018; Nanni et al., 2021***). It is these corridors of high hydraulic connectivity that are envisaged to produce SMC (**Fig. 1**) (see also ***Lewington et al., 2020; Ojala et al., 2021***).

*6.1.1. Water erosion and deposition-dominated SMC (***Fig. 11B***)*

The landforms in SMC are interpreted to record variations in ice-water-sediment coupling caused by fluctuations in water supply and water pressure. Large inputs of meltwater to the bed during rapid (likely surface) lake drainage events (***Das et al., 2008***) and from diurnal and seasonal fluctuations in melt and rainfall events (***Hubbard et al., 1995; Andrews et al., 2014; Smith et al., 2021***) can overwhelm the subglacial drainage system facilitating cavity expansion (***Cowton et al., 2016***), ice-bed separation (e.g., as blisters: ***Lai et al., 2021***) and active drainage through the hydraulically-connected drainage system (**Fig. 11B**) (e.g., ***Nanni et al., 2021***).

During periods of high-hydraulic connectivity geomorphic processes will be dominated by water erosion and (re-) deposition in the corridors (see also ***Lewington et al., 2020***). The landform and sediment record indicates a range of drainage configurations, including laterally-restricted floods scouring till and bedrock surfaces (e.g., ***Rampton, 2000***), producing "fishscale" hummocks and gravel megadunes, and depositing reworked till as hummocks and ridges in basal ice cavities (and see ***Brennand, 1994; Burke et al., 2012b; Utting et al., 2009; Haiblen, 2017; DesRosiers, 2021***), scouring of the ice base, and crevasses produced by hydrofracture (***St-Onge, 1984; Evans et al., 2022***); to smaller-scale braided or

anastomosing channel networks (see also ***Peterson et al., 2018; Kirkham et al., 2021***). The rare examples of megadunes likely record bankfull floods down corridors (e.g., ***Burke et al., 2012b***), while the hummocks and ridges arise from water flow through a broad network of variably active conduits (e.g., ***Vore et al. 2015***), cavities and crevasses, with ice partially coupled with the substrate. In the latter case, deposition, predominantly by hyperconcentrated flows, is likely to be controlled by variations in accommodation space due to cavity expansion, sediment choking and hydrofracture (basal crevasses), likely during waning of high velocity flood conditions. Discrete hummock and ridge swarms are interpreted to be deposited roughly synchronously during individual flood events, with repeated sequences of hummock tracts along a corridor forming time transgressively as the margin receded. We also note the progressive emergence of geometric patterns caused by fragmentation of the adjacent till plain and pre-existing bedforms, such as ribbed moraines and streamlined bedforms, into erosional till ridges (e.g., fragmented ribbed moraines) and hummocks (e.g., fragmented lineations). More complex, naturally arising cross-hatched patterns associated with meltwater erosion are possibly linked to drainage of a shallow water layer (***Daerr et al., 2003***) and/or erosion of murtoo fields. Although depositional and erosional hummocks and ridges are produced by different processes, with patterning more evident in the erosional features, they exhibit overlapping morphological envelopes, implying some equifinality of form.

As the lateral extent of the hydraulically-connected region varies in space and time, for example, narrowing due to more efficient drainage later in the melt season and towards the margin (***Rada & Schoof, 2018; Vore et al., 2019; Nanni et al., 2021***), we also expect the extent of geomorphic work to vary laterally. This is consistent with the formation of inset channels and greater thinning of ridges and fragmentation of subglacial bedforms into hummocks and small-scale ridges towards the centre of corridors. The tendency for depositional landforms to concentrate along narrow zones on top of eroded till/ bedrock is interpreted to represent either formation closer to the ice margin or waning flow conditions. The rare occurrence of some meltwater landforms beyond the bounds of the corridors likely indicates formation during infrequent high magnitude event(s) when the rate of melt supply vastly exceeded the drainage capacity of the hydrological system.

The dominant overall landform type in SMC appears to be erosional, suggesting that sediment from SMC is transported down flow and probably evacuated from under the ice, at the ice margin. However, at a regional scale, depositional landforms are common indicating local variability in erosion and deposition along individual systems. Outside of SMC, the poor hydraulic connectivity of the weakly connected distributed drainage system limits sediment mobilisation and restricts transport by meltwater (***Alley et al., 1997***).

6.1.2. Deformation-dominated SMC (**Fig. 11C**)

Till deformation is strongly controlled by porewater pressure and ice-bed coupling (***Boulton et al., 2001; Iverson et al., 2003, 2007; Kavanaugh & Clark, 2006; Truffer & Harrison, 2006; Bougamont et al., 2014; Damsgaard et al., 2016, 2020***). It therefore follows that fluctuating subglacial water pressure within the hydraulically-connected drainage system (meltwater corridors) (**Fig. 11A**) will generate complex meltwater drainage configurations and geomorphic imprints that differs from the surrounding weakly-connected regions where high-water pressure in the till and widespread ice-bed coupling is maintained. Deformation is generally facilitated by increasing pore-water pressures weakening the till, although at high water pressures the basal ice will decouple from the underlying till, increasing sliding and reducing till deformation.

Our results suggest that bed-forming processes (i.e., growth of lineations, drumlins and ribbed moraines) are generally reduced along hydraulically-connected corridors due to repeated ice-bed decoupling when the drainage system becomes overwhelmed (e.g., during spring) (***Davison et al., 2019***). This allows distinct ribbed and streamlined tracts to be partially preserved along hydraulically connected corridors with ice-related deformation outside the corridors able to keep reshaping the landscape.

Although we suggest there is less cumulative deformation within active SMC compared to the surrounding weakly connected distributed drainage areas, repeated ice-bed (re-) coupling in response to fluctuating surface meltwater inputs (e.g., ***Truffer & Harrison, 2006; Bougamont et al., 2014; Damsgaard et al., 2020; Becher and Johnson, 2021***) can also result in deformation of existing bedforms within the corridor. This ice-water-sediment (re-) coupling manifests as stubbier lineations, potentially smaller ribs within corridors (***Dunlop and Clark, 2006***) and a continuum of morphologies distinct to meltwater corridors (e.g., murtoos; remobilised ribbed moraines, murtoo-related ridges, proto murtoos)

(**Fig. 11C**). The cumulative deformation in corridors depends on the degree of ice-bed coupling, modulating factors such as grain size, till thickness, ice thickness and surface-slope, ice velocity, and the duration that the corridor was active.

6.1.3. SMC evolution in response to changing ice-water-sediment coupling

SMC are a composite imprint of spatio-temporal variations in ice-water-sediment coupling (i.e., a time-transgressive landsystem) (**Fig. 12**). The time-transgressive nature of the geomorphological assemblages found in SMC is best illustrated by the occurrence of eskers (youngest subglacial conduits) that crosscut SMC (oldest subglacial drainage) at significant angles (>30° angles, **Figs. 9C, 10C**). Within the SMC longitudinal and lateral transitions in landform morphology (e.g., from hummocks to ridges; and inset channels) also suggest that the geomorphic record results from multiple episodes of modification linked to variations in ice-water-sediment coupling. Overall, where and when ice-bed decoupling dominates, meltwaters scour till and bedrock producing channels and progressively fragmenting the adjacent till sheet and existing bedforms (e.g., ribbed moraines or lineations). The eroded sediment is ultimately either evacuated from under the ice to the ice margin or re-deposited down-ice in cavities and crevasses (Section 6.1.1). Conversely, where and when ice-bed coupling occurs (Section 6.1.2), new bedforms (e.g., murtoos, streamlined hummocks) are generated by deforming existing subglacial bedforms (e.g., streamlined tracts) in the direction of palaeo-ice flow.

A simple explanation for variations in coupling could be that water pressure fluctuates hourly-to-seasonally (as seen at present-day glaciers and ice sheets, ***Rada & Schoof, 2018; Davison et al., 2019***). Hence, these fluctuations provoke alternation between meltwater erosion-deposition processes and glacially-induced deformation processes, which in turn leads to the formation, transformation and then fragmentation of bedforms. For example, the transformation of existing bedforms into murtoos and ridges appears to be the combined result of fluctuations in ice-water and ice-bed coupling related to repetitive flooding along SMC (***Mäkinen et al., 2017; Ojala et al., 2019, 2021; Becher Peterson & Johnson, 2021; Vérité et al. 2022***). Similarly, streamlined hummocks are interpreted to record deposition during ice-bed decoupling followed by deformation during recoupling (***Haiblen, 2017***); the increase in elongation and frequency of streamlining towards the edge of corridors being concomitant

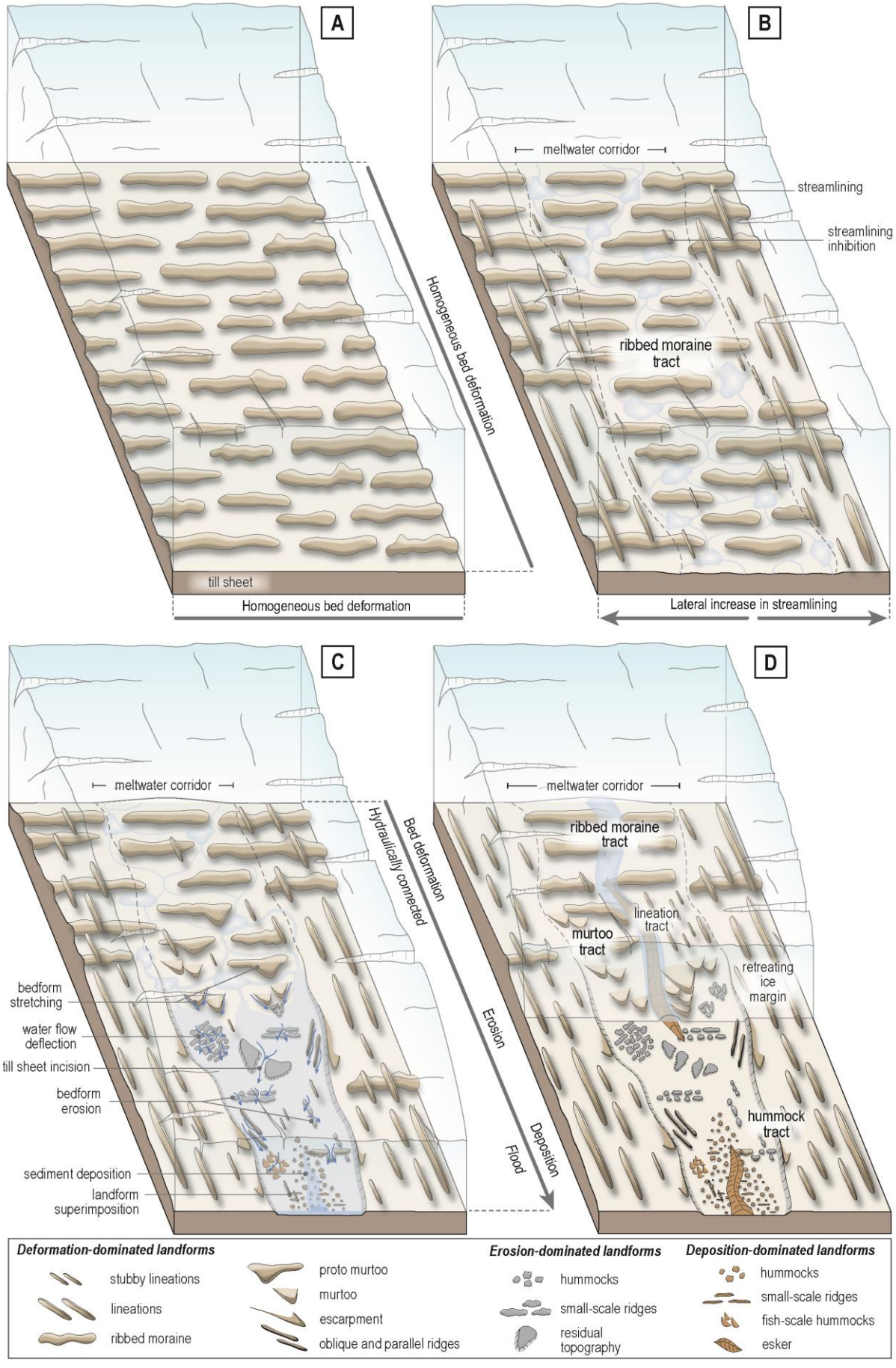
A
B
meltwater corridor
streamlining
streamlining inhibition
ribbed moraine tract
Homogeneous bed deformation
till sheet
Homogeneous bed deformation
Lateral increase in streamlining
C
D
meltwater corridor
meltwater corridor
Hydraulically connected
Bed deformation
ribbed moraine tract
lineation tract
murtoo tract
retreating ice margin
bedform stretching
water flow deflection
till sheet incision
bedform erosion
sediment deposition
landform superimposition
Erosion
Flood
Deposition
hummock tract
Deformation-dominated landforms
stubby lineations
lineations
ribbed moraine
proto murtoo
murtoo
escarpment
oblique and parallel ridges
Erosion-dominated landforms
hummocks
small-scale ridges
residual topography
Deposition-dominated landforms
hummocks
small-scale ridges
fish-scale hummocks
esker

Figure 12. Potential evolution of a SMC in response to ice-water-sediment coupling. A. *Ribbed moraines form widely across the bed* ***B.*** *Water flow becomes organised down a corridor inhibiting streamlining due to evacuation of sediment and reduced pore-water pressures (greater connectivity). This hydraulically well-connected drainage may involve interaction with a central conduit. The ribs are largely preserved in the corridor apart from minor streamlining.* ***C.*** *Continued variations in ice-water-sediment coupling result in modification (deformation) and fragmentation (e.g., due to dissection by water flow) of bedforms, and also deposition of new features (although note these are not included here). Erosion (e.g., by minor channels) results in the emergence of geometric patterning.* ***D.*** *Deposition in the conduit close to the margin produces an esker as ice recedes back across the region. See the main text for other possible landform signature evolutions.*

with greater ice-bed coupling away from the main drainage axis.

The evolution and final landform signature of SMC is conditioned by the pre-existing landform assemblage. A first scenario, identified in SW Keewatin and Finland, is where fields of ribbed moraines (**Fig. 12A**) are locally preserved/ modified in the SMC, forming ribbed tracts (**Fig. 12B**), while outside the corridor the ribs transform into lineations or lineations are superimposed on ribs. The degree to which the ribbed moraine tracts are subsequently modified (**Fig. 12C-D**) and evolve into other tracts depends on the dominant modification process: (1) erosion/deposition (hummock tracts) or (2) deformation (murtoo tracts). The spatio-temporal operation of these processes is controlled by changing water pressure and drainage conditions along the subglacial meltwater corridor. A second scenario is when an initial field of lineations is penecontemporaneously reworked during meltwater corridor development, via fragmentation into longitudinally-organised hummocks and deposition of hummock tracts. Corridor development can also occur concurrently with subglacial bed-forming, as evidenced by lateral gradations into stubbier streamlined bedforms towards and into corridors. Thus, the timing of streamlining proposed in Fig. 12B, C may either predate or occur contemporaneously with subglacial meltwater corridor formation. Finally, streamlined tracts could represent the differential response of streamlining after the cessation of subglacial meltwater corridor activity, although this relationship is less clear.

6.2. Implications for understanding subglacial meltwater drainage and its broader impact

Our model for subglacial meltwater corridors, and their widespread occurrence in Canada and Fennoscandia (***Peterson et al., 2017; Lewington et al., 2020; McMartin et al., 2021; Ahokangas et al., 2021; Dewald et al., 2022***) suggests that subglacial meltwater is typically organised into broad (up to km-wide) corridors of well-connected drainage, with the intervening (often streamlined) till sheets likely characterized by high pore-water pressures in a weakly connected drainage system. This concept of

spatially varying water content, pressure and till properties is consistent with the idea of a transient mosaic of bed conditions (***Piotrowski, 2004; Lee and Philips, 2008; Murray et al., 2008***). It also suggests that water is a key control on the production of subglacial bedforms and ice-dynamic processes across wide regions of the bed, with the SMC in Keewatin estimated to comprise 5-36% of the bed (***Lewington et al., 2020***) except under large ice divide zones or relict cold-based landscapes where they are rare or absent (e.g., ***McMartin et al., 2021***). Lateral gradations in streamlined bedform size and elongation, and bedform types (e.g., murtoos) in association with SMC are interpreted to reflect variations in ice-water-sediment coupling rather than ice flow speed. Thus, the lateral extent and density of corridors are likely to be key controls governing bedforming processes.

As SMC are interpreted to record variations in ice-water-sediment coupling, our model requires pulsed delivery of water at the bed, which could be caused by surface melt inputs and/ or subglacial lake draining. Given the limited evidence for subglacial lakes in Keewatin (***Livingstone et al., 2013***), and the ice-sheet scale organisation and occurrence of SMC (***Dewald et al., 2022***) we favour a surface meltwater source associated with enhanced surface ablation during deglaciation (e.g., ***Carlson et al., 2008, 2009***). This is consistent with modern observations of ice sheet hydrological processes, specifically, the formation of broad hydraulically connected 'corridors' during the melt season (e.g., ***Nanni et al., 2021***). Indeed, in the absence of surface-melt contributions to the bed, SMC on the deglaciated Antarctic continental shelf are rare (although see ***Simkins et al., 2021***).

Palaeo-studies suggest that meltwater landform patterning is likely to reflect both local (e.g., topography - ***Simkins et al., 2021***) and external controls (e.g., increased water inputs as air temperatures rise – ***Storrar et al., 2014***). Although the full range of meltwater corridors and associated landform signature types are found in both northern Canada and Fennoscandia, murtoo tracts are noticeably more common in the latter. These murtoos tend to be associated with former ice lobes and occur in locations corresponding to periods of rapid ice-margin retreat and delivery of large volumes of supraglacial meltwater to the bed (***Ojala et al., 2019***). More detailed mapping and field investigations of these and other discrete tracts (e.g., depositional and erosional hummock tracts) would likely provide insights into the controls governing meltwater corridor formation, density and spacing.

The palimpsest signature of SMC and bedform formation allows the relative timing and style of subglacial drainage activity to be unravelled. SMC formed both contemporaneously and penecontemporaneously to streamlined bedforms, with eskers formed later as a final signature of deglaciating meltwater drainage at or near the ice-margin. The repetition of diverse bedform signatures both between and within individual corridors, and evidence that bedforms and subglacial meltwater landforms are reworked, deformed and eroded by repeated ice-bed and ice-water coupling implies time-transgressive formation. The implication is that corridors were probably not all active at the same time and thus that whole networks were not formed synchronously by large sheet floods (e.g., see ***Sharpe et al., 2017, 2021***). Bedform superposition relationships suggest that wide erosional corridors largely formed up-ice, with increased channelisation (e.g., eskers) and narrower, largely depositional corridors towards the ice margin. It might therefore be possible to use the palimpsest record, and the width and repetition of discrete tracts to infer the style and rates of ice retreat.

Further work is required to better connect our interpretation of subglacial water drainage down corridors to mathematical treatments of the stability of various types of water drainage configurations. For example, ***Walder and Fowler (1994)*** and ***Ng (2000)*** showed theoretically that a water film over deformable sediment is unstable and would either collapse to R-channels (i.e. esker type conduits) or wider sediment-floored 'canals', according to controls of effective pressure and water discharge. Interestingly, a prediction that arose is that R-channels are favoured under steeper ice surface slopes and canals under flatter slopes. This is exactly the circumstance we deduce from the evolution of meltwater corridors to eskers over time, whereupon wider canal type flow is replaced by R-channel flow as the ice margin withdrew, noting that surface slopes are typically steeper close the ice margin. It is also worth noting that ***Carter et al. (2017)*** found that drainage through sediment floored canals rather than R-channels allowed them to better match some Antarctic subglacial lake drainage and refilling events. We suggest that our observations and data especially on the size and spacing of meltwater corridors and transitions between corridor to R-channel configurations may be useful in building or testing theory.

7. Conclusions

Building on previous work, this paper has used high-resolution (2-m) DEMs and field-based observations in selected areas in northern Canada and Fennoscandia to describe and interpret the landform assemblages (tracts) that together form networks of SMC. We identify tracts of depositional and erosional hummocks and small-scale ridges, murtoos and murtoo-related bedforms, and ribbed and streamlined bedforms, often connected by or containing eskers or minor meltwater channels.

The diversity of landforms found within SMC is interpreted to record variations in ice-water-sediment coupling in response to meltwater forcing. During periods of enhanced melt supply, water floods the drainage system forming broad hydraulically-connected SMC. These flood events modify existing streamlined bedforms, ribbed moraines and murtoos by meltwater erosion, yielding geometric ridge and hummock patterns. Eroded sediments are partially redeposited downstream in cavities and basal crevasses and as megadunes. During periods of reduced water supply the ice will recouple with the bed resulting in the deformation of existing landforms. Repeated cycles of flooding (ice-bed decoupling) and deformation (ice-bed recoupling) produce a continuum of morphologies associated with the formation, transformation and fragmentation of bedforms. Following previous work, we suggest that the transformation of existing bedforms into murtoos and ridges is the combined result of fluctuations in ice-bed coupling related to repetitive flooding along subglacial meltwater corridors (Vérité et al. 2022). As cumulative deformation is lower within corridors compared to the surrounding weakly connected drainage system, bed-forming processes are typically reduced producing stubbier lineations and enabling older bedforms (ribs and streamlined bedforms) to be partially preserved.

The evolution and final landform signature of SMC is conditioned by the pre-existing landform assemblage, and represents a time-integrated pattern of changing conditions during ice retreat and fluctuating melt forcing. The record is a palimpsest, often with broad erosional corridors containing a narrower zone of depositional hummocks and ridges, sometimes partially deformed, and then eskers and minor channels, some of which are misaligned or cut obliquely across the corridors. Combined with the repetition of tracts and both contemporaneous and penecontemporaneous relationships with the surrounding bedforms, we suggest that not all corridors were active at once, and that formation was time-transgressive, with erosion more prevalent up ice and deposition closer to the margin.

Our findings have implications for understanding the impact of subglacial hydrological processes on bed-forming and the stability of drainage configurations on soft and hard-bedded ice sheets. The impact of the drainage configuration on cumulative deformation (ice-water-sediment coupling) and sediment availability is shown to play a key role in controlling bedform formation and morphology. This study demonstrates the importance of examining the geomorphic record of past ice sheets to understand the glaciological dynamics of present day ice sheets. SMC provide an important record for understanding subglacial hydrological processes beneath the Greenland and Antarctic ice sheets, including the relative importance of the hydraulically-connected and weakly-connected drainage components, their spatio-temporal evolution with warming and their impact on ice dynamics.

Data Availability

Publicly available high-resolution DEMs were used to identify and describe subglacial bedforms and meltwater landforms, including national 2-m LiDAR datasets in Sweden (https://www.lantmateriet.se) and Finland (https://www.maanmittauslaitos.fi/en) and the 2-m ArcticDEM mosaic v7 (https://www.pgc.umn.edu/data/arcticdem) in northern Canada.

Acknowledgements

This project benefitted from the PALGLAC team of researchers and received funding from the ERC to CDC under the European Union's Horizon 2020 research and innovation programme (Grant agreement No. 787263). ELML was funded through "Adapting to the Challenges of a Changing Environment" (ACCE), a NERC-funded doctoral training partnership ACCE DTP (NE/L002450/1). This study has benefited from the ANR Ice Collapse team of researchers funded by the French Agence Nationale de la Recherche through grant ANR-18-CE01-0009. Field work in northern Canada for IM and JC is a contribution to Natural Resources Canada Geomapping for Energy and Minerals (GEM) - GeoNorth Program (NRCan contribution number 20220127). We thank Etienne Brouard for constructive feedback and edits on an earlier draft.

Author Contributions

EL and ND carried out the initial large-sale mapping of subglacial meltwater corridors. SJL, ER, JV, IM, JC, CDC identified and described individual landforms and landform tracts. SJL, ER, JV, ND IM, JC produced the figures. IM and JC collected the field data. The model was conceptualised by JV, ER, SJL, CDC, with contributions from all authors. SJL wrote the paper with contributions from all authors.

References

Ahokangas, E., Ojala, A.E., Tuunainen, A., Valkama, M., Palmu, J.P., Kajuutti, K. and Mäkinen, J., 2021. The distribution of glacial meltwater routes and associated murtoo fields in Finland. Geomorphology, p.107854.

Allen, J.R.L. 1982. Developments in Sedimentology, vol. 30B, Sedimentary Structures—Their Character and Physical Basis, vol. 1, Elsevier, Amsterdam.

Alley, R.B., Cuffey, K.M., Evenson, E.B., Strasser, J.C., Lawson, D.E. and Larson, G.J., 1997. How glaciers entrain and transport basal sediment: physical constraints. Quaternary Science Reviews, 16(9), pp.1017-1038.

Alley, R.B., Cuffey, K.M. and Zoet, L.K., 2019. Glacial erosion: status and outlook. Annals of Glaciology, 60(80), pp.1-13.

Anandakrishnan, S. and Alley, R.B., 1997. Stagnation of ice stream C, West Antarctica by water piracy. Geophysical Research Letters, 24(3), pp.265-268.

Andrews, L.C., Catania, G.A., Hoffman, M.J., Gulley, J.D., Lüthi, M.P., Ryser, C., Hawley, R.L. and Neumann, T.A., 2014. Direct observations of evolving subglacial drainage beneath the Greenland Ice Sheet. Nature, 514(7520), pp.80-83.

Bartholomew, I., Nienow, P., Mair, D., Hubbard, A., King, M.A. and Sole, A., 2010. Seasonal evolution of subglacial drainage and acceleration in a Greenland outlet glacier. Nature Geoscience, 3(6), pp.408-411.

Becher Peterson, G. and Johnson, M.D., 2021. Sedimentology and internal structure of murtoos-V-shaped landforms indicative of a dynamic subglacial hydrological system. Geomorphology, 380, p.107644.

Bendixen, M., Iversen, L.L., Bjørk, A.A., Elberling, B., Westergaard-Nielsen, A., Overeem, I., Barnhart, K.R., Khan, S.A., Box, J.E., Abermann, J. and Langley, K., 2017. Delta progradation in Greenland driven by increasing glacial mass loss. Nature, 550(7674), pp.101-104.

Bougamont, M., Christoffersen, P., A L, H., Fitzpatrick, A.A., Doyle, S.H. and Carter, S.P., 2014. Sensitive response of the Greenland Ice Sheet to surface melt drainage over a soft bed. Nature communications, 5(1), pp.1-9.

Boulton, G.S., Dobbie, K.E. and Zatsepin, S., 2001. Sediment deformation beneath glaciers and its coupling to the subglacial hydraulic system. Quaternary International, 86(1), pp.3-28.

Brennand, T.A., 1994. Macroforms, large bedforms and rhythmic sedimentary sequences in subglacial eskers, south-central Ontario: implications for esker genesis and meltwater regime. Sedimentary Geology, 91(1-4), pp.9-55.

Bunce, C., Nienow, P., Sole, A., Cowton, T. and Davison, B., 2021. Influence of glacier runoff and near-terminus subglacial hydrology on frontal ablation at a large Greenlandic tidewater glacier. Journal of Glaciology, 67(262), pp.343-352.

Burke, M.J., Brennand, T.A. and Perkins, A.J., 2012a. Transient subglacial hydrology of a thin ice sheet: insights from the Chasm esker, British Columbia, Canada. Quaternary Science Reviews, 58, pp.30-55.

Burke, M.J., Brennand, T.A. and Perkins, A.J., 2012b. Evolution of the subglacial hydrologic system beneath the rapidly decaying Cordilleran Ice Sheet caused by ice-dammed lake drainage: implications for meltwater-induced ice acceleration. Quaternary Science Reviews, 50, pp.125-140.

Campbell, J.E., Lauzon, G., Dyke, A.S., Haiblen, A.M., and Roy, M. 2016. Report of 2016 activities for the regional surficial geological mapping of the south Rae Craton, southeast NWT: GEM 2 South Rae Quaternary and Bedrock Project; Geological Survey of Canada, Open File 8143. 13p. doi:10.4095/299391

Campbell, J.E., McCurdy, M.W., Lauzon, G., Regis, D., and Wygergangs, M., 2020. Field data, till composition, and ice-flow history, south Rae Craton, Northwest Territories: results from the GEM-2 South Rae project — Surficial Mapping activity; Geological Survey of Canada, Open File 8714, 1 .zip file. https://doi.org/10.4095/327218

Carlson, A.E., LeGrande, A.N., Oppo, D.W., Came, R.E., Schmidt, G.A., Anslow, F.S., Licciardi, J.M. and Obbink, E.A., 2008. Rapid early Holocene deglaciation of the Laurentide ice sheet. Nature Geoscience, 1(9), pp.620-624.

Carlson, A.E., Anslow, F.S., Obbink, E.A., LeGrande, A.N., Ullman, D.J. and Licciardi, J.M., 2009. Surface-melt driven Laurentide Ice Sheet retreat during the early Holocene. Geophysical Research Letters, 36(24).

Carter, S.P., Fricker, H.A. and Siegfried, M.R., 2017. Antarctic subglacial lakes drain through sediment-floored canals: theory and model testing on real and idealized domains. The Cryosphere, 11(1), pp.381-405.

Chandler, D.M., Wadham, J.L., Nienow, P.W., Doyle, S.H., Tedstone, A.J., Telling, J., Hawkings, J., Alcock, J.D., Linhoff, B. and Hubbard, A., 2021. Rapid development and persistence of efficient subglacial drainage under 900 m-thick ice in Greenland. Earth and Planetary Science Letters, 566, p.116982.

Clark, C.D., Ely, J.C., Spagnolo, M., Hahn, U., Hughes, A.L.C., Stokes, C.R., 2018. Spatial organization of drumlins. Earth Surf. Processes Landforms 43, pp.499–513.

Cook, S.J., Swift, D.A., Kirkbride, M.P., Knight, P.G. and Waller, R.I., 2020. The empirical basis for modelling glacial erosion rates. Nature communications, 11(1), pp.1-7.

Cowton, T., Nienow, P., Bartholomew, I., Sole, A. and Mair, D., 2012. Rapid erosion beneath the Greenland ice sheet. Geology, 40(4), pp.343-346.

Cowton, T., Nienow, P., Sole, A., Bartholomew, I. and Mair, D., 2016. Variability in ice motion at a land-terminating Greenlandic outlet glacier: the role of channelized and distributed drainage systems. Journal of Glaciology, 62(233), pp.451-466.

Daerr, A., Lee, P., Lanuza, J. and Clément, É., 2003. Erosion patterns in a sediment layer. Physical Review E, 67(6), p.065201.

Dahlgren, S., 2013, Subglacially eroded meltwater hummocks: Master of Science thesis, University of Gothenburg, Gothenburg, Sweden, 49 pp.

Dalton, A.S., Margold, M., Stokes, C.R., Tarasov, L., Dyke, A.S., Adams, R.S., Allard, S., Arends, H.E., Atkinson, N., Attig, J.W. and Barnett, P.J., 2020. An updated radiocarbon-based ice margin chronology for the last deglaciation of the North American Ice Sheet Complex. Quaternary Science Reviews, 234, p.106223.

Damsgaard, A., Egholm, D.L., Beem, L.H., Tulaczyk, S., Larsen, N.K., Piotrowski, J.A. and Siegfried, M.R., 2016. Ice flow dynamics forced by water pressure variations in subglacial granular beds. Geophysical Research Letters, 43(23), pp.12-165.

Damsgaard, A., Goren, L. and Suckale, J., 2020. Water pressure fluctuations control variability in sediment flux and slip dynamics beneath glaciers and ice streams. Communications Earth & Environment, 1(1), pp.1-8.

Das, S.B., Joughin, I., Behn, M.D., Howat, I.M., King, M.A., Lizarralde, D. and Bhatia, M.P., 2008. Fracture propagation to the base of the Greenland Ice Sheet during supraglacial lake drainage. Science, 320(5877), pp.778-781.

Davison, B.J., Sole, A.J., Livingstone, S.J., Cowton, T.R. and Nienow, P.W., 2019. The influence of hydrology on the dynamics of land-terminating sectors of the Greenland ice sheet. Frontiers in Earth Science, 7, p.10.

DesRosiers, P., 2021. The effect of deglacial meltwater processes on kimberlite indicator mineral concentrations in glacial sediments (Doctoral dissertation, Science: Department of Earth Sciences).

Dewald, N., Livingstone, S.J. and Clark, C.D., 2022. Subglacial meltwater routes of the Fennoscandian Ice Sheet. Journal of Maps, pp.1-15.

Dredge, L., Nixon, F., and Richardson, R. 1985. Surficial Geology, Northwestern Manitoba: Geological Survey of Canada, Series Map 1608A, 1 : 500 000.

Dredge, L.A., Campbell, J.E. and McMartin, I., 2016: Surficial geology, Walker Lake south, Nunavut, NTS 56J-south; Geological Survey of Canada, CGM-151, (ed.2, Prelim.) scale 1:100 000, https://doi.org/10.4095/298698

Dunlop, P. and Clark, C.D., 2006. The morphological characteristics of ribbed moraine. Quaternary Science Reviews, 25(13-14), pp.1668-1691.

Dunlop, P., Clark, C.D. and Hindmarsh, R.C., 2008. Bed ribbing instability explanation: testing a numerical model of ribbed moraine formation arising from coupled flow of ice and subglacial sediment. Journal of Geophysical Research: Earth Surface, 113(F3).

Ely, J.C., Clark, C.D., Spagnolo, M., Stokes, C.R., Greenwood, S.L., Hughes, A.L., Dunlop, P. and Hess, D., 2016. Do subglacial bedforms comprise a size and shape continuum? Geomorphology, 257, pp.108-119.

Evans, D.J., Ewertowski, M., Roberts, D.H. and Tomczyk, A.M., 2022. The historical emergence of a geometric and sinuous ridge network at the Hørbyebreen polythermal glacier snout, Svalbard and its use in the interpretation of ancient glacial landforms. Geomorphology, p.108213.

Fannon, J.S., Fowler, A.C. and Moyles, I.R., 2017. Numerical simulations of drumlin formation. Proceedings of the Royal Society A: Mathematical, Physical and Engineering Sciences, 473(2204), p.20170220.

Fisher, T.G. and Shaw, J., 1992. A depositional model for Rogen moraine, with examples from the Avalon Peninsula, Newfoundland. Canadian Journal of Earth Sciences, 29(4), pp.669-686.

Fowler, A.C. and Chapwanya, M., 2014. An instability theory for the formation of ribbed moraine, drumlins and mega-scale glacial lineations. Proceedings of the Royal Society A: Mathematical, Physical and Engineering Sciences, 470(2171), p.20140185.

Fried, M.J., Catania, G.A., Bartholomaus, T.C., Duncan, D., Davis, M., Stearns, L.A., Nash, J., Shroyer, E. and Sutherland, D., 2015. Distributed subglacial discharge drives significant submarine melt at a Greenland tidewater glacier. Geophysical Research Letters, 42(21), pp.9328-9336.

Greenwood, S.L., Clason, C.C., Helanow, C. and Margold, M., 2016. Theoretical, contemporary observational and palaeo-perspectives on ice sheet hydrology: processes and products. Earth-Science Reviews, 155, pp.1-27.

Haiblen, A.M., 2017. Glacial history and landform genesis in the Lac de Gras area, Northwest Territories (Doctoral dissertation, Science: Department of Earth Sciences).

Hewitt, I. J. 2011. Modelling distributed and channelized subglacial drainage: the spacing of channels. Journal of Glaciology, 57, pp.302-314.

Hewitt, I.J. and Creyts, T.T., 2019. A model for the formation of eskers. Geophysical Research Letters, 46(12), pp.6673-6680.

Hindmarsh, R. C. A. 1998a. The stability of a viscous till sheet coupled with ice flow, considered at wavelengths less than ice thickness, J. Glaciol., 44, 288 – 292.

Hindmarsh, R. C. A. 1998b. Drumlinization and drumlin-forming instabilities: Viscous till mechanisms, J. Glaciol., 44, 293 – 314.

Hindmarsh, R. C. A. 1998c. Ice-stream surface texture, sticky-spots, waves and breathers: The coupled flow of ice, till and water, J. Glaciol., 44, 589 – 614.

Hoffman, M.J., Andrews, L.C., Price, S.F., Catania, G.A., Neumann, T.A., Lüthi, M.P., Gulley, J., Ryser, C., Hawley, R.L. and Morriss, B., 2016. Greenland subglacial drainage evolution regulated by weakly connected regions of the bed. Nature communications, 7(1), pp.1-12.

Hubbard, B.P., Sharp, M.J., Willis, I.C., Nielsen, M. and Smart, C.C., 1995. Borehole water-level variations and the structure of the subglacial hydrological system of Haut Glacier d'Arolla, Valais, Switzerland. Journal of Glaciology, 41(139), pp.572-583.

Hughes, A.L., Gyllencreutz, R., Lohne, Ø.S., Mangerud, J. and Svendsen, J.I., 2016. The last Eurasian ice sheets–a chronological database and time-slice reconstruction, DATED-1. Boreas, 45(1), pp.1-45.

Iken, A. and Bindschadler, R.A., 1986. Combined measurements of subglacial water pressure and surface velocity of Findelengletscher, Switzerland: conclusions about drainage system and sliding mechanism. Journal of Glaciology, 32(110), pp.101-119.

Iverson, N.R., Cohen, D., Hooyer, T.S., Fischer, U.H., Jackson, M., Moore, P.L., Lappegard, G. and Kohler, J., 2003. Effects of basal debris on glacier flow. Science, 301(5629), pp.81-84.

Iverson, N.R., Hooyer, T.S., Fischer, U.H., Cohen, D., Moore, P.L., Jackson, M., Lappegard, G. and Kohler, J., 2007. Soft-bed experiments beneath Engabreen, Norway: regelation infiltration, basal slip and bed deformation. Journal of Glaciology, 53(182), pp.323-340.

Jenkins, A., 2011. Convection-driven melting near the grounding lines of ice shelves and tidewater glaciers. Journal of Physical Oceanography, 41(12), pp.2279-2294.

Kavanaugh, J.L. and Clarke, G.K., 2006. Discrimination of the flow law for subglacial sediment using in situ measurements and an interpretation model. Journal of Geophysical Research: Earth Surface, 111(F1).

Kerr, D., Knight, R., Sharpe, D., and Cummings, D. 2014a. Reconnaissance surficial geology, Lynx Lake, Northwest Territories, NTS 75-J, Geological Survey of Canada, 1:125000.

Kerr, D., Knight, R., Sharpe, D., and Cummings, D. 2014b. Reconnaissance surficial geology, Walmsley Lake, Northwest Territories, NTS 75-N, Canadian Geoscience Map-140, Geological Survey of Canada, 1:125000.

Kirkham, J.D., Hogan, K.A., Larter, R.D., Self E., Games, K., Huuse, M., Stewart, M.A., Ottesen, D., Arnold, N.S., Dowdeswell, J.A. 2021. Tunnel valley infill and genesis revealed by high-resolution 3-D seismic data. Geology 2021; doi: https://doi.org/10.1130/G49048.1

Lai, C.Y., Stevens, L.A., Chase, D.L., Creyts, T.T., Behn, M.D., Das, S.B. and Stone, H.A., 2021. Hydraulic transmissivity inferred from ice-sheet relaxation following Greenland supraglacial lake drainages. Nature communications, 12(1), pp.1-10.

Lauzon, G. and Campbell, J.E. 2018. Surficial geology, Wholdaia Lake south, Northwest Territories, NTS 75-A south; Geological Survey of Canada, Canadian Geoscience Map 342, (ed. prelim.); 1 sheet, doi:10.4095/ 306373.

Lewington, E.L., Livingstone, S.J., Sole, A.J., Clark, C.D. and Ng, F.S., 2019. An automated method for mapping geomorphological expressions of former subglacial meltwater pathways (hummock corridors) from high resolution digital elevation data. Geomorphology, 339, pp.70-86.

Lewington, E.L., Livingstone, S.J., Clark, C.D., Sole, A.J. and Storrar, R.D., 2020. A model for interaction between conduits and surrounding hydraulically connected distributed drainage based on geomorphological evidence from Keewatin, Canada. The Cryosphere, 14(9), pp.2949-2976.

Lewington, E.L.M., 2020. New insights into subglacial meltwater drainage pathways from the ArcticDEM. Ph.D.. University of Sheffield. Sheffield.

Livingstone, S.J., Lewington, E.L., Clark, C.D., Storrar, R.D., Sole, A.J., McMartin, I., Dewald, N. and Ng, F., 2020. A quasi-annual record of time-transgressive esker formation: implications for ice-sheet reconstruction and subglacial hydrology. The Cryosphere, 14(6), pp.1989-2004.

Mäkinen, J., 2003. Time-transgressive deposits of repeated depositional sequences within interlobate glaciofluvial (esker) sediments in Köyliö, SW Finland. Sedimentology, 50(2), pp.327-360.

McMartin, I., Campbell, J.E., Dredge, L.A., LeCheminant, A.N.., McCurdy, M.W., and Scromeda, N., 2015a. Quaternary geology and till composition north of Wager Bay, Nunavut: Results from the GEM Wager Bay Surficial Geology Project; Geological Survey of Canada, Open File 7748, doi:10.4095/296419.

McMartin, I., Campbell, J.E. and Dredge, L.A. 2015b: Surficial geology, Curtis Lake north, Nunavut, NTS 56I-north; Geological Survey of Canada, CGM-205, (ed. prelim.), scale 1:100 000, https://doi.org/10.4095/295851.

McMartin, I., Godbout, P.M., Campbell, J.E., Tremblay, T. and Behnia, P., 2021. A new map of glacigenic features and glacial landsystems in central mainland Nunavut, Canada. Boreas, 50(1), pp.51-75.

Mejía, J.Z., Gulley, J.D., Trunz, C., Covington, M.D., Bartholomaus, T.C., Xie, S. and Dixon, T.H., 2021. Isolated cavities dominate Greenland ice sheet dynamic response to lake drainage. Geophysical Research Letters, 48(19), p.e2021GL094762.

Morton, R.A., 1978. Large-scale rhomboid bed forms and sedimentary structures associated with hurricane washover. Sedimentology, 25(2), pp.183-204.

Murray, T., Corr, H., Forieri, A. and Smith, A.M., 2008. Contrasts in hydrology between regions of basal deformation and sliding beneath Rutford Ice Stream, West Antarctica, mapped using radar and seismic data. Geophysical Research Letters, 35(12).

Nanni, U., Gimbert, F., Roux, P. and Lecointre, A., 2021. Observing the subglacial hydrology network and its dynamics with a dense seismic array. Proceedings of the National Academy of Sciences, 118(28).

Ng, F.S., 2000. Canals under sediment-based ice sheets. Annals of Glaciology, 30, pp.146-152.

Ojala, A.E., Peterson, G., Mäkinen, J., Johnson, M.D., Kajuutti, K., Palmu, J.P., Ahokangas, E. and Öhrling, C., 2019. Ice-sheet scale distribution and morphometry of triangular-shaped hummocks (murtoos): a subglacial landform produced during rapid retreat of the Scandinavian Ice Sheet. Annals of Glaciology, 60(80), pp.115-126.

Ojala, A.E., Mäkinen, J., Kajuutti, K., Ahokangas, E. and Palmu, J.P., Subglacial evolution from distributed to channelized drainage: evidence from the Lake Murtoo area in SW Finland. Earth Surface Processes and Landforms.

Overeem, I., Hudson, B.D., Syvitski, J.P., Mikkelsen, A.B., Hasholt, B., Van Den Broeke, M.R., Noël, B.P.Y. and Morlighem, M., 2017. Substantial export of suspended sediment to the global oceans from glacial erosion in Greenland. Nature Geoscience, 10(11), pp.859-863.

Peterson, G. and Johnson, M.D., 2018. Hummock corridors in the south-central sector of the Fennoscandian ice sheet, morphometry and pattern. Earth Surface Processes and Landforms, 43(4), pp.919-929.

Peterson, G., Johnson, M.D. and Smith, C.A., 2017. Glacial geomorphology of the south Swedish uplands–focus on the spatial distribution of hummock tracts. Journal of Maps, 13(2), pp.534-544.

Peterson, G., Johnson, M.D., Dahlgren, S., Påsse, T. and Alexanderson, H., 2018. Genesis of hummocks found in tunnel valleys: an example from Hörda, southern Sweden. GFF, 140(2), pp.189-201.

Piotrowski, J.A. and Kraus, A.M., 1997. Response of sediment to ice-sheet loading in northwestern Germany: effective stresses and glacier-bed stability. Journal of Glaciology, 43(145), pp.495-502.

Rada, C. and Schoof, C., 2018. Channelized, distributed, and disconnected: subglacial drainage under a valley glacier in the Yukon. The Cryosphere, 12(8), pp.2609-2636.

Rampton, V.N., 2000. Large-scale effects of subglacial meltwater flow in the southern Slave Province, Northwest Territories, Canada. Canadian Journal of Earth Sciences, 37(1), pp.81-93.

Rattas, M. and Piotrowski, J.A., 2003. Influence of bedrock permeability and till grain size on the formation of the Saadjärve drumlin field, Estonia, under an east-Baltic Weichselian ice stream. Boreas, 32(1), pp.167-177.

Roberts, M.J., 2005. Jökulhlaups: a reassessment of floodwater flow through glaciers. Reviews of Geophysics, 43(1).

Schoof, C., 2007. Pressure-dependent viscosity and interfacial instability in coupled ice–sediment flow. Journal of Fluid Mechanics, 570, pp.227-252.

Sharpe, D.R., Kjarsgaard, B.A., Knight, R.D., Russell, H.A.J. and Kerr, D.E., 2017. Glacial dispersal and flow history, east arm area of Great Slave Lake, NWT, Canada. Quaternary Science Reviews, 165, pp.49-72.

Sharpe, D., Lesemann, J., Knight, R. and Kjarsgaard, B., 2021. Regional stagnation of the western Keewatin ice sheet and the significance of meltwater corridors and eskers, northern Canada. Canadian Journal of Earth Sciences, (ja).

Shaw, J., 2002. The meltwater hypothesis for subglacial bedforms. Quaternary International, 90(1), pp.5-22.

Simkins, L.M., Anderson, J.B., Greenwood, S.L., Gonnermann, H.M., Prothro, L.O., Halberstadt, A.R.W., Stearns, L.A., Pollard, D. and DeConto, R.M., 2017. Anatomy of a meltwater drainage system beneath the ancestral East Antarctic ice sheet. Nature Geoscience, 10(9), pp.691-697.

Simkins, L.M., Greenwood, S.L., Munevar Garcia, S., Eareckson, E.A., Anderson, J.B. and Prothro, L.O., 2021. Topographic controls on channelized meltwater in the subglacial environment. Geophysical Research Letters, 48(20), p.e2021GL094678.

Slater, D.A., Nienow, P.W., Cowton, T.R., Goldberg, D.N. and Sole, A.J., 2015. Effect of near-terminus subglacial hydrology on tidewater glacier submarine melt rates. Geophysical Research Letters, 42(8), pp.2861-2868.

Smith, L.C., Andrews, L.C., Pitcher, L.H., Overstreet, B.T., Rennermalm, Å.K., Cooper, M.G., Cooley, S.W., Ryan, J.C., Miège, C., Kershner, C. and Simpson, C.E., 2021. Supraglacial river forcing of subglacial water storage and diurnal ice sheet motion. Geophysical Research Letters, 48(7), p.e2020GL091418.

Smith, M.J. and Clark, C.D., 2005. Methods for the visualization of digital elevation models for landform mapping. Earth Surface Processes and Landforms, 30(7), pp.885-900.

Sole, A., Nienow, P., Bartholomew, I., Mair, D., Cowton, T., Tedstone, A. and King, M.A., 2013. Winter motion mediates dynamic response of the Greenland Ice Sheet to warmer summers. Geophysical Research Letters, 40(15), pp.3940-3944.

St-Onge, D.A., 1984. Surficial deposits of the Redrock Lake area, District of Mackenzie. Current Research, Part A; Geological Survey of Canada, Paper, pp.271-276.

Storrar, R.D. and Livingstone, S.J., 2017. Glacial geomorphology of the northern Kivalliq region, Nunavut, Canada, with an emphasis on meltwater drainage systems. Journal of Maps, 13(2), pp.153-164.

Swift, D.A., Nienow, P.W. and Hoey, T.B., 2005. Basal sediment evacuation by subglacial meltwater: suspended sediment transport from Haut Glacier d'Arolla, Switzerland. Earth Surface Processes and Landforms, 30(7), pp.867-883.

Tedstone, A.J., Nienow, P.W., Gourmelen, N. and Sole, A.J., 2014. Greenland ice sheet annual motion insensitive to spatial variations in subglacial hydraulic structure. Geophysical Research Letters, 41(24), pp.8910-8917.

Trommelen, M.S., Ross, M. and Ismail, A., 2014. Ribbed moraines in northern Manitoba, Canada: characteristics and preservation as part of a subglacial bed mosaic near the core regions of ice sheets. Quaternary Science Reviews, 87, pp.135-155.

Truffer, M. and Harrison, W.D., 2006. In situ measurements of till deformation and water pressure. Journal of Glaciology, 52(177), pp.175-182.

Utting, D.J., Ward, B.C. and Little, E.C., 2009. Genesis of hummocks in glaciofluvial corridors near the Keewatin Ice Divide, Canada. Boreas, 38(3), pp.471-481.

Vérité, J., Ravier, É., Bourgeois, O., Pochat, S., Lelandais, T., Mourgues, R., Clark, C.D., Bessin, P., Peigné, D. and Atkinson, N., 2021. Formation of ribbed bedforms below shear margins and lobes of palaeo-ice streams. The Cryosphere, 15(6), pp.2889-2916.

Vérité, J., Ravier, É., Bourgeois, O., Bessin, P., Livingstone, S.J., Clark, C.D., Pochat, S. and Mourgues, R., 2022. Formation of murtoos by repeated flooding of ribbed bedforms along subglacial meltwater corridors. Geomorphology, 408, p.108248.

Vore, M.E., Bartholomaus, T.C., Winberry, J.P., Walter, J.I. and Amundson, J.M., 2019. Seismic tremor reveals spatial organization and temporal changes of subglacial water system. Journal of Geophysical Research: Earth Surface, 124(2), pp.427-446.

Wagner, K. 2014: Ribbed moraines and subglacial geomorphological signatures of interior-sector palaeo-ice sheet dynamics. M.Sc. thesis, Brock University, 274 pp.

Walder, J.S. and Fowler, A., 1994. Channelized subglacial drainage over a deformable bed. Journal of glaciology, 40(134), pp.3-15.

Ward, B.C., Dredge, L.A., Kerr, D.E. and Kurfurst, D., 1997. Surficial geology, Lac de Gras, District of Mackenzie, Northwest Territories. Geological Survey of Canada.

Williams, J.J., Gourmelen, N. and Nienow, P., 2020. Dynamic response of the Greenland ice sheet to recent cooling. Scientific reports, 10(1), pp.1-11.

Wright, P.J., Harper, J.T., Humphrey, N.F. and Meierbachtol, T.W., 2016. Measured basal water pressure variability of the western Greenland Ice Sheet: Implications for hydraulic potential. Journal of Geophysical Research: Earth Surface, 121(6), pp.1134-1147.

Synthèse des principaux résultats

Partie A. Formation des murtoos par inondation répétée de ribbed bedforms le long des routes de drainage d'eau de fonte sous-glaciaire mise en évidence par un continuum morphométrique et génétique.

→ Quelle est la nature de l'association spatiale entre les murtoos, la variété de bedforms morphologiquement proches ('murtoo-related bedforms') et les ribbed bedforms ? Suggère-t-elle l'existence d'une relation génétique entre ces bedforms au sein des routes de drainage d'eau de fonte sous-glaciaire ?

L'analyse morphométrique des bedforms cartographiés le long de corridors d'eau de fonte a mis en évidence une relation géographique et un continuum morphologique entre des ribbed bedforms, des ribbed bedforms en partie lobés, des bedforms lobés à sub-triangulaires et des murtoos.

Les expériences de modélisation analogique démontrent que des bedforms décrits dans la littérature comme des ribbed bedforms recoupées par des murtoos (***Ojala et al., 2019***) ou des '*murtoo-related bedforms'* (***Ojala et al., 2021***) sont des bedforms de transition – correspondant respectivement à des ribbed bedforms partiellement remobilisés et des proto-murtoos – dans un processus génétique continu aboutissant à la formation de murtoos.

→ Comment la périodicité de l'écoulement d'eau de fonte et des processus de couplage/découplage module-t-elle les caractéristiques morphologiques et les processus de formation des murtoos au sein des routes de drainage ?

Le continuum morphologique et génétique, correspondant à l'expression de la remobilisation progressive de ribbed bedforms en murtoos, est dépendant de la récurrence de crues sous-glaciaires, responsable de réorganisations périodiques et transitoires des routes de drainage d'eau de fonte. Ces réorganisations produisent alternativement :

- (i) des phases de circulation massive d'eau de fonte sous-glaciaire dans un système à forte connectivité hydraulique qui favorisent le découplage de l'interface glace-sédiments et les processus de

remobilisation d'origine fluvio-glaciaire (i.e. érosion des ribbed bedforms, dépôt de sédiments érodés et chenalisation en bordure des proto-murtoos et murtoos)

- (ii) des phases de circulation limitée d'eau de fonte sous-glaciaire dans un système à faible connectivité hydraulique qui favorisent le couplage de l'interface glace-sédiments et les processus de remobilisation d'origine glaciogénique (i.e. déformation/étirement du lit sédimentaire et des bedforms).

Ce processus de remobilisation progressive à l'origine du continuum morphologique et génétique entre les ribbed bedforms, les murtoos et une variété de bedforms de transition est matérialisé par un paramètre quantitatif nommé « degré de remobilisation », dépendant des caractéristiques morphologiques de ces bedforms et calculé à partir de leurs indices de sinuosité et de circularité.

→ En quoi ces processus font des murtoos et autres bedforms associés ('murtoo-related bedforms') des marqueurs de la dynamique d'écoulement de l'eau de fonte à la base des calottes glaciaires ?

Les processus composites – à la fois d'origine fluvio-glaciaire et glaciogénique – enregistrés par ce continuum morphométrique et génétique et matérialisés par le « degré de remobilisation » permettent de préciser (i) l'évolution et la dynamique des routes de drainage d'eau de fonte sous-glaciaire, notamment durant les périodes de déglaciation et de retrait des calottes glaciaires et (ii) d'affiner leur distribution spatiale.

- **Partie B. Un modèle d'évolution des bedforms observés le long des corridors d'eau de fonte sous-glaciaires basé sur les variations de couplage glace-eau-sédiments.**

→ Quelle diversité d'assemblages morphologiques existe-t-il le long des corridors d'eau de fonte sous-glaciaire ?

La cartographie haute résolution (2 m) a mis en évidence une diversité d'assemblages morphologiques au sein des corridors d'eau de fonte sous-glaciaires (dits '*tracts*') associés aux (i) hummocks et rides sédimentaires (i.e. *hummock tracts*), (ii) aux murtoos et bedforms associés (i.e. *murtoo tracts*), et aux (iii) ribbed bedforms et linéations glaciaires (i.e. *ribbed and streamlined tracts*).

→ Comment ces différents assemblages morphologiques permettent-ils de caractériser les processus de remobilisation de sédiments, les interactions glace-eau-sédiments et les variations de circulation d'eau de fonte de fonte le long des routes de drainage sous-glaciaires ?

Durant les périodes de forts débits d'eau de fonte, le système de drainage n'est pas suffisamment efficace pour transférer l'intégralité de l'eau de fonte ce qui favorise la formation de crues sous-glaciaires, l'extension des zones en découplage et les processus d'érosion et de dépôt par l'eau de fonte le long de l'interface glace-sédiments. Les bedforms sous-glaciaires préexistants (i.e. linéations, ribbed bedforms ou murtoos) sont érodés, ce qui induit la formation de hummocks et de rides sédimentaires de petites dimensions (< 100 m de long et <10^{nes} m de large) alignés ou formant des motifs géométriques. Lorsque les sédiments érodés ne sont pas évacués vers la marge, ces derniers sont redéposés au sein de cavités, de conduits ou de crevasses formant des hummocks et des rides sédimentaires aux motifs plus chaotiques mais morphologiquement identiques à leurs homologues « érosifs ». Tandis que les bedforms « en dépôt » se forment – comme les eskers ou les chenaux – proche de la marge des calottes glaciaires en raison de la diminution de la pression d'eau de fonte basale, les bedforms « érosifs » se développent plus en amont au sein des routes de drainage sous de plus fortes pressions d'eau de fonte basale.

Durant les périodes de faibles débits d'eau de fonte, le système de drainage est suffisamment efficace pour permettre le transfert de l'intégralité de l'eau de fonte ce qui favorise une réduction des zones en découplage, une extension des zones enregistrant du recouplage et l'activation des processus de déformation par l'écoulement de la glace le long de l'interface glace-sédiments. Des ribbed bedforms (ou de linéations glaciaires) préexistants peuvent alors être préservés ou remodelés, formant progressivement des proto-murtoos ('*murtoos-related bedforms*') et des murtoos. Des ribbed bedforms et des linéations glaciaires peuvent également s'y former, mais la faible quantité de déformation enregistrée par le lit sédimentaire le long des corridors d'eau de fonte (en raison du plus faible taux de couplage) implique de plus petites dimensions et longueurs d'onde que leurs homologues situés en dehors des corridors.

→ Est-il possible de construire un modèle de continuum génétique permettant de relier la diversité morphologique observé le long des corridors d'eau de fonte à la dynamique spatio-temporelle d'écoulement de l'eau de fonte au sein des routes de drainage ?

Un modèle de continuité génétique propose ainsi que l'alternance des phases de découplage et de recouplage – dépendante des variations spatio-temporelles de circulation d'eau de fonte – permet d'expliquer l'amplitude des processus de déformation, d'érosion, de transformation, de fragmentation et de chenalisation et ainsi d'expliquer la diversité morphologique des bedforms et landforms observé le long des corridors d'eau de fonte sous-glaciaires. Le modèle de continuité génétique propose également que la diversité morphologique observée le long des corridors d'eau de fonte est conditionnée par la nature des bedforms préexistants au moment de la mise en place de la route de drainage (i.e. ribbed bedforms ou linéations glaciaires).

CHAPITRE V

CONCLUSIONS & PERSPECTIVES

Synthesis

In this thesis, a new morphometric analysis has been developed to jointly study subglacial bedforms (i) mapped along palaeo-ice sheet beds and (ii) reproduced by analog modeling. The morphological characteristics, spatial distribution and formation processes of these bedforms, re-investigated in the light of this new method, revealed morphometric continuums and evolutionary sequences depending on ice-meltwater-bed interactions.

- The analog model designed to simulate subglacial bedforms reproduces at a reduced scale processes of sediment remobilization such as erosion, transport, deposition and deformation, which, following the principle of "unreasonable effectiveness" defined by ***Paola et al.*** (***2009***), are similar to processes operating at larger scales in natural subglacial systems. Although imperfectly scaled according to dynamic scaling principles and with many limitations (e.g. non-reproducibility of streamlined bedforms and depositional hummocks and depositional ridges), the analog model is able to reproduce subglacial bedforms such as ribbed bedforms and murtoos, which are morphologically similar to their natural counterparts. Analog modeling of subglacial bedforms therefore unables the temporal variability of ice-water-bed interactions responsible for their formation and evolution to be deciphered.

- Analog modeling demonstrated that spatial and temporal variations in ribbed bedform shape and orientation depend on the direction and quantity of bed deformation generated by the overlying and shearing ice flow, in a similar way the shape and orientation of finite strain ellipses along shear bands in natural systems evolve through time (**Figure 5.**1). Experiments also demonstrated that the transient activity of subglacial meltwater drainage routes induces a periodicity of coupling (low meltwater pressure and low hydraulic connectivity) and decoupling (high meltwater pressure and high hydraulic connectivity) phases. This periodicity results in alternating deformation and erosion, transport and deposition processes responsible for the progressive remobilization of existing bedforms (i.e. linear

to sinuous ribbed bedforms) into new ones (i.e. fragmented and remobilized ribbed bedforms, proto-murtoos and murtoos).

- Considering the morphometric approach commonly defined for subglacial bedforms accounted for sizes and proportions (length, width, elongation ratio), assumed an orientation relative to the ice flow direction (transverse or parallel) and ignored complex bedforms (i.e. sinuous and/or oblique), we develop a new morphometric analysis to integrate and compare all subglacial bedforms together with the least amount of preconceptions. This morphometric analysis better takes into account complexities of contours and crestlines through sinuosity and circularity indexes, and uses transverse and longitudinal elongation components relative to the ice flow direction (oriented elongation index) rather than classical elongation ratio. The compilation of morphometric characteristics from ~ 41 000 murtoos, murtoo-related bedforms, ribbed, streamlined and complex bedforms, mapped in a variety of glaciological context (e.g. ice stream, ice dome, drainage routes), reveals a single bedform continuum in a oriented elongation vs. sinuosity scatter plot. Within this bedform continuum, a sequence of ribbed bedforms ranging from circular to linear forms constitute an end-member from which two distinct morphological sequences are rooted. These two morphological sequences materialize evolutionary trajectories either toward streamlined bedforms or murtoos, respectively depending on (i) increasing cumulative bed deformation (ice flow-induced) or (ii) increasing bedform remobilization (meltwater flow-induced) (**Figure 5.2**).

- The diversity of subglacial bedforms populating these two morphological sequences can therefore be interpreted through a single evolutionary model depending on alternating ice-bed coupling and decoupling under fluctuating pore-water pressure, respectively responsible for either glaciogenic (deformation) or glacio-fluvial (erosion, deposition) sediment remobilization (**Figure 5.3**). These subglacial conditions allow us to define subglacial bedforms resulting from :

  - (i) ice-bed coupling and bed deformation (i.e. circular to linear ribbed bedforms, sinuous transitional bedforms and low to highly-elongated streamlined bedforms),

  - (ii) transitory ice-bed coupling/decoupling and bedform deformation and erosion (i.e. fragmented to partially remobilized ribbed bedforms, proto-murtoos, escarpments, murtoos and stubby

lineations),

- (iii) ice-bed decoupling, high pore-water pressure and bedform erosion (i.e. geometric patterns of erosional hummocks and ridges)

- (iv) ice-bed decoupling, low pore-water pressure and sediment deposition (i.e. chaotic patterns of depositional hummocks and ridges).

○ During glacial maximum (**Figure 5.4**), low meltwater supply and few high-magnitude drainage events due to limited solar radiation combined with a restricted ablation zone would imply the development of a narrow marginal channelization fringe. At the ice sheet scale, this reduced meltwater input implies a lower density of drainage routes and channelized features, resulting to an overall distributed and inefficient drainage system. These hydrological conditions would certainly favor higher ice flow velocities and higher density of ice streams, while cold-based conditions are assumed to be pervasive at the base of ice domes.

Thus, ice sheet bed would be essentially populated by subglacial bedforms resulting from ice-bed coupling and bed deformation. Their degree of evolution, depending on cumulative bed deformation, is mainly controlled by ice flow velocity: streamlined bedforms (MSGLs, drumlins) below fast-flowing ice streams and ribbed bedforms below slow-flowing inter-ice stream and interior areas. Subglacial environments recording ice flow velocity and deformation gradients, such as onset areas (i.e. longitudinal extension, coaxial strain), shear margins (i.e. lateral shear, non-coaxial strain) and lobe margins (i.e. longitudinal compression, coaxial strain), would be evidenced by linear to sinuous bedforms whose the orientation depends on deformation directions. Local changes in pore-water pressure or bed strength can also modulate cumulative bed deformation, forming sticky spots.

○ During deglaciation periods (**Figure 5.5**), thinning of the ice sheet margin by ablation combined with increasing supraglacial melt rates would result in (i) the upstream expansion of the marginal channelization fringe and (ii) higher meltwater inputs and frequent high-magnitude drainage events. These subglacial hydrological conditions promote an increased density of channelized features and drainage routes, and a channelized and more efficient drainage system at ice-sheet scale. This ice-sheet scale drainage efficiency would certainly imply a lower density of ice streams, along which

channelized features and drainage routes are rare. Changes in the basal thermal regime could participate in a propagation of warm-based conditions beneath ice domes. In this configuration, the ice sheet bed would mainly be populated by meltwater-related bedforms, whose the morphological characteristics depend on (i) their position relative to the ice (modulating the pore-water pressure), (ii) the shape of pre-existing bedforms along the path of drainage routes, and (iii) the frequency/intensity of meltwater inputs along drainage routes.

Drainage routes located along the marginal channelization fringe would be essentially characterized by bedforms and landforms formed by sediment deposition under ice-bed decoupling and low pore-water pressure conditions, such as hummocks and ridges with chaotic patterns, and eskers.

Beyond this fringe, drainage routes associated with high and constant meltwater inputs focus bedforms that are formed from the erosion of existing bedforms under ice-bed decoupling and high pore-water pressure conditions. These bedforms typically correspond to erosional hummocks and ridges, whose transverse, parallel or oblique alignment could result from the remobilization of ribbed bedforms, streamlined bedforms or murtoos respectively.

Drainage routes associated with high and episodic meltwater inputs would be characterized by transitory ice-bed coupling and decoupling, responsible for alternating bed deformation and erosion (and deposition in a minor extent). These drainage routes tend to be populated by murtoos, proto-murtoos, escarpments, resulting from the stretching and re-shaping of existing bedforms by ice and meltwater. Along these drainage routes, the reduction of ice-bed coupling surface because of high meltwater pressure is also potentially recorded through ribbed bedform corridors. These corridors indeed record a lower quantity of bed deformation.

1. Synthèse

Dans ce travail, un nouveau protocole d'analyse morphométrique a été développé pour étudier conjointement les bedforms (i) cartographiés le long de paléo-lits sous-glaciaires et (ii) reproduits par un modèle analogique. L'analyse et l'interprétation des caractéristiques morphologiques, de la distribution spatiale et des processus de formation des bedforms en réponse aux variations spatio-temporelles des interactions glace-eau-sédiments et des processus de remobilisation du lit sédimentaire, a révélé l'existence de continuums morphologiques et de modèles d'évolution unifiant différentes populations de bedforms. Une synthèse de ce travail est réalisée ci-après.

1.1. Une approche méthodologique combinée utilisant la cartographie et la modélisation analogique au moyen d'analyses morphométriques

1.1.1. Un nouveau modèle analogique pour l'étude des bedforms sous-glaciaires

La reproduction de bedforms sous-glaciaires a été rendue possible grâce à un nouveau modèle analogique inspiré du dispositif expérimental mis en place par ***Lelandais et al. (2016, 2018)*** et ***Lelandais (2018)***, et développé afin reproduire les interactions fondamentales entre une calotte de silicone (analogue de la glace), un écoulement d'eau (analogue du système hydrologique sous-glaciaire) et une couche de sable (analogue du lit sédimentaire sous-glaciaire). Ce modèle analogique – bien qu'imparfaitement dimensionné selon les principes de dimensionnement dynamique (Chapitre II - §2.4.1) et possédant certaines limites (Chapitre II - §2.4.2 & Chapitre V - §1.2.3) – reproduit à une échelle réduite des processus d'érosion, de transport, de dépôt et de déformation des sédiments, semblables aux processus opérant à plus grande échelle dans les systèmes sous-glaciaires naturels. En comparant les résultats expérimentaux à de nouvelles données cartographiques issues de paléo-lits glaciaires, une similitude morphométrique a été démontrée entre les bedforms naturels et expérimentaux résultant tous deux de ces processus fondamentaux de remobilisation sédimentaire. Cette similitude justifie ainsi l'intérêt d'utiliser la modélisation analogique pour étudier les processus et formes sous-glaciaires (***Paola et al., 2009***). Le contrôle spatio-temporel des processus sous-glaciaires et des

interactions glace-eau-sédiments sur l'évolution morphologique offert par la modélisation analogique pour certains bedforms (ribbed bedforms, murtoos et bedforms associés) (Chapitre V - §1.1.3 et Chapitre V - §1.1.4) a ainsi permis de proposer dans ce travail des continuums morphologiques et de modèles d'évolution (Chapitre V - §1.2).

1.1.2. Une nouvelle méthode d'analyse morphométrique des bedforms

Les analyses morphométriques utilisées jusqu'à présent pour les bedforms sous-glaciaires ne prenaient en compte que leurs dimensions, leurs proportions et leurs degrés d'allongement ; elles se basaient sur l'hypothèse que les bedforms étaient soit parallèles soit perpendiculaires à la direction d'écoulement de la glace (e.g. ***Clark et al., 2009 ; Stokes et al., 2013 ; Ely et al., 2016***). Cette approche participait à l'absence d'une caractérisation morphométrique des bedforms dits « complexes » aussi précise que pour les drumlins, MSGLs, ribbed bedforms ou murtoos et d'une représentation partielle du véritable spectre de variabilité morphologique des bedforms sous-glaciaires (***Carl, 1978 ; Markgren & Lassila, 1980 ; Lundqvist, 1981 ; Knight, 1997 ; Dunlop & Clark, 2006 ; Wagner, 2014 ; Eyles et al., 2016 ; Ojala et al., 2019 ; Sookhan et al., 2021***).

Considérant ces lacunes, une nouvelle méthode d'analyse morphométrique reposant sur des paramètres de forme non-dimensionnés a été développée et appliquée aux bedforms associés indistinctement aux dynamiques d'écoulement de la glace et de l'eau de fonte. Pour chaque bedform, les indices de circularité (I_{CIR}), de sinuosité (I_{SIN}) et d'élongation orientée (I_{OE}) permettent de quantifier respectivement la forme de son contour (circulaire ou non) et de sa ligne de crête (linéaire ou sinueuse), et des composantes de son allongement parallèle et transverse à la direction de déplacement de la glace. Cette nouvelle méthode a permis la comparaison morphologique des bedforms naturels et expérimentaux en s'affranchissant du saut d'échelle entre leurs dimensions respectives, démontrant ainsi la pertinence de l'utilisation combinée de la modélisation analogique et de la cartographie glaciaire. En suivant l'évolution des bedforms expérimentaux au cours du temps, cette méthode a également permis de reconstruire l'évolution morphologique des bedforms et de déterminer les relations entre leurs caractéristiques morphologiques et les dynamiques d'écoulement de la glace et de l'eau de fonte.

1.1.3. Quantité et direction de déformation enregistrées par le lit sédimentaire : facteurs de contrôle de forme et de l'orientation des bedforms sous-glaciaires associés au couplage glace-sédiments

Ce travail a démontré que la forme (rectiligne à sinueuse) et l'orientation (perpendiculaire à oblique) des ribbed bedforms par rapport à la direction de déplacement de la glace étaient contrôlées par la déformation d'un lit sédimentaire meuble induite par l'écoulement cisaillant de la glace sus-jacente (***Smalley & Unwin, 1968 ; Smith et al., 2007 ; Linden et al., 2008 ; Stokes et al., 2008 ; King et al., 2009 ; Clark, 2010 ; O Cofaigh et al., 2013 ; Fannon et al., 2017***). Les variations spatiales et temporelles de forme et d'orientation des bedforms dépendent ainsi des quantités et directions de déformation enregistrées dans le lit sédimentaire. Ces quantités et directions de déformation sont directement contrôlées par l'amplitude et les directions des champs de déplacement de la glace à la base, le couplage/découplage entre la glace et les sédiments (modulé par la pression d'eau de fonte basale), et les caractéristiques lithologiques du lit sédimentaire. Les bedforms sous-glaciaires peuvent donc évoluer – en fonction de la déformation finie – en des formes complexes d'orientations obliques par rapport à la direction de déplacement de la glace, sans invoquer nécessairement de multiples trajectoires d'écoulement de la glace successives (***Clark, 1993 ; Knight et al., 1999 ; Dunlop & Clark, 2006 ; Stokes et al., 2006 ; De Angelis & Kleman, 2007 ; Greenwood & Clark, 2009 ; Brown et al., 2011***).

○ <u>*Relation entre l'orientation des bedforms et les axes de déformation du lit sédimentaire*</u>

Dans les matériaux qui se déforment de façon homogène, la déformation en deux dimensions est décrite par le changement de forme (i.e. allongement, raccourcissement) d'un cercle en une ellipse (***Ramsay & Huber, 1983***). Considérant un plan horizontal sur lequel opère un écoulement cisaillant horizontal, tel que cela intervient le long de l'interface basale entre la glace et les sédiments, des variations d'amplitudes et de directions des champs de déplacement horizontaux génèrent de la déformation coaxiale ou non-coaxiale, modulant longitudinalement et transversalement la déformation enregistrée.

Lorsque la déformation est coaxiale ('*pure strain*'), en relation avec de l'extension ou de la compression, les axes d'allongement et de raccourcissement de l'ellipse de déformation finie ('*finite strain'*) conservent leur orientation quel que soit l'intensité de la déformation. Dans les systèmes

glaciaires, des écoulements de glace compressifs (i.e. lobe de glace) ou extensifs (i.e. onset area) génèrent ainsi des gradients longitudinaux de l'amplitude des champs de déplacement à la base, modulant ainsi longitudinalement la quantité de déformation enregistrée par les sédiments. La quantité de déformation controllant directement le degré d'évolution des bedforms, des variations de forme interviennent ainsi longitudinalement entre des bedforms dont les axes d'allongement sont perpendiculaires (ribbed bedforms) ou parallèles (linéations) aux champs de déplacement de la glace (Chapitre III – Partie C).

Au sein des bandes de cisaillement, enregsitrant de la déformation non-coaxiale *('simple shear')*, l'orientation et l'allongement des objets déformés varient dans le temps et dans l'espace en fonction de l'intensité de la déformation. Les axes d'allongement et de raccourcissement de l'ellipse de déformation instantanée ('*instantaneous strain'*) se situent ainsi en permanence à 45° de la direction de déplacement tandis que ceux de l'ellipse de déformation finie tournent progressivement au cours de la déformation, depuis 45°, pour se paralléliser (axe d'allongement fini) ou se perpendiculariser (axe de raccourcissement fini) à la direction de déplacement lorsque la déformation est infinie. Par conséquent, les objets déformés s'étirent de plus en plus à mesure que leurs axes d'allongement et de raccourcissement finis deviennent respectivement parallèles et perpendiculaires à la direction de déplacement. Dans une bande de cisaillement hétérogène, ceci se traduit par le fait que les objets déformés sont à la fois plus allongés et plus parallèles à la direction de déplacement dans les zones de forte déformation finie que dans celles de faible déformation finie.

Une analogie peut ainsi être faite entre (i) l'orientation des ellipses de déformation finie dans les bandes de cisaillement hétérogènes (**Figure 5.1A**) et (ii) l'orientation des bedforms sous-glaciaires dans les zones soumises à des gradients latéraux de déformation (**Figure 5.1B**) : cette analogie permet d'expliquer l'obliquité de certains bedforms par rapport à la direction de déplacement de la glace (Chapitre III – Partie C). L'indice d'élongation orientée (I_{OE}), qui intègre les composantes d'allongement parallèle et transverse des bedforms par rapport à la direction de déplacement de la glace, peut donc être considéré comme un proxy de la quantité de déformation enregistrée par le lit sédimentaire sous-glaciaire. En raison de la variabilité morphologique (et de l'hétérogénéité sédimentaire) des bedforms les plus précoces – notamment des ribbed bedforms (circulaires à linéaires) (Chapitre III – Partie B) –

l'amplitude de l'étirement dans la direction de déplacement, à mesure que la quantité de déformation accommodée par le lit sédimentaire augmente, n'est pas nécessairement homogène au sein d'un même bedform. Ces hétérogénéités d'étirement engendrent une augmentation de la sinuosité de la ligne de crête (I_{SIN}), qui doit donc être prise en compte afin de caractériser l'évolution morphologique des bedforms en fonction de la déformation finie.

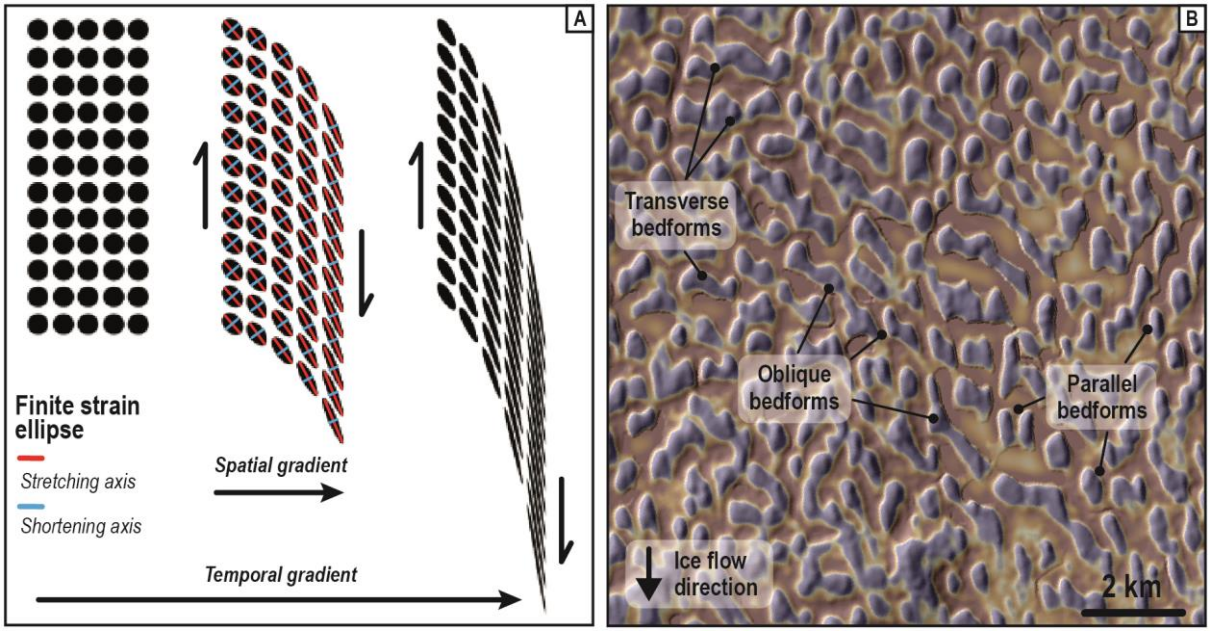

***Figure 5.1**. Analogy between the progressive rotation of strain ellipses along heterogeneous shear bands and the lateral variations in subglacial bedforms orientation (from flow-transverse to flow-parallel through oblique), which are here inferred to underline the position of a palaeo-shear margin of an ice stream (Irish Ice Sheet).*

○ *Marges cisaillantes des fleuves de glace : bedforms obliques et 'lateral shear moraines'*

Cette analogie permet ainsi d'interpréter les bedforms obliques comme des marqueurs morphologiques des marges cisaillantes des fleuves de glace, dont le principal critère de reconnaissance était jusqu'à présent les '*lateral shear moraines*'. Par extrapolation de la relation entre l'orientation des bedforms et les ellipses de déformation, les *'lateral shear moraines'* pourraient résulter de l'agglomération de bedforms obliques ayant enregistré une déformation finie suffisante pour permettre leur coalescence et leur alignement par rapport à la direction de déplacement de la glace. Le processus de formation des '*lateral shear moraines'* serait ainsi analogue à celui des mylonites dans les roches. Cette hypothèse permettrait d'expliquer pourquoi des bedforms obliques et des '*lateral shear moraines'* ne sont pas systématiquement observés le long des paléo-fleuves de glace. Alors que les deux principaux modèles de formation des *'lateral shear moraines'* sont liés à (i) un différentiel d'érosion généré par un gradient de vitesse de déplacement de la glace et (ii) l'accrétion de rides sédimentaires situés dans les

zones inter-fleuves de glace (***Stokes & Clark, 2002 ; Batchelor & Dowdeswell, 2016***), un effet de succion des sédiments résultant du cisaillement et de l'amincissement de la glace a aussi été proposée et concorde avec l'hypothèse proposée (***Hindmarsh & Stokes, 2008***). Cette hypothèse pourrait notamment être explorée au travers d'une étude structurale et de la recherche de motifs périodiques – correspondant à de potentielles reliques d'anciens bedforms obliques – à l'intérieur des *'lateral shear moraines'*, dont les plusieurs dizaines de km de longueur dépassent largement l'ordre de grandeur de dimensions des bedforms sous-glaciaires.

1.1.4. Pression d'eau de fonte basale et connectivité hydraulique : facteurs de contrôle de la diversité morphologique des bedforms le long des routes de drainage sous-glaciaires

Ce travail a également démontré que le caractère transitoire des routes de drainage d'eau de fonte sous-glaciaires résultant de variations de la pression d'eau de fonte basale induisait une périodicité des phases de couplage (faible connectivité hydraulique) et de découplage (forte connectivité hydraulique) et des processus de remobilisation sédimentaire : déformation, érosion, transport et dépôt. La mise en place de routes de drainage au sein de champs de ribbed bedforms préexistants est ainsi associée à des phases transitoires d'inondations et de quiescences responsables de leur érosion et du dépôt des sédiments érodés, et de leur déformation. Ces processus de remobilisation des matériaux constitutifs des ribbed bedforms sont à l'origine de la formation successive de ribbed bedforms fragmentés ou en partie remobilisés, de proto-murtoos (i.e. '*murtoo-related bedforms'*) et de murtoos. Ces travaux ont permis de confirmer des hypothèses de formation des murtoos par le dépôt et la déformation de sédiments triés et de tills sous-glaciaires basées sur des observations sédimentaires (***Makïnen et al., 2017 ; Peterson Becher & Johnson, 2021***). Enfin, ces travaux ont donné lieu à des hypothèses de significations génétiques expliquant les relations spatiales et morphométriques observées entre les corridors de murtoos, '*murtoo-related bedforms'* et ribbed bedforms (***Peterson et al., 2017 ; Ojala et al., 2019 ; Ahokangas et al., 2021***).

1.2. Vers un modèle unificateur selon lequel les interactions glace-eau-sédiments expliqueraient la diversité et la continuité morphologique des bedforms sous-glaciaires ?

1.2.1. Un continuum morphologique intégrant les ribbed bedforms (circulaires / linéaires), les bedforms sinueux, les linéations (drumlins/MSGLs), les murtoos et les 'murtoos-related bedforms'

Ce travail a permis d'intégrer dans une même caractérisation morphométrique des bedforms déjà bien décrits dans la littérature (i.e. bedforms circulaires, drumlins, MSGLS, ribbed bedforms, murtoos, hummocks) et des bedforms moins bien décrits car possédant des formes plus complexes (i.e. bedforms sinueux, murtoo-related bedforms). Les caractéristiques morphométriques de ~ 41 000 bedforms cartographiés dans cette thèse sont compilées dans un unique graphique en trois dimensions dont les axes correspondent aux indices de sinuosité I_{SIN}, de circularité I_{CIR} et d'élongation orientée I_{OE} (**Figure 5.2A**). La compilation des caractéristiques morphométriques met en évidence un unique nuage de points continu, i.e. continuum morphologique, au sein duquel les ribbed bedforms (de forme circulaire à linéaire) constituent un pôle intermédiaire où s'enracinent deux séquences morphologiques. Les caractéristiques morphométriques de chaque bedform au sein de ce graphique et le long de chaque séquence d'évolution sont ainsi dépendantes de la nature et de l'intensité du processus d'évolution.

La première séquence morphologique, qui couvre des bedforms communément associés à la dynamique d'écoulement de la glace, est interprétée comme témoignant d'une augmentation de la quantité de déformation enregistrée par le lit sédimentaire. Cette séquence est matérialisée par une infinité de trajectoires d'évolution – qui dépendent de la longueur du bedform initial – entre des ribbed bedforms, des bedforms sinueux et des linéations glaciaires (i.e. drumlins, MSGLs) (**Figure 5.2B**).

La deuxième séquence morphologique, qui regroupe des bedforms communément associés aux dynamiques d'écoulement de l'eau de fonte, a été interprétée comme témoignant de la remobilisation progressive de ribbed bedforms par l'eau de fonte en relation avec des cycles de découplage/recouplage à l'interface glace-eau-sédiments. Cette séquence est matérialisée une trajectoire d'évolution entre des ribbed bedforms, des bedforms de transitions ('*murtoo-related bedforms'*) et des murtoos (**Figure 5.2C**).

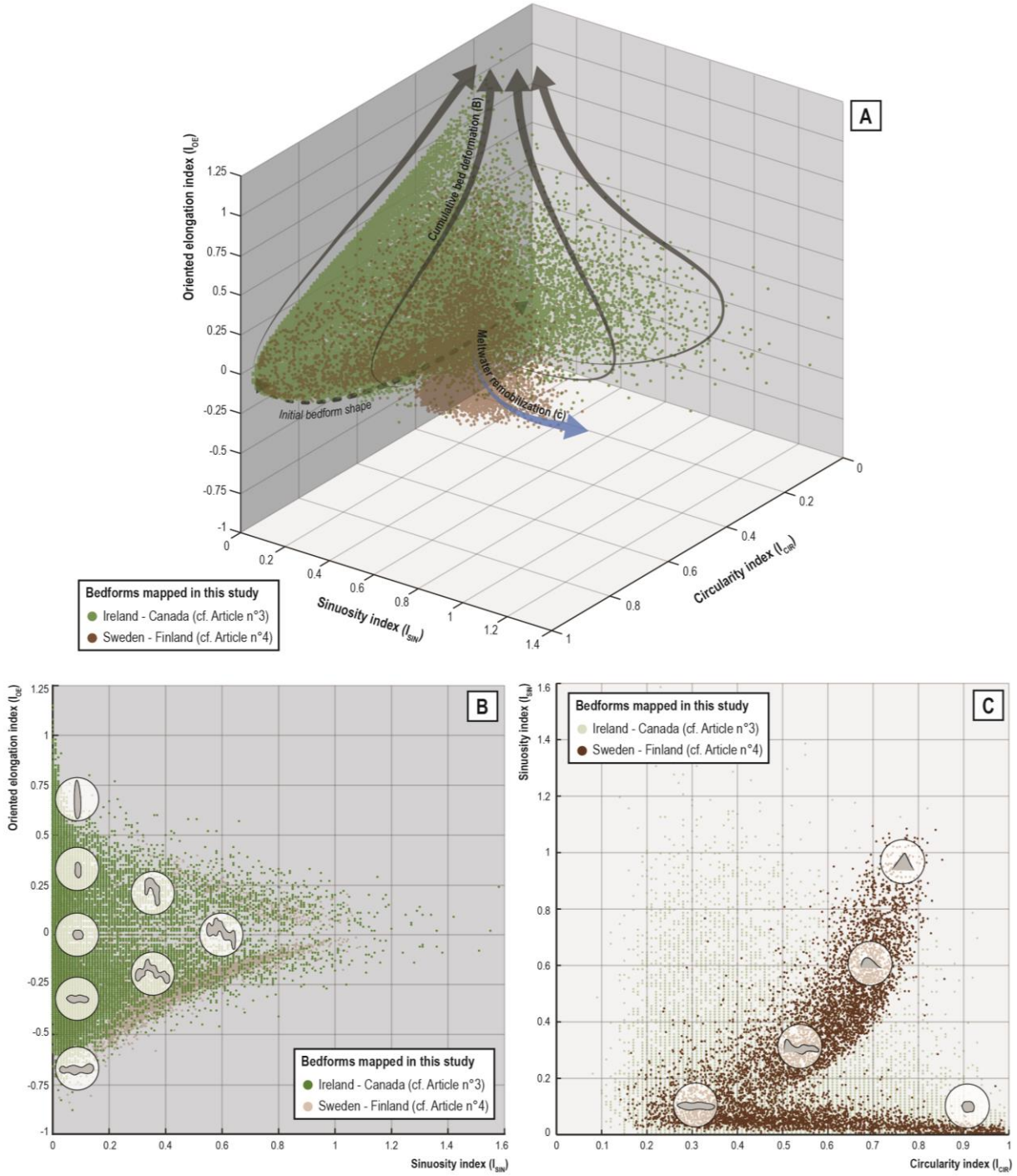

Figure 5.2. *Plots of oriented elongation (I_{OE}), sinuosity (I_{SIN}) and circularity (I_{CIR}) indexes. (A) 3D-plots with all subglacial bedforms mapped in this study highlight the existence of a single point cloud of bedform metrics and a single morphological continuum. Within this continuum, morphological sequences materializing the evolution of subglacial bedforms from the 'ribbed bedform' end-member are constituted of multiple morphological evolution trajectories that depend on ice/meltwater-induced processes. (B) Subglacial bedforms (n ~ 33 700) mapped in Ireland and Canada (Boyd Lake and Poorfish Lake) (green dots), for which the continuum between ribbed bedforms (circular to linear forms), sinuous transitional bedforms and streamlined bedforms has been interpreted as reflecting a degree of cumulative bed deformation (cf. Article n°3). (C) Subglacial bedforms (n ~ 7 200) mapped in Sweden and Finland (brown dots, for which the continuum between ribbed bedforms (circular to linear forms), murtoo-related bedforms and murtoos has been interpreted as reflecting a degree of bedform remobilization by meltwater flow (cf. Article n°4).*

En réalité une troisième séquence morphologique, correspondant au pôle intermédiaire de ribbed bedforms de forme circulaire à linéaire, est mise en évidence dans ce graphique. À partir de travaux de modélisation numérique (***Fannon, 2020 p.139-140***) et analogique (Chapitre III – Partie A ; Chapitre IV – Partie A), un continuum morphologique de ribbed bedforms circulaires à linéaires a été interprété comme résultant d'un stade préliminaire de déformation du lit sédimentaire sous-glaciaire. Bien que leurs distributions spatiales et les modèles numériques/analogiques suggèrent que la composante transverse des ribbed bedforms croisse de façon aléatoire, la signification de cette séquence morphologique en termes de dynamique d'écoulement de la glace ou de caractéristiques du lit sédimentaire reste à explorer (Chapitre V - §2).

1.2.2. Variations spatio-temporelles des interactions glace-eau-sédiments et des processus de déformation/érosion/dépôt : facteurs de contrôle d'un modèle de formation unifiant la diversité de bedforms sous-glaciaires

L'existence d'un continuum morphologique au sein de la **Figure 5.2A** a révélé des séquences d'évolution morphologique, qui – hormis la séquence d'évolution des ribbed bedforms circulaires à linéaires définissant la forme initiale des bedforms – sont interprétables au travers d'un modèle d'évolution unificateur. Ce modèle d'évolution, schématiquement illustré en **Figure 5.3**, est gouverné la couplage/découplage entre la glace et le lit sédimentaire, la pression d'eau de fonte basale et la quantité de déformation accommodée par le lit sédimentaire.

○ *Bedforms associés à la dynamique d'écoulement de la glace : couplage glace-sédiments*

Lorsque l'interface glace-sédiments est couplée, la formation et l'évolution des bedforms sont dominées par des processus de remobilisation glaciogénique, i.e. la déformation du lit sédimentaire. À mesure que la déformation cumulée enregistrée par le lit sédimentaire augmente – en raison d'une augmentation de la vitesse de déplacement de la glace, de la déformabilité du lit sédimentaire ou de la durée du processus – des ribbed bedforms (circulaires à linéaires) se développent initialement avant d'évoluer en bedforms sinueux, puis se fragmentent pour former des linéations glaciaires de plus en plus allongées (Chapitre III – Partie C). Considérant une préservation du volume de sédiments au cours du processus de déformation et de fragmentation, j'ai proposé qu'un ribbed bedform évolue en moyenne en 3 à 4 linéations glaciaires au sein de cette séquence d'évolution morphologique (**Figure 5.2B**).

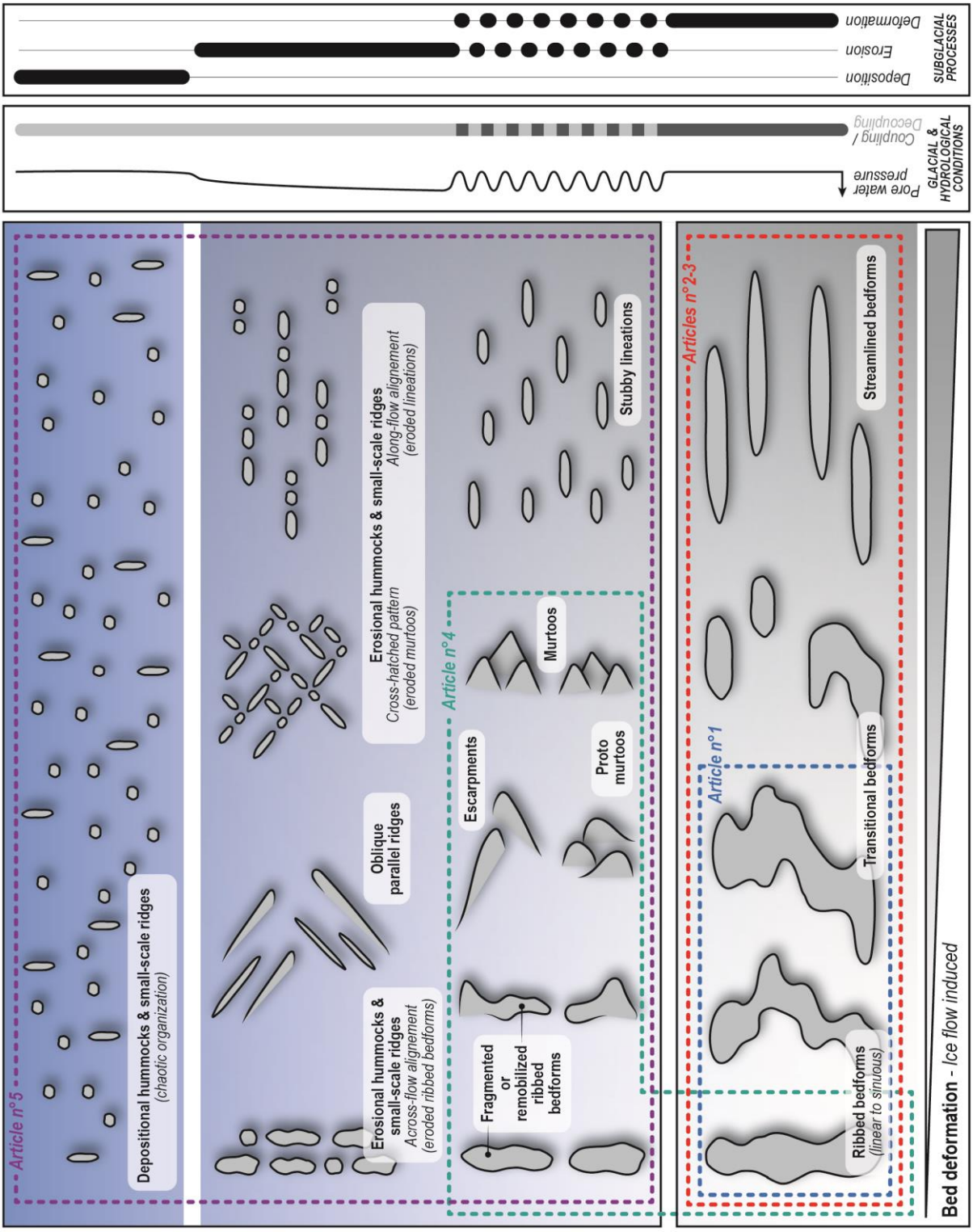

Figure 5.3. *Schematic representation of a unifying model for the diversity and the continuity of subglacial bedforms. Depending on ice-bed coupling/decoupling and pore water pressure, the genesis and the evolution of subglacial bedforms are associated to sustainable ice-bed coupling (i.e. deformation), transitory ice-bed coupling/decoupling (i.e. deformation / erosion) and sustainable ice-bed decoupling with high (i.e. erosion) or low pore-water pressure (i.e. deposition). In this unifying model, the formation of subglacial bedforms formed under sustained ice-bed coupling conditions (i.e. related to ice flow dynamic) is anterior; the shape of these preliminary bedforms therefore control the shape of subglacial bedforms related to ice flow dynamics along evolutionary sequences. Given that the morphological evolution of subglacial bedforms depends on the preliminary bedform shape and on the progressive varitations in ice-bed coupling and pore-water pressure, we consider that all these bedforms gather along a single morphological continuum; probably except for bedforms associated with sediment deposition since they are formed in-situ and do not necessarily result from bedform remobilization.*

○ *Bedforms associés à la dynamique d'écoulement de l'eau de fonte*

En considérant que les bedforms associés à la dynamique d'écoulement de l'eau de fonte à la base des calottes sont formés postérieurement aux bedforms sous-glaciaires associés à des conditions de couplage glace-sédiments, les caractéristiques morphologiques des bedforms nouvellement formés sont conditionnées par la géométrie des bedforms préexistants, la perennité de l'écoulement d'eau de fonte et du découplage glace-sédiments, et par la pression d'eau de fonte basale.

Découplage glace-sédiments transitoire

Lorsque la pression d'eau de fonte basale alterne, entre (i) de fortes pressions (i.e. forte connectivité hydraulique, découplage) et (i) de faibles pressions (i.e. faible connectivité hydraulique, couplage), la formation et l'évolution des bedforms sont dominées par des processus de remobilisation sédimentaire composites associant déformation glaciogénique, érosion, transport et dans une moindre mesure sédimentation fluvio-glaciaire. Par exemple, par itération, les processus périodiques d'érosion et de déformation sur des ribbed bedforms (ou éventuellement sur tout autre type de bedforms transverses préexistants) permettent successivement de former des bedforms de taille inférieure : des ribbed bedforms fragmentés à partiellement remobilisés, des proto-murtoos (i.e. '*murtoo-related bedforms*' et escarpements) et des murtoos (Chapitre IV – Partie A). Dans cette configuration, des processus de dépôt sédimentaire peuvent également intervenir, participant à l'incorporation de sédiments triés dans les bedforms précédemment cités, mais ne participent pas directement au façonnage des bedforms. Dans une configuration où des linéations longitudinales préexistent, l'écoulement de l'eau de fonte induit à la fois de l'érosion et une réduction de la surface de couplage – réduisant ainsi la quantité de déformation enregistrée par le lit sédimentaire – et génère des linéations de taille réduite.

Découplage glace-sédiments permanent & forte pression d'eau de fonte

A mesure que la pression d'eau de fonte devient élevée, les processus d'érosion et le découplage deviennent prédominants, et l'évolution des bedforms est contrôlée par une fragmentation intense liée à l'érosion fluvio-glaciaire. L'écoulement d'eau de fonte induit la formation de hummocks et de rides sédimentaires décamétriques à hectométriques. Ces hummocks et rides sédimentaires peuvent présenter des motifs d'organisation spatiale transverses, obliques/hachurés ou parallèles suggérant qu'ils correspondant respectivement à des reliques érodées de ribbed bedforms, de murtoos ou de linéations

(Chapitre IV – Partie B). En plus de la fragmentation et de l'érosion des bedforms préexistants, l'écoulement d'eau de fonte peut induire une chenalisation entre les bedforms, aboutissant par exemple à la formation de rides sédimentaires obliques et parallèles les unes aux autres, et dont les bordures sont façonnées par des chenaux d'eau de fonte. Cette proposition est cohérente avec une étude sédimentaire récente qui démontre que les rides obliques et parallèles et les escarpements sont des structures essentiellement associées à l'érosion, situées à la transition entre des systèmes de drainage (i) distribués marqués par la déformation (murtoos) et (ii) chenalisés marqués par le dépôt sédimentaire (eskers) (***Ojala et al., 2022***).

Découplage glace-sédiments permanent & faible pression d'eau de fonte

Enfin, lorsque la pression et le débit d'eau de fonte diminuent le long d'une interface glace-sédiments découplée, les processus de dépôt sédimentaire deviennent prédominants. Ainsi les sédiments issus de l'érosion du lit sédimentaire et/ou des bedforms sont redéposés pour former un continuum morphologique de monticules sédimentaires « en dépôt », de formes circulaires à linéaires. Ces monticules sédimentaires correspondent typiquement à de hummocks et des rides sédimentaires de tailles décamétriques à hectométriques, sans organisation spatiale notable (Chapitre IV – Partie B).

1.2.3. Limites actuelles de la méthode pour l'exploration de continuums morphologiques et d'un modèle de formation unificateur

○ *Méthode d'analyse morphométrique*

Bien que cette nouvelle méthode d'analyse morphométrique fondée sur des paramètres de forme non-dimensionnés ait permis de démontrer la continuité morphologique des bedforms sous-glaciaires malgré leur diversité et leur complexité, l'absence de critères dimensionnés ne permet pas de différencier des bedforms de forme similaire mais de dimensions distinctes. Les hummocks et rides sédimentaires (10^1 m) liés à l'érosion ou au dépôt de sédiments par l'eau de fonte – non pris en compte dans le continuum morphométrique présenté en **Figure 5.2**C – ne sont ainsi pas distinguables des ribbed bedforms subcirculaires ou linéaires (10^2-10^3 m) liés à la déformation glaciogénique du lit sédimentaire, bien que les ordres de grandeurs de leurs tailles soient très différents. Afin de distinguer ces bedforms et d'étudier la signification de la distribution statistique des caractéristiques morphologiques des bedforms au sein d'un unique continuum morphologique (Chapitre IV – Partie B; **Figure 5.3**),

l'intégration d'un critère dimensionné (par exemple longueur, largeur, aire) est donc nécessaire (Chapitre V - §2).

Par ailleurs, même si cette méthode d'analyse morphométrique réduit les aprioris initiaux sur l'orientation et la forme des bedforms sous-glaciaires, le calcul de l'indice d'élongation orientée – basé sur une reconstitution des trajectoires de déplacement de la glace – repose sur un échantillonnage de linéations glaciaires et sur le postulat qu'elles sont parallèles à la direction de déplacement. Bien que ce postulat soit cohérent avec l'observation de linéations glaciaires parallèles à la direction de déplacement de la glace sous la calotte Antarctique (e.g. ***King et al., 2007***) et sous des lobes fraîchement retirés d'une calotte islandaise (e.g. ***Johnson et al., 2010***), des linéations glaciaires obliques par rapport à la direction de déplacement de la glace ont déjà été identifiées à proximité de hauts topographiques (***Kleman & Borgström, 1994 ; Greenwood & Clark, 2009***). Ainsi, une caractérisation des bedforms sous-glaciaires totalement dépourvue d'aprioris en termes de classification ou d'orientation par rapport à la direction de déplacement de la glace reste à explorer (Chapitre V - §2).

○ *Modélisation analogique*

De nombreux bedforms sous-glaciaires – tels que les drumlins, les MSGLs ou les hummocks et rides sédimentaires formés par le dépôt de sédiments – ne sont à l'heure actuelle pas reproduits par le modèle analogique utilisé durant cette thèse. L'absence de drumlins et de linéations résulte probablement en partie de la nécessité d'un découplage total entre la silicone et son substrat pour initier de fortes vitesses de déplacement dans l'expérience ; l'étirement des ribbed bedforms initiaux par écoulement de la silicone n'est ainsi pas possible dans les zones d'écoulement rapide de l'expérience. Il est aussi possible que l'absence de drumlins et de MSGLs résulte de l'incapacité à générer dans l'expérience des vitesses de déplacement de la silicone d'ordres de grandeur 10^1 à 10^2 fois plus élevés que celles qui permettent la reproduction des ribbed bedforms dans les zones couplées. Ces faibles différences de vitesses expérimentales résultent potentiellement de l'absence de boucles de rétroactions thermomécaniques et du caractère non-newtonien et non-rhéofluidifiant de la silicone comparé à la glace (***Payne & Dongelmans, 1997 ; Hindmarsh, 2009***).

L'absence de hummocks et rides formés uniquement par le dépôt de sédiments dans l'expérience résulte probablement d'une combinaison entre (i) la forte granulométrie des sédiments (100 µm), (ii) les faibles

vitesses d'écoulement d'eau (~10^1 cm/s) et (iii) la faible viscosité de la silicone et de l'absence de fonte basale empêchant la formation d'espaces d'accommodation disponibles et pérennes (cavités) pour le dépôt (e.g. ***Dufresne et al., 2010***).

Ces lacunes induisent des incertitudes sur les interprétations proposées pour expliquer les séquences d'évolution morphologique, notamment pour les bedforms associés à la dynamique d'écoulement de l'eau de fonte n'ayant pas fait l'objet d'études de modélisation numérique (hummocks et rides formés par l'érosion et le dépôt de sédiments) (***Barchyn et al., 2016 ; Fannon et al., 2017 ; Fannon, 2020***). Par ailleurs, les expériences de modélisation analogique ont été réalisées avec des configurations initiales identiques de régime thermique (basé tempérée, entre 15-20°C) et de lithologie du substrat sédimentaire (sable meuble et perméable, de granulométrie homogène d_{50} = 100 µm, saturé en eau), permettant systématiquement la circulation d'eau dans la porosité et le long de l'interface basale. Ces conditions limitent l'exploration des facteurs contrôlant la formation et l'évolution des bedforms associés à la dynamique d'écoulement de l'eau de fonte lorsque le substrat sédimentaire est peu déformable, mais aussi des bedforms pouvant se former sous des calottes à base froide marquées par l'absence d'eau de fonte basale.

Faire varier les conditions expérimentales initiales (i.e. régie thermique et lithologie) permettrait par exemple d'explorer les différences d'abondance des murtoos entre le dôme de la paléo-calotte Fennoscandinave (Suède, Finlande) et le dôme Keewatin de la paléo-calotte Laurentide (Canada) – reposant tous deux sur des socles cristallins archéens et interprétés comme ayant accueilli des bases froides (***Kleman & Hattestrand, 1999 ; Kleman & Glasser, 2007***). Dans les expériences de modélisation, et dans les modèles d'évolution proposés, la formation des murtoos est contrôlée par la déformation et l'érosion des ribbed bedforms. En revanche certaines études ont suggéré que les murtoos puissent se former à partir d'un lit sédimentaire sans remobilisation de bedforms existants (***Mäkinen et al., 2017 ; Peterson Becher & Johnson, 2021***) ; configuration qui n'est actuellement pas reproduite par le modèle expérimental.

Les différentes limites du modèle analogique énoncées dans cette sous-partie font l'objet de perspectives présentées dans le Chapitre V - §2.

1.3. Evolutions spatio-temporelles des dynamiques d'écoulement de la glace et des systèmes hydrologiques sous-glaciaires : implications sur la diversité morphologique et les processus de formation des bedforms

Les travaux menés durant cette thèse ont permis de proposer un modèle de formation unificateur intégrant l'ensemble des bedforms sous-glaciaires et dépendant du couplage/découplage entre la glace et le lit sédimentaire, de la pression d'eau de fonte basale et de la quantité de déformation accommodée par le lit sédimentaire. Selon ce modèle, la forme des bedforms est ainsi directement contrôlée par les variations de la dynamique d'écoulement de la glace et des systèmes hydrologiques sous-glaciaires, dans le temps (par exemple depuis une période de maximum glaciaire jusqu'à période de déglaciation) et dans l'espace (par exemple entre les dômes de glace, les fleuves de glace et les routes de drainage ou entre les zones d'enracinement, les '*trunks*' et les lobes des fleuves de glace). En considérant les variabilités d'environnements sous-glaciaires et de dynamiques d'écoulement de la glace et de l'eau de fonte communément admises dans l'espace et dans le temps, deux modèles d'assemblages morphologiques ('landform systems') à l'échelle d'une portion de calotte glaciaire sont proposés pour une période de maximum glaciaire (**Figure 5.4**) et une période de déglaciation (**Figure 5.5**).

1.3.1. Contexte temporel type « maximum glaciaire » (Figure 5.4)

○ *Conditions glaciodynamiques et hydrologiques*

En période de maximum glaciaire, la moindre irradiation par le rayonnement solaire tend à induire une plus faible production d'eau de fonte (***Lewis et al., 1998 ; Zeng et al., 2012***). Conjuguées à une zone d'ablation restreinte, ces faibles productions d'eau de fonte tendent au développement d'une frange de chenalisation marginale étroite. L'extension de cette frange de chenalisation ne dépasse pas 50 km en amont de la marge ou se limite à des régions où l'épaisseur de la colonne de glace est inférieure à 1 km (***Bartholomew et al., 2011 ; Chandler et al., 2013 ; Schroeder et al., 2013 ; Dow et al., 2014 ; de Fleurian et al., 2016 ; Koziol & Arnold, 2018***). À l'échelle de la calotte glaciaire, ces plus faibles apports d'eau de fonte favorise aussi une plus faible densité de routes de drainage et autres structures chenalisées de grandes dimensions (***Greenwood et al., 2016 ; Davison et al., 2019***). Compte tenu du degré de chenalisation plus faible, le système de drainage est considéré comme davantage distribué et

inefficace à grande échelle (i.e. lit sédimentaire saturé en eau, film d'eau et cavités sous-glaciaires), favorisant des vitesses d'écoulement de la glace plus importantes (***Alley et al., 1986 ; Engelhardt & Kamb, 1997 ; King et al., 2004 ; Smith et al., 2007 ; Murray et al., 2008***) et une densité spatiale de fleuves de glace accrue (***Margold et al., 2015, 2018 ; Clark et al., 2022***). Des conditions de base froide sont supposées être répandues à la base des dômes de glace (***Sollid & Sørbel, 1994 ; Engelhardt, 2004 ; Kleman & Glasser, 2007***).

○ *Assemblages de bedforms sous-glaciaires*

En période de maximum glaciaire, les bedforms formés dans les environnements sous-glaciaires à base tempérée et marqués par la présence d'un lit sédimentaire meuble tendent à être essentiellement associés au couplage glace-sédiments. Parmi ces bedforms, des variations morphologiques témoignent de différents gradients d'évolution et de différentiels de déformation cumulée enregistrée par le lit sédimentaire. Des ribbed bedforms circulaires à linéaires se forment dans les zones intérieures des calottes et dans les zones inter-fleuves de glace marquées par de faibles vitesses de déplacement de la glace tandis que des linéations glaciations (i.e. drumlins et MSGLs) se forment à la base des fleuves de glace marqués par de fortes vitesses d'écoulement. Les zones de transition entre ces environnements sont marquées par des gradients de vitesses de déplacement de la glace et de déformation du lit sédimentaire : des gradients latéraux (déformation non-coaxiale) opèrent par exemple à la base des marges latérales cisaillantes et des gradients longitudinaux (déformation coaxiale) extensifs et compressifs opèrent respectivement à la base des zones d'enracinement des fleuves de glace et des lobes frontaux. Ces gradients de déformation sont illustrés par des bedforms sinueux, prédominamment transverse et parallèle à la direction de déplacement de la glace lorsque la déformation est coaxiale et essentiellement oblique lorsque la déformation est non-coaxiale.

Pour les fleuves de glace à terminaisons terrestres, l'existence d'une terminaison lobée induit une diminution de la vitesse d'écoulement de la glace au niveau de la zone marginale et la formation de gradients longitudinaux compressifs. En fonction du niveau de développement des structures chenalisées sous le lobe – qui influent directement sur l'efficacité de drainage – les assemblages morphologiques diffèrent. Des structures chenalisées peu développées favorisent la formation de systèmes de drainage distribués/inefficaces sous le lobe, des vitesses d'écoulement de la glace fortes

mais plus faible qu'au sein des fleuves de glace et la formation de linéations glaciaires faiblement allongées (drumlins) (***Stokes & Clark, 2001***). Des structures chenalisées bien développées favorisent quant à elle une concentration des écoulements d'eau de fonte au sein de systèmes de drainage efficace, des vitesses d'écoulement de la glace faibles et la formation de ribbed bedforms. À plus petite échelle, la présence d'un substrat sédimentaire rigide et/ou avec une plus faible pression d'eau interstitielle (*sticky spot*) peut être associée à des ribbed bedforms et des bedforms sinueux au sein de champs de linéations marquant la présence de fleuves de glace (***Stokes, 2018***).

Les quelques routes de drainage potentielles existant en période de maximum glaciaire tendent à être contrôlées par l'érosion – voire le dépôt au sein de la frange de chenalisation marginale – en raison du faible apport d'eau de fonte et de l'absence de cycles de couplage/découplage liés aux rares épisodes de drainage de forte amplitude (***Greenwood et al., 2016 ; Davison et al., 2019***). Ces routes de drainage sont ainsi essentiellement marquées par des hummocks et rides sédimentaires et des topographies résiduelles, tous associés à l'érosion de bedform préexistants ou du lit sédimentaire.

Considérant l'absence de processus de remobilisation de sédiments sous les dômes de glaces, en raison des conditions de base froide, des vitesses d'écoulement de la glace nulle à la base et l'absence d'eau de fonte, la formation de bedforms est certainement inhibée dans ces régions.

1.3.2. Contexte temporel type « déglaciation » (Figure 5.5)

○ *Conditions glaciodynamiques et hydrologiques*

En période de déglaciation, l'irradiation croissante par le rayonnement solaire tend à induire une plus forte production d'eau de fonte qu'en période de maximum glaciaire et à générer un amincissement des calottes glaciaires par ablation (***Lewis et al., 1998 ; Zeng et al., 2012***). L'amincissement des calottes favorisant la réduction de la pente de surface des régions marginales et du gradient hydraulique, les calottes glaciaires enregistrent une expansion de la frange de chenalisation marginale vers l'amont et une augmentation de la densité des structures chenalisées en période de déglaciation (***Carlson et al., 2008, 2009 ; Livingstone et al., 2015*** ; ***Greenwood et al., 2016***). L'augmentation de la densité des structures chenalisées durant la période de déglaciation serait également accompagnée d'une croissance de leur activité dans le temps, notamment à l'échelle annuelle, favorisant certainement le développement par incrémentation de réseaux de chenaux et d'eskers linéaires à mesure que la marge de la calotte

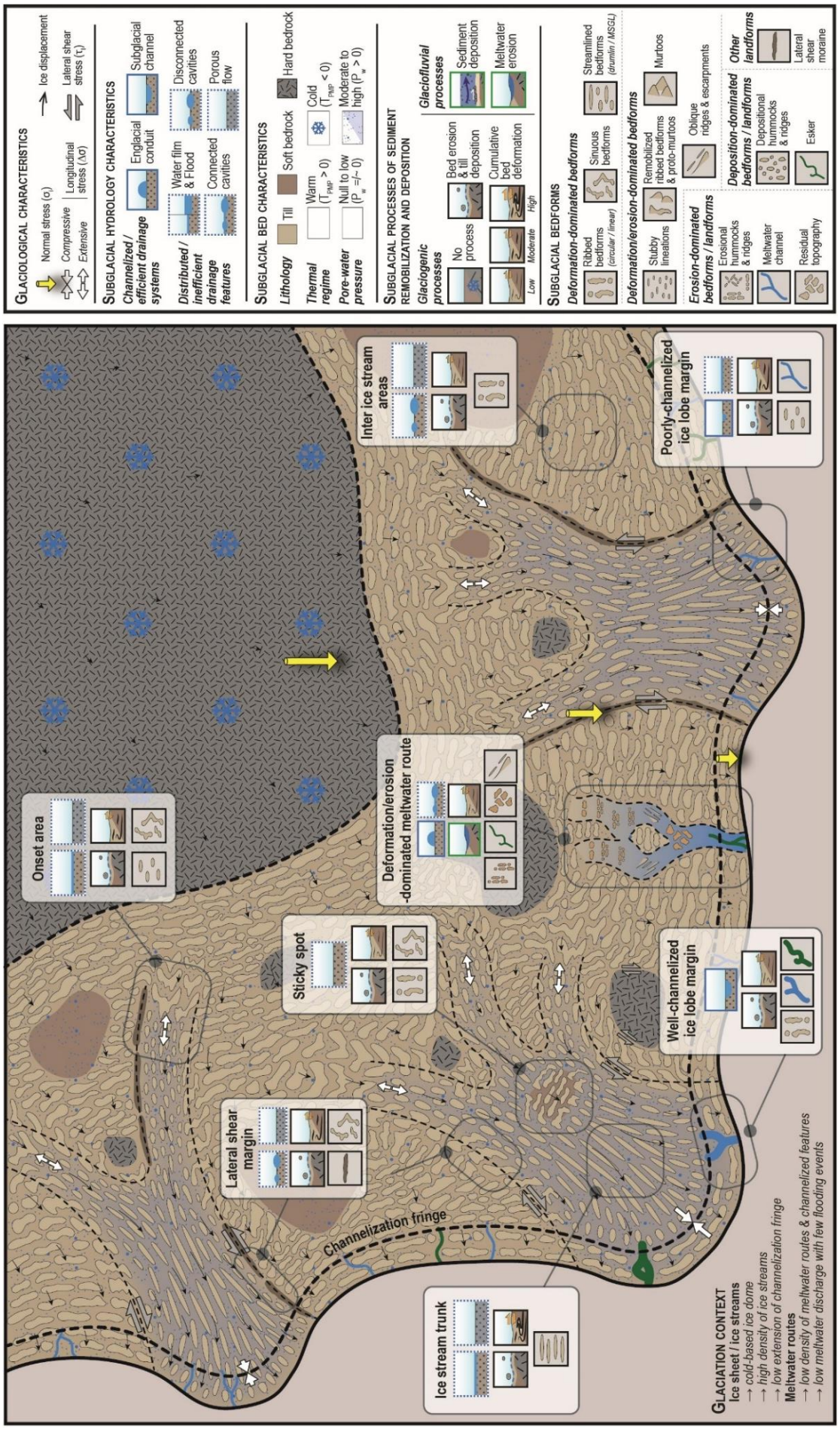

***Figure 5.4**. Diversity and spatial distribution of subglacial bedforms depending on glaciological, hydrological and lithological environments of an ice sheet during a maximum glacial period.*

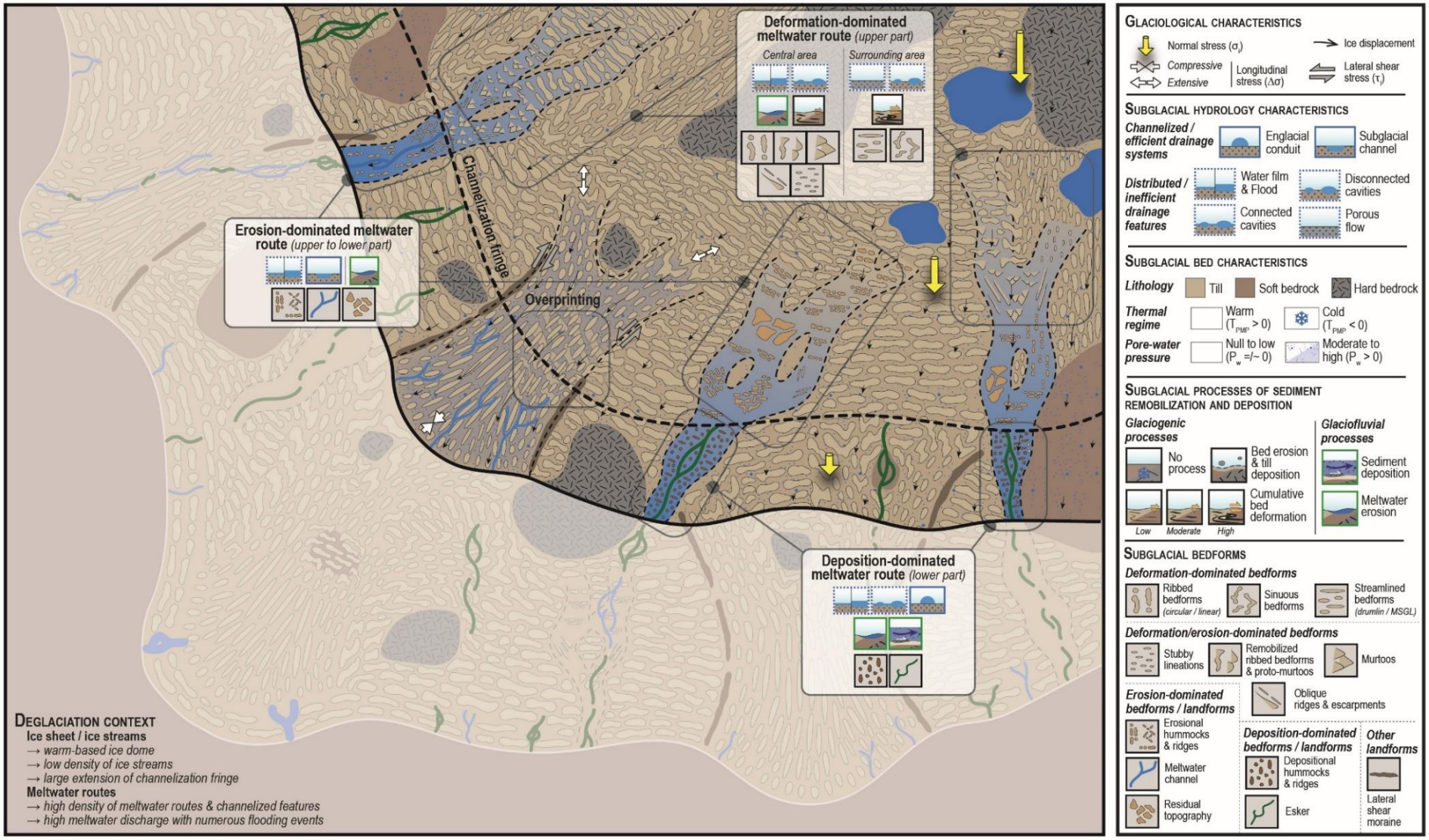

***Figure 5.5**. Diversity and spatial distribution of subglacial bedforms depending on glaciological, hydrological and lithological environments of an ice sheet during a deglaciation period.*

glaciaire se retire (***Clark & Walder, 1994 ; Punkari, 1997 ; Mäkinen, 2003 ; Livingstone et al., 2015***). La linéarité de ces réseaux serait donc un témoin direct du comportement transgressif dans le temps des processus sous-glaciaires.

La forte densité de routes de drainage et structures chenalisées en raison de l'apport croissant d'eau de fonte et de l'augmentation du nombre d'évènements de drainage de forte amplitude (i.e. vidange de lacs supra-glaciaires) suggère l'existence d'un système de drainage davantage chenalisé et efficace à grande échelle (***Greenwood et al., 2016 ; Davison et al., 2019***); les routes de drainage distribuées et hydrauliquement connectées étant considérées comme des structures chenalisées de grande échelle (***Peterson et al., 2017*** ; ***Lewington et al., 2020***). Cette efficacité de drainage à grande échelle implique plus de couplage et donc une plus faible densité de fleuves de glace durant les périodes de déglaciation (***Sole et al., 2013 ; Tedstone et al., 2014 ; Margold et al., 2015 ; Lelandais et al., 2018 ; Davison et al., 2019***). À la base de ces fleuves de glace, les structures chenalisées et les routes de drainage sont en revanche peu fréquentes, probablement en raison de la faible pente de surface et du faible gradient hydraulique (***Kleman & Glasser, 2007 ; Bell, 2008 ; Storrar et al., 2013, 2014 ; Livingstone et al., 2015 ; Lewington et al., 2020***). Les modifications du régime thermique basal participent à une propagation des conditions de base tempérée sous les dômes de glace, caractérisés par des bases froides en période de maximum glaciaire.

○ *Assemblages de bedforms sous-glaciaires*

En période de déglaciation, l'augmentation des apports d'eau de fonte et la forte densité de routes de drainage impliqueraient que la majorité des bedforms formés sont associés à des remobilisations sédimentaires fluvio-glaciaires induites par la circulation d'eau de fonte. La variabilité morphologique des bedforms observés au sein des routes de drainage dépend alors (i) des bedforms formés avant la mise en place de la route de drainage, (ii) de la position par rapport à la marge, et (iii) des variations temporelles d'écoulement de l'eau de fonte (i.e. apports d'eau de fonte élevés et constants ou épisodiques). Des apports d'eau de fonte élevés et constants, combinés à de fortes pressions d'eau de fonte basale, favorisent les processus d'érosion de bedform préexistants (ribbed bedforms, linéations, murtoos) ou du lit sédimentaire à l'origine (i) de hummocks et rides sédimentaires formant des assemblages géométriques et (ii) des topographies résiduelles.

Des apports d'eau de fonte forts épisodiques, impliquant une périodicité des phases de découplage/ couplage, favorisent une combinaison de processus d'érosion et de déformation, illustrés par des ribbed bedforms fragmentés à partiellement remobilisés, des proto-murtoos, des murtoos et des linéations de petits tailles. Le long de ces routes de drainage, les fortes pressions d'eau de fonte basale et connectivités hydrauliques tendent localement à limiter le couplage glace-sédiments et ainsi préserver les bedforms précédemment formés, tels que des ribbed bedforms. En périphérie de ces zones, la diminution de la pression d'eau de fonte basale et de la connectivité hydraulique favorise le couplage et la remobilisation des bedforms préexistants par des processus de déformation ; des bedforms sinueux et des linéations glaciaires se forment à mesure que l'on s'éloigne de l'axe de la route de drainage.

Au sein de la zone marginale de chenalisation des calottes glaciaires, où la pression et la vitesse d'écoulement d'eau de fonte basale diminuent, les processus de dépôt dominent. Ces portions de routes de drainage sont illustrées par des hummocks et rides sédimentaires aux assemblages chaotiques (les distinguant ainsi des motifs plus géométriques dessinés par les hummocks et rides sédimentaires issus des processus d'érosion) et des eskers.

À la base des fleuves de glace, moins nombreux et suivant potentiellement d'autres trajectoires d'écoulement qu'en période de maximum glaciaire, des linéations glaciaires témoignant de fortes déformations cumulées enregistrées par le lit sédimentaire se forment et peuvent apparaitre en superposition ou recoupement par rapport aux bedforms précédemment formés, illustrant la nature transgressive dans le temps des calottes glaciaires. La propagation des conditions de base tempérée sous les dômes de glace, caractérisés par des bases froides en période de maximum glaciaire, favorisent l'érosion du substrat et la formation d'un lit sédimentaire. Les faibles vitesses d'écoulement de la glace et la durée limitée des processus opérant sous le centre d'une calotte en retrait sont associées au développement de bedforms peu évolués issus de processus de déformation, i.e. les ribbed bedforms. Les ribbed bedforms observés au centre des paléo-calottes glaciaires (e.g. Laurentide, Fennoscandinave, Irlandaise) tendent donc à se former tardivement lors de leur retrait, à mesure que les conditions de base tempérée se propagent vers le cœur de la calotte.

2. Perspectives

De nombreuses perspectives découlant de ce travail ou questions scientifiques n'ayant pas été résolues sont encore à explorer :

- **La méthode d'analyse morphométrique permet-elle de tester les modèles d'assemblage morphologique à l'échelle d'une calotte glaciaire ?**

  Combiné à des méthodes de cartographie automatique, le protocole d'analyse morphométrique des bedforms sous-glaciaires pourrait permettre d'étudier à plus grande échelle les interactions glace-eau-sédiments à la base des paléo-calottes glaciaires. L'utilisation des paramètres quantitatifs matérialisant des séquences d'évolution morphologiques et dérivés des indices morphométriques permettrait d'explorer avec une plus grande précision les dynamiques d'écoulement de glace et d'eau de fonte à l'échelle d'une calotte glaciaire, lors du maximum glaciaire et de son retrait (***Margold et al., 2015 ; Lewington et al., 2019 ; Dewald et al., 2022***).

- **Comment distinguer des bedforms formés en dehors (i.e. déformation) ou au sein (i.e. déformation / érosion / dépôt dominées) des routes de drainage d'eau de fonte ?**

  Dans le Chapitre IV – Partie B, l'hypothèse a été proposée que les ribbed bedforms et les linéations glaciaires observés le long des routes de drainage d'eau de fonte sous-glaciaires se distinguent de leurs homologues formés en dehors (e.g. fleuves ou dômes de glace) par de plus petites dimensions et longueurs d'onde. Il a également été proposé que des bedforms de formes identiques mais de dimensions distinctes pouvaient coexister au sein d'une même zone d'étude, en dehors (i.e. ribbed bedforms circulaires à linéaires ; 10^2 – 10^3 m) et au sein (i.e. hummocks et rides sédimentaires ; 10^1 – 10^2 m) des routes de drainage. L'exploration de ces hypothèses pourrait s'effectuée par (i) l'intégration de paramètres dimensionnés au protocole d'analyse morphométrique et (ii) par une caractérisation sédimentaire et structurale de bedforms.

  L'intégration d'un critère dimensionné au protocole d'analyse morphométrique permettrait de filtrer et de distinguer au préalable des bedforms de formes identiques formés par la déformation du lit sous-glaciaire sous l'action de l'écoulement de la glace (i.e. fluide de forte viscosité ; grandes dimensions) ou par l'érosion ou le dépôt de sédiments sous l'action de l'écoulement d'eau de fonte

(i.e. fluide de faible viscosité ; petites dimensions). La caractérisation sédimentaire et structurale de bedforms pourrait être réalisée en Amérique du Nord (***Aylsworth & Shilts, 1989 ; Dunlop & Clark, 2006 ; Lewington et al., 2019***) ou en Islande (***Helgadottir, 2020 ; Benjaminsdottir, 2021***) où des corridors de ribbed bedforms et de linéations – indiquant apriori des routes de drainage – ont été identifiés. Ces études complémentaires permettraient notamment d'explorer les distinctions entre des ribbed bedforms et des linéations glaciaires (i) déformation dominée et (ii) déformation/érosion dominée, afin de valider le modèle de formation unificateur proposé dans cette étude.

- **Comment améliorer le dispositif de modélisation analogique afin d'explorer l'origine de la diversité morphologique à la base des calottes glaciaires et au sein des routes de drainage ?**

  Comme énoncé dans le Chapitre V - §1.2.3, les linéations et les hummocks/rides sédimentaires en dépôt ne sont actuellement pas reproductible par le modèle analogique en raison de la granulométrie des sédiments, des vitesses d'écoulement d'eau et de l'absence de processus thermiques (limitant la vitesse d'écoulement de la glace et la formation de cavités). Considérant le modèle analogique actuel dont les propriétés mécaniques de la gomme de silicone sont difficilement modifiables, l'impact des variations des températures et l'initiation de fortes vitesses d'écoulement de la silicone ne sont pas simulables. En revanche, il serait pertinent d'explorer l'impact des variations de pression d'eau basale, de lithologie, de granulométrie et de topographie – positive (bedforms préexistants) ou négtaive (cavités pré-existantes) – du lit sédimentaire sur les caractéristiques morphologiques des bedforms formés le long des routes de drainage. Par ailleurs, il serait intéressant d'étudier le contrôle de la vitesse de déformation de la glace sur les caractéristiques morphologiques des bedforms associés au couplage glace-sédiments (i.e. forme, longueur d'onde, sinuosité). Ces perspectives pourraient être explorées en controllant et en forcant mécaniquement le déplacement de la silicone, actuellement stimulé de façon in-situ par l'écoulement d'eau le long de l'interface basale.

  Par ailleurs, aucune explication – hormis l'hypothèse d'un processus aléatoire d'instabilité – n'a été proposée pour expliquer le continuum morphologique entre les ribbed bedforms circulaires à linéaires, bien que ces derniers soient reproduits avec le modèle expérimental. Considérant que les volumes de sédiments sont préservés au sein du modèle d'évolution entre des ribbed bedforms

d'allongements divers et des linéations gouverné par la quantité de déformation, l'hypothèse que la géométrie initiale des ribbed bedforms – circulaires ou linéaires – puisse être contrôlée par le stock sédimentaire disponible mérite d'être explorée. Cette hypothèse pourrait par exemple être testée en faisant variable la quantité de sédiments disponible au sein du modèle expérimental.

- **Comment préciser la relation entre la direction de déformation de la glace et l'orientation des bedforms afin de contraindre leur modalité, leur lieu et leur timing de formation ?**

  L'exploration de l'évolution morphologique des bedforms sous les calottes glaciaires actuelles est actuellement limitée par les difficultés d'observations sur de grandes échelles d'espace et de temps. Face à ces difficultés, la relation entre les directions de déformation enregistrées dans le lit sédimentaire et les orientations des bedforms s'avère être un proxy intéressant pour préciser la relation entre l'évolution morphologique des beforms et la dynamique d'écoulement des fleuves de glace et des calottes glaciaires.

  Actuellement seules des ellipses horizontales de déformation de la surface de la silicone sont calculées à partir des données expérimentales du modèle analogique. La reconstruction d'ellipsoides de déformation de la surface et de la base de la silicone ainsi que du lit sédimentaire permettrait de contraindre la relation entre la déformation de la glace, la déformation enregistrée par le lit sédimentaire et les caractéristiques morphologiques des bedforms. Les variabilités spatiales de cette relation notamment en fonction des différents contextes glaciodynamiques simulables par le modèle analogique (fleuves et lobes de glace, marges latérales cisaillantes) permettraient notamment d'expliquer la nature de la diversité morphologique des bedforms. La reconstruction d'ellispoides de deformation nécessiterait de développer une méthode de photogramétrie suffisamment précise pour étudier les composantes de déplacement vertical du lit sédimentaire et de la silicone. L'extraction de ces composantes pour la silicone nécessiterait aussi l'intégration d'un réseau de marqueurs – potentiellement UV – à la base de la calotte de silicone.

  Par ailleurs, l'augmentation croissante de la résolution des données topographiques permet la cartographie d'objets sous-glaciaires de petites dimensions (10^1-10^2 m), tels que les rides sédimentaires de remplissage de crevasses ('*crevasse-squeeze ridges*') dont l'orientation témoigne

également des directions de déformation de la glace (***Evans et al., 2015, 2016***). L'étude combinée des '*crevasse-squeeze ridges*' – formés à la base des régions marginales lors du retrait des calottes glaciaires – et des bedforms sous-glaciaires pourrait ainsi permettre de contraindre avec plus de précision la temporalité et le lieu de formation des bedforms sous-glaciaires.

- **Comment la relation entre l'orientation des bedforms sous-glaciaires et les directions de déformation – et non de déplacement – proposée dans cette étude remet-elle en question certaines méthodes de reconstitutions paléoglaciologiques ?**

  Ce travail a permis de démontrer que l'orientation des bedforms était contrôlée par les directions de déformation enregistrée dans le lit sédimentaire – et non par les directions de déplacement de la glace – et pouvait être variable (et notamment oblique) sous une même direction de déplacement de la glace. Par conséquent, certaines reconstitutions de paléogéographiques proposant de multiples trajectoires d'écoulement basées sur l'interpréation de relations de recoupement de bedforms ou de superposition pour expliquer des bedforms de forme complexe d'orientation oblique sont possiblement à réviser (***Clark, 1993 ; Knight et al., 1999 ; Dunlop & Clark, 2006 ; Stokes et al., 2006 ; De Angelis & Kleman, 2007 ; Greenwood & Clark, 2009 ; Brown et al., 2011***).

  Tester la méthode d'analyse morphométrique et le modèle d'évolution des bedforms sur des régions où des bedforms complexes/obliques/sinueux ont été interprétés comme résultant du recoupement de plusieurs générations de bedforms permettrait de vérifier si un nombre réduit de trajectoires d'écoulement de la glace est compatible avec l'intégralité des orientations et formes de bedforms cartographiés. En parallèle, le développement d'une méthode d'inversion des orientations des bedforms pour remonter aux directions de déformation permettrait de tester l'existence d'une ou plusieurs trajectoire(s) d'écoulement dans ces mêmes régions peuplées de bedforms complexes (***Cobbold & Percevault, 1982 ; Hindle & Burkhard, 1999 ; Gumiaux et al., 2003***).

  Par ailleurs, bien que des processus de superposition et de recoupement de bedforms résultent du caractère transgressif dans le temps des calottes glaciaires, ce travail a démontré que l'âge de formation des bedforms était en moyenne de plus en plus jeune à mesure que ces derniers sont observés proche du cœur des paléo-calottes glaciaires. Ce travail a notamment mis en évidence que

les ribbed bedforms observés au cœur des paléo-calottes glaciaires étaient vraisemblablement tardifs et formés au cours de leur retrait, en raison de la propagation vers l'amont des conditions de base tempérée en période de déglaciation. Ce modèle questionne alors une théorie datant de la fin des années 1990 suggérant que la position des dômes de glace à base froide durant les périodes de maximum glaciaire est reconstructible à partir de l'identification de champs de ribbed bedforms, en considérant que leur formation résulte de la fracturation par extension d'un substrat sédimentaire gelé (***Hättestrand & Kleman, 1997 ; Kleman & Hättestrand, 1999***). Ce modèle suggère ainsi une révision partielle des méthodes de reconstructions des régimes thermiques à la base des calottes glaciaires quaternaires, ainsi que certaines reconstitutions glaciodynamiques associées.

- **L'orientation et la forme des bedforms éoliens et aquatiques dépendent-elles des directions de déformation résultant des interactions fluide-sédiments ?**

  De nombreux modèles d'évolution des bedforms éoliens et subaquatiques ont été développés afin de mettre en relation les caractéristiques morphologiques avec la direction et la vitesse de déplacement du fluide, le stock sédimentaire ou le type de transport (e.g. ***McKee, 1979 ; Kleinhans et al., 2002***). Comme pour les bedforms sous-glaciaires, tester l'hypothèse que l'orientation et la forme des bedforms éoliens et subaquatiques dépendent de la direction et de la quantité de déformation finie enregistrée par le lit sédimentaire pourrait permettre d'explorer leurs diversités de forme. L'observation de dunes obliques par rapport à la direction de déplacement du vent ou de l'eau au sein d'environnements éoliens (e.g. ***Zarate & Tripaldi, 2012***) ou le long de bordures de rivières (e.g. ***Venditti et al., 2019***), vont dans le sens de cette hypothèse et suggère potentiellement de la déformation cisaillante résultant de différentiels de vitesse de déplacement.

BIBLIOGRAPHIE

A

Aario, R. (1997). Classification and terminology of morainic landforms in Finland. Boreas, 6(2), 87–100.

Ahokangas, E., Ojala, A. E., Tuunainen, A., Valkama, M., Palmu, J. P., Kajuutti, K., & Mäkinen, J. (2021). The distribution of glacial meltwater routes and associated murtoo fields in Finland. Geomorphology, 389, 107854.

Alley, K. E., Scambos, T. A., Anderson, R. S., Rajaram, H., Pope, A., & Haran, T. M. (2018). Continent-wide estimates of Antarctic strain rates from Landsat 8-derived velocity grids. Journal of Glaciology, 64(244), 321-332.

Alley, R. B. (1993). In search of ice-stream sticky spots. Journal of Glaciology, 39(133), 447–454.

Alley RB. (2000). Continuity comes first: recent progress in understand- ing subglacial deformation. In Deformation of Glacial Materials, Maltman AJ, Hubbard B, Hambrey MJ (eds), Vol. 176. The Geologi- cal Society of London Special Publication; 171–179.

Allen, J. R. L. (1968). The nature and origin of bed-form hierarchies. Sedimentology, 10(3), 161-182.

Anandakrishnan, S. and Alley, R.B. (1997). Stagnation of ice stream C, West Antarctica by water piracy. Geophysical Research Letters, 24(3), pp.265-268.

Anderson, J. B., & Fretwell, L. O. (2008). Geomorphology of the onset area of a paleo-ice stream, Marguerite Bay, Antarctic Peninsula. Earth Surface Processes and Landforms: The Journal of the British Geomorphological Research Group, 33(4), 503-512.

Andrews, L. C., Catania, G. A., Hoffman, M. J., Gulley, J. D., Lüthi, M. P., Ryser, C., Hawley, R.L. & Neumann, T. A. (2014). Direct observations of evolving subglacial drainage beneath the Greenland Ice Sheet. Nature, 514(7520), 80-83.

Andrews, L. C., Hoffman, M. J., Neumann, T. A., Catania, G. A., Lüthi, M. P., Hawley, R. L., ... & Morriss, B. F. (2018). Seasonal evolution of the subglacial hydrologic system modified by supraglacial lake drainage in western Greenland. Journal of Geophysical Research: Earth Surface, 123(6), 1479-1496.

Atkinson, N., Utting, D. J., and Pawley, S. M. (2018). An Update to the Glacial Landforms Map of Alberta. In Alberta Geological Survey

Atkinson, N., Pawley, S., and Utting, D. J. (2016). Flow-pattern evolution of the Laurentide and Cordilleran ice sheets across west-central Alberta, Canada: implications for ice sheet growth, retreat and dynamics during the last glacial cycle. Journal of Quaternary Science, 31(7), 753–768

Aylsworth, J. M., and Shilts, W. W. (1989). Bedforms of the Keewatin Ice Sheet, Canada. Sedimentary Geology, 62(2–4), 407–428.

B

Bamber, J. L., Vaughan, D. G., and Joughin, I. (2000). Widespread complex flow in the interior of the antarctic ice sheet. Science, 287(5456), 1248–1250.

Banwell, A., Hewitt, I., Willis, I., & Arnold, N. (2016). Moulin density controls drainage development beneath the Greenland ice sheet. Journal of Geophysical Research: Earth Surface, 121(12), 2248-2269.

Barchyn, T. E., Dowling, T. P. F., Stokes, C. R., and Hugenholtz, C. H. (2016). Subglacial bed form morphology controlled by ice speed and sediment thickness. Geophysical Research Letters, 43(14), 7572–7580

Bartholomew, I., Nienow, P., Sole, A., Mair, D., Cowton, T., & King, M. A. (2012). Short-term variability in Greenland Ice Sheet motion forced by time-varying meltwater drainage: Implications for the relationship between subglacial drainage system behavior and ice velocity. Journal of Geophysical Research: Earth Surface, 117(F3).

Batchelor, C. L., & Dowdeswell, J. A. (2016). Lateral shear-moraines and lateral marginal-moraines of palaeo-ice streams. Quaternary Science Reviews, 151, 1-26.

Batchelor, C. L., Margold, M., Krapp, M., Murton, D. K., Dalton, A. S., Gibbard, P. L., ... & Manica, A. (2019). The configuration of Northern Hemisphere ice sheets through the Quaternary. Nature communications, 10(1), 1-10.

Bell, R. E., Studinger, M., Shuman, C. A., Fahnestock, M. A., & Joughin, I. (2007). Large subglacial lakes in East Antarctica at the onset of fast-flowing ice streams. Nature, 445(7130), 904-907.

Bell, R. E. (2008). The role of subglacial water in ice-sheet mass balance. Nature Geoscience, 1(5), 297-304.

Benediktsson, Í. Ö. et al (2016). Progressive formation of modern drumlins at Múlajökull, Iceland: stratigraphical and morphological evidence. Boreas 45, 567–583.

Benediktsson, Í. Ö., Aradóttir, N., Ingólfsson, Ó., & Brynjólfsson, S. (2022). Cross-cutting palaeo-ice streams in NE-Iceland reveal shifting Iceland Ice Sheet dynamics. Geomorphology, 396, 108009.

Benjamínsdóttir, M. M (2021). Rifjagarðar í Bakkaflóa-landmótun, setgerð og myndun (Master's Thesis).

Benn, D. I., & Evans, D. J. A. (2010). Glaciers and glaciation, 2nd Edition, Hodder Arnold Publication

Benn, D.I. (1992). The genesis and significance of hummocky moraine: evidence frome the isle of Skye, Scotland. Quaternary Research (United States), 11, 781–799.

Bennett, M. R., Huddart, D., & Waller, R. I. (2006). Diamict fans in subglacial water-filled cavities—a new glacial environment. Quaternary Science Reviews, 25(21-22), 3050-3069.

Bennett, M., & Glasser, N. (2009). Glacial Sedimentation in Water. Glacial Geology: Ice sheet and Lanforms.

Bestmann, M., & Prior, D. J. (2003). Intragranular dynamic recrystallization in naturally deformed calcite marble: Diffusion accommodated grain boundary sliding as a result of subgrain rotation recrystallization. Journal of Structural Geology, 25(10), 1597–1613

Bindschadler, R. (1983). The importance of pressurized subglacial water in separation and sliding at the glacier bed. Journal of Glaciology, 29(101), 3-19.

Bluemle, J. P., Lord, M. L., and Hunke, N. T. (1993). Exceptionnaly long, narrow drumlins formed in subglacial cavities, North Dakota. Boreas, 22, 15–24

Boone, S. J., and Eyles, N. (2001). Geotechnical model for great plains hummocky moraine formed by till deformation below stagnant ice, Geomorphology, 38(1–2), 109–124

Bouchard, M. A. (1989). Subglacial landforms and deposits in central and northern Québec, Canada, with emphasis on Rogen moraines. Sedimentary Geology, 62(2–4), 293–308

Bougamont, M., Price, S. F., Christoffersen, P., and Payne, A. J. (2011). Dynamic patterns of ice stream flow in a 3-D higher-order ice sheetmodel with plastic bed and simplified hydrology. Journal of Geophysical Research, 116, 1–13.

Bougamont, M., Christoffersen, P., Hubbard, A. L., Fitzpatrick, A. A., Doyle, S. H., & Carter, S. P. (2014). Sensitive response of the Greenland Ice Sheet to surface melt drainage over a soft bed. Nature communications, 5(1), 1-9.

Boulton, G. S. (1976). The origin of glacially fluted surfaces-observations and theory. Journal of Glaciology, 17(76), 287-309.

Boulton, G. S. (1982). Processes and patterns of glacial erosion. In Glacial geomorphology (pp. 41-87). Springer, Dordrecht.

Boulton, G. S. (1986). Push-moraines and glacier-contact fans in marine and terrestrial environments. Sedimentology, 33(5), 677–698

Boulton, G. S. (1987). A theory of drumlin formation by subglacial sediment deformation. In Drumlin symposium. Manchester, 1985 (pp. 25–80).

Boulton, G. S. (1996). Theory of glacial erosion, transport and deposition as a consequence of subglacial sediment deformation. Journal of Glaciology, 42(140), 43-62.

Boulton, G. S., and Hindmarsh, R. C. A. (1987). Sediment deformation beneath glaciers: rheology and geological consequences. Journal of Geophysical Research, 92(B9), 9059–9082

Boulton, G. S., Caban, P. E., & Van Gijssel, K. (1995). Groundwater flow beneath ice sheets: Part I—Large scale patterns. Quaternary Science Reviews, 14(6), 545-562.

Boyce, J. I., & Eyles, N. (1991). Drumlins carved by deforming till streams below the Laurentide Ice Sheet. Geology, 19(8), 787–790

Boyce, J. I., & Eyles, N. (2000). Architectural element analysis applied to glacial deposits: internal geometry of a late Pleistocene till sheet, Ontario, Canada. GSA Bulletin, 112(1), 98-118.

Boyes, B. M., Pearce, D. M., & Linch, L. D. (2021). Glacial geomorphology of the Kola Peninsula and Russian Lapland. Journal of Maps, 17(2), 497-515.

Breemer, C. W., Clark, P. U., & Haggerty, R. (2002). Modeling the subglacial hydrology of the late Pleistocene Lake Michigan lobe, Laurentide Ice Sheet. Geological Society of America Bulletin, 114(6), 665-674.

Brennand, T. A. (2000). Deglacial meltwater drainage and glaciodynamics: inferences from Laurentide eskers, Canada. Geomorphology, 32(3-4), 263-293.

Briner, J. P. (2007). Supporting evidence from the New York drumlin field that elongate subglacial bedforms indicate fast ice flow. Boreas, 36(2), 143–147.

Brown, V. H., Stokes, C. R., & O'Cofaigh, C. (2011). The glacial geomorphology of the north-west sector of the Laurentide Ice Sheet. Journal of Maps, 7(1), 409-428.

Bryce, J. (1833). On the evidences of diluvial action in the north of Ireland. J. R. Geol. Soc. Dublin, 1, 34-44.

Burgess, D. O., Shaw, J., & Eyton, J. R. (2003). Morphometric comparisons between Rogen terrain and hummocky terrain. Physical Geography, 24(4), 319-336.

Burke, M. J., Brennand, T. A., & Perkins, A. J. (2012). Evolution of the subglacial hydrologic system beneath the rapidly decaying Cordilleran Ice Sheet caused by ice-dammed lake drainage: implications for meltwater-induced ice acceleration. Quaternary Science Reviews, 50, 125-140.

C

Campbell, J.E., McCurdy, M.W., Lauzon, G., Regis, D., and Wygergangs, M., 2020. Field data, till composition, and ice-flow history, south Rae Craton, Northwest Territories: results from the GEM-2 South Rae project — Surficial Mapping activity; Geological Survey of Canada.

Canals, M., Urgeles, R., & Calafat, A. M. (2000). Deep sea-floor evidence of past ice streams off the Antarctic Peninsula. Geology, 28(1), 31-34.

Carl, J. D. (1978). Ribbed moraine–drumlin transition belt, St. Lawrence Valley, New York. Geology, 6(9), 562-566.

Carlson, A. E., LeGrande, A. N., Oppo, D. W., Came, R. E., Schmidt, G. A., Anslow, F. S., ... & Obbink, E. A. (2008). Rapid early Holocene deglaciation of the Laurentide ice sheet. Nature Geoscience, 1(9), 620-624.

Catania, G., & Paola, C. (2001). Braiding under glass. Geology, 29(3), 259-262.

Chamberlain, T.C. (1883): Preliminary paper on the Terminal Moraine of the second glaciar epoch. U.S. Geological Survey, Third Annual Report, 1881-1882, pp. 219-402.

Chandler, D. M., Wadham, J. L., Lis, G. P., Cowton, T., Sole, A., Bartholomew, I., ... & Hubbard, A. (2013). Evolution of the subglacial drainage system beneath the Greenland Ice Sheet revealed by tracers. Nature Geoscience, 6(3), 195-198.

Chandler, B. M. P., Evans, D. J. A., & Roberts, D. H. (2016). Characteristics of recessional moraines at a temperate glacier in SE Iceland: Insights into patterns, rates and drivers of glacier retreat. Quaternary Science Reviews, 135, 171–205.

Chandler, B. M. P., & Evans, D. J. A. (2019). Glacial processes and sediments. In Encyclopedia of Geology, 2nd Edition. Earth Systems and Environmental Sciences Elsevier.

Chandler, D. M., Wadham, J. L., Nienow, P. W., Doyle, S. H., Tedstone, A. J., Telling, J., ... & Hubbard, A. (2021). Rapid development and persistence of efficient subglacial drainage under 900 m-thick ice in Greenland. Earth and Planetary Science Letters, 566, 116982.

Chapwanya, M., Clark, C. D., & Fowler, A. C. (2011). Numerical computations of a theoretical model of ribbed moraine formation. Earth Surface Processes and Landforms, 36(8), 1105–1112.

Clark, C. D. (1993). Mega-scale glacial lineations and cross-cutting ice-flow landforms. Earth Surface Processes and Landforms, 18, 1–29.

Clark, C. D. (1999). Glaciodynamic context of subglacial bedform generation and preservation. Annals of Glaciology, 28, 23–32.
Clark, C. D., & Stokes, C. R. (2001). Extent and basal characteristics of the M'Clintock Channel Ice Stream. Quaternary International, 86(1), 81–101.
Clark, C. D. & Stokes, C. R. (2003). Palaeo-ice stream landsystem. In Glacial Landsystems, pp. 204–227.
Clark, C. D., Tulaczyk, S. M., Stokes, C. R., and Canals, M. (2003). A groove-ploughing theory for the production of mega-scale glacial lineations, and implications for ice-stream mechanics. Journal of Glaciology, 49(165), 240–256.
Clark, C. D., Hughes, A. L., Greenwood, S. L., Spagnolo, M., & Ng, F. S. (2009). Size and shape characteristics of drumlins, derived from a large sample, and associated scaling laws. Quaternary Science Reviews, 28(7-8), 677-692.
Clark, C. D. (2010). Emergent drumlins and their clones: from till dilatancy to flow instabilities. Journal of Glaciology, 56(200), 1011-1025.
Clark, C. D., Hughes, A. L., Greenwood, S. L., Jordan, C., & Sejrup, H. P. (2012). Pattern and timing of retreat of the last British-Irish Ice Sheet. Quaternary Science Reviews, 44, 112-146.
Clark, C. D., Ely, J. C., Spagnolo, M., Hahn, U., Hughes, A. L., and Stokes, C. R. (2018). Spatial organization of drumlins. Earth Surface Processes and Landforms, 43(2), 499-513.
Clark, C. D., Ely, J. C., Hindmarsh, R. C., Bradley, S., Ignéczi, A., Fabel, D., ... & Wilson, P. (2022). Growth and retreat of the last British–Irish Ice Sheet, 31 000 to 15 000 years ago: the BRITICE-CHRONO reconstruction. Boreas.
Clark, P. U., & Walder, J. S. (1994). Subglacial drainage, eskers, and deforming beds beneath the Laurentide and Eurasian ice sheets. Geological Society of America Bulletin, 106(2), 304-314.
Clarke, G. K. (1987). Fast glacier flow: Ice streams, surging, and tidewater glaciers. Journal of Geophysical Research: Solid Earth, 92(B9), 8835-8841.
Clerc, S., Buoncristiani, J. F., Guiraud, M., Desaubliaux, G., & Portier, E. (2012). Depositional model in subglacial cavities, Killiney Bay, Ireland. Interactions between sedimentation, deformation and glacial dynamics. Quaternary Science Reviews, 33, 142-164.
Cobbold, P. R., & Percevault, M. N. (1983). Spatial integration of strains using finite elements. In Strain Patterns in Rocks (pp. 299-305). Pergamon.
Colgan, W., Rajaram, H., Abdalati, W., McCutchan, C., Mottram, R., Moussavi, M. S., & Grigsby, S. (2016). Glacier crevasses: Observations, models, and mass balance implications. Reviews of Geophysics, 54(1), 119-161.
Collins, D. N. (1989). Seasonal development of subglacial drainage and suspended sediment delivery to melt waters beneath an Alpine glacier. Annals of Glaciology, 13, 45-50.
Corti, G., Zeoli, A., Belmaggio, P., & Folco, L. (2008). Physical modeling of the influence of bedrock topography and ablation on ice flow and meteorite concentration in Antarctica. Journal of Geophysical Research: Earth Surface, 113(F1).
Corti, G., Zeoli, A., & Iandelli, I. (2014). Small-scale modeling of ice flow perturbations induced by sudden ice shelf breakup. Global and Planetary Change, 119, 51-55.
Corti, G., & Zeoli, A. (2018). Analogue modelling of the influence of ice shelf collapse on the flow of ice sheets grounded below sea-level. Annals of Geophysics, 61(3), OC332-OC332.
Coughlan, M., Tóth, Z., Van Landeghem, K. J., Mccarron, S., & Wheeler, A. J. (2020). Formational history of the Wicklow Trough: a marine-transgressed tunnel valley revealing ice flow velocity and retreat rates for the largest ice stream draining the late-Devensian British–Irish Ice Sheet. Journal of Quaternary Science, 35(7), 907-919.
Cowan, W. R. (1968). Ribbed moraine: Till-fabric analysis and origin. Canadian Journal of Earth Sciences, 5(5), 1145–1159.
Cowton, T., Nienow, P., Sole, A., Wadham, J., Lis, G., Bartholomew, I., ... & Chandler, D. (2013). Evolution of drainage system morphology at a land-terminating Greenlandic outlet glacier. Journal of Geophysical Research: Earth Surface, 118(1), 29-41.
Cowton, T., Nienow, P., Sole, A., Bartholomew, I., & Mair, D. (2016). Variability in ice motion at a land-terminating Greenlandic outlet glacier: the role of channelized and distributed drainage systems. Journal of Glaciology, 62(233), 451-466.
Cuffey, K. M., & Paterson, W. S. B. (2010). The physics of glaciers. Academic Press.
Cutler, P. M., Colgan, P. M., & Mickelson, D. M. (2002). Sedimentologic evidence for outburst floods from the Laurentide Ice Sheet margin in Wisconsin, USA: implications for tunnel-channel formation. Quaternary International, 90(1), 23-40.

D

Dahlgren S. 2013. Subglacially eroded meltwater hummocks. Master of Science thesis. Gothenburg University, Department of Earth Sciences B741.
Damsgaard, A., Egholm, D. L., Beem, L. H., Tulaczyk, S., Larsen, N. K., Piotrowski, J. A., & Siegfried, M. R. (2016). Ice flow dynamics forced by water pressure variations in subglacial granular beds. Geophysical Research Letters, 43(23), 12-165.
Das, S. B., Joughin, I., Behn, M. D., Howat, I. M., King, M. A., Lizarralde, D., & Bhatia, M. P. (2008). Fracture propagation to the base of the Greenland Ice Sheet during supraglacial lake drainage. Science, 320(5877), 778-781.
Davis, W. M. (1884). The distribution and origin of drumlins. American Journal of Science, 3(168), 407-416.
Davison, B. J., Sole, A. J., Livingstone, S. J., Cowton, T. R., & Nienow, P. W. (2019). The influence of hydrology on the dynamics of land-terminating sectors of the Greenland Ice Sheet. Frontiers in Earth Science, 10.
De Angelis, H., and Kleman, J. (2007). Palaeo-ice streams in the Foxe/Baffin sector of the Laurentide Ice Sheet. Quaternary Science Reviews, 26(9–10), 1313–1331.
De Fleurian, B., Morlighem, M., Seroussi, H., Rignot, E., van den Broeke, M. R., Kuipers Munneke, P., ... & Tedstone, A. J. (2016). A modeling study of the effect of runoff variability on the effective pressure beneath Russell Glacier, West Greenland. Journal of Geophysical Research: Earth Surface, 121(10), 1834-1848.

Denis, M., Guiraud, M., Konaté, M., & Buoncristiani, J. F. (2010). Subglacial deformation and water-pressure cycles as a key for understanding ice stream dynamics: evidence from the Late Ordovician succession of the Djado Basin (Niger). International Journal of Earth Sciences, 99(6), 1399-1425.

Denton, G. H., and Hughes, T. (1981). The last great ice sheets.

DesRosiers, P., 2021. The effect of deglacial meltwater processes on kimberlite indicator mineral concentrations in glacial sediments (Doctoral dissertation, Science: Department of Earth Sciences).

Dewald, N., Livingstone, S. J., & Clark, C. D. (2022). Subglacial meltwater routes of the Fennoscandian Ice Sheet. Journal of Maps, 1-15.

Depoorter, M. A., Bamber, J. L., Griggs, J. A., Lenaerts, J. T., Ligtenberg, S. R., van den Broeke, M. R., & Moholdt, G. (2013). Calving fluxes and basal melt rates of Antarctic ice shelves. Nature, 502(7469), 89-92.

Doornkamp, J. C., & King, C. A. (1971). Numerical analysis in geomorphology: an introduction. Hodder Education.

Dow, C. F., Kulessa, B., Rutt, I. C., Doyle, S. H., & Hubbard, A. (2014). Upper bounds on subglacial channel development for interior regions of the Greenland ice sheet. Journal of Glaciology, 60(224), 1044-1052.

Dowdeswell, J. A., Ó Cofaigh, C., & Pudsey, C. J. (2004). Continental slope morphology and sedimentary processes at the mouth of an Antarctic palaeo-ice stream. Marine Geology, 204(1–2), 203–214.

Dowling, T. P., Spagnolo, M., & Möller, P. (2015). Morphometry and core type of streamlined bedforms in southern Sweden from high resolution LiDAR. Geomorphology, 236, 54-63.

Dreimanis, A. (1989). Tills: their genetic terminology and classification. Genetic classification of glacigenic deposits, 17-83.

Dufresne, M., Dewals, B. J., Erpicum, S., Archambeau, P., & Pirotton, M. (2010). Experimental investigation of flow pattern and sediment deposition in rectangular shallow reservoirs. International Journal of Sediment Research, 25(3), 258-270.

Dunlop, P., and Clark, C. D. (2006). The morphological characteristics of ribbed moraine. Quaternary Science Reviews, 25(13–14), 1668–1691.

Dunse, T., Schellenberger, T., Hagen, J. O., Kääb, A., Schuler, T. V., and Reijmer, C. H. (2015). Glacier-surge mechanisms promoted by a hydro-thermodynamic feedback to summer melt. Cryosphere, 9(1), 197–215.

Dyke, A. S. (1993). Landscapes of cold-centred Late Wisconsinan ice caps, Arctic Canada. Progress in Physical Geography, 17(2), 223-247.

Dyke, A. S., Morris, T. F., Green, D. E. C., and England, J. (1992). Quaternary geology of Prince of Wales Island, Arctic Canada. In Memoir - Geological Survey of Canada (Vol. 433).

Dyke, A. S. & Morris, T. F. (1988). Drumlin fields, dispersal trains and ice streams in Arctic Canada. Canadian Geographer / Le Géographe Canadien, 32(1), 86–90.

Dyke, A. S., Vincent, J. S., Andrews, J. T., Dredge, L. A., & Cowan, W. R. (1989). The Laurentide Ice Sheet and an introduction to the Quaternary geology of the Canadian Shield.

E

Ebert, K., & Kleman, J. (2004). Circular moraine features on the Varanger Peninsula, northern Norway, and their possible relation to polythermal ice sheet coverage. Geomorphology, 62(3–4), 159–168.

Echelmeyer, K. A., Harrison, W. D., Larsen, C., and Mitchell, J. E. (1994). The role of the margins in the dynamics of an active ice stream. Journal of Glaciology, 40(136), 527–538.

Ely, J. C., Clark, C. D., Spagnolo, M., Stokes, C. R., Greenwood, S. L., Hughes, A. L. C., Dunlop, P., and Hess, D. (2016). Do subglacial bedforms comprise a size and shape continuum? Geomorphology, 257, 108–119.

Ely, J. C., Graham, C., Barr, I. D., Rea, B. R., Spagnolo, M., & Evans, J. (2017). Using UAV acquired photography and structure from motion techniques for studying glacier landforms: application to the glacial flutes at Isfallsglaciären. Earth Surface Processes and Landforms, 42(6), 877-888.

Embleton, C., & King, C. A. M. (1968). Glacial and periglacial geomorphology.

Engelhardt, H., Humphrey, N., Kamb, B., and Fahnestock, M. (1990). Physical conditions at the base of a fast moving Antarctic ice stream. Science, 248(4951), 57–59.

Engelhardt, H. (1998). Basal sliding of Ice Stream B, West Antarctica. Journal of Glaciology, 44(147), 223–230.

Engelhardt, H. (2004). Ice temperature and high geothermal flux at Siple Dome, West Antarctica, from borehole measurements. Journal of Glaciology, 50(169), 251-256.

Evans, D. J., Owen, L. A., & Roberts, D. (1995). Stratigraphy and sedimentology of Devensian (Dimlington Stadial) glacial deposits, east Yorkshire, England. Journal of Quaternary Science, 10(3), 241-265.

Evans, I. S. (1996). Abraded rock landforms (whalebacks) developed under ice streams in mountain areas. Annals of Glaciology, 22, 9-16.

Evans, D. J. A. (1996). A possible origin for a mega-fluting complex on the southern Alberta prairies, Canada. Zeitschrift für Geomorphologie. Supplementband, (106), 125-148.

Evans, D. J., & Hansom, J. D. (1996). The Edinburgh Castle crag-and-tail. Scottish Geographical Magazine, 112(2), 129-131.

Evans, D. J., & Twigg, D. R. (2002). The active temperate glacial landsystem: a model based on Breiðamerkurjökull and Fjallsjökull, Iceland. Quaternary science reviews, 21(20-22), 2143-2177.

Evans, D. J., & Hiemstra, J. F. (2005). Till deposition by glacier submarginal, incremental thickening. Earth Surface Processes and Landforms, 30(13), 1633–1662.

Evans, D. J., Phillips, E. R., Hiemstra, J. F., & Auton, C. A. (2006). Subglacial till: formation, sedimentary characteristics and classification. Earth-Science Reviews, 78(1-2), 115-176.

Evans, D. J., Clark, C. D., and Rea, B. R. (2008). Landform and sediment imprints of fast glacier flow in the southwest Laurentide Ice Sheet. Journal of Quaternary Science, 23(3), 249–272.

Evans, D. J., Young, N. J. P., and Cofaigh, C. O. (2014). Glacial geomorphology of terrestrial-terminating fast flow lobes/ice stream margins in the southwest Laurentide Ice Sheet. Geomorphology, 204, 86–113.

Evans, D.J., Ewertowski, M., Orton, C. (2015).. Fláajökull (north lobe), Iceland: active temperate piedmont lobe glacial landsystem. Journal of Maps.
Evans, D. J., Storrar, R. D., and Rea, B. R. (2016). Crevasse-squeeze ridge corridors: diagnostic features of late-stage palaeo-ice stream activity. Geomorphology, 258, 40-50.
Evans, D. J. (2017). Till: A glacial process sedimentology. John Wiley & Sons.
Evans, D. J., Atkinson, N., and Phillips, E. (2020). Glacial geomorphology of the Neutral Hills Uplands, southeast Alberta, Canada: The process-form imprints of dynamic ice streams and surging ice lobes. Geomorphology, 350, 106910.
Eyles, N., Sladen, J. A., & Gilro, S. (1982). A depositional model for stratigraphic complexes and facies superimposition in lodgement tills. Boreas, 11(4), 317-333.
Eyles, N., Eyles, C. H., & Miall, A. D. (1983). Lithofacies types and vertical profile models; an alternative approach to the description and environmental interpretation of glacial diamict and diamictite sequences. Sedimentology, 30(3), 393-410.
Eyles, N., Boyce, J. I., and Barendregt, R. W. (1999). Hummocky moraine: Sedimentary record of stagnant Laurentide Ice Sheet lobes resting on soft beds. Sedimentary Geology, 123(3–4), 163–174.
Eyles, N. (2012). Rock drumlins and megaflutes of the Niagara Escarpment, Ontario, Canada: a hard bed landform assemblage cut by the Saginaw–Huron Ice Stream. Quaternary Science Reviews, 55, 34-49.
Eyles, N., Boyce, J. I., & Putkinen, N. (2015). Neoglacial (< 3000 years) till and flutes at Saskatchewan Glacier, Canadian Rocky Mountains, formed by subglacial deformation of a soft bed. Sedimentology, 62(1), 182-203.
Eyles, N., Putkinen, N., Sookhan, S., & Arbelaez-Moreno, L. (2016). Erosional origin of drumlins and megaridges. Sedimentary Geology, 338, 2-23.

F

Fannon, J. S., Fowler, A. C., and Moyles, I. R. (2017). Numerical simulations of drumlin formation. Proceedings of the Royal Society A: Mathematical, Physical and Engineering Sciences, 473(2204).
Fannon, J. S. (2020). Mathematical modelling of subglacial bedform formation and dense granular flows (PhD Thesis).
Farinotti, D., Huss, M., Fürst, J. J., Landmann, J., Machguth, H., Maussion, F., & Pandit, A. (2019). A consensus estimate for the ice thickness distribution of all glaciers on Earth. Nature Geoscience, 12(3), 168-173.
Fisher, T. G., & Taylor, L. D. (2002). Sedimentary and stratigraphic evidence for subglacial flooding, south-central Michigan, USA. Quaternary International, 90(1), 87-115.
Fitzpatrick, A. A., Hubbard, A., Joughin, I., Quincey, D. J., Van As, D., Mikkelsen, A. P., ... & Jones, G. A. (2013). Ice flow dynamics and surface meltwater flux at a land-terminating sector of the Greenland ice sheet. Journal of Glaciology, 59(216), 687-696.
Flowers, G. E. (2015). Modelling water flow under glaciers and ice sheets. Proceedings of the Royal Society A: Mathematical, Physical and Engineering Sciences, 471(2176), 20140907.
Folk, R. L. (1968). Petrology of sedimentary rocks: Hemphill's. Austin, Texas, 170, 85.
Fountain, A. G., & Walder, J. S. (1998). Water flow through temperate glaciers. Reviews of Geophysics, 36(3), 299-328.
Fowler, A. C. (1987). Sliding with cavity formation. Journal of Glaciology, 33(115), 255-267.
Fowler, A. C. (2000). An instability mechanism for drumlin formation. Geological Society Special Publication, 176(1987), 307–319.
Fowler, A. C. (2009). Instability modelling of drumlin formation incorporating lee-side cavity growth. Proceedings of the Royal Society A: Mathematical, Physical and Engineering Sciences, 465(2109), 2681-2702.
Fowler, A. C. (2010). The formation of subglacial streams and mega-scale glacial lineations. Proceedings of the Royal Society A: Mathematical, Physical and Engineering Sciences, 466(2123), 3181-3201.
Fowler, A. C., & Chapwanya, M. (2014). An instability theory for the formation of ribbed moraine, drumlins and mega-scale glacial lineations. Proceedings of the Royal Society A: Mathematical, Physical and Engineering Sciences, 470(2171).
Fowler, A. C. (2018). The philosopher in the kitchen: the role of mathematical modelling in explaining drumlin formation. Gff, 140(2), 93–105.
Francek, M., & Blish, R. (1991). Glacio-Dynamic Variations in Central New York Drumlins: A Morphometric Analysis. The Geographical Bulletin, 33(2), 105.
Franke, S., Jansen, D., Binder, T., Dörr, N., Helm, V., Paden, J., Steinhage, D., & Eisen, O. (2020). Bed topography and subglacial landforms in the onset region of the Northeast Greenland Ice Stream. Annals of Glaciology, 1–11.
Fried, M. J., Carroll, D., Catania, G. A., Sutherland, D. A., Stearns, L. A., Shroyer, E. L., & Nash, J. D. (2019). Distinct frontal ablation processes drive heterogeneous submarine terminus morphology. Geophysical Research Letters, 46(21), 12083-12091.

G

Glen, J. W. (1955). The creep of polycrystalline ice. Proceedings of the Royal Society of London. Series A. Mathematical and Physical Sciences, 228(1175), 519-538.
Goldstein, R., Engelhardt, H. F., Kamb, B., and Frolich, R. (1993). Satellite Radar lnterferometry for Monitoring lce-sheet Motion: application to Antarctic Ice Stream. Science, 262(5139), 1525–1530.
Gordon, J. E., Whalley, W. B., Gellatly, A. F., & Vere, D. M. (1992). The formation of glacial flutes: assessment of models with evidence from Lyngsdalen, North Norway. Quaternary Science Reviews, 11(7-8), 709-731.
Greenwood, S. L., Clark, C. D., & Hughes, A. L. (2007). Formalising an inversion methodology for reconstructing ice-sheet retreat patterns from meltwater channels: application to the British Ice Sheet. Journal of Quaternary Science: Published for the Quaternary Research Association, 22(6), 637-645.

Greenwood, S. L., & Clark, C. D. (2008). Subglacial bedforms of the Irish ice sheet. Journal of Maps, 4(1), 332-357.
Greenwood, S. L., & Clark, C. D. (2009a). Reconstructing the last Irish Ice Sheet 1: changing flow geometries and ice flow dynamics deciphered from the glacial landform record. Quaternary Science Reviews, 28(27-28), 3085-3100.
Greenwood, S. L., & Clark, C. D. (2009b). Reconstructing the last Irish Ice Sheet 2: a geomorphologically-driven model of ice sheet growth, retreat and dynamics. Quaternary Science Reviews, 28(27-28), 3101-3123.
Greenwood, S. L., & Clark, C. D. (2010). The sensitivity of subglacial bedform size and distribution to substrate lithological control. Sedimentary Geology, 232(3–4), 130–144.
Greenwood, S. L., & Kleman, J. (2010). Glacial landforms of extreme size in the Keewatin sector of the Laurentide Ice Sheet. Quaternary Science Reviews, 29(15–16), 1894–1910.
Greenwood, S. L., Gyllencreutz, R., Jakobsson, M., & Anderson, J. B. (2012). Ice-flow switching and East/West Antarctic Ice Sheet roles in glaciation of the western Ross Sea. Bulletin of the Geological Society of America, 124(11–12), 1736–1749.
Greenwood, S.L., Clason, C.C., Helanow, C. & Margold, M. (2016). Theoretical, contemporary observational and palaeo-perspectives on ice sheet hydrology: processes and products. Earth-Science Reviews, 155, pp.1-27.
Gumiaux, C., Gapais, D., & Brun, J. P. (2003). Geostatistics applied to best-fit interpolation of orientation data. Tectonophysics, 376(3-4), 241-259.

H

Haiblen, A. M. (2017). Glacial history and landform genesis in the Lac de Gras area, Northwest Territories (Doctoral dissertation, Science: Department of Earth Sciences).
Hall, J. (1815). V. On the Revolutions of the Earth's Surface. Earth and Environmental Science Transactions of The Royal Society of Edinburgh, 7(1), 169-211.
Hallet, B. (1979). Subglacial regelation water film. Journal of Glaciology, 23(89), 321-334.
Hamilton, N., Owens, W. H., and Rees, A. I. (1968). Laboratory experiments on the production of grain orientation in shearing sand. Journal of Geology, 76, 465–472.
Hart, J. K., & Roberts, D. H. (1994). Criteria to distinguish between subglacial glaciotectonic and glaciomarine sedimentation, I. Deformation styles and sedimentology. Sedimentary Geology, 91(1-4), 191-213.
Hart, J. K. (1999). Identifying fast ice flow from landform assemblages in the geological record: a discussion. Annals of Glaciology, 28, 59-66.
Hart, J. K., Clayton, A. I., Martinez, K., & Robson, B. A. (2018). Erosional and depositional subglacial streamlining processes at Skálafellsjökull, Iceland: an analogue for a new bedform continuum model. Gff, 140(2), 153-169.
Hättestrand, C. (1997). Ribbed moraines in Sweden—distribution pattern and palaeoglaciological implications. Sedimentary Geology, 111(1-4), 41-56.
Hättestrand, C., and Kleman, J. (1999). Ribbed moraine formation. Quaternary Science Reviews, 18(1), 43–61.
Hättestrand, C., Götz, S., Näslund, J. O., Fabel, D., & Stroeven, A. P. (2004). Drumlin formation time: evidence from northern and central Sweden. Geografiska Annaler: Series A, Physical Geography, 86(2), 155-167.
Helgadóttir, E. G (2020). Ribbed moraines in the Vopnafjörður region, Iceland. (Master's Thesis).
Hermanowski, P., Piotrowski, J. A., & Szuman, I. (2019). An erosional origin for drumlins of NW Poland. Earth Surface Processes and Landforms, 44(10), 2030-2050.
Hewitt, I. J. (2011). Modelling distributed and channelized subglacial drainage: the spacing of channels. Journal of Glaciology, 57(202), 302-314.
Hewitt, I. J., & Creyts, T. T. (2019). A model for the formation of eskers. Geophysical Research Letters, 46(12), 6673-6680.
Hill, A. R. (1973). The distribution of drumlins in County Down, Ireland. Annals of the Association of American Geographers, 63(2), 226-240.
Hiller, J. K., & Smith, M. (2008). Residual relief separation: digital elevation model enhancement for geomorphological mapping. Earth Surface Processes and Landforms, 33(14), 2266-2276.
Hillier, J. K., Kougioumtzoglou, I. A., Stokes, C. R., Smith, M. J., Clark, C. D., & Spagnolo, M. S. (2016). Exploring explanations of subglacial bedform sizes using statistical models. Plos one, 11(7), e0159489.
Hindle, D., & Burkhard, M. (1999). Strain, displacement and rotation associated with the formation of curvature in fold belts; the example of the Jura arc. Journal of structural Geology, 21(8-9), 1089-1101.
Hindmarsh, R. C. A. (1998a). Drumlinization and drumlin-forming instabilities: Viscous till mechanisms. Journal of Glaciology, 44(147), 293–314.
Hindmarsh, R. C. A. (1998b). The stability of a viscous till sheet coupled with ice flow, considered at wavelengths less than the ice thickness. Journal of Glaciology, 44(147), 285–292.
Hindmarsh, R. C., & Stokes, C. R. (2008). Formation mechanisms for ice-stream lateral shear margin moraines. Earth Surface Processes and Landforms: The Journal of the British Geomorphological Research Group, 33(4), 610-626.
Hindmarsh, R. C. A. (2009). Consistent generation of ice-streams via thermo-viscous instabilities modulated by membrane stresses. Geophysical Research Letters, 36(6), 1–6.
Hodgson DA. (1993). Surficial Geology, Storkerson Peninsula, Victoria Island and Stefansson Island, Northwest Territories. Geological Survey of Canada, Map 1817A, Scale 1:250 000.
Hoffman, M. J., Andrews, L. C., Price, S. F., Catania, G. A., Neumann, T. A., Lüthi, M. P., ... & Morriss, B. (2016). Greenland subglacial drainage evolution regulated by weakly connected regions of the bed. Nature communications, 7(1), 1-12.
Hollingworth, S. E. (1931). The glaciation of western Edenside and adjoining areas and the drumlins of Edenside and the Solway basin. Quarterly Journal of the Geological Society of London, Vol. 87, Pt. 2, p. 28 1- 359.
Hooke, R. L., Laumann, T., & Kohler, J. (1990). Subglacial water pressures and the shape of subglacial conduits. Journal of Glaciology, 36(122), 67-71.
Hooke, R. L. (2005). Principles of Glacier Mechanics, 763 pp.

Hooke, R. L., and Jennings, C. E. (2006). On the formation of the tunnel valleys of the southern Laurentide ice sheet. Quaternary Science Reviews, 25(11-12), 1364-1372.
Horton, R. E. (1945). Erosional development of streams and their drainage basins; hydrophysical approach to quantitative morphology. Geological society of America bulletin, 56(3), 275-370.
Hubbard, B. P., Sharp, M. J., Willis, I. C., Nielsen, M., & Smart, C. C. (1995). Borehole water-level variations and the structure of the subglacial hydrological system of Haut Glacier d'Arolla, Valais, Switzerland. Journal of Glaciology, 41(139), 572-583.
Huddart, D., Bennett, M. R., & Glasser, N. F. (1999). Morphology and sedimentology of a high-arctic esker system: Vegbreen, Svalbard. Boreas, 28(2), 253-273.
Hughes, O. L. (1964). Surficial geology, Nichicun-Kaniapiskau map area, Quebec. Geological Survey of Canada Bulletin, 106, 18pp.
Hughes, A. L., Gyllencreutz, R., Lohne, Ø. S., Mangerud, J., & Svendsen, J. I. (2016). The last Eurasian ice sheets–a chronological database and time-slice reconstruction, DATED-1. Boreas, 45(1), 1-45.
Hunter, P., Meyer, C., Minchew, B., Haseloff, M., & Rempel, A. (2021). Thermal controls on ice stream shear margins. Journal of Glaciology, 67(263), 435-449.

I

Iken, A., & Bindschadler, R. A. (1986). Combined measurements of subglacial water pressure and surface velocity of Findelengletscher, Switzerland: conclusions about drainage system and sliding mechanism. Journal of Glaciology, 32(110), 101-119.
Irvine-Fynn, T. D., Hodson, A. J., Moorman, B. J., Vatne, G., & Hubbard, A. L. (2011). Polythermal glacier hydrology: a review. Reviews of Geophysics, 49(4).
Ives, L. R. W., & Iverson, N. R. (2019). Genesis of glacial flutes inferred from observations at Múlajökull, Iceland. Geology, 47(5), 387-390.

J

Jakobsen, P. R. (2012). Rock-cored drumlins on Bornholm, Denmark. GEUS Bulletin, 26, 17-20.
Jansson, K. N., & Glasser, N. F. (2005). Using Landsat 7 ETM+ imagery and Digital Terrain Models for mapping glacial lineaments on former ice sheet beds. International Journal of Remote Sensing, 26(18), 3931-3941.
Jennings, S. J., & Hambrey, M. J. (2021). Structures and deformation in glaciers and ice sheets. Reviews of Geophysics, 59(3), e2021RG000743.
Johnson, M. D., & Clayton, L. (2003). Supraglacial landsystems in lowland terrain. In Glacial Landsystems, pp. 228–258.
Johnson, M. D., Schomacker, A., Benediktsson, Í. Ö., Geiger, A. J., Ferguson, A., & Ingólfsson, Ó. (2010). Active drumlin field revealed at the margin of Múlajökull, Iceland: a surge-type glacier. Geology, 38(10), 943-946.
Jørgensen, F. & Piotrowski, J. Signature of the Baltic Ice Stream on Funen Island, Denmark during the Weichselian glaciation. Boreas 32, 242–255 (2003).
Joughin, I., Das, S. B., King, M. A., Smith, B. E., Howat, I. M., & Moon, T. (2008). Seasonal speedup along the western flank of the Greenland Ice Sheet. Science, 320(5877), 781-783.

K

Kamb, B. (1987). Glacier surge mechanism based on linked cavity configuration of the basal water conduit system. Journal of Geophysical Research: Solid Earth, 92(B9), 9083-9100.
Kamb, B. (1991). Rheological nonlinearity and flow instability in the deforming bed mechanism of ice stream motion. Journal of Geophysical Research, 96(B10).
Kehew, A. E., Piotrowski, J. A., & Jørgensen, F. (2012). Tunnel valleys: Concepts and controversies—A review. Earth-Science Reviews, 113(1-2), 33-58.
Kerr, M., & Eyles, N. (2007). Origin of drumlins on the floor of Lake Ontario and in upper New York State. Sedimentary Geology, 193(1-4), 7-20.
Kim, B.-H., Lee, C.-K., Seo, K.-W., Lee, W. S., and Scambos, T. (2016). Active subglaical lakes beneath the stagnant trunk of Kamb Ice Stream: evidence of channelized subglacial flow. The Cryosphere Discussions, April, 1–15.
King, E. C., Woodward, J., & Smith, A. M. (2007). Seismic and radar observations of subglacial bed forms beneath the onset zone of Rutford Ice Stream, Antarctica. Journal of Glaciology, 53(183), 665-672.
King, E. C., Hindmarsh, R. C., & Stokes, C. R. (2009). Formation of mega-scale glacial lineations observed beneath a West Antarctic ice stream. Nature Geoscience, 2(8), 585-588.
Kirkham, J. D., Hogan, K. A., Larter, R. D., Arnold, N. S., Nitsche, F. O., Kuhn, G., ... & Dowdeswell, J. A. (2020). Morphometry of bedrock meltwater channels on Antarctic inner continental shelves: Implications for channel development and subglacial hydrology. Geomorphology, 370, 107369.
Kjær, K. H., and Krüger, J. (2001). The final phase of dead-ice moraine development: processes and sediment architecture, Kötlujökull , Iceland. Sedimentology, 48, 935–952.
Kjær, K. H., Krüger, J., & van der Meer, J. J. (2003). What causes till thickness to change over distance? Answers from Mýrdalsjökull, Iceland. Quaternary Science Reviews, 22(15-17), 1687-1700.
Kjær, K. H., Larsen, E., van der Meer, J., Ingólfsson, Ó., Krüger, J., Benediktsson, Í. Ö., ... & Schomacker, A. (2006). Subglacial decoupling at the sediment/bedrock interface: a new mechanism for rapid flowing ice. Quaternary Science Reviews, 25(21-22), 2704-2712.

Kleinhans, M. G., Wilbers, A. W. E., De Swaaf, A., & Van Den Berg, J. H. (2002). Sediment supply-limited bedforms in sand-gravel bed rivers. Journal of sedimentary research, 72(5), 629-640.
Kleman, J., & Borgström, I. (1994). Glacial land forms indicative of a partly frozen bed. Journal of Glaciology, 40(135), 255-264.
Kleman, J., and Borgström, I. (1996). Reconstruction of palaeo-ice sheets: The use of geomorphological data. Earth Surface Processes and Landforms, 21(10), 893–909.
Kleman, J., & Hättestrand, C. (1999). Frozen-bed Fennoscandian and Laurentide ice sheets during the Last Glacial Maximum. Nature, 402(6757), 63-66.
Kleman, J., & Glasser, N. F. (2007). The subglacial thermal organisation (STO) of ice sheets. Quaternary Science Reviews, 26(5-6), 585-597.
Knight, J. (1997). Morphological and morphometric analyses of drumlin bedforms in the Omagh Basin, north central Ireland. Geografiska Annaler: Series A, Physical Geography, 79(4), 255-266.
Knight, J., Stephen, G. M., & McCabe, A. M. (1999). Landform modification by palaeo-ice streams in east-central Ireland. Annals of Glaciology, 28, 161-167.
Koistinen, T., Stephens, M. B., Bogatchev, V., Nordgulen, Ø., Wennerström, M., & Korhonen, J. (2001). Geological map of the Fennoscandian Shield 1: 2 000 000. Espoo: Geological Survey of Finland, Trondheim: Geological Survey of Norway, Uppsala: Geological Survey of Sweden, Moscow: Ministry of Natural Resources of Russia.
Koziol, C. P., & Arnold, N. (2018). Modelling seasonal meltwater forcing of the velocity of land-terminating margins of the Greenland Ice Sheet. The Cryosphere, 12(3), 971-991.
Kyrke-Smith, T. M., & Fowler, A. C. (2014). Subglacial swamps. Proceedings of the Royal Society A: Mathematical, Physical and Engineering Sciences, 470(2171), 20140340.
Kyrke-Smith, T. M., Katz, R. F., & Fowler, A. C. (2014). Subglacial hydrology and the formation of ice streams. Proceedings of the Royal Society A: Mathematical, Physical and Engineering Sciences, 470(2161).

L

Lai, C. Y., Stevens, L. A., Chase, D. L., Creyts, T. T., Behn, M. D., Das, S. B., & Stone, H. A. (2021). Hydraulic transmissivity inferred from ice-sheet relaxation following Greenland supraglacial lake drainages. Nature communications, 12(1), 1-10.
Lappegard, G., Kohler, J., Jackson, M., & Hagen, J. O. (2006). Characteristics of subglacial drainage systems deduced from load-cell measurements. Journal of Glaciology, 52(176), 137-148.
Larsen, N. K., Piotrowski, J. A., & Kronborg, C. (2004). A multiproxy study of a basal till: a time-transgressive accretion and deformation hypothesis. Journal of Quaternary Science: Published for the Quaternary Research Association, 19(1), 9-21.
Larson, G. J., Menzies, J., Lawson, D. E., Evenson, E. B., & Hopkins, N. R. (2016). Macro-and micro-sedimentology of a modern melt-out till–Matanuska Glacier, Alaska, USA. Boreas, 45(2), 235-251.
Larter, R. D., Graham, A. G. C., Gohl, K., Kuhn, G., Hillenbrand, C. D., Smith, J. A., Deen, T. J., Livermore, R. A., & Schenke, H. W. (2009). Subglacial bedforms reveal complex basal regime in a zone of paleo-ice stream convergence, Amundsen Sea embayment, West Antarctica. Geology, 37(5), 411–414.
Le Brocq, A. M., Payne, A. J., Siegert, M. J., & Alley, R. B. (2009). A subglacial water-flow model for West Antarctica. Journal of Glaciology, 55(193), 879-888.
Le Heron, D. P., Sutcliffe, O. E., Whittington, R. J., & Craig, J. (2005). The origins of glacially related soft-sediment deformation structures in Upper Ordovician glaciogenic rocks: implication for ice-sheet dynamics. Palaeogeography, Palaeoclimatology, Palaeoecology, 218(1-2), 75-103.
Lelandais, T., Mourgues, R., Ravier, É., Pochat, S., Strzerzynski, P., and Bourgeois, O. (2016). Experimental modeling of pressurized subglacial water flow: Implications for tunnel valley formation. Journal of Geophysical Research: Earth Surface, 121(11), 2022–2041.
Lelandais, T., Ravier, É., Pochat, S., Bourgeois, O., Clark, C., Mourgues, R., and Strzerzynski, P. (2018). Modelled subglacial floods and tunnel valleys control the life cycle of transitory ice streams. Cryosphere, 12(8), 2759–2772.
Lelandais, T. (2018). Modélisation analogique des écoulements d'eau sous-glaciaire: implications sur les relations entre vallées tunnels et dynamique glaciaire (Doctoral dissertation, Le Mans).
Lesemann, J. E., Alsop, G. I., & Piotrowski, J. A. (2010). Incremental subglacial meltwater sediment deposition and deformation associated with repeated ice-bed decoupling: a case study from the Island of Funen, Denmark. Quaternary Science Reviews, 29(23-24), 3212-3229.
Lewington, E.L., Livingstone, S.J., Sole, A.J., Clark, C.D. and Ng, F.S. (2019). An automated method for mapping geomorphological expressions of former subglacial meltwater pathways (hummock corridors) from high resolution digital elevation data. Geomorphology, 339, pp.70-86.
Lewington, E.L., Livingstone, S.J., Clark, C.D., Sole, A.J. and Storrar, R.D. (2020). A model for interaction between conduits and surrounding hydraulically connected distributed drainage based on geomorphological evidence from Keewatin, Canada. The Cryosphere, 14(9), pp.2949-2976.
Lewington, E. L. M. (2020). New insights into subglacial meltwater drainage pathways from the ArcticDEM (Doctoral dissertation, University of Sheffield).
Lewis, K. J., Fountain, A. G., & Dana, G. L. (1998). Surface energy balance and meltwater production for a Dry Valley glacier, Taylor Valley, Antarctica. Annals of Glaciology, 27, 603-609.
Lindén, M., Möller, P., and Adrielsson, L. (2008). Ribbed moraine formed by subglacial folding, thrust stacking and lee-side cavity infill. Boreas, 37(1), 102–131.
Livingstone, S. J., Clark, C. D., Piotrowski, J. A., Tranter, M., Bentley, M. J., Hodson, A., ... & Woodward, J. (2012). Theoretical framework and diagnostic criteria for the identification of palaeo-subglacial lakes. Quaternary Science Reviews, 53, 88-110.

Livingstone, S. J., Cofaigh, C. Ó., Stokes, C. R., Hillenbrand, C. D., Vieli, A., & Jamieson, S. S. (2013). Glacial geomorphology of Marguerite Bay palaeo-ice stream, western Antarctic Peninsula. Journal of Maps, 9(4), 558-572.
Livingstone, S. J., Storrar, R. D., Hillier, J. K., Stokes, C. R., Clark, C. D., & Tarasov, L. (2015). An ice-sheet scale comparison of eskers with modelled subglacial drainage routes. Geomorphology, 246, 104-112.
Livingstone, S. J., Vérité, J., Ravier, É., McMartin, I., Campbell, J. E., Lewington, E. L. M., Dewald, N., Clark, C. D., Sole, A. J., & Storrar, R. D. (submitted). Diversity of landforms in subglacial meltwater corridors and a potential unifying explanation. Earth Surface Processes and Landforms, 1–46.
Lliboutry, L. (1968). General theory of subglacial cavitation and sliding of temperate glaciers. Journal of Glaciology, 7(49), 21-58.
Lliboutry, L. (1979). Local friction laws for glaciers: a critical review and new openings. Journal of Glaciology, 23(89), 67-95.
Lundqvist, J. (1969). Problems of the so-called Ribbed moraines, 1969.
Lundqvist, J. (1981). Moraine morphology: terminological remarks and regional aspects. Geografiska Annaler: Series A, Physical Geography, 63(3-4), 127-138.
Lundqvist, J. (1986). Late Weichselian glaciation and deglaciation in Scandinavia. Quaternary Science Reviews, 5, 269-292.
Lundqvist, J. (1989). Rogen (ribbed) moraine-identification and possible origin. Sedimentary Geology, 62(2–4), 281–292.
Lundqvist, J., & Wohlfarth, B. (2000). Timing and east–west correlation of south Swedish ice marginal lines during the Late Weichselian. Quaternary Science Reviews, 20(10), 1127-1148.

M

MacGregor, J. A., Catania, G. A., Conway, H., Schroeder, D. M., Joughin, I., Young, D. A., ... & Blankenship, D. D. (2013). Weak bed control of the eastern shear margin of Thwaites Glacier, West Antarctica. Journal of Glaciology, 59(217), 900-912.
Maclachlan, J. C., & Eyles, C. H. (2013). Quantitative geomorphological analysis of drumlins in the Peterborough drumlin field, Ontario, Canada. Geografiska Annaler: Series A, Physical Geography, 95(2), 125-144.
Mäkinen, J. (2003). Time-transgressive deposits of repeated depositional sequences within interlobate glaciofluvial (esker) sediments in Köyliö, SW Finland. Sedimentology, 50(2), 327-360.
Mäkinen, J., Kajuutti, K., Palmu, J. P., Ojala, A., & Ahokangas, E. (2017). Triangular-shaped landforms reveal subglacial drainage routes in SW Finland. Quaternary Science Reviews, 164, 37-53.
Margold, M., Stokes, C. R., and Clark, C. D. (2015). Ice streams in the Laurentide Ice Sheet: Identification, characteristics and comparison to modern ice sheets. Earth-Science Reviews, 143, 117–146.
Margold, M., Stokes, C. R., and Clark, C. D. (2018). Reconciling records of ice streaming and ice margin retreat to produce a palaeogeographic reconstruction of the deglaciation of the Laurentide Ice Sheet. Quaternary Science Reviews, 189, 1–30.
Marich, A., Batterson, M., and Bell, T. (2005). The Morphology and Sedimentological Analyses of Rogen Moraines, Central Avalon Peninsula, Newfoundland. Current Research, 1–14.
Markgren, M., & Lassila, M. (1980). Problems of moraine morphology: Rogen moraine and Blattnick moraine. Boreas, 9(4), 271-274.
Mayer, C., Lambrecht, A., Hagg, W., & Narozhny, Y. (2011). Glacial debris cover and melt water production for glaciers in the Altay, Russia. The Cryosphere Discussions, 5(1), 401-430.
McCabe, A. M., & Ó Cofaigh, C. (1994). Sedimentation in a subglacial lake, Enniskerry, eastern Ireland. Sedimentary Geology, 91(1-4), 57-95.
McGrath, D., Colgan, W., Steffen, K., Lauffenburger, P., & Balog, J. (2011). Assessing the summer water budget of a moulin basin in the Sermeq Avannarleq ablation region, Greenland ice sheet. Journal of Glaciology, 57(205), 954-964.
McKee, E. D. (1979). A study of global sand seas (Vol. 1052). US Government Printing Office.
McKenzie, M. A., Simkins, L. M., Principato, S. M., & Munevar Garcia, S. (2022). Streamlined subglacial bedform sensitivity to bed characteristics across the deglaciated Northern Hemisphere. Earth Surface Processes and Landforms.
McMartin, I., Campbell, J.E., Dredge, L.A., LeCheminant, A.N.., McCurdy, M.W., and Scromeda, N., (2015a). Quaternary geology and till composition north of Wager Bay, Nunavut: Results from the GEM Wager Bay Surficial Geology Project; Geological Survey of Canada.
McMartin, I., Campbell, J.E. and Dredge, L.A. (2015b). Surficial geology, Curtis Lake north, 1067 Nunavut, NTS 56I-north; Geological Survey of Canada, CGM-205, (ed. prelim.), scale 1:100 1068 000.
Meierbachtol, T., Harper, J., & Humphrey, N. (2013). Basal drainage system response to increasing surface melt on the Greenland ice sheet. Science, 341(6147), 777-779.
Meierbachtol, T. W., Harper, J. T., Humphrey, N. F., & Wright, P. J. (2016). Mechanical forcing of water pressure in a hydraulically isolated reach beneath Western Greenland's ablation zone. Annals of Glaciology, 57(72), 62-70.
Mejía, J. Z., Gulley, J. D., Trunz, C., Covington, M. D., Bartholomaus, T. C., Xie, S., & Dixon, T. (2021). Isolated cavities dominate Greenland Ice Sheet dynamic response to lake drainage. Geophysical Research Letters, e2021GL094762.
Menzies, J. (1979). A review of the literature on the formation and location of drumlins. Earth Science Reviews, 14(4), 315–359.
Menzies, J., & Rose, J. (1987). Drumlin symposium. In Drumlin Symposium (1985: Manchester, England); International Conference on Geomorphology 1985: Manchester, England). AA Balkema.
Menzies, J. (1989). Subglacial hydraulic conditions and their possible impact upon subglacial bed formation. Sedimentary Geology, 62(2–4), 125–150.
Menzies, J., & Ellwanger, D. (2011). Insights into subglacial processes inferred from the micromorphological analyses of complex diamicton stratigraphy near Illmensee-Lichtenegg, Höchsten, Germany. Boreas, 40(2), 271-288.

Middleton, M., Nevalainen, P., Hyvönen, E., Heikkonen, J., & Sutinen, R. (2020). Pattern recognition of LiDAR data and sediment anisotropy advocate a polygenetic subglacial mass-flow origin for the Kemijärvi hummocky moraine field in northern Finland. Geomorphology, 362, 107212.

Mills, H. H. (1987). Morphometry of drumlins in the northeastern and north-central USA. In Drumlin symposium (pp. 131-147).

Minchew, B., and Joughin, I. (2020). Toward a universal glacier slip law. Science, 368(6486), 29–30.

Moellering, H., & Rayner, J. N. (1979). Measurement of shape in geography and cartography. Reports of the Numerical Cartography Laboratory, Ohio State University, NSF Report# SOC77-11318

Møller, J. J., Danielsen, T. K., & Fjalstad, A. (1992). Late Weichselian glacial maximum on Andøya, north Norway. Boreas, 21(1), 1-13.

Möller, P. (2006). Rogen moraine: An example of glacial reshaping of pre-existing landforms. Quaternary Science Reviews, 25(3–4), 362–389.

Möller, P. (2010). Melt-out till and ribbed moraine formation, a case study from south Sweden. Sedimentary Geology, 232(3–4), 161–180.

Möller, P., & Dowling, T. P. (2015). The importance of thermal boundary transitions on glacial geomorphology; mapping of ribbed/hummocky moraine and streamlined terrain from LiDAR, over Småland, South Sweden. Gff, 137(4), 252-283.

Möller, P., & Dowling, T. P. (2016). Streamlined subglacial bedforms on the Närke plain, south-central Sweden–areal distribution, morphometrics, internal architecture and formation. Quaternary Science Reviews, 146, 182-215.

Möller, P., & Dowling, T. P. F. (2018). Equifinality in glacial geomorphology: instability theory examined via ribbed moraine and drumlins in Sweden. Gff, 140(2), 106–135.

Moon, T., Joughin, I., Smith, B., Van Den Broeke, M. R., Van De Berg, W. J., Noël, B., and Usher, M. (2014). Distinct patterns of seasonal Greenland glacier velocity. Geophysical Research Letters, 41(20), 7209–7216.

Morlighem, M., Williams, C. N., Rignot, E., An, L., Arndt, J. E., Bamber, J. L., ... & Zinglersen, K. B. (2017). BedMachine v3: Complete bed topography and ocean bathymetry mapping of Greenland from multibeam echo sounding combined with mass conservation. Geophysical research letters, 44(21), 11-051.

Morlighem, M., Rignot, E., Binder, T., Blankenship, D., Drews, R., Eagles, G., ... & Young, D. A. (2020). Deep glacial troughs and stabilizing ridges unveiled beneath the margins of the Antarctic ice sheet. Nature Geoscience, 13(2), 132-137.

Murray, T., Corr, H., Forieri, A. and Smith, A.M., 2008. Contrasts in hydrology between regions of basal deformation and sliding beneath Rutford Ice Stream, West Antarctica, mapped using radar and seismic data. Geophysical Research Letters, 35(12).

N

Nanni, U., Gimbert, F., Roux, P., & Lecointre, A. (2021). Observing the subglacial hydrology network and its dynamics with a dense seismic array. Proceedings of the National Academy of Sciences, 118(28).

Napieralski, J., & Nalepa, N. (2010). The application of control charts to determine the effect of grid cell size on landform morphometry. Computers & geosciences, 36(2), 222-230.

Newton, M., Evans, D. J. A., Roberts, D. H., and Stokes, C. R. (2018). Bedrock mega-grooves in glaciated terrain: A review. Earth-Science Reviews, 185(March 2017), 57–79.

Norris, S. L., Margold, M. & Froese, D. G (2017). Glacial landforms of northwest saskatchewan. J. Maps 13, 600–607.

Nye, J. F. (1959). The motion of ice sheets and glaciers. Journal of Glaciology, 3(26), 493–507.

Nye, J. F. (1976). Water flow in glaciers: jökulhlaups, tunnels and veins. Journal of Glaciology, 17(76), 181-207.

O

Ó Cofaigh, C. (1996). Tunnel valley genesis. Progress in physical geography, 20(1), 1-19.

Ó Cofaigh, C., Pudsey, C. J., Dowdeswell, J. A., & Morris, P. (2002). Evolution of subglacial bedforms along a paleo-ice stream, Antarctic Peninsula continental shelf. Geophysical Research Letters, 29(8), 41-1.

Ó Cofaigh, C. O., Dowdeswell, J. A., Allen, C. S., Hiemstra, J. F., Pudsey, C. J., Evans, J., & Evans, D. J. A. (2005). Flow dynamics and till genesis associated with a marine-based Antarctic palaeo-ice stream. In Quaternary Science Reviews (Vol. 24, Issues 5–6).

Ó Cofaigh, C., Evans, J., Dowdeswell, J. A., & Larter, R. D. (2007). Till characteristics, genesis and transport beneath Antarctic paleo-ice streams. Journal of Geophysical Research: Earth Surface, 112(F3).

O Cofaigh, C., Stokes, C. R., Lian, O. B., Clark, C. D., & Tulacyzk, S. (2013). Formation of mega-scale glacial lineations on the Dubawnt Lake Ice Stream bed: 2. Sedimentology and stratigraphy. Quaternary science reviews, 77, 210-227.

O Connor, J. E., Baker, V. R., Waitt, R. B., Smith, L. N., Cannon, C. M., George, D. L., & Denlinger, R. P. (2020). The Missoula and Bonneville floods—A review of ice-age megafloods in the Columbia River basin. Earth-Science Reviews, 208, 103181.

O'Neel, S., Pfeffer, W. T., Krimmel, R., & Meier, M. (2005). Evolving force balance at Columbia Glacier, Alaska, during its rapid retreat. Journal of Geophysical Research: Earth Surface, 110(F3).

Oda, M., & Konishi, J. (1974). Microscopic deformation mechanism of granular material in simple shear. Soil and Foundations, 14(4), 25–38.

Ojala, A.E., Peterson, G., Mäkinen, J., Johnson, M.D., Kajuutti, K., Palmu, J.P., Ahokangas, E. & Öhrling, C. (2019). Ice-sheet scale distribution and morphometry of triangular-shaped hummocks (murtoos): a subglacial landform produced during rapid retreat of the Scandinavian Ice Sheet. Annals of Glaciology, 60(80), pp.115-126.

Ojala, A. E., Mäkinen, J., Ahokangas, E., Kajuutti, K., Valkama, M., Tuunainen, A., & Palmu, J. P. (2021). Diversity of murtoos and murtoo-related subglacial landforms in the Finnish area of the Fennoscandian Ice Sheet. Boreas.

Ojala, A. E., Mäkinen, J., Kajuutti, K., Ahokangas, E., & Palmu, J. P. (2022). Subglacial evolution from distributed to channelized drainage: evidence from the Lake Murtoo area in SW Finland. Earth Surface Processes and Landforms.

Owen, G. (1987). Deformation processes in unconsolidated sands. Geological Society Special Publication, 29(29), 11–24.

P

Palmer, S., Shepherd, A., Nienow, P., & Joughin, I. (2011). Seasonal speedup of the Greenland Ice Sheet linked to routing of surface water. Earth and Planetary Science Letters, 302(3-4), 423-428.

Paola, C., Straub, K., Mohrig, D., and Reinhardt, L. (2009). The "unreasonable effectiveness" of stratigraphic and geomorphic experiments. Earth-Science Reviews, 97(1–4), 1–43.

Paterson, W. S. B. (1994). The Physics of Glaciers, 3rd Edition, Pergamon, 1994.

Patterson, C. J., & Hooke, R. L. (1995). Physical environment of drumlin formation. Journal of Glaciology, 41(137), 30-38.

Patterson, C. J. (1997). Southern Laurentide ice lobes were created by ice streams: Des Moines Lobe in Minnesota, USA. Sedimentary Geology, 111(1–4), 249–261.

Paul, M. A., & Eyles, N. (1990). Constraints on the preservation of diamict facies (melt-out tills) at the margins of stagnant glaciers. Quaternary Science Reviews, 9(1), 51-69.

Payne, A. J., & Dongelmans, P. W. (1997). Self-organization in the thermomechanical flow of ice sheets. Journal of Geophysical Research: Solid Earth, 102(B6), 12219–12233.

Perol, T., and Rice, J. R. (2015). Shear heating and weakening of the margins of West Antarctic ice streams. May, 3406–3413.

Perol, T., Rice, J. R., Platt, J. D., and Suckale, J. (2015). Subglacial hydrology and ice stream margin locations Special Section : Journal of Geophysical Research: Earth Surface, 1352–1368.

Peterson, G., Johnson, M.D. and Smith, C.A. (2017). Glacial geomorphology of the south Swedish uplands–focus on the spatial distribution of hummock tracts. Journal of Maps, 13(2), pp.534-544.

Peterson, G. & Johnson, M.D. (2018). Hummock corridors in the south-central sector of the Fennoscandian ice sheet, morphometry and pattern. Earth Surface Processes and Landforms, 43(4), pp.919-929.

Peterson Becher, G.P. and Johnson, M.D. (2021). Sedimentology and internal structure of murtoos-V-shaped landforms indicative of a dynamic subglacial hydrological system. Geomorphology, 380, p.107644.

Pimentel, S., & Flowers, G. E. (2011). A numerical study of hydrologically driven glacier dynamics and subglacial flooding. Proceedings of the Royal Society A: Mathematical, Physical and Engineering Sciences, 467(2126), 537-558.

Piotrowski, J. A., Larsen, N. K., & Junge, F. W. (2004). Reflections on soft subglacial beds as a mosaic of deforming and stable spots. Quaternary Science Reviews, 23(9–10), 993–1000.

Piotrowski, J. A., Larsen, N. K., Menzies, J., & Wysota, W. (2006). Formation of subglacial till under transient bed conditions: deposition, deformation, and basal decoupling under a Weichselian ice sheet lobe, central Poland. Sedimentology, 53(1), 83-106.

Porter, C., Morin, P., Howat, I., Noh, M.-J., Bates, B., Peterman, K., Keesey, S., Schlenk, M., Gardiner, J., Tomko, K., Willis, M., et al., (2018). ArcticDEM. Harvard Dataverse, V1.

Punkari, M. (1980). The ice lobes of the Scandinavian ice sheet during the deglaciation in Finland. Boreas, 9(4), 307-310.

Punkari, M. (1995). Glacial flow systems in the zone of confluence between the Scandinavian and Novaja Zemlya Ice Sheets. Quaternary Science Reviews, 14(6), 589-603.

Punkari, M. (1997). Glacial and glaciofluvial deposits in the interlobate areas of the Scandinavian Ice Sheet. Quaternary Science Reviews, 16(97), 741–753.

R

Rabassa, J., Ercolano, B., & Estaña, P. M. (2022). Geomorphology of subglacial ribbed-Rogen moraines of Early Pleistocene age, southernmost Patagonia, Argentina (No. ICG2022-70). Copernicus Meetings.

Rada, C., & Schoof, C. (2018). Channelized, distributed, and disconnected: subglacial drainage under a valley glacier in the Yukon. The Cryosphere, 12(8), 2609-2636.

Rampton, V.N. (2000). Large-scale effects of subglacial meltwater flow in the southern Slave Province, Northwest Territories, Canada. Canadian Journal of Earth Sciences, 37(1), pp.81-93.

Ramsay, J., and Huber, M. (1987). The techniques of modern structural geology: Folds and fractures, Elsevier Science.

Rattas, M., & Piotrowski, J. A. (2003). Influence of bedrock permeability and till grain size on the formation of the Saadjärve drumlin field, Estonia, under an east-Baltic Weichselian ice stream. Boreas, 32(1), 167-177.

Ravier, E., Buoncristiani, J. F., Clerc, S., Guiraud, M., Menzies, J., & Portier, E. (2014). Sedimentological and deformational criteria for discriminating subglaciofluvial deposits from subaqueous ice-contact fan deposits: AP leistocene example (I reland). Sedimentology, 61(5), 1382-1410.

Ravier, E., & Buoncristiani, J. F. (2018). Glaciohydrogeology. In Past glacial environments (pp. 431-466). Elsevier.

Raymond, C. F. (1987). How Do Glaciers Surge? A Review. Journal of Geophysical Research, 92(B9), 9121–9134.

Raymond, C. (1996). Shear margins in glaciers and ice sheets. Journal of Glaciology, 42(140), 90-102.

Raymond, C. F., Echelmeyer, K. A., Whillans, I. M., and Doake, C. S. M. (2001). Ice stream shear margins. Antarctic Research Series, 77, 137–155.

Reed, B., Galvin, C. J., & Miller, J. P. (1962). Some aspects of drumlin geometry. American Journal of Science, 260(3), 200-210.

Reinardy, B. T., Larter, R. D., Hillenbrand, C. D., Murray, T., Hiemstra, J. F., & Booth, A. D. (2011). Streaming flow of an Antarctic Peninsula palaeo-ice stream, both by basal sliding and deformation of substrate. Journal of Glaciology, 57(204), 596-608.

Remmert, I., & Kristiansson, J. (2018). Murtoo–Associated landforms, positioning, and cross-cutting relationships.

Rignot, E., Jacobs, S., Mouginot, J., & Scheuchl, B. (2013). Ice-shelf melting around Antarctica. Science, 341(6143), 266-270.

Rolstad, C., Whillans, I. M., Hagen, J. O., & Isaksson, E. (2000). Large-scale force budget of an outlet glacier: Jutulstraumen, Dronning Maud Land, East Antarctica. Annals of Glaciology, 30, 35-41.

Rose, J., & Letzer, J. M. (1977). Superimposed drumlins. Journal of Glaciology, 18(80), 471-480.

Rose, J. (1987). Drumlins as part of a glacier bedform continuum. In Drumlin symposium. Balkema, Rotterdam.

Rose, J. (1992). Boulder clusters in glacial flutes. Geomorphology, 6(1), 51-58.

Röthlisberger, H. (1972). Water pressure in intra-and subglacial channels. Journal of Glaciology, 11(62), 177-203.

Ryan, J. C., Smith, L. C., Cooley, S. W., Pearson, B., Wever, N., Keenan, E., & Lenaerts, J. T. M. (2022). Decreasing surface albedo signifies a growing importance of clouds for Greenland Ice Sheet meltwater production. Nature Communications, 13(1), 1-8.

S

Sarala, P. (2006). Ribbed moraine stratigraphy and formation in southern Finnish Lapland. Journal of Quaternary Science, 21(4), 387–398.

Schellenberger, T., Dunse, T., Kääb, A., Schuler, T. V., Hagen, J. O., and Reijmer, C. H. (2017). Multi-year surface velocities and sea-level rise contribution of the Basin-3 and Basin-2 surges, Austfonna, Svalbard. The Cryosphere Discussions, February, 1–27.

Schroeder, D. M., Blankenship, D. D., & Young, D. A. (2013). Evidence for a water system transition beneath Thwaites Glacier, West Antarctica. Proceedings of the National Academy of Sciences, 110(30), 12225-12228.

Schomacker, A., Johnson, M. D., & Möller, P. (2018). Drumlin formation: a mystery or not?. GFF, 140(2), 91-92.

Schoof, C. (2004). On the mechanics of ice-stream shear margins. Journal of Glaciology, 50(169), 208-218.

Schoof, C. (2007). Pressure-dependent viscosity and interfacial instability in coupled ice-sediment flow. Journal of Fluid Mechanics, 570(February), 227–252.

Schoof, C. (2010). Ice-sheet acceleration driven by melt supply variability. Nature, 468(7325), 803-806.

Sergienko, O. V., and Hindmarsh, R. C. A. (2013). Regular patterns in frictional resistance of ice-stream beds seen by surface data inversion. Science, 342(November), 1086–1089.

Sergienko, O. V., Creyts, T. T., and Hindmarsh, R. C. A. (2014). Similarity of organized patterns in driving and basal stresses of Antarctic and Greenland ice sheets beneath extensive areas of basal sliding. Geophysical Research Letters, 41(11), 3925–3932.

Sevestre, H., Benn, D. I., Luckman, A., Nuth, C., Kohler, J., Lindbäck, K., and Pettersson, R. (2018). Tidewater Glacier Surges Initiated at the Terminus. Journal of Geophysical Research: Earth Surface, 123(5), 1035–1051.

Sharp, M.J. (1985). "Crevasse-fill" ridges — a landform type characteristic of surging? Geogr. Ann. A67, 213–220.

Sharp, M., Gemmell, J. C., & Tison, J. L. (1989). Structure and stability of the former subglacial drainage system of the Glacier de Tsanfleuron, Switzerland. Earth Surface Processes and Landforms, 14(2), 119-134.

Sharpe, D.R., Kjarsgaard, B.A., Knight, R.D., Russell, H.A.J. and Kerr, D.E., (2017). Glacial dispersal and flow history, east arm area of Great Slave Lake, NWT, Canada. Quaternary Science Reviews, 165, pp.49-72.

Sharpe, D. R., Lesemann, J. E., Knight, R. D., & Kjarsgaard, B. A. (2021). Regional stagnation of the western Keewatin ice sheet and the significance of meltwater corridors and eskers, northern Canada. Canadian Journal of Earth Sciences, 99(999), 1-22.

Shaw, J. (1977). Till body morphology and structure related to glacier flow. Boreas, 6(2), 189-201.

Shaw, J. (1979). Genesis of the Sveg tills and Rogen moraines of central Sweden: a model of basal melt out. Boreas, 8(4), 409–426.

Shaw, J. (1983). Drumlin formation related to inverted melt-water erosional marks. Journal of Glaciology, 29(103), 461–479.

Shaw, J., & Sharpe, D. R. (1987). Drumlin formation by subglacial meltwater erosion. Canadian Journal of Earth Sciences, 24(11), 2316-2322.

Shaw, J. (1989). Drumlins, subglacial meltwater floods, and ocean responses. Geology, 17(9), 853-856.

Shaw, J., Faragini, D. M., Kvill, D. R., & Rains, R. B. (2000). The Athabasca fluting field, Alberta, Canada: implications for the formation of large-scale fluting (erosional lineations). Quaternary Science Reviews, 19(10), 959-980.

Shaw, J. (2002). The meltwater hypothesis for subglacial bedforms. Quaternary International, 90, 5–22.

Shaw, J., Pugin, A., & Young, R. R. (2008). A meltwater origin for Antarctic shelf bedforms with special attention to megalineations. Geomorphology, 102(3-4), 364-375.

Shilts, W. W., Cunningham, C. M., & Kaszycki, C. A. (1979). Keewatin Ice Sheet—Re-evaluation of the traditional concept of the Laurentide Ice Sheet. Geology, 7(11), 537-541.

Shilts, W. W., Aylsworth, J. M., Kaszycki, C. A., & Klassen, R. A. (1987). Canadian shield. In Geomorphic Systems of North America (Vol. 2, pp. 119-161). Geological Society of America Boulder, Colorado.

Simkins, L. M., Anderson, J. B., Greenwood, S. L., Gonnermann, H. M., Prothro, L. O., Halberstadt, A. R. W., ... & DeConto, R. M. (2017). Anatomy of a meltwater drainage system beneath the ancestral East Antarctic ice sheet. Nature Geoscience, 10(9), 691-697.

Sjogren, D. B., Fisher, T. G., Taylor, L. D., Jol, H. M., & Munro-Stasiuk, M. J. (2002). Incipient tunnel channels. Quaternary International, 90(1), 41-56.

Slater, D. A., Nienow, P. W., Cowton, T. R., Goldberg, D. N., & Sole, A. J. (2015). Effect of near-terminus subglacial hydrology on tidewater glacier submarine melt rates. Geophysical Research Letters, 42(8), 2861-2868.

Smalley, I. J., & Unwin, D. J. (1968). The Formation and Shape of Drumlins and their Distribution and Orientation in Drumlin Fields. Journal of Glaciology, 7(51), 377–390.

Smalley, I., & Warburton, J. (1994). The shape of drumlins, their distribution in drumlin fields, and the nature of the sub-ice shaping forces. Sedimentary geology, 91(1-4), 241-252.

Smith, E. C., Smith, A. M., White, R. S., Brisbourne, A. M., & Pritchard, H. D. (2015). Mapping the ice-bed interface characteristics of Rutford Ice Stream, West Antarctica, using microseismicity. Journal of Geophysical Research: Earth Surface, 120(9), 1881–1894.

Smith, L. C., Andrews, L. C., Pitcher, L. H., Overstreet, B. T., Rennermalm, Å. K., Cooper, M. G., Cooley, S.W., Ryan, J.C., Miège, C., Kershner, C. & Simpson, C. E. (2021). Supraglacial river forcing of subglacial water storage and diurnal ice sheet motion. Geophysical Research Letters, 48(7), e2020GL091418.

Smith-Johnsen, S., Fleurian, B. D., Schlegel, N., Seroussi, H., & Nisancioglu, K. (2020). Exceptionally high heat flux needed to sustain the Northeast Greenland Ice Stream. The Cryosphere, 14(3), 841-854.

Smith, A. M., Murray, T., Nicholls, K. W., Makinson, K., Adalgeirsdóttir, G., Behar, A. E., and Vaughan, D. G. (2007). Rapid erosion, drumlin formation, and changing hydrology beneath an Antarctic ice stream. Geology, 35(2), 127–130.

Smith, A. M., & Murray, T. (2009). Bedform topography and basal conditions beneath a fast-flowing West Antarctic ice stream. Quaternary Science Reviews, 28(7-8), 584-596.

Smith, M. J., & Wise, S. M. (2007). Problems of bias in mapping linear landforms from satellite imagery. International Journal of Applied Earth Observation and Geoinformation, 9(1), 65-78.

Smith, M. J., Rose, J. & Gousie, M. B. The Cookie Cutter: A method for obtaining a quantitative 3D description of glacial bedforms. Geomorphology 108, 209–218 (2009).

Smith, H. T. U. (1948). Giant glacial grooves in northwest Canada. American Journal of Science, 246(8), 503–514.

Sollid, J. L., & Sørbel, L. (1994). Distribution of glacial landforms in southern Norway in relation to the thermal regime of the last continental ice sheet. Geografiska Annaler: Series A, Physical Geography, 76(1-2), 25-35.

Sommerkorn, J. (2020). Distribution of ribbed moraines and their connection to subglacial water-in the Oppland region of Norway (Master's thesis).

Sookhan, S., Eyles, N., & Putkinen, N. (2016). LiDAR-based volume assessment of the origin of the Wadena drumlin field, Minnesota, USA. Sedimentary Geology, 338, 72-83.

Sookhan, S., Eyles, N., Bukhari, S., & Paulen, R. C. (2021). LiDAR-based quantitative assessment of drumlin to mega-scale glacial lineation continuums and flow of the paleo Seneca-Cayuga paleo-ice stream. Quaternary Science Reviews, 263, 107003.

Sookhan, S., Eyles, N., & Bukhari, S. (2022). Drumlins and mega-scale glacial lineations as a continuum of subglacial shear marks: A LiDAR based morphometric study of streamlined surfaces on the bed of a Canadian paleo-ice stream. Quaternary Science Reviews, 292, 107679.

Souček, O., Bourgeois, O., Pochat, S., and Guidat, T. (2015). A 3 Ga old polythermal ice sheet in Isidis Planitia, Mars: Dynamics and thermal regime inferred from numerical modeling. Earth and Planetary Science Letters, 426, 176–190.

Spagnolo, M., Clark, C. D., Hughes, A. L., Dunlop, P., & Stokes, C. R. (2010). The planar shape of drumlins. Sedimentary Geology, 232(3-4), 119-129.

Spagnolo, M., Clark, C. D., Hughes, A. L., & Dunlop, P. (2011). The topography of drumlins; assessing their long profile shape. Earth Surface Processes and Landforms, 36(6), 790-804.

Spagnolo, M., Clark, C. D. & Hughes, A. L. C (2012). Drumlin relief. Geomorphology 153–154, 179–191.

Spagnolo, M. et al (2014). Size, shape and spatial arrangement of mega-scale glacial lineations from a large and diverse dataset. Earth Surf. Process. Landforms 39, 1432–1448.

Stewart, M. A., Lonergan, L., & Hampson, G. (2013). 3D seismic analysis of buried tunnel valleys in the central North Sea: morphology, cross-cutting generations and glacial history. Quaternary Science Reviews, 72, 1-17.

St-Onge, D.A. (1984). Surficial deposits of the Redrock Lake area, District of Mackenzie. Current Research, Part A; Geological Survey of Canada, Paper, pp.271-276.

Stone, D. B., & Clarke, G. K. (1993). Estimation of subglacial hydraulic properties from induced changes in basal water pressure: a theoretical framework for borehole-response tests. Journal of Glaciology, 39(132), 327-340.

Stokes, C. R. (2018). Geomorphology under ice streams: Moving from form to process. Earth Surface Processes and Landforms, 43(1), 85–123.

Stokes, C. R., & Clark, C. D. (1999). Geomorphological criteria for identifying Pleistocene ice streams. Annals of glaciology, 28, 67-74.

Stokes, C. R, & Clark, C. D. (2001). Palaeo-ice streams. Quaternary Science Reviews, 20, 1437–1457.

Stokes, C. R., & Clark, C. D. (2002a). Are long subglacial bedforms indicative of fast ice flow? Boreas, 31(3), 239–249.

Stokes, C. R., & Clark, C. D. (2002b). Ice stream shear margin moraines. Earth Surface Processes and Landforms, 27(5), 547–558.

Stokes, C.R., & Clark, C.D. (2003). The Dubawnt Lake palaeo-ice stream: evidence for dynamic ice sheet behaviour on the Canadian Shield and insights regarding the controls on ice-stream location and vigour. Boreas, 32(1), 263–279.

Stokes, C. R., & Clark, C. D. (2004). Evolution of late glacial ice-marginal lakes on the northwestern Canadian Shield and their influence on the location of the Dubawnt Lake palaeo-ice stream. Palaeogeography, Palaeoclimatology, Palaeoecology, 215(1-2), 155-171.

Stokes, C. R., Clark, C. D., Lian, O. B., and Tulaczyk, S. (2006a). Geomorphological map of ribbed moraines on the Dubawnt Lake Palaeo-Ice Stream bed: A signature of ice stream shut-down? Journal of Maps, 2(1), 1–9.

Stokes, C. R., Clark, C. D., and Winsborrow, C. M. (2006b). Subglacial bedform evidence for a major palaeo-ice stream and its retreat phases in Amundsen Gulf, Canadian Arctic Archipelago. Journal of Quaternary Science, 21(4), 399–412.

Stokes, C. R., Clark, C. D., Lian, O. B., and Tulaczyk, S. (2007). Ice stream sticky spots: A review of their identification and influence beneath contemporary and palaeo-ice streams. Earth-Science Reviews, 81(3–4), 217–249.

Stokes, C. R., Lian, O. B., Tulaczyk, S., and Clark, C. D. (2008). Superimposition of ribbed moraines on a palaeo-ice-stream bed: implications for ice stream dynamics and shutdown. Earth Surface Processes and Landforms, 33, 593–609.
Stokes, C. R., Spagnolo, M., & Clark, C. D. (2011). The composition and internal structure of drumlins: complexity, commonality, and implications for a unifying theory of their formation. Earth-Science Reviews, 107(3-4), 398-422.
Stokes, C. R., Spagnolo, M., Clark, C. D., Ó Cofaigh, C., Lian, O. B., and Dunstone, R. B. (2013a). Formation of mega-scale glacial lineations on the Dubawnt Lake Ice Stream bed: 1. size, shape and spacing from a large remote sensing dataset. Quaternary Science Reviews, 77, 190–209.
Stokes, C. R., Fowler, A. C., Clark, C. D., Hindmarsh, R. C., and Spagnolo, M. (2013b). The instability theory of drumlin formation and its explanation of their varied composition and internal structure. Quaternary Science Reviews, 62, 77-96.
Stokes, C. R., Margold, M., and Creyts, T. T. (2016). Ribbed bedforms on palaeo-ice stream beds resemble regular patterns of basal shear stress ('traction ribs') inferred from modern ice streams. Journal of Glaciology, 62(234), 696–713.
Storrar, R. D., Stokes, C. R., & Evans, D. J. (2013). A map of large Canadian eskers from Landsat satellite imagery. Journal of maps, 9(3), 456-473.
Storrar, R. D., Stokes, C. R., & Evans, D. J. (2014). Morphometry and pattern of a large sample (> 20,000) of Canadian eskers and implications for subglacial drainage beneath ice sheets. Quaternary Science Reviews, 105, 1-25.
Storrar, R.D. and Livingstone, S.J. (2017). Glacial geomorphology of the northern Kivalliq region, Nunavut, Canada, with an emphasis on meltwater drainage systems. Journal of Maps, 13(2), pp.153-164.
Stroeven, A.P., Hättestrand, C., Kleman, J., Heyman, J., Fabel, D., Fredin, O., Goodfellow, B.W., Harbor, J.M., Jansen, J.D., Olsen, L. and Caffee, M.W. (2016). Deglaciation of fennoscandia. Quaternary Science Reviews, 147, pp.91- 121.
Sugden, D. E., & John, B. S. (1976). Glaciers and landscape: a geomorphological approach (Vol. 365). London: Edward Arnold.
Sugden, D. E., Denton, G. H., & Marchant, D. R. (1991). Subglacial meltwater channel systems and ice sheet overriding, Asgard Range, Antarctica. Geografiska Annaler: Series A, Physical Geography, 73(2), 109-121.
Sundal, A. V., Shepherd, A., Nienow, P., Hanna, E., Palmer, S., & Huybrechts, P. (2011). Melt-induced speed-up of Greenland ice sheet offset by efficient subglacial drainage. Nature, 469(7331), 521-524.
Synge, F. M., & Stephens, N. (1960). The Quaternary period in Ireland—an assessment, 1960. Irish Geography, 4(2), 121-130.
Szuman, I., Kalita, J. Z., Ewertowski, M. W., Clark, C. D., and Livingstone, S. J. (2021). Dynamics of the last Scandinavian Ice Sheet's southernmost sector revealed by the pattern of ice streams. Boreas.

T

Tedstone, A. J., Nienow, P. W., Gourmelen, N., & Sole, A. J. (2014). Greenland ice sheet annual motion insensitive to spatial variations in subglacial hydraulic structure. Geophysical Research Letters, 41(24), 8910-8917.
Tedstone, A. J., Nienow, P. W., Gourmelen, N., Dehecq, A., Goldberg, D., & Hanna, E. (2015). Decadal slowdown of a land-terminating sector of the Greenland Ice Sheet despite warming. Nature, 526(7575), 692-695.
Terzaghi, C. (1931). The Static Rigidity of Plastic Clays. Journal of Rheology, 2(3), 253–262.
Thielicke, W., & Sonntag, R. (2021). Particle Image Velocimetry for MATLAB: Accuracy and enhanced algorithms in PIVlab. Journal of Open Research Software, 9(1).
Thomas, G. S., & Chiverrell, R. C. (2007). Structural and depositional evidence for repeated ice-marginal oscillation along the eastern margin of the Late Devensian Irish Sea Ice Stream. Quaternary Science Reviews, 26(19-21), 2375-2405.
Thomason, J. F., & Iverson, N. R. (2008). A laboratory study of particle ploughing and pore-pressure feedback: a velocity-weakening mechanism for soft glacier beds. Journal of Glaciology, 54(184), 169-181.
Totten, S. M. (1969). Overridden Recessional Moraines of North-Central Ohio. GSA Bulletin ; 80 (10): 1931–1946.
Trenhaile, A. S. (1971). Drumlins: their distribution, orientation, and morphology. Canadian Geographer/Le Géographe canadien, 15(2), 113-126.
Trommelen, M. S., Ross, M., and Ismail, A. (2014). Ribbed moraines in northern Manitoba, Canada: Characteristics and preservation as part of a subglacial bed mosaic near the core regions of ice sheets. Quaternary Science Reviews, 87, 135–155.
Tulaczyk, S., Kamb, W. B., & Engelhardt, H. F. (2000a). Basal mechanics of ice stream B, West Antarctica: 1. Till mechanics. Journal of Geophysical Research: Solid Earth, 105(B1), 463-481.
Tulaczyk, S. M., Kamb, W. B., and Engelhardt, H. F. (2000b). Basal mechanics of Ice Stream B, West Antarctica 2. Undrained plastic bed model. Journal of Geophysical Research, 105(B1), 483–494.
Tulaczyk, Slawek M., Scherer, R. P., and Clark, C. D. (2001). A ploughing model for the origin of weak tills beneath ice streams: A qualitative treatment. Quaternary International, 86(1), 59–70.

U

Utting, D.J., Ward, B.C. and Little, E.C. (2009). Genesis of hummocks in glaciofluvial corridors near the Keewatin Ice Divide, Canada. Boreas, 38(3), pp.471-481.

V

Van Landeghem, K. J., & Chiverrell, R. C. (2020). Bed erosion during fast ice streaming regulated the retreat dynamics of the Irish Sea Ice Stream. Quaternary Science Reviews, 245, 106526.
van der Meer, J. J., Menzies, J., & Rose, J. (2003). Subglacial till: the deforming glacier bed. Quaternary Science Reviews, 22(15-17), 1659-1685.

van der Veen, C. J., & Payne, A. J. (2004). Modelling land-ice dynamics. Mass Balance of the Cryosphere Observations and Modelling of Contemporary and Future Changes, 169-219.
Venditti, J. G., Nittrouer, J. A., Allison, M. A., Humphries, R. P., & Church, M. (2019). Supply-limited bedform patterns and scaling downstream of a gravel–sand transition. Sedimentology, 66(6), 2538-2556.
Vérité, J., Ravier, É., Bourgeois, O., Pochat, S., Lelandais, T., Mourgues, R., Clark, C. D., Bessin, P., Peigné, D., & Atkinson, N. (2021). Formation of ribbed bedforms below shear margins and lobes of palaeo-ice streams. Cryosphere, 15(6), 2889–2916.
Vérité, J., Ravier, É., Bourgeois, O., Bessin, P., Livingstone, S. J., Clark, C. D., Pochat, S., & Mourgues, R. (2022). Formation of murtoos by repeated flooding of ribbed bedforms along subglacial meltwater corridors. Geomorphology, 408(April), 108248.
Vérité, J., Ravier, É., Bourgeois, O., Bessin, P., & Pochat, S. (submitted). A new morphometric approach revealing the morphological diversity and evolution of subglacial bedforms. 1–29.
Vernon, P. (1966). Drumlins and Pleistocene ice flow over the Ards Peninsula/Strangford Lough area, County Down, Ireland. Journal of Glaciology, 6(45), 401-409.
Vijay, S., King, M. D., Howat, I. M., Solgaard, A. M., Khan, S. A., & Noël, B. (2021). Greenland ice-sheet wide glacier classification based on two distinct seasonal ice velocity behaviors. Journal of Glaciology, 67(266), 1241-1248.
Vore, M. E., Bartholomaus, T. C., Winberry, J. P., Walter, J. I., & Amundson, J. M. (2019). Seismic tremor reveals spatial organization and temporal changes of subglacial water system. Journal of Geophysical Research: Earth Surface, 124(2), 427-446.

W

Wagner (2014), K. Ribbed moraines and subglacial geomorphological signatures of interior-sector palaeo-ice sheet dynamics.
Walder, J., & Hallet, B. (1979). Geometry of former subglacial water channels and cavities. Journal of Glaciology, 23(89), 335-346.
Waller, R., Phillips, E., Murton, J., Lee, J., & Whiteman, C. (2011). Sand intraclasts as evidence of subglacial deformation of Middle Pleistocene permafrost, North Norfolk, UK. Quaternary Science Reviews, 30(23-24), 3481-3500.
Weertman, J. (1972). General theory of water flow at the base of a glacier or ice sheet. Reviews of Geophysics, 10(1), 287-333.
Wellner, J. S., Lowe, A. L., Shipp, S. S., & Anderson, J. B. (2001). Distribution of glacial geomorphic features on the Antarctic continental shelf and correlation with substrate: Implications for ice behavior. Journal of Glaciology, 47(158), 397–411.
Whillans, I. M., & van der Veen, C. J. (1997). The role of lateral drag in the dynamics of Ice Stream B, Antarctica. Journal of Glaciology, 43(144), 231-237.
Williams, J. J., Gourmelen, N., & Nienow, P. (2020). Dynamic response of the Greenland ice sheet to recent cooling. Scientific reports, 10(1), 1-11.
Winsborrow, M. C. M., Clark, C. D., and Stokes, C. R. (2004). Ice streams of the Laurentide Ice Sheet. Geographie Physique et Quaternaire, 58(2–3), 269–280.
Winsborrow, M. C. M., Clark, C. D., and Stokes, C. R. (2010). What controls the location of ice streams? Earth-Science Reviews, 103(1–2), 45–59.
Winsborrow, M. C. M., Stokes, C. R. & Andreassen, K (2012). Ice-stream flow switching during deglaciation of the southwestern Barents Sea. Bull. Geol. Soc. Am. 124, 275–290.
Wysota, W (1994). Morphology, internal composition and origin of drumlins in the southeastern part of the Chelmno-Dobrzyń Lakeland, North Poland. Sediment. Geol. 91, 345–364.

Y

Young, T. J., Schroeder, D. M., Jordan, T. M., Christoffersen, P., Tulaczyk, S. M., Culberg, R., & Bienert, N. L. (2021). Inferring ice fabric from birefringence loss in airborne radargrams: Application to the eastern shear margin of Thwaites Glacier, West Antarctica. Journal of Geophysical Research: Earth Surface, 126(5), e2020JF006023.

Z

Zárate, M. A., & Tripaldi, A. (2012). The aeolian system of central Argentina. Aeolian research, 3(4), 401-417.
Zeng, C., Gremaud, V., Zeng, H., Liu, Z., & Goldscheider, N. (2012). Temperature-driven meltwater production and hydrochemical variations at a glaciated alpine karst aquifer: implication for the atmospheric CO2 sink under global warming. Environmental Earth Sciences, 65(8), 2285-2297.
Zheng, W., Pritchard, M. E., Willis, M. J., and Stearns, L. A. (2019). The Possible Transition From Glacial Surge to Ice Stream on Vavilov Ice Cap. Geophysical Research Letters, 46(23), 13892–13902.
Zoet, L. K., Rawling III, J. E., Woodard, J. B., Barrette, N., & Mickelson, D. M. (2021). Factors that contribute to the elongation of drumlins beneath the Green Bay Lobe, Laurentide Ice Sheet. Earth Surface Processes and Landforms, 46(13), 2540-2550.
Zwally, H. J., Abdalati, W., Herring, T., Larson, K., Saba, J., & Steffen, K. (2002). Surface melt-induced acceleration of Greenland ice-sheet flow. Science, 297(5579), 218-222.

ANNEXES

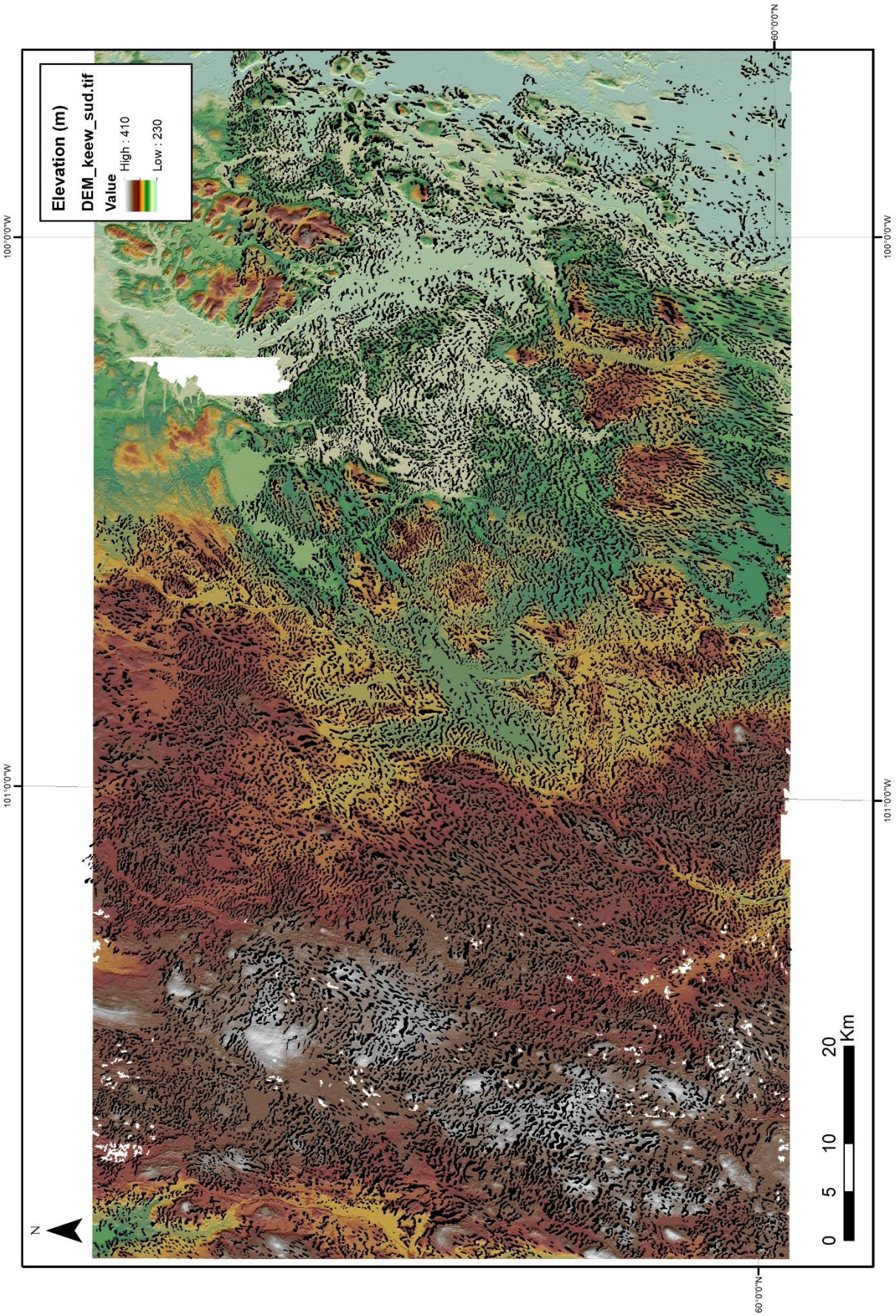

Annexe 1 *– Digital Elevation Model and digitized bedforms of Poorfish Lake area (Canada)*

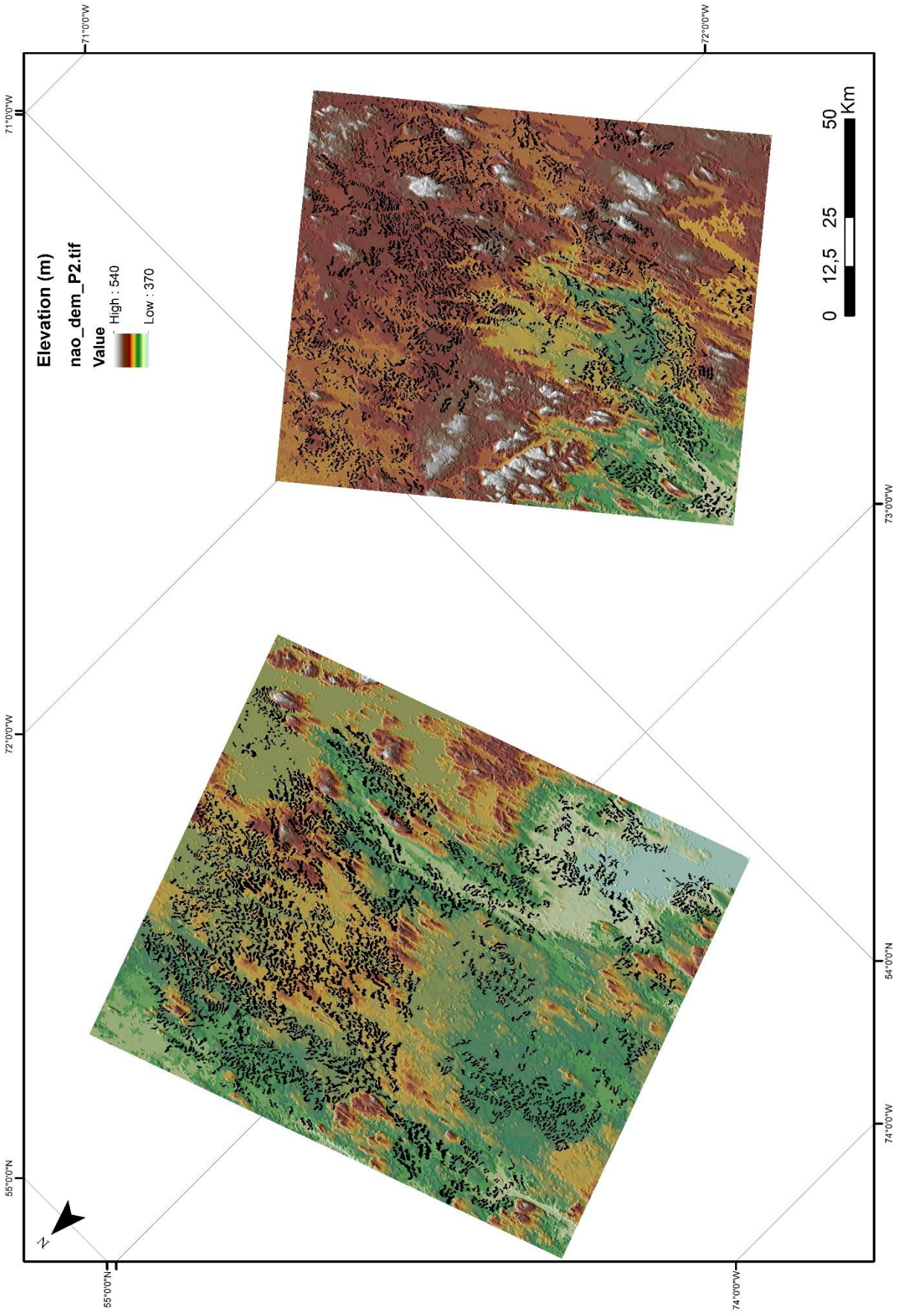

Annexe 2 *– Digital Elevation Model and digitized bedforms of Naococane Lake area (Canada)*

DOCTORAT ECOLOGIE
BRETAGNE GEOSCIENCES
LOIRE AGRONOMIE ALIMENTATION

Le Mans Université

université angers

Titre : **Diversité morphologique, formation et évolution des bedforms sous-glaciaires : implications pour la compréhension des interactions glace-eau-sédiments**

Mots clés : géomorphologie / modélisation analogique / bedforms sous-glaciaires / calottes glaciaires / fleuves de glace / routes de drainage sous-glaciaires

Résumé : En raison de l'inaccessibilité des environnements sous-glaciaires actuels, les bedforms découverts après le retrait glaciaire constituent d'excellents témoins interactions glace-eau-sédiments. Leur étude permet notamment d'appréhender les relations entre les caractéristiques de la dynamique d'écoulement de la glace, de l'hydrologie sous-glaciaire et des sédiments sous-glaciaires. Ce travail présente une nouvelle méthode d'étude des bedforms sous-glaciaires combinant la modélisation analogique et de la géomorphologie glaciaire. Au travers d'une analyse morphométrique inédite permettant de caractériser la diversité des bedforms, deux continuums morphologiques ont été découverts (i) entre les ribbed bedforms, les bedforms sinueux/obliques et les linéations glaciaires et (ii) entre les ribbed bedforms, les proto-murtoos et les murtoos. Ces continuums ont mis en évidence des séquences d'évolution de bedforms contrôlées par (i) la quantité et les directions de déformation transmises au lit sédimentaire par l'écoulement de glace sus-jacent et (ii) le degré de remobilisation généré par l'écoulement d'eau de fonte. Considérant les variations spatio-temporelles des interactions glace-eau-sédiments et des processus de déformation, d'érosion et de dépôt à la base des calottes glaciaires, un unique modèle d'évolution est proposé afin d'expliquer la formation de la plupart des bedforms sous-glaciaires actuellement identifiés.

Title : **Morphological diversity, formation and evolution of subglacial bedforms : implications for the understanding of ice-meltwater-bed interactions**

Keywords : geomorphology / analog modeling / subglacial bedforms / ice sheet / ice streams / subglacial meltwater routes

Abstract : Considering the inaccessibility of modern subglacial environments, bedforms discovered after the retreat of ice sheets are critical relics of subglacial processes. Their thorough investigation allows the relationships between the characteristics of ice flow dynamics, subglacial hydrology and subglacial sediments to be unraveled. This work presents a new method for studying subglacial bedforms combining analog modeling and glacial geomorphology. We developed an innovative morphometric analysis enlightening the diversity of subglacial bedforms and morphological continuums (i) between ribbed bedforms, sinuous/oblique bedforms and streamlined bedforms and (ii) between ribbed bedforms, proto-murtoos and murtoos. These bedform continuums highlight several morphological evolutionary sequences controlled by (i) the quantity and directions of deformation transmitted to the bed by the ice flow and (ii) the degree of remobilization induced by meltwater flow. Considering the spatio-temporal variations of ice-meltwater-bed interactions and deformation, erosion and deposition processes at the base of ice sheets, a unifying evolutionary model is proposed to explain the formation of the most subglacial bedforms currently observed.